Role of Fused Ring Size in Organocatalysis by Bicyclic Triazolium Salts

JIAYUN ZHU

Role of Fused Ring Size in Organocatalysis by Bicyclic Triazolium Salts

Jiayun Zhu

A thesis submitted in partial fulfillment of the requirements for the degree of Doctor of Philosophy

Department of Chemistry

Durham University

Mar 2019

Declaration

This work described in this thesis was carried out at the Department of Chemistry, Durham Univeristy between Oct 2016 and Mar 2019, under the supervision of Dr. AnnMarie O'Donoghue. The material contained has not been previously submitted for a degree at this or any other university. All work has been carried out by the author unless otherwise indicated.

Jiayun Zhu

Copyright

Abstract

Despite many advances in synthetic organocatalysis by N-heterocyclic carbenes (NHCs), it is not understood why product distributions often differ dramatically with catalyst scaffold or with subtle substituent variation within a catalyst family. We herein focused on the kinetic and structural analysis of the origins of the NHC-catalytic behavior.

Overall, sixteen N-aryl substituted bicyclic triazolium satls were attempted, and twelve of them were successfully isolated and purified, and ten crystal structures of them were obtained. During the preparation of these triazolium salts, novel dialkoxy acetal adduct was isolated. We modified the synthetic procedure of triazolium and successfully obtained three pure dialkoxy acetal analogues, and four crystal strucutres of this category. In parallel, three synthetic trials of bis(amino)cyclopropenium salts, precursors of a new class of carbene, were performed.

We used the triazolium salts as carbene precursors to kinetically evaluate the influence of backbone structures towards the catalytic properties. In total, seventeen aryl-substituted aldehydes and fifteen N-aryl bicyclic triazolium salts were used to conduct over one hundred benzoin condensation experiments. The formation and decay of reactants, intermediates, products and by-products were monitored *in situ* by ^{1}H NMR spectroscopy, and reaction parameters were calculated and fitted by three parallel methonds.

Changing the fused ring size of triazolium salts shows dramatic differences on reaction paraemters of benzoin condensation. Increasing fused ring size from n=1 to n=2 largely decreased the formation rate constant, k_1, $M^{-1}s^{-1}$, of a key intermediate (4.2-7.8 fold), while the formation rate constant with n=2 and n=3 are comparable. The opposite trend

can be observed for the dissociation constant, k_{-1}, s^{-1}, of the intermediate, with increased fused ring size decreases the dissociation rate constants. The combined variation of k_1 and k_{-1} lead to the overall equilibrium constant of the intermediate formation, K, M^{-1}, decreases with increased fused ring size of triazolium salts.

We found the electron-withdrawing aryl-substituents of both triazolium salts and aldehydes increases the formation rate constants, k_1, of the intermediate. The electron-withdrawing aryl-substituents of triazolium salts also increase the dissociation rate constants, k_{-1}, of the intermediate, while the aryl-subsituents of aldehyde only have small influence on k_{-1}.

We also aimed to find a catalytic route towards the synthesis of d_1-deuterated aledehydes. The extent of deuterium incorporation into reactant aldehyde was evaluated under different reaction conditions. We found the best deuterium exchange result at 2.2 hours with 0.02 M of pentafluorophenyl triazolium salt loading and 0.08 M of aldehyde in d_4-methanol at 25 °C, with 0.16 M NEt_3. 73% of aldehyde remained, with 99% of deuterium incorporation, and only 14% of the initial aldehyde formed benzoin product.

Contents

Abbreviations

aq.	Aqueous
Ar	aryl
Bu	butyl
Boc	butoxycarbonyl
^{13}C NMR	carbon nuclear magnetic resonance
Δ	chemical shift
D_2O	deuterium oxide
D_2	deuterium gas
DBAD	di-*tert*-butyl azodicarboxylate
DBU	1,8-diazabicycloundec-7-ene
DCM	dichloromethane
DMSO	dimethylsulfoxide
DIPEA	*N*,*N*-diisopropylethylamine
EA	elemental analysis
ee.	enantiomeric excess
ESI-MS	Electrospray Ionisation Mass Spectrometry
equiv.	equivalent
Et	ethyl
HCl	hydrogen chloride
^{1}H NMR	proton nuclear magnetic resonance
h	hour (s)
HOMO	Highest occupied molecular orbital
IR	Infrared
i-	*iso-*
J	coupling constant
k	rate constant
K	equilibrium constant
K_a	acidity constant
λ	wavelength
ln	natural logarithm
Me	methyl
MeO	methoxy
MeOD	methanol-d_4
m/z	mass to charge ratio
NaOH	sodium hydroxide
NMR	nuclear magnetic resonance
NHC	nitrogen heterocyclic carbene
Ph	phenyl
pH	acidity of aqueous solution
ppm	parts per million
R	alkyl group
t-	*tert-*
TMS	trimethylsilyl
r_{vdW}	Van de Waals' radius

Chapter 1. Introduction

1.1. Carbene: Structure and Stability

Defined as neutral compounds with a divalent carbon centre, carbenes have long been recognised as prototypical reactive intermediates[1, 2]. Depending on their spin multiplicities and ground states, carbenes can be formally classified as singlet and triplet[3, 4]. In triplet carbenes, the two valence electrons have parallel spins and accommodate different orbitals, theoretically owing to a small singlet-triplet (S-T) energy gap, *e.g.* with adjacent aromatic ring substituents (Figure 1.1)[5-9].

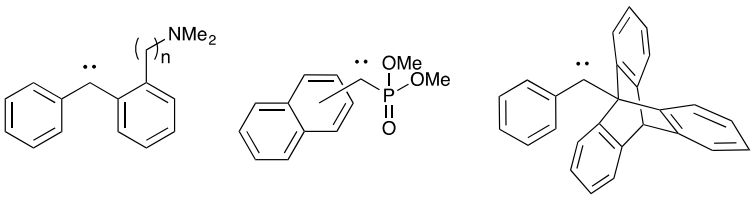

Figure 1.1. Typical triplet carbenes: a) diphenylcarbene, b) naphthyl(phosphonyl)carbene, c) phenyl(triptycyl)carbene

This project is mainly focused on isolable singlet carbene derivatives and particularly including bicyclic N-heterocyclic carbenes (NHCs) **1**. NHCs are defined as formally neutral compounds with the carbenic centre directly connected to at least one nitrogen center in a heterocyclic system[10-13]. Depending on the electronic and steric properties of NHCs, the S-T energy gap are relatively large, thereby confining the two valence electrons in the HOMO and reducing 1,1-dimerisation. The suppression of dimerization is an essential factor underpinning the versatility and stability of carbenes[14-16].

Regarding NHCs, the size of the S-T energy gap is largely influenced by the inductive and mesomeric effects of the adjacent nitrogen atom (Figure 1.2b). The reduction of

electron deficiency caused by the neighbouring nitrogen atom was thought to be indispensable, and singlet carbenes were supposed to be isolable only when at least one π-donor heteroatom was directly attached to the carbene centre[1].

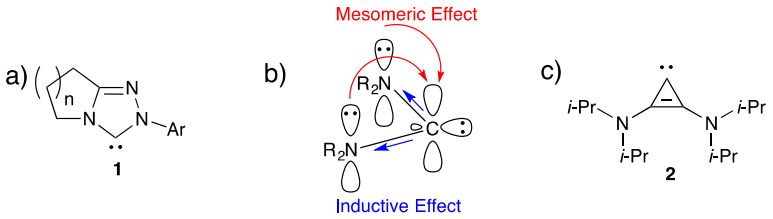

Figure 1.2. a) Bicyclic NHC **1**, b) Inductive and mesomeric effects of neighbouring substituents in NHC, c) bis(diisopropylamino)cyclopropenylidene **2**.

This concept was disproved by the preparation, isolation and single X-ray crystal diffraction study of bis(diisopropylamino)cyclopropenylidene (BAC) **2**, which will be mainly introduced in Chapter 5. Meanwhile, apart from the electronic stabilisation for NHCs, sterically bulky N-substituents could also favour higher stability by increasing the dimerization energy barrier[14, 15, 17].

1.2. NHCs in Organocatalysis:

1.2.1. Umpolung Reaction Catalysed by N-Heterocyclic Carbenes (NHCs)

The catalytic nature of carbenes relies on their accessibility towards several "Umpolung" transformations. "Umpolung", first introduced by Seebach, represents a series of reactions that proceed *via* reversed conventional functional group polarity[18]. For a number of decades, cyanide was utilised as the main source of umpolung reactivity for the reaction of aldehydes[19, 20]. As Scheme 1.1a shows, the negatively charged cyanide attacks the carbonyl group of aldehydes, and donates electron density to the C=O bond, thereby facilitating the development of a partial negative charge on carbon[21]. Another

classical example of umpolung reaction involves a dithiane for inversion of polarity (Scheme 1.1b)[22]. With the assistance of *n*-butyl lithium, a bisthio masked aldehyde can be generated into a nucleophilic source, which can be applied as d^1 keto synthons[23, 24].

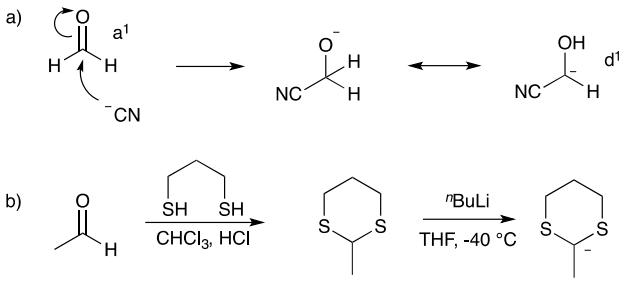

Scheme 1.1. Umpolung process involving a) cyanide anion, b) dithiane and aldehyde

Umpolung reactions utilising carbenes as organocatalysts typically involve the *in situ* deprotonation of a precursor cation **3** to form the catalytic carbene **4**, followed by the addition to an electrophilic moiety (Scheme 1.2). Depending on the nature of reagents, four possible discrete reactive intermediates could be generated. The four synthons are classified as nucleophiles (acyl anion, enolate, and homoenolate) and electrophiles (acyl azolium), often with remarkable chemo-, regio-, and stereo-selectivities. An overview of typical reactions of NHCs containing these intermediates will be introduced in the following section, and particular attention will be devoted to acyl anion equivalents according to the project aim[25, 26].

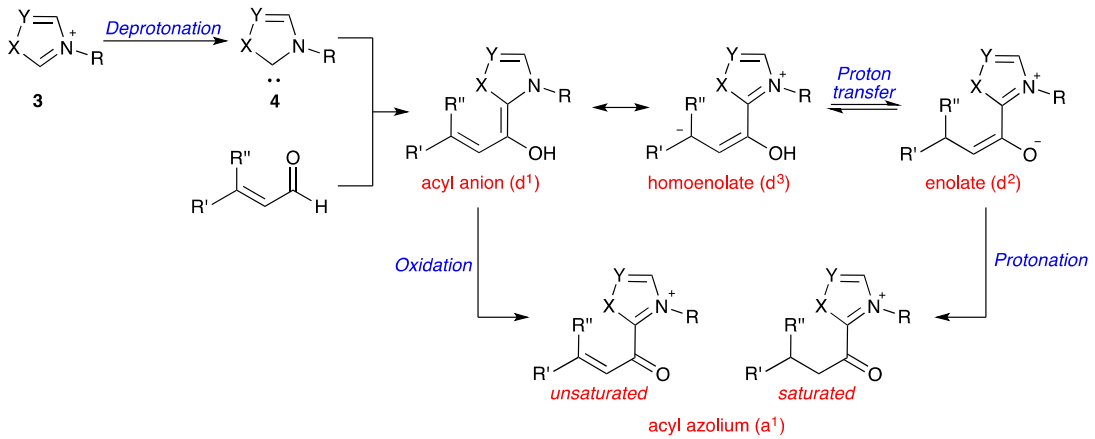

Scheme 1.2. Four possible synthons generated by NHCs and α,β-unsaturated aldehyde.

1.2.2. Acyl Anion Equivalents (d^1 Synthons)

Hydroxyaryl adduct **5**, formed by the reaction of NHC and aldehyde, can generate an acyl anion equivalent **6** via deprotonation, which is commonly referred to "Breslow intermediate" (Scheme 1.3). This d^1 synthon could either react with another aldehyde to undergo a benzoin condensation, or it may combine with an α,β-unsaturated ketone or ester through the Stetter reaction[2, 26]. The combination of Breslow intermediate with other electron-acceptors (*e.g.* ketone, olefin) will be introduced briefly in Section 1.2.2.2.

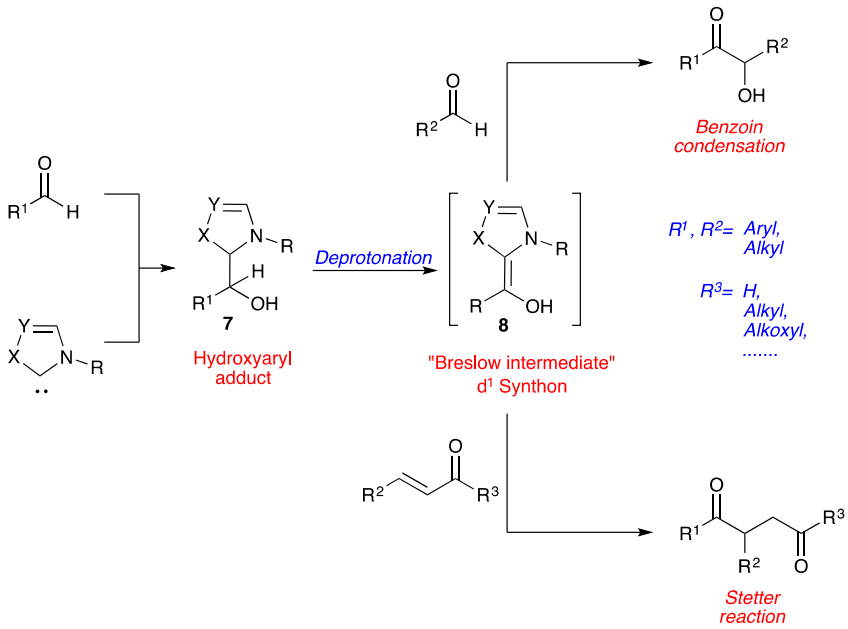

Scheme 1.3. Brief description of the benzoin condensation and Stetter reaction.

1.2.2.1. The Homobenzoin Condensation

Although the dimerization of aldehydes was first reported by Liebig in 1832, it was not until 1943 that Ukai replaced the cyanide group by using the NHC as an organocatalyst in the benzoin condensation[27, 28]. Ukai used a naturally occurring thiazolium salt, vitamin B_1 (**7**, Scheme 1.4), as the precursor to generate the corresponding thiazolyl carbene for aldehyde dimerization. Later on, Mizuhara suggested the catalytic activity

was derived from the thiazolium centre[29, 30], and the groundbreaking mechanistic study was published by Breslow in 1958[31]. Although Breslow represented the active catalytic centre with ylidic structure **8**, the thiazolyl carbene **9** is now known also to be a significant resonance structure. These early studies underpin a massive volume of research focusing on organocatalysis of the benzoin and related reactions catalysed by NHCs and derivatives[32-35].

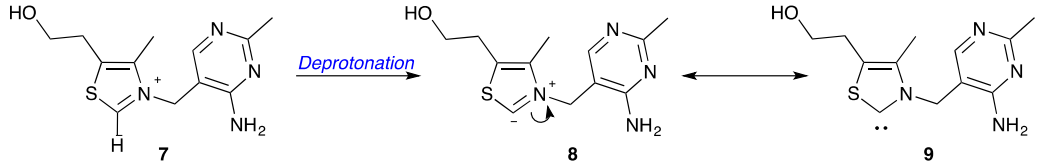

Scheme 1.4. First synthetic generation of thiazolyl carbene **9** from Vitamin B_1 precursor **7**.

Sheehan reported the first asymmetric benzoin condensation in 1966 catalysed by thiazolyl carbene **10** with poor results (22% *ee.*). Further artificial modifications of thiazolium derivatives increased the enantioselectivity of the benzoin product up to 52% *ee*., however, in very low yield (Figure 1.3)[36, 37].

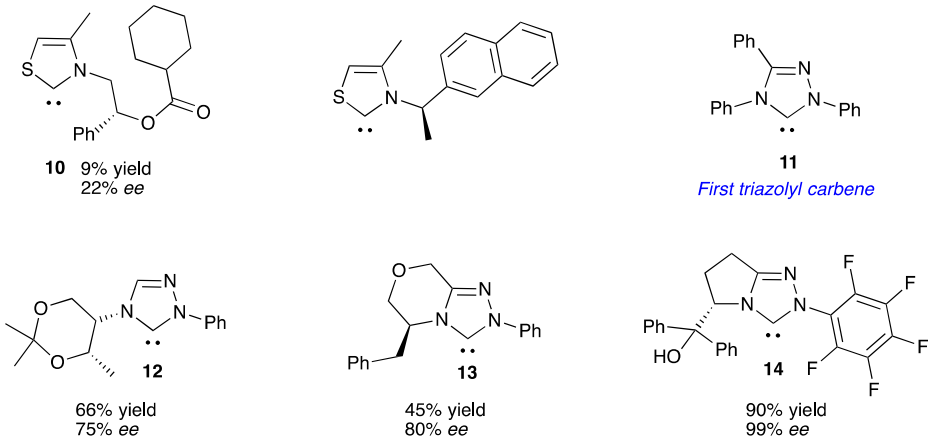

Figure 1.3. Development of chiral NHCs.

After Enders designed the first triazolyl carbene **11** in 1995[38], triazolium-derived NHCs have been shown to outperform related thiazolium salts considering efficacies and selectivities. In 1996, Enders introduced the first chiral triazolyl carbene **12**-catalysed

benzoin condensation and achieved the product in 75% *ee* and 66% yield[39]. Two years later, Leeper showed that the bicyclic triazolyl carbenes **13** resulted in better enantioselectivities (80% *ee*), which led to the development of NHCs with fundamental bicyclic structures[40, 41]. Among the bicyclic NHCs, Connon reported that the most efficacious triazolyl carbene **14** (4 mol%) could afford a benzoin product in excellent yield (90%) and high enantioselectivity (99% *ee*) in 2009[42]. The formation of a hydrogen bond between adduct **5** and aldehyde was proposed to explain the high selectivity. Compared with thiazolyl derivatives, the higher stability and the extra sterically-occupied substituent on nitrogen was proposed to result in the better yields and enantioselectivities[26, 40].

Interestingly, the enantioselectivity of structurally similar triazolium and thiazolium salts are often opposite to each other. For instance, the triazolium salt **15** generates (*S*)-benzoin product with 80% *ee*, while thiazolium salt **16** provides (*R*)-benzoin, however, with only 19.6% *ee*[26]. It was suggested that the steric hindrance provided by the extra-aryl group of the triazolium salt impedes the approach of the aldehyde with the carbenic and aldehydic phenyl groups on the same side (Figure 1.4). Subsequent computational study also agreed with the stereo-control caused by the unfavoured *N*-aryl interactions between the catalyst and aldehyde[43].

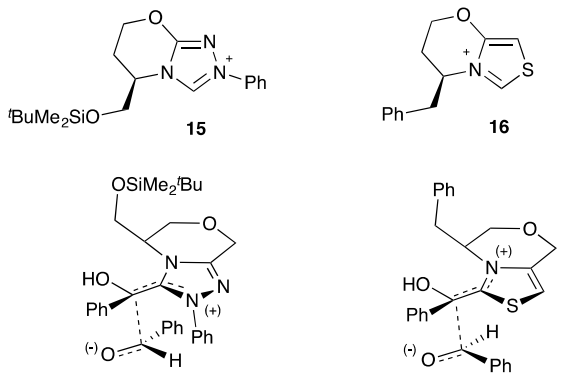

Figure 1.4. Structurally similar triazolium salt **15** and thiazolium salt **16** and their preferred transition state.

1.2.2.2. Extension of Carbene-Derived d[1] Synthon Methodology

The use of an alternative second acceptor expands the catalytic prospects of carbenes, *e.g.* aldehyde, Michael acceptor, ester, and olefins[2, 26, 44]. The inclusion of an alternative second electrophile, however, introduces chemoselectivity issues relating to the formation of the homobenzoin product[45].

The cross-benzoin reaction was first reported in 1976 utilising two different aldehydes[45], and various catalyst types have been studied to investigate the chemoselectivity[46, 47]. In 2003, Suzuki reported the first cross-benzoin reaction with ketone acceptors, which involved an intramolecular hetero-coupling between aldehydes and ketones (Scheme 1.5a)[48]. Later on, several groups investigated the enantioselectivites of the aldehyde-ketone cross benzoin reactions, and all suggested excellent catalytic efficacies of NHCs[49-52]. In particular, Rovis reported a cascade system catalysed by NHC **17** along with a secondary amine (Jørgensen–Hayashi catalyst **18**), and showed perfect cooperation of the two catalysts with excellent yields and selectivities (Scheme 1.5b)[53, 54]. In 2001, Frantz first coupled the Breslow intermediate to an imine, and created the precedent of an aza-cross-benzoin reaction (Scheme 1.5c)[55]. Both aliphatic and aromatic aldehyde and imine substrates are well suited towards this reaction type[56-59].

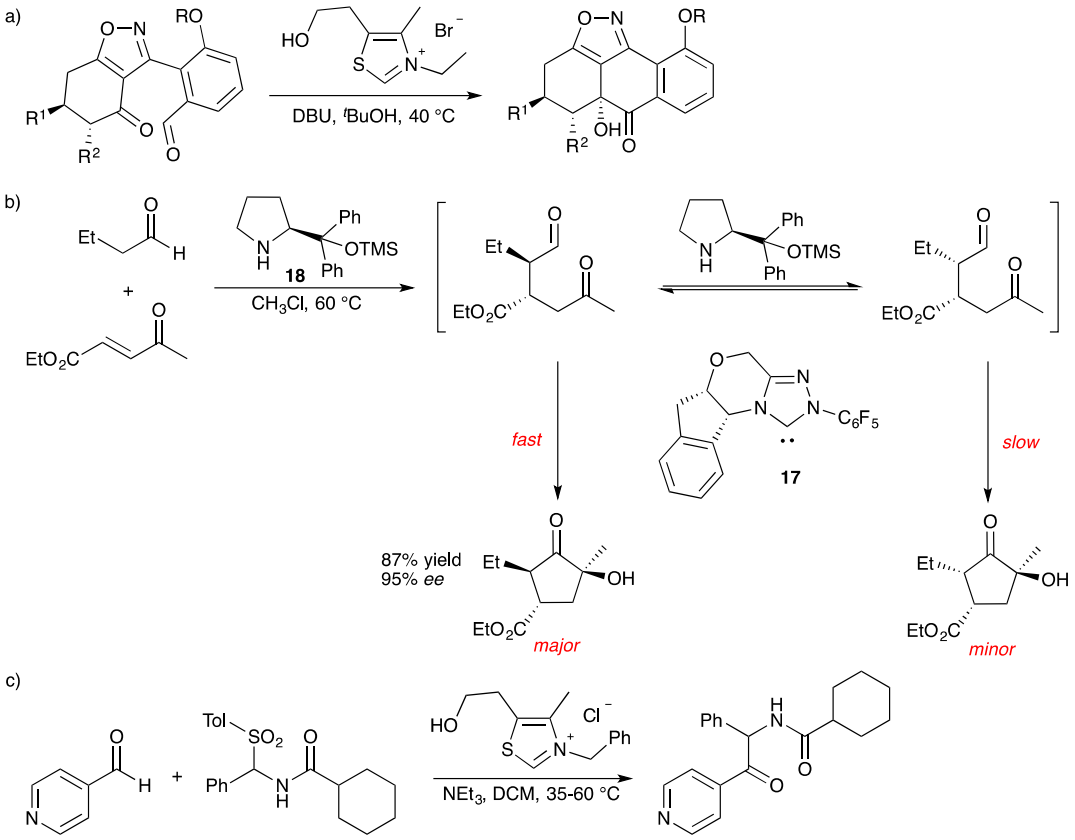

Scheme 1.5. a) The intramolecular cross-benzoin reaction with a ketone acceptor, b) a cascade enantioselective Stetter reaction using an amine co-catalyst, c) a typical aza-cross-benzoin condensation reaction *via* reaction with an imine formed *in situ*

The intermolecular Stetter reaction provides important access to many organic precursors[44]. This NHC-catalysed addition of an aldehyde to a Michael acceptor, presumed to be *via* Breslow intermediate formation, was first reported by Stetter in 1976 (Scheme 1.6a)[60], and several alternative Michael acceptors have been subsequently employed. For instance, You reported arylsulfonyl-indoles as precursors of α,β-unsaturated iminium ions (Scheme 1.6b)[61], and Massi demonstrated the use of alkyl α-diketones as acetaldehyde donors (Scheme 1.6c)[62]. Moreover, the enantioselectivity of the intermolecular Stetter reaction can also be modified by using different types of carbene catalysts[35, 63-65], which was first analysed by Enders in 1989[26].

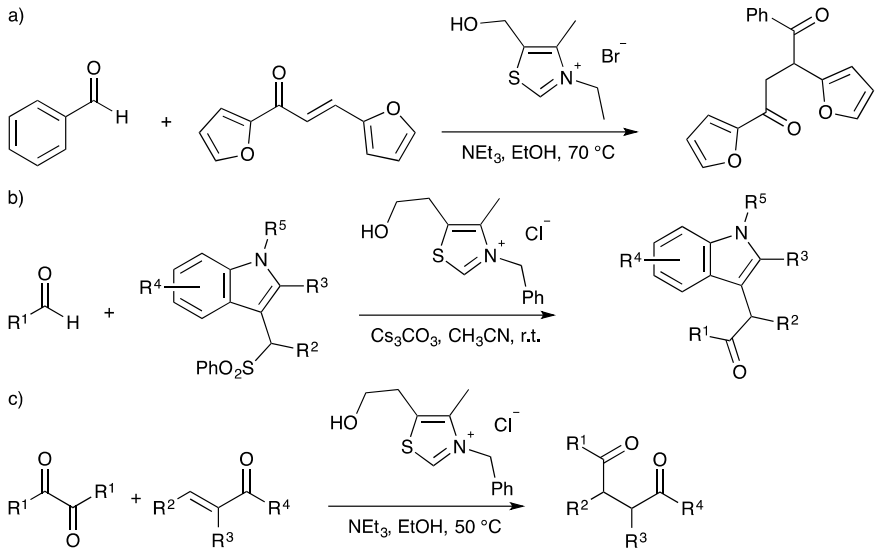

Scheme 1.6. a) Earliest Stetter reaction reported in 1976, b) Stetter reaction using arylsulfonyl-indoles as reagent precursor, c) Stetter reaction with alkyl α-diketones

It was not until 1995 that the first intramolecular Stetter reaction was reported by Ciganek[66], followed by an enantioselective variant in the next year[39], which has been one of the most attractive areas of research recently (Scheme 1.7)[67]. The O'Donoghue and Smith groups focused on the mechanistic insight of Stetter reactions, and the rate and equilibrium constants of formation of the adduct, and Breslow intermediate were measured[68].

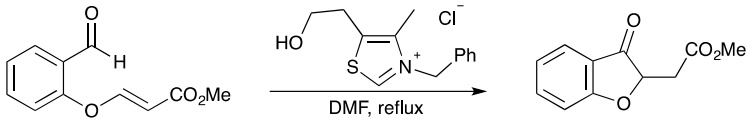

Scheme 1.7. First intramolecular Stetter reaction

NHC-derived d^1 synthon activity towards unactivated olefins was discovered serendipitously by Pan in 2006 as they found the reaction selectivity of a tethered alkyl tosylate **19** changed with the addition of phenyl group (Scheme 1.8a)[69]. Later on, using an isotope labelling method, the detailed mechanism of this reaction *via* olefin formation was proposed by She in 2008 (Scheme 1.8b)[70]. Based on this mechanism, Glorius raised the possible coupling of aldehydes to unactivated alkenes and alkynes, and also

described the enantioselective hydroacylation of tethered styrenes[71].

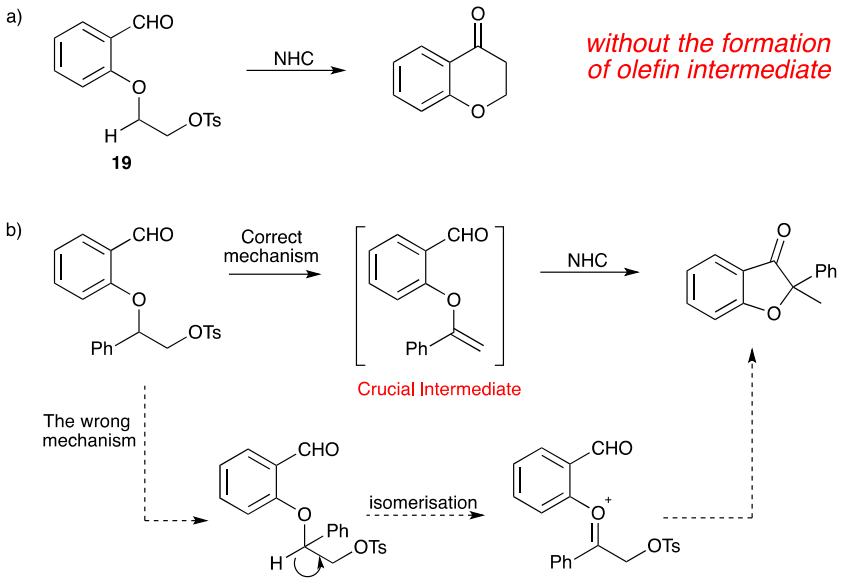

Scheme 1.8. Selectivity of tethered tosylate **19** change by introduction of a phenyl group

1.2.3. Enolate (d^2), Homoenolate (d^3) and Acyl Azolium (a^1) Derivatives

Apart from the benzoin and Stetter reactions *via* acyl anion formation, substrates with an α-reducible functional group, a leaving group, or with unsaturation adjacent to the carbonyl group, can also be applied. These reactions are proposed to involve three alternative intermediates: azolium enol, homoenolate, and acyl azolium, which can be recognised as d^2, d^3, and a^1 synthons, respectively.

1.2.3.1. Azolium Enolate Equivalents (d^2 Synthons)

Azolium enolates, typical d^2 synthons, can be generated through two key pathways: proton transfer from homoenolate analogues, or *via* direct coupling of a NHC to a ketene (Scheme 1.9)[26].

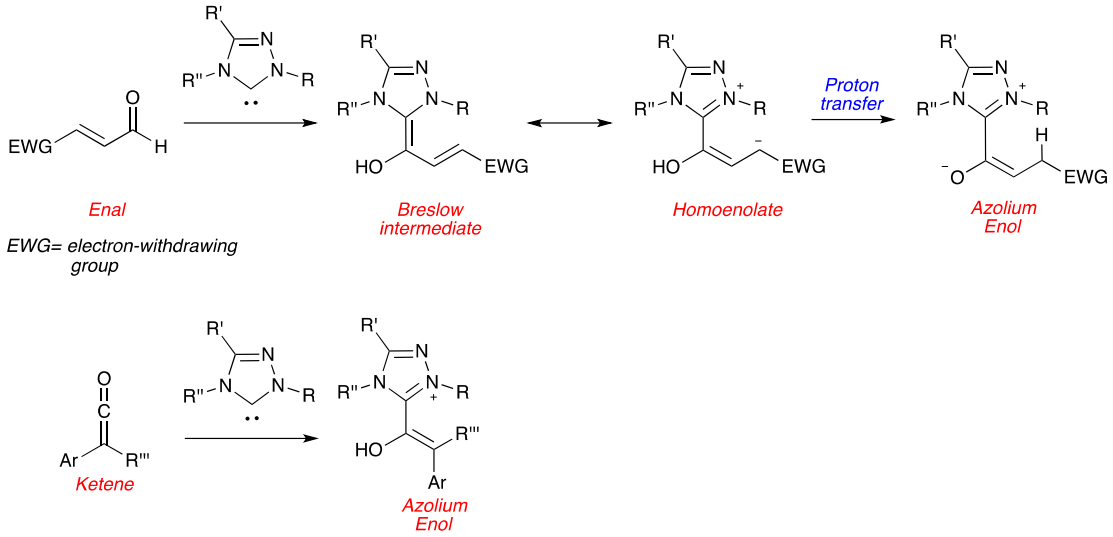

Scheme 1.9. Two pathways towards azolium enolate formation

In 2006, Bode reported the first analysis of an azolium enolate in a hetero-Diels-Alder transformation[72]. The combination of a NHC and an electrophilic enal traps the Breslow intermediate in its enol form *via* a highly reactive homoenolate. The following OH-Cγ proton transfer generates the azolium enolate. Notably, the formation of the azolium enolate is assumed to be the crucial divergence point compared to the reaction with homoenolate derivatives[73]. A computational modelling experiment suggest the proton transfer towards homoenolate is most efficient with the assistance of base (*e.g.* Hunig's base)[74]. By controlling the reaction parameters (*e.g.* solvent, base), Berkessel achieved two azolium enolates, and demonstrated the first X-ray characterization of azolium enolate derivatives (Figure 1.5).

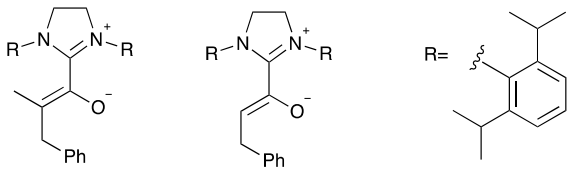

Figure 1.5. Berkessel achieved azolium enolates derivatives

The direct formation of an azolium enol was first suggested by Ye *et al*. during an asymmetric Staudinger reaction[75]. This reaction couples a ketene with an imine to

generate α,β-lactam, and there are two potential mechanisms for this process (Scheme 1.10, mechanism A and B) as NHCs react sluggishly with less electron-deficient imines (*e.g.* N-Boc imines). Ye suggested that the mechanism *via* azolium enol formation (mechanism A) should be favoured in these cases.

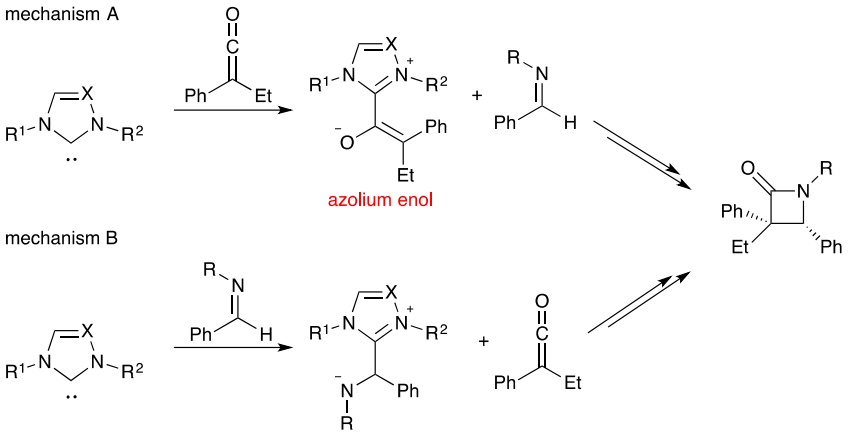

Scheme 1.10. Two potential mechanisms for the NHC-catalysed asymmetric Staudinger reaction

Apart from Ye's report, this d^2 synthon may react with an electrophile to undergo [4+2] or [2+2] cycloadditions, *e.g.* the nucleophilic attack towards aldimines or ketamines to yield the corresponding activated carboxylates **20** and **21**[76-78].

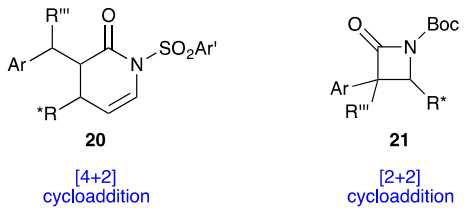

Figure 1.6. [4+2] and [2+2] cycloaddition product of azolium enolate derivatives

1.2.3.2. Homoenolate Equivalents (d^3 Synthons)

The combination of NHCs with an α,β-unsaturated aldehyde allows negative charge transfer through the conjugate system, and yields the homoenolate form of Breslow

intermediate (Scheme 1.11)[79].

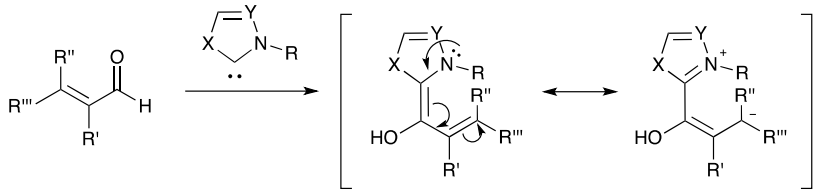

Scheme 1.11. Transformation from Breslow intermediate to homoenolate equivalent

The homoenolate equivalent was first reported in 2004, and was found to be a key intermediate in many reactions[80, 81]. For instance, the coupling of a homoenolate with an aryl-aldehyde or a protected ketamine could afford the corresponding γ-butyrolactones or γ-lactams[82, 83]. Moreover, in the presence of a less nucleophilic carbene and mild base (*e.g.* DIPEA), homoenolate derivatives can be protonated and undergo a redox esterification process[34, 84].

In 2004, Glorius and Bode individually reported NHC-catalysed annulation reactions between enals and aryl aldehydes, which involve homoenolate derivatives and afford γ-lactone products (Scheme 1.12)[81, 85]. Their results suggest that diarylimidazolium precatalyst **22** is the most efficient towards annulation products, while the thiazolium precatalyst **23** only gave several benzoin products without the formation of the γ-lactone product.

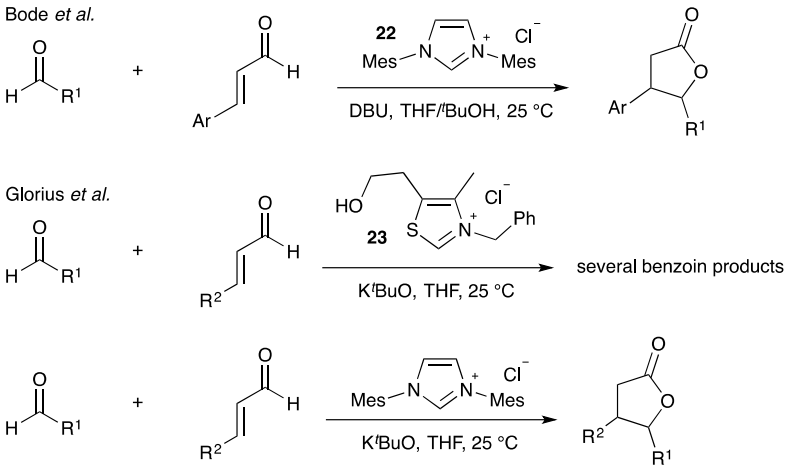

Scheme 1.12. First NHC-catalysed annulation reaction which involves homoenolate derivatives

The nitrogen heterocyclic process involving a proposed homoenolate intermediate to afford a γ-lactam was first reported in 2005, while with the imine N-substituent limited to the 4-methoxyphenylsulfonamide group (Scheme 1.13a)[82]. Later, additional ranges of imines were discovered to be suitable for γ-lactam generation, including cyclic sulfonyl ketimine **24**[83], diazene **25**[86], N-acyl hydrazone **26**[87], aza-diene **27**[88], and azomethine ylide **28**[89].

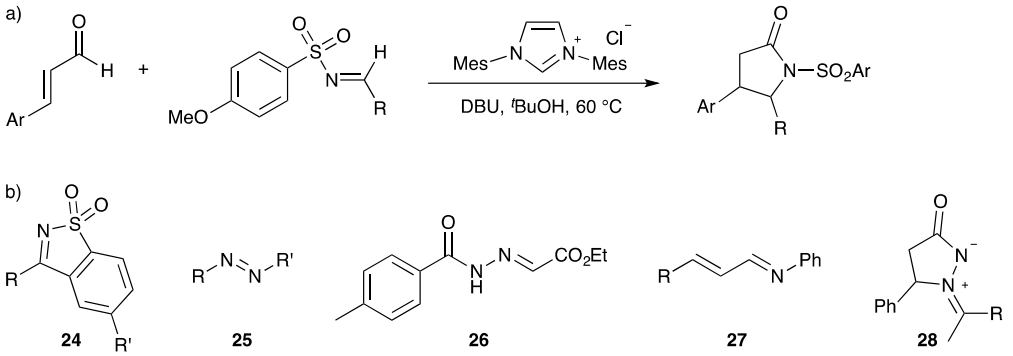

Scheme 1.13. a) First nitrogen heterocyclic process involving a homoenolate intermediate, b) several imines suitable for coupling with NHC-based homoenolate derivatives.

The homoenolate derivatives can also undergo non-annulative processes, such as the β-functionalization of enals. Scheit suggested the utilisation of an alcohol as nucleophile could trap homoenolate derivatives and form a saturated ester (Scheme 1.14a). Bode

further demonstrated this concept by showing the less nucleophilic carbenes and mild bases resulted in esterification product as Scheit's work, while the more nucleophilic NHCs preferred the formation of self-condensation product **29** (Scheme 1.14b)[34, 84].

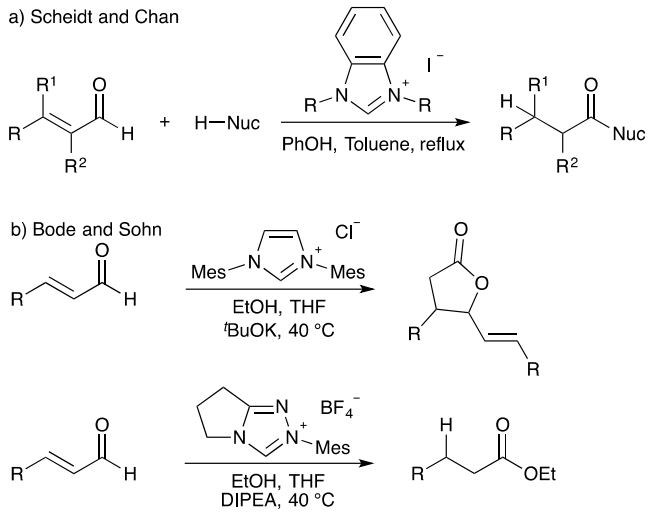

Scheme 1.14. Redox esterification of α,β-unsaturated aldehyde introduced by a) Scheidt and b) Bode

The application scope of homoenolate was mainly limited by the preparation of the starting enal. Thus, the alternative ways to afford homoenolate derivatives were studied and many other compounds were found to be suitable precursors towards homoenolates. Bode introduced the α'-hydroxyenone **30** as an efficient surrogate for an enal to undergo annulation reactions (Scheme 1.15a)[90]. The preparation of these α'-hydroxyenones is straightforward, and their utilisation bears nitrogen heterocycles (Scheme 1.15b). Notably, in contrast to other aldehydes, the Breslow intermediate formation with the α'-hydroxyenone derivatives is suggested to be irreversible.

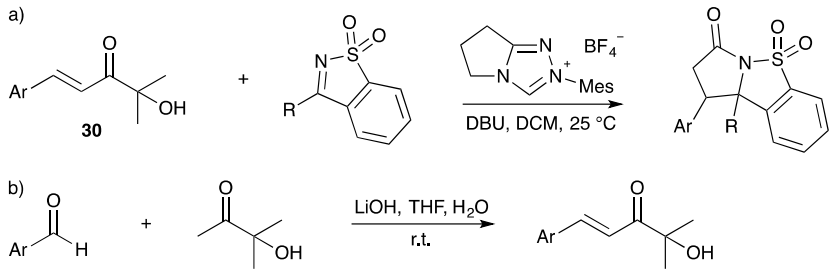

Scheme 1.15. a) Nitrogen heterocycle involved annulation reaction *via* formation of a homoenolate using α'-hydroxyenone **30** as precursor, b) straightforward synthesis of α'-hydroxyenone derivative

Chi *et al*. reported a NHC-activation of saturated carboxylic esters to generate the nucleophilic ester β-carbons, which also is proposed to involve a homoenolate intermediate (Scheme 1.16)[91]. They illustrated typical reactions generating cyclopropentenes, γ-lactones and γ-lactams, *via* homoenolate, and with good chemoselectivities. Moreover, the application of chiral triazolium salt **31** show good enantioselectivity (>87% *ee*.).

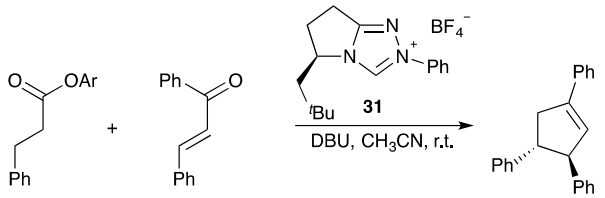

Scheme 1.16. Activation of the β-carbon of saturated esters by NHC catalysis

1.2.3.3. Acyl Azolium Equivalents (a^1 Synthons)

The above three NHC-based reactions all involved an umpolung process of the carbonyl group. NHCs can also behave as competent catalysts in non-umpolung reactions, for instance, NHC-based acyl azolium derivatives are typical a^1 synthons.

Starting with the Nolan's and Hedrick's transesterification reactions (Scheme 1.17)[33, 92], a large number of NHC-catalysed transformations *via* acyl azolium equivalents **32** have

been discovered. Based on the structure of acyl azolium salts, Rovis *et al.* classified these NHC-based acyl azolium intermediates into three different categories α,β-unsaturated acyl azolium intermediates, NHC-bound allenoate intermediate, and saturated acyl azolium intermediate[44].

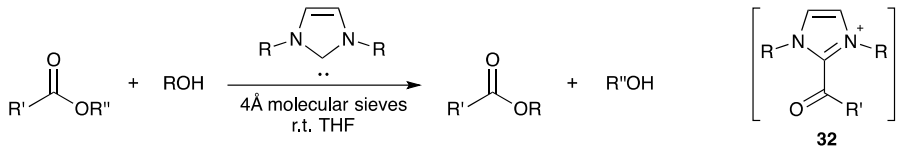

Scheme 1.17. First transesterification reaction proposed to involve acyl azolium intermediate **32**[I]

The most commonly used synthetic protocol to afford α,β-unsaturated acyl azolium salt is the oxidation of aldehydes with an oxidizable α-functional group, and most commonly using ynals **33** (Scheme 1.18). Zeitler reported the conversion of ynal **33** to α,β-unsaturated esters *via* the oxidation of the unsaturated Breslow intermediate **34** and the following protonation and tautomerisation affords the α,β-unsaturated acyl azolium ion **35**[93].

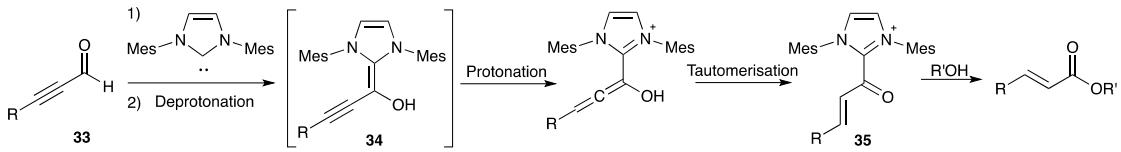

Scheme 1.18. Brief preposed mechanism of the NHC-catalysed synthesis of α,β-unsaturated esters *via* acyl azolium intermediate **35**.

In 2010, Bode demonstrated an intramolecular Claisen rearrangement of the hemiacetal **36** formed by the NHC-based acyl azolium salt and enol **37**, with good

[I] Limited experimental detail for catalyst preparation can be obtained. The deprotonation of the imidazolium precursor probably used K^{t}BuO or NaH as base. The counter ion of the acyl azolium salt **32** thus is unknown.

enantioselectivity[94]. Their kinetic study and a following computational study suggest a 1,2-addition followed by [3,3]-sigmatropic rearrangement (Scheme 1.19, mechanism B). Meanwhile, a DFT study from the Mayr group suggested a 1,4-Michael addition pathway (Scheme 1.19, mechanism A)[95]. The later on observation of the by-product of 1,2-addition from Lupton group support the Bode's mechanism (B) in certain substrate classes[96]. Digressively, Bode claimed the addition of aldehyde **38** to NHC **39** to be irreversible, the validity of which remains questionable.

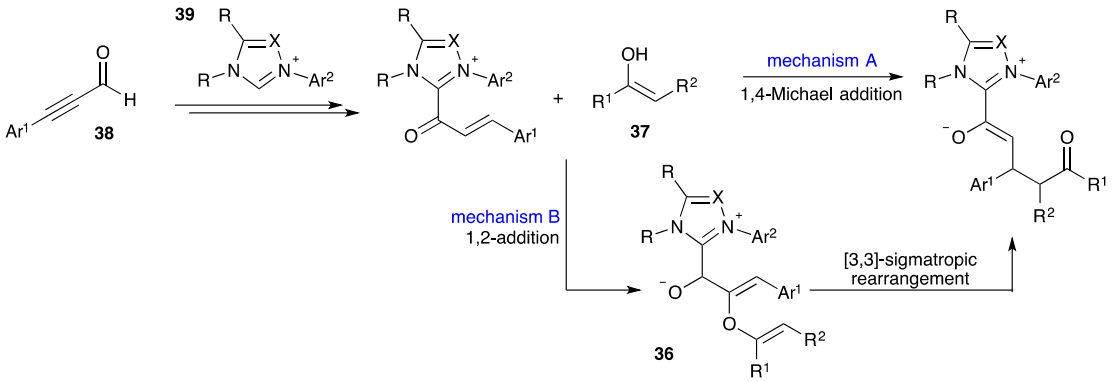

Scheme 1.19. Mechanistic study for the reaction between aldehyde **38** and enol **37**.

Apart from ynals, coupling α-bromo enals with α,β-unsaturated esters[97], or oxidation from acyl azolium precursors (*e.g.* allylic alcohols)[98] can be the alternative ways to access the acyl azolium derivatives.

Allenoates are synthetically important structural motifs, while the original synthetic method has many drawbacks[99]. Sun *et al*. demonstrated the NHC-catalysed allenoate synthesis *via* an allenoate acyl azolium intermediate[100]. The condensation between thiazolium salt **40** with an ynal aldehydes with a γ-leaving group followed by the isomerization afford the NHC-allenoyl azolium salt.

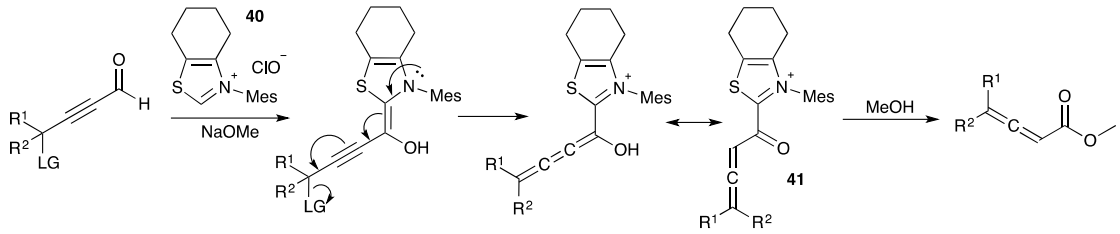

Scheme 1.20. Mechanism of the synthesis of allenoate *via* NHC-based allenoyl azolium salt **40**.

The commonly-used pathway to afford saturated acyl azolium intermediates is through transesterification or amidation from the corresponding esters. Apart from Nolan's and Hedrick's work (*e.g.* Scheme 1.17), many other groups contribute to this type of synthetic approach, including the computational study from Hu *et al.*, who demonstrated the NHC worked as Brønsted base rather than the nucleophilic reagent to afford the acyl azolium salt in their cases (Scheme 1.21)[101].

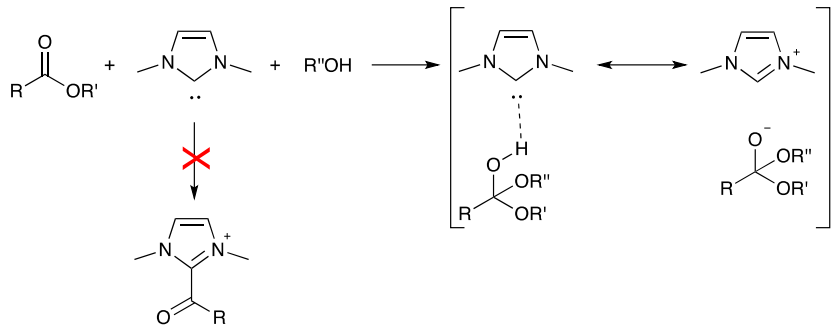

Scheme 1.21. Computational study which suggest the NHC works as a Brønsted base

1.3. Project Aims

This PhD project is divided into four parts: synthesis of triazolium salts and novel dialkoxy acetal adducts (Chapter 2); the mechanistic study of the N-heterocyclic carbene-catalysed benzoin condensation (Chapter 3); H/D-exchange of aldehydic proton and retro-benzoin condensation (Chapter 4); and the synthesis of bis(amino)cyclopropenium salts (Chapter 5). All four parts are relevant to the synthesis, mechanistic evaluation and applications of stable carbenes.

Gravel in 2014 introduced the chemoselectivity variation of cross-benzoin condensation based on catalyst fused ring size, however, with limited kinetic and mechanistic evaluation. Thus, sixteen N-aryl substituted bicyclic triazolium salts was attempted to prepare as NHC precursors, and their catalytic properties towards benzoin condensation of various aryl aldehydes are investigated. The reaction parameters of these reactions are analysed and compared to establish the general idea about the impact of backbone variation on both aldehyde and catalyst towards benzoin condensation.

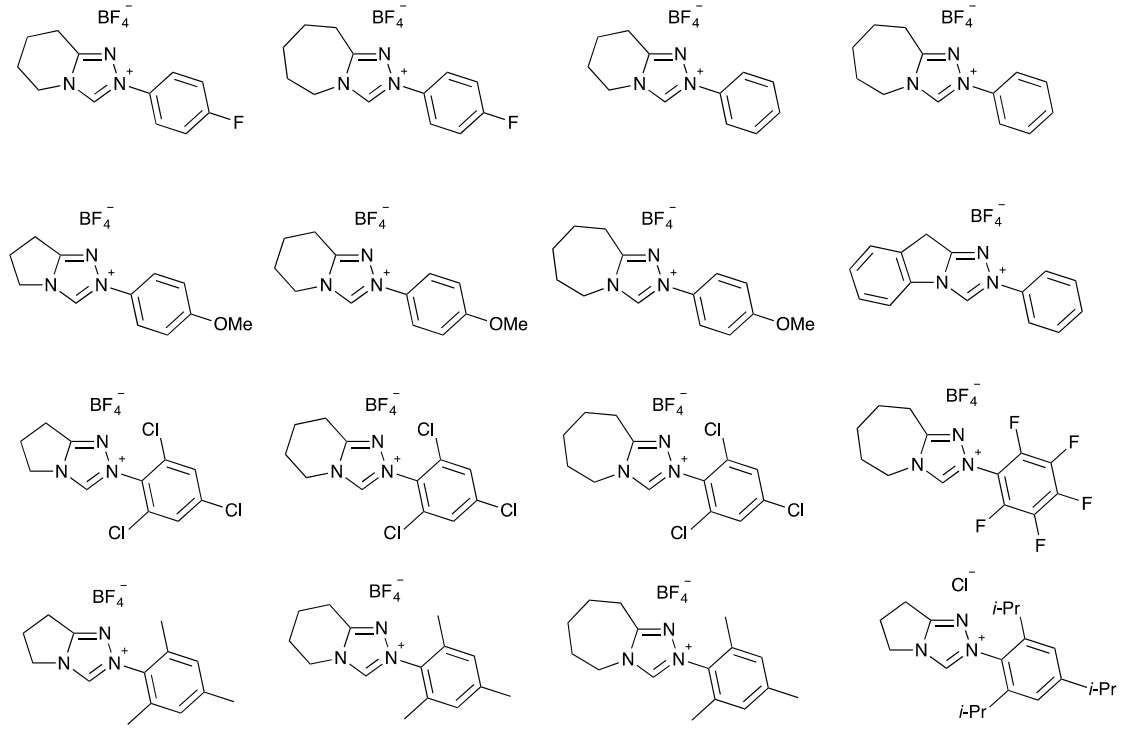

During the kinetic study of the benzoin condensation, traced amounts of d^1-deuterated aldehyde were generated. Although results of the previous study show low levels of deuterium incorporation, we still hypothesize the modification of NHC backbones can potentially suppress the equilibrium constants of the formation of Breslow intermediate and allow the reverse deuteration of aldehydes. Thus, the ^{1}H NMR probed deuterium exchange of aldehydic d^1 position was probed to evaluate the potential of an NHC organocatalytic route to d_1-aldehyde.

According to our group's unpublished results, bis(amino)cyclopropyildene (BAC) are considered to have comparable pK_a values with imidazolyl carbenes. Three bis(amino)cyclopropenium salt are therefore attempted to syntheses to further extend these studies.

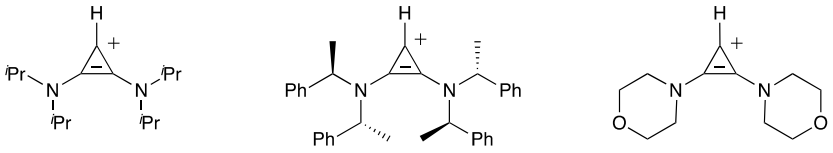

1.4. Reference

1. V. Lavallo, Y. Canac, B. Donnadieu, W. W. Schoeller and G. Bertrand, *Science*, 2006, **312**, 722-724.
2. M. N. Hopkinson, C. Richter, M. Schedler and F. Glorius, *Nature*, 2014, **510**, 485-496.
3. W. A. Herrmann and C. Koecher, *Angewandte Chemie International Edition in English*, 1997, **36**, 2162-2187.
4. M. Fevre, J. Pinaud, Y. Gnanou, J. Vignolle and D. Taton, *Chem Soc Rev*, 2013, **42**, 2142-2172.
5. K. Hirai, T. Itoh and H. Tomioka, *Chem Rev*, 2009, **109**, 3275-3332.
6. S. Morgan, M. S. Platz, M. Jones and D. R. Myers, *J. Org. Chem.*, 1991, **56**, 1351-1353.
7. H. Tomioka, J. Nakajima, H. Mizuno, T. Sone and K. Hirai, *J. Am. Chem. Soc.*, 1995, **117**, 11355-11356.
8. H. Tomioka, K. Hirai and Y. Tanimoto, *J. Chem. Soc., Perkin Trans. 2*, 1994, 633-641.
9. H. Tomioka, S. Yamada and K. Hirai, *J. Org. Chem.*, 1995, **60**, 1298-1302.
10. G. J. LaBonia, The University of Mississippi, 2014.
11. D. Bourissou, O. Guerret, F. P. Gabbai and G. Bertrand, *Chem Rev*, 2000, **100**, 39-92.
12. L. Benhamou, E. Chardon, G. Lavigne, S. Bellemin-Laponnaz and V. Cesar, *Chem Rev*, 2011, **111**, 2705-2733.
13. D. Martin, M. Melaimi, M. Soleilhavoup and G. Bertrand, *Organometallics*, 2011, **30**, 5304-5313.
14. A. Poater, F. Ragone, S. Giudice, C. Costabile, R. Dorta, S. P. Nolan and L. Cavallo, *Organometallics*, 2008, **27**, 2679-2681.
15. W. W. Schoeller, G. D. Frey and G. Bertrand, *Chemistry*, 2008, **14**, 4711-4718.
16. G. Kuchenbeiser, B. Donnadieu and G. Bertrand, *J Organomet Chem*, 2008, **693**, 899-904.

17. S. C. Carbenes, *Angew. Chem., Int. Ed.*, 2010, **49**, 8810-8849.
18. D. Seebach, *Angew. Chem.-Int. Edit. Engl.*, 1979, **18**, 239-258.
19. D. Enders and T. Balensiefer, *Acc Chem Res*, 2004, **37**, 534-541.
20. J. S. Johnson, *Angew Chem Int Edit*, 2004, **43**, 1326-1328.
21. B. Goldfuss and M. Schumacher, *J Mol Model*, 2006, **12**, 591-595.
22. P. S. Tobin, S. K. Basu, R. S. Grosserode and D. M. S. Wheeler, *J. Org. Chem.*, 1980, **45**, 1250-1253.
23. B.-T. Gröbel and D. SEEBACH, *Synthesis*, 1977, **1977**, 357-402.
24. E. J. Corey and D. Crouse, *J. Org. Chem.*, 1968, **33**, 298-300.
25. R. A. Moss and M. P. Doyle, *Contemporary Carbene Chemistry*, John Wiley & Sons, 2013.
26. R. MASSEY, Durham University, 2013.
27. T. Ukai, R. Tanaka and T. Dokawa, *J. Pharm. Soc. Jpn*, 1943, **63**, 296-300.
28. T. Ukai, R. Tanaka and T. Dokawa, *J. Am. Chem. Soc*, 1958, **80**, 3719.
29. S. MIZUHARA, R. TAMURA and H. ARATA, *Proc. Japan Acad. Sci.-Chem. Sci.*, 1951, **27**, 302-308.
30. S. MIZUHARA and H. ARATA, *Proc. Japan Acad. Sci.-Chem. Sci.*, 1951, **27**, 700-704.
31. R. Breslow, *J. Am. Chem. Soc.*, 1958, **80**, 3719-3726.
32. J. E. Thomson, K. Rix and A. D. Smith, *Org Lett*, 2006, **8**, 3785-3788.
33. G. A. Grasa, R. M. Kissling and S. P. Nolan, *Org Lett*, 2002, **4**, 3583-3586.
34. A. Chan and K. A. Scheidt, *Org. Lett.*, 2005, **7**, 905-908.
35. D. Enders, J. Han and A. Henseler, *Chem Commun (Camb)*, 2008, DOI: 10.1039/b809913h, 3989-3991.
36. J. C. Sheehan and D. H. Hunneman, *J. Am. Chem. Soc.*, 1966, **88**, 3666-+.
37. J. C. Sheehan and T. Hara, *J. Org. Chem.*, 1974, **39**, 1196-1199.
38. D. Enders, K. Breuer, G. Raabe, J. Runsink, J. H. Teles, J. P. Melder, K. Ebel and S. Brode, *Angew. Chem.-Int. Edit. Engl.*, 1995, **34**, 1021-1023.
39. D. Enders, K. Breuer, J. Runsink and J. H. Teles, *Helv. Chim. Acta*, 1996, **79**, 1899-1902.
40. R. L. Knight and F. J. Leeper, *J. Chem. Soc.-Perkin Trans. 1*, 1998, DOI: DOI 10.1039/a803635g, 1891-1893.
41. O. Holloczki, Z. Kelemen and L. Nyulaszi, *J Org Chem*, 2012, **77**, 6014-6022.
42. L. Baragwanath, C. A. Rose, K. Zeitler and S. J. Connon, *J Org Chem*, 2009, **74**, 9214-9217.
43. X. Lu and U. Schneider, *Chem Commun (Camb)*, 2016, **52**, 12980-12983.
44. D. M. Flanigan, F. Romanov-Michailidis, N. A. White and T. Rovis, *Chem Rev*, 2015, **115**, 9307-9387.
45. R. C. Cookson and R. M. Lane, *J. Chem. Soc., Chem. Commun.*, 1976, 804-805.
46. C. A. Rose, S. Gundala, S. J. Connon and K. Zeitler, *Synthesis*, 2011, **2011**, 190-198.
47. I. Piel, M. D. Pawelczyk, K. Hirano, R. Frohlich and F. Glorius, *Eur. J. Org. Chem.*, 2011, **2011**, 5475-5484.
48. Y. Hachisu, J. W. Bode and K. Suzuki, *J. Am. Chem. Soc.*, 2003, **125**, 8432-8433.
49. T. Ema, Y. Oue, K. Akihara, Y. Miyazaki and T. Sakai, *Org Lett*, 2009, **11**, 4866-4869.
50. T. Ema, K. Akihara, R. Obayashi and T. Sakai, *Adv. Synth. Catal.*, 2012, **354**, 3283-3290.
51. S. Kankala, R. Edulla, S. Modem, R. Vadde and C. S. Vasam, *Tetrahedron Lett.*, 2011, **52**, 3828-

3831.

52. F. Pichiorri, D. Palmieri, L. De Luca, J. Consiglio, J. You, A. Rocci, T. Talabere, C. Piovan, A. Lagana, L. Cascione, J. Guan, P. Gasparini, V. Balatti, G. Nuovo, V. Coppola, C. C. Hofmeister, G. Marcucci, J. C. Byrd, S. Volinia, C. L. Shapiro, M. A. Freitas and C. M. Croce, *J Exp Med*, 2013, **210**, 951-968.
53. S. P. Lathrop and T. Rovis, *J. Am. Chem. Soc.*, 2009, **131**, 13628-13630.
54. K. E. Ozboya and T. Rovis, *Chem Sci*, 2011, **2**, 1835-1838.
55. J. A. Murry, D. E. Frantz, A. Soheili, R. Tillyer, E. J. Grabowski and P. J. Reider, *J. Am. Chem. Soc.*, 2001, **123**, 9696-9697.
56. G. Q. Li, Y. Li, L. X. Dai and S. L. You, *Org Lett*, 2007, **9**, 3519-3521.
57. D. Enders, A. Henseler and S. Lowins, *Synthesis*, 2009, **2009**, 4125-4128.
58. L. H. Sun, Z. Q. Liang, W. Q. Jia and S. Ye, *Angew Chem Int Edit*, 2013, **52**, 5803-5806.
59. D. A. DiRocco and T. Rovis, *J. Am. Chem. Soc.*, 2012, **134**, 8094-8097.
60. H. Stetter, *Angew. Chem., Int. Ed.*, 1976, **15**, 639-647.
61. Y. Li, F. Q. Shi, Q. L. He and S. L. You, *Org Lett*, 2009, **11**, 3182-3185.
62. O. Bortolini, G. Fantin, M. Fogagnolo, P. P. Giovannini, A. Massi and S. Pacifico, *Org Biomol Chem*, 2011, **9**, 8437-8444.
63. D. Enders and J. W. Han, *Synthesis*, 2008, **2008**, 3864-3868.
64. D. A. DiRocco, K. M. Oberg, D. M. Dalton and T. Rovis, *J. Am. Chem. Soc.*, 2009, **131**, 10872-10874.
65. J. M. Um, D. A. DiRocco, E. L. Noey, T. Rovis and K. N. Houk, *J. Am. Chem. Soc.*, 2011, **133**, 11249-11254.
66. E. Ciganek, *Synthesis*, 1995, **1995**, 1311-&.
67. M. S. Kerr, J. Read de Alaniz and T. Rovis, *J. Am. Chem. Soc.*, 2002, **124**, 10298-10299.
68. C. J. Collett, R. S. Massey, O. R. Maguire, A. S. Batsanov, A. C. O'Donoghue and A. D. Smith, *Chem. Sci.*, 2013, **4**, 1514-1522.
69. J. He, J. Zheng, J. Liu, X. She and X. Pan, *Org Lett*, 2006, **8**, 4637-4640.
70. J. M. He, S. C. Tang, J. Liu, Y. P. Su, X. F. Pan and X. G. She, *Tetrahedron*, 2008, **64**, 8797-8800.
71. A. T. Biju, N. E. Wurz and F. Glorius, *J. Am. Chem. Soc.*, 2010, **132**, 5970-5971.
72. M. He, J. R. Struble and J. W. Bode, *J. Am. Chem. Soc.*, 2006, **128**, 8418-8420.
73. A. Berkessel, V. R. Yatham, S. Elfert and J. M. Neudorfl, *Angew Chem Int Edit*, 2013, **52**, 11158-11162.
74. Y. Reddi and R. B. Sunoj, *Org Lett*, 2012, **14**, 2810-2813.
75. Y. R. Zhang, L. He, X. Wu, P. L. Shao and S. Ye, *Org Lett*, 2008, **10**, 277-280.
76. L. He, H. Lv, Y. R. Zhang and S. Ye, *J Org Chem*, 2008, **73**, 8101-8103.
77. Y. R. Zhang, H. Lv, D. Zhou and S. Ye, *Chemistry*, 2008, **14**, 8473-8476.
78. N. Duguet, C. D. Campbell, A. M. Slawin and A. D. Smith, *Org Biomol Chem*, 2008, **6**, 1108-1113.
79. A. Grossmann and D. Enders, *Angew Chem Int Edit*, 2012, **51**, 314-325.
80. C. Berthelette and J. Scheigetz, *Journal of Labelled Compounds & Radiopharmaceuticals*, 2004, **47**, 891-894.
81. S. S. Sohn, E. L. Rosen and J. W. Bode, *J. Am. Chem. Soc.*, 2004, **126**, 14370-14371.
82. M. He and J. W. Bode, *Org Lett*, 2005, **7**, 3131-3134.

83. M. Rommel, T. Fukuzumi and J. W. Bode, *J. Am. Chem. Soc.*, 2008, **130**, 17266-17267.
84. S. S. Sohn and J. W. Bode, *Org. Lett.*, 2005, **7**, 3873-3876.
85. C. Burstein and F. Glorius, *Angew Chem Int Edit*, 2004, **43**, 6205-6208.
86. A. Chan and K. A. Scheidt, *J. Am. Chem. Soc.*, 2008, **130**, 2740-2741.
87. D. E. Raup, B. Cardinal-David, D. Holte and K. A. Scheidt, *Nat Chem*, 2010, **2**, 766-771.
88. X. Zhao, D. A. DiRocco and T. Rovis, *J. Am. Chem. Soc.*, 2011, **133**, 12466-12469.
89. A. Chan and K. A. Scheidt, *J. Am. Chem. Soc.*, 2007, **129**, 5334-5335.
90. P.-C. Chiang, M. Rommel and J. W. Bode, *J. Am. Chem. Soc.*, 2009, **131**, 8714-8718.
91. Z. Fu, J. Xu, T. Zhu, W. W. Y. Leong and Y. R. J. N. c. Chi, 2013, **5**, 835.
92. G. W. Nyce, J. A. Lamboy, E. F. Connor, R. M. Waymouth and J. L. Hedrick, *Org Lett*, 2002, **4**, 3587-3590.
93. K. Zeitler, *Org Lett*, 2006, **8**, 637-640.
94. J. Kaeobamrung, J. Mahatthananchai, P. Zheng and J. W. Bode, *J. Am. Chem. Soc.*, 2010, **132**, 8810-8812.
95. R. C. Samanta, B. Maji, S. De Sarkar, K. Bergander, R. Frohlich, C. Muck-Lichtenfeld, H. Mayr and A. Studer, *Angew Chem Int Edit*, 2012, **51**, 5234-5238.
96. S. J. Ryan, L. Candish and D. W. Lupton, *J. Am. Chem. Soc.*, 2009, **131**, 14176-14177.
97. F. G. Sun, L. H. Sun and S. Ye, *Adv. Synth. Catal.*, 2011, **353**, 3134-3138.
98. M. Christmann, *Angew Chem Int Edit*, 2010, **49**, 9580-9586.
99. A. Hoffmann-Roder and N. Krause, *Angew Chem Int Edit*, 2004, **43**, 1196-1216.
100. Y. M. Zhao, Y. Tam, Y. J. Wang, Z. Li and J. Sun, *Org Lett*, 2012, **14**, 1398-1401.
101. C. L. Lai, H. M. Lee and C. H. Hu, *Tetrahedron Lett.*, 2005, **46**, 6265-6270.

Chapter 2. Synthesis of Triazolium Salts and Novel Dialkoxy Acetal Adducts

2.1. Procedures Towards NHCs and Their Procursors

Carbenes have long been recognised as a type of unstable intermediate with short life-times because of their unsaturated coordination and incomplete electron octet[1]. There have been debates on their isolabilities for one hundred years since the evidence of their existence was first established by Buchner and Curtius in 1885[2]. In 1988, Bertrand reported the first isolable free carbene **42**, and three years later, the synthesis of the first commercially available carbene **43** by Arduengo initiated the broader usage of carbenes in organic synthesis and catalysis (Figure 2.1)[3, 4].

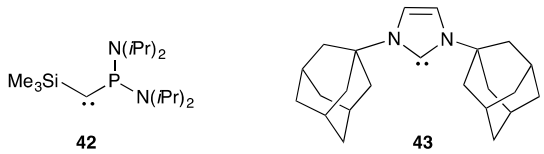

42 **43**

Figure 2.1. First stable phosphinosilyl carbene **42** and first crystallised stable imidazolyl carbene **43**

Since then, hundreds of persistent free carbenes have been isolated, and the modification of carbene backbones has been popular in recent years, with various substituents, ring sizes, and element components (Figure 2.2)[5-13]. Among these carbenes, N-heterocyclic carbenes (NHCs) are one of the most common types.

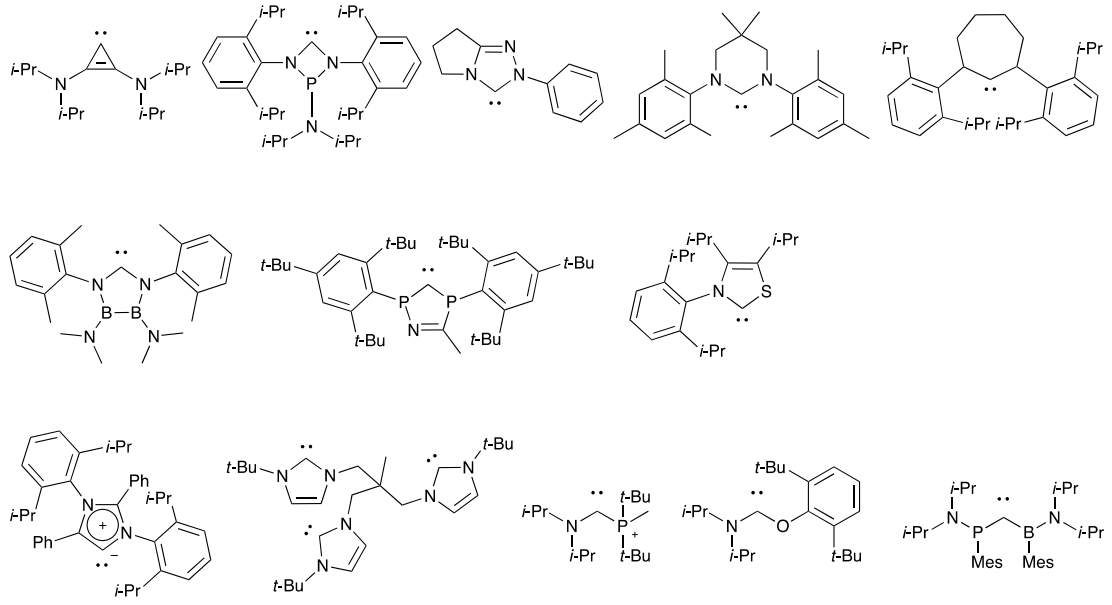

Figure 2.2. Selected examples of stable crystalline carbenes.

Several methods can be used to obtain free NHCs, including NHC-volatile compound pyrolysis under vacuum[14], thiourea reduction[11], *in situ* release of NHCs from NHC-metal adducts or NHC-CO_2[12], chloroformamidinium salt reduction[13, 15], and, the most common way, from the deprotonation of the corresponding azolium precursors.

César *et al*. disassembled NHC precursors into three parts: the precarbenic unit, the amino part, and the backbone moiety (Figure 2.3)[16]. They thus classified the syntheses of NHC precursors into three types by the latest assembled subunit in the final ring closure step (precarbenic, amino, and backbone). I agree with this classification method and this introduction will follow the same logic to introduce several typical syntheses of the NHC precursors.

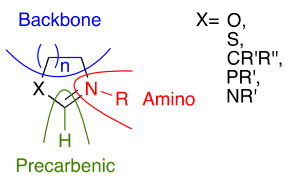

Figure 2.3. Disassembly of the NHC precursor.

2.1.1. Final Cyclisation by Introducing the Backbone Moiety

The precursor of the first commercially available carbene, the 1,3-disubstituted imidazolium salt, can be obtained from the direct substitution of an imidazole unit (still with many contemporary applications)[4, 17], dialkylation on an unsubstituted imidazolium salt[18], or desulfurization of 1,3-disubstituted imidazole-2-thiones[19]. Remarkably, Arduengo demonstrated a straightforward pathway towards an imidazolium salt *via* a one-pot condensation of formaldehyde, amine and glyoxal in 1991 (Scheme 2.1)[4]. This method is efficient towards the preparation of a range of aryl and alkyl-substituted imidazolium salts[20-23]. However, sterically hindered amines gave low yields or even did not react. Meanwhile, the harsh purification of the imidazolium salts also limited its applications.

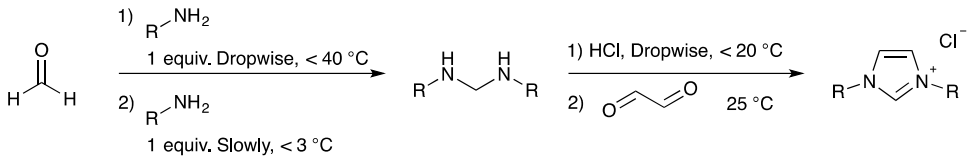

Scheme 2.1. One-pot synthetic procedure of imidazolium salts

To obtain more complicated structures of NHC precursors, the final ring closure procedure could involve a pre-modified formamidine. Aryl-formamidines can be easily obtained from the condensation of triethyl orthoformate with primary anilines (Scheme 2.2. Route a)[24]. By controlling the equivalents of the anilines used during the synthesis, asymmetric diarylformamidines can also be obtained easily (Scheme 2.2. Route b)[25, 26]. The acid-free conditions ensure the irreversibility of the addition of the second aniline which prevent the thermodynamic selection. Meanwhile, alkyl-formamidine formation is similar to the procedure for aryl-formamidine, however requires the addition of acetic acid[27].

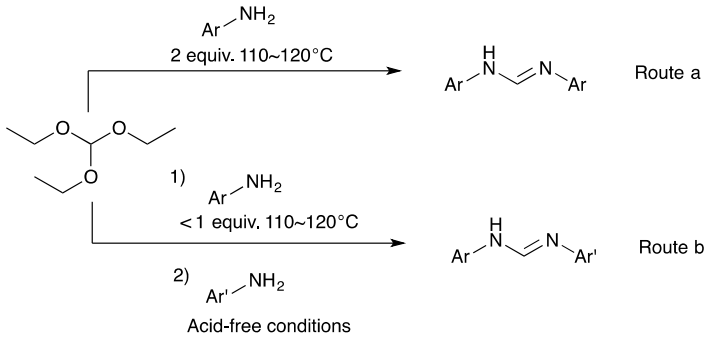

Scheme 2.2. Route a, preparation of symmetric diaryl-formamidines. Route b, preparation of asymmetric diaryl-formamidines

Depending on the desired structure of the NHC precursors, various reagents have been reported for the final cyclisation with formamidines. Dibromopropane **44**[9, 14], 2-bis(bromomethyl)benzene **45**, 1,3,2-dioxathiolane-2,2-dioxide **46**[28], dichloroethane **47**[29], α-haloketone **48**[30], dichlone **49**[31], chloroacetyl chloride **50**[32], α-bromo methylester **51**[33] are all typical backbone resources, and their reactions with pre-modified formamidines are briefly shown in Scheme 2.3.

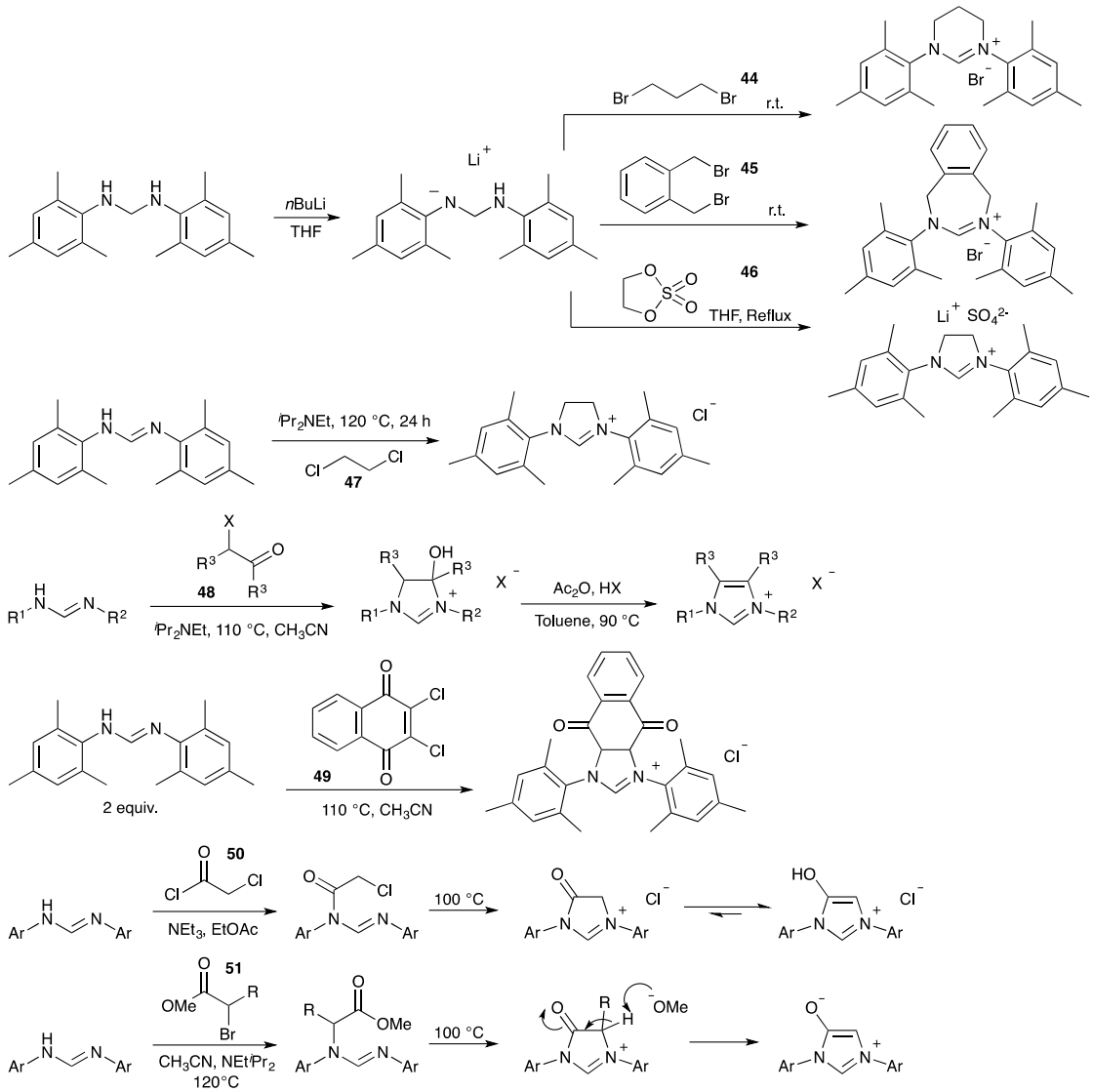

Scheme 2.3. Synthetic approach towards NHC precursors using different backbone sources **44**-**51**.

Many NHC precursors with inorganic backbones can be generated through this synthetic pathway, like **52**-**54**, which all use a corresponding trimethylsilyl iminium **55** as starting materials (Figure 2.4)[6, 34, 35]. Unfortunately, triazolium salt synthesis cannot be approached through the final introducing of the backbone.

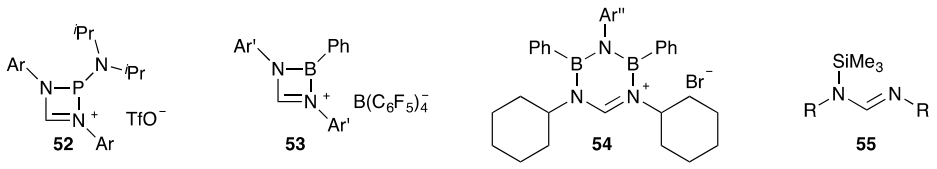

Figure 2.4. Typical NHC precursors with inorganic backbones **52**-**54** and their starting material **55**.

2.1.2. Final Ring-Closure by Assembly of the Amino Moiety

The insertion of the amino moiety in the final ring cyclisation process can be divided into two categories: *via* the interconversion of the heterocyclic ring, or *via* the condensation with aryl hydrazine[16].

The interconversion process of the heterocyclic ring may involve sigmatropic rearrangement or dehydration processes. Lassaletta *et al.* prepared the isoquinolinium salt **56** through a Zincke reaction. The aromatic nucleophilic substitution between chloro-dinitrobenzene **57** and isoquinoline **58** gives a pyridinium salt **59**. The following addition of phenylethylamine **60** forces aryl ring opening, and probably a subsequent sigmatropic rearrangement on the intermediate **61** to generate the desired NHC precursor **56** (Scheme 2.4)[36-38].

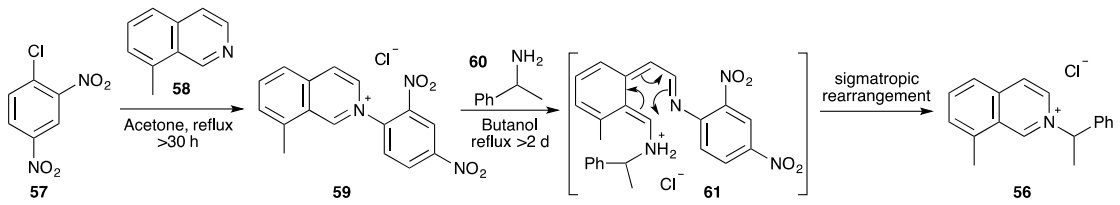

Scheme 2.4. Formation of NHC precursor **61** through a Zincke reaction.

Interconversion through a dehydration process was also reported to generate several NHC precursors. Boyd *et al.* reported the first synthetic route towards a disubstituted triazolium salt **62** (Scheme 2.5). Hydrazines **63** are first formylated by reaction with an anhydride (*e.g.* acetic anhydride) in perchloric acid, and subsequent dehydration leads

to the oxadiazolium salt **64**. Further reaction with a primary amine generates the triazolium salt **62**[39, 40].

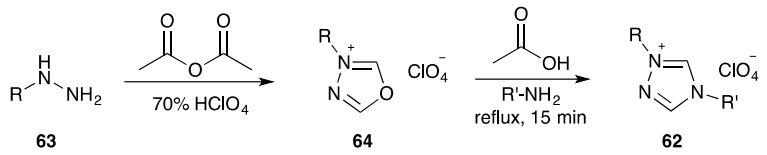

Scheme 2.5. Synthesis of triazolium salt **62**

Fürstner *et al.* reported the Zincke reaction failed to generate asymmetric imidazolium salts as the nucleophilic attack of phenylethylamine did not work (Scheme 2.6a). Adapted from Boyd's work, Fürstner *et al.* demonstrated another method using oxazolium salts as more reactive nucleophiles[41]. The α-aminoketone **65** was first formed and its formylated product **66** can cyclize easily with the addition of acid. Different from the formation of triazolium salt **62** in Boyd's work, the cyclized salt **67** showed good acid-stability and did not undergo the desired aromatization. The following alkylation of compound **67** using a primary amine generated an imidazolinium salt, which can further dehydrate to the imidazolium salt **68** with acid-catalysis (Scheme 2.6b).

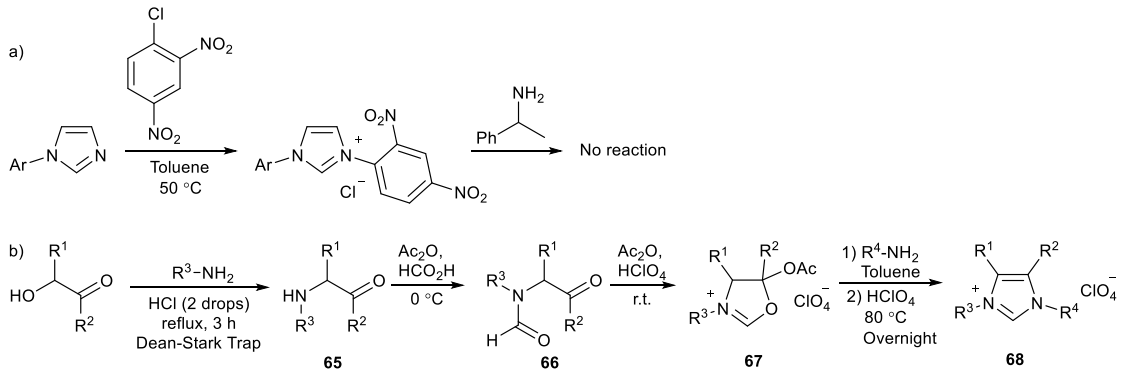

Scheme 2.6. a) Unsuccessful Zincke reaction in an attempted synthesis of an asymmetric imidazolium salt; b) intramolecular dehydration for the synthesis of asymmetric imidazolium salt **68**

It is known that the overlap of the nitrogen lone pair of electrons and the carbene's empty *p*-orbital contribute to the NHC's stability. To investigate if other substituents with

similar electronic properties can still tolerate carbene formation, Fürstner in 2008 reported an NHC precursor **69**. This precursor was generated using a vinamidinium salt **70** *via* a condensation process with a mono-substituted hydrazine (Scheme 2.7)[42]. By analysing its crystal structure, Fürstner suggested the polarized π bonds of ylides are suitable for carbene stabilisation, and the positive charge could be largely localized on the triphenylphosphine group.

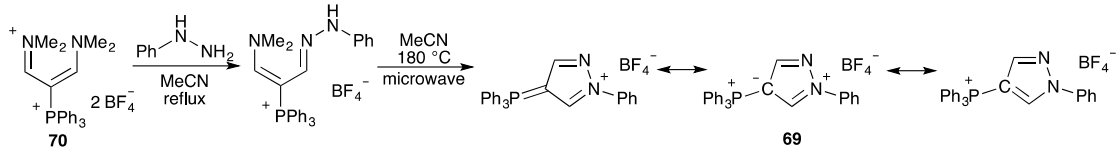

Scheme 2.7. Synthetic procedure of NHC precursor **69** with the positive charge localized on the phosphorous group.

2.1.3. Final Cyclisation by Introducing the Precarbenic Moiety

The final cyclisation process by introducing a pre-carbenic moiety (C_1) is the most widely used synthetic route towards NHC precursors. Bis-electrophile compounds, paraformaldehyde, and the trialkyl orthoformate are all widely used pre-carbenic sources[16]. The following paragraphs will briefly introduce some typical synthetic routes using such pre-carbenic sources.

Bis-electrophiles, or a methylene compound connected with two leaving groups, can easily react with bis-nucleophiles to form NHC precursors. Dipyridoimidazolium salt **71** and **72** can be prepared using methylene iodide and α-haloketone **73**[43]. Different from the direct double nucleophilic substitution of methylene iodide, the reaction of α-haloketone **73** first undergoes the aromatization then followed by the deacylation using aluminum oxide (Scheme 2.8)[44, 45]. Other bis-electrophile sources include Weiss' reagent **74**[46], chloromethyl ether **75**[47], and Glorius' reagent **76**[48].

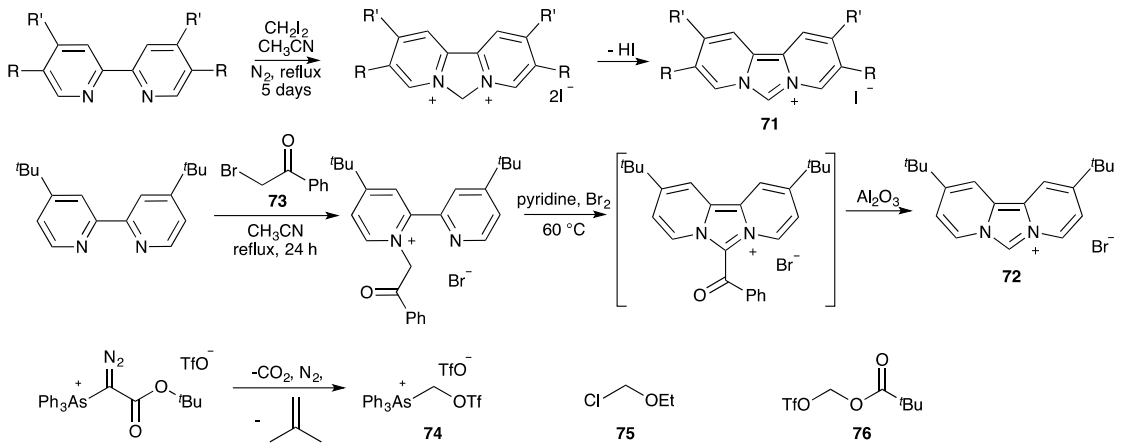

Scheme 2.8. Synthesis of NHC precursors **71** and **72**, and several typical bis-electrophile sources **74**-**76**.

Paraformaldehyde can be used as a pre-carbenic building block to synthesize both saturated and unsaturated NHC precursors[16]. Nucleophilic substitution between anilines and glyoxal gives diazabutadiene, and its condensation with paraformaldehyde under anhydrous conditions with anhydrous hydrogen chloride precipitate out the imidazolium chloride (Scheme 2.9)[49]. Apart from the amines with strong electron-withdrawing aryl-substituents, this synthetic pathway works for range of anilines including alkylamines. This procedure can be further improved by replacing anhydrous hydrogen chloride with chlorotrimethylsilane as the chloride source[50]. Paraformaldehyde can also first react with a diamine to form a saturated tetrahydropyrimidinium ion, followed by oxidation using halosuccinimide to generate the corresponding NHC precursor[51].

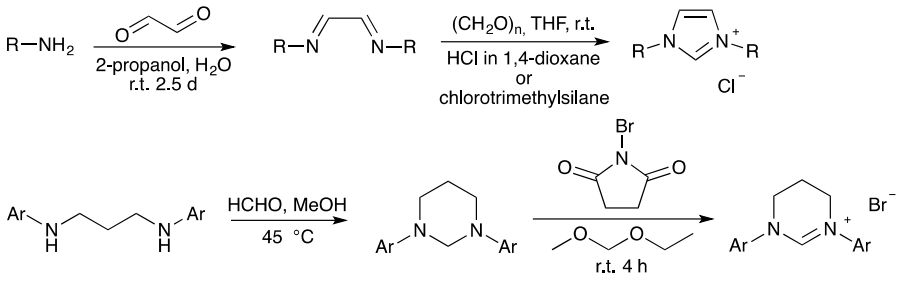

Scheme 2.9. Paraformaldehyde used as pre-carbenic sources.

The use of trialkyl orthoformate as the pre-carbenic source was first demonstrated by

Saba and Kaloustain in 1991 (Scheme 2.10)[52]. This method is reported to be highly efficient and, theoretically, could lead to NHC precursors with any secondary diamine. The most challenging aspect of this synthetic route is the preparation of the diamine. Based on the different target backbone structures, many synthetic pathways have been discovered to approach substituted diamines, and subsequent condensation with trialkyl orthoformate affords the final NHC precursors. The diamine of a symmetrical imidazolinium salt could be obtained from the condensation between primary amines with glyoxal, followed by reduction using sodium borohydride (Scheme 2.10a)[53]. Nucleophilic substitution of dialkyl halides (*e.g.* 1,2-dibromoethane) with primary amines have also been reported (Scheme 2.10b)[54], and the use of amino acids as practical building block (Scheme 2.10c)[55]. Adapted from Rovis' work (Scheme 2.10d)[56], this project uses trialkyl orthoformate as the pre-carbenic source to generate a series of triazolium salts.

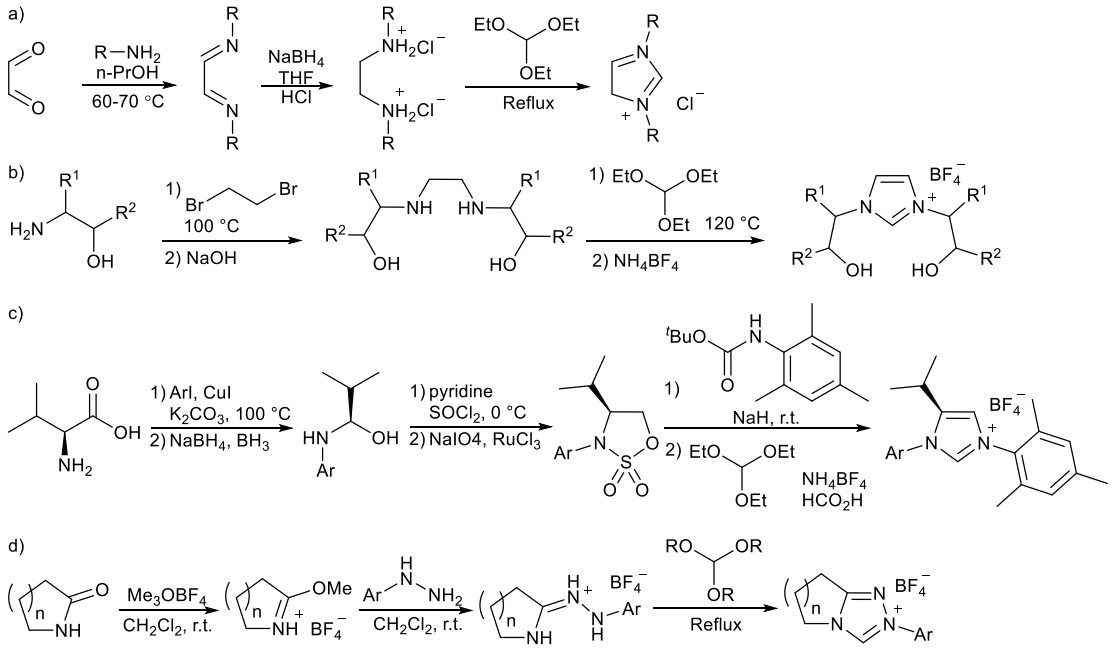

Scheme 2.10. Syntheses of NHC precursors using trialkyl orthoformate as pre-carbenic source.

2.2. Syntheses of the Triazolium Salts

During this project, the syntheses of sixteen N-aryl substituted bicyclic triazolium salts **77-92** were attempted (Figure 2.5). These sixteen triazolium salts were chosed to be synthesized to investigate the reason of the chemoselectivity variation of benzoin condensation caused by the structural difference of catalyst, and will be mainly discussed in the next chapter. Among these triazolium salts, **88** was first designed in my MSc degree, and the synthetic procedures of **81, 84-87, 89** have been published previously[57-70], while there are no previous reports of the preparation of **77-80, 82, 83, 90-92**. Among the sixteen triazolium salts, the 2,4,6-trichlorophenyl triazolium salt **82, 83,** and mesityl triazolium salt **87** could not be purified as only trace amounts were identified by mass spectrometry, the indole triazolium **92** was not detected by mass spectrometry, and the other twelve triazolium salts were successfully isolated and purified.

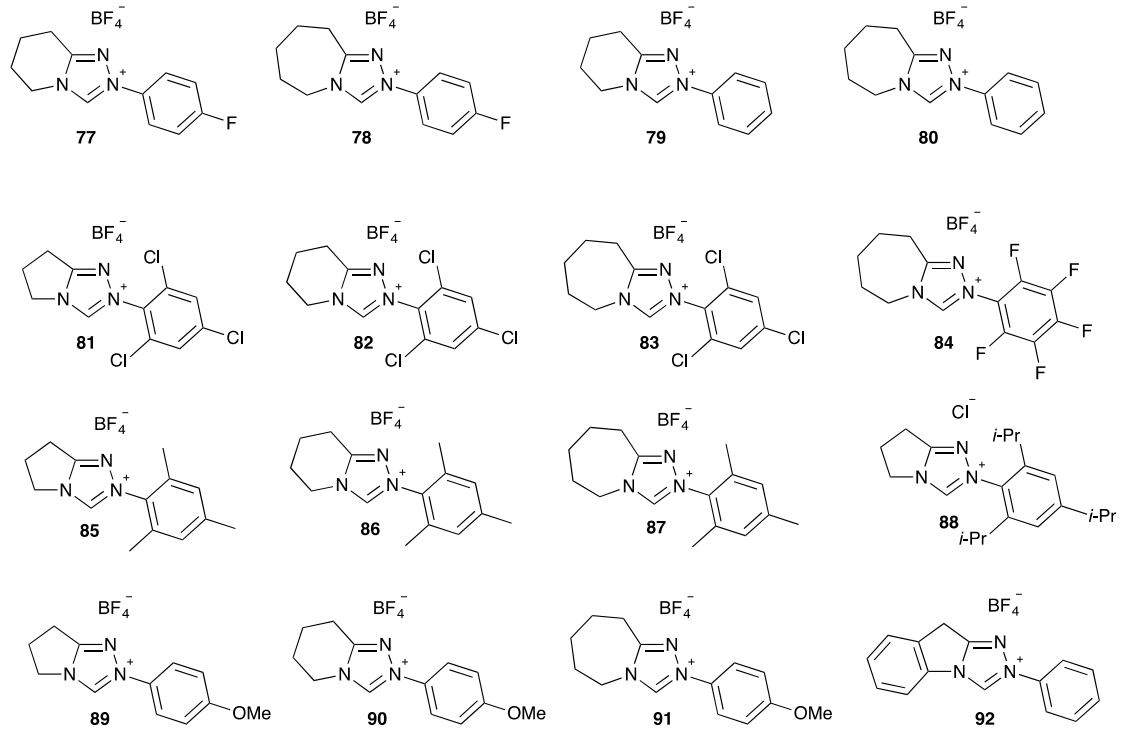

Figure 2.5. Selectively prepared bicyclic N-aryl triazolium salts **77-92**.

Based on previous research[57, 66], two synthetic pathways were applied for different triazolium salts (Scheme 2.11). These two procedures all require the methylation of the lactam **93**, followed by the addition of the hydrazine **94** or hydrazine hydrochloride salt **95** to form the amidrazone **96**, and the final cyclisation with trialkyl orthoformate generates the N-aryl triazolium salts. The diversity of the triazolium salts are achieved by varying the aryl-substituents of hydrazine and hydrazine hydrochloride salt, or using different sizes of lactam (n= 1, 2, 3).

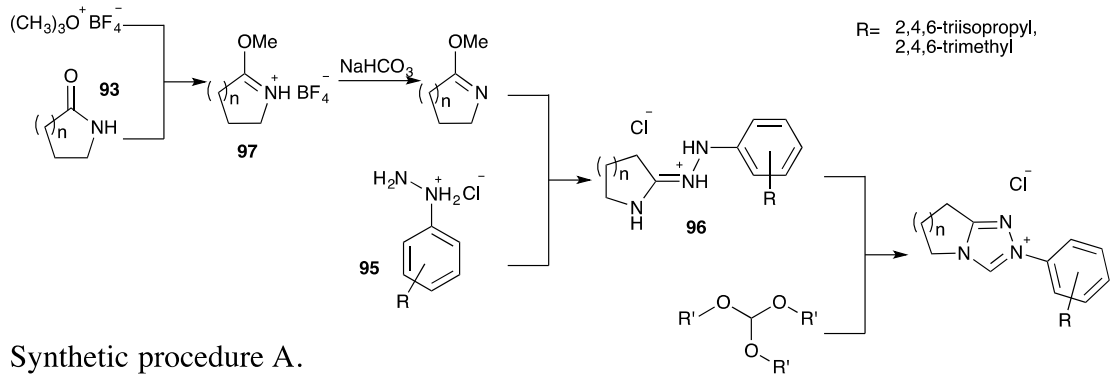

Scheme 2.11. General procedures utilised for the preparation of bicyclic N-aryl triazolium salts.

Apart from the 2,4,6-triisopropylphenyl triazolium salt **88**, the corresponding hydrazines or hydrazine hydrochloride salts of other triazolium salts are commercially available. To obtain the 2,4,6-triisopropyl hydrazine hydrochloride, three different routes were tried during my MSc degree (Scheme 2.12)[58], and the procedure *via* use of a Grignard reagent

proved to be most successful (Route C). I further improved the synthetic procedure during this project, such as adding in the iodide in granular form for the initiation of Grignard reagent and lengthening reaction times. The optimized reaction procedure is provided in the Experimental section (Section 7.3.2).

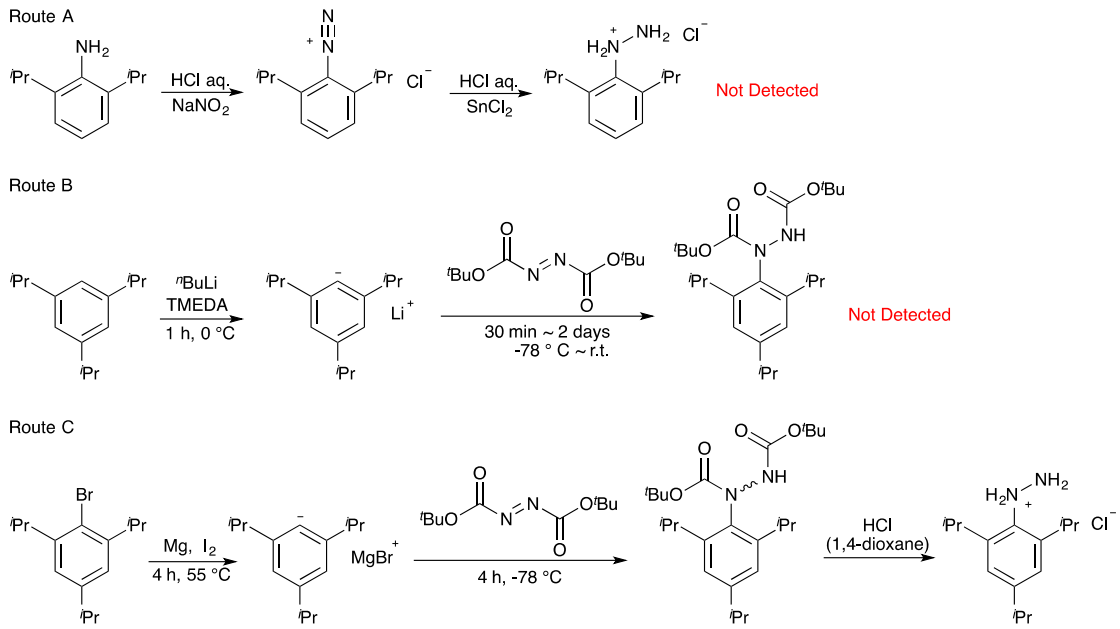

Scheme 2.12. Three synthetic approaches towards 2,4,6-triisopropylphenyl hydrazine hydrochloride[I].

The nucleophilic substitution between hydrazine and the carboximidate **97** is not favoured in acidic conditions, as either the imidate or the hydrazine should be in its neutral form. Meanwhile, depending on the aryl-substituents of hydrazine, the neutralization of hydrazine hydrochloride salt **95** has the possibility to decompose the hydrazine to aniline. Thus, the stability and accessibility of hydrazine or hydrazine hydrochloride decide the synthetic pathway used for amidrazone (**96**) syntheses. Table 2.1 summarized the synthetic procedures and yields of triazolium salts **77-91,** and **98-**

[I] The aim of synthesizing the triisopropylphenyl triazolium salt **88** is to investigate the *ortho*-aryl substituents effect of the triazolyl salts' catalytic behavior, and the aryl-substituent on the *para*-position has limited effects.

101 obtained.

LC-MS showed the formation of amidrazone salts was straightforward, and complete conversion could be achieved. There is no need to purify the amidrazone, and the final triazolium salts could be obtained directly by adding trialkyl orthoformate into the amidrazone mixture and refluxed for two hours to over one week.

Table 2.1. Summary of synthetic procedures and product yield of selected bicyclic N-aryl triazolium salts **77-91**, **98-101**.

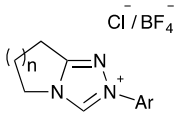

	Ar=		Procedure[a), b)]	Yield
98		n= 1	B	67%[c)]
99	Pentafluorophenyl	n= 2	B	56% [c)]
84		n= 3	B	27%
88	2,4,6-Triisopropylphenyl	n= 1	A	29%
85		n= 1	A and B	92%
86	Mesityl	n= 2	A and B	13%
87		n= 3	B	-
100		n= 1	B	58% [d)]
77	4-Fluorophenyl	n= 2	B	49%
78		n= 3	B	11%
101		n= 1	B	52% [c)]
79	Phenyl	n= 2	B	42%
80		n= 3	B	86%
89		n= 1	B	85%
90	4-Methoxyphenyl	n= 2	B	65%
91		n= 3	B	22%
81		n= 1	B	14%
82	2,4,6-Trichlorophenyl	n= 2	B	-
83		n= 3	B	-

a) Brief details of procedure A refer to Scheme 2.11A. b) Brief details of procedure B refer to Scheme 2.11B. c) Yield obtained from my MSc degree. d) Yield obtained by Richard Massey.

With the increment of fused ring size, the difficulty of triazolium salts purification increased. Most of the triazolium salts with five-membered fused rings (n=1) can be precipitated simply by washing with ethyl acetate or diethyl ether; while six membered analogues (n=2) require recrystallisation from methanol: diethyl ether or dichloromethane: diethyl ether. Triazolium salts with seven-membered fused rings (n=3) required several recrystallisations with varied solvent systems to yield the pure compounds (up to 10 times recrystallisation should be expected). Interestingly, the recrystallisation of *para*-fluorophenyl triazolium salt (n= 3, **78**) from dichloromethane: toluene yielded a white gel (Figure 2.6), while other triazolium salts with seven-membered fused rings gave needle-like crystals even in the same solvent system.

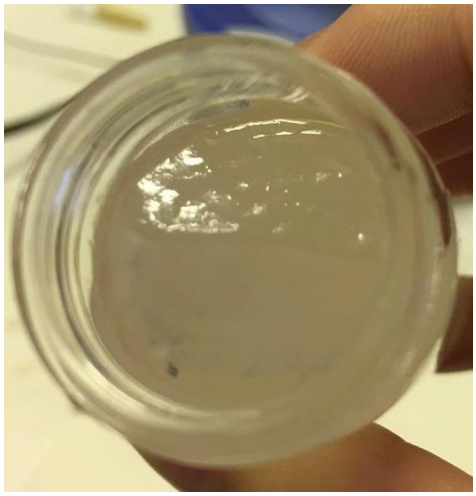

Figure 2.6. White gel of *para*-fluorophenyl triazolium salt with seven-membered fused ring (n= 3, **88**).

I found that two typical methods could be used to obtain single crystals of triazolium salts, which involve slow evaporation from methanol, or dissolution of the salt with low solubility (*e.g. para*-methoxyphenyl triazolium salts **89-91**) in warm methanol (30 to 40 °C) and naturally cooling down the solution to room temperature. Using the above two methods, a total of ten crystal structures were obtained (Figure 2.7), where the *para*-bromophenyl triazolium salt **104** (n= 1), *meta*-chlorophenyl triazolium salt **103** (n= 1) were synthesized by Hector Macrae, *para*-trifluoromethylphenyl triazolium salt **105** (n=

1) were synthesized by Jinyi Xuan, mesityl triazolium salt **85** (n= 1) and pentafluorophenyl triazolium salt **78** (n= 3) was obtained during my MSc degree.

The crystal structures clearly suggest the addition of CH_2 groups to the fused ring have impacts on the structure of the triazolium salt. For instance, the bond angle of N-C-N follows the trend of n= 1< n= 2 ≈ n= 3, and Table 2.2 lists the N-C-N bond angle of each triazolium salt. Although the increasing of this angle is quite small[I] (with an average of 0.8° increase by changing n= 1 to 2; 0.2° increase by changing n= 2 to 3), it might leads to a significant change in terms of influencing NHC reactivity. Meanwhile, additional structural variation between different triazolium salts will be discussed in detail in Chapter 3, Section 3.7.1.4.

[I] Average N-C-N bond angle for triazolium salts with n=1 equals to 106.1 ± 0.3°, this angle changed into 106.9 ± 0.3° with n=2, and 107.1 ± 0.3° with n=3. Notably, the bond angles were obtained from the direct measurement of crystal structure data using software Mercury. According to the single X-ray crystal structure data collected by the Crystallography Department of Durham University, the standard deviation of the bond angles are smaller than 0.3°, and the standard deviations for the bond lengths are smaller than 0.01 angstrom.

Table 2.2. Summary of N-C-N bond angle of ten N-aryl triazolium salts.

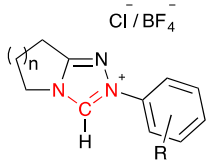

n=	R=	N-C-N bond angle (°)
1 [a]	4-OMe	105.6
1 [a]	4-F	106.2
1[a]	pentafluoro	105.9
1[a]	2,4,6-triCl	105.9
1[b]	4-Br	105.9
1[b]	3-Cl	106.5
1[c]	4-CF_3	106.2
1	2,4,6-triMe	106.3
2	4-F	106.6
2	4-OMe	106.6
2	H	107.2
2	2,4,6-triMe	107.2
3	pentafluoro	106.9
3	4-OMe	107.4

[a] Crystal structure obtained by Peter Quinn, [b] Triazolium synthesised by Hector Macrae. [c] Triazolium synthesised by Jinyi Xuan.

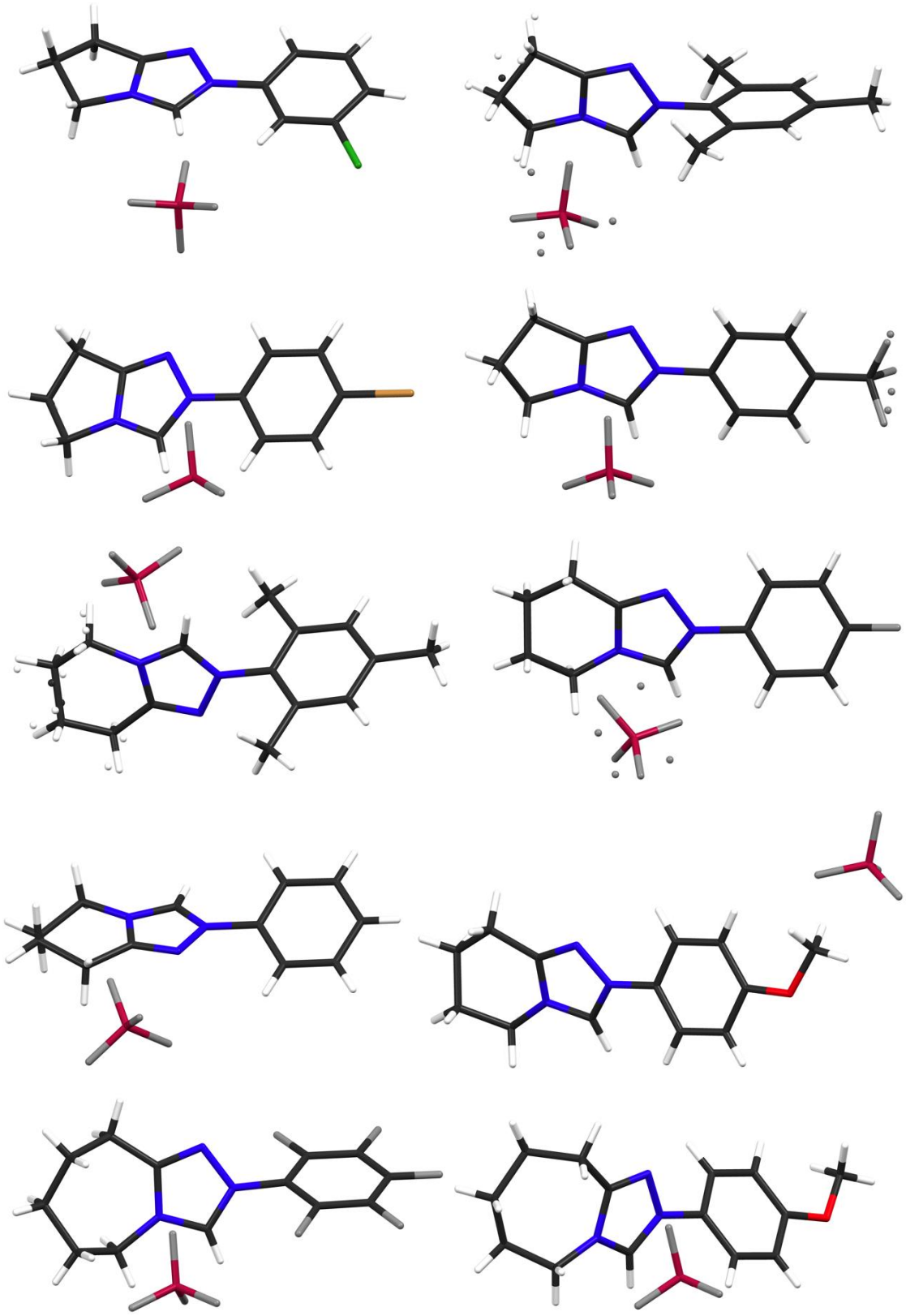

Figure 2.7. Crystal structures of ten triazolium salts **77-81, 84-86, 88-91**.

2.3. Novel Dialkoxy Acetal Adducts

2.3.1. Syntheses of the Novel Dialkoxy Acetal Adducts

As introduced in Table 2.1, the yields of triazolium salts decreased with the increment of fused ring size (apart from the phenyl triazolium salts **79, 80,** and **101**). Additional peaks present in NMR and Mass spectra suggested the formation of by-products, however, these were initially difficult to identify.

During the synthesis of 2,4,6-triisopropylphenyl triazolium salt **88** (n=1) and pentafluorophenyl triazolium salt **84** (n=3), two crystals were obtained serendipitously[58]. The first corresponds to the N-methylformanilide **106** (Figure 2.8), and the formation mechanism of this compound still remains elusive.

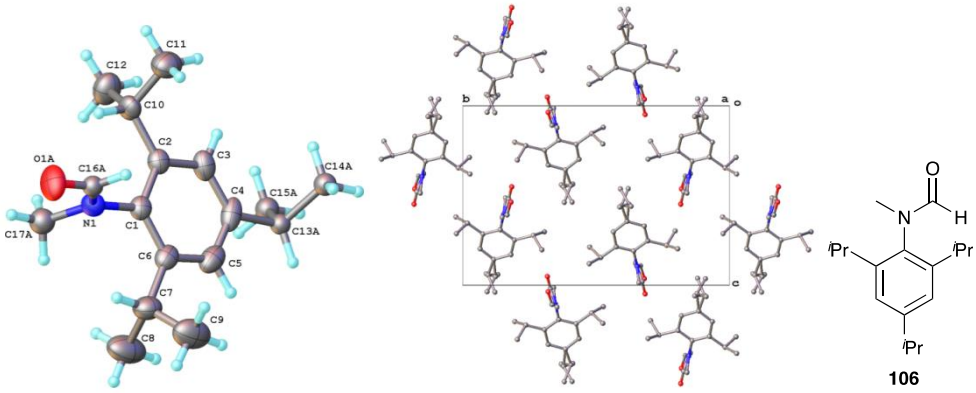

Figure 2.8. Crystal structure of the methylformanilide **106** obtained during the preparation of 2,4,6-triisopropylphenyl triazolium salt **88**.

The second crystal obtained was of a dimethoxy acetal adduct of the pentafluorophenyl triazolium salt (n=3, Figure 2.9). This type of NHC-adduct had not been previously reported, and the NMR spectrum suggested it to be the major by-product of the preparation of pentafluorophenyl triazolium salt (n=3). The solubility and polarity of this acetal adduct were similar to the triazolium salt, and recrystallisation could not

achieve separation.

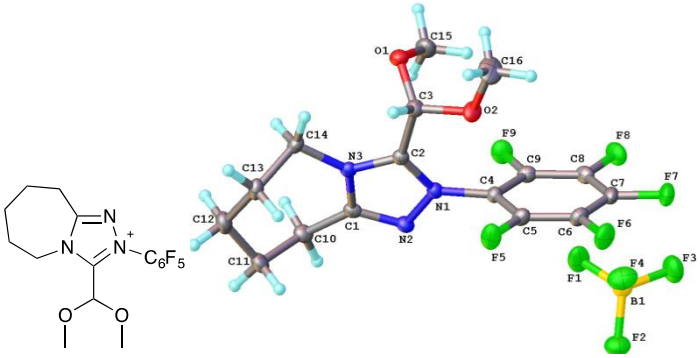

Figure 2.9. Crystal structure of dimethoxy acetal adduct of 2-perfluorophenyl- 6,7,8,9-tetrahydro-5H-3-dimethylacetal-[1,2,4] triazolo[4,3-a]azepin-2-ium tetrafluoroborate

Based on the formation of this adduct, the mass spectra (high resolution mass spectra in some cases) of the reaction mixtures obtained during the preparation of other triazolium salts were subsequently re-checked, and trace amounts of dialkoxy adducts were also detected. Table 2.3 summarises the range of potential adducts explored, which suggest that the adduct formation is possibly favoured by electron-withdrawing N-aryl groups and *ortho*-substituted aryl rings.

Table 2.3. Summarised dimethoxy- and diethoxy-adduct formation detected by MS analysis of final reaction mixtures in triazolium salt syntheses.

	Catalyst		Adduct
	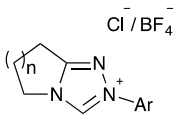		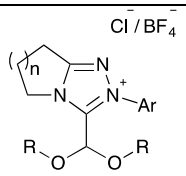
84	Ar= Pentafluorophenyl	n= 3	R= Me
88	Ar= 2,4,6-Triisopropylphenyl	n= 1	R= Me and Et
85	Ar= Mesityl	n= 1	R= Et
86		n= 2	R= Me and Et
87		n= 3	R= Me
77	Ar= 4-Fluorophenyl	n= 2	R= Et
78		n= 3	R= Me
79	Ar= Phenyl	n= 2	-
80		n= 3	-
89	Ar= 4-Methoxyphenyl	n= 1	-
90		n= 2	-
91		n= 3	-
81	Ar= 2,4,6-Trichlorophenyl	n= 1	R= Me
82		n= 2	R= Et
83		n= 3	R= Et

Fortuitously, for the reaction of 2,4,6-trichlorophenyl aryl substituted amidrazones **81**-**83**, a much larger ratio of adduct to triazolium salt was observed by LC-MS. Thus, trial syntheses of the diethoxy adduct **111**, **112**, and diisopropoxy adduct **113**, **114** and **115**, and the dimethoxy pentafluorophenyl adduct **116** were conducted.

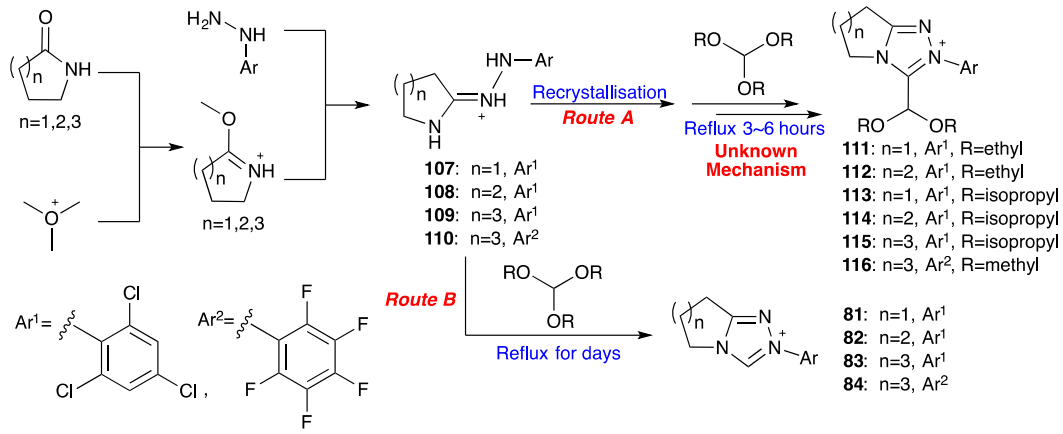

Scheme 2.13. Synthesis of 2,4,6-trichlorophenyl dialkoxy adducts and triazolium salts.

Adapted from the synthetic procedures of triazolium salts (Scheme 2.13, Route B), the modifications to improve dialkoxy adduct synthesis involves the purification of amidrazone (**107-110**) and the shortened reflux duration with orthoformates (Scheme 2.13, Route A). Traditional triazolium synthesis has no restriction on amidrazone purity, and diethyl orthoformate was added directly into the amidrazone mixture followed by reflux for several days. The good stabilities of these amidrazones, however, allows their purification by recrystallisation from methanol: diethyl ether systems. Subsequent slow evaporation from methanol provided crystals for all four amidrazones (**107-110**), and their crystal structures were obtained by single X-ray crystallography (Figure 2.10-2.13).

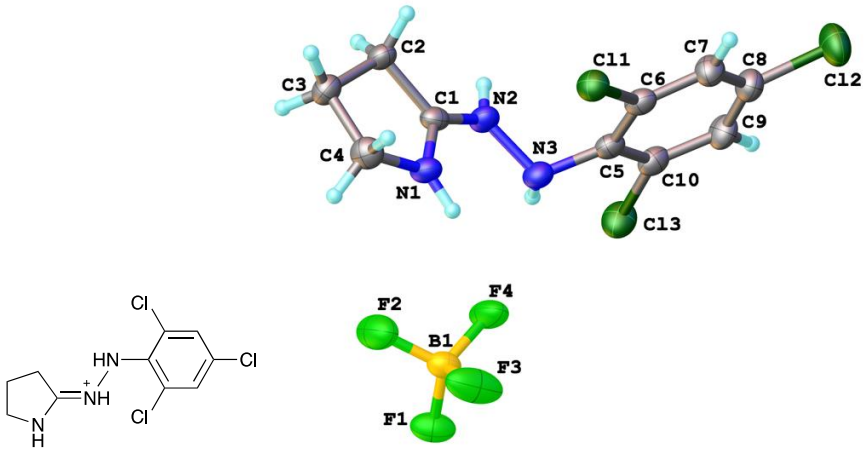

Figure 2.10. Crystal structures of 2,4,6-trichlorophenyl amidrazone **107**.

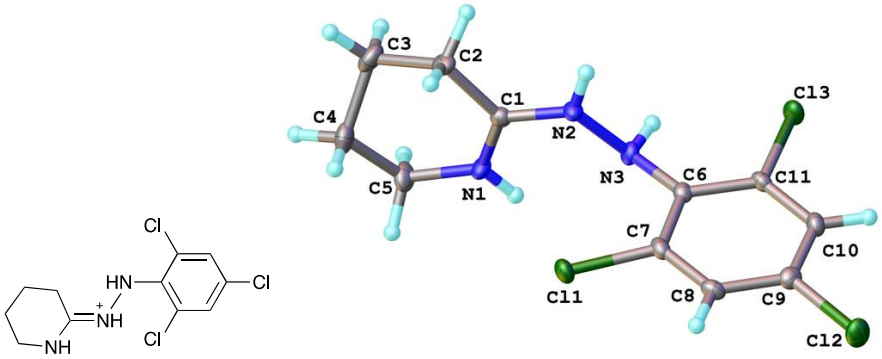

Figure 2.11. Crystal structures of 2,4,6-trichlorophenyl amidrazone **108**

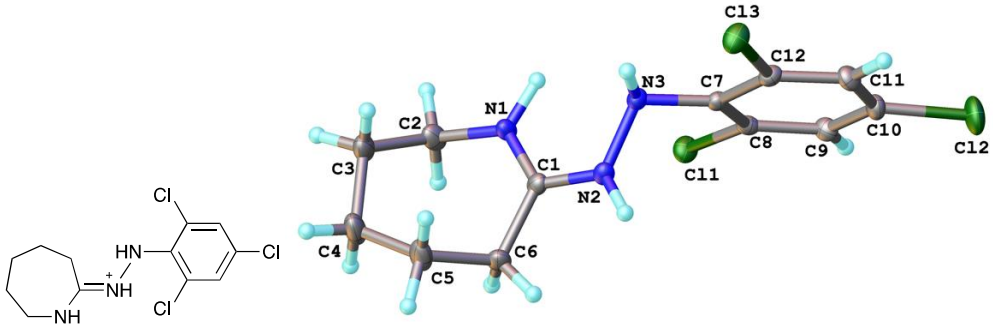

Figure 2.12. Crystal structures of 2,4,6-trichlorophenyl amidrazone **109**.

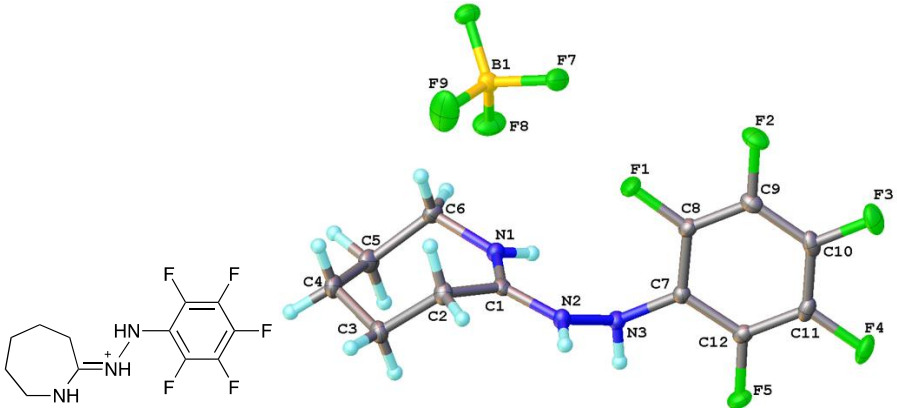

Figure 2.13. Crystal structures of pentafluorophenyl amidrazone **110**.

All four crystal structures suggest similar bond lengths between C1-N1 and C1-N2, indicating the positive charge of the amidrazone being stabilized by the resonance among the three atoms (C1, N1, and N2). Meanwhile, the high purity of amidrazones decreases additional by-product formation and the associated difficulty in probing the reaction time course.

After refluxing for 4 to 6 hours, LC-MS clearly shows that most of amidrazones were consumed with limited triazolium formation. Orthoformates were removed and dialkoxy adducts **111, 112, 114** were purified by careful recrystallisation from methanol/diethyl ether/hexane systems. Slow evaporation from methanol followed by single X-ray crystallography gave crystal structures of dialkoxy adducts (Figure 2.14-2.17). NMR analysis suggested the diethoxy adduct **111** (76% yield), **112** (52% yield), and diisopropoxy adduct **114** (60% yield) are pure, while the 7-membered diisopropoxy adduct **115**, and 7-membered dimethoxy pentafluorophenyl adduct **116** contains certain quantity of the corresponding triazolium salts **83** and **84** (10-20%), which could not be separated by recrystallisation (Figure 2.18a and 2.18b). Meanwhile, diisopropoxy adduct **113** could not be precipitated using recrystallisation.

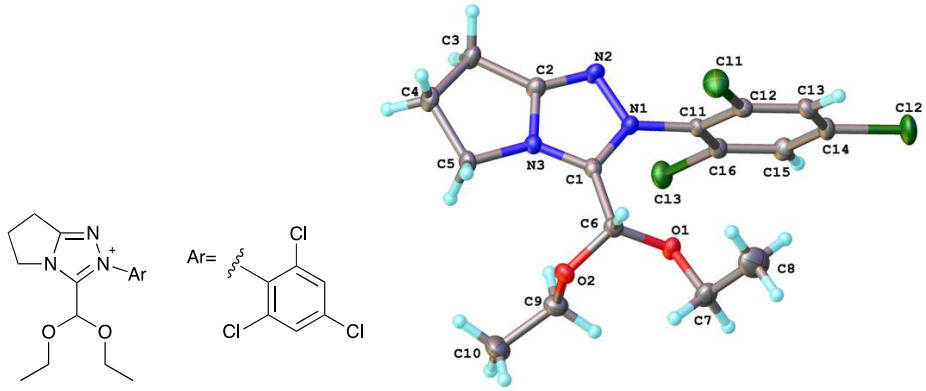

Figure 2.14. Crystal structure of pyrrol-2,4,6-trichlorophenyl triazolium diethoxy adduct **111**.

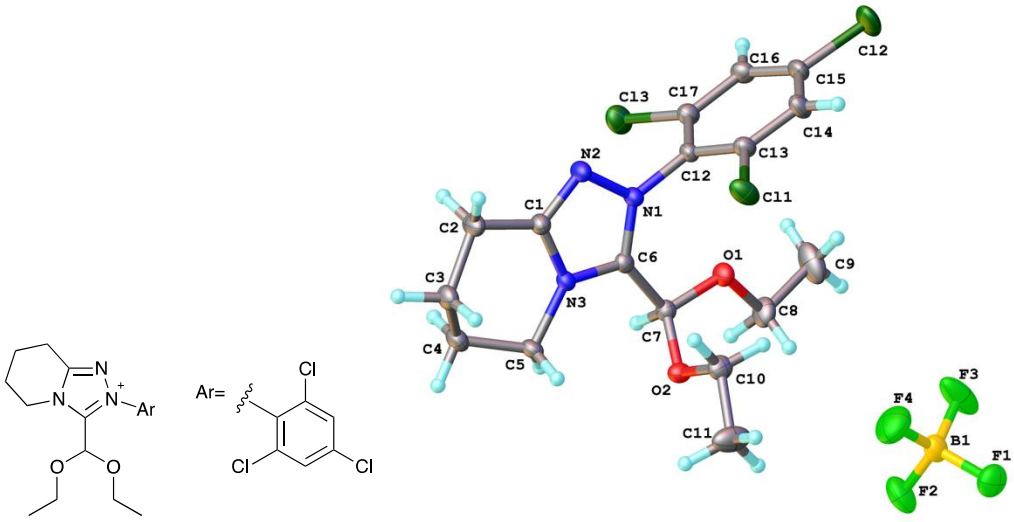

Figure 2.15. Crystal structure of 2,4,6-trichlorophenyl triazolium diethoxy adduct **112** with six membered fused ring.

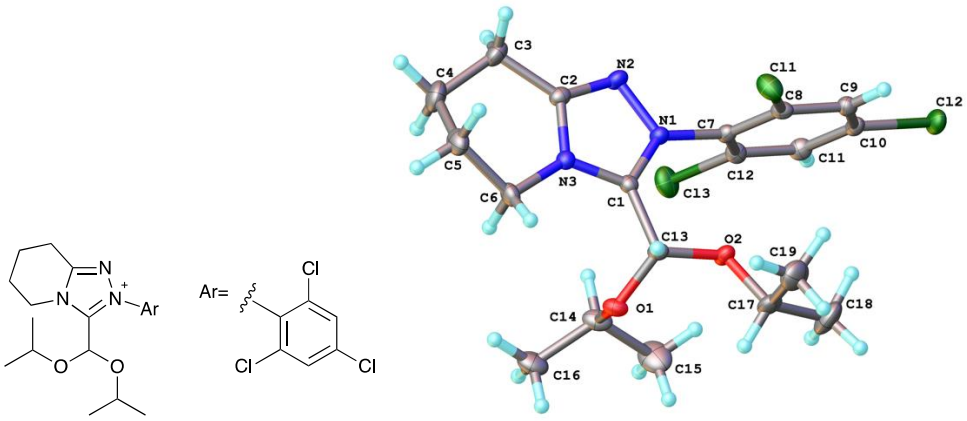

Figure 2.16. Crystal structure of 2,4,6-trichlorophenyl triazolium diisopropoxy adduct **114** with six membered fused ring.

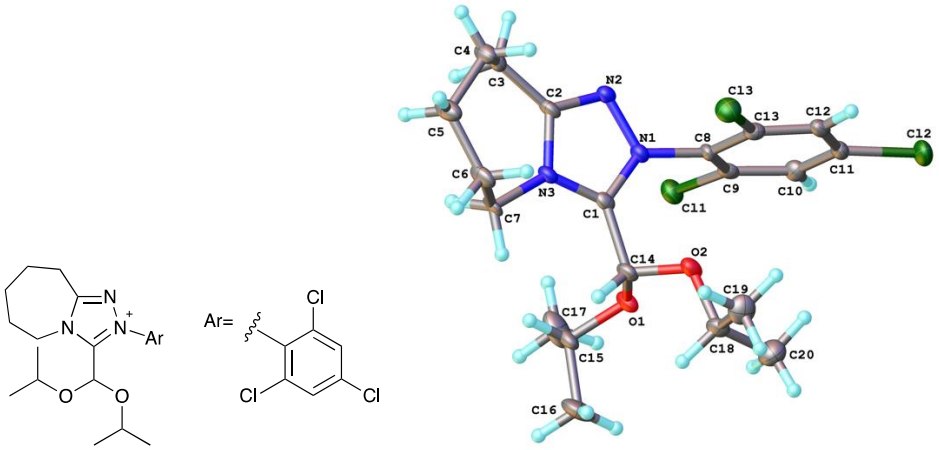

Figure 2.17. Crystal structure of 2,4,6-trichlorophenyl triazolium diisopropoxy adduct **115** with seven membered fused ring

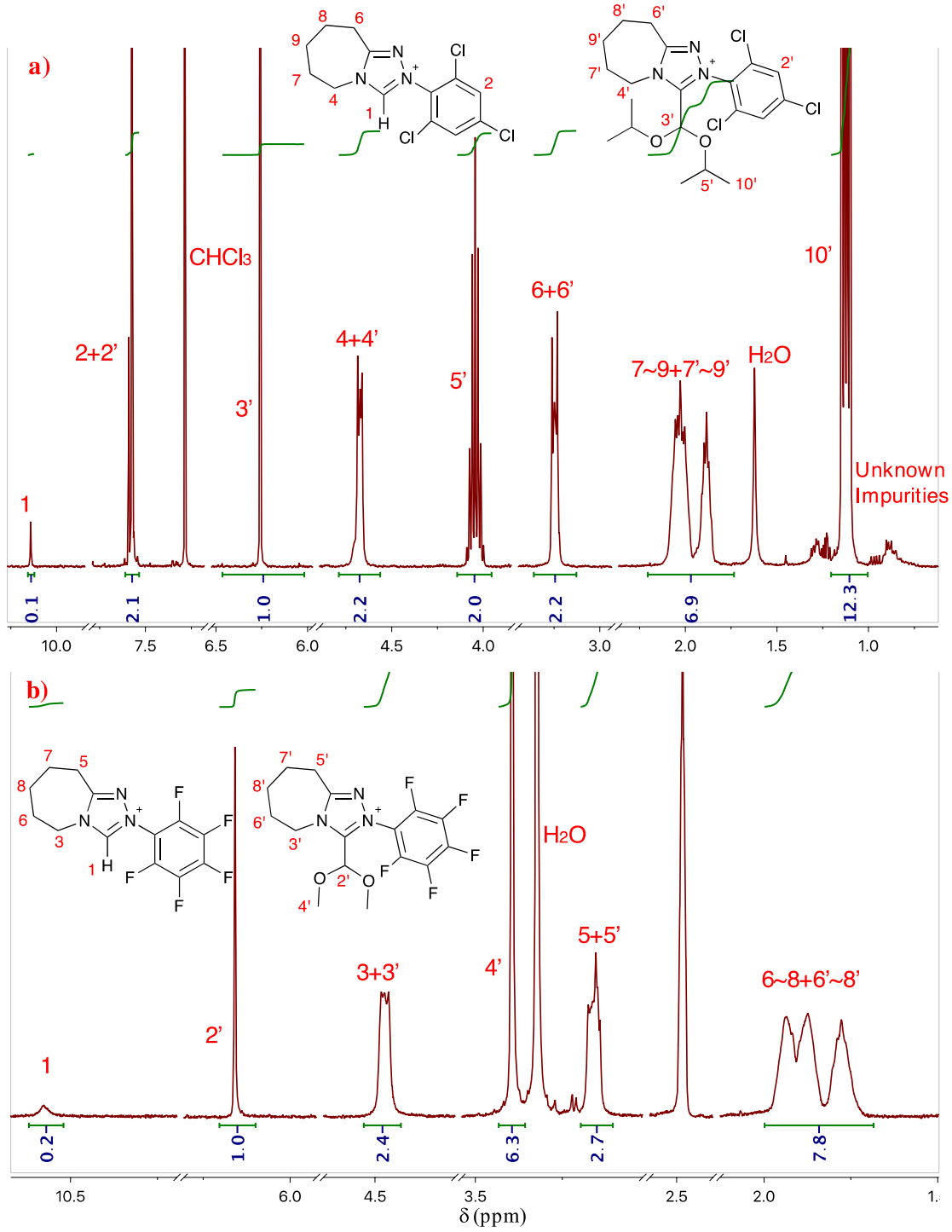

Figure 2.18. a) NMR spectrum in $CDCl_3$ of the diisopropoxy acetal adduct **115** along with the 2,4,6-trichlorophenyl triazolium salt **83** (n=3); b) NMR spectrum in DMSO-d_6 of the dimethoxy acetal adduct **116** along with the pentafluorophenyl triazolium salt **84** (n=3).

2.3.2. Mechanistic Analysis of the Dialkoxy Acetal Adduct Formation

The synthetic mechanism of dialkoxy adduct formation is unknown, thus, the reflux with trialkyl orthoformate was quenched intermittently to check the adduct formation by LC-MS. Mass spectrometry clearly showed the formation of triazolium salts, followed by their disappearance, probably owing to the formation of the dialkoxy acetal adducts. Meanwhile, mass spectra suggested the formation rate of dialkoxy acetal adducts was larger with increased fused ring size, when smaller amounts of triazolium salt could be observed. This might be an explanation for the generally reported poorer yields of triazolium salts with larger fused rings.

We assume the dialkoxy adduct probably forms *via* the reaction of the corresponding carbene and orthoformate (Scheme 2.14). Single X-ray crystal structures suggest the aryl ring of all 2,4,6-trichlorophenyl adduct **111, 112, 114, 115**, and the pentafluorophenyl adduct **116** are almost perpendicular to the triazolyl ring (Table 2.4). Meanwhile, *ortho*-aryl substituted triazolium salts also have larger dihedral angles (Figure 2.19) between aryl and triazolyl rings (Table 2.5). The steric hindrance of *ortho*-aryl substituents may block the free rotation of the aryl ring and provide easier access to the C(3) position and better accommodation of the relatively large dialkoxyacetal moiety. Thus, the formation of dialkoxy acetal adduct favours the *ortho*-substituted aryl rings.

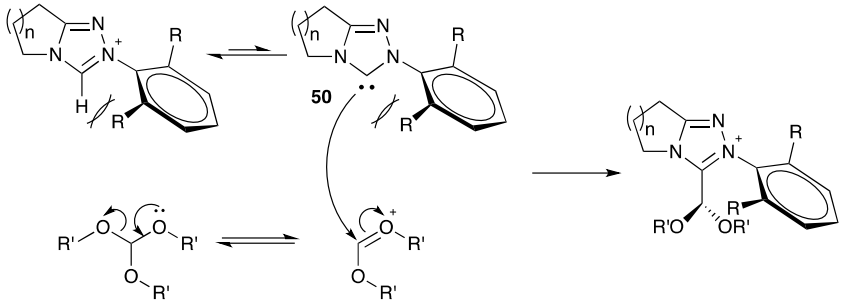

Scheme 2.14. Potential mechanism of formation of dialkoxyacetal adduct and the free N-aryl rotation blocked by steric hindrance of *ortho*-aryl substituents.

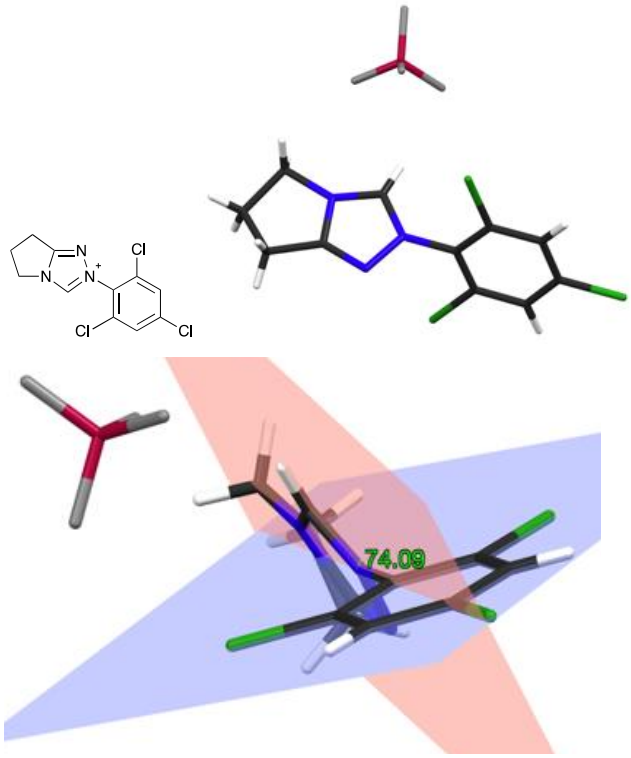

Figure 2.19. Dihedral angle measurement of 2,4,6-trichlorophenyl triazolium salt **83** (n=1); the trichlorophenyl group locates on the blue-plane, while the triazolyl group on the red-phase.

Table 2.4. Dihedral angles of dialkoxy acetal adduct between aryl and triazolyl ring obtained by single crystal X-ray crystallography at 120 K.

	Adduct			Dihedral Angle/ °
	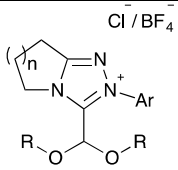			
116	Ar= Pentafluorophenyl	n= 3	R= Me	79.79
111	Ar= 2,4,6-Trichlorophenyl	n= 1	R= Et	72.63
112		n= 2	R= Et	89.55
114		n= 2	R= ^{i}Pr	84.76
115		n= 3	R= ^{i}Pr	83.96

Table 2.5. Dihedral angles of triazolium salt between aryl and triazolyl ring obtained by single X-ray crystallography at 120 K.

	Triazolium		Dihedral Angle/ °
	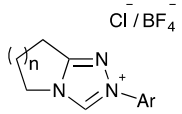		
85	Ar= Mesityl	n= 1	69.98
81[a]	Ar= 2,4,6-Trichlorophenyl	n= 1	74.35
117[a]	Ar= 2,6-Dimethoxyphenyl	n= 1	78.80
98[a]	Ar= Pentafluorophenyl	n= 1	58.83
84		n= 3	74.13
89[a]	Ar= 4-methoxyphenyl	n= 1	15.55
90		n= 3	43.43
100[a]	Ar= 4-fluorophenyl	n= 1	25.45
104[b]	Ar= 4-bromophenyl	n= 1	7.21
79	Ar= phenyl	n= 2	31.51

[a] Crystal structure obtained by Peter Quinn, [b] Triazolium synthesised by Hector Macrae.

To further investigate the mechanism of the dialkoxy acetal adduct formation, diethoxy acetal adduct **111** was dissolved into trimethyl orthoformate, and the solution was refluxed and probed by mass spectrometry. After 48 hours' refluxing, only traced amount of the dimethoxy acetal adduct **117** were detected, while the formation of triazolium salt was not observed (Scheme 2.15). This suggests, for the triazolium salts with electron-deficient *ortho*-aryl substituents, the formation rate constant of the dialkoxy acetal adduct is much larger than its dissociation rate constant.

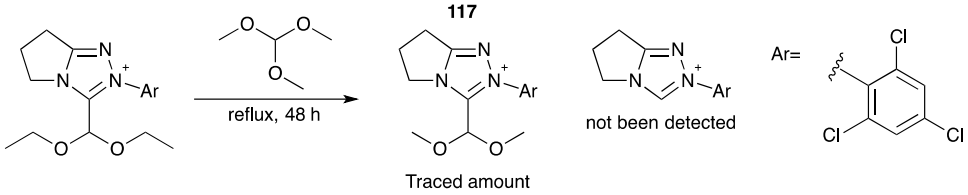

Scheme 2.15. Further mechanistic study of dialkoxy acetal adduct

During the synthesis of diethoxy acetal adduct **111** (n=1), at the very beginning of the reflux (< 1 h), several by-products were observed by LC-MS, and their peak intensity gradually decreased in the following few hours. The identification of those by-products was initially difficult until the crystal structure **118** was obtained (Figure 2.20).

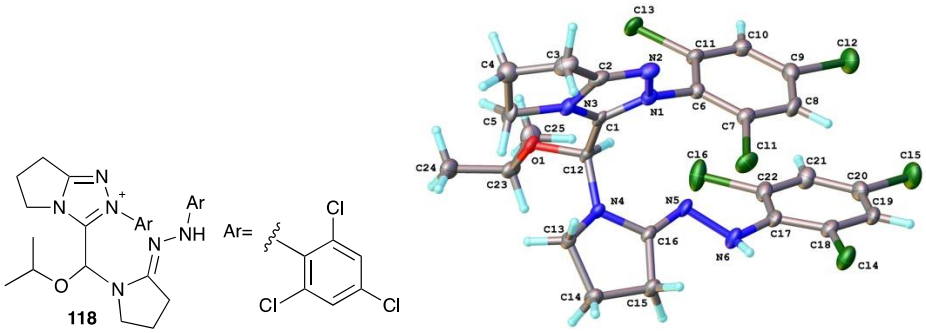

Figure 2.20. Crystal structure of condensed by-product **118** of diisopropoxy adduct and 2,4,6-trichlorophenyl amidrazone.

By mass spectrometry, at the very early reaction stage, relatively large peak intensities of the by-product **118**, amidrazone **107** are observed, whereas small peak intensities of the triazolium salt **81**, and dialkoxy acetal adduct **111** are observed. At late times, the by-product's (**118**) and amidrazone's (**107**) peak intensities significantly decreased, with the dialkoxy acetal adduct's peak intensity increased while the triazolium salt's remain at a relatively low level. According to these observations, the following reaction scheme is possible.

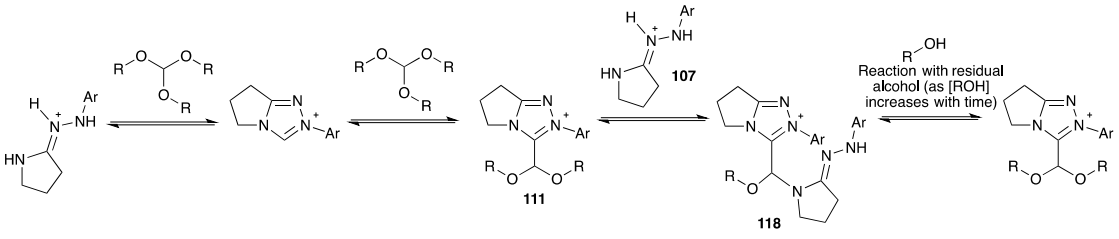

Scheme 2.16. Mechanistic flow chart illustrating reactions involving by-product **118.**

In scheme 2.16, the by-product **118** forms *via* the substitution between dialkoxy acetal adduct **111** and the amidrazone salt **107**. At the very beginning, the reaction solution

contains high concentrations of amidrazone and orthoformate (as both solvent and reagent). As discussed before, the formation rate of dialkoxy acetal adduct from orthoformate and triazolium salt could be quite fast in case of trichlorophenyl aryl substituent. Thus, the formed triazolium salt directly adds to the orthoformate and affords the dialkoxy acetal adduct. The remaining high concentration of amidrazone then undergoes a further substitution reaction with the acetal adduct to afford by-product **118**. With the accumulation of alcohol, subsequent decomposition of **118** can occur. The alcohol could displace the amidrazone by substitution resulting again in adduct (Scheme 2.16).

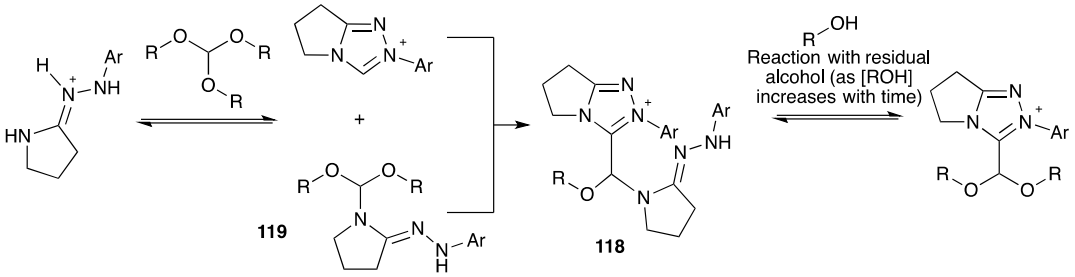

Scheme 2.17. Additional mechanistic possibilities involve by-product **118.**

Scheme 2,17 includes a second formation pathway of byproduct **118**, where the amidrazone first forms a formamide **119**, and the triazolium salt **111** adds to the formamide to afford by-product **118**. The accumulation of the later alcohol cleaved the amidrazone, and further formed dialkoxy acetal adduct **111**.

2.3.3. Prospective Applications of the Novel Dialkoxy Acetal Adducts

2.3.3.1. Formation of the Simplest NHC a[1] Synthon in Acidic Conditions

The dialkoxy acetal adducts could potentially be precursors to NHC-formaldehyde adducts under acidic conditions, which can be seen as the simplest NHC-based a[1]

synthon **120** (Scheme 2.18). Alternative routes to afford NHC-based a[1] synthons are challenging and difficult to access. Thus, the diethoxy acetal adduct **111** was added into the deuterium chloride solution (1M). Limited by the adduct solubility in deuterium oxide, deuterated acetonitrile was used as co-solvent, and NMR spectrometry was applied to probe the reaction process. Interestingly, the dialkoxy acetal adduct showed good stability in acidic conditions, and no reaction happened even by increasing the reaction temperature to 60 °C. This probably could be attributed to the positive charge of the adduct, which impedes the further protonation to a dication intermediate.

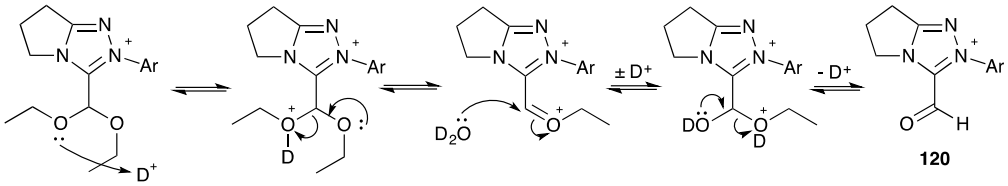

Scheme 2.18. Possible mechanism towards NHC a[1] synthons **120**.

2.3.3.2. Formation of NHC d[1] Synthons in Basic Conditions

Currently, several groups have recently reported the isolation and characterization of the Breslow intermediate (Figure 2.21)[71-73]. However, to date, there has been no report of the synthesis and characterization of an unprotected triazolyl-derived Breslow intermediate.

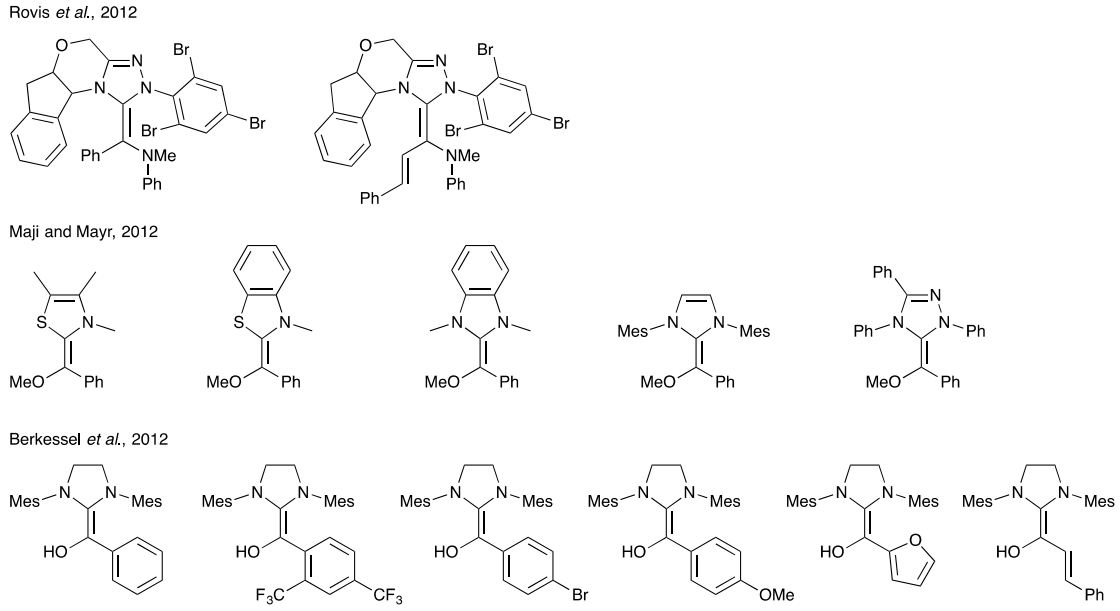

Figure 2.21. Typical isolable Breslow intermediates.

We predicted the ortho-formate-derived proton could be deprotonated to afford a new type of isolable bicyclic triazolyl Breslow intermediate (Scheme 2.19). Thus, H/D-exchange could be used to assess the acidity at this position. The trichlorophenyl diethoxy acetal adduct **111** (n=1) was added into the acetic acid buffered solution (*p*D ~ 6), and NMR spectroscopy suggest no reaction occurred. The diethoxy acetal adduct **111** was then added into a more basic solution, buffered with $KDCO_3/K_2CO_3$ (*p*D ~11). The color of the solution turned yellow immediately and gradually faded. NMR spectroscopy gave interesting results (Figure 2.22).

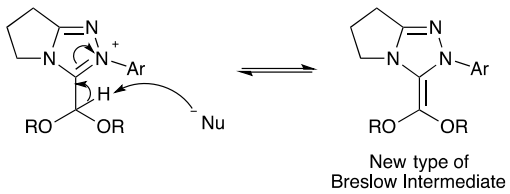

Scheme 2.19. Deprotonation of dialkoxy acetyl adduct.

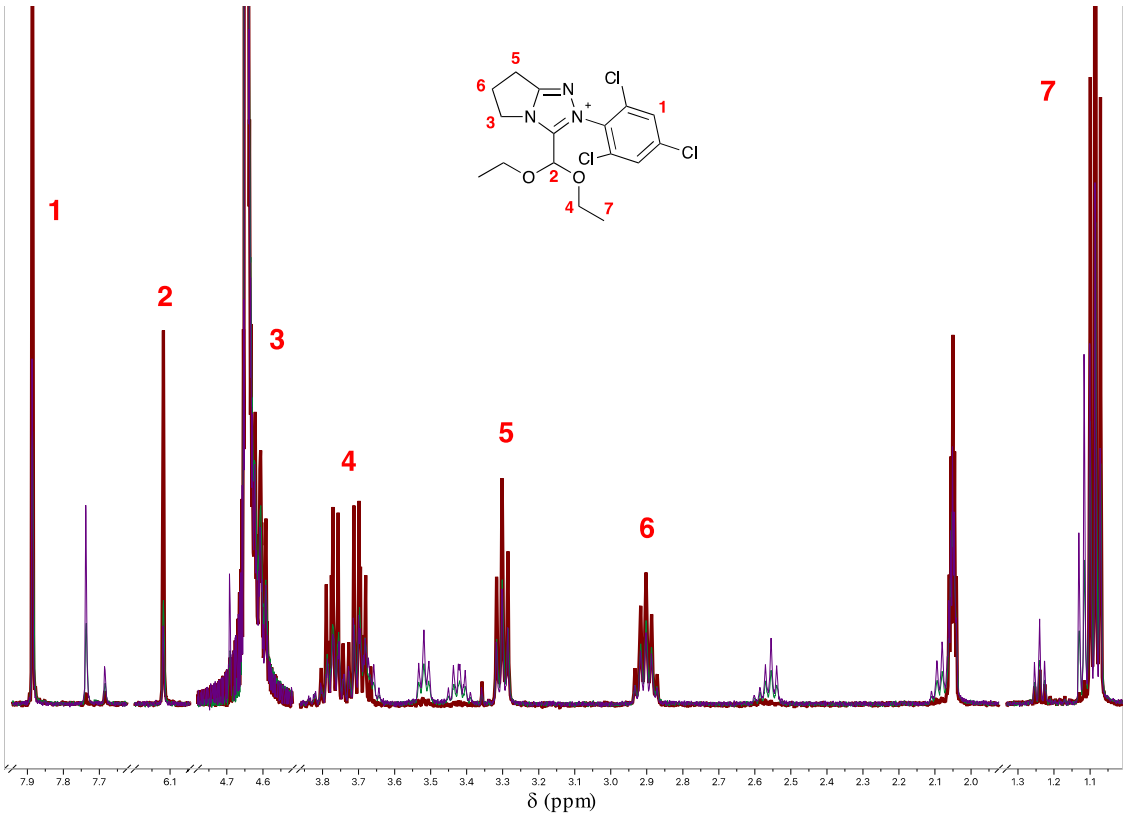

Figure 2.22. Superimposed NMR spectra for the deprotonation of diethoxy acetal adduct **111**. Unlabeled peaks belongs to two unknown compounds.

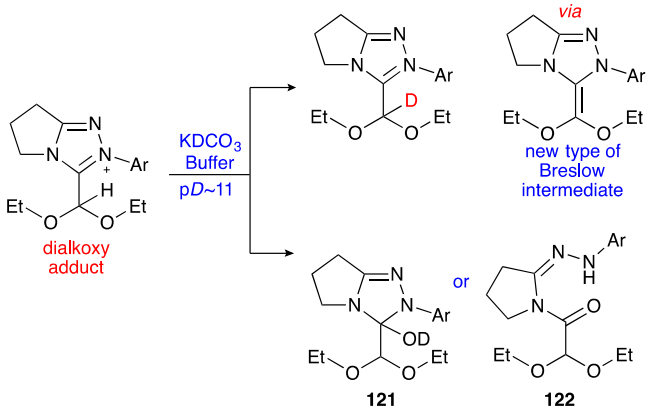

Scheme 2.20. Hydrolysis of diethoxy acetal adduct and the formation evidence of the new type of Breslow intermediate.

Figure 2.22 superimposes 3 individual NMR spectra, which covered the first 3.5 hours of reaction time. Both the aryl region (7.6~7.9 ppm) and the methyl groups (0.9~1.3 ppm) suggest that during the reaction time, two new compounds gradually accumulate, with the disappearance of the original diethoxy acetal adduct **111**. These two new

compounds might be the hydrolysis and ring opening by-products **121** and **122** of the adduct (Scheme 2.20), or alternatively be the oxidised product of the Breslow intermediate. It also demonstrates the faster disappearance of the orthoformic proton compared to the aryl and alkyl protons of the diethoxy acetal adduct. This faster disappearance could be attributed to the H/D-exchange on the orthoformic position, which can be seen as an evidence of the Breslow intermediate formation.

2.4. Summary

Adapted from literature procedures, the syntheses of sixteen N-aryl bicyclic triazolium salts was attempted *via* two synthetic pathways. These triazolium salts were designed with different backbone structures, including the fused ring size and the N-aryl substituents. Twelve salts were successfully isolated and purified, and ten crystal structures were obtained by using single X-ray crystallography. The analysis of these crystal structures shows the N-C-N bond angle changed with the increment of fused ring size. They follow the order of n= 1> n= 2 ≈ n= 3.

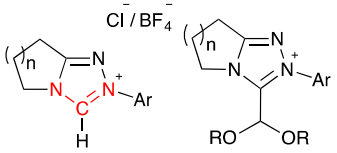

During the preparation of these triazolium salts, a novel dialkoxy acetal adduct was isolated, whose formation probably can explain the difficult access towards certain triazolium salts. LC-MS reaction monitoring suggests the formation of this dialkoxy acetal adduct is favoured by electron-withdrawing N-aryl groups and *ortho*-substituted aryl rings. We thus modified the original synthetic procedure towards triazolium salts, and successfully isolated and purified three dialkoxy acetal adducts with 2,4,6-trichlorophenyl as N-aryl substituent. The crystal structure of a pentafluorophenyl-

substituted adduct was also obtained, however, the crude sample salt could not be purified by recrystallisation. Moreover, crystal structures of four amidrazones and two additional by-products were also achieved from single X-ray crystallography.

Several experiments were performed to explore the mechanism of formation of the novel NHC-catalysts. From our results, it is most likely that the NHC-acetals are formed after triazolium salt formation. In addition, the reactivity of the acetal adducts under acidic and basic conditions was explored. In the presence of 1 M DCl, the acetals were stable over 4 days even at 60 °C. ^{1}H NMR spectra suggest the H/D-exchange at the orthoformic position, which can be seen as an evidence of the Breslow intermediate formation, in parallel with hydrolysis and/or oxidation.

2.5. Reference

1. G. J. LaBonia, The University of Mississippi, 2014.
2. E. Buchner and T. Curtius, *Ber. Dtsch. Chem. Ges.*, 1885, **18**, 2377-2379.
3. A. Igau, H. Grutzmacher, A. Baceiredo and G. Bertrand, *J. Am. Chem. Soc.*, 1988, **110**, 6463-6466.
4. A. J. Arduengo III, R. L. Harlow and M. Kline, *J. Am. Chem. Soc.*, 1991, **113**, 361-363.
5. F. E. Hahn, *Angew Chem Int Edit*, 2006, **45**, 1348-1352.
6. E. Despagnet-Ayoub and R. H. Grubbs, *J. Am. Chem. Soc.*, 2004, **126**, 10198-10199.
7. D. Martin, A. Baceiredo, H. Gornitzka, W. W. Schoeller and G. Bertrand, *Angew Chem Int Edit*, 2005, **44**, 1700-1703.
8. J. Yun, E. R. Marinez and R. H. Grubbs, *Organometallics*, 2004, **23**, 4172-4173.
9. M. Iglesias, D. J. Beetstra, J. C. Knight, L. L. Ooi, A. Stasch, S. Coles, L. Male, M. B. Hursthouse, K. J. Cavell, A. Dervisi and I. A. Fallis, *Organometallics*, 2008, **27**, 3279-3289.
10. A. Kausamo, H. M. Tuononen, K. E. Krahulic and R. Roesler, *Inorg Chem*, 2008, **47**, 1145-1154.
11. V. Lavallo, Y. Canac, B. Donnadieu, W. W. Schoeller and G. Bertrand, *Science*, 2006, **312**, 722-724.
12. K. E. Krahulic, G. D. Enright, M. Parvez and R. Roesler, *J. Am. Chem. Soc.*, 2005, **127**, 4142-4143.
13. E. Aldeco-Perez, A. J. Rosenthal, B. Donnadieu, P. Parameswaran, G. Frenking and G. Bertrand, *Science*, 2009, **326**, 556-559.
14. Y. Ishida, B. Donnadieu and G. Bertrand, *Proc Natl Acad Sci U S A*, 2006, **103**, 13585-13588.
15. J. E. Thomson, K. Rix and A. D. Smith, *Org Lett*, 2006, **8**, 3785-3788.
16. L. Benhamou, E. Chardon, G. Lavigne, S. Bellemin-Laponnaz and V. Cesar, *Chem Rev*, 2011,

111, 2705-2733.

17. E. A. Barsa and R. Richter, *J. Org. Chem.*, 1986, **51**, 4483-4485.
18. J. S. Mccallum, J. R. Gasdaska, L. S. Liebeskind and S. J. Tremont, *Tetrahedron Lett.*, 1989, **30**, 4085-4088.
19. H. W. Wanzlick and Schonher.Hj, *Angew. Chem.-Int. Edit.*, 1968, **7**, 141-&.
20. W. A. Herrmann, L. J. Goossen, G. R. J. Artus and C. Kocher, *Organometallics*, 1997, **16**, 2472-2477.
21. C. L. Winn, F. Guillen, J. Pytkowicz, S. Roland, P. Mangeney and A. Alexakis, *J. Organomet. Chem.*, 2005, **690**, 5672-5695.
22. M. H. Voges, C. Romming and M. Tilset, *Organometallics*, 1999, **18**, 529-533.
23. I. C. Stewart, T. Ung, A. A. Pletnev, J. M. Berlin, R. H. Grubbs and Y. Schrodi, *Org Lett*, 2007, **9**, 1589-1592.
24. M. L. Cole and P. C. Junk, *Journal of organometallic chemistry*, 2003, **666**, 55-62.
25. A. Binobaid, M. Iglesias, D. J. Beetstra, B. Kariuki, A. Dervisi, I. A. Fallis and K. J. Cavell, *Dalton Trans*, 2009, DOI: 10.1039/b909834h, 7099-7112.
26. R. H. DeWOLFE, *J. Org. Chem.*, 1962, **27**, 490-493.
27. E. C. Taylor and W. A. Ehrhart, *J. Org. Chem.*, 1963, **28**, 1108-1112.
28. R. Jazzar, H. Liang, B. Donnadieu and G. Bertrand, *J Organomet Chem*, 2006, **691**, 3201-3205.
29. K. M. Kuhn and R. H. Grubbs, *Org Lett*, 2008, **10**, 2075-2077.
30. K. Hirano, S. Urban, C. Wang and F. Glorius, *Org Lett*, 2009, **11**, 1019-1022.
31. A. J. Boydston, J. D. Rice, M. D. Sanderson, O. L. Dykhno and C. W. Bielawski, *Organometallics*, 2006, **25**, 6087-6098.
32. L. Benhamou, V. Cesar, H. Gornitzka, N. Lugan and G. Lavigne, *Chem Commun (Camb)*, 2009, DOI: 10.1039/b907908d, 4720-4722.
33. A. T. Biju, K. Hirano, R. Frohlich and F. Glorius, *Chem Asian J*, 2009, **4**, 1786-1789.
34. V. Lavallo, Y. Ishida, B. Donnadieu and G. Bertrand, *Angew. Chem., Int. Ed.*, 2006, **45**, 6652-6655.
35. V. Lavallo, Y. Canac, C. Prasang, B. Donnadieu and G. Bertrand, *Angew. Chem., Int. Ed.*, 2005, **44**, 5705-5709.
36. S. Gómez-Bujedo, M. Alcarazo, C. Pichon, E. Álvarez, R. Fernández and J. M. Lassaletta, *Chem. Commun.*, 2007, 1180-1182.
37. D. Barbier, C. Marazano, B. C. Das and P. Potier, *J. Org. Chem.*, 1996, **61**, 9596-9598.
38. Y. Genisson, C. Marazano, M. Mehmandoust, D. Gnecco and B. C. Das, *Synlett*, 1992, **1992**, 431-434.
39. D. Enders and H. Gielen, *J. Organomet. Chem.*, 2001, **617**, 70-80.
40. G. Boyd and A. Summers, *J. Chem. Soc. C*, 1971, 409-414.
41. A. Furstner, M. Alcarazo, V. Cesar and C. W. Lehmann, *Chem Commun (Camb)*, 2006, DOI: 10.1039/b604236h, 2176-2178.
42. A. Furstner, M. Alcarazo, K. Radkowski and C. W. Lehmann, *Angew Chem Int Edit*, 2008, **47**, 8302-8306.
43. I. Calder, W. Sasse and T. Spotswood, 1963.
44. I. Calder and W. Sasse, *Aust. J. Chem.*, 1965, **18**, 1819-1833.
45. I. Calder and W. Sasse, *Aust. J. Chem.*, 1968, **21**, 2951-2965.

46. R. Weiss, S. Reichel, M. Handke and F. Hampel, *Angew. Chem.-Int. Edit.*, 1998, **37**, 344-347.
47. A. J. Arduengo III, R. Krafczyk, R. Schmutzler, H. A. Craig, J. R. Goerlich, W. J. Marshall and M. Unverzagt, *Tetrahedron*, 1999, **55**, 14523-14534.
48. S. Wurtz and F. Glorius, *Acc Chem Res*, 2008, **41**, 1523-1533.
49. L. Jafarpour, E. D. Stevens and S. P. Nolan, *J. Organomet. Chem.*, 2000, **606**, 49-54.
50. L. Hintermann, *Beilstein J Org Chem*, 2007, **3**, 22.
51. R. A. DONIA, J. A. SHOTTON, L. O. BENTZ and G. E. SMITH JR, *J. Org. Chem.*, 1949, **14**, 952-961.
52. S. Saba, A. Brescia and M. K. Kaloustian, *Tetrahedron Lett.*, 1991, **32**, 5031-5034.
53. A. J. Arduengo III, R. Krafczyk, R. Schmutzler, H. A. Craig, J. R. Goerlich, W. J. Marshall and M. J. T. Unverzagt, 1999, **55**, 14523-14534.
54. V. Jurčík, M. Gilani and R. Wilhelm, *Eur. J. Org. Chem.*, 2006, **2006**, 5103-5109.
55. S. Tiede, A. Berger, D. Schlesiger, D. Rost, A. Luhl and S. Blechert, *Angew Chem Int Edit*, 2010, **49**, 3972-3975.
56. M. S. Kerr, J. Read de Alaniz and T. Rovis, *J. Am. Chem. Soc.*, 2002, **124**, 10298-10299.
57. R. MASSEY, Durham University, 2013.
58. J. ZHU, Durham University, 2016.
59. S. M. Langdon, M. M. Wilde, K. Thai and M. Gravel, *J. Am. Chem. Soc.*, 2014, **136**, 7539-7542.
60. F. Liu, X. Bugaut, M. Schedler, R. Frohlich and F. Glorius, *Angew Chem Int Edit*, 2011, **50**, 12626-12630.
61. M. Schedler, R. Frohlich, C. G. Daniliuc and F. Glorius, *Eur. J. Org. Chem.*, 2012, **2012**, 4164-4171.
62. U. Tilstam and H. Weinmann, *Org. Process Res. Dev.*, 2002, **6**, 906-910.
63. K. Jones, R. F. Newton and C. J. Yarnold, *Tetrahedron*, 1996, **52**, 4133-4140.
64. V. R. Yatham, W. Harnying, D. Kootz, J. r.-M. Neudörfl, N. E. Schlörer and A. Berkessel, *J. Am. Chem. Soc.*, 2016, **138**, 2670-2677.
65. J. P. Demers and D. H. Klaubert, *Tetrahedron Lett.*, 1987, **28**, 4933-4934.
66. M. S. Kerr, J. Read de Alaniz and T. Rovis, *J Org Chem*, 2005, **70**, 5725-5728.
67. P.-C. Chiang, M. Rommel and J. W. Bode, *J. Am. Chem. Soc.*, 2009, **131**, 8714-8718.
68. R. W. Davidson and M. J. Fuchter, *Chem. Commun.*, 2016, **52**, 11638-11641.
69. J. E. Thomson, C. D. Campbell, C. Concellon, N. Duguet, K. Rix, A. M. Slawin and A. D. Smith, *J Org Chem*, 2008, **73**, 2784-2791.
70. Z. I. Yoshida and Y. Tawara, *J. Am. Chem. Soc.*, 1971, **93**, 2573-&.
71. A. Berkessel, V. R. Yatham, S. Elfert and J. M. Neudorfl, *Angew Chem Int Edit*, 2013, **52**, 11158-11162.
72. D. A. DiRocco, K. M. Oberg and T. Rovis, *J. Am. Chem. Soc.*, 2012, **134**, 6143-6145.
73. B. Maji and H. Mayr, *Angew Chem Int Edit*, 2012, **51**, 10408-10412.

Chapter 3. Fused Ring Size and Kinetic Evaluation

3.1. Introduction

3.1.1. Benzoin Condensation

As introduced in Chapter 1, aldehyde analogues can undergo self-condensation catalysed by N-heterocyclic carbenes *via* an umpolung process[1]. Recent work from the O'Donoghue and Smith groups has explored the mechanism of the bicyclic triazolium-catalysed benzoin reaction (Scheme 3.1)[2, 3]. The triazolyl NHC **1** first combines with the aldehyde **123** to afford the Breslow intermediate **124**, followed by reaction with another molecule of aldehyde to form the benzoin product **125**. During their studies, ^{1}H NMR spectroscopy was used to probe the reaction, which suggested the hydroxy aryl adduct **126** to be the only observed intermediate.

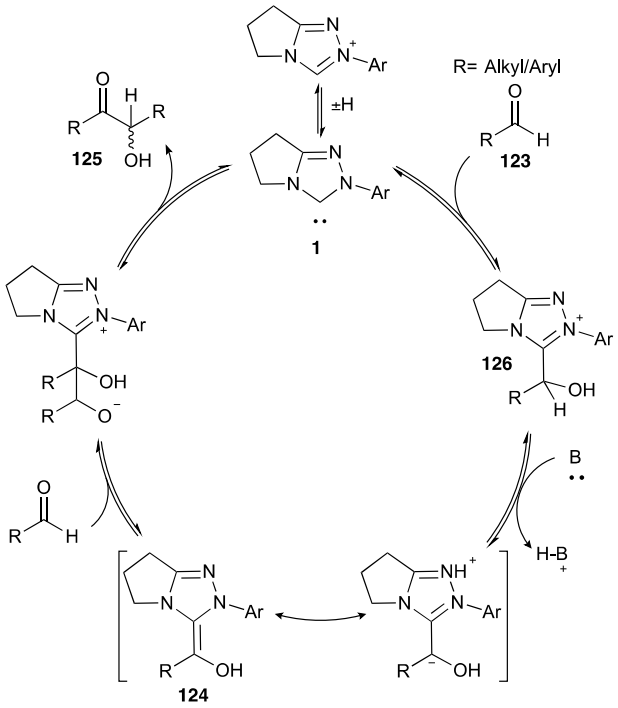

Scheme 3.1. Mechanism of NHC-catalysed benzoin condensation.

Moreover, the rate constants of the three main steps in benzoin condensation (formation of the adduct, Breslow intermediate, and benzoin) were also measured by the O'Donoghue and Smith groups[4]. They focused on a quantitative evaluation of the effect of the N-aryl substituent on the benzoin condensation, as the role of the N-aryl substituent in NHC **1** has been shown synthetically to be key to the catalytic efficiency of various NHC-processes[2, 3].

3.1.2. Chemoselectivity of NHCs

Traced back to 1976, Cookson and Lane demonstrated the first cross-benzoin reactions catalysed by thiazolium salts, which emphasised the lack of chemoselectivity between two aldehydes (Scheme 3.2)[5]. Although previous studies suggested the ratio of the preferred product can be increased by using an excess amount of the corresponding aldehyde (10 equivalents), the selectivity was still unsatisfactory[6].

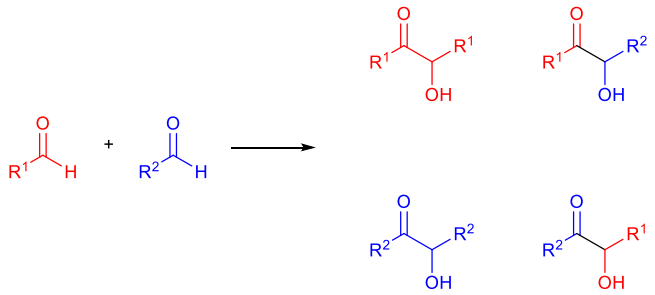

Scheme 3.2. Four potential products generated in a cross-benzoin condensation.

Glorius investigated the cross-benzoin condensation of benzaldehyde and metachlorobenzaldehyde catalysed by thiazolium salt **127**, and suggested the chemoselectivity was based on the steric hindrance of aldehydes (Scheme 3.3). The formation of Breslow intermediate favours benzaldehyde as a result of its small steric requirement, while the Breslow intermediate prefers to react with the *ortho*-substituted benzaldehydes, possibly due to electronic effects[7].

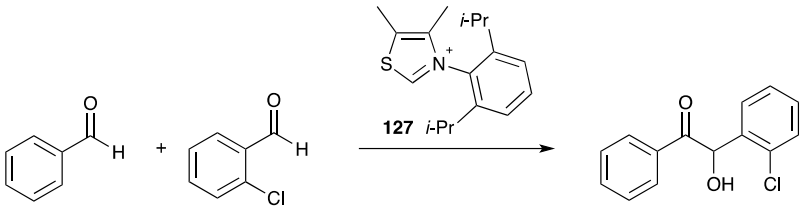

Scheme 3.3. Chemoselectivity of the cross-benzoin reaction due to *ortho*-substituents.

Yang and co-workers noted an interesting difference in selectivity between thiazolyl carbene **128** and triazolyl carbene derivatives **1**. They suggested the nucleophilic attack of thiazolyl carbene prefers the aromatic aldehyde rather than acetaldehyde due to the formation of the most stable Breslow intermediate **129**. In contrast, the nucleophilic attack of triazolyl carbene favours the less sterically demanding acetaldehyde and forms the intermediate **130**. Moreover, the following attachment of the second aldehyde towards the d^1 synthon liberates the hybrid benzoin products. Remarkably, this chemoselectivity could not be contravened even with ten equivalents of acetaldehyde[8].

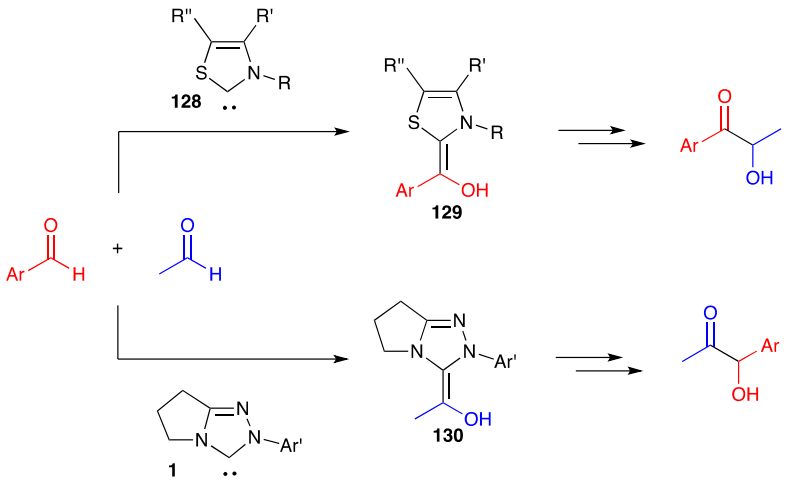

Scheme 3.4. Difference in chemoselectivity between thiazolyl **128** and triazolyl **1** carbenes.

Apart from Glorius' and Yang's work, other research groups also demonstrated methods to undergo chemoselective cross-benzoin condensation using specific aldehydes[9]. In particular, Mennen and Miller suggest a series of macrocyclizations of α,ω-dialdehydes in a relatively short reaction time (90 min)[8, 10, 11]. Similar to Yang's work, Connon

reported selective condensation of the 2-bromophenylaldehyde with aliphatic aldehyde in excellent yield (90%)[12]. Enders[13, 14], Connon[15] and Anand[16] applied Michael acceptors (*e.g.* trifluoroacetophenone, benzyl-α-ketoesters, and trifluoroacetaldehyde ethyl hemiacetal) to replace one of the aldehydes to direct the chemoselectivity[6]. Müller[17], Johnson[18], and Xin[19] contributed excellent chemoselectivities by introducing enzymes, or using acylsilanes and acylphosphonates as replacement of acyl anion equivalents[13]. However, none of these advances provide a general method to afford chemoselective cross-benzoin condensations[9].

In 2014, Gravel designed the first comprehensive catalytic system which selectively forms the cross-benzoin product between aromatic and aliphatic aldehydes[9]. Previous results from this group showed that a triazolyl carbene with a morpholine fused ring preferred to react with aliphatic aldehyde rather than aromatic aldehyde, and Gravel attributed this chemoselectivity mostly to structures of catalysts[20].

NHC	Product ratio			
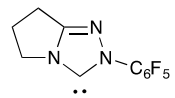	2	59	25	14
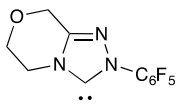	2	93	0	5
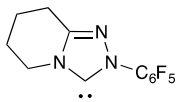	2	94	0	4
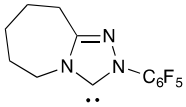	21	68	9	2

Scheme 3.5. Comparison of chemoselectivities in cross-benzoin reactions.

By analysis of the reaction between benzaldehyde and hydrocinnamaldehyde catalysed

by triazolyl carbenes with different fused rings, Gravel concluded the chemoselectivity is possibly influenced by the fused ring size of carbene, with the six-membered fused ring being optimal (Scheme 3.5). They expanded this chemoselectivity by utilising various aryl- and alkyl-aldehydes in different conditions. With small excesses of aliphatic aldehydes (1.5 equivalents), the 6-membered-fused triazolyl carbene prefers to react with alkyl-aldehydes to afford the Breslow intermediate, and followed by subsequent reaction with the aryl-aldehyde. Remarkably, Gravel's work obviated the requirement for a large excess of one aldehyde, and was further developed towards an enantioselective intermolecular cross-benzoin condensation by using related chiral triazolyl carbene **131** (Scheme 3.6)[9, 21].

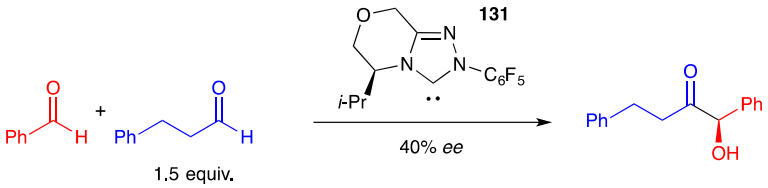

Scheme 3.6. Enantioselective intermolecular cross-benzoin condensation.

To suggest the substantial reason for the chemoselectivity variation caused by fused ring sizes of catalyst, this project focused on the systematic kinetic evaluation of the homo-benzoin condensation catalysed by various triazolium salts.

3.2. Reaction Profiles and ^{1}H NMR Analysis of Stoichiometric Reaction Between Triazolium and Aldehyde

Adapted from Leeper and White's kinetic experiments in 2001[22], ^{1}H NMR spectroscopy was used to analyse the reaction parameters of the benzoin condensation. Stoichiometric quantities of aldehyde and triazolium salt were added to a triethylamine buffered methanol-d_4 solution at 25 °C to facilitate the identification of reaction intermediates. The concentration of aldehyde **123**, benzoin product **125**, unreacted azolium **132** and adduct **133** (formed by direct combination of aldehyde and carbene) were probed by ^{1}H

NMR spectroscopy. The utilisation of methanol-d_4 allowed the concurrent H/D-exchange of the benzylic hydrogens of intermediate and therefore, the formation rate of Breslow intermediate can be crucially calculated. Additionally, the existence of solvent adduct **134** from aldehydes was taken into consideration, which generally occupies 1~10% of total aldehyde concentration[2, 4].

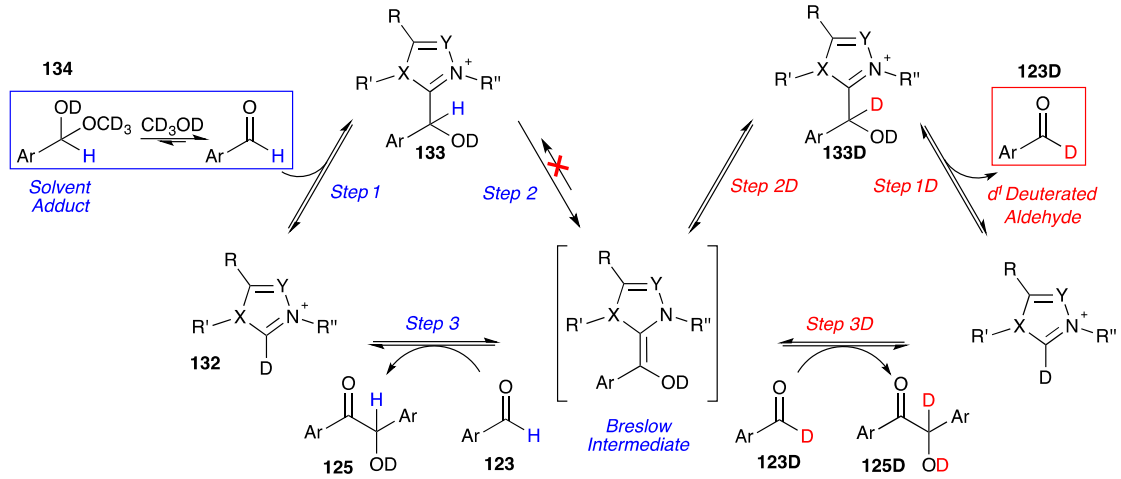

Scheme 3.7. Mechanistic model for the self-condensation of aldehyde **123** catalysed by NHC precatalyst **132** in methanol-d_4 solution.

Based on Leeper's mechanistic studies and the previous joint work from the O'Donoghue and Smith groups, the reaction profiles of triazolium salts **77-80**, **89-91**, **100, 101** towards the homobenzoin condensation of aldehyde **135-139** in triethylamine-buffered (2:1 NEt_3: NEt_3·HCl) methanol-d_4 solution were investigated (Figure 3.1). The representative method, the self-condensation of 2-methoxybenzaldehyde **138** catalysed by 4-fluorophenyl triazolium salt **100** (n= 1), will be introduced to demonstrate the calculations of concentrations of each component during the course of reaction. Although NMR spectra varied with catalysts and aldehydes, similar procedures could be employed for each reaction studied.

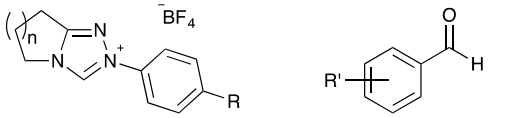

101: n=1, R= H **78** : n=3, R= F
79 : n=2, R= H **89** : n=1, R= OMe
80 : n=3, R= H **90** : n=2, R= OMe
100: n=1, R= F **91** : n=3, R= OMe
77 : n=2, R= F

135: R= H
136: R= 2-Me
137: R= 4-Me
138: R= 2-OMe
139: R= 4-OMe

Figure 3.1. Range of triazolium salts **77-80**, **89-91**, **100, 101** and aldehydes **135-139** used in kinetic experiments.

3.3. The Stoichiometric Reaction of 2-[4-Fluorophenyl]-6,7-dihydro-5H-pyrrolo[2,1-c][1,2,4]triazol-2-ium Tetrafluoroborate 100 and 2-Methoxybenzaldehyde 138

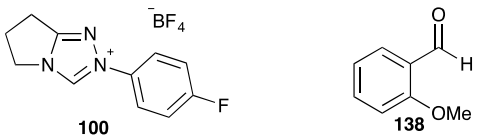

100 **138**

Solutions of *para*-fluorophenyl triazolium salt **100** (0.08 M) and 2-methoxybenzaldehyde **138** (0.08 M) in triethylamine buffered (0.18 M) methanol-d_4 were mixed in an NMR tube to initiate reaction. The reaction was followed in the NMR probe where the temperature was thermostatted at 25 °C. The solution components were analysed by ^{1}H NMR spectroscopy at regular intervals of ~ 5 min, and three representative spectra taken at different time points during the procedure are shown in Figure 3.3.

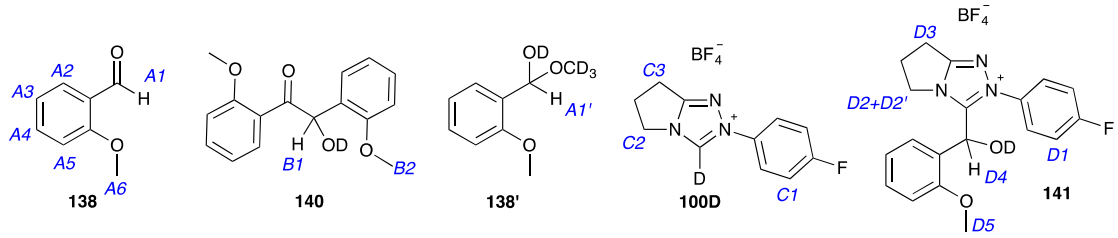

Figure 3.2. Five components involved in the kinetic study of the self-condensation of 2-methoxybenzaldehyde **138** catalysed by N-4-fluorophenyl triazolium precatalyst **100**.

Five main components can be assigned from ^{1}H NMR spectra: 2-methoxybenzaldehyde **138**, benzoin product **140**, hemiacetal **138'**, remaining triazolium salt **100D**, and the

tetrahedral adduct **141** (Figure 3.2). Under our experimental conditions, the absence of any other intermediate apart from the adduct **141** indicated the fast decay of the Breslow intermediate relative to its formation. Although the formation of Breslow intermediate **124** was not observed, the appearance of deuterated adduct **141D** and the deuterated aldehyde **138D** also supports the catalytic cycle of benzoin condensation *via* a Breslow-like intermediate **124** (Scheme 3.8).

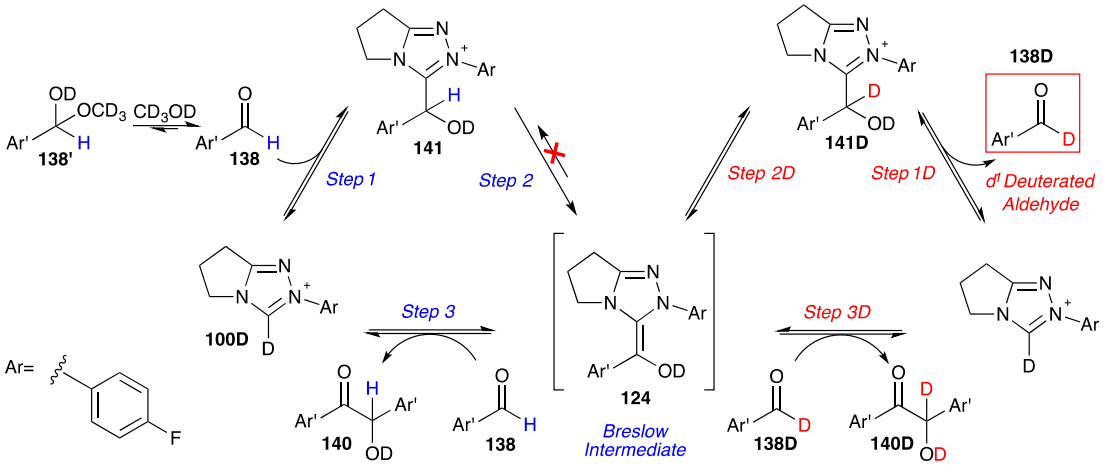

Scheme 3.8. Mechanistic model for the self-condensation of 2-methoxybenzaldehyde **138** catalyzed by 4-fluorophenyl triazolium precatalyst **100D** in d4-methanol solution.

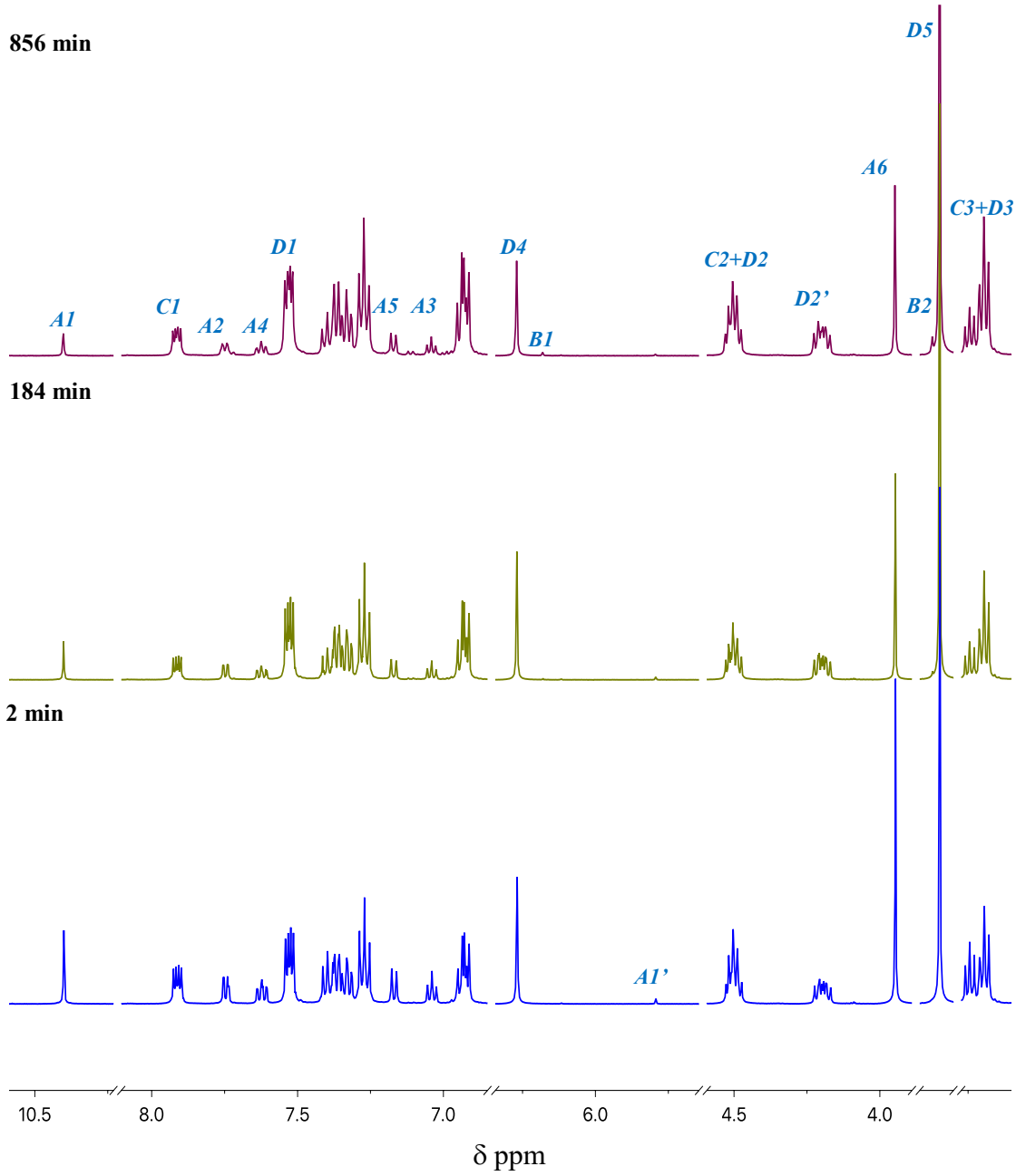

Figure 3.3. Representative ^{1}H NMR spectra at 500 MHz showing progress of the benzoin condensation of 2-methoxybenzaldehyde **138**, catalysed by *para*-fluorophenyl triazolium salt **100**, in triethylamine-buffered methanol-d_4 solution at 25 °C.

In the buffered methanol-d_4 solution, the NCN-H of the precatalyst ion **100** was deuterated rapidly to give the C1-deuterated triazolium **100D**. After the addition of 2-methoxybenzaldehyde **138**, the integration of triazolium precatalyst and aldehyde decreased, and the peak corresponding to adduct **141** (the only observable intermediate) appeared immediately. Currently, no adduct has been directly isolated, and the peak

identification was based on the comparison with related compounds previously studied in our group.

Minimally-overlapped peaks were chosen for integration purposes, and in most cases, a single peak could be utilized with baseline resolution to access the concentration of the relevant species. From the NMR spectra, the multiplet at 7.91 ppm (***C1***), representing two aryl protons was used to calculate the concentration of remaining triazolium precatalyst **100D** (Equation 3.1). In adduct **141**, the ***C1*** signal transformed to a multiplet at 7.52 ppm (***D1***) *in situ*, however, overlapping with peaks due to other aryl protons.

In the triazolium precatalyst, the multiplet signal at 4.50 ppm (***C2***) corresponding to one pair of the CH_2 protons on the five-membered fused ring (adjacent to the N atom), split into two multiplet signals at 4.50 (***D2***) and 4.19 ppm (***D2'***) for the analogous hydrogens of adduct **141**. The 4.19 ppm (***D2'***) peak can be directly used to calculate the adduct concentration (Equation 3.2), while the ***C2*** and ***D2*** peaks overlapped with each other, and circuitously provided the concentration of remaining triazolium salt by Equation 3.3. Moreover, the overlapped signals at 3.24 (***C3***) and 3.19 ppm (***D3***), representing triazolium and adduct respectively, can also be used to calculate triazolium concentration independently (Equation 3.4).

An independent estimate of total adduct concentration could potentially be obtained using the signal at 3.66 ppm (***D5***), which represents the methoxyl protons on the phenyl ring (Equation 3.5). In the case of N-*para*-fluorophenyl triazolium **100** with a five-membered fused ring, this was not possible due to the overlap between methoxyl protons in benzoin at 3.68 ppm (***B2***) and adduct. For the estimation of total adduct concentration, Equation 3.5 can be applied to cases without overlap between benzoin and adduct, or without observable benzoin formation.

$$[\text{catalyst}] = \frac{A_{\text{C1}}/2}{(A_{C2\&D2}+A_{D2\prime})/2} \times 0.08 \qquad \textbf{Equation 3.1}$$

$$[\text{adduct (tot)}] = \frac{A_{\text{D2}\prime}}{(A_{C2\&D2}+A_{D2\prime})/2} \times 0.08 \qquad \textbf{Equation 3.2}$$

$$[\text{catalyst}]' = \frac{(A_{\text{C2\&D2}}-A_{\text{D2}\prime})/2}{(A_{C2\&D2}+A_{D2\prime})/2} \times 0.08 \qquad \textbf{Equation 3.3}$$

$$[\text{catalyst}]'' = \frac{A_{C3\&D3}/2-A_{D2\prime}}{(A_{C2\&D2}+A_{D2\prime})/2} \times 0.08 \qquad \textbf{Equation 3.4}$$

$$[\text{adduct(tot)}]' = \frac{A_{\text{D5}}/3}{(A_{C2\&D2}+A_{D2\prime})/2} \times 0.08 \qquad \textbf{Equation 3.5}$$

The singlet at 6.27 ppm (***D4***) corresponds to the exchangeable tetrahedral proton on the adduct **141**. The concentration of the unexchanged adduct **141** could be determined by utilising this signal (Equation 3.6), and the concentration of deuterated adduct **141D** was obtained from the difference between that of total and non-deuterated adduct species (Equation 3.7).

$$[\text{adduct (H)}] = \frac{A_{\text{D4}}}{(A_{C2\&D2}+A_{D2\prime})/2} \times 0.08 \qquad \textbf{Equation 3.6}$$

$$[\text{adduct (D)}] = [\text{adduct (tot)}] - [\text{adduct(H)}] \qquad \textbf{Equation 3.7}$$

2-Methoxybenzaldehyde **138** exists in an equilibrium with corresponding methanol solvent adduct **138'** (Scheme 3.9). Leeper neglected this solvent adduct, and our previous work used the fraction of aldehyde f_{ald} to rectify the concentration of aldehyde[3, 4].

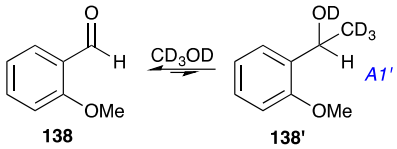

Scheme 3.9. Existing equilibrium between 2-methoxybenzaldehyde **138** and solvent adduct **138**'.

$$f_{ald} = \frac{A_{A1}}{(A_{A1'}+A_{A1})} = \frac{[aldehyde]}{([aldehyde]+[hemiacetal])} \qquad \textbf{Equation 3.8}$$

A singlet signal at 5.79 ppm (***A1'***) corresponding to the benzylic proton of hemiacetal **138'** was observed in the buffered methanol-d_4 solution. From the integrations of the aldehyde (***A1***) and hemiacetal (***A1'***) protons, values for the fraction of the aldehyde present, f_{ald}, can be obtained by Equation 3.8. Richard Massey calculated f_{ald} of 2-methoxybenzaldehyde to be 0.940 by NMR spectroscopy, and the average f_{ald} value obtained within this project was 0.943, which are identical within the experimental error of the method employed. Table 3.1 summarises the five aldehydes' average f_{ald} values determined within this project from the ratio of integrals of aldehyde and hemiacetal protons.

Table 3.1. Fraction of aldehyde f_{ald} calculated for the five aldehydes.

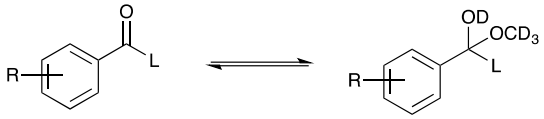

R=	No.[a]	f_{ald} (Ave.)	SD.[b]
2-OMe	31	0.943	0.004
4-OMe	17	0.991	0.003
H	16	0.916	0.002
2-Me	14	0.924	0.001
4-Me	14	0.966	0.001

a. Indicates the number of experiments measured for calculating the average fraction of aldehyde.

b. SD = $\sqrt{\frac{\sum(x-\bar{x})^2}{(n-1)}}$.

The proportional total amount of 2-methoxybenzaldehyde **138** was calculated from the doublet of doublet signal at 7.74 ppm (***A2***), corresponding to the *ortho*-aryl CH proton (Equation 3.9). The doublet of triplet signal at 7.62 ppm (***A4***), doublet signal at 7.17 ppm (***A5***), and triplet signal at 7.04 ppm (***A3***) represent other aryl-protons respectively, and can be used for independent evaluation of concentration. Moreover, the aldehyde concentration can also be obtained independently by using the integration of the singlet signal at 3.94 ppm (***A6***), corresponding to methoxyl protons.

Both of the aryl- and alkyl-signals of benzoin product **140** were overlapped with other components, and integration of total benzoin product was roughly calculated from one of the methoxyl proton signals at 3.68 ppm (***B2***) by Equation 3.12. In the experiment catalysed by N-*para*-fluorophenyl triazolium **100**, the total amount of benzoin product **140** had to be neglected due to the overlap of the methoxyl protons between benzoin and adduct (***B2*** and ***D5***).

Integration of protonated 2-methoxybenzaldehyde **138** was achieved using the signal at 10.40 ppm (***A1***), recognised as the aldehydic hydrogen atom (Equation 3.10). The concentration of protonated benzoin product **140** was obtained from the singlet peak at 6.18 ppm (***B1***), identified as the tetrahedral proton on benzoin (Equation 3.13). Moreover, quantities of deuterated aldehyde **138D** and benzoin product **140D** were determined from the concentration difference between total and protonated components (Equation 3.11 and 3.14).

$$[\text{aldehyde (tot)}] = \frac{1}{f_{\text{ald}}} \times \frac{A_{A2}}{(A_{C2\&D2}+A_{D2\prime})/2} \times 0.08 \qquad \textbf{Equation 3.9}$$

$$[\text{aldehyde (H)}] = \frac{1}{f_{\text{ald}}} \times \frac{A_{\text{A1}}}{(A_{C2\&D2}+A_{D2\prime})/2} \times 0.08 \qquad \textbf{Equation 3.10}$$

$$[\text{aldehyde (D)}] = [\text{aldehyde (tot)}] - [\text{aldehyde(H)}] \qquad \textbf{Equation 3.11}$$

$$[\text{benzoin (tot)}] = \frac{A_{B2}/3}{(A_{C2\&D2}+A_{D2\prime})/2} \times 0.08 \qquad \textbf{Equation 3.12}$$

$$[\text{benzoin (H)}] = \frac{A_{B1}}{(A_{C2\&D2}+A_{D2\prime})/2} \times 0.08 \qquad \textbf{Equation 3.13}$$

$$[\text{benzoin (D)}] = [\text{benzoin (tot)}] - [\text{benzoin (H)}] \qquad \textbf{Equation 3.14}$$

3.4. Concentration Profiles.

As representative examples, concentration profiles for the self-condensation of 2-methoxybenzaldeyde **138** catalysed by *p*-fluorophenyl triazolium **77** (n= 2) are provided (Figure 3.4). Profiles for all other reactions are presented in Appendix.

Figure 3.4. Concentration profile for the self-condensation of 2-methoxybenzaldehyde **138** (0.08 M), catalysed by *para*-fluorophenyl triazolium precatalyst **77** (n= 2, 0.08 M), in 0.107 M NEt_3 and 0.053 M NEt_3·HCl in methanol-d_4.

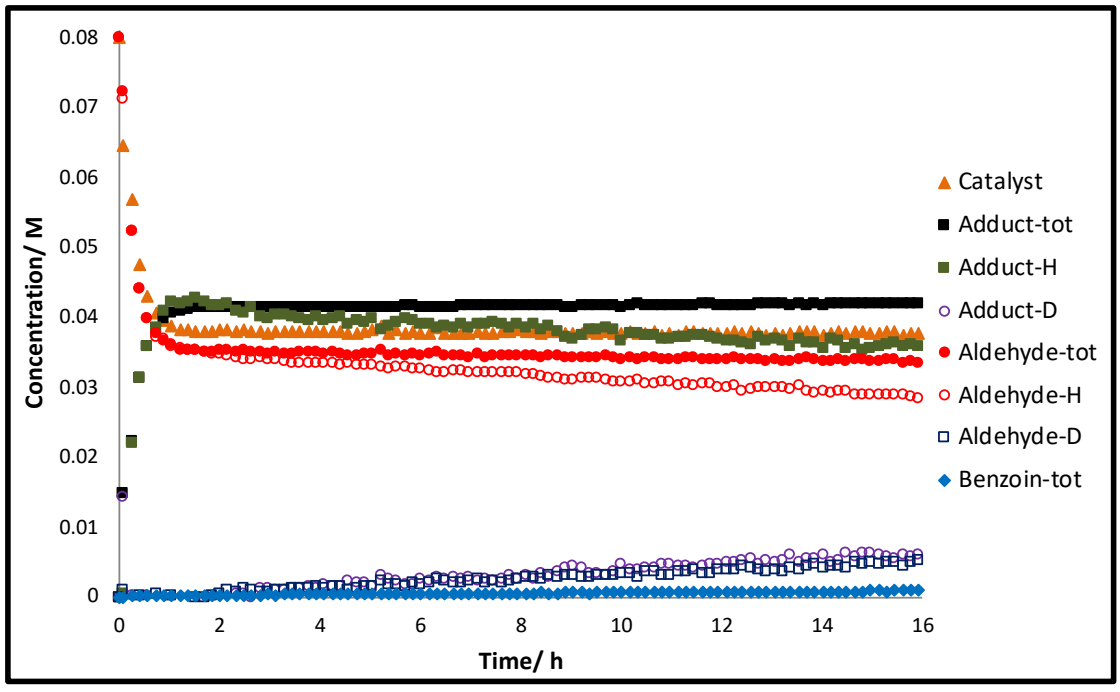

For most of the reactions, a stock solution of triazolium salt was used to control the concentration of catalyst. Meanwhile, the preparation of aldehyde stock solutions with degassed methanol-d_4 in a glove box suggested the formation of non-identified by-product, which was generated only by methanol and aldehyde. Therefore, the aldehydes were measured by a Hamilton syringe and added into the methanol-d_4 solution with triazolium salts and triethylamine buffer directly. Fortunately, during our kinetic experiments, the formation rate of this by-product was relatively small compared to the rate of reaction between aldehyde and triazolium[I], therefore is negligible. In addition, oxidation of aldehyde was also initially detected on occasion, however could be carefully suppressed through preparation of solutions under an inert atmosphere.

As explained above, stock solutions of aldehydes cannot be prepared in advance due to the formation of the non-identified by-product, and the usage of a Hamilton syringe to measure aldehyde may lead to a concentration deviation[II]. The aldehyde concentration variability of up to ± 10% could potentially contribute up to 27.5% error in calculation of reaction parameters. Moreover, the NMR probed kinetic experiments were also restricted by the solubility of triazolium salt. For example, only 0.06 M of 4-methoxyphenyl triazolium **91** (n= 3) and aldehyde were used due to the low solubility of the former, which enlarged the analytical and experimental error percentage by using the traditional calculation method introduced in the following section (Section 2.5.2).

[I] Generally, the formation of the by-product cannot be observed after a few hours, with the exception of reactions with benzaldehyde, for which the by-product's formation is quicker but still after the pre-equilibrium state.

[II] According to the guide (https://www.hamiltoncompany.com/laboratory-products/syringes#support), "Hamilton syringes are manufactured to be accurate within ±1% of nominal volume, and with precision within 1%, measured at 80% of total scale volume". However, due to the large surface tension and viscosity of aldehydes, up to ± 10% error should be expected.

3.5. Determination of Rate Constants for Adduct Formation and Dissociation

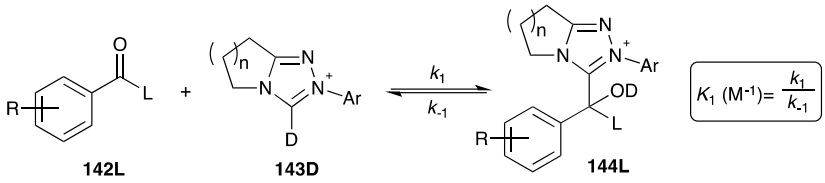

Scheme 3.10. Equilibrium for the formation of adduct **144L** from arylaldehyde **142L** and NHC precatalyst **143D**[I].

Before significant benzoin product formation (< 10%), the combination of aldehyde **142L** and triazolium precatalyst **143D** towards adduct **144L** can be considered as pseudo second order, and Scheme 3.10 can be applied to achieve the rate constant k_1 (M^{-1} s^{-1}). The rate expression of the reaction is provided in Equation 3.15.

$$\frac{d[\text{cat}]}{dt} = -k_1[\text{cat}][\text{ald}] + k_{-1}[\text{add}] \qquad \textbf{Equation 3.15}$$

This project applies two integration equations and Berkeley Madonna, the global fitting software, to determine the adduct formation reaction parameters. The traditional calculation method (Section 3.5.1) used in previous joint work from the O'Donoghue and Smith groups assumed the initial concentration of catalyst and aldehyde to be the same, which simplified the calculation, however, restricts the reaction conditions (*e.g.* catalyst and aldehyde concentrations)[4]. This project then applied the second integration equation (Section 3.5.2), which gave better correlation with the results obtained *via* global fitting software (Section 3.5.3). The summary of reaction parameters is in Section

[I] In this Chapter, the letter "L" included in all compound structures and their numbers indicates this position could either be a proton or a deuterium.

3.5.4.

3.5.1. Previous Calculation Equation

Previously, by assuming the concentration of aldehyde equals to catalyst, the adduct formation rate constant k_1 (M^{-1} s^{-1}) can be calculated *via* a simplified Equation 3.16, where subscript '$_e$' represents the equilibrated concentration.

$$\frac{d[\mathrm{cat}]}{dt} = -k_1[\mathrm{cat}]^2 + k_1 \frac{[\mathrm{cat}]_e^2}{([\mathrm{cat}]_0 - [\mathrm{cat}]_e)}([\mathrm{cat}]_0 - [\mathrm{cat}]) \qquad \textbf{Equation 3.16}$$

By setting $[\mathrm{cat}]_0 = [\mathrm{ald}]_0 = b$, $y = ([\mathrm{cat}]_0 - [\mathrm{cat}]) = ([\mathrm{ald}]_0 - [\mathrm{ald}])$ and $y_e = ([\mathrm{cat}]_0 - [\mathrm{cat}]_e) = ([\mathrm{ald}]_0 - [\mathrm{ald}]_e)$, the k_1 value can be expressed as the slope of a semilogarithmic plot of $(y_e(b^2 - yy_e)/(b^2(y_e - y))$ against time (Equation 3.17), where 'b' equals the initial concentration of catalyst and aldehyde. A detailed proof is included in Appendix.

$$\frac{y_e}{(b^2 - y_e^2)} \ln \frac{y_e(b^2 - yy_e)}{b^2(y_e - y)} = k_1 t \qquad \textbf{Equation 3.17}$$

The equilibrium constant K (M^{-1}) can be estimated from the concentration profile by Equation 3.18, and k_{-1} (s^{-1}), representing the dissociation rate constant of adduct, could be evaluated using values for K and k_1 (Equation 3.19).

$$K = \frac{[\mathrm{add\ (tot)}]_e}{[\mathrm{cat}]_e^{\ 2}} \qquad \textbf{Equation 3.18}$$

$$k_{-1} = k_1/K \qquad \textbf{Equation 3.19}$$

3.5.2. New k_1, k_{-1} and K Calculation Method

Due to the relatively large potential errors the old calculation method might introduce if

the initial concentrations of catalyst and aldehyde are different (Section 2.5.1), another new method was also applied to obtain the reaction parameters. Within this method, the equilibrium constant of adduct formation, K (M^{-1}), was obtained by Equation 3.20. Meanwhile, differing from the previous methodology, the aldehyde concentration is no longer assumed to be the same as catalyst concentration to give the simplified rate expression (Equation 3.16). The current aldehyde concentration can be expressed by Equation 3.21. The introduction of aldehyde initial concentration $[ald]_0$ removes the impact of concentration deviation imposed by aldehyde measurement. Equation 3.15 can then be integrated with the application of Equation 3.21-2.23.

$$K = \frac{[\text{add (tot)}]_e}{[\text{cat}]_e \times [\text{ald (tot)}]_e} \quad \textbf{Equation 3.20}$$

$$\frac{d[\text{cat}]}{dt} = -k_1[\text{cat}][\text{ald}] + k_{-1}[\text{add}] \quad \textbf{Equation 3.15}$$

$$[\text{ald}] = [\text{ald}]_0 - ([\text{cat}]_0 - [\text{cat}]) \quad \textbf{Equation 3.21}$$

$$[\text{add}] = [\text{cat}]_0 - [\text{cat}] \quad \textbf{Equation 3.22}$$

$$k_{-1} = \frac{k_1}{K} \quad \textbf{Equation 3.23}$$

To simplify the equations, the initial concentration of catalyst, $[cat]_0$, was set to x_0, the initial concentration of aldehyde, $[ald]_0$, to y_0, current concentration of catalyst, [cat], to x. Equation 3.15 can then be rewritten into Equation 3.24, and the k_1 can be obtained as the slope of the function of x against time (Equation 3.25). By replacing catalyst concentration for aldehyde (or *vice versa*), a similar equation can be applied to obtain the k_1 value as the slope of the function of y against time.

$$\frac{dx}{dt} = -k_1 x(y_0 - x_0 + x) + \frac{k_1}{K}(x_0 - x) \qquad \textbf{Equation 3.24}$$

$$k_1 \mathrm{t} = \frac{1}{\sqrt{(y_0 - x_0 + \frac{1}{K})^2 + \frac{4x_0}{K}}} \left| \ln\left(\frac{x - x_1}{x - x_2}\right) \right|_{x_0}^{x}, \text{ where}$$

$$x_1 = \frac{-(y_0 - x_0 + \frac{1}{K}) + \sqrt{(y_0 - x_0 + \frac{1}{K})^2 + \frac{4x_0}{K}}}{2},$$

$$x_2 = \frac{-\left(y_0 - x_0 + \frac{1}{K}\right) - \sqrt{(y_0 - x_0 + \frac{1}{K})^2 + \frac{4x_0}{K}}}{2} \qquad \textbf{Equation 3.25}$$

The concentration of adduct can also be applied for calculation of k_1. By setting the current concentration of adduct to z, Equation 3.15 can be rewritten into Equation 3.26, and the k_1 can be obtained as the slope of the function of z against time (Equation 3.27).

$$-\frac{dz}{dt} = -k_1(x_0 - z)(y_0 - z) + \frac{k_1}{K} z \qquad \textbf{Equation 3.26}$$

$$k_1 \mathrm{t} = \frac{1}{\sqrt{(x_0 + y_0 + \frac{1}{K})^2 - 4x_0 y_0}} \left| \ln\left(\frac{z - z_1}{z - z_2}\right) \right|_{0}^{z}, \text{ where}$$

$$z_1 = \frac{(x_0 + y_0 + \frac{1}{K}) + \sqrt{(x_0 + y_0 + \frac{1}{K})^2 - 4x_0 y_0}}{2},$$

$$z_2 = \frac{\left(x_0 + y_0 + \frac{1}{K}\right) - \sqrt{(x_0 + y_0 + \frac{1}{K})^2 - 4x_0 y_0}}{2} \qquad \textbf{Equation 3.27}$$

Moreover, a similar method can be used to calculate k_{-1}. Equation 3.15 can be rewritten into Equation 3.28, and k_{-1} can be obtained as the slope of function of z against time (Equation 3.29). The entire proofs of Equation 3.25, 3.27 and 3.29 are included in Appendix.

$$-\frac{dz}{dt} = -Kk_{-1}(x_0 - z)(y_0 - z) + k_{-1} z \qquad \textbf{Equation 3.28}$$

$$k_{-1}\mathrm{t} = \frac{1}{K\sqrt{(x_0+y_0+\frac{1}{K})^2-4x_0y_0}}\left|\ln\left(\frac{z-z_1}{z-z_2}\right)\right|_0^z, \text{ where}$$

$$z_1 = \frac{(x_0+y_0+\frac{1}{K})+\sqrt{(x_0+y_0+\frac{1}{K})^2-4x_0y_0}}{2},$$

$$z_2 = \frac{\left(x_0+y_0+\frac{1}{K}\right)-\sqrt{(x_0+y_0+\frac{1}{K})^2-4x_0y_0}}{2} \qquad \textbf{Equation 3.29}$$

In a few cases, as a result of unavoidable NMR peak overlap, the calculated adduct formation constant, k_1, could carry a degree of imprecision. By comparing the three individual k_1 values obtained from the concentrations of aldehyde, catalyst, and adduct, respectively, the most reasonable values[I] would be selected as the final result.

3.5.3. Global Fitting Software: Berkeley Madonna

Based on the concentration profile obtained *via* ^{1}H NMR spectroscopy, Global fitting software Berkeley Madonna was used to fit the data and suggest reaction parameters as a parallel method. A simplified reaction model was applied for data fitting (Scheme 3.11). As the concentration of deuterated adduct **144D**, aldehyde **142D** and benzoin **140D** in Scheme 3.11 are relatively small compared with the spectrum analysing errors, this model only accounts for the total concentration of triazolium **143D**, adduct **144L**, aldehyde **142L**, and benzoin **140L**, which include both deuterated and protonated components. This simplified model only included components whose concentrations over time may be analysed by NMR. The benzoin formation process actually combines the deprotonation of adduct, the attachment of the second aldehyde, and the dissociation between benzoin and triazolium. Among these processes, the reaction parameters of

[I] "Most reasonable values" means the value was obtained by the concentrations of substrates calculated from the least overlapped NMR peaks, or, in case of the *para*-methoxybenzaldehyde **139** catalysed by triazolium salt **80** and **91**, the most similar results as all peaks overlapped.

each individual steps cannot be obtained from both the concentration profile or the global fitting software, and the retro-benzoin was also dismissed because of the small reaction rate.

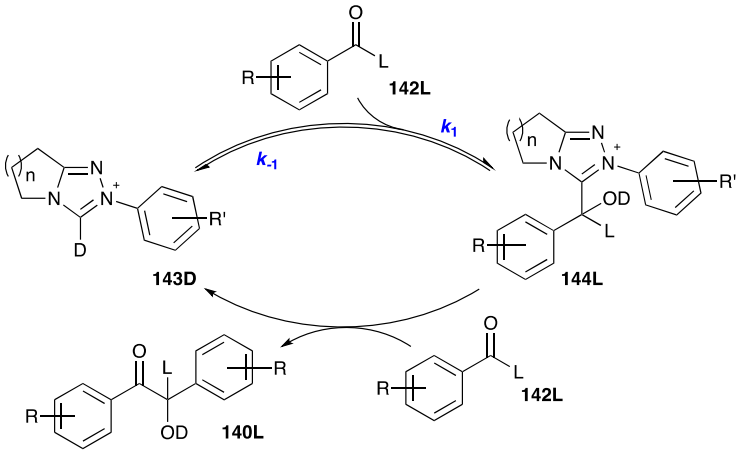

Scheme 3.11. Simplified model of benzoin condensation used for data fitting

As a representative example, the data fitting based on the concentration profile for the self-condensation of 2-methoxybenzaldehyde **138** catalysed by 4-fluorophenyl triazolium **77** (n=2) are provided (Figure 3.5). Profiles for all other reactions are presented in Appendix.

Figure 3.5. Global fitting profile for the self-condensation of 2-methoxybenzaldehyde **138** (0.08 M), catalysed by *para*-fluorophenyl triazolium precatalyst **77** (n= 2, 0.08 M), in 0.107 M NEt_3 and 0.053 M NEt_3·HCl in methanol-d_4.

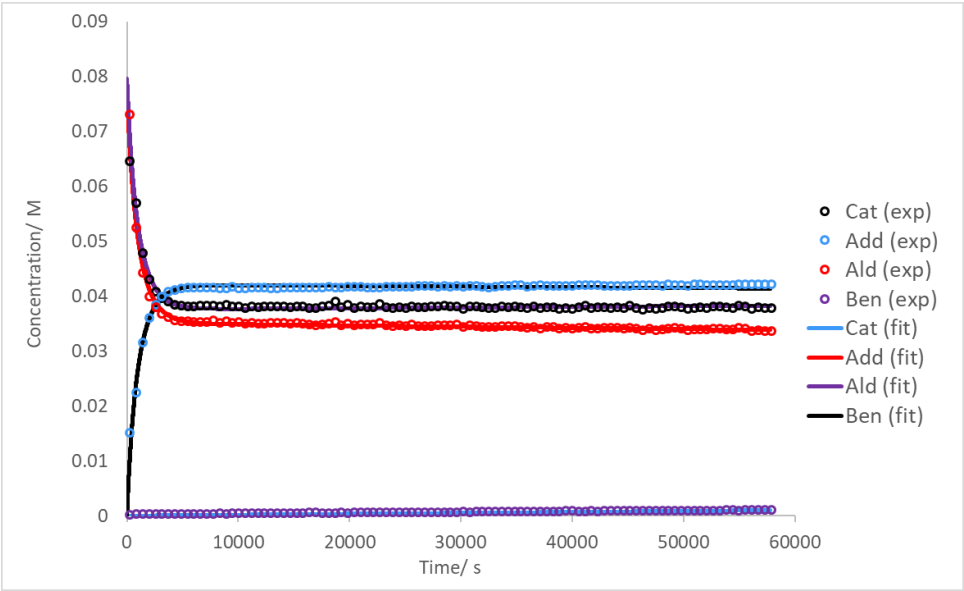

3.5.4. Summary of the Kinetic Parameters

Table 3.3-3.7 summarises the kinetic parameters obtained among triazolium **77-80**, **89-91**, **100, 101** and aldehydes **135-139** by using three methods introduced above. Reaction parameters of benzaldehyde **135** and 4-methoxybenzaldehyde **139** catalysed by all three triazolium salts **89, 100,** and **101** (n= 1) were obtained by another PhD student, Peter Quinn (PQ), in our research group. Table 3.2 summarises Peter's reaction parameters obtained *via* global fitting software Berkeley Madonna.

Table 3.2. Summary of Peter Quinn's reaction parameters obtained from global fitting software for the self-condensation of one equivalent of aldehyde **135**, **139**, in the presence of stoichiometric triazolium precatalyst **89**, **100**, and **101** (0.08 M), in 0.107 M NEt_3 and 0.053 M NEt_3·HCl in methanol-d_4 at 25 °C.

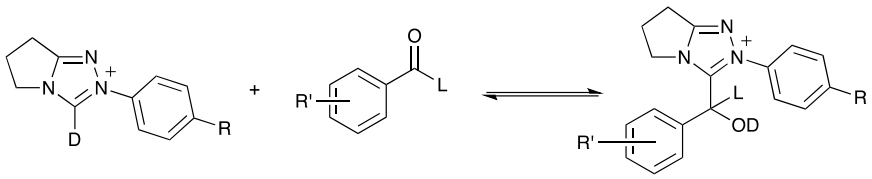

R=	R'=	k_1 ($M^{-1}s^{-1}$)	k_{-1} (s^{-1})	K (M^{-1})
H		9.86×10^{-3}	7.30×10^{-4}	1.35×10^{1}
F	H	2.92×10^{-2}	1.62×10^{-3}	1.80×10^{1}
OMe		9.53×10^{-3}	3.79×10^{-4}	2.51×10^{1}
H		1.80×10^{-3}	7.56×10^{-4}	2.38×10^{0}
F	4-OMe	5.10×10^{-3}	1.72×10^{-3}	2.97×10^{0}
OMe		1.85×10^{-3}	5.37×10^{-4}	3.45×10^{0}
H		2.11×10^{-2}	1.44×10^{-4}	1.47×10^{2}
F	2-OMe	5.15×10^{-2}	2.23×10^{-4}	2.31×10^{2}
OMe		1.46×10^{-2}	6.61×10^{-5}	2.21×10^{2}

In Table 3.5, adduct association (k_1) and dissociation constants (k_{-1}) of 4-methoxybenzaldehyde **139** catalysed by phenyl triazolium **79, 80** (n= 2, 3), 4-fluorophenyl (n= 3), and 4-methoxyphenyl (n= 3) triazolium **78, 91** could not be obtained due to the low conversion of adduct, and the limited data points collected within

pre-equilibrium state.

Table 3.3. Summary of reaction parameters and reagent concentrations for the self-condensation of 2-methoxybenzaldehyde **138**, in the presence of triazolium precatalyst **77-80**, **89-91**, **100, 101**, in 0.108 M NEt_3 and 0.053 M NEt_3·HCl in methanol-d_4 at 25 °C.

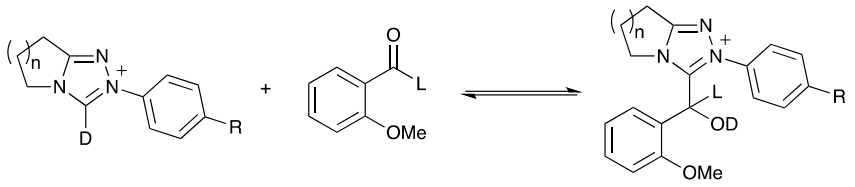

R=	n=	$[Cat]_0$	$[Ald]_0$	Method	k_1 ($M^{-1}s^{-1}$)	k_{-1} (s^{-1})	K (M^{-1})
H	1	0.079 M	0.079 M	*Old*	2.44×10^{-2}	1.78×10^{-4}	1.35×10^{2}
				New	2.02×10^{-2}	1.48×10^{-4}	1.36×10^{2}
				Fitting	2.07×10^{-2}	1.43×10^{-4}	1.45×10^{2}
	2	0.080 M	0.080 M	*Old*	3.23×10^{-3}	1.57×10^{-4}	2.06×10^{1}
				New	3.08×10^{-3}	1.49×10^{-4}	2.06×10^{1}
				Fitting	3.14×10^{-3}	1.48×10^{-4}	2.12×10^{1}
	3	0.080 M	0.081 M	*Old*	3.43×10^{-3}	4.25×10^{-4}	8.07×10^{0}
				New	3.54×10^{-3}	4.47×10^{-4}	7.92×10^{0}
				Fitting	4.43×10^{-3}	5.59×10^{-4}	7.93×10^{0}
F	1	*N.D.*[a]					
	2	0.080 M	0.077 M	*Old*	1.01×10^{-2}	3.77×10^{-4}	2.69×10^{1}
				New	8.09×10^{-3}	2.79×10^{-4}	2.90×10^{1}
				Fitting	7.81×10^{-3}	2.44×10^{-4}	3.20×10^{1}
	3	0.080 M	0.081 M	*Old*	4.96×10^{-3}	5.42×10^{-4}	9.44×10^{0}
				New	5.28×10^{-3}	5.77×10^{-4}	9.15×10^{0}
				Fitting	5.14×10^{-3}	5.53×10^{-4}	9.29×10^{0}
OMe	1	0.080 M	0.080 M	*Old*	1.41×10^{-2}	6.67×10^{-5}	2.11×10^{2}
				New	1.41×10^{-2}	6.72×10^{-5}	2.10×10^{2}
				Fitting	1.35×10^{-2}	6.03×10^{-5}	2.24×10^{2}
	2	0.039 M	0.038 M	*Old*	2.34×10^{-3}	6.43×10^{-5}	3.64×10^{1}
				New	2.32×10^{-3}	6.18×10^{-5}	3.75×10^{1}
				Fitting	2.40×10^{-3}	6.28×10^{-5}	3.82×10^{1}
	3	0.060 M	0.062 M	*Old*	2.35×10^{-3}	1.83×10^{-4}	1.28×10^{1}
				New	2.16×10^{-3}	1.76×10^{-4}	1.23×10^{1}
				Fitting	2.21×10^{-3}	1.78×10^{-4}	1.24×10^{1}

[a] This experiment was not performed by the present author.

Table 3.4. Summary of reaction parameters and reagent concentrations for the self-condensation of benzaldehyde **135**, in the presence of triazolium precatalyst **77-80**, **89-91**, **100, 101**, in 0.108 M NEt_3 and 0.053 M $NEt_3 \cdot HCl$ in methanol-d_4 at 25 °C.

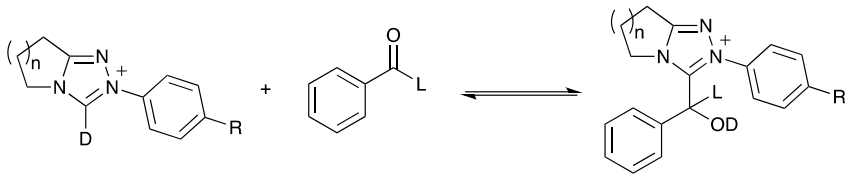

R=	n=	$[Cat]_0$	$[Ald]_0$	Method	k_1 ($M^{-1}s^{-1}$)	k_{-1} (s^{-1})	K (M^{-1})
H	1	*N.D.*[a]					
	2	0.081 M	0.080 M	*Old*	1.68×10^{-3}	1.15×10^{-4}	1.46×10^{0}
				New	1.55×10^{-3}	1.06×10^{-3}	1.46×10^{0}
				Fitting	1.30×10^{-3}	8.15×10^{-4}	1.59×10^{0}
	3	0.080 M	0.071 M	*Old*	1.21×10^{-3}	2.88×10^{-4}	4.21×10^{-1}
				New	1.21×10^{-3}	2.53×10^{-4}	4.79×10^{-1}
				Fitting	1.18×10^{-3}	2.39×10^{-4}	4.94×10^{-1}
F	1	*N.D.*[a]					
	2	0.080 M	0.068 M	*Old*	2.93×10^{-3}	1.80×10^{-3}	1.63×10^{0}
				New	3.40×10^{-3}	1.76×10^{-3}	1.93×10^{0}
				Fitting	3.70×10^{-3}	1.81×10^{-3}	2.05×10^{0}
	3	0.080 M	0.069 M	*Old*	1.49×10^{-3}	3.41×10^{-3}	4.36×10^{-1}
				New	1.28×10^{-3}	2.56×10^{-3}	5.00×10^{-1}
				Fitting	1.27×10^{-3}	2.46×10^{-3}	5.16×10^{-1}
OMe	1	*N.D.*[a]					
	2	0.040 M	0.063 M	*Old*	2.04×10^{-3}	4.24×10^{-4}	4.81×10^{0}
				New	1.26×10^{-3}	4.36×10^{-4}	2.88×10^{0}
				Fitting	1.28×10^{-3}	4.34×10^{-4}	2.95×10^{0}
	3	0.060 M	0.053 M	*Old*	7.56×10^{-4}	1.00×10^{-3}	7.54×10^{-1}
				New	6.83×10^{-4}	7.80×10^{-4}	8.76×10^{-1}
				Fitting	6.74×10^{-4}	7.22×10^{-4}	9.32×10^{-1}

[a] This experiment was not performed by the present author.

Table 3.5. Summary of reaction parameters and reagent concentrations for the self-condensation of 4-methoxybenzaldehyde **139**, in the presence of triazolium precatalyst **77-80**, **89-91**, **100, 101**, in 0.108 M NEt_3 and 0.053 M NEt_3·HCl in methanol-d_4 at 25 °C.

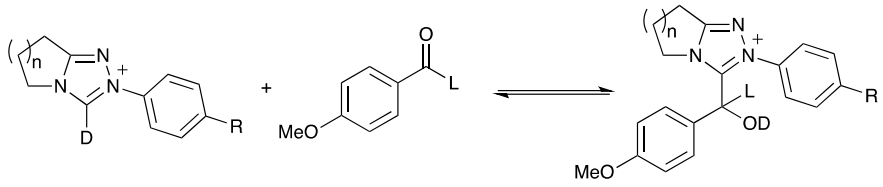

R=	n=	$[Cat]_0$	$[Ald]_0$	Method	k_1 ($M^{-1}s^{-1}$)	k_{-1} (s^{-1})	K (M^{-1})
H	1				*N.D.*[a]		
	2	0.080 M	0.082 M	*Old*	*N.D.*[b]	*N.D.*[b]	2.13×10^{-1}
				New	*N.D.*[b]	*N.D.*[b]	2.08×10^{-1}
				Fitting	*N.D.*[b]	*N.D.*[b]	*N.D.*[b]
	3	0.080 M	0.082 M	*Old*	*N.D.*[b]	*N.D.*[b]	6.78×10^{-2}
				New	*N.D.*[b]	*N.D.*[b]	6.64×10^{-2}
				Fitting	*N.D.*[b]	*N.D.*[b]	*N.D.*[b]
F	1				*N.D.*[a]		
	2	0.077 M	0.073 M	*Old*	2.77×10^{-3}	3.77×10^{-4}	2.69×10^{-1}
				New	1.73×10^{-3}	3.94×10^{-3}	4.40×10^{-1}
				Fitting	2.77×10^{-3}	6.34×10^{-3}	4.37×10^{-1}
	3	0.059 M	0.067 M	*Old*	*N.D.*[b]	*N.D.*[b]	1.00×10^{-1}
				New	*N.D.*[b]	*N.D.*[b]	1.06×10^{-1}
				Fitting	*N.D.*[b]	*N.D.*[b]	*N.D.*[b]
OMe	1				*N.D.*[a]		
	2	0.040 M	0.093 M	*Old*	6.37×10^{-4}	7.30×10^{-4}	8.73×10^{-1}
				New	2.17×10^{-4}	5.84×10^{-4}	3.72×10^{-1}
				Fitting	2.35×10^{-4}	6.20×10^{-4}	3.79×10^{-1}
	3	0.060 M	0.060 M	*Old*	*N.D.*[b]	*N.D.*[b]	6.71×10^{-3}
				New	*N.D.*[b]	*N.D.*[b]	6.40×10^{-3}
				Fitting	*N.D.*[b]	*N.D.*[b]	*N.D.*[b]

[a] This experiment was not performed by the present author.

[b] This reaction parameter could not be obtained owing to the limited data points obtained during the pre-equilibrium state.

Table 3.6. Summary of reaction parameters and reagent concentrations for the self-condensation of 2-methylbenzaldehyde **136**, in the presence of triazolium precatalyst **77-80**, **89-91**, **100, 101**, in 0.108 M NEt_3 and 0.053 M NEt_3·HCl in methanol-d_4 at 25 °C.

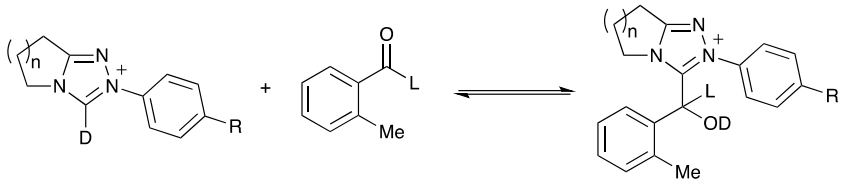

R=	n=	$[Cat]_0$	$[Ald]_0$	Method	k_1 ($M^{-1}s^{-1}$)	k_{-1} (s^{-1})	K (M^{-1})
H	1	0.080 M	0.077 M	*Old*	1.18×10^{-2}	7.91×10^{-4}	1.50×10^{1}
				New	1.14×10^{-2}	7.33×10^{-4}	1.56×10^{1}
				Fitting	1.15×10^{-2}	6.77×10^{-4}	1.69×10^{1}
	2	0.080 M	0.079 M	*Old*	2.16×10^{-3}	1.79×10^{-3}	1.21×10^{0}
				New	1.97×10^{-3}	1.61×10^{-3}	1.22×10^{0}
				Fitting	2.00×10^{-3}	1.57×10^{-3}	1.27×10^{0}
	3	0.080 M	0.074 M	*Old*	6.57×10^{-4}	2.53×10^{-3}	2.59×10^{-1}
				New	6.26×10^{-4}	2.30×10^{-3}	2.86×10^{-1}
				Fitting	6.30×10^{-4}	2.20×10^{-3}	2.86×10^{-1}
F	1	0.080 M	0.076 M	*Old*	2.31×10^{-2}	1.14×10^{-3}	2.03×10^{1}
				New	2.14×10^{-2}	1.01×10^{-3}	2.12×10^{1}
				Fitting	2.24×10^{-2}	9.74×10^{-4}	2.30×10^{1}
	2	0.080 M	0.076 M	*Old*	2.49×10^{-3}	1.25×10^{-3}	1.99×10^{0}
				New	2.64×10^{-3}	1.25×10^{-3}	2.12×10^{0}
				Fitting	3.20×10^{-3}	1.58×10^{-3}	2.03×10^{0}
	3	0.078 M	0.077 M	*Old*	5.12×10^{-4}	1.42×10^{-3}	3.60×10^{-1}
				New	1.06×10^{-3}	2.90×10^{-3}	3.67×10^{-1}
				Fitting	1.02×10^{-3}	2.79×10^{-3}	3.66×10^{-1}
OMe	1	0.080 M	0.122 M	*Old*	1.03×10^{-2}	2.70×10^{-4}	3.82×10^{1}
				New	5.45×10^{-3}	3.16×10^{-4}	1.72×10^{1}
				Fitting	5.45×10^{-3}	2.78×10^{-4}	1.96×10^{1}
	2	0.040 M	0.036 M	*Old*	1.14×10^{-3}	6.23×10^{-4}	1.83×10^{0}
				New	1.37×10^{-3}	6.72×10^{-4}	2.03×10^{0}
				Fitting	1.27×10^{-3}	6.33×10^{-4}	2.01×10^{0}
	3	0.060 M	0.082 M	*Old*	3.46×10^{-4}	5.36×10^{-4}	6.46×10^{-1}
				New	4.92×10^{-4}	1.05×10^{-3}	4.68×10^{-1}
				Fitting	4.91×10^{-4}	9.85×10^{-4}	4.98×10^{-1}

Table 3.7. Summary of reaction parameters and reagent concentrations for the self-condensation of 4-methylbenzaldehyde **137**, in the presence of triazolium precatalyst **77-80**, **89-91**, **100, 101**, in 0.108 M NEt_3 and 0.053 M NEt_3·HCl in methanol-d_4 at 25 °C.

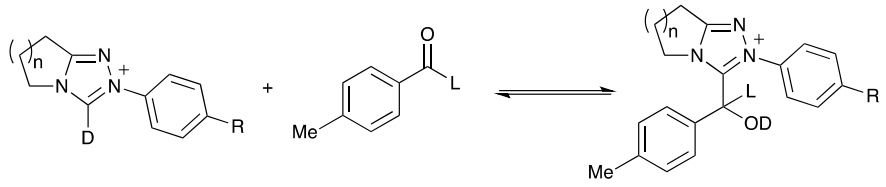

R=	n=	$[Cat]_0$	$[Ald]_0$	Method	k_1 ($M^{-1}s^{-1}$)	k_{-1} (s^{-1})	K (M^{-1})
H	1	0.080 M	0.092 M	*Old*	8.91×10^{-3}	1.05×10^{-3}	8.48×10^{0}
				New	6.92×10^{-3}	9.70×10^{-4}	7.13×10^{0}
				Fitting	7.34×10^{-3}	9.82×10^{-4}	7.48×10^{0}
	2	0.080 M	0.081 M	*Old*	1.02×10^{-3}	1.15×10^{-3}	8.86×10^{-1}
				New	1.04×10^{-3}	1.20×10^{-3}	8.73×10^{-1}
				Fitting	1.24×10^{-3}	1.44×10^{-3}	8.61×10^{-1}
	3	0.080 M	0.073 M	*Old*	7.05×10^{-4}	2.96×10^{-3}	2.38×10^{-1}
				New	6.96×10^{-4}	2.66×10^{-3}	2.65×10^{-1}
				Fitting	6.79×10^{-4}	2.55×10^{-3}	2.66×10^{-1}
F	1	0.080 M	0.081 M	*Old*	1.32×10^{-2}	1.42×10^{-3}	9.25×10^{0}
				New	1.05×10^{-2}	1.11×10^{-3}	9.43×10^{0}
				Fitting	1.09×10^{-2}	1.08×10^{-3}	1.00×10^{1}
	2	0.080 M	0.076 M	*Old*	1.51×10^{-3}	1.56×10^{-3}	9.65×10^{-1}
				New	1.17×10^{-3}	2.11×10^{-3}	1.03×10^{0}
				Fitting	2.19×10^{-3}	2.10×10^{-3}	1.04×10^{0}
	3	0.077 M	0.077 M	*Old*	1.49×10^{-4}	4.90×10^{-3}	3.04×10^{-1}
				New	1.17×10^{-3}	3.85×10^{-3}	3.04×10^{-1}
				Fitting	6.09×10^{-4}	2.01×10^{-3}	3.03×10^{-1}
OMe	1	0.080 M	0.110 M	*Old*	3.18×10^{-3}	3.53×10^{-4}	1.37×10^{1}
				New	3.05×10^{-3}	3.56×10^{-4}	8.56×10^{0}
				Fitting	3.18×10^{-3}	3.56×10^{-4}	8.93×10^{0}
	2	0.040 M	0.041 M	*Old*	1.14×10^{-3}	6.23×10^{-4}	1.83×10^{0}
				New	1.37×10^{-3}	6.72×10^{-4}	2.03×10^{0}
				Fitting	7.66×10^{-4}	5.21×10^{-4}	1.47×10^{0}
	3	0.060 M	0.082 M	*Old*	9.78×10^{-5}	1.80×10^{-4}	5.42×10^{-1}
				New	1.06×10^{-4}	2.76×10^{-4}	3.83×10^{-1}
				Fitting	1.14×10^{-4}	2.44×10^{-4}	4.66×10^{-1}

Comparing the data obtained *via* three different methods, they all gave comparable

values of reaction parameters in most of the cases, with differences smaller than 25%. However, the traditional calculation method using Equation 3.17 gives a poorer correlation with the data obtained by the other two, especially for cases with an unavoidable larger difference between aldehyde and catalyst initial concentrations (*e.g.* Table 3.6, R= OMe, n= 1). The new calculation method using Equation 3.25, 3.27, and 2.29 is more suitable for calculating k_1, and gave more comparable results with fitted data compared with the values obtained from old method. Comparing the reaction parameters measured by Peter Quinn and author, the results of 2-methoxybenzaldehyde **138** catalysed by 5-membered phenyl and 4-methoxyphenyl triazolium salts **101**, **89** correlate well with each other, which suggest the measurement and calculation are reproducible (Table 3.2, R= H and OMe, R'= 2-OMe; and Table 3.3, n= 1, R= H and OMe).

3.5.5. Pre-equilibrium Study

Limited by the NMR parameters used (transient number = 32, acquisition time = 2s, relaxation delay = 5s), the time interval between two NMR spectra was set to 224 seconds. For certain reactants under these conditions, only very few spectra could be taken within the pre-equilibrium state, and limited data points can be used for k_1 calculation, thus, larger errors of rate constants would be expected. This problem can be solved by changing the transient number from 32 to 8 to decrease the time interval between two NMR spectra to 56 seconds, and quadrupled the data points obtained during the pre-equilibrium state.

The concentration profiles of the *ortho*-methylbenzaldehyde **137** catalysed by 4-fluorophenyl triazolium salt **78** (n= 3) are present below. Figure 3.6 is obtained from the experiment with the transient number, nt = 32, while nt= 8 data is shown in Figure 3.7. Both of the timescales of the profiles were 2.5 hours, and these two profiles clearly

suggest the difference of the data quantity with different transient number, and the shift of the end point of the pre-equilibrium state. The fluctuation of the aldehyde concentration was caused by the NMR peak overlap.

Figure 3.6. Concentration profiles for the self-condensation of 2-methylbenzaldehyde **137** catalysed by 4-fluorophenyl triazolium **78** (n= 3), in 0.107 M NEt_3 and 0.053 M NEt_3·HCl in methanol-d_4, with transient number set to be 32.

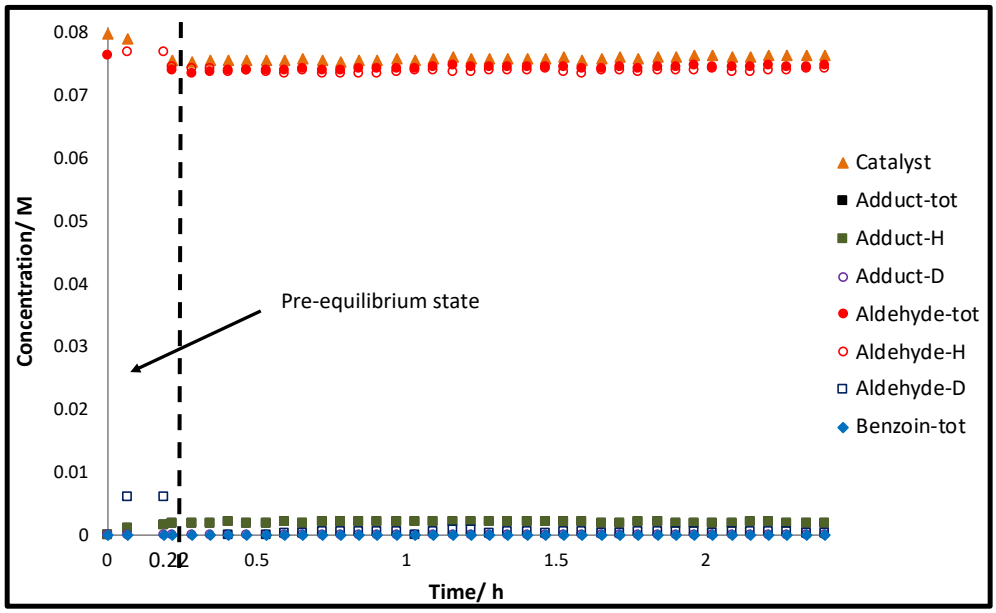

Figure 3.7. Concentration profiles for the self-condensation of 2-methylbenzaldehyde **137** catalysed by 4-fluorophenyl triazolium **78** (n= 3), in 0.107 M NEt_3 and 0.053 M NEt_3·HCl in methanol-d_4, with transient number set to be 8.

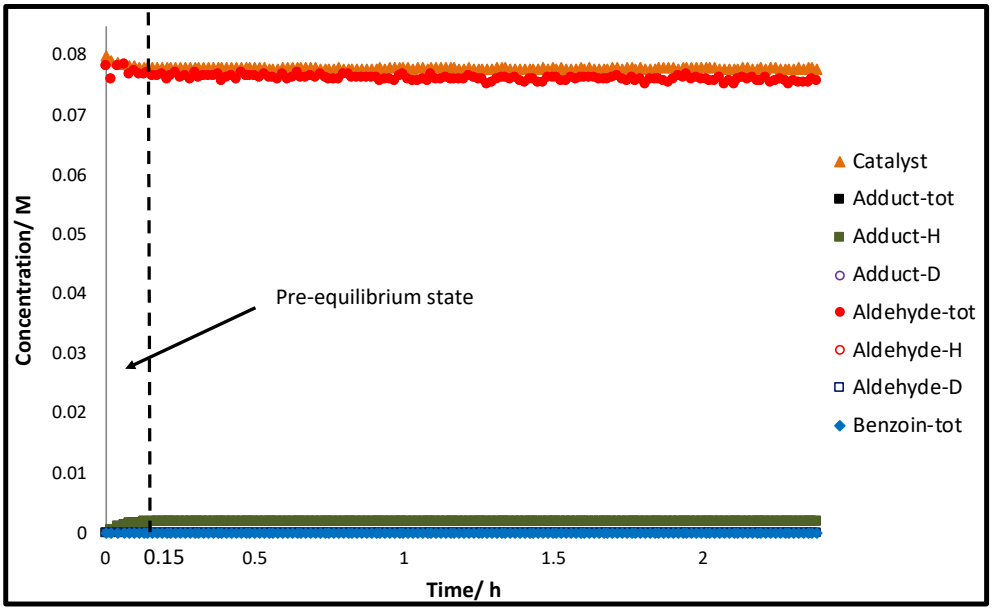

Lowering down the transient number enlarged the influence of the noise in NMR spectra. To check the effects of the reduced scan times towards the reaction parameters, two experiments with relatively long pre-equilibrium duration were chosen as representatives. The reaction parameters of benzaldehyde **135** and 2-methoxybenzaldehyde **138** catalysed by 4-methoxyphenyl triazolium **89** (n= 1) were summarised in Table 3.8. The long pre-equilibrium durations of these two reactions ensures the accuracy of the reaction parameters obtained from previous experiments with nt= 32, and therefore, the precision of the results obtained from experiments with nt= 8 can be judged by comparing with the previous results.

Table 3.8. Summary of reaction parameters and reagent concentrations for the self-condensation of aldehyde **135** and **138** and, in the presence of 4-methoxyphenyl triazolium precatalyst **89** (n= 1), in 0.108 M NEt_3 and 0.053 M NEt_3·HCl in methanol-d_4 at 25 °C (n= 8).

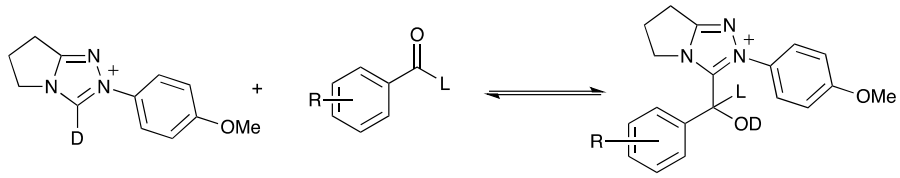

R=	$[Cat]_0$	$[Ald]_0$	Method	k_1 ($M^{-1}s^{-1}$)	k_{-1} (s^{-1})	K (M^{-1})
H	0.080 M	0.065 M	*Old*	6.80×10^{-3}	2.71×10^{-4}	2.51×10^{1}
			New	8.10×10^{-3}	3.23×10^{-4}	2.51×10^{1}
			Fitting	8.07×10^{-3}	3.98×10^{-4}	2.03×10^{1}
2-OMe	0.080 M	0.075 M	*Old*	1.49×10^{-2}	6.16×10^{-5}	2.24×10^{2}
			New	1.38×10^{-2}	6.61×10^{-5}	2.24×10^{2}
			Fitting	1.37×10^{-2}	6.65×10^{-5}	2.06×10^{2}

The relatively similar results for a given catalyst in Table 3.8 and 3.2 suggest the decrease of transient number only has small effects on reaction parameter measurements. Therefore, specific reactants with short pre-equilibrium period are chosen to obtain more precise results *via* pre-equilibrium study (nt= 8) due to the limited data points gathered by using previous NMR parameters (nt= 32). The initial concentration of both aldehyde and triazolium salts were also changed to extend the pre-equilibrium state. The reaction

parameters obtained are summarised in Table 3.9-3.11. The results obtained from Section 3.5.4. are also listed for comparison.

The following tabulated pre-equilibrium results only listed the reaction parameters which could be obtained in good precision. The rate constants of certain reactions like 4-methoxybenzaldehyde **139**, and 4-methylbenzaldehyde **137** could not be measured under pre-equilibrium conditions as the pre-equilibrium period is too short.

Table 3.9. Summary of reaction parameters and reagent concentrations for the self-condensation of aldehyde **136, 137, 139** and, in the presence of piperidine 4-fluorophenyl triazolium precatalyst **77**, in 0.108 M NEt_3 and 0.053 M NEt_3·HCl in methanol-d_4 at 25 °C.

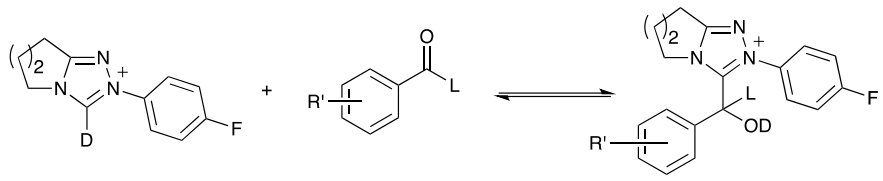

R'=	nt	$[Cat]_0$	$[Ald]_0$	Method	k_1 ($M^{-1}s^{-1}$)	k_{-1} (s^{-1})	K (M^{-1})
2-Me	32	0.080 M	0.076 M	*Old*	2.49×10^{-3}	1.25×10^{-3}	1.99×10^{0}
				New	2.64×10^{-3}	1.25×10^{-3}	2.12×10^{0}
				Fitting	3.20×10^{-3}	1.58×10^{-3}	2.03×10^{0}
	8	0.038 M	0.039 M	*Old*	8.17×10^{-3}	4.42×10^{-3}	1.85×10^{0}
				New	4.30×10^{-3}	2.38×10^{-3}	1.81×10^{0}
				Fitting	4.42×10^{-3}	2.30×10^{-3}	1.92×10^{0}
	8	0.080 M	0.075 M	*Old*	7.48×10^{-3}	4.36×10^{-3}	1.71×10^{0}
				New	4.05×10^{-3}	2.11×10^{-3}	1.92×10^{0}
				Fitting	4.23×10^{-3}	2.34×10^{-3}	1.81×10^{0}
4-Me	32	0.080 M	0.076 M	*Old*	1.51×10^{-3}	1.56×10^{-3}	9.65×10^{-1}
				New	1.17×10^{-3}	2.11×10^{-3}	1.03×10^{0}
				Fitting	2.19×10^{-3}	2.10×10^{-3}	1.04×10^{0}
	8	0.080 M	0.074 M	*Old*	1.63×10^{-3}	1.89×10^{-3}	8.62×10^{-1}
				New	1.69×10^{-3}	1.80×10^{-3}	9.38×10^{-1}
				Fitting	1.70×10^{-3}	1.74×10^{-3}	9.75×10^{-1}
4-OMe	32	0.077 M	0.073 M	*Old*	2.77×10^{-3}	3.77×10^{-4}	2.69×10^{-1}
				New	1.73×10^{-3}	3.94×10^{-3}	4.40×10^{-1}
				Fitting	2.77×10^{-3}	6.34×10^{-3}	4.37×10^{-1}
	8	0.040 M	0.039 M	*Old*	3.82×10^{-4}	1.18×10^{-3}	3.23×10^{-1}
				New	1.04×10^{-3}	3.22×10^{-3}	3.24×10^{-1}
				Fitting	7.89×10^{-4}	3.34×10^{-3}	2.36×10^{-1}
	8	0.080 M	0.078 M	*Old*	2.77×10^{-3}	1.16×10^{-2}	2.39×10^{-1}
				New	7.09×10^{-4}	2.91×10^{-3}	2.44×10^{-1}
				Fitting	7.35×10^{-4}	2.65×10^{-3}	2.77×10^{-1}

Table 3.10. Summary of reaction parameters and reagent concentrations for the self-condensation of aldehyde **136, 137, 138** and, in the presence of ε-caprolactam phenyl triazolium precatalyst **80**, in 0.108 M NEt_3 and 0.053 M NEt_3·HCl in methanol-d_4 at 25 °C.

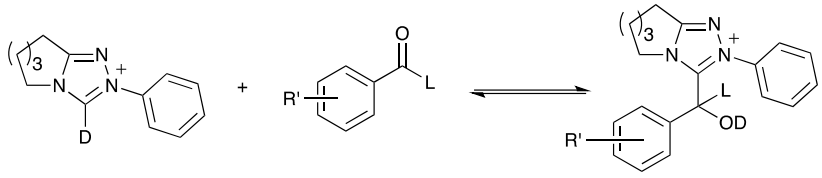

R'=	nt	$[Cat]_0$	$[Ald]_0$	Method	k_1 ($M^{-1}s^{-1}$)	k_{-1} (s^{-1})	K (M^{-1})
2-Me	32	0.080 M	0.074 M	*Old*	6.57×10^{-4}	2.53×10^{-3}	2.59×10^{-1}
				New	6.26×10^{-4}	2.30×10^{-3}	2.86×10^{-1}
				Fitting	6.30×10^{-4}	2.20×10^{-3}	2.86×10^{-1}
	8	0.044 M	0.043 M	*Old*	*N.D.*[a]	*N.D.*[a]	2.31×10^{-1}
				New	3.55×10^{-4}	1.51×10^{-3}	2.35×10^{-1}
				Fitting	7.64×10^{-4}	3.13×10^{-3}	2.44×10^{-1}
	8	0.044 M	0.081 M	*Old*	*N.D.*[a]	*N.D.*[a]	4.72×10^{-1}
				New	5.49×10^{-4}	2.14×10^{-3}	2.57×10^{-1}
				Fitting	9.61×10^{-4}	3.46×10^{-3}	2.78×10^{-1}
2-OMe	32	0.080 M	0.081 M	*Old*	3.43×10^{-3}	4.25×10^{-4}	8.07×10^{0}
				New	3.54×10^{-3}	4.47×10^{-4}	7.92×10^{0}
				Fitting	4.43×10^{-3}	5.59×10^{-4}	7.93×10^{0}
	8	0.043 M	0.043 M	*Old*	4.31×10^{-3}	5.48×10^{-4}	7.86×10^{0}
				New	4.03×10^{-3}	5.12×10^{-4}	7.87×10^{0}
				Fitting	4.05×10^{-3}	4.76×10^{-4}	8.50×10^{0}
	8	0.043 M	0.087 M	*Old*	4.31×10^{-3}	2.11×10^{-4}	2.04×10^{1}
				New	3.89×10^{-3}	4.91×10^{-4}	7.92×10^{0}
				Fitting	3.86×10^{-3}	4.52×10^{-4}	8.54×10^{0}
4-Me	32	0.080 M	0.073 M	*Old*	7.05×10^{-4}	2.96×10^{-3}	2.38×10^{-1}
				New	6.96×10^{-4}	2.66×10^{-3}	2.65×10^{-1}
				Fitting	6.79×10^{-4}	2.55×10^{-3}	2.66×10^{-1}
	8	0.043 M	0.032 M	*Old*	7.05×10^{-4}	4.65×10^{-3}	1.51×10^{-1}
				New	6.05×10^{-4}	2.99×10^{-3}	2.02×10^{-1}
				Fitting	5.94×10^{-4}	2.54×10^{-3}	2.35×10^{-1}
	8	0.043 M	0.077 M	*Old*	7.05×10^{-4}	1.46×10^{-3}	4.81×10^{-1}
				New	7.20×10^{-4}	2.71×10^{-3}	2.66×10^{-1}
				Fitting	7.03×10^{-4}	2.56×10^{-3}	2.75×10^{-1}

[a] Concentration of catalyst fluctuated and no data point can be used for k_1 calculation.

Table 3.11. Summary of reaction parameters and reagent concentrations for the self-condensation of aldehyde 136, 137 and, in the presence of ε-caprolactam 4-fluorophenyl triazolium precatalyst 78, in 0.108 M NEt3 and 0.053 M NEt3·HCl in methanol-d4 at 25 °C.

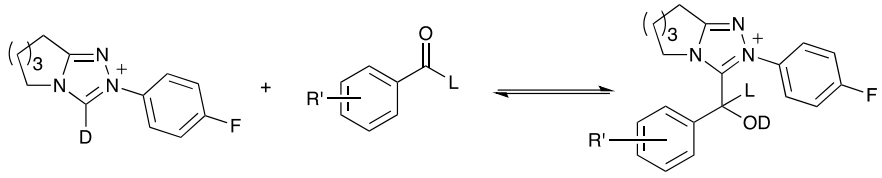

R'=	nt	$[Cat]_0$	$[Ald]_0$	Method	k_1 ($M^{-1}s^{-1}$)	k_{-1} (s^{-1})	K (M^{-1})
2-Me	32	0.078 M	0.077 M	*Old*	5.12×10^{-4}	1.42×10^{-3}	3.60×10^{-1}
				New	1.06×10^{-3}	2.90×10^{-3}	3.67×10^{-1}
				Fitting	1.02×10^{-3}	2.79×10^{-3}	3.66×10^{-1}
	8	0.080 M	0.078 M	*Old*	1.92×10^{-3}	6.01×10^{-3}	3.19×10^{-1}
				New	1.74×10^{-3}	5.40×10^{-3}	3.22×10^{-1}
				Fitting	1.66×10^{-3}	4.81×10^{-3}	3.45×10^{-1}
4-Me	32	0.077 M	0.077 M	*Old*	1.49×10^{-4}	4.90×10^{-3}	3.04×10^{-1}
				New	1.17×10^{-3}	3.85×10^{-3}	3.04×10^{-1}
				Fitting	6.09×10^{-4}	2.01×10^{-3}	3.03×10^{-1}
	8	0.077 M	0.077 M	*Old*	7.86×10^{-4}	2.61×10^{-3}	3.00×10^{-1}
				New	1.00×10^{-3}	3.73×10^{-3}	2.69×10^{-1}
				Fitting	1.04×10^{-3}	3.48×10^{-3}	2.99×10^{-1}

3.6. Kinetics of Breslow intermediate Formation

Owing to the relatively short life-time of the Breslow intermediate **124**, direct kinetic probing of its formation and decay are difficult[22]. However, the deuteration of Breslow intermediate towards deuterated adduct **144D** is essentially irreversible with a deuterium source (d_4-methanol solvent). This allows the crucial calculation of the pseudo first order rate constant, k_2 (s^{-1}), of Breslow intermediate formation from the consumption of protonated adduct **144H** after the equilibrium concentrations have been achieved (Scheme 3.12)[I]. Figure 3.8 present the concentration profile of 2-methylbenzaldehyde

[1] Note: the k_2 values were obtained from the same experiments as for k_1, k_{-1}, and K (Section 3.5)

136 catalysed by phenyl triazolium salt **101** (n= 1), which shows the concentration of protonated adduct, adduct-H (green), used for k_2 calculation after 0.63 hours. The excess of buffer concentration over adduct allows the assumption of k_2 being pseudo first order, and the expression of the adduct consumption rate is shown in Equation 3.30.

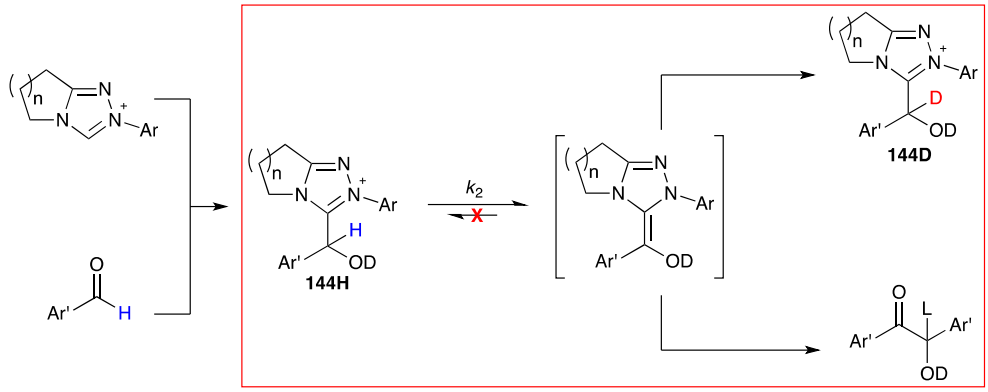

Scheme 3.12. Mechanism of Breslow intermediate formation and consumption by onward reactions.

Figure 3.8. Concentration profiles for the self-condensation of 2-methylbenzaldehyde **136** catalysed by phenyl triazolium **101** (n= 1), in 0.107 M NEt_3 and 0.053 M NEt_3·HCl in methanol-d_4.

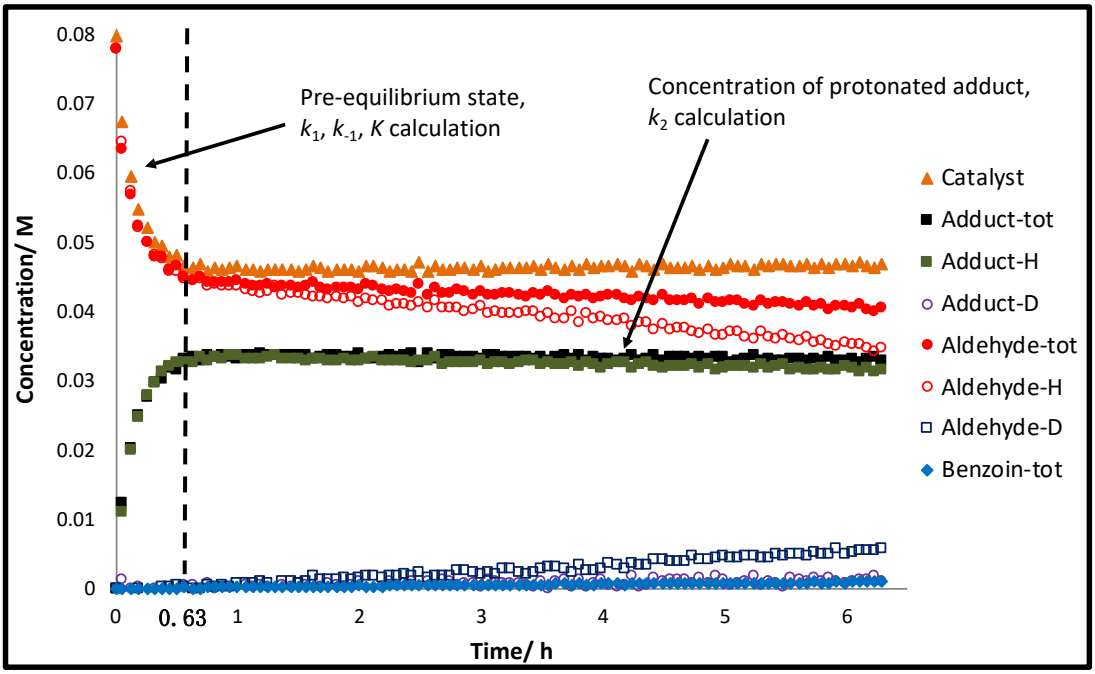

$$-\frac{d[\text{add (H)}]}{dt} = k_2[\text{add(H)}] \qquad \textbf{Equation 3.30}$$

$$[\text{add (H)}] = [\text{add (H)}]_0 e^{-k_2 t} \qquad \textbf{Equation 3.31}$$

The integrated form of Equation 3.30 is given in Equation 3.31, and the k_2 value can be obtained as the slope of the semilogarithmic plots of the protonated adduct concentration against time. The linear correlation obtained between the function of protonated adduct concentration, [add(H)], and time confirmed k_2 to be a pseudo first order rate constant. Table 3.12-3.14 summarizes the k_2 values for aldehyde **135-139** catalysed by triazolium **77-80**, **89-91**, **100, 101**. The k_2 values obtained from triazoliums salts with 7-membered fused rings have large unavoidable errors as the decrease in area of the benzylic protons is extremely small, and in some cases the value of k_2 was too small to be reliably measured.

Table 3.12. Summary of k_2 (s^{-1}) for the self-condensation of aldehyde **135-139** in the presence of phenyl triazolium precatalyst **77-80**, **89-91**, **100, 101**, in 0.107 M NEt_3 and 0.053 M $NEt_3 \cdot HCl$ in methanol-d_4 at 25 °C.

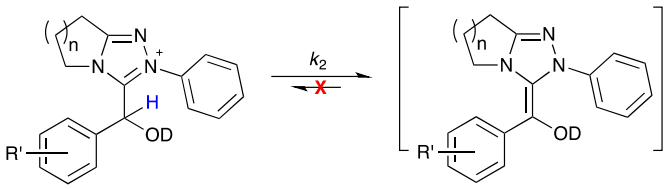

R'=	n=	k_2 (s^{-1})	R'=	n=	k_2 (s^{-1})
2-OMe	1	4.85×10^{-6}	4-OMe	1[a]	2.67×10^{-6}
	2	9.58×10^{-7}		2	*N.D.*[b]
	3	3.27×10^{-7}		3	*N.D.*[b]
2-Me	1	2.80×10^{-6}	4-Me	1	4.21×10^{-6}
	2	4.37×10^{-7}		2	5.30×10^{-8}
	3	*N.D.*[b]		3	*N.D.*[b]
H	1[a]	7.35×10^{-6}			
	2	1.88×10^{-7}			
	3	4.46×10^{-8}			

[a] Reaction parameter obtained by Peter Quinn.

[b] k_2 value could not be calculated due to the small decrease of the concentration of protonated adduct.

Table 3.13. Summary of k_2 (s^{-1}) for the self-condensation of aldehyde **135-139** in the presence of phenyl triazolium precatalyst **77-80**, **89-91**, **100, 101**, in 0.107 M NEt_3 and 0.053 M $NEt_3 \cdot HCl$ in methanol-d_4 at 25 °C.

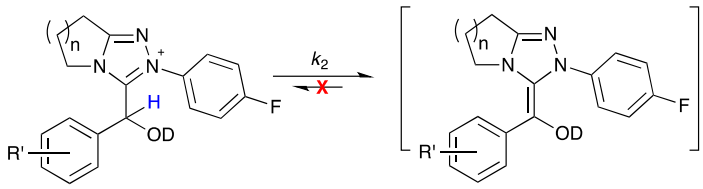

R'=	n=	k_2 (s^{-1})	R'=	n=	k_2 (s^{-1})
2-OMe	1	1.17×10^{-5}	4-OMe	1[a]	3.28×10^{-6}
	2	2.62×10^{-6}		2	2.55×10^{-7}
	3	1.78×10^{-6}		3	*N.D.*[b]
2-Me	1	6.02×10^{-6}	4-Me	1	7.04×10^{-6}
	2	5.25×10^{-7}		2	5.64×10^{-7}
	3	*N.D.*[b]		3	*N.D.*[b]
H	1[a]	2.10×10^{-5}			
	2	2.05×10^{-6}			
	3	7.21×10^{-7}			

[a] Reaction parameter obtained by Peter Quinn.

[b] k_2 value could not be calculated due to the small decrease of the concentration of protonated adduct.

Table 3.14. Summary of k_2 (s^{-1}) for the self-condensation of aldehyde **135-139** in the presence of phenyl triazolium precatalyst **77-80**, **89-91**, **100, 101**, in 0.107 M NEt_3 and 0.053 M $NEt_3 \cdot HCl$ in methanol-d_4 at 25 °C.

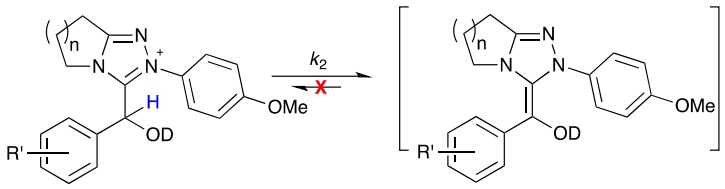

R'=	n=	k_2 (s^{-1})	R'=	n=	k_2 (s^{-1})
2-OMe	1	3.31×10^{-6}	4-OMe	1[a]	4.80×10^{-7}
	2	4.27×10^{-7}		2	*N.D.*[b]
	3	*N.D.*[b]		3	*N.D.*[b]
2-Me	1	1.45×10^{-6}	4-Me	1	2.16×10^{-6}
	2	*N.D.*[b]		2	1.36×10^{-7}
	3	*N.D.*[b]		3	*N.D.*[b]
H	1[a]	8.25×10^{-6}			
	2	*N.D.*[b]			
	3	*N.D.*[b]			

[a] Reaction parameter obtained by Peter Quinn.
[b] k_2 value could not be calculated due to the small decrease of the concentration of protonated adduct.

3.7. Impact of Catalyst Structure

From previous research, the variation of the aryl-substituents on both aldehyde and catalyst influences the reaction parameters. Meanwhile, Gravel demonstrated that the fused ring size of triazoliums has significant effects on the chemoselectivity of the cross benzoin condensation, which raised our interest on the trend of reaction parameters by changing the triazolyl fused ring size[1-4, 9, 21].

In Section 3.5 and 3.6, Table 3.2-3.14 show the absolute values of k_1, k_{-1}, K, and k_2. To provide a more direct comparison of the reaction parameters, some experiments were chosen as reference, and the relative reaction parameters k_1^{rel}, k_{-1}^{rel}, and K^{rel} were defined as the ratio of the kinetic parameters of each experiment divided by the relevant

reference value[I]. Table 3.15 gives the relative reaction parameters obtained from both fitted data (Section 3.5.3) and calculation (New Calculation Method, Section 3.5.2) for comparison of catalyst fused ring size towards benzoin condensation of 2-methoxybenzaldehyde **138**. Although the absolute value of the relative reaction parameters for fitted and calculated data are not identical, there is excellent overall agreement, and the trends are similar. Therefore, only fitted data were used for all other comparisons in the main thesis (Table 3.16-3.19).

3.7.1. Effects of Catalyst Fused Ring Size upon Reaction Parameters

3.7.1.1. Data Analyses and X-ray Crystal Structures

Table 3.15-3.19 summarises the relative reaction parameters of aldehyde **135-139** catalysed by triazolium salts **77-80**, **89-91**, **100, 101**. All the original data are obtained from Table 3.2-3.14 (Section 3.5 and 3.6). The "≈" symbol suggest the reaction parameter used might involve relatively large inaccuracy. The relative reaction parameters that could not be obtained are not listed here.

[I] Reaction parameters obtained from phenyl triazolium salts or benzaldehyde are chosen as references for the study of the substituent effects.

Table 3.15. Summary of reaction parameter ratios for the self-condensation of 2-methoxybenaldehyde **138**, in the presence of stoichiometric triazolium precatalyst **77-80**, **89-91**, **100, 101**, in 0.107 M NEt_3 and 0.053 M $NEt_3 \cdot HCl$ in methanol-d_4 at 25 °C.

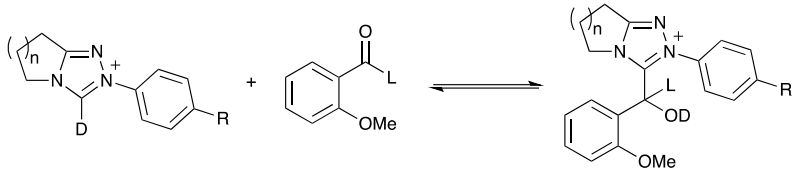

R=	Method	n=1/n=2	n=2/n=3	n=1/n=3
H	*Fitting*	k_1^{rel} = 6.60	k_1^{rel} = 0.813	k_1^{rel} = 5.27
		k_{-1}^{rel} = 0.966	k_{-1}^{rel} = 0.328	k_{-1}^{rel} = 0.317
		K^{rel} = 6.83	K^{rel} = 2.48	K^{rel} = 16.9
	Calculated	k_1^{rel} = 6.56	k_1^{rel} = 0.870	k_1^{rel} = 5.71
		k_{-1}^{rel} = 0.993	k_{-1}^{rel} = 0.333	k_{-1}^{rel} = 0.331
		K^{rel} = 6.60	K^{rel} = 2.60	K^{rel} = 17.2
4-F	*Fitting*	k_1^{rel} = 4.60	k_1^{rel} = 1.52	k_1^{rel} = 6.98
		k_{-1}^{rel} = 0.737	k_{-1}^{rel} = 0.441	k_{-1}^{rel} = 0.325
		K^{rel} = 6.25	K^{rel} = 3.44	K^{rel} = 21.5
	Calculated	k_1^{rel} = 4.86	k_1^{rel} = 1.53	k_1^{rel} = 7.44
		k_{-1}^{rel} = 0.742	k_{-1}^{rel} = 0.484	k_{-1}^{rel} = 0.359
		K^{rel} = 6.52	K^{rel} = 3.17	K^{rel} = 20.7
4-OMe	*Fitting*	k_1^{rel} = 5.71	k_1^{rel} = 1.09	k_1^{rel} = 6.20
		k_{-1}^{rel} = 1.06	k_{-1}^{rel} = 0.353	k_{-1}^{rel} = 0.374
		K^{rel} = 5.39	K^{rel} = 3.08	K^{rel} = 16.6
	Calculated	k_1^{rel} = 6.08	k_1^{rel} = 1.07	k_1^{rel} = 6.53
		k_{-1}^{rel} = 1.09	k_{-1}^{rel} = 0.351	k_{-1}^{rel} = 0.382
		K^{rel} = 5.60	K^{rel} = 3.05	K^{rel} = 17.1

Table 3.16. Summary of reaction parameter ratios for the self-condensation of benzaldehyde **135**, in the presence of stoichiometric triazolium precatalyst **77-80**, **89-91**, **100, 101**, in 0.107 M NEt_3 and 0.053 M $NEt_3 \cdot HCl$ in methanol-d_4 at 25 °C.

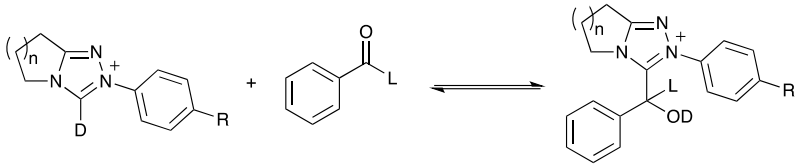

R=	n=1/n=2	n=2/n=3	n=1/n=3
H	$k_1^{rel} = 7.61$ $k_{-1}^{rel} = 0.896$ $K^{rel} = 8.50$	$k_1^{rel} = 1.10$ $k_{-1}^{rel} = 0.341$ $K^{rel} = 3.22$	$k_1^{rel} = 8.36$ $k_{-1}^{rel} = 0.305$ $K^{rel} = 27.3$
4-F	$k_1^{rel} = 7.88$ $k_{-1}^{rel} = 0.895$ $K^{rel} = 8.80$	$k_1^{rel} = 2.92$ $k_{-1}^{rel} = 0.736$ $K^{rel} = 3.96$	$k_1^{rel} = 23.0$ $k_{-1}^{rel} = 0.659$ $K^{rel} = 34.9$
4-OMe	$k_1^{rel} = 7.45$ $k_{-1}^{rel} = 0.873$ $K^{rel} = 8.52$	$k_1^{rel} = 1.09$ $k_{-1}^{rel} = 0.353$ $K^{rel} = 3.08$	$k_1^{rel} = 6.20$ $k_{-1}^{rel} = 0.374$ $K^{rel} = 16.6$

Table 3.17. Summary of reaction parameter ratios for the self-condensation of 4-methoxybenzaldehyde **139**, in the presence of stoichiometric triazolium precatalyst **77-80**, **89-91**, **100, 101**, in 0.107 M NEt_3 and 0.053 M $NEt_3 \cdot HCl$ in methanol-d_4 at 25 °C.

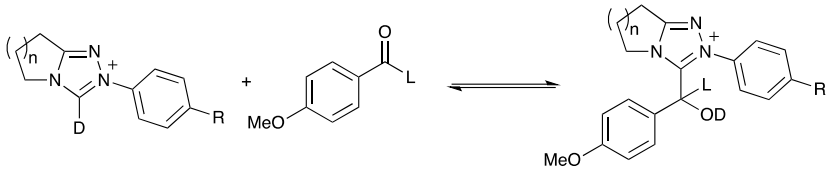

R=	n=1/n=2	n=2/n=3	n=1/n=3
H	$K^{rel} \approx 11.4$	$K^{rel} \approx 3.13$	$K^{rel} \approx 35.8$
4-F	$k_1^{rel} = 6.94$ $k_{-1}^{rel} = 0.649$ $K^{rel} = 10.7$	$K^{rel} \approx 2.61$	$K^{rel} \approx 28.0$
4-OMe	$k_1^{rel} \approx 7.89$ $k_{-1}^{rel} \approx 0.867$ $K^{rel} \approx 9.11$	$K^{rel} \approx 59.2$	$K^{rel} \approx 539$

Table 3.18. Summary of reaction parameter ratios for the self-condensation of 2-methylbenzaldehyde **136**, in the presence of stoichiometric triazolium precatalyst **77-80**, **89-91**, **100, 101**, in 0.107 M NEt_3 and 0.053 M $NEt_3 \cdot HCl$ in methanol-d_4 at 25 °C.

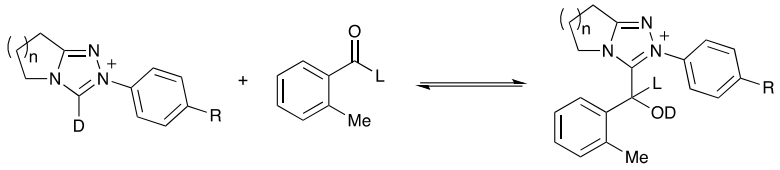

R=	n=1/n=2	n=2/n=3	n=1/n=3
H	$k_1^{rel} = 5.73$ $k_{-1}^{rel} = 0.431$ $K^{rel} = 13.3$	$k_1^{rel} = 2.62$ $k_{-1}^{rel} = 0.502$ $K^{rel} = 5.22$	$k_1^{rel} = 15.0$ $k_{-1}^{rel} = 0.216$ $K^{rel} = 69.4$
4-F	$k_1^{rel} = 5.29$ $k_{-1}^{rel} = 0.416$ $K^{rel} = 12.7$	$k_1^{rel} = 2.55$ $k_{-1}^{rel} = 0.486$ $K^{rel} = 5.25$	$k_1^{rel} = 13.5$ $k_{-1}^{rel} = 0.202$ $K^{rel} = 66.5$
4-OMe	$k_1^{rel} \approx 4.29$ $k_{-1}^{rel} \approx 0.439$ $K^{rel} \approx 9.77$	$k_1^{rel} \approx 2.59$ $k_{-1}^{rel} \approx 0.643$ $K^{rel} \approx 4.03$	$k_1^{rel} \approx 11.1$ $k_{-1}^{rel} \approx 0.282$ $K^{rel} \approx 39.4$

Table 3.19. Summary of reaction parameter ratios for the self-condensation of 4-methylbenzaldehyde **137**, in the presence of stoichiometric triazolium precatalyst **77-80**, **89-91**, **100, 101**, in 0.107 M NEt_3 and 0.053 M $NEt_3 \cdot HCl$ in methanol-d_4 at 25 °C.

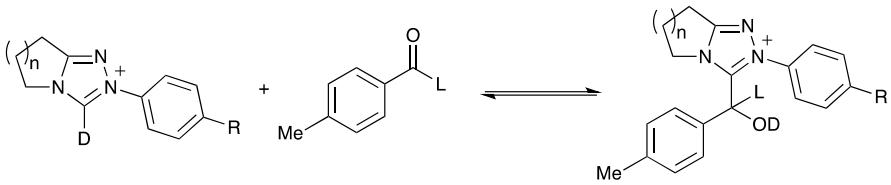

R=	n=1/n=2	n=2/n=3	n=1/n=3
H	$k_1^{rel} = 5.92$ $k_{-1}^{rel} = 0.682$ $K^{rel} = 8.68$	$k_1^{rel} = 1.76$ $k_{-1}^{rel} = 0.563$ $K^{rel} = 3.13$	$k_1^{rel} = 10.4$ $k_{-1}^{rel} = 0.383$ $K^{rel} = 27.2$
4-F	$k_1^{rel} = 6.38$ $k_{-1}^{rel} = 0.621$ $K^{rel} = 10.3$	$k_1^{rel} = 1.63$ $k_{-1}^{rel} = 0.500$ $K^{rel} = 3.26$	$k_1^{rel} = 10.4$ $k_{-1}^{rel} = 0.310$ $K^{rel} = 33.6$
4-OMe	$k_1^{rel} \approx 4.15$ $k_{-1}^{rel} \approx 0.684$ $K^{rel} \approx 6.07$	$k_1^{rel} \approx 6.72$ $k_{-1}^{rel} \approx 2.13$ $K^{rel} \approx 3.16$	$k_1^{rel} \approx 27.9$ $k_{-1}^{rel} \approx 1.46$ $K^{rel} \approx 19.2$

Changing catalyst fused ring size from 5 (n= 1) to 6 (n= 2) largely decreased the adduct

formation rate constants. The association constants of adduct formation with 5-membered fused rings are at 4.2-7.8 fold larger than those with 6-membered fused rings[I] (k_1^{rel}: n= 1/ n= 2). The relative adduct association values of triazolium salts with six- and seven-membered fused ring sizes are more comparable. Apart from the reaction of 2-methoxybenzaldehyde **138** catalysed by phenyl triazolium salts **101, 79**, the association constants with 6-membered fused rings are only 1.1-2.9 fold larger than those with 7-membered fused ring[II] (k_1^{rel}: n= 2/ n= 3).

Meanwhile, opposite trends can be observed for the dissociation constants of adduct (k_{-1}). Apart from the reaction of 4-methylbenzaldehyde **137** catalysed by 4-methoxyphenyl triazolium **89, 90**, the adducts with 7-membered fused ring size have the largest dissociation rate constants, and 5-membered analogues have the smallest values[III]. Furthermore, for k_{-1}, the differences between n=2 and 3 are larger than n=1 and 2. Statistically, the changing of k_1 values is larger than k_{-1}[IV] (0.328-0.736 fold for k_1, 0.416-0.966 fold for k_{-1}).

With the combined effects of both association and dissociation rate constants, equilibrium constants decreased more significantly with the increment of fused ring sizes. Overall, equilibrium constants decrease in the order: $K^{n=1} >> K^{n=2} > K^{n=3}$. Equilibrium constants of triazolium salts with 6-membered fused ring are 11~16% of

---

[I] k_1^{rel} (changing n= 1 to 2) in range of 4.15 (4-OMe-Ph NHC and 4-Me PhCHO) to 7.89 (4-OMe-Ph NHC and 4-OMe-PhCHO)

[II] Apart from reaction of 4-Me-PhCHO catalysed by 4-OMe-Ph NHC ($k_1^{rel} \approx 6.72$) and 2-OMe-PhCHO catalysed by Ph NHC ($k_1^{rel} = 0.813$), k_1^{rel} (changing n= 2 to 3) all in range of 1.09 (4-OMe-Ph-NHC and PhCHO) to 2.92 (4-F-Ph NHC and PhCHO).

[III] Apart from reaction of 2-OMe-PhCHO catalysed by 4-OMe-Ph NHC ($k_{-1}^{rel} = 1.06$), changing n= 1 to 2, k_{-1}^{rel} in range of 0.416 (4-F-Ph NHC and 2-Me-PhCHO) to 0.966 (Ph-NHC and 2-OMe-PhCHO).

[IV] Apart from reaction of 4-Me-PhCHO catalysed by 4-OMe-Ph NHC ($k_{-1}^{rel} = 2.13$), changing n= 2 to 3, k_{-1}^{rel} in range of 0.328 (Ph NHC and 2-OMe-PhCHO) to 0.736 (4-F-Ph-NHC and PhCHO).

the triazolium salts with 5-membered fused ring[I] (K^{rel}: n= 1/ n= 2). The values of *K* for triazolium salts with 7-membered fused rings only account for 2~5% of those with n=1, and 20~40% of those with n=2[II] (K^{rel}: n= 2/ n= 3).

We postulated that the relatively smaller steric occupancy of the 5-membered fused ring (n=1) than that of the 6-membered (n=2) and 7-membered (n=3) fused rings may potentially facilitate the formation of the sterically bulky adduct. Existing crystal structures of triazolium salts obtained in our laboratory suggest the hydrogen atoms adjacent to the nitrogen (H_1 and H_1') may provide steric hindrance to the reaction center (Figure 3.9). Table 3.9 lists bond angles of $H_1C_1H_1$', and torsion angles between C_1H_1, C_1H_1', C_2H_2, while Table 3.10 provides the distance between three hydrogen atoms obtained using the available crystallographic data. Changing fused ring size from 5 to 6 to 7 lowers down the torsion angles between C_1H_1 and C_2H_2 from 43.8° (± 1.9°) to 38.5° (± 1.6°) to almost 0°, and the distances between H_1H_2 from 3.05 Å (± 0.04 Å) to 2.75 Å (± 0.03 Å) to 2.48 Å (± 0.05 Å).

Although limited crystal structures are available for the triazolium salts with 6- and 7-membered fused ring, a crucial conclusion can be made that the protons on the 6-and 7-membered fused ring are closer to the reaction center, which might prevent the deprotonation on the C2 position to form the carbene and reduce the reaction rates.

[I] K^{rel} (changing n= 1 to 2) in range of 5.39 (4-OMe-Ph NHC and 2-OMe PhCHO) to 13.3 (Ph NHC and 2-Me-PhCHO)

[II] Apart from reaction of 4-OMe-PhCHO catalysed by 4-OMe-Ph NHC (K^{rel}≈ 59.2), K^{rel} (changing n= 2 to 3) in range of 2.48 (Ph NHC and 2-OMe PhCHO) to 5.25 (4-F-Ph NHC and 2-Me-PhCHO).

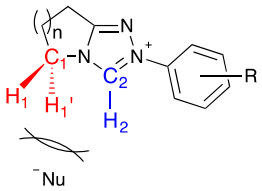

Figure 3.9. Potential steric hindrance provided by adjacent proton.

Table 3.20. Bond angles and torsion angles of triazolium salts measured from crystal structures by using software Mercury.

		Bond angle	Torsion angles (°)	
n=	R=	$H_1C_1H_1$'	C_1H_1, C_2H_2	C_1H_1', C_2H_2
1 [a]	4-OMe	109.50	44.19	64.95
1 [a]	2,6-dimethoxy	109.25	43.22	65.64
1 [a]	4-F	112.80	46.34	64.45
1[a]	pentafluoro	109.32	42.75	69.65
1[a]	2,4,6-triCl	112.36	46.45	65.35
1[b]	4-Br	109.38	42.18	66.49
1[b]	3-Cl	111.88	43.90	70.44
1[c]	4-CF_3	111.61	41.15	72.48
2	4-F	108.16	39.81	67.56
2	4-OMe	108.53	36.73	70.00
2	H	108.33	38.82	68.53
3	pentafluoro	109.22	2.71	75.75
3	4-OMe	107.95	0.6	72.47

[a] Crystal structure obtained by Peter Quinn, [b] Triazolium salt synthesised by Hector Macrae. [c] Triazolium salt synthesised by Jinyi Xuan.

Table 3.21. Hydrogen atom distances of triazolium salts measured from crystal structures by using software Mercury.

		Distance (Å)		
n=	R=	H_1H_1'	H_1H_2	H_2H_1'
1 [a]	4-OMe	1.617	3.059	3.298
1 [a]	2,6-dimethoxy	1.614	3.122	3.318
1 [a]	4-F	1.629	3.041	3.230
1[a]	pentafluoro	1.615	3.072	3.315
1[a]	2,4,6-triCl	1.567	3.017	3.236
1[b]	4-Br	1.616	3.078	3.339
1[b]	3-Cl	1.530	3.040	3.220
1[c]	4-CF_3	1.570	2.991	3.237
2	4-F	1.604	2.768	3.095
2	4-OMe	1.607	2.717	3.136
2	H	1.605	2.760	3.100
3	pentafluoro	1.579	2.445	3.308
3	4-OMe	1.602	2.510	3.427

[a] Crystal structure obtained by Peter Quinn, [b] Triazolium salt synthesised by Hector Macrae. [c] Triazolium salt synthesised by Jinyi Xuan.

This kinetic explanation is based on the solid-state structures of the triazolium salts. Thermodynamically, the increment of the fused ring size could also destabilise the hydroxy-aryl adduct due to the electrostatic repulsion and steric hindrance between fused ring proton and the aldehydic moiety depending on the conformation of the aldehyde (Figure 3.10). Moreover, the attachment of the aldehyde to the carbene probably involves the twisting of fused ring to afford enough space for the accommodation of the aldehydic moiety.

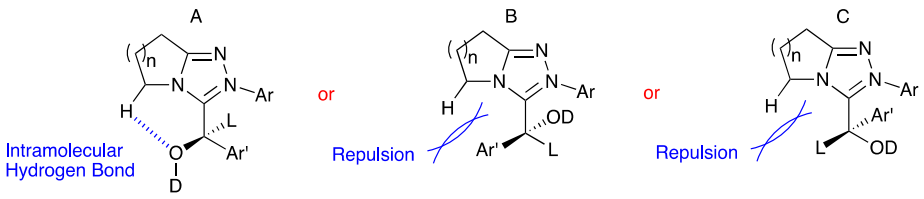

Figure 3.10. Potential electrostatic effects between fused ring and aldehydic moiety[I].

Density Functional Theory (DFT) calculations were performed to attempt to further understand these problems. Adapted from Gravel's work, all systems were studied *via* Gaussview using the Durham University Hamilton HPC. The level of theory applied was B3LYP/6-31(g), with solvent methanol modelled using an implicit polarizable continuum model (PCM). Limited by the research time, all the models ignored intermolecular Van de Waals interaction, and the counter ions were excluded during the calculation. The computational data may also be compared with earlier analogous data from Peter Quinn in our group[21, 23].

3.7.1.2. Role of Conformational Flexibility of the Fused Ring

With an increase in ring size, the fused ring of triazolium is likely to be more flexible. By fixing the dihedral angle between C_1H_1 and C_2H_2 to a certain degree, the energy increments caused by the twisting of the fused ring were obtained and are listed in Table 3.22-3.24. The symbol 'Γ'represents the torsion angle between bond C_1H_1 and C_2H_2; E_{diff} is the calculated energy difference between the original and current conformations. The initial calculation models were based on the experimental X-ray crystal structures of triazolium salts obtained in our laboratory, and the similar dihedral angles of the calculated and the experimental models suggest the reliability of this computational

[I] There is currently no crystal structure of hydroxy aryl adducts with 6- and 7-fused ring sizes, and the conformation of the adduct has three different possibilities (A-C). Notably, if the hydroxy group is localized as A, the energy of the system could be decreased by a potential intramolecular hydrogen bond.

study. The Boltzmann distribution of conformer mole fraction can be obtained from the energy differences by using Equation 3.32, which indirectly indicate the potential steric hindrance provided by the fused ring proton H_1 to the reaction centre.

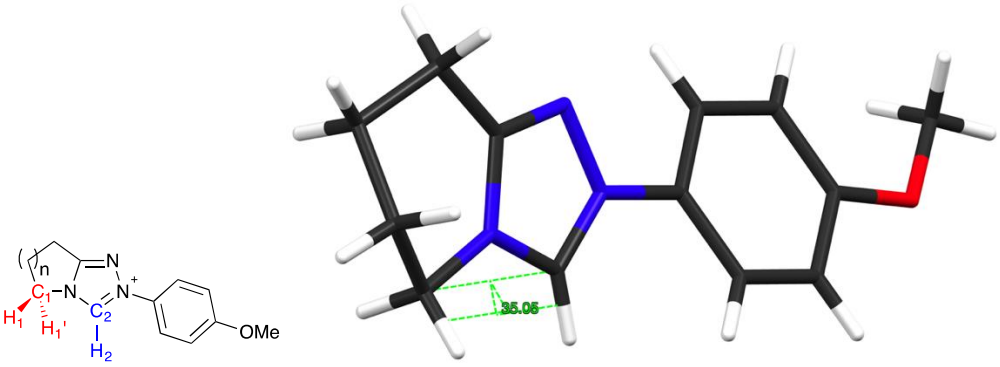

Figure 3.11. DFT calculation model with fixed dihedral angle between bond C_1H_1 and C_2H_2.

$$\frac{p_i}{p_j} = e^{\frac{e_j - e_i}{RT}} \qquad \text{Equation 3.32}$$

Table 3.22. Energy and conformer distribution of *para*-methoxyphenyl triazolium (n= 1, **89**) obtained from DFT calculations.

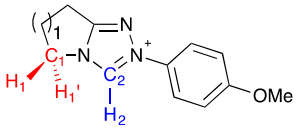

Γ(°)	$\Delta\Gamma$(°)	E_{diff} (kJ/mol)	p_i/p_j	Γ(°)	$\Delta\Gamma$(°)	E_{diff} (kJ/mol)	p_i/p_j
57.16	14.00	2.078	0.432	41.16	-2.00	0.049	0.981
55.16	12.00	1.598	0.525	39.16	-4.00	0.200	0.922
53.16	10.00	1.146	0.630	37.16	-6.00	0.456	0.832
51.16	8.00	0.754	0.737	35.16	-8.00	0.816	0.719
49.16	6.00	0.436	0.839	33.16	-10.00	1.285	0.595
47.16	4.00	0.199	0.923	31.16	-12.00	1.867	0.471
45.16	2.00	0.052	0.979	29.16	-14.00	2.563	0.355
43.16[a]	0.00	0.000	1.000	27.16	-16.00	3.374	0.256

[a] The initial model calculated from experimental X-ray crystal structures obtained in our laboratory.

Table 3.23. Energy and conformer distribution of *para*-methoxyphenyl triazolium (n= 2, **90**) obtained from DFT calculations.

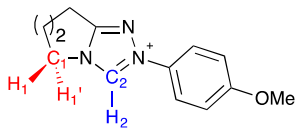

Γ(°)	$\Delta\Gamma$(°)	E_{diff} (kJ/mol)	p_i/p_j	Γ(°)	$\Delta\Gamma$(°)	E_{diff} (kJ/mol)	p_i/p_j
53.47	14.00	2.051	0.437	37.47	-2.00	0.045	0.982
51.47	12.00	1.519	0.542	35.47	-4.00	0.182	0.929
49.47	10.00	1.061	0.652	33.47	-6.00	0.411	0.847
47.47	8.00	0.684	0.759	31.47	-8.00	0.729	0.745
45.47	6.00	0.390	0.854	29.47	-10.00	1.136	0.632
43.47	4.00	0.178	0.931	27.47	-12.00	1.632	0.518
41.47	2.00	0.046	0.982	25.47	-14.00	2.216	0.409
39.47[a]	0.00	0.000	1.000	23.47	-16.00	2.888	0.312

[a] The initial model calculated from experimental X-ray crystal structures obtained in our laboratory.

Table 3.24. Energy and conformer distribution of *para*-methoxyphenyl triazolium (n= 3, **91**) obtained from DFT calculations.

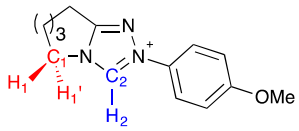

Γ(°)	$\Delta\Gamma$(°)	E_{diff} (kJ/mol)	p_i/p_j	Γ(°)	$\Delta\Gamma$(°)	E_{diff} (kJ/mol)	p_i/p_j
14.63	14.00	2.387	0.382	-1.37	-2.00	0.051	0.980
12.63	12.00	1.756	0.492	-3.37	-4.00	0.205	0.921
10.63	10.00	1.225	0.610	-5.37	-6.00	0.446	0.835
8.63	8.00	0.790	0.727	-7.37	-8.00	0.753	0.738
6.63	6.00	0.448	0.835	-9.37	-10.00	1.136	0.632
4.63	4.00	0.200	0.922	-11.37	-12.00	1.604	0.523
2.63	2.00	0.050	0.980	-13.37	-14.00	2.162	0.418
0.63[a]	0.00	0.000	1.000	-15.37	-16.00	2.806	0.322

[a] The initial model calculated from experimental X-ray crystal structures obtained in our laboratory.

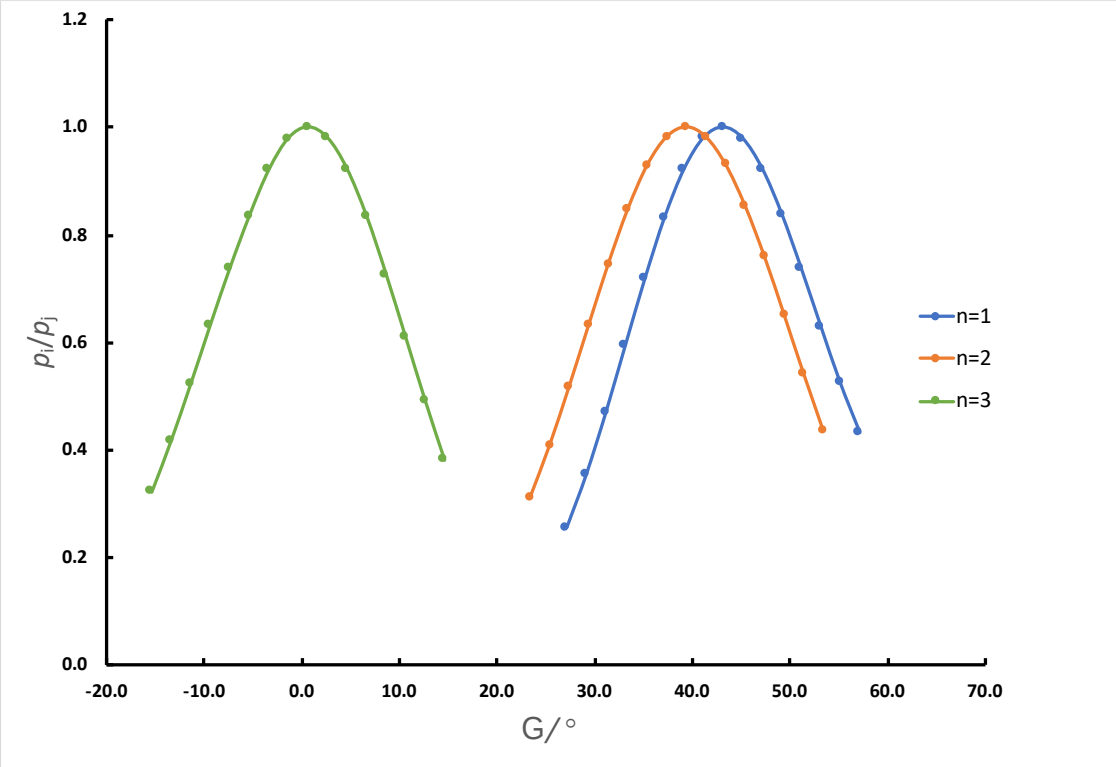

Figure 3.12. Population variation of triazolium salts (n= 1-3) against torsion angles between C_1H_1 and C_2H_2.

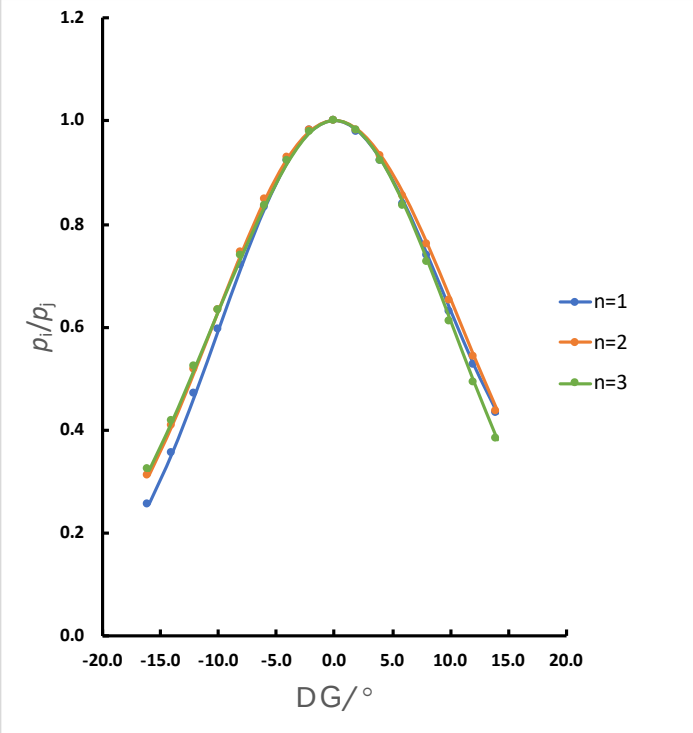

Figure 3.13. Population variation of triazoliums against torsion angle differences between C_1H_1 and C_2H_2.

To give a more direct comparison of the populational differences, Figure 3.12 presents the populational ratio (p_i/p_j) against the torsion angles (Γ), while Figure 3.13 shows the populational ratio (p_i/p_j) against the torsion angle differences ($\Delta\Gamma$) of the triazolium salts with different fused ring sizes. From Figure 3.12, the change of population ratio against dihedral angle clearly shows the conformers' population accumulated around three different positions, and the torsion angle p_i/p_j follows the order: $\Gamma_{n=1} > \Gamma_{n=2} >> \Gamma_{n=3}$. Figure 3.13 states the proportional variation of triazoliums with different fused ring sizes are highly similar and are essentially superimposable. This analysis suggests that incremental CH_2 addition does not change the conformational flexibility of the fused ring. Flipping of 7-membered fused ring is however closer to the reaction centre, which provides largest steric hindrance towards the reaction center than 5- and 6-membered fused ring.

3.7.1.3. Hydroxyaryl Adduct Conformation

Richard Massey, a previous PhD student in our research group obtained the crystal structures of three hydroxyaryl adducts with five-membered fused rings (Figure 3.14)[4] , which suggest the rigid conformations of these adducts in solid state.

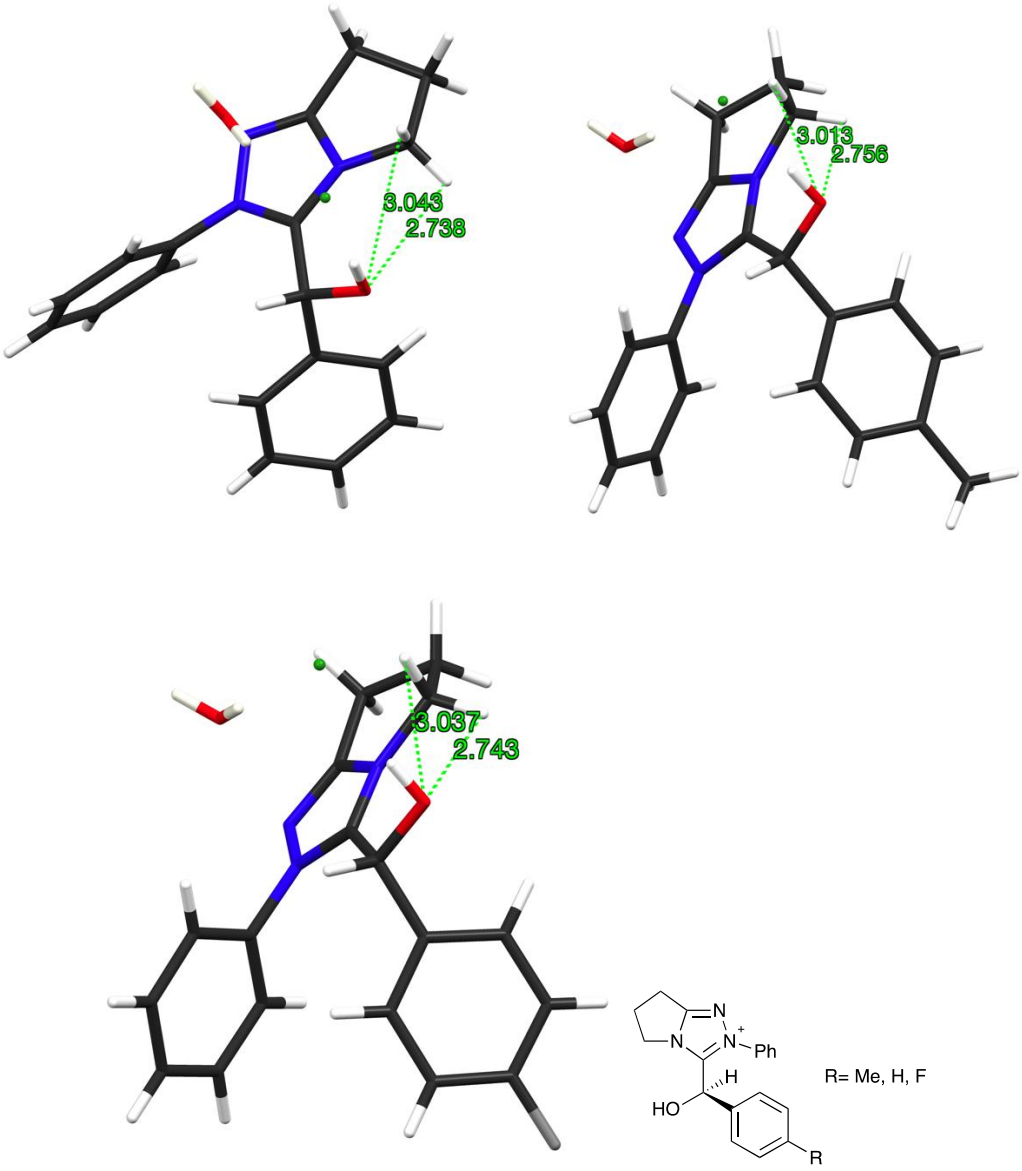

Figure 3.14. Crystal structure of Richard Massey's hydroxy aryl adducts.

Previously, I suggested that the steric hindrance and static repulsion provided by the protons on the fused ring may have impact on the accommodation of the aldehydic moiety of the adduct. Table 3.25 lists torsion angles among C_1H_1, C_1H_1', C_2C_3, and the distance among atom H_1, H_1', O measured from the X-ray crystal structures.

Table 3.25. Torsion angles, and distances between atoms measured from Richard Massey's crystal structures by using software Mercury.

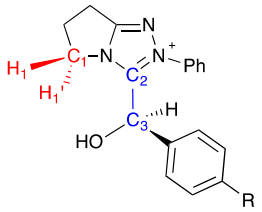

	Torsion angles (°)		Distance (Å)		
R=	C_1H_1, C_2C_3	C_1H_1', C_2C_3	H_1H_1'	H_1O	H_1'O
Me	67.06	39.78	1.616	3.013	2.756
H	67.90	40.98	1.618	3.043	2.738
F	67.46	41.09	1.616	3.037	2.743

The torsion angles between C_1H_1, C_2C_3, and C_1H_1', C_2C_3, and the distance between H_1H_2 do not change when comparing catalyst versus adduct. Meanwhile, the distances between proton and oxygen are larger than the sum of their Van de Waals radii ($r_{vdW}H$ = 1.20 Å, $r_{vdW}O$ = 1.50 Å), suggesting there are no (or very low) intramolecular interactions and repulsions between proton and oxygen in the adduct systems with 5-membered fused rings.

Synthetic-based structural analyses of hydroxy aryl adduct with larger fused ring sizes are difficult. The decreased equilibrium constants of adduct formation caused by the increment of fused ring size hindered the isolation of adduct with six- and seven-membered fused rings. Currently, no X-ray crystal structures for those hydroxy-aryl adducts are available. Meanwhile, the hydroxy-aryl adducts' conformations with lowest energy may be different in solution phase compared to the solid state. Therefore, DFT was again applied to obtain the lowest energy conformers of hydroxy-aryl adducts with different fused ring sizes.

To check the possible conformations of hydroxy-aryl adducts with different fused ring

sizes, Avogadro software was used for the conformational calculation using MMFF94 as the force field. Structures with local energy minima are used as initial points for DFT calculations[24], and the conformations obtained with lowest energies are given in Figure 3.15. Limited by the DFT approach used, the structures obtained still have the possibility to be conformations with local minimum energies but not global minima.

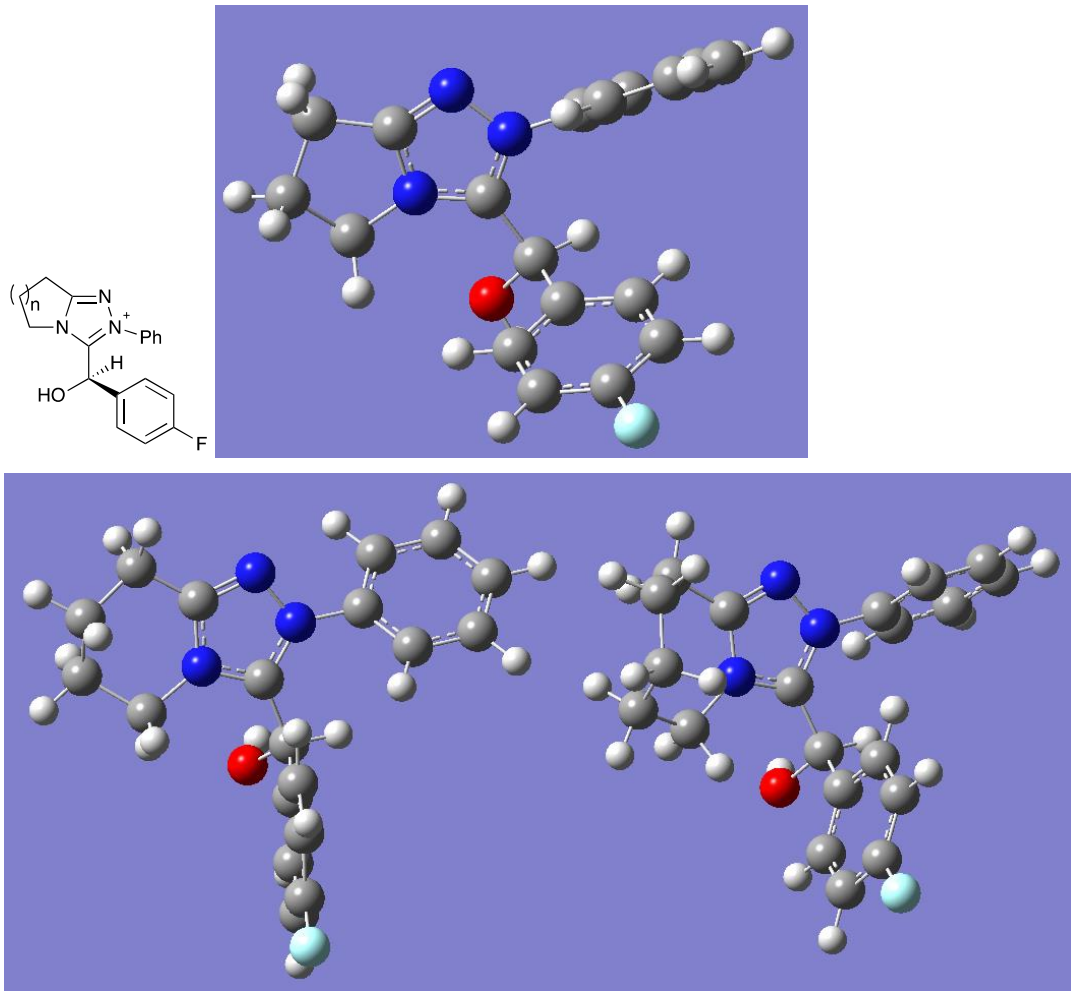

Figure 3.15. The lowest energy conformations of hydroxy-aryl adducts with five-, six-, and seven-membered fused rings.

Table 3.26 lists torsion angles among C_1H_1, C_1H_1', C_2C_3, and the distance among atoms H_1, H_1', O measured from the computer modelling structures. Compared with the data obtained from the calculated models of triazolium salts (Table 3.27), the C_1H_1' bond twists more with larger fused ring sizes during the formation of adducts.

Setting the triazolium ring as the reference plane, during the formation of the hydroxy aryl adduct, the C_1H_1 bond twists +5.14° for n=1, +6.64° for n=2, -37.54° for n=3 versus initial catalyst. For systems with n=1 and n=2, the decreasing of the torsion angles potentially suggests the existence of an intramolecular hydrogen bond (mentioned in Figure 3.10) which lowers down the energy of the whole system. Meanwhile, the largely increased torsion angle of the 7-membered fused ring shows the impact of the steric hindrance of the hydroxy groups. The combined effect of the intramolecular hydrogen bond and the steric hindrance provided by the hydroxy group lead to the overall twist of the fused ring during the formation of the hydroxy aryl adducts. Moreover, the degree of the twist of torsion angles could be related to a higher energy barrier of adduct formation with a larger fused ring size.

NMR spectra showed that during the formation of the adduct, the chemical shifts of proton H_1 and H_1' splits into two separate values due to the formation of the chiral centre. For the reaction with non-*ortho*-substituted aldehyde, the differences of the chemical shifts of the two protons are largest in case of 6-membered fused ring system (~0.45 ppm), while comparable in 5- (~0.15 ppm) and 7-membered (~0.12 ppm) fused ring systems. Relevant or not, the calculated structure of hydroxy aryl adducts suggests the torsion angles between C_1H_1' and C_2C_3 are smallest in 6-membered fused ring system, and comparable in 5- and 7-membered fused ring adducts (Table 3.26).

Table 3.26. Torsion angles, and distances between atoms measured from DFT calculated structures by using software Gaussview for hydroxy aryl adducts.

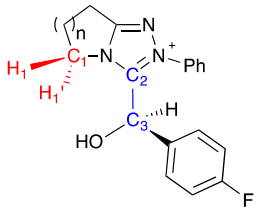

	Torsion angles (°)		Distance (Å)		
n=	C_1H_1, C_2C_3	C_1H_1', C_2C_3	H_1H_1'	H_1O	H_1'O
1	73.19	38.02	1.775	2.883	2.683
2	76.03	32.83	1.776	3.595	2.396
3	69.19	38.17	1.764	2.815	2.717

Table 3.27. Torsion angles, and distances between atoms measured from DFT calculated structures by using software Gaussview for triazolium salts.

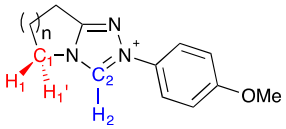

	Torsion angles (°)		Distance (Å)		
n=	C_1H_1, C_2H_2	C_1H_1', C_2H_2	H_1H_1'	H_1H_2	H_1'H_2
1	68.53	43.16	1.783	3.368	3.156
2	69.46	39.47	1.777	3.122	2.776
3	106.11	0.63	1.768	3.547	2.483

To study the influence of conformational change, DFT software was used to calculate the energy of certain conformations of hydroxy aryl adducts. Similar to Section 2.7.1.2, the dihedral angles between bond C_1H_1 and C_2H_2 was set to a certain degree, and the calculated conformers with minimum energies were used as the starting points. The energy increments caused by the twisting of the fused ring were obtained and are listed in Table 3.28-3.30. The Boltzmann distribution of conformer mole fraction (p_i/p_j) can be

obtained from the energy differences by using Equation 3.32. The symbol 'Γ'represents the torsion angle between bond C_1H_1 and C_2H_2, and, E_{diff}, the calculated energy difference between the original and current conformations.

Table 3.28. Energy and conformer distribution of hydroxy-aryl adduct with five-membered fused ring obtained from DFT calculations.

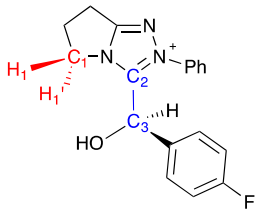

Γ(°)	$\Delta\Gamma$(°)	E_{diff} (kJ/mol)	p_i/p_j
38.02	0.00	0	1.000
36.02	-2.00	0.047	0.981
34.02	-4.00	0.213	0.918
32.02	-6.00	0.492	0.820
30.02	-8.00	0.878	0.702
28.02	-10.00	1.371	0.575
26.02	-12.00	1.975	0.451
24.02	-14.00	2.698	0.337
22.02	-16.00	3.545	0.239
20.02	-18.00	4.498	0.163
18.02	-20.00	5.547	0.107

Table 3.29. Energy and conformer distribution of hydroxy-aryl adduct with six-membered fused ring obtained from DFT calculations.

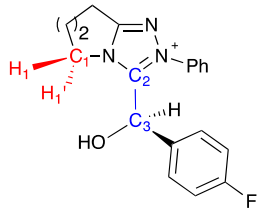

Γ (°)	$\Delta\Gamma$ (°)	E_{diff} (kJ/mol)	p_i/p_j
32.83	0.00	0	1.000
30.83	-2.00	0.030	0.988
28.83	-4.00	0.164	0.936
26.83	-6.00	0.413	0.847
24.83	-8.00	0.757	0.737
22.83	-10.00	1.199	0.616
20.83	-12.00	1.750	0.493
18.83	-14.00	2.414	0.377
16.83	-16.00	3.189	0.276
14.83	-18.00	4.069	0.194
12.83	-20.00	5.042	0.131

Table 3.30. Energy and conformer distribution of hydroxy-aryl adduct with seven-membered fused ring obtained from DFT calculations.

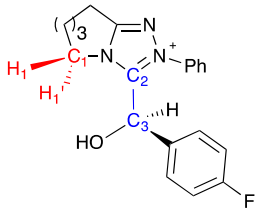

Γ(°)	$\Delta\Gamma$(°)	E_{diff} (kJ/mol)	p_i/p_j
38.17	0.00	0	1.000
36.17	-2.00	0.023	0.991
34.17	-4.00	0.087	0.965
32.17	-6.00	0.197	0.924
30.17	-8.00	0.349	0.869
28.17	-10.00	0.535	0.806
26.17	-12.00	0.747	0.740
24.17	-14.00	0.976	0.674
22.17	-16.00	1.213	0.613
20.17	-18.00	1.439	0.559
18.17	-20.00	1.644	0.515

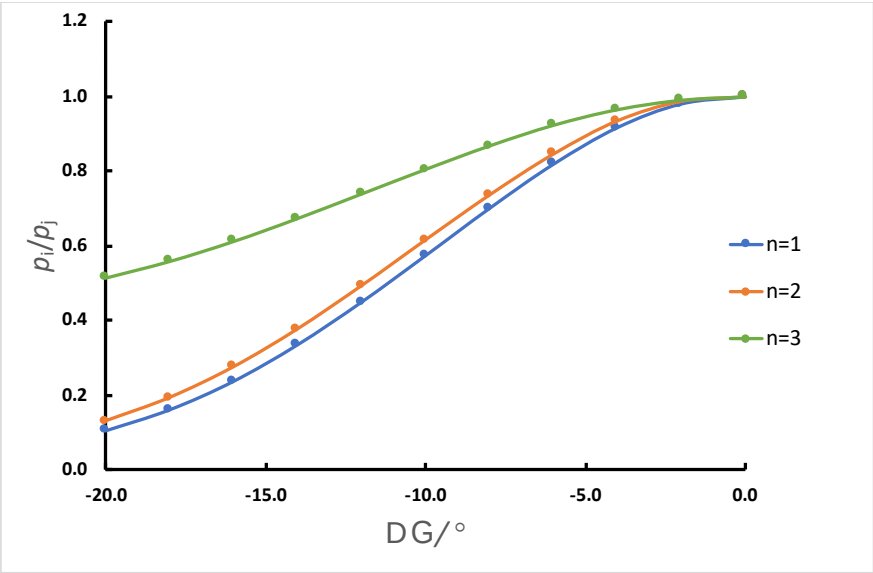

Figure 3.16. Boltzmann distribution of hydroxy-aryl adducts with different conformations.

From the population distribution (Figure 3.16), p_i/p_j values are relatively smaller as a function of $\Delta\Gamma$ for n= 3, whereas they change more for n= 1 and 2. The results of calculations suggest the smaller fused ring size (n= 1 and 2) gives more rigid structures, with the 7-membered fused ring twisted most easily. Compared with the superimposable conformer's populational variation of triazolium fused ring showed in Figure 3.13, the altered behavior in Figure 3.16 could only be a result of the steric occupancy of the aldehydic moiety of adducts.

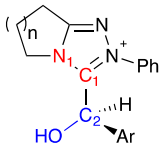

Figure 3.17. DFT calculation models with fixed dihedral angle between bond N_1C_1 and C_2O.

To further check the influence of the steric effects between fused ring and aldehydic moiety in the hydroxy aryl adduct, the dihedral angle between N_1C_1 and C_2O was incrementally changed by DFT (Figure 3.17), and the obtained energy differences were further applied to calculate the ratio of conformational populations by using a Boltzmann Distribution (Equation 3.32). The calculations were started from the dihedral angle obtained from the conformations listed in Figure 3.15, and the data obtained are shown in 3.31-3.33. The ratio of conformers' molar population distributions is shown in Figure 3.18.

Table 3.31. Energy and conformer distribution of hydroxy-aryl adduct with five membered fused ring obtained from DFT calculations.

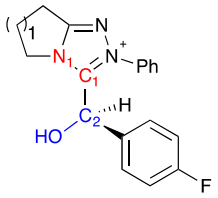

Γ(°)	$\Delta\Gamma$(°)	E_{diff} (kJ/mol)	p_i/p_j	Γ(°)	$\Delta\Gamma$(°)	E_{diff} (kJ/mol)	p_i/p_j
0.00	-22.15	1.745	0.494	67.15	45.00	0.074	0.970
2.15	-20.00	1.343	0.581	72.15	50.00	-0.268	1.114
7.15	-15.00	0.626	0.777	77.15	55.00	-0.759	1.358
12.15	-10.00	0.332	0.875	82.15	60.00	-1.142	1.586
17.15	-5.00	0.074	0.971	87.15	65.00	-1.501	1.832
22.15[a]	0.00	0.000	1.00	92.15	70.00	-1.250	1.656
27.15	5.00	0.250	0.904	97.15	75.00	-0.592	1.270
32.15	10.00	0.914	0.691	102.15	80.00	0.484	0.822
37.15	15.00	1.059	0.652	107.15	85.00	1.951	0.455
42.15	20.00	0.880	0.701	112.15	90.00	3.627	0.231
47.15	25.00	0.574	0.793	117.15	95.00	5.067	0.129
52.15	30.00	0.543	0.803	127.15	105.00	7.159	0.056
57.15	35.00	0.599	0.785	137.15	115.00	7.184	0.055
62.15	40.00	0.273	0.896	147.15	125.00	7.742	0.044

[a] The initial model calculated by GaussView.

Table 3.32. Energy and conformer distribution of hydroxy-aryl adduct with six membered fused ring obtained from DFT calculations.

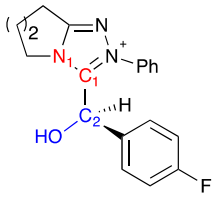

Γ(°)	$\Delta\Gamma$(°)	E_{diff} (kJ/mol)	p_i/p_j	Γ(°)	$\Delta\Gamma$(°)	E_{diff} (kJ/mol)	p_i/p_j
0.00	-50.45	12.928	0.005	50.45[a]	0.00	0.000	1.000
0.45	-50.00	12.842	0.006	55.45	5.00	0.191	0.926
5.45	-45.00	11.489	0.010	60.45	10.00	1.077	0.647
10.45	-40.00	10.655	0.014	70.45	20.00	3.961	0.202
20.45	-30.00	7.780	0.043	80.45	30.00	7.470	0.049
25.45	-25.00	5.881	0.093	90.45	40.00	2.504	0.364
30.45	-20.00	4.108	0.191	100.45	50.00	5.535	0.107
35.45	-15.00	2.142	0.421	110.45	60.00	10.000	0.018
40.45	-10.00	1.186	0.620	120.45	70.00	14.138	0.003
45.45	-5.00	0.224	0.914				

[a] The initial model calculated by GaussView.

Table 3.33. Energy and conformer distribution of hydroxy-aryl adduct with seven membered fused ring obtained from DFT calculations.

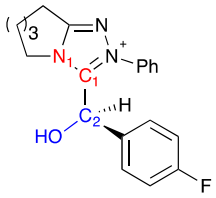

Γ(°)	$\Delta\Gamma$(°)	E_{diff} (kJ/mol)	p_i/p_j	Γ(°)	$\Delta\Gamma$(°)	E_{diff} (kJ/mol)	p_i/p_j
12.22	-40.00	10.536	0.014	52.22[a]	0.00	0.000	1.000
17.22	-35.00	9.110	0.025	57.22	5.00	0.478	0.825
22.22	-30.00	9.563	0.021	62.22	10.00	1.343	0.581
27.22	-25.00	9.118	0.025	72.22	20.00	5.165	0.124
32.22	-20.00	6.322	0.078	82.22	30.00	3.765	0.219
37.22	-15.00	3.702	0.224	92.22	40.00	6.592	0.070
42.22	-10.00	1.711	0.501	102.22	50.00	10.290	0.016
47.22	-5.00	0.456	0.832	112.22	60.00	14.798	0.003

[a] The initial model calculated by GaussView.

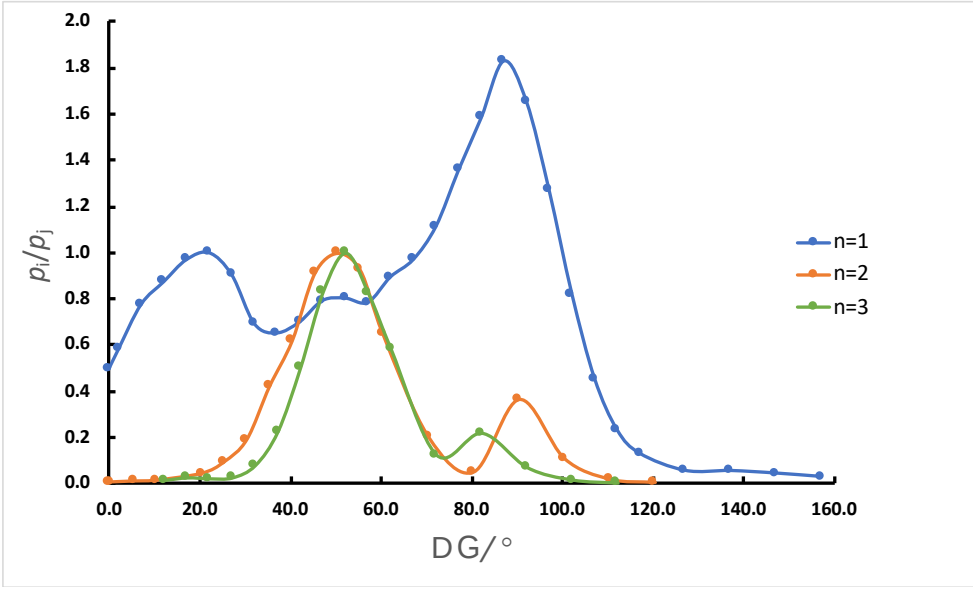

Figure 3.18. Boltzmann distribution of hydroxy-aryl adducts with different conformations.

The Boltzmann distribution suggest the population of adduct decreases quickly when the aldehydic moiety is rotated in piperidine and caprolactam systems (n=2 and 3), while

in pyrrole adduct (n=1), the changing of dihedral angle has less effect. This faster decreasing of adduct population with larger fused ring size suggest the increased fused ring size blocks the rotation of the hydroxy aryl adduct, and decreases the space to accommodate the aldehydic moiety. Meanwhile, since the rotation of C_1C_2 bond occurs much more freely in the adduct with n= 1 than in the adducts with n= 2 and 3, similar to the free catalyst, the entropic penalty is smaller in the systems with n= 1.

3.7.1.4. Impact of Fused Ring Size on Breslow intermediate Formation

Overall, an increase in fused ring size of triazolium salts largely decreased the rate constant of formation of the Breslow intermediate. The k_2 values of the system with n= 1 are up to 10-fold larger than the derivatives with 6-membered fused rings (n= 2). Most of the k_2 values with 7-membered fused ring sizes (n= 3) could not be obtained, as their values were too small to be reliable. Current data suggests the extra CH_2 group leads to a further ~50%-75% decrease in k_2 values versus n= 2.

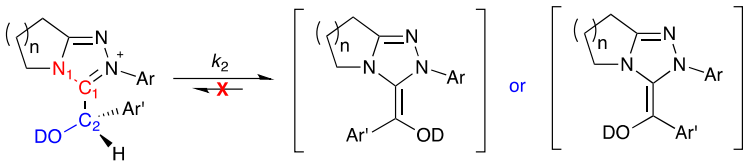

Scheme 3.13. Tetrahedral intermediate and Breslow intermediate.

This decreasing of k_2 ($k_2^{n=1} > k_2^{n=2} > k_2^{n=3}$) probably can be recognised as indirect evidence of the formation of Breslow intermediate. Compared to the tetrahedral intermediate **144**, the formation of the Breslow intermediate involves the formation of a carbon-carbon double bond, which forces the hydroxy group and the aldehydic aryl ring to be more co-planar with the triazolyl moiety (Scheme 3.13). As discussed in Section 3.7.1.3, the increment of fused ring size significantly limited the rotation of the aldehydic moiety. Taking the adduct with 7-membered fused ring as an example, the most

favorable conformation has the dihedral angle between N_1C_1 and C_2O equals to 52.2° (Table 3.33), while the formation of the Breslow intermediate requires this dihedral angle to be decreased to almost 0. On this basis, the Breslow formation rate constant should be suppressed with the increased fused ring size. Meanwhile, if the H/D-exchange process proceed without the formation of double bond, and the intermediate is more ylidic, the increased fused ring size would be predicted to have smaller influences on k_2.

3.7.2. Influences of Aryl-substituents on Aldehyde.

Previous research from our group suggested that both electron deficient *para*-aryl and *ortho*-aryl substituents on aldehyde increased the adduct formation rate constants[4, 25]. Remarkably, moving the *para*-methoxy group to the *ortho*-position on aldehyde, the hydroxy aryl adduct formation constants increased more than for methyl groups. This extra variation of reaction parameters (also have impacts on K and k_{-1}) could be potentially a result of the intramolecular hydrogen bond formation between the developing adduct OH and the *ortho*-substituent on aldehyde (Figure 3.19).

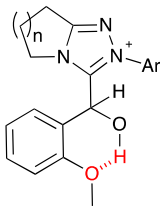

Figure 3.19. Proposed intramolecular hydrogen bond.

3.7.2.1. Reaction Parameter Comparison

To further investigate the influence of the aldehydic aryl-substituents, the relative reaction parameters of aldehyde **136-139** catalysed by triazolium **77-80**, **89-91**, **100, 101** compared to benzaldehyde **135** are listed in Table 3.34-3.37.

Table 3.34. Summary of relative reaction parameter ratios for the self-condensation of 2-methoxybenzaldehyde **138**, in the presence of triazolium precatalyst **77-80**, **89-91**, **100, 101**, in 0.107 M NEt_3 and 0.053 M NEt_3·HCl in methanol-d_4 at 25 °C.

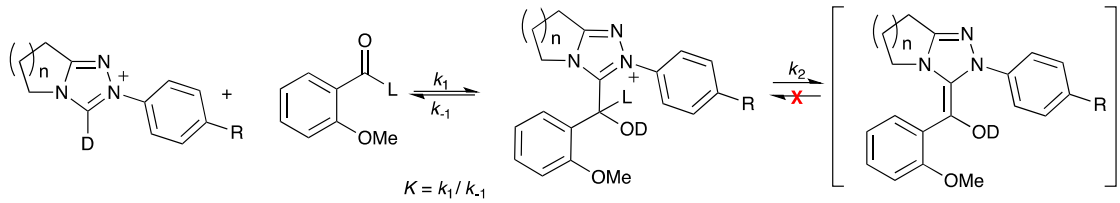

R=	n	k_1^{rel}	k_{-1}^{rel}	K^{rel}	k_2^{rel}
H	1	2.10	0.197	10.7	0.659
	2	2.42	0.182	13.3	5.09
	3	3.27	0.189	17.3	7.34
F	1	1.76	0.138	12.8	0.559
	2	2.11	0.135	15.6	0.960
	3	4.05	0.225	18.0	2.46
OMe	1	1.44	0.175	8.21	0.401
	2	1.88	0.145	13.0	*N.D.*[a]
	3	3.28	0.246	13.3	*N.D.*[a]

[a] Ratio cannot be determined due to the lack of the reaction parameter (Section 3.5-3.6)

Table 3.35. Summary of relative reaction parameter ratios for the self-condensation of 4-methoxybenzaldehyde **138**, in the presence of triazolium precatalyst **77-80**, **89-91**, **100, 101**, in 0.107 M NEt_3 and 0.053 M NEt_3·HCl in methanol-d_4 at 25 °C.

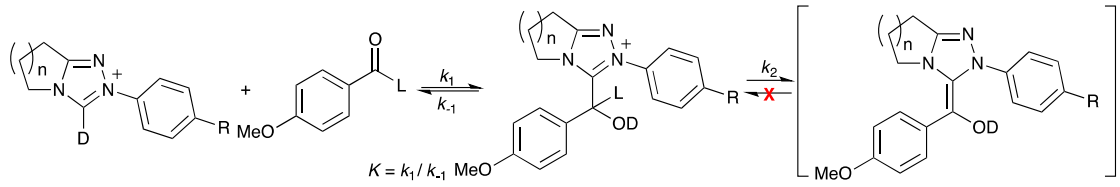

R=	n	k_1^{rel}	k_{-1}^{rel}	K^{rel}	k_2^{rel}
H	1	0.183	1.04	0.176	0.363
	2	*N.D.*[a]	*N.D.*[a]	0.131	*N.D.*[a]
	3	*N.D.*[a]	*N.D.*[a]	0.135	*N.D.*[a]
F	1	0.175	1.06	0.165	0.156
	2	0.198	1.46	0.135	0.0932
	3	*N.D.*[a]	*N.D.*[a]	0.206	*N.D.*[a]
OMe	1	0.194	1.42	0.137	0.0582
	2	0.183	1.43	0.129	*N.D.*[a]
	3	*N.D.*[a]	*N.D.*[a]	≈ 0.00686	*N.D.*[a]

[a] Ratio cannot be determined due to the lack of the reaction parameter (Section 3.5-3.6)

Table 3.36. Summary of relative reaction parameter ratios for the self-condensation of 2-methylbenzaldehyde **136**, in the presence of triazolium precatalyst **77-80**, **89-91**, **100, 101**, in 0.107 M NEt_3 and 0.053 M NEt_3·HCl in methanol-d_4 at 25 °C.

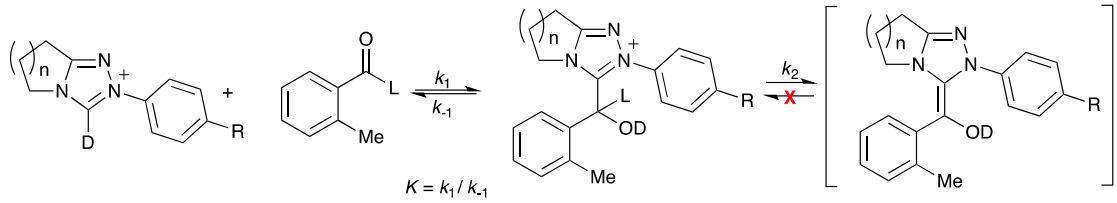

R=	n	k_1^{rel}	k_{-1}^{rel}	K^{rel}	k_2^{rel}
H	1	1.16	0.927	1.25	0.381
	2	1.54	1.93	0.802	2.32
	3	0.647	1.31	0.494	*N.D.*[a]
F	1	0.766	0.601	1.28	0.287
	2	1.14	1.29	0.884	0.192
	3	1.31	1.96	0.668	*N.D.*[a]
OMe	1	0.572	0.734	0.781	0.176
	2	0.993	1.46	0.681	*N.D.*[a]
	3	0.728	1.36	0.534	*N.D.*[a]

[a] Ratio cannot be determined due to the lack of the reaction parameter (Section 3.5-3.6)

Table 3.37. Summary of relative reaction parameter ratios for the self-condensation of 4-methoxybenzaldehyde **139**, in the presence of triazolium precatalyst **77-80**, **89-91**, **100, 101**, in 0.107 M NEt_3 and 0.053 M NEt_3·HCl in methanol-d_4 at 25 °C.

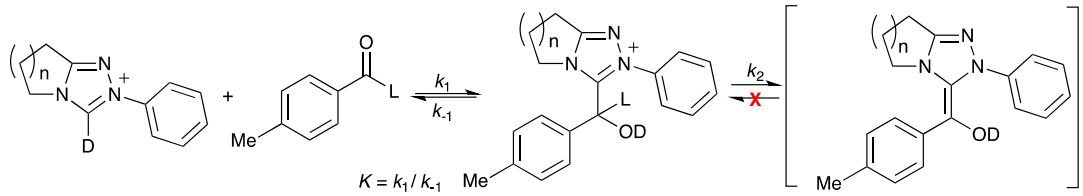

R=	n	k_1^{rel}	k_{-1}^{rel}	K^{rel}	k_2^{rel}
H	1	0.744	1.34	0.554	0.573
	2	0.958	1.77	0.542	0.282
	3	0.596	1.07	0.557	*N.D.*[a]
F	1	0.372	0.667	0.558	0.335
	2	0.459	0.961	0.476	0.206
	3	0.819	1.41	0.579	*N.D.*[a]
OMe	1	0.334	0.939	0.356	0.262
	2	0.598	1.20	0.499	*N.D.*[a]
	3	0.169	0.338	0.500	*N.D.*[a]

[a] Ratio cannot be determined due to the lack of the reaction parameter (Section 3.5-3.6)

Regardless of the triazolium backbone structures (fused ring size and aryl-substituent), electron donating *para*-aryl substituents on aldehyde decrease the adduct formation rate constants, k_1. Meanwhile, there is no simple conclusion about the influence of the aldehydic *para*-aryl substituents towards the variation trend of adduct dissociation rate constants (k_{-1}). However, the variation of k_{-1} are overall smaller than k_1, and the combined effects of k_1 and k_{-1} leads to the decrease in equilibrium constants (K) with more electron-donating *para*-aryl substituents on aldehyde. Meanwhile, the Breslow intermediate formation rate constant (k_2) also decreased with electron-donating *para*-substituents, and this difference gets larger with increased fused ring sizes.

The reaction parameters obtained from *ortho*-substituted aryl-aldehydes provides a larger range of values for adduct formation, dissociation and Breslow intermediate formation. The rate constant of adduct association (k_1) and the Breslow intermediate formation (k_2) of the *ortho*-substituted aldehydes decreased less or even increased compared with benzaldehyde **135**. In *ortho*-methoxybenzaldehyde **138** systems, the adduct dissociation constant (k_{-1}) decreased to around 20% of the value of benzaldehyde **135**, while the k_{-1} value of *ortho*-methylbenzaldehyde **138** is relatively comparable to benzaldehyde. The combined effect of adduct association and dissociation constants lead to the overall changes of equilibrium constants, K. These extra variations will be further discussed in Section 3.7.2.3.

3.7.2.2. Kinetic Analysis of Additional Reactions

Previous research only focused on limited aryl-substituted aldehydes, and the effects of *meta*-substituents have never been considered[3, 4, 25]. Our aim was to do a Hammett analysis of reaction data to obtain further insight into the aryl-substituent effect of aldehydes. This required additional data to that discussed in Section 3.5. Thus, reactions

with ranges of aldehydes **146-157** catalysed by phenyl triazolium **101** (n= 1) were studied (Figure 3.20). The NMR transient number, nt, was set to 8 to obtain more data points before the reaction reaches equilibrium. However, in the reaction of nitrophenyl aldehydes, and *ortho*-trifluoromethylphenyl aldehyde (**146-148, 150**), the aldehydes are too reactive to collect any data. The reaction parameters of *meta-, para*-trifluoromethylphenyl, and *ortho*-, *meta*-fluorophenyl aldehyde (**151, 152, 154, 155**) involve large errors, probably caused by the NMR peak overlap between aldehyde and its solvent adduct. The k_2 value of *para*-dimethyl(amino)benzaldehyde **157** could not be obtained because of the low concentration of adduct.

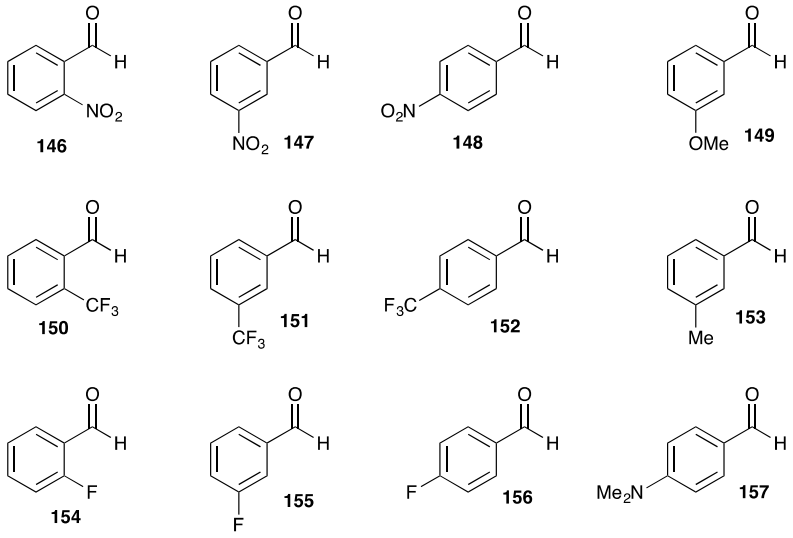

Figure 3.20. Range of additional aldehydes **146-157** used in kinetic evaluation

Table 3.38 summarises the aldehydes' f_{ald} values determined from the ratio of integrals of aldehyde and hemiacetal protons by using Equation 3.8. Table 3.39 summarises the reaction parameters of aldehyde **146-157** obtained from the kinetic profiles by using global fitting software Berkeley Madonna. Reaction parameters obtained from Equation 3.17 and 3.25, the initial concentration of catalysts and aldehydes, reaction concentration profiles, and the global fitting profiles are all included in Appendix.

Table 3.38. Fraction of aldehyde f_{ald} calculated from aldehyde **146-157**.

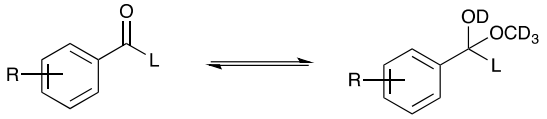

R=	f_{ald}	R=	f_{ald}
2-NO_2	*N.D.*[a]	2-F	0.569
3-NO_2	*N.D.*[a]	3-F	0.679
4-NO_2	*N.D.*[a]	4-F	0.908
2-CF_3	0.461	3-OMe	0.913
3-CF_3	0.547	3-Me	0.937
4-CF_3	0.456	4-NMe_2	0.100

[a] Various peaks observed, not be able to identify the proton signal belongs to hemiacetal.

Table 3.39. Summary of reaction parameters and reagent concentrations for the self-condensation of aldehydes **146-157**, in the presence of phenyl triazolium precatalyst **101**, in 0.108 M NEt_3 and 0.053 M NEt_3·HCl in methanol-d_4 at 25 °C.

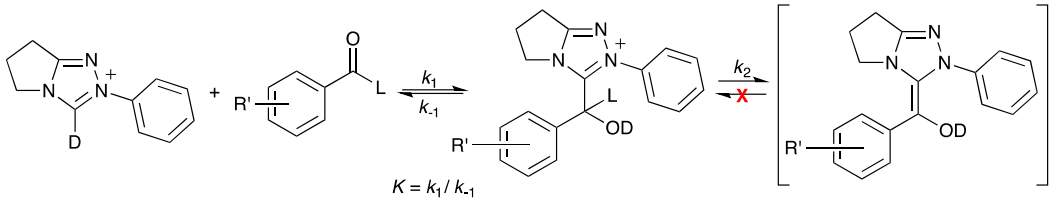

$K = k_1 / k_{-1}$

R=	k_1 ($M^{-1}s^{-1}$)	k_{-1} (s^{-1})	K (M^{-1})	k_2 (s^{-1})
3-CF_3	3.55×10^{-2}	1.66×10^{-3}	2.14×10^{1}	9.82×10^{-5}
4-CF_3	5.27×10^{-2}	1.11×10^{-3}	4.75×10^{1}	1.30×10^{-4}
2-F	7.08×10^{-2}	5.32×10^{-4}	1.33×10^{2}	8.47×10^{-5}
3-F	2.62×10^{-2}	1.26×10^{-3}	2.08×10^{1}	4.56×10^{-5}
4-F	1.28×10^{-2}	1.28×10^{-3}	9.96×10^{0}	1.13×10^{-5}
3-OMe	1.66×10^{-2}	1.08×10^{-3}	1.54×10^{1}	1.23×10^{-5}
3-Me	9.51×10^{-3}	6.60×10^{-4}	1.44×10^{1}	5.24×10^{-6}
4-NMe_2	2.60×10^{-4}	1.25×10^{-3}	2.05×10^{-1}	

Table 3.40 summarises the *meta*-, *para*-substituent constants, σ[26], and the logarithmic ratio of reaction parameters of all the *meta*-, *para*-substituents. The reaction parameters obtained from benzaldehyde **135** (k_1', k_{-1}', K', and k_2', obtained from Section 3.5-3.6) are used as references. The reaction constant, ρ, was obtained as the slope of the

semilogarithmic plot of the ratio of reaction parameters against substituent constant, σ (Equation 3.33). The semilogarithmic plots of the ratios of all four reaction parameters *versus* substituent constants are shown in Figure 3.21, and the summary of the reaction constants are shown in Table 3.41.

$$\log_{10}\left(\frac{k}{k'}\right) = \rho \times \sigma \qquad \textbf{Equation 3.33}$$

Table 3.40. Substituent constants and the logarithmic ratio of reaction parameters of substituents.

R=	σ	lg(k_1/k_1')	lg(k_{-1}/k_{-1}')	lg(K/K')	lg(k_2/k_2')
3-OMe	0.115	0.23	0.17	0.06	0.22
4-OMe	-0.268	-0.74	0.02	-0.75	-0.44
3-Me	-0.069	-0.02	-0.04	0.03	-0.15
4-Me	-0.17	-0.13	0.13	-0.26	-0.24
4-NMe_2	-0.83	-1.59	0.23	-1.82	*N.D.*[a]
3-CF_3	0.43	0.56	0.36	0.20	1.13
4-CF_3	0.54	0.73	0.18	0.55	1.25
3-F	0.34	0.42	0.24	0.19	0.79
4-F	0.06	0.11	0.24	-0.13	0.19

[a] k_2 value could not be calculated due to the small decrease of the concentration of protonated adduct.

Figure 3.21. Semilogarithmic plots of $\log_{10}(k/k')$ against substituent constant, σ, for the reaction of a range of substituted aryl-aldehyde **146-157** with phenyl triazolium **101** (n= 1).

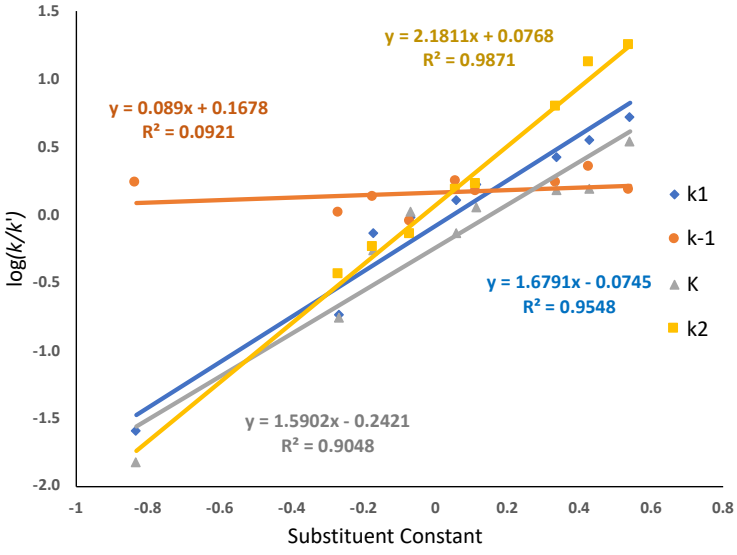

Table 3.41. Summary of the reaction constants, ρ, of each reaction parameters.

	k_1	k_{-1}	K	k_2
ρ	1.7	0.1	1.6	2.2

The positive reaction constants, ρ, suggest the hydroxy aryl adduct formation, and the Breslow intermediate formation steps can be accelerated by electron-withdrawing aryl-substituents of aldehyde. The positive slopes also suggest that there is an increase in electron density near the N-substituted aryl ring at the transition state (for correlations of k), or in the product (for correlation of K), relative to the reactant state.

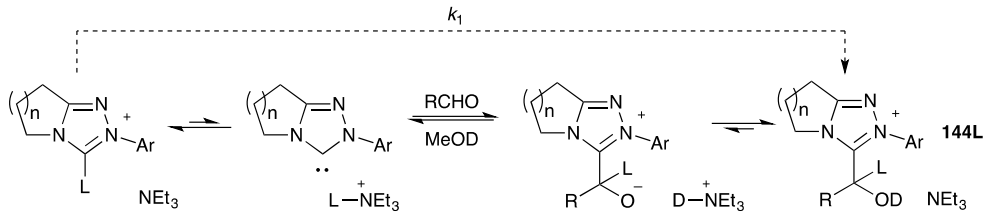

Scheme 3.14. Detailed mechanism of formation of adduct **144L**.

Within this project, the adduct formation steps are simplified, and a pseudo second order reaction model directly from triazolium **143** and aldehyde **142** to adduct **144** was used. Scheme 3.14 presents the original reaction mechanism, and triethylamine base is catalytically regenerated upon the formation of hydroxy aryl-adduct. The positive sign of the reaction constant suggests the rate limiting step of these processes to be the combination of carbene and aldehyde. This further supports our methodology to study the mechanism of adduct formation *via* the simplified model.

The reaction constant value obtained from k_{-1} suggests the adduct dissociation is non-sensitive towards the aldehydic aryl substituents. Previous crystal structures of hydroxy aryl-adducts obtained in our group confirmed the adducts' tetrahedral construction with the aldehydic aryl-moieties being twisted out of conjugation. Therefore, only inductive effects of aldehydic *para*-, and *meta*-aryl substituents towards adduct dissociation can

likely contribute.

3.7.2.3. Effects of *Ortho*-aryl Substituents

From previous research, *ortho*-substituents of aryl-aldehyde provide extra effects towards hydroxy aryl-adduct formation, dissociation and Breslow intermediate formation. To give a more direct comparison, reaction parameters obtained from *ortho*-substituted aldehyde are divided by the reaction parameters obtained from the corresponding *para*-substituted aldehydes ($k_1^{o/p}$, $k_{-1}^{o/p}$, $K^{o/p}$, and $k_2^{o/p}$). Table 3.42 summarises these reaction parameter ratios.

In methoxy aryl-aldehyde systems, regardless of fused ring sizes, changing substituents from *para* to *ortho* position increased the equilibrium constants, *K* ($K^{o/p}$= 59.7~1942). In most cases, larger differences are obtained with increased fused ring sizes ($K^{o/p,\ n=1} < K^{o/p,\ n=2} < K^{o/p,\ n=3}$). Although it is difficult to obtain the ratio of rate constants in systems with n= 2 and 3, the existing data suggests that changing the methoxy group from *para* to *ortho* position, increases the adduct association constant, k_1 ($k_1^{o/p}$= 7.41-11.5 fold), and decreases the adduct dissociation constant, k_{-1} ($k_{-1}^{o/p}$ = 10~20%). The Breslow intermediate formation rate, k_2, is 1.8-10.3 fold larger in *ortho*-methoxybenzaldehyde, and this difference typically gets larger with increased fused ring sizes ($k_2^{o/p,\ n=1} > k_2^{o/p,\ n=2}$).

Table 3.42. Summary of relative reaction parameter ratios for the self-condensation of aldehyde 136-139, in the presence of triazolium precatalyst 77-80, 89-91, 100, 101, in 0.107 M NEt3 and 0.053 M NEt3·HCl in methanol-d4 at 25 °C.

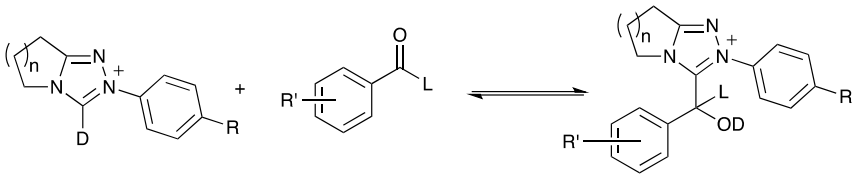

R=	R'=	n	$k_1^{o/p}$	$k_{-1}^{o/p}$	$K^{o/p}$	$k_2^{o/p}$
H	OMe	1	11.5	0.189	60.8	1.81
		2	*N.D.*[a]	*N.D.*[a]	102	*N.D.*[a]
		3	*N.D.*[a]	*N.D.*[a]	128	*N.D.*[a]
	Me	1	1.56	0.689	2.26	0.666
		2	1.61	1.09	1.48	8.25
		3	1.09	1.22	0.887	*N.D.*[a]
F	OMe	1	10.1	0.130	77.8	3.58
		2	10.6	0.0921	115	10.3
		3	*N.D.*[a]	*N.D.*[a]	87.5	*N.D.*[a]
	Me	1	2.06	0.902	2.29	0.855
		2	2.49	1.34	1.86	0.931
		3	1.60	1.38	1.15	*N.D.*[a]
OMe	OMe	1	7.41	0.124	59.7	6.90
		2	10.2	0.101	101	*N.D.*[a]
		3	*N.D.*[a]	*N.D.*[a]	1942	*N.D.*[a]
	Me	1	1.71	0.781	2.19	0.671
		2	1.66	1.22	1.36	*N.D.*[a]
		3	4.30	4.03	1.07	*N.D.*[a]

[a] Ratio cannot be achieved due to the lack of the reaction parameter (Section 3.5-3.6)

In methyl-substituted aldehydes, the k_1 values of *ortho*-methylbenzaldehyde are 10% to 4.3-fold larger than the *para*-methylbenzaldehyde. The k_{-1} obtained from triazolium with n= 1 (**101, 100, 89**) and *ortho*-methylbenzaldehyde **136** are all smaller than the *para*-methylbenzaldehyde, while in systems with n= 2 and 3, the k_{-1} of *para*-aldehyde are smaller than *ortho*-aldehyde. Overall, the $k_{-1}^{o/p}$ increased with larger fused ring size ($k_{-1}^{o/p,\ n=1} > k_{-1}^{o/p,\ n=2} > k_{-1}^{o/p,\ n=3}$). The equilibrium constant, *K*, of *ortho*-methylbenzaldehyde is larger than *para*-methylbenzaldehyde in most of the cases, and in contrast to the 2-

methoxybenzaldehyde case, the ratio of K decreased with larger fused ring size ($K^{o/p,\ n=1} < K^{o/p,\ n=2} < K^{o/p,\ n=3}$). Meanwhile, the Breslow intermediate formation rate, k_2, of *ortho*-substituted aldehyde is smaller than *para*-substituted aldehyde in most of the cases. The ratio of k_2 also gets larger with increased fused ring size.

Considering all the reaction parameter changing trends (Section 2.7.2.1 and this section), both the increment of fused ring size and steric occupancy on *ortho* position lead to extra variations. Notably, different aldehydic aryl substituents give different impacts. For instance, the k_1 values of *ortho*-methoxybenzaldehyde **138** have larger incremental changes compared to the methyl-substituted aldehyde, and larger sensitivity towards fused ring size. The k_{-1} values of *ortho*-methoxybenzaldehyde **138** decreased more, however, with less sensitivity towards fused ring size.

The variation of equilibrium constant, K, gives opposite trends in methoxy- and methyl-benzaldehyde. Theoretically, if only accounting for the electronic properties of the aldehydic aryl-substituents, both methyl- and methoxy-substituted aldehydes should have smaller K values compared to the benzaldehyde. Experimental data suggest that the K values of *ortho*-methylbenzaldehyde **136** are smaller as predicted in most of the cases, however, the *ortho*-methoxybenzaldehyde **138** gives opposite results. Meanwhile, the larger fused ring size clearly increased the variation of K in *ortho*-methoxybenzaldehyde, however, the larger fused ring size decreased the variation of K in *ortho*-methylbenzaldehyde.

For the *ortho-para* ratio of Breslow intermediate formation rate, $k_2^{o/p}$, *ortho*-methoxybenzaldehyde **138** has larger values than *ortho*-methylbenzaldehyde **136**, and the fused ring size impacts in both cases, while the *ortho*-methoxybenzaldehyde are more sensitive to fused ring size.

All the observations listed above suggest extra driving forces apart from electronic properties of aldehydic aryl-substituents. Our group previously suggested the intramolecular hydrogen bond formation between the adduct OH and the *ortho*-substituent on aldehyde could be a potential candidate to explain the observed effects. However, the observations of *ortho*-methylbenzaldehyde **136** cannot be explained by the presence of an intramolecular hydrogen bond. To further explore the underpinning origins of the substituent effects, Table 3.43 and 3.44 are used to illustrate and compare the reaction parameter ratios of fluoro-substituted-phenyl aldehyde **154** (*ortho*) and **156** (*para*). The fluorophenyl aldehydes were chosen because the fluorine group could potentially accept a hydrogen bond, while the steric occupancy of fluorine is relatively small. Table 3.43 presents the ratio of reaction parameters using benzaldehyde as reference (k_1^{rel}, k_{-1}^{rel}, K^{rel}, k_2^{rel}), while Table 3.44 presents the ratio between *ortho*- and *para*-substituted aldehyde ($k_1^{o/p}$, $k_{-1}^{o/p}$, $K^{o/p}$, and $k_2^{o/p}$).

Table 3.43. Summary of reaction parameter ratios for the self-condensation of aldehyde **138, 154, 136**, in the presence of phenyl triazolium precatalyst **101** in 0.107 M NEt_3 and 0.053 M NEt_3·HCl in methanol-d_4 at 25 °C.

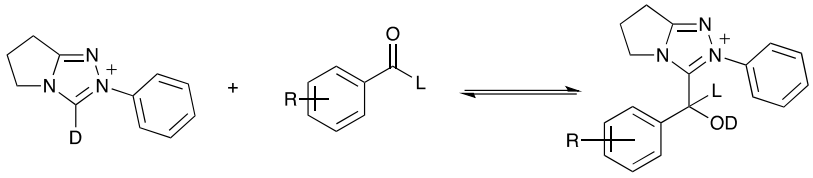

R=	k_1^{rel}	k_{-1}^{rel}	K^{rel}	k_2^{rel}
2-OMe	2.10	0.197	10.7	0.659
2-F	7.18	0.729	9.85	11.5
2-Me	1.16	0.927	1.25	0.381

Table 3.44. Summary of relative reaction parameter ratios for the self-condensation of aldehyde **136-139, 154, 156**, in the presence of phenyl triazolium precatalyst **101**, in 0.107 M NEt_3 and 0.053 M NEt_3·HCl in methanol-d_4 at 25 °C.

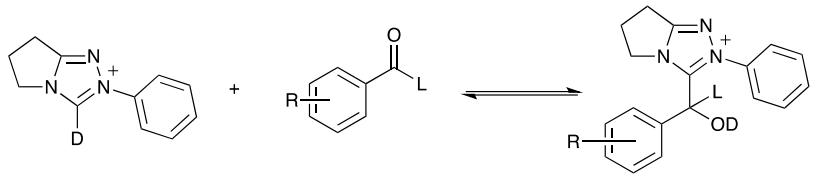

R=	$k_1^{o/p}$	$k_{-1}^{o/p}$	$K^{o/p}$	$k_2^{o/p}$
OMe	11.5	0.189	60.8	1.81
F	5.55	0.416	13.4	7.52
Me	1.56	0.689	2.26	0.666

Unfortunately, limited by the fast reaction speed and the large quantity of aldehydic hemiacetal adduct, the absolute values of reaction parameters of *ortho*-fluorophenyl aldehyde **154** involves errors, but the trends of reaction parameters are still reliable.

It is clear that compared to methyl substituents, the *ortho*-fluorophenyl aldehyde provides extra effects on reaction parameters. Considering the relatively small size of fluorine atom, the steric hindrance could only provide limited effects on adduct formation and dissociation, and all the extra effects should also owing to additional factors. Considering the sensitivity of fused ring size depends on different *ortho*-aldehydic substituents as discussed previously, the intramolecular hydrogen bond should be a reasonable candidate (Figure 3.22a).

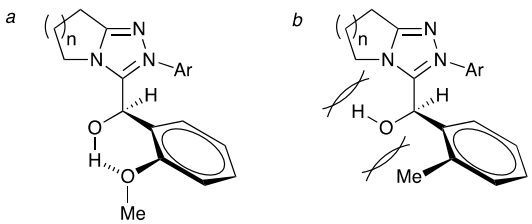

Figure 3.22. a. Intramolecular bond, b. intramolecular repulsion.

As illustrated above, the larger fused ring size increased the adduct formation rate

constants more in *ortho*-methoxybenzaldehyde. This could be owing to the increased fused ring size restricting the movement of the oxygen and hydrogen of the hydroxy group, thus favouring the formation of a hydrogen bond to the methoxy substituent and hence favouring adduct formation (Figure 3.22a). Therefore, the increased fused ring size largely increased the variation of k_1 in this case. For the adduct dissociation constant, as the methoxy group pulls the hydroxy group away from the fused ring, the increased steric hindrance caused by the extra CH_2 only has limited influences on the hydroxy group. Therefore, the k_{-1} variation trend of *ortho*-methoxybenzaldehyde is less sensitive.

In contrast, in the case of *ortho*-methylbenzaldehyde **136** (Figure 3.22b), the methyl group pushes the hydroxy group towards the fused ring, leading to the competition of repulsion between the steric hindrance provided by the fused ring and aldehydic methyl group. For adduct dissociation, the increased repulsion between fused ring and the aldehydic moiety of adduct forces the leaving of the aldehydic moiety, and leads to the larger incremental changes of k_{-1}.

3.7.3. Influences of Catalyst Aryl-substituents

Similar to aldehydic aryl-substituents, previous studies also suggest that the aryl-substituents of the catalysts influence the benzoin condensation reaction parameters[2-4, 25]. To further obtain insight, a Hammett analysis of these N-aryl substituent effects was conducted which required the determination of additional kinetic parameters for a more complete data set.

3.7.3.1. Reaction Parameters Obtained for Additional Reactions

Apart from the kinetic profile studied in Section 3.5.4, we investigated *ortho*- and *para*-methoxybenzaldehyde, and benzaldehyde **135, 138, 139** with the presence of 4-

trifluoromethylphenyl, 4-bromophenyl, and 3-chlorophenyl triazolium pre-catalysts **103-105** (Figure 3.23).

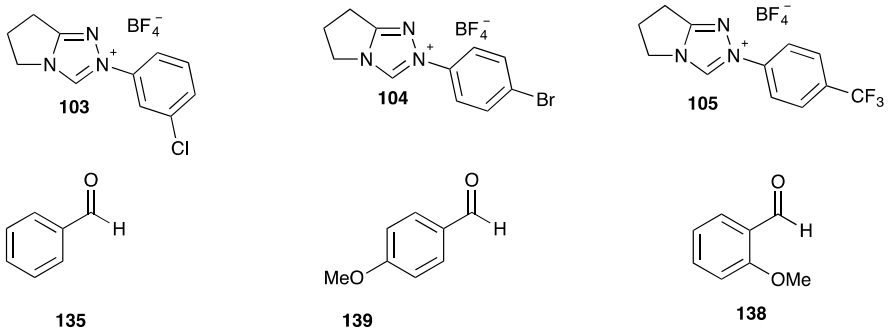

Figure 3.23. Aldehyde and triazolium salts used for linear free energy relationship analyses.

To obtain relatively accurate reaction parameters, the nine kinetic experiments were performed twice with NMR, transient number being set to 32 and 8. Table 3.45 summarises the reaction parameters of these experiments obtained from global fitting software Berkeley Madonna. The reaction parameters obtained by using Equation 3.17 and 3.25, the initial concentration of catalysts and aldehydes, the concentration profiles, and the global fitting profiles are all in Appendix.

Table 3.45. Summary of reaction parameters and reagent concentrations for the self-condensation of aldehyde **135, 138, 139**, in the presence of triazolium precatalyst **103-105**, in 0.108 M NEt_3 and 0.053 M NEt_3·HCl in methanol-d_4 at 25 °C.

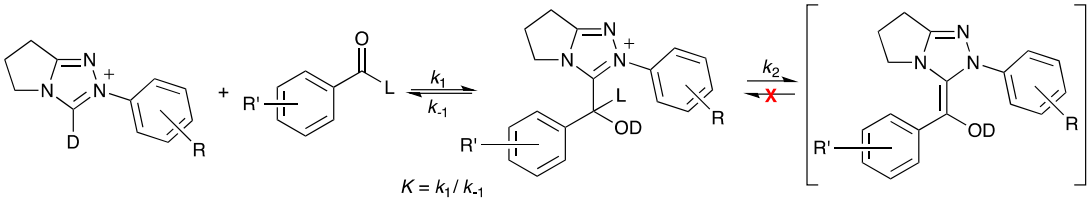

R=	R'=	nt=	k_1 ($M^{-1}s^{-1}$)	k_{-1} (s^{-1})	K (M^{-1})	k_2 (s^{-1})
4-Br	2-OMe	8	9.39×10^{-2}	6.07×10^{-4}	1.55×10^{2}	1.39×10^{-5}
		32	8.57×10^{-2}	6.06×10^{-4}	1.41×10^{2}	2.24×10^{-5}
	H	8	4.10×10^{-2}	2.91×10^{-3}	1.41×10^{1}	1.25×10^{-5}
		32	3.56×10^{-2}	1.93×10^{-3}	1.84×10^{1}	2.37×10^{-5}
	4-OMe	8	9.54×10^{-3}	3.85×10^{-3}	2.48×10^{0}	*N.D.*[a]
		32	5.62×10^{-3}	2.30×10^{-3}	2.44×10^{0}	2.75×10^{-6}
3-Cl	2-OMe	8	1.45×10^{-1}	8.44×10^{-4}	1.71×10^{2}	1.41×10^{-5}
		32	1.11×10^{-1}	9.00×10^{-4}	1.24×10^{2}	7.28×10^{-6}
	H	8	5.20×10^{-2}	3.67×10^{-3}	1.42×10^{1}	1.56×10^{-5}
		32	4.73×10^{-2}	4.00×10^{-3}	1.18×10^{1}	1.43×10^{-5}
	4-OMe	8	1.23×10^{-2}	5.44×10^{-3}	2.26×10^{0}	*N.D.*[a]
		32	2.25×10^{-2}	2.80×10^{-3}	8.04×10^{0}	2.04×10^{-6}
4-CF_3	2-OMe	8	2.21×10^{-1}	1.61×10^{-3}	1.37×10^{2}	3.23×10^{-5}
		32	1.34×10^{1}	9.22×10^{-2}	1.45×10^{2}	3.22×10^{-5}
	H	8	9.03×10^{-2}	8.24×10^{-3}	1.10×10^{1}	2.75×10^{-5}
		32	1.11×10^{-1}	9.00×10^{-3}	1.24×10^{1}	7.28×10^{-6}
	4-OMe	8	1.28×10^{-2}	8.36×10^{-3}	1.53×10^{0}	2.91×10^{-6}
		32	4.82×10^{0}	2.42×10^{0}	2.00×10^{0}	3.64×10^{-6}

[a] k_2 value are not be able to obtain because of too small variation of protonated adduct

Previous research in our group suggests that the *ortho*-substituents on catalyst aryl ring dramatically increase the k_1 and K values. The *ortho*-substituents on triazolium aryl rings force the aryl group out of plane with the central triazole thereby allowing easier accommodation of the hydroxy aryl moiety. To check if the further extension of steric hindrance of triazolium aryl *ortho*-position, and the increased fused ring size will change the influence of the *ortho*-substituents, kinetic reactions of *ortho*-, *para*-methoxybenzaldehyde, and benzaldehyde **135, 138, 139** catalysed by triisopropylphenyl

triazolium **88** (n= 1) and mesityl triazolium **85** (n= 1) were performed (Figure 3.24).

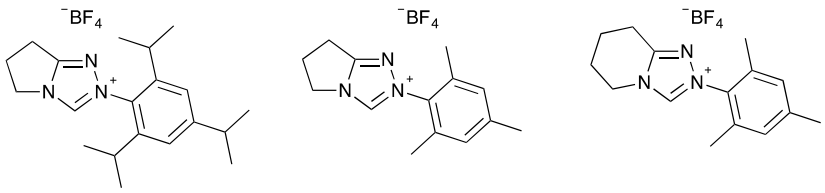

Figure 3.24. Triazoliums used for investigate the influence of catalysts' *ortho*-substituents

Table 3.46 summarises the reaction parameters of these experiments obtained from global fitting software Berkeley Madonna. The reaction parameters of pyrrole mesityl triazolium **85** (n= 1) obtained by Peter Quinn are also included inside Table 3.46 for more direct comparison. The reaction parameters obtained in this project by using Equation 3.17 and 3.25, the initial concentration of catalysts and aldehydes, the concentration profiles, and the global fitting profiles are all in Appendix.

Table 3.46. Summary of reaction parameters and reagent concentrations for the self-condensation of aldehyde **135, 138, 139**, in the presence of triazolium precatalyst **85, 86, 88**, in 0.108 M NEt_3 and 0.053 M NEt_3·HCl in methanol-d_4 at 25 °C.

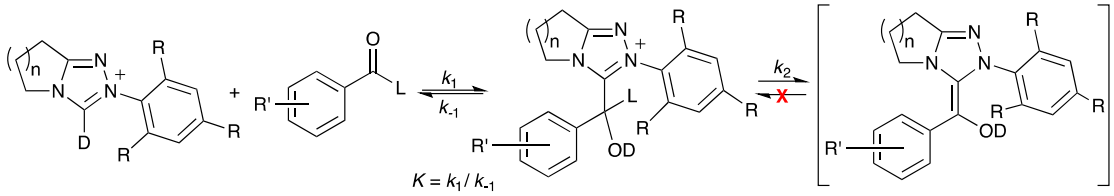

R=	n=	R'=	k_1 ($M^{-1}s^{-1}$)	k_{-1} (s^{-1})	K (M^{-1})	k_2 (s^{-1})
		2-OMe	1.23×10^{-2}	3.14×10^{-5}	3.92×10^{2}	5.65×10^{-7}
Me[a]	1	H	9.32×10^{-3}	7.21×10^{-5}	1.29×10^{2}	3.53×10^{-6}
		4-OMe	2.04×10^{-3}	8.94×10^{-5}	2.28×10^{1}	2.01×10^{-6}
		2-OMe	2.04×10^{-2}	1.81×10^{-5}	1.13×10^{3}	4.14×10^{-7}
^{i}Pr	1	H	1.49×10^{-2}	1.15×10^{-4}	1.29×10^{2}	5.27×10^{-6}
		4-OMe	3.01×10^{-3}	1.42×10^{-4}	2.11×10^{1}	1.55×10^{-6}
		2-OMe	1.13×10^{-2}	5.60×10^{-5}	2.01×10^{2}	6.76×10^{-7}
Me	2	H	7.58×10^{-3}	3.64×10^{-4}	2.08×10^{1}	2.91×10^{-6}
		4-OMe	1.52×10^{-3}	4.93×10^{-4}	3.29×10^{0}	6.76×10^{-7}

[a]Reaction parameters obtained by Peter Quinn

3.7.3.2. N-(*para*-aryl) Triazolium Substituent Effects and Hammett Analysis

To give a more direct view of the influence of the catalyst substituent effect, the relative reaction rate or equilibrium constants of aldehyde **135- 139** catalysed by triazolium **89, 100, 103-105** divided by the corresponding values of the relevant phenyl triazolium **101, 79, 80** (n= 1- 3) are listed in Table 3.47-3.51 (calculated using the data reported in Table 3.2-3.14).

Table 3.47. Summary of relative reaction parameter ratios for the self-condensation of 2-methoxybenzaldehyde **138**, in the presence of triazolium precatalyst **89, 100, 103-105**, in 0.107 M NEt_3 and 0.053 M NEt_3·HCl in methanol-d_4 at 25 °C.

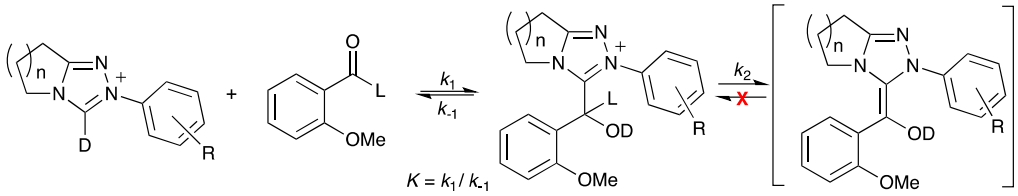

R=	n	$k_1^{R/H}$	$k_{-1}^{R/H}$	$K^{R/H}$	$k_2^{R/H}$
4-F	1	2.49	1.56	1.60	2.42
	2	2.49	1.65	1.51	2.74
	3	1.16	0.990	1.17	5.43
4-OMe	1	0.652	0.421	1.55	0.684
	2	0.764	0.424	1.80	0.446
	3	0.499	0.318	1.57	2.40
4-Br	1	4.53	4.24	1.07	2.87
4-CF_3	1	10.7	11.3	0.949	6.66
3-Cl	1	6.98	5.90	1.18	2.92

Table 3.48. Summary of relative reaction parameter ratios for the self-condensation of 4-methoxybenzaldehyde **139**, in the presence of triazolium precatalyst **89, 100, 103-105**, in 0.107 M NEt_3 and 0.053 M NEt_3·HCl in methanol-d_4 at 25 °C.

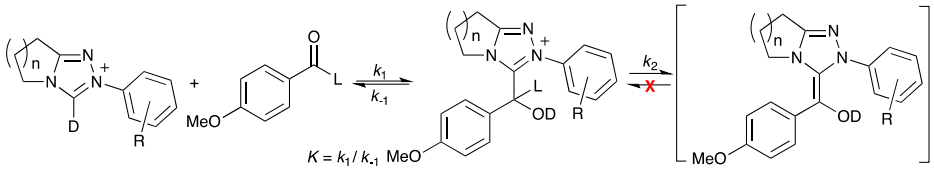

R=	n	$k_1^{R/H}$	$k_{-1}^{R/H}$	$K^{R/H}$	$k_2^{R/H}$
4-F	1	2.83	2.28	1.25	1.23
	2	*N.D.*[a]	*N.D.*[a]	2.10	*N.D.*[b]
	3	*N.D.*[a]	*N.D.*[a]	1.60	*N.D.*[b]
4-OMe	1	1.03	0.710	1.45	0.180
	2	*N.D.*[a]	*N.D.*[a]	1.82	*N.D.*[b]
	3	*N.D.*[a]	*N.D.*[a]	0.0962	*N.D.*[b]
4-Br	1	5.30	5.09	1.04	1.03
4-CF_3	1	7.12	11.1	0.644	1.09
3-Cl	1	6.83	7.20	0.949	0.764

[a] Value could not be obtained owing to limited data points collected during pre-equilibrium state.

[b] Value could not be obtained because of too small variation of protonated adduct.

Table 3.49. Summary of relative reaction parameter ratios for the self-condensation of benzaldehyde **135**, in the presence of triazolium precatalyst **89, 100, 103-105**, in 0.107 M NEt_3 and 0.053 M NEt_3·HCl in methanol-d_4 at 25 °C.

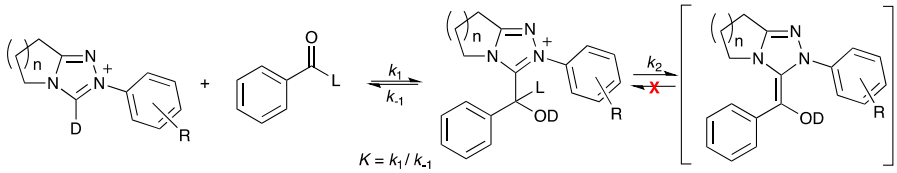

R=	n	$k_1^{R/H}$	$k_{-1}^{R/H}$	$K^{R/H}$	$k_2^{R/H}$
4-F	1	2.96	2.22	1.33	2.86
	2	2.86	2.22	1.29	14.5
	3	1.08	1.03	1.05	16.2
4-OMe	1	0.967	0.519	1.86	1.12
	2	0.988	0.533	1.85	*N.D.*[a]
	3	0.571	0.302	1.89	4.22
4-Br	1	4.16	3.99	1.04	1.70
4-CF_3	1	9.16	11.3	0.812	3.74
3-Cl	1	5.27	5.03	1.05	2.13

[a] Value could not be obtained because of too small variation of protonated adduct.

Table 3.50. Summary of relative reaction parameters' ratios for the self-condensation of 2-methylbenzaldehyde **136**, in the presence of triazolium precatalyst **89, 100, 103-105**, in 0.107 M NEt_3 and 0.053 M NEt_3·HCl in methanol-d_4 at 25 °C.

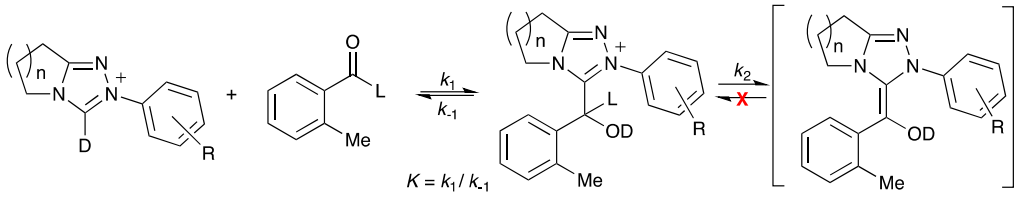

R=	n	$k_1^{R/H}$	$k_{-1}^{R/H}$	$K^{R/H}$	$k_2^{R/H}$
4-F	1	1.95	1.44	1.36	2.15
	2	1.60	1.01	1.59	1.20
	3	2.63	2.19	1.21	*N.D.*[a]
4-OMe	1	0.476	0.411	1.16	0.517
	2	0.635	0.403	1.57	*N.D.*[a]
	3	0.779	0.448	1.74	*N.D.*[a]

[a] Value could not be obtained because of too small variation of protonated adduct.

Table 3.51. Summary of relative reaction parameters' ratios for the self-condensation of 4-methylbenzaldehyde **137**, in the presence of triazolium precatalyst **89, 100, 103-105**, in 0.107 M NEt_3 and 0.053 M NEt_3·HCl in methanol-d_4 at 25 °C.

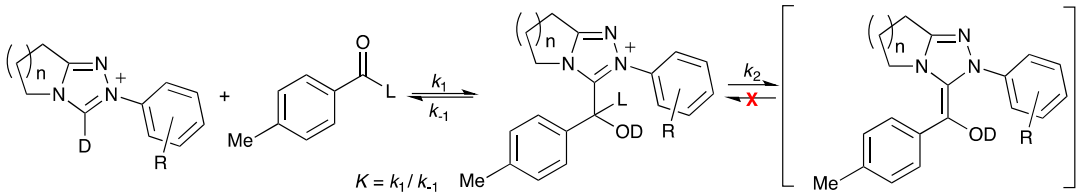

R=	n	$k_1^{R/H}$	$k_{-1}^{R/H}$	$K^{R/H}$	$k_2^{R/H}$
4-F	1	1.48	1.10	1.34	1.67
	2	1.77	1.46	1.21	10.6
	3	1.53	1.36	1.12	2.60
4-OMe	1	0.433	0.363	1.19	0.513
	2	0.618	0.361	1.71	2.58
	3	0.168	0.0959	1.75	*N.D.*[a]

[a] Value could not be obtained because of too small variation of protonated adduct.

Our data suggests that the electron-withdrawing N-aryl substituents (R) accelerate both the adduct association and dissociation rate constants irrespective of ring size. Equation 3.33 is applied to probe the linear free energy relationship between the catalyst aryl-substituents and the σ reaction parameter. As a representative example, Table 3.52

summarises the *meta*- and *para*-substituent constants, σ, and the logarithmic ratio of reaction parameters of 2-methoxybenzaldehyde **138** catalysed by a range of triazolium salts **89, 100, 103-105**. The reaction parameters obtained from phenyl triazolium with a 5-membered fused ring **101** (k_1^H, k_{-1}^H, K^H, and k_2^H) are used as reference values. Tables for other aldehydes are concluded in Appendix. The reaction constant, ρ, was obtained as the slope of the semilogarithmic plot of ratio of reaction parameters against substituent constant, σ (Equation 3.33). Three representative semilogarithmic plots of ratios reaction parameters sets *versus* substituent constants are shown in Figure 3.25-3.27. Meanwhile, the semilogarithmic plots of the Breslow intermediate formation rate, k_2, yield an interesting curve but not straight lines, thus their semilogarithmic plots are shown in Figure 3.28, with no approximate reaction constants or ρ values suggested.

$$\log_{10}\left(\frac{k}{k'}\right) = \rho \times \sigma \qquad \textbf{Equation 3.33}$$

Table 3.52. Substituent constants and the logarithmic ratio of reaction parameters of 2-methoxybenzaldehyde **138** in the presence of triazolium **89, 100, 103-105**.

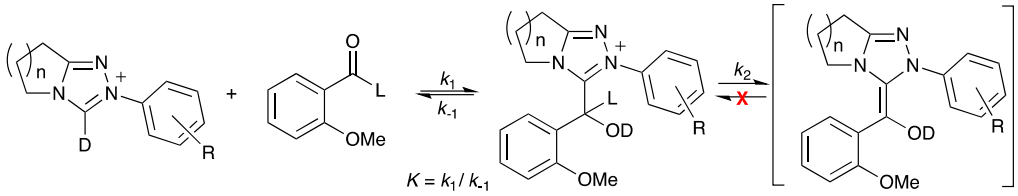

R=	σ	lg(k_1/k_1^H)	lg(k_{-1}/k_{-1}^H)	lg(K/K^H)
4-OMe	-0.268	-0.186	-0.375	0.190
4-F	0.062	0.396	0.193	0.203
4-Br	0.232	0.656	0.628	0.029
3-Cl	0.373	0.844	0.771	0.073
4-CF_3	0.54	1.029	1.051	-0.023

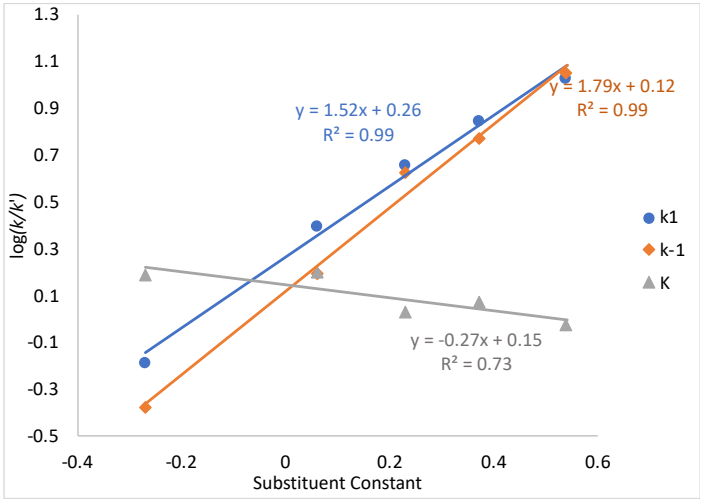

Figure 3.25. Semilogarithmic plots of $\log_{10}(k/k^{H})$ against substituent constant, σ, for the reaction of *ortho*-methoxybenzaldehyde **138** with triazolium salts with five-membered fused ring **89, 100, 103-105** (n= 1).

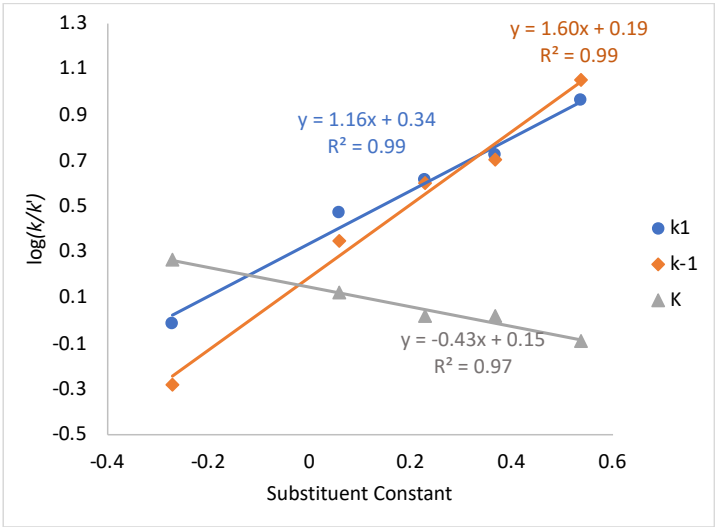

Figure 3.26. Semilogarithmic plots of $\log_{10}(k/k^{H})$ against substituent constant, σ, for the reaction of benzaldehyde **135** with triazolium salt with five-membered fused ring **89, 100, 103-105** (n= 1).

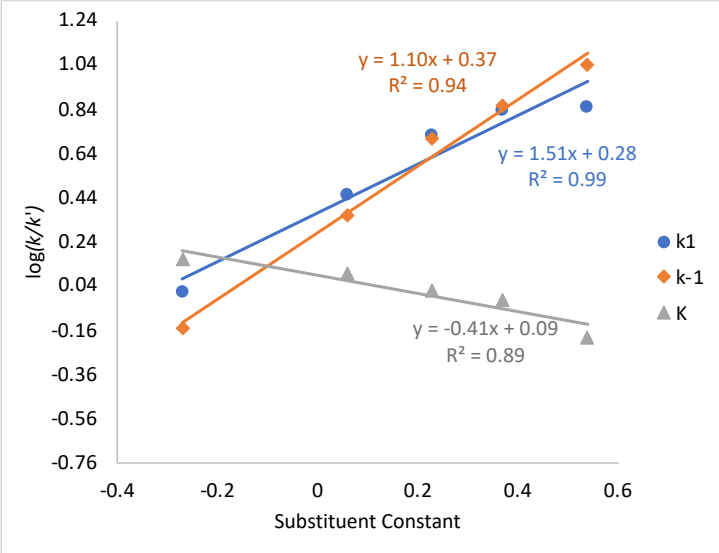

Figure 3.27. Semilogarithmic plots of $\log_{10}(k/k^{H})$ against substituent constant, σ, for the reaction of *para*-methoxybenzaldehyde **139** with triazolium salt with five-membered fused ring **89, 100, 103-105** (n= 1).

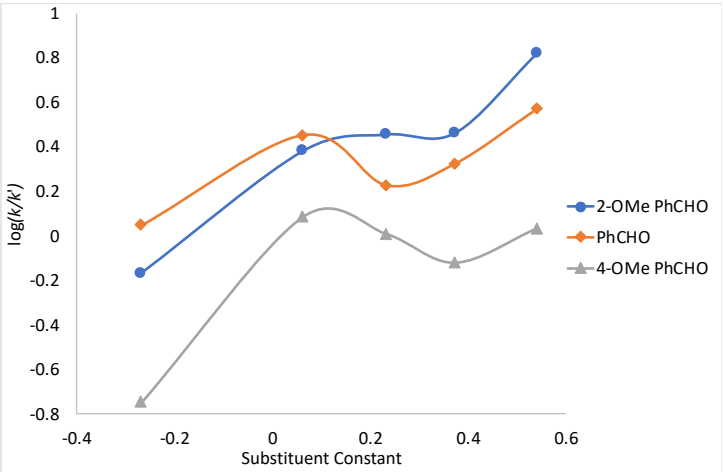

Figure 3.28. Semilogarithmic plots of $\log_{10}(k_2/k_2^{H})$ against substituent constant, σ, for the reaction of aldehyde **135, 138, 139** catalysed by triazolium salt with five-membered fused ring **89, 100, 103-105** (n= 1)

Due to the difficulty of triazolium syntheses, some kinetic analyses of triazolium salts with 6- and 7-membered fused rings (n= 2 and 3) could not be performed. Thus, reaction constants, ρ, for certain reactions can only be calculated from two data points. These reaction constant values, and their semilogarithmic plots are summarized in Appendix.

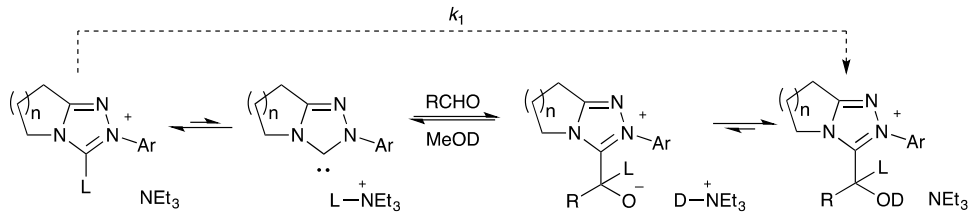

Scheme 3.15. Detailed mechanism of formation of adduct **144**.

As introduced in Section 3.7.2.3, the k_1 value we observe is a combination of three individual processes, and should equal the product of the equilibrium constant of carbene formation and the rate constant of formation of alkoxide. Thus, the influence of electron-withdrawing catalyst aryl-substituents should be divided into two parts: the increased equilibrium constant of carbene formation which is favoured by electron withdrawing substituents, and the reduced nucleophilicity of the carbene likely decreasing the rate constant for addition to form alkoxide. Overall N-aryl electron withdrawing substituents increase k_1 thus the substituent effect on the first pre-equilibrium must dominate. In the reverse direction, the k_{-1} value we observe is the product of the equilibrium constant of O-deprotonation of adduct and the rate constant of loss of NHC from alkoxide. Both of these processes will be favoured by N-aryl electron withdrawing substituents explaining the positive ρ-value also observed for k_{-1}.

In all the cases, the reaction constants of K are substantially smaller than 1, which suggest the combined effect of variation of k_1 and k_{-1} leads to the position of equilibrium being relatively independent with the catalyst aryl substituents compared to the aldehydic aryl substituents.

3.7.3.3. *Ortho*-substituent Effect

As introduced in Section 3.7.3.1, *ortho*-aryl substituents of catalyst dramatically change the catalytic performance. To further investigate this, benzoin condensation reactions of aldehyde **135, 138, 139** catalysed by triazolium **85, 86, 88** were performed. Table 3.53

summarises the relative reaction parameters of these reactions, which used the corresponding reaction parameters of phenyl triazolium **101** (n= 1) as references. Table 3.54 summarises the relative reaction parameters of aldehyde **135, 138, 139** catalysed by mesityl triazolium salt with 5-membered fused ring **85** (n= 1) divided by mesityl triazolium salt with 6-membered fused ring **86**.

Table 3.53. Summary of relative reaction parameters for the self-condensation of aldehyde **135, 138, 139**, in the presence of triazolium precatalyst **85, 86**, in 0.107 M NEt_3 and 0.053 M NEt_3·HCl in methanol-d4 at 25 °C.

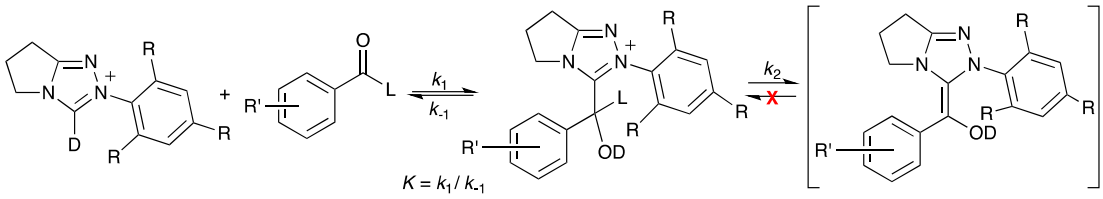

R=	R'=	$k_1^{R/H}$	$k_{-1}^{R/H}$	$K^{R/H}$	$k_2^{R/H}$
Me	2-OMe	0.594	0.219	2.71	0.117
	H	0.945	0.0988	9.56	0.480
	4-OMe	1.13	0.118	9.58	0.753
^{i}Pr	2-OMe	0.986	0.126	7.80	0.0855
	H	1.50	0.157	9.56	0.717
	4-OMe	1.67	0.189	8.85	0.579

Table 3.54. Summary of relative reaction parameters for the self-condensation of aldehyde **135, 138, 139**, in the presence of triazolium precatalyst **85, 86**, in 0.107 M NEt_3 and 0.053 M NEt_3·HCl in methanol-d_4 at 25 °C.

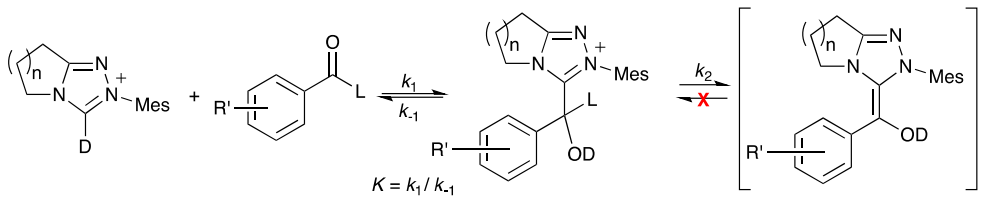

R'=	$k_1^{n=1/n=2}$	$k_{-1}^{n=1/n=2}$	$K^{n=1/n=2}$	$k_2^{n=1/n=2}$
2-OMe	1.09	0.561	1.95	0.836
H	1.23	0.198	6.20	1.21
4-OMe	1.34	0.181	7.39	3.80

Compared to the N-phenyl triazolium salt with n= 1 (**101**), the mesityl triazolium salt

(n= 1, **85**) has comparable k_1 values in case of benzaldehyde and 4-methoxybenzaldehyde, while the $k_1^{R/H} = 0.59$ in the reaction of 2-methoxybenzaldehyde **138**. In contrast, the triisopropyl triazolium salt (n= 1, **88**) gives comparable k_1 values for 2-methoxybenzaldehyde, however, this k_1 values are 1.50- and 1.67-folds higher in case of the benzaldehyde and 4-methoxybenzaldehyde.

This variation of the adduct association constant could be owing to the steric hindrance of the combined effect of the *ortho*-substituents on aldehyde and triazoliums. The steric hindrance of catalytic *ortho*-aryl substituents has the potential to force the aryl ring perpendicular to the triazolyl centre to provide a better accommodation for the aldehydic moiety during the development of the adduct formation. However, the steric hindrance provided by mesityl group is smaller than the isopropyl group, and is not enough to fix the triazolium to a relatively rigid conformation. In other words, there is still relatively free rotation of the mesityl group, whereas the isopropylphenyl group is more rigid and perpendicular to the triazolyl centre.

As introduced in section 3.7.2.3, the *ortho*-methoxy aldehydic group could possibly form an intramolecular hydrogen bond during the formation of adduct (Section 3.7.2, Figure 3.19), which limits the rotation of the aldehydic aryl ring. The extra steric hindrance provided by the *ortho*-substituents of the triazolium then has a larger possibility to impede the approach of the aldehydic moiety than the cases without the intramolecular hydrogen bonds. Therefore, the relative $k_1^{R/H}$ values of *ortho*-methoxybenzaldehyde catalysed by mesityl and triisopropylphenyl triazoliums are smaller than the reactions of benzaldehyde and *para*-methoxybenzaldehyde. Meanwhile, the relatively rigid structure of triisopropyl phenyl triazolium **88** limits the rotation of the aryl ring, and limits the impeding effects towards the aldehyde.

The comparison of the reaction parameters between aldehydic substituents could also

improve this. In the case of triazolium salts with 5-membered fused rings **85**, **88**, **101**, changing methoxy group from *para*-position to *ortho* on aldehyde increased the k_1 values by 10-fold for mesityl triazolium salt **85**, 6-fold for phenyl triazolium salt **101**, and 6.8-fold for triisopropylphenyl triazolium salt **88**. Clearly, *ortho*-substituents on both catalyst and aldehyde have extra effects on adduct formation.

Influenced also by the better accommodation of aldehydic moiety caused by the perpendicular conformation between aryl and triazolyl ring of triazolium, all the dissociation constants of mesityl- and triisopropyl-triazoliums decreased to 10-20% of phenyl triazolium. The equilibrium constants of *para*-substituted aldehydes increased by 9-fold, while the reaction of *ortho*-methoxybenzaldehyde catalysed by mesityl triazolium salt only increased 2.7-fold, and 7.8-fold in the triisopropylphenyl case. Meanwhile, the rate constants of formation of the Breslow intermediate are decreased for *ortho*-substituted triazoliums, probably caused by the extra steric hindrance and the donating electronic properties of the substituents of triazoliums.

3.8. Summary

The benzoin condensation of various aldehydes catalysed by NHCs was studied at 25 °C in triethylamine-buffered methanol-d_4 solutions. The formation and consumption of reactants, and intermediates and products were probed by ^{1}H NMR spectroscopy *in situ*. The formation and decomposition rate constants, equilibrium constants of the hydroxy aryl adduct **144** were determined by using three parallel methods from the concentration profiles. The structural data obtained from single X-ray crystallography and computer modelling (DFT) were also analysed.

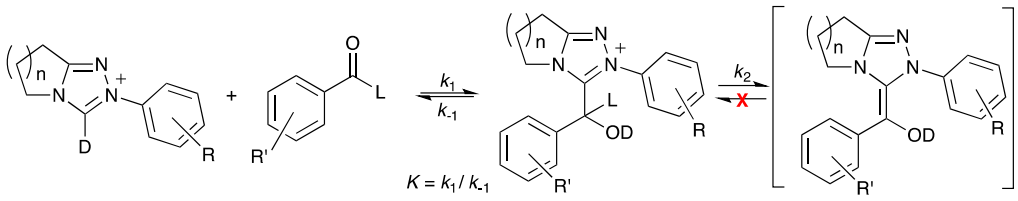

Three aspects (fused ring size of catalyst, aryl-substitution variation of catalyst, and aryl-substitution variation of aldehyde) which influence the reaction parameters (k_1, k_{-1}, K, k_2) of the formation and consumption of hydroxy aryl adduct were investigated.

Increasing fused ring size from 5 (n= 1) to 6 (n= 2) largely decreased the adduct formation rate constants ($k_1^{n=1/n=2}$ = 4.2-7.8 fold), while the k_1 values for n= 2 and 3 are comparable ($k_1^{n=2/n=3}$ = 1.1-2.9 fold). Opposite trends for the adduct dissociation constants (k_{-1}) can be observed ($k_{-1}^{n=1/n=2}$ = 0.42-0.97 fold, $k_{-1}^{n=2/n=3}$ = 0.33-0.74 fold). The combined variation of k_1 and k_{-1} lead to the overall equilibrium constants decreasing in the order $K^{n=1} >> K^{n=2} > K^{n=3}$ ($K^{n=1/n=2}$ = 5.4-13.3 fold, $K^{n=2/n=3}$ = 2.5-5.3 fold). By analysing the existing crystal structures of triazolium salts with different fused ring sizes, the first structural based explanation towards the catalyst performance could be suggested. We postulated that the relatively small steric occupancy of the 5-membered fused ring (n= 1) compared to the 6- (n= 2) and 7-membered fused ring (n= 3) may facilitate the formation of the hydroxy aryl adduct **144** due to the better accommodation of the hydroxy aryl moiety. The following DFT modelling also support this postulation.

Results from DFT calculation suggest that the incremental CH_2 addition does not change the conformational flexibility of the fused ring of triazolium salt. Flipping of the 7-membered fused ring is however closer to the reaction centre, which provides largest steric hindrance towards the reaction center than 5- and 6-membered fused ring. Meanwhile, the altered behavior of ring flipping in hydroxy aryl adduct with 7-membered fused ring could only be a result of the steric occupancy of the aldehydic moiety of adducts. Moreover, the rotation of aldehydic moiety of adduct occurs more

freely in adduct with 5-membered fused ring than 6- and 7-membered analogues, thus, with larger space to accommodate the aldehydic moiety.

The formation rate constants of Breslow intermediate (k_2) largely decreased with the increment of fused ring size[I]. This can be interpreted as indirect evidence of the formation of a Breslow-type intermediate as the larger steric hindrance provided by larger fused rings impede the planarization required for double bond formation.

Regardless of the triazolium salt backbone structures (fused ring size and aryl-substituent), electron donating *para*-aryl substituents on aldehyde decrease the adduct formation rate constant, k_1, the equilibrium constant, K, and the formation rate constant of Breslow intermediate, k_2. Further Hammett analysis of the reaction data also support these general trends. The positive reaction constants, σ, for all three parameters, suggest the increased electron density near the N-substituted aryl ring at the transition state, or in the product, relative to the reactant state, which is favoured by electron withdrawing substituents on aldehyde. Meanwhile, no simple rules can explain the trends observed for the dissociation constant, k_{-1}.

The *ortho*-substituents of aryl-aldehyde were shown to exhibit extra effects in addition to normal electronic properties towards the reaction parameters, with the natural of the o-substituent effect also related to the different aldehydic aryl substituents. We suggest intramolecular hydrogen bond formation and steric hindrance provided by *ortho*-aryl aldehydic substituents as two crucial factors.

We also performed a Hammett linear free energy analysis of the catalyst *para*-/*meta*-N-

---

[I] Limited data obtained due to the small values of k_2 being observed, thus, the variation range of k_2 was not state here.

aryl-substituents and the reaction parameters. Our data suggest that, regardless of the fused ring size of triazolium salts, the electron-withdrawing N-aryl substituents accelerate both the adduct association and dissociation rate constants (positive □-values). Meanwhile, the □ values of the equilibrium constants *K* are substantially smaller than 1, which suggest the position of equilibrium being relatively independent on the catalyst aryl substituents. Moreover, the Hammett analyses of k_2 show non-linear relationships.

Finally, the *ortho*-aryl-substituents of triazolium salts impede the approach of the aldehydic moiety towards catalyst, with extra impact on *ortho*-aryl substituted aldehydes. Thus, a decrease of adduct formation rate constant should be expected. Meanwhile, we also suggest the extra steric hindrance provided by *ortho*-aryl substituents force the aryl ring perpendicular to the triazolyl centre to provide a better accommodation for the aldehydic moiety during the development of the adduct formation. These two combined effects lead to the complicated effect of catalyst *ortho*-aryl substituents towards the reaction parameters.

3.9. Reference

1. R. S. Massey, C. J. Collett, A. G. Lindsay, A. D. Smith and A. C. O'Donoghue, *J. Am. Chem. Soc.*, 2012, **134**, 20421-20432.
2. C. J. Collett, R. S. Massey, O. R. Maguire, A. S. Batsanov, A. C. O'Donoghue and A. D. Smith, *Chem. Sci.*, 2013, **4**, 1514-1522.
3. C. J. Collett, R. S. Massey, J. E. Taylor, O. R. Maguire, A. C. O'Donoghue and A. D. Smith, *Angew Chem Int Edit*, 2015, **54**, 6887-6892.
4. R. MASSEY, Durham University, 2013.
5. R. C. Cookson and R. M. Lane, *J. Chem. Soc., Chem. Commun.*, 1976, 804-805.
6. D. M. Flanigan, F. Romanov-Michailidis, N. A. White and T. Rovis, *Chem Rev*, 2015, **115**, 9307-9387.
7. I. Piel, M. D. Pawelczyk, K. Hirano, R. Frohlich and F. Glorius, *Eur. J. Org. Chem.*, 2011, **2011**, 5475-5484.
8. M. Y. Jin, S. M. Kim, H. Han, D. H. Ryu and J. W. Yang, *Org Lett*, 2011, **13**, 880-883.
9. S. M. Langdon, M. M. Wilde, K. Thai and M. Gravel, *J. Am. Chem. Soc.*, 2014, **136**, 7539-7542.
10. S. M. Mennen and S. J. Miller, *J Org Chem*, 2007, **72**, 5260-5269.

11. M. Y. Jin, S. M. Kim, H. Mao, D. H. Ryu, C. E. Song and J. W. Yang, *Org Biomol Chem*, 2014, **12**, 1547-1550.
12. S. Toole, C. Rose, S. Gundala, K. Zeitler and S. Connon, *J. Org. Chem*, 2011, **76**, 347-357.
13. D. Enders and A. Henseler, *Adv. Synth. Catal.*, 2009, **351**, 1749-1752.
14. D. Enders, A. Grossmann, J. Fronert and G. Raabe, *Chem Commun (Camb)*, 2010, **46**, 6282-6284.
15. C. A. Rose, S. Gundala, C. L. Fagan, J. F. Franz, S. J. Connon and K. Zeitler, *Chem. Sci.*, 2012, **3**, 735-740.
16. B. T. Ramanjaneyulu, S. Mahesh and R. V. Anand, *Org Lett*, 2015, **17**, 3952-3955.
17. P. Dunkelmann, D. Kolter-Jung, A. Nitsche, A. S. Demir, P. Siegert, B. Lingen, M. Baumann, M. Pohl and M. Muller, *J. Am. Chem. Soc.*, 2002, **124**, 12084-12085.
18. X. Linghu, C. C. Bausch and J. S. Johnson, *J. Am. Chem. Soc.*, 2005, **127**, 1833-1840.
19. X. Linghu and J. S. Johnson, *Angew Chem Int Edit*, 2003, **42**, 2534-2536.
20. K. Thai, S. M. Langdon, F. Bilodeau and M. Gravel, *Org Lett*, 2013, **15**, 2214-2217.
21. S. M. Langdon, C. Y. Legault and M. Gravel, *J Org Chem*, 2015, **80**, 3597-3610.
22. M. J. White and F. J. Leeper, *J Org Chem*, 2001, **66**, 5124-5131.
23. P. QUINN, Durham University, 2018.
24. M. D. Hanwell, D. E. Curtis, D. C. Lonie, T. Vandermeersch, E. Zurek and G. R. Hutchison, *J Cheminform*, 2012, **4**, 17.
25. J. ZHU, Durham University, 2016.
26. C. D. Johnson and C. D. Johnson, *The Hammett Equation*, CUP Archive, 1973.

Chapter 4. H/D-exchange of Aldehyde

4.1. Introduction

4.1.1. General Deuterated Sources

Deuterium, known as the stable isotope of hydrogen, contains one more neutron than a proton, leading to its property variation. The detectability of the deuterium label in molecules by NMR, IR spectroscopy, and mass spectrometry, and the absence of radioactivity lead to the wide applications of deuterated compounds, like the NMR solvents[1-3]. Meanwhile, the kinetic isotope effects between R-H and R-D could suggest possible mechanism of reactions, suppress the formation of the undesired by-products (Scheme 4.1), and also, impact drugs' stabilities and toxicities[4].

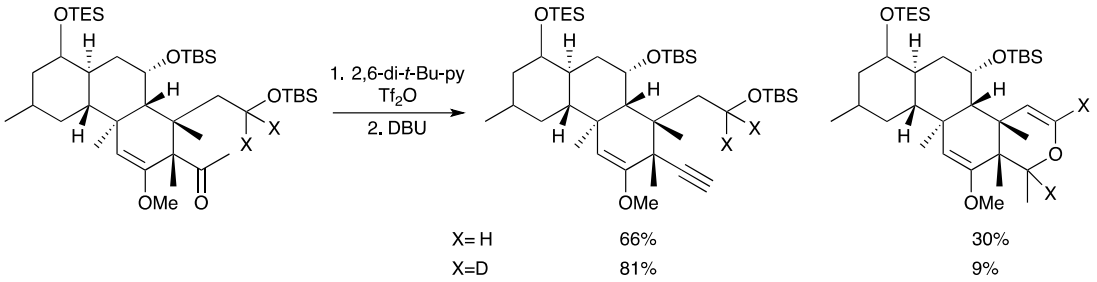

Scheme 4.1. Deuterium suppresses the formation of by-product.

Figure 4.1 presents three deuterated drugs. Tamoxifen can be used for breast cancer treatment, while it forms adducts with DNA in rats and leads to liver cancer[5, 6]. The replacement of the ethyl-protons by deuteria lowers down the genotoxicity by reducing adduct formation by around 2-fold. The metabolism of the reverse transcriptase inhibitor, Efavirenz, involves a toxic metabolite in rats' urine via propargylic oxidation. The introduction of the single deuterium atom at the site of propargylic oxidation reduces the formation of the metabolite from 28.1 μg/mL to 4.0 μg/mL[7]. For the hepatitis C protease inhibitor, Telaprevir, the deuterium atom significantly suppresses the formation of R-

epimer, which is 30-fold less active[7].

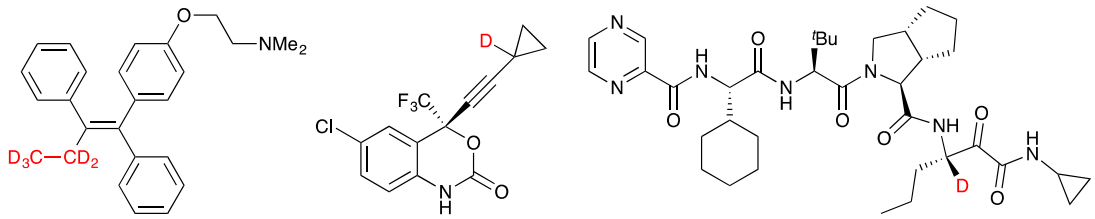

Figure 4.1. Three typical deuterated drugs.

4.1.2. General H/D-exchange Methods Towards Deuterated Compounds.

Hydrogen-deuterium exchange of protons attached to heteroatoms is facile and this process occurs rapidly in deuterium sources, *e.g.* d_4-methanol or deuterium oxide. By contrast, H/D-exchange at carbon is substantially slower thus requiring harsher conditions[8].

Generally, two methodologies are commonly used to afford isotopically labeled compounds. First, commercially available isotopically labeled precursors can be used in synthetic preparations. However, this method is limited by the high cost and restricted range of available precursors[9, 10]. The second and more common approach is to label compounds by the direct H/D-exchange. In the mid-1990s, due to the development of C-H bond activation catalysts and the growing demand for isotopically labeled reagents to facilitate the evaluation of catalytic mechanism, this research area experienced resurgence[10].

To date, two main strategies are followed for H/D-exchange: transition metal-catalysed H/D-exchange, and p*H*-dependent H/D-exchange. Metal complex catalysts usually require mild conditions, and have wide application ranges, generating products with

good regio- and stereo-selectivity[11]. However, the complicated preparation, poor control of by-product formation, and the high expense can limit the utilisation of metal-complexes. Meanwhile, p*H*-dependent H/D-exchange can achieve relatively pure product, but the reliance on relatively high kinetic acidities largely limits its development[12-17]. Scheme 4.2 shows three general pathways for the metal-catalysed H/D-exchange, and two typical examples of metal-catalysed and p*H*-dependent H/D-exchange.

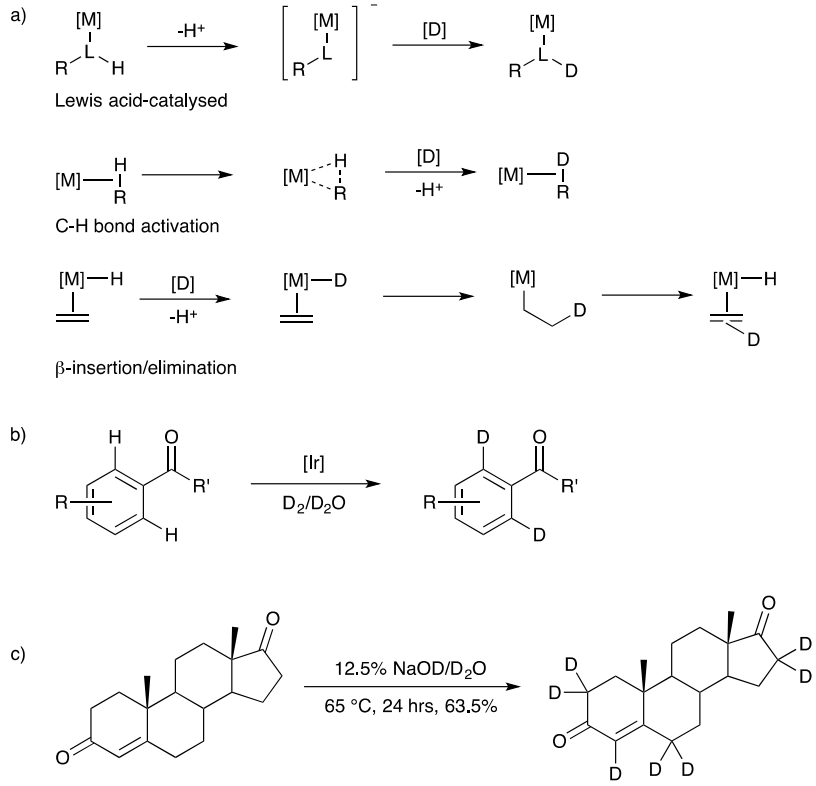

Scheme 4.2. a) Three general pathways for the metal-catalysed H/D-exchange[11], b) cationic iridium catalysed *ortho*-deuteration of aryl-ketones[18, 19], c) base catalysed deuteration of testosterone[20].

4.1.3. Syntheses and Applications of Deuterated Aldehydes

Compared with other deuterated compounds, access to d^1-aldehydes is difficult and expensive due to the extremely low acidity of the aldehydic hydrogens. The first deuterated aldehyde was acetaldehyde-d_4, synthesised by Zanetti and Sickman in 1936

via the hydration (D_2O) of acetylene-d_2[21]. Three years later, Thompson and Cromwell introduced the first synthetic routes towards two d^1-deuterated aryl-aldehydes through the reduction of *para*-phenylbenzoyl chloride and benzoyl chloride with Pd-$BaSO_4$ as catalyst[22]. Unfortunately, in Thompson and Cromwell's work, the accumulation of hydrogen ion in the system limited the deuterium incorporation of the products.

Recently, to study the mechanism of the oxidation of alcohols to the corresponding carbonyl compounds catalysed by ferrate (VI), Lau *et al.* investigated the kinetic isotope effects of the reaction *via* a range of deuterated alcohols[23]. Their kinetic experiments suggest the formation of acetaldehyde-d_4 and formaldehyde-d_2 from ethanol-d_6 and methanol-d_4, however, without isolated yields. Scheme 4.3 shows the mechanism proved by their kinetic work, which was also supported by the DFT calculations.

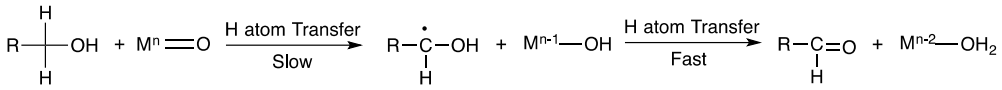

Scheme 4.3. Hydrogen atom transfer mechanism in the metal oxo catalysed oxidation of alcohol.

Acetaldehyde-d_4 can also be obtained from non-catalytic routes. Oxidation of ethanol-d_4 by using $Na_2Cr_2O_7 \cdot H_2O$ in concentrated sulfuric acid provides acetaldehyde-d_4 with 14% yield[24]. The kinetic experiment of aquachromium (IV) (CrO^{2+}) suggests the oxidation of deuterated alcohols towards acetaldehyde-d_4 and formaldehyde-d_2 through hydride transfer, with the consumption of CrO^{2+} to Cr^{2+} [25]. The paraldehyde-d_{12}, warmed up in xylene and concentrated sulfuric acid generates acetaldehyde-d_4 as an isotopic reactant for mechanistic studies[26].

Similar to the syntheses of acetaldehyde-d_4, deuterated aromatic aldehydes can also be obtained from the corresponding deuterated precursors. The oxidation of benzenemethanol-d_7 by manganese (IV) oxide[27], or using the aluminium oxide

supported ruthenium as a solvent-free catalyst[28] show the formation of benzaldehyde-d_6. Addition of anisole-d_5 to the dimethylformaldehyde-d_1 followed by the pyrophosphoryl chloride gives *ortho*- and *para*-regioisomers of methoxy-benzaldehyde-d_5 [29].

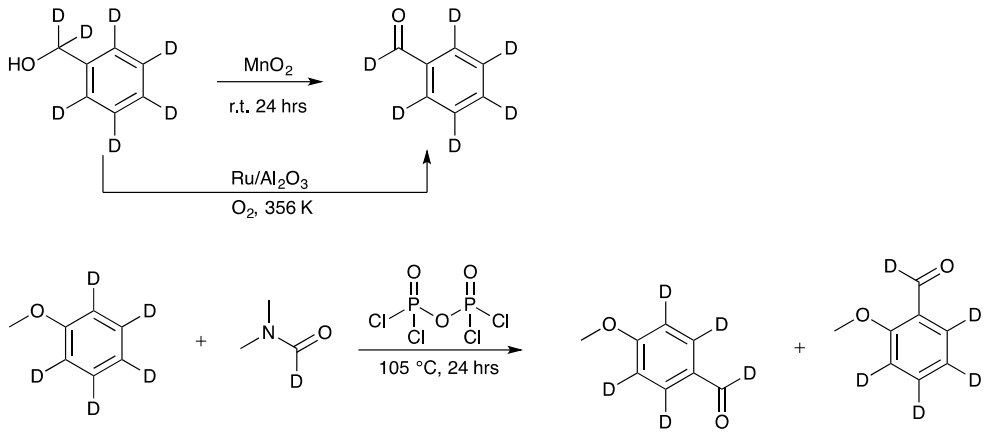

Scheme 4.4. Syntheses of benzaldehyde-d_6 and methoxy-benzaldehyde-d_5.

4.1.3.1. d_1-Deuterated Aliphatic Aldehyde

Owing to resonance stabilisation of the conjugate base, the pK_a value of the protons on the alpha positions of aldehyde is lower than the aldehydic proton. This leads to the difficulty of the traditional p*H*-dependent H/D-exchange of the aldehydic proton specifically. Limited synthetic procedures can be found for the preparation of acetaldehyde-d_1.

Rappoli and Bullock suggest the reaction of $DMn(CO)_5$ with $CH_3Mn(CO)_5$ gives $Mn_2(CO)_9(\eta_1\text{-}CH_3CDO)$ complex, and the aldehyde can undergo facile replacement by other ligands, however, without isolated yield (Scheme 4.5a)[30]. Banerji *et al.* introduced the mechanistic study of the oxidation of alcohols by quinolinium fluorochromate, which forms acetaldehyde-d_1 kinetically (Scheme 4.5b)[31]. The P450 2A6 enzyme has also been reported to form the d_1-deuterated acetaldehyde from deuterated *N,N*-diethylnitrosamine, however, this enzyme also oxidised acetaldehyde to the carboxylic acid *in situ* (Scheme 4.5c)[32].

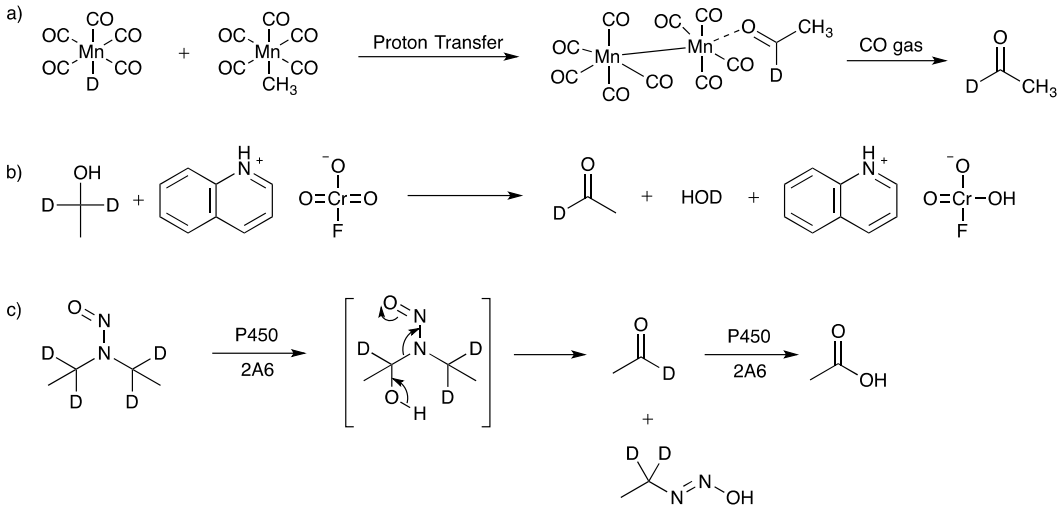

Scheme 4.5. a) Preparation of acetaldehyde-d_1 *via* the formation of a manganese complex, b) quinolinium fluorochromate oxidised acetaldehyde-d_1 formation, c) P450 2A6-catalysed acetaldehyde-d_1 formation.

4.1.3.2. d_1-Deuterated Aryl Aldehyde

Owing to the lack of the □-carbonyl protons, potentially, the p*H*-dependent H/D-exchange of the aryl aldehydic proton is easier compared to aliphatic aldehydes. However, the low acidity of the aldehydic proton still limits the direct formation of d_1-deuterated aryl aldehyde *via* a simple H/D-exchange route.

Since 1939, a range of d_1-deuterated aryl aldehydes have been synthesized (Figure 4.2). However, most of the routes towards these examples are based on the direct synthesis from other reagents. Reactions to synthesize d_1-deuterated aryl aldehydes might require harsh conditions, metal catalysts, irradiations, multi-reaction steps, expensive or toxic reagents, and the product outcomes might still be unsatisfying[33-41]. Some of these reactions give low yield or low deuterium incorporation, further oxidation to carboxylic acid or unavoidable side products. Studies focused on the kinetics of deuteration lacked the isolated yields. The following paragraphs will selectively introduce several reactions towards d_1-deuterated aryl aldehydes and their applications.

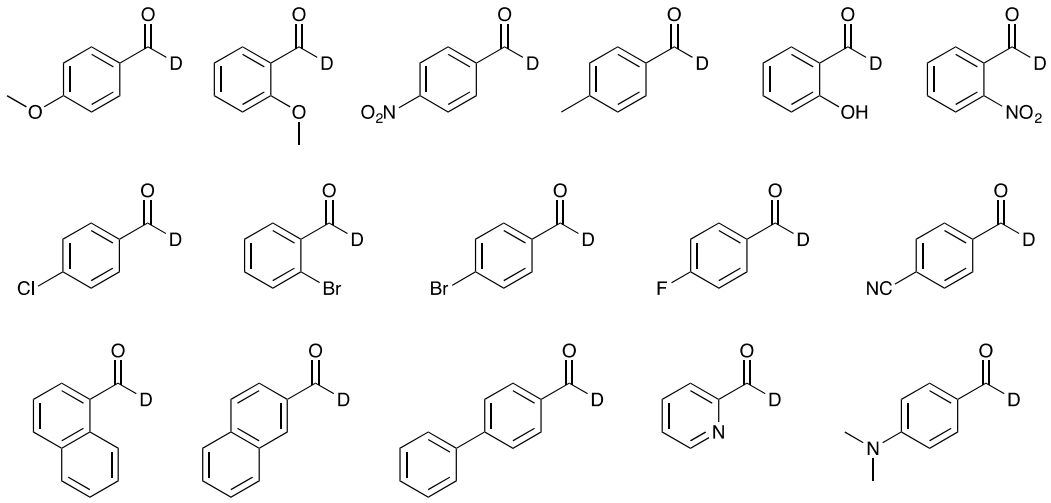

Figure 4.2. Selected examples of d_1-deuterated aryl aldehydes.

In 1986, Kuhn and Görner reported the photo-deuteriation of aryl aldehydes. The laser flash photolysis of aryl aldehydes activates the aldehyde to the corresponding α-hydroxybenzyl radical, and the subsequent quenching by deuterium oxide forms the deuterated aryl aldehyde (deuterium incorporation: 1%~ 98%). They reported that deuterium incorporation of aryl-aldehydes depends on both the concentration of deuterium oxide and the substituent of the aldehyde[33].

Curley *et al*. reported a multi-step synthetic pathway towards d_1-deuterated aryl aldehydes (Scheme 4.6a). The addition of morpholine, perchloric acid and potassium cyanide to the aldehyde forms the α-aryl-4-morpholine acetonitrile. The deprotonation, deuteration, and subsequent cleavage of morpholine and cyanide groups lead to the corresponding d_1-deuterated aldehyde. These deuterated aldehydes were reported as reagents towards enantioselective benzyl-chloride derivatives *via* the corresponding benzyl-alcohols, and can be used as precursors towards enantioselective amino acids, *e.g.* tyrosine (Scheme 4.6b)[34, 35].

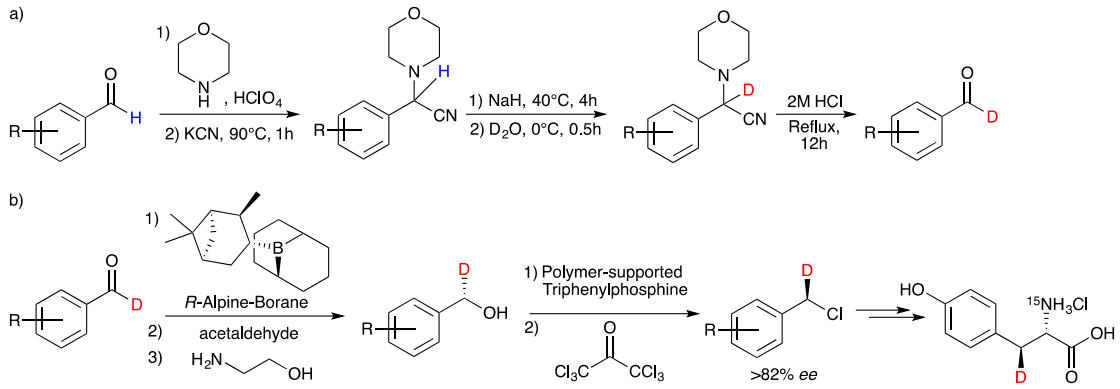

Scheme 4.6. a) Synthetic procedure towards deuterated benzaldehyde, b) d_1-deuterated aldehyde used as precursors towards tyrosine derivatives

In 2018, Denmark and Ibrahim introduced a cooperative Pd/Rh dual-metallic catalytic route towards reductive carbonylation of aryl halides to form hindered aryl aldehydes, where CO was used as carbonyl source (15-25 bar). The utilisation of deuterium oxide allows the formation of d_1-deuterated aldehydes (Scheme 4.7a)[36]. In 2019, Xie *et al.* demonstrated a cascade catalytical route from aromatic and aliphatic carboxylic acids to d_1-deuterated aldehydes using deuterium oxide as the deuterium source[37]. In their work, an Ir-complex is used as photocatalyst, and a thiol compound is employed as deuterium-atom transfer catalyst (Scheme 4.7b). Moreover, selectively labeled deuterated aldehydes can also be produced by Ru- (Scheme 4.7c) and Ir-catalysed (Scheme 4.7d) hydrogen isotope exchange[I, 38, 39], reductive carbonylation of aryl halides with iron pentacarbonyl catalysed by a Pd complex (Scheme 4.7e)[40], or from the corresponding amide with deuterated Schwartz's reagent (Scheme 4.7f)[41]. In all the above metal-catalysed routes, some of the yields are still unsatisfying.

[I] H/D-exchange on the aryl ring can also been observed.

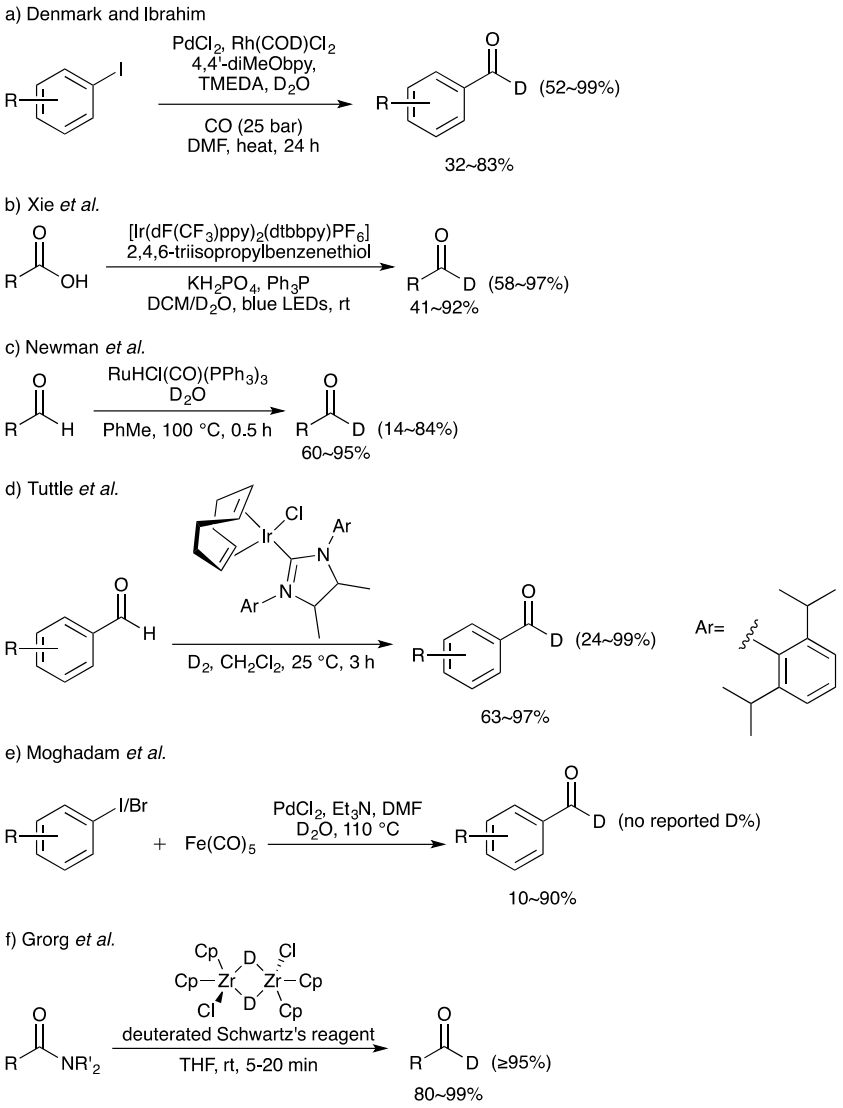

Scheme 4.7. Selective routes towards d_1-deuterated aldehyde using metal complex as catalysts or reagents

4.1.4. New Organocatalytic Pathway towards d_1-Deuterated Aldehydes

During our group's recent kinetic and mechanistic study of benzoin condensation, trace amounts of d_1-deuterated aldehyde were observed, although with limited deuterated aldehyde percentage[42]. Based on the mechanism of the benzoin condensation, the reversal of the deprotonation of the tetrahedral intermediate **144** in deuterated protic solvents results in deuteration due to the large excess of deuterium (protic solvents used as deuterium source, *e.g.* D_2O, MeOD), which can lead to the corresponding d_1-aldehyde.

Theoretically, a similar catalytic cycle may be envisaged for aliphatic aldehydes.

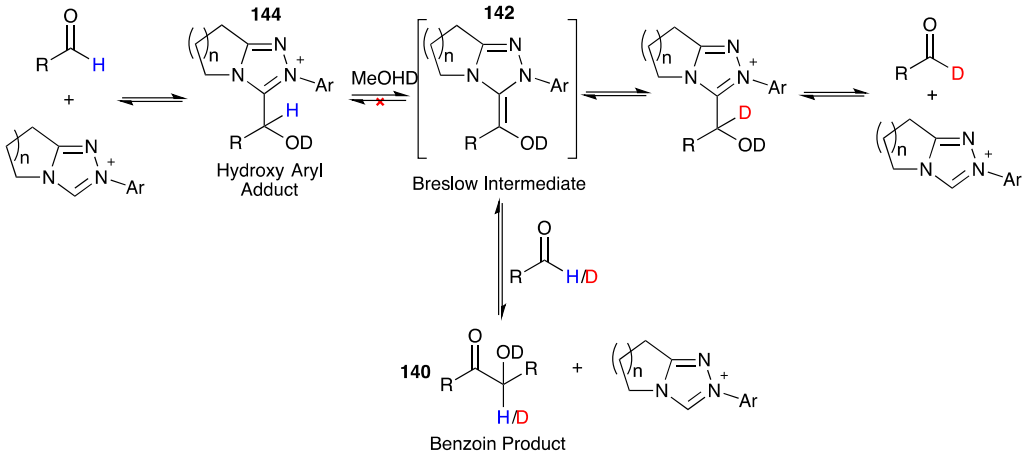

Scheme 4.8. Benzoin condensation based d_1-deuterated aldehyde synthesis

From the benzoin condensation mechanism, the percentage of d_1-deuterated aldehyde depends on the formation rate of Breslow intermediate **124**, the stability of hydroxy aryl adduct **144**, and the formation rate of benzoin product **140** from Breslow intermediate. One of my project aims was to modify the NHC backbone structure, to suppress the formation of Breslow intermediate and benzoin product, and increase the formation and dissociation rate of the hydroxy aryl adduct **144**.

4.2. Overview of Methodology

Adapted from the kinetic analysis of the triazolium salt-catalysed benzoin condensation introduced in Chapter 3, Section 3.3, ^{1}H NMR spectroscopy was used to trace the concentration of each component. All the concentrations are obtained from the Equations 3.1-3.14, which are introduced in Section 3.5. To show results more directly, the percentage remaining of each components are used in this section. The "Ald%" represents the remaining concentration percentage of aldehyde, "Add%" for hydroxy aryl adduct **144**, and "Ben%" for benzoin product **140**. These % values are calculated by Equation 4.1-4.4, and the percentage deuterium incorporation of aryl-aldehydes D%

is calculated by Equation 4.4 from the area of the remaining aldehydic peak.

$$Ald\% = \frac{[Ald]}{[Ald]_0} = \frac{[Ald]}{[Ald]+[Add]+2\times[Ben]} \times 100\% \quad \textbf{Equation 4.1}$$

$$Add\% = \frac{[Add]}{[Ald]_0} = \frac{[Add]}{[Ald]+[Add]+2\times[Ben]} \times 100\% \quad \textbf{Equation 4.2}$$

$$Ben\% = \frac{2\times[Ben]}{[Ald]_0} = \frac{2\times[Ben]}{[Ald]+[Add]+2\times[Ben]} \times 100\% \quad \textbf{Equation 4.3}$$

$$D\% = \frac{[Ald]_D}{[Ald]} \times 100\% \quad \textbf{Equation 4.4}$$

4.3. Catalyst Backbone Selection

4.3.1. *Ortho*-substituents Effects of Catalyst Aryl Ring

During my MSc research project, we initially assumed that the sterically bulky *ortho*-substituents of catalyst may kinetically suppress the formation of benzoin product by impeding the aldehyde approach towards Breslow intermediate. By analysis of kinetic profiles of reactions between benzaldehyde **135** and 2,4,6-trisubstituted triazolium salts **85** and **88** (Figure 4.3), a crucial conclusion was obtained that *ortho*-substituents on catalyst's aryl ring did decrease the formation of benzoin product, however, also suppressed the decomposition of deuterated adduct **144** towards d_1-deuterated aldehyde [43].

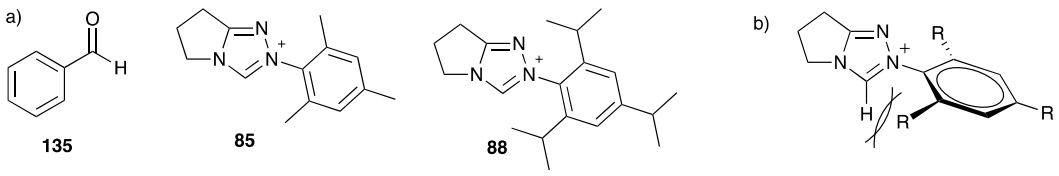

Figure 4.3. a) benzaldehyde **135** and 2,4,6-trisubsituted triazolium salt **85** and **88**, b) *ortho*-aryl substituents force the aryl-moiety out of triazolyl plane.

The existing single X-ray crystallographic data for an *ortho*-substituted N-aryl triazolium salt during the MSc project highlighted the non-coplanarity between the N-aryl moiety and triazolyl ring in the presence of *ortho*-substituents, which leads to the better accommodation of the hydroxyaryl moiety in adduct **144** thereby increasing its stability. These observations formed the basis for further studies during my PhD project.

4.3.2. Effect of Fused Ring Size and Aryl-Substituents of Catalysts

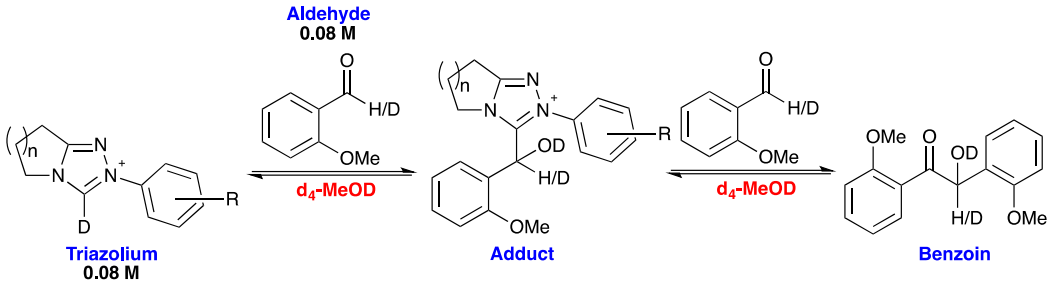

Considering the relatively fast oxidation rate of benzaldehyde, 2-methoxybenzaldehyde **138** was instead used for a systematic deuterium exchange investigation. Stoichiometric quantities of 2-methoxy benzaldehyde **138** (0.08 M) and triazolium salts **77-80**, **89-91**, **100, 101** (0.08 M) were added to a d_4-methanol solution with buffered triethylamine (2:1 NEt_3: $NEt_3 \cdot HCl$). ^1H NMR spectroscopy was employed to probe the deuterium incorporation and the concentrations of components at 25 °C. Table 4.1 provides the results obtained from experiments catalysed by 2,4,6-triisopropyl, phenyl, 4-methoxyphenyl, and 4-fluorophenyl triazolium salts salts **77-80**, **89-91**, **100, 101**.

Table 4.1.% Component distribution of the reaction of 2-methoxybenzaldehyde **138** catalysed by 2,4,6-triisopropyl, phenyl, 4-methoxyphenyl, and 4-fluorophenyl triazolium salts salts **77-80**, **89-91**, **100, 101** in d_4-methanol at 25 °C.

R=	n	Time/ h	D%	Ald%	Add%	Ben%
2,4,6-^{i}Pr	1	16.2	1	9	91	0
	1	16.0	26	22	76	2
H	2	14.6	5	52	47	1
	3	13.3	7	70	30	1
	1	14.6	8	21	80	0
4-OMe	2	15.2	~0	54	46	0
	3	14.7	4	67	33	0
	1	15.4	61	19	77	4
4-F	2	15.0	15	44	54	2
	3	15.3	3	65	33	2

* The percentage of components distribution were calculated from Equation 4.1-4.4.

Similar to previous results, the *ortho*-substituted catalyst was found to stabilise the hydroxy aryl-adduct, and suppress both the onward benzoin formation and the backward dissociation of adduct (Add%=91). The results suggest relative quantities of components to be most dependent on the triazolium fused ring size. The reaction catalysed by 5-membered triazolium salts **89, 100, 101** only yielded ~20% aldehyde, with ~77% reacted to the adduct stage. Triazolium salts with 6-membered fused ring **77, 79, 90** gave ~50% aldehyde and adduct, whereas the 7-membered analogues **78, 80, 91** resulted in ~67% aldehyde and 31% adduct. The quantities of benzoin are relatively small, however, still suggest the increased fused ring size suppresses benzoin formation.

Deuterium exchange is favoured by electron-withdrawing N-aryl-substituents of catalyst, owing to the increased association and dissociation rates of adduct (Section 3.7.3.2). Meanwhile, triazolium salts with 5-membered fused ring provided the highest D%, although with the lowest Ald%. Kinetic analyses suggest, in the self-condensation reaction of 2-methoxybenzaldehyde **138**, reaction rates of adduct formation with triazolium salts with a 5-membered fused ring are highest, whereas the corresponding

dissociation rates are comparable to adducts with 6-membered fused ring, and lower than for the adduct with 7-membered fused ring.

Initially, we assumed the D% should decrease with the incremental fused ring size. However, in cases of phenyl and 4-methoxyphenyl triazolium salt **101, 79, 80, 89-91**, D% is favoured by the triazolium salts with 7-membered fused ring (**80**, and **91**) rather than those with a 6-membered fused ring (**79** and **90**), while *para*-fluorophenyl triazolium salts (**100, 77, 78**) follows the expected trend.

For phenyl triazolium salts, the relatively lower formation rate of adduct with 7-membered fused ring ($k_1^{n=2}/\ k_1^{n=3}= 0.81$) leads to the lower D% (Chapter 3, Section 3.7.1); while for *para*-methoxyphenyl triazolium salts, the relatively low Breslow intermediate formation rate of adduct with 7-membered ring ($k_1^{n=2}/\ k_1^{n=3}= 0.81$, Chapter 3, Section 3.7.1) limited the H/D-exchange rate of the benzylic proton of adduct, and result in the smaller D% value.

4.3.3. Effects of Solution Basicity and Triazolyl Fused Ring Size

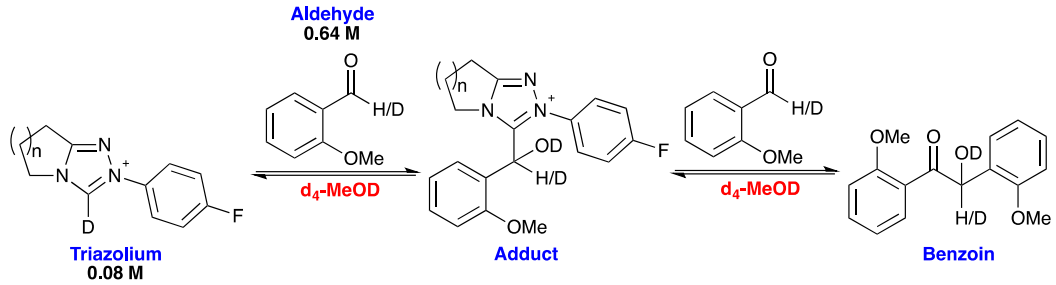

The ratio of triethylamine and triethylamine hydrochloride was changed from 2:1 to 1:1 and 1:2 to decrease the effective p*D* whilst maintaining a constant total buffer concentration (0.16 M). The 4-fluorophenyl triazolium salts with 5- and 6-membered fused rings **100** and **77** were used based on results from previous experiments; **100** suggests highest deuterium incorporation, while **77** provides relatively more remaining

aldehyde. In this case, an 8-fold excess of aldehyde was employed. Table 4.2 shows the results of reactions conducted at 50 °C[I]. These reactions were further incubated at 25 °C for four days followed by component analysis, and the results are provided in Table 4.3.

Table 4.2.% Component distribution for the of self-condensation reaction of 2-methoxybenzaldehyde **138** (0.64 M) catalysed by *para*-fluorophenyl triazolium salts **100, 77** (0.08 M) at 50 °C in d_4-methanol.

	n	NEt_3: NEt_3·HCl	Time/ h	D%	Ald%	Add%	Ben%
		1:2	5.2	3	83	14	3
100	1	1:1	4.9	11	81	14	5
		2:1	4.7	23	76	13	11
		1:2	3.7	0	89	10	0
77	2	1:1	4.0	2	87	11	2
		2:1	3.8	7	86	12	3

* The percentage of components distribution were calculated from Equation 4.1-4.4.

Table 4.3.% Component distribution for the reaction of 2-methoxybenzaldehyde **138** (0.64 M) catalysed by *para*-fluorophenyl triazolium salts **100, 77** (0.08 M) after four further days of incubation at 25 °C in d_4-methanol.

	n	NEt_3: NEt_3·HCl	D%	Ald%	Add%	Ben%
		1:2	42	57	14	29
100	1	1:1	66	43	14	43
		2:1	90	26	14	61
		1:2	2	85	12	3
77	2	1:1	35	72	12	17
		2:1	51	59	12	29

* The percentage of components distribution were calculated from Equation 4.1-4.4.

Due to the excess amount of aldehyde, the formation of adduct is more favoured in all cases and equilibrium is reached. Thus, the percentage of hydroxy aryl-adducts should theoretically be close to 13% (with all triazolium salt formed adduct), while the fluctuation was due to the experimental and analytical errors. After four days, the small

[I] The reaction temperature was increased to 50 °C to increase the reaction speed.

change in Add% should owe to the oxidation of aldehyde, while the oxidised aldehyde was not included in the total aldehyde amount.

The results suggest the more basic conditions favour both deuterium exchange and the formation of benzoin product. Moreover, irrespective of solution basicity, the larger fused ring size of catalyst suppresses the formation of benzoin product and H/D-exchange.

4.3.4. Comparison Between *Para*-fluorophenyl and Pentafluorophenyl Triazolium 100, 77, 78, 98, 99, 84

Previous experiments show either too low deuterium incorporation or too high benzoin percentage with long reaction times. Thus, the use of a triazolium salt with a more electron-deficient pentafluorophenyl aryl-substituent was investigated. Pentafluorophenyl triazolium **98, 99, 84** (0.04 M) and 2-methoxybenzaldehyde **138** (0.16 M) were added into a solution of d_4-methanol with 0.16 M of triethylamine. Experiments using *para*-fluorophenyl triazolium **100, 77, 78** (0.08 M) and 0.32 M of aldehyde **138** were also probed for comparison, with the temperature increased to 50 °C. Table 4.4 summarises the results, and the end point of the reaction was chosen when the increment of D% levelled.

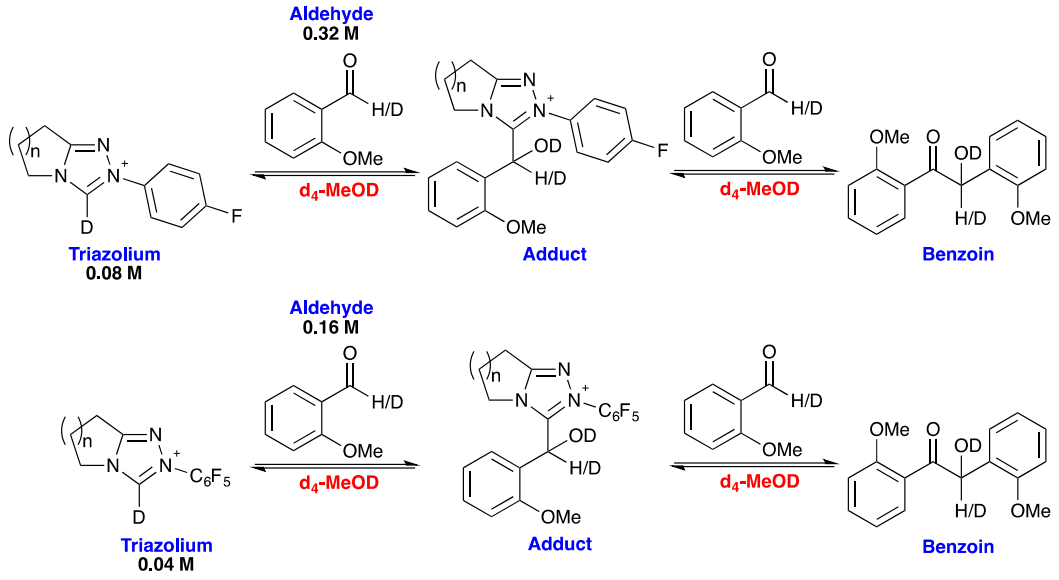

Table 4.4. Components concentration percentage of self-condensation reaction of 2-methoxybenzaldehyde **138** catalysed by *para*-fluorophenyl triazolium salt **100, 77, 78**, and pentafluorophenyl triazolium salt **98, 99, 84**.

R=	n	Temp.	Time/ h	D%	Ald%	Add%	Ben%
	1		2	90	35	28	37
4-F	2	50 °C	5.3	82	42	22	36
	3		5.3	33	67	16	17
	1		0.7	99	42	12	46
Pentafluorophenyl	2	25 °C	0.7	94	73	11	16
	3		10.0	95	63	2	35

* The percentage of components distribution were calculated from Equation 4.1-4.4.

Results suggest that the highly electron-withdrawing aryl-substituents increase the triazolium salt's reactivity and shorten the reaction duration. As observed for the other N-aryl triazolium salts, an increased fused ring size of pentafluorophenyl derivatives decreases the Add% and Ben%, but also decreases the rate of the deuterium exchange process for the 4-fluorophenyl catalyst.

Conspicuously, pentafluorophenyl triazolium salts **98, 99, 84** all suggest good deuterium incorporation at room temperature with relatively short reaction times. The pentafluorophenyl triazolium salts with a 5-membered fused ring (**98)** gave the best

deuterium incorporation (D%= 99%), however, 46% of aldehyde formed benzoin, while triazolium **84** (n=3) requires long reaction time to achieve comparable deuterium incorporation. However, for pentafluorophenyl triazolium salts **98, 99, 84**, under these conditions over time, there is a reduction of corresponding triazolium salt's intensities and the shift of triethylamine peaks can be observed. Thus, a side reaction of pentafluorophenyl triazolium salt occurs, possibly owing to a ring-opening reaction, which limits the reaction time of deuterium exchange. The pentafluorophenyl triazolium salt **99** (n=2) suggests relatively high deuterium incorporation (94%) and highest remaining aldehyde percentage (73%) with short reaction time (0.7 h), hence has the potential to be the ideal candidate to catalyse the deuteration of the aldehydic proton.

4.3.5. Further Deuteration Studies Catalysed by Pentafluorophenyl Triazolium Salt 99 (n=2)

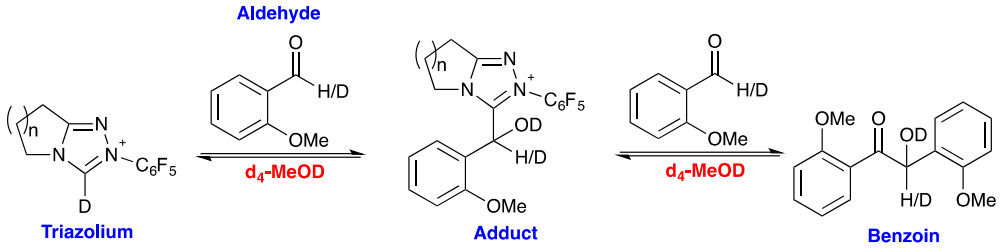

To obtain the highest efficacy of aldehydic deuteration, further reactions of 2-methoxybenzaldehyde **138** catalysed by pentafluorophenyl triazolium salt with 6-membered fused ring (**99)** under various reaction conditions were probed by ^{1}H NMR spectroscopy. Table 4.5 summarises the results with various concentrations of both aldehyde and triazolium, reaction temperature, and buffer concentration.

Table 4.5.% Conponent distribution of the reaction of 2-methoxybenzaldehyde **138** catalysed by pentafluorophenyl triazolium salt with 6-membered fused ring **99** in d_4-methanol.

Exp	[Cat]/ M	[Ald]/ M	Time/ h	D%	Ald%	Add%	Ben%
1	0.04	0.16	1.2	94	68	18	15
2[a]	0.04	0.16	2.4	88	63	25	13
3[b]	0.04	0.16	1.0	59	68	26	6
4	0.02	0.16	1.9	87	77	6	17
5	0.02	0.16	6.3	96	76	4	21
6	0.02	0.08	0.7	94	70	21	10
7	0.02	0.08	2.2	99	73	14	14
8	0.01	0.08	4.8	95	83	2	15
9	0.005	0.08	15.6	85	87	<1%	12

% Yield determined by ^{1}H NMR spectroscopy with 0.16 M triethylamine, 25 °C, except *a*: 0 °C, *b*: 2:1 triethylamine: triethylamine hydrochloride. The percentage of components distribution were calculated from Equation 4.1-4.4.

A lower reaction temperature and basicity favour adduct formation and reduce the Ben%, however, also decrease the D% (Exp 1, 2 & 3). Lower triazolium salt concentrations require longer reaction times for deuterium exchange, however, result in similar deuterium incorporation levels (Exp 1, 4 & 5). By limiting the quantity of adduct that can be formed, lower initial triazolium concentrations increase the amount of remaining aldehyde (Exp 1, 5 & 7).

However, the disappearance of the pentafluorophenyl triazolium salt can still be observed during the reaction, and the reduction in Add% also confirmed this (Exp 4, 5, 6 & 7). ^{1}H NMR spectra show the triazolium and adduct concentration decreased at the same rate, and the concomitant increasing concentration of aldehyde suggests the side reaction happens on the triazolium rather than the adduct (Exp 6 & 7). Experiments 8 and 9 prove that the further reduction of the triazolium salt concentration decreases deuterium incorporation as a direct consequence of the consumption of triazolium.

The best deuterium exchange result was found at 2.2 hours with 0.02 M of triazolium

salt loading and 0.08 M of aldehyde. 73% of aldehyde remained with 99% of deuterium incorporation, and only 14 Ben%. To confirm the deuteration at the aldehydic position, ^{2}D NMR spectroscopy was performed and confirmed the aldehydic proton at 10.41 ppm did exchange for deuterium. Unfortunately, the resolution of ^{2}D NMR is relatively low compared to the background noise and acquisition times are quite long, which limits its broader application for analysis in this case.

4.4. Deuterium Exchange for Other Aldehydes

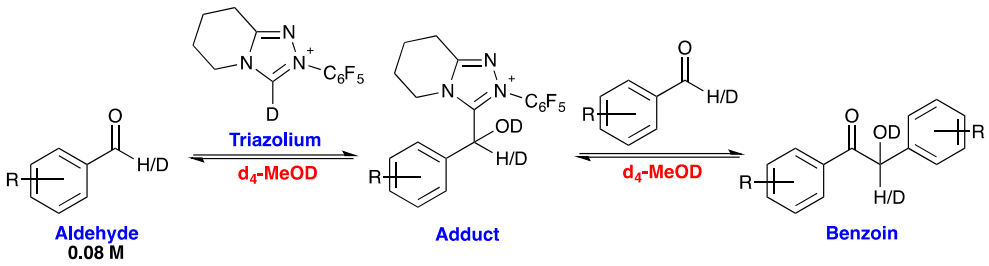

Deuterium exchange experiments of 4-methoxybenzaldehyde **137** and 2-methylbenzaldehyde **136** were also investigated by using pentafluorophenyl triazolium **99** (n=2) as catalyst, and Table 4.6 summaries the results at different time. For these two reactions, 0.01 M of triazolium **99** was added into 0.08 M of aldehyde d_4-methanol solution with 0.16 M of triethylamine as base.

Table 4.6.% Component distribution of reaction of 4-methoxybenzaldehyde **139** (0.08 M), and 2-methylbenzaldehyde **136** (0.08 M) catalysed pentafluorophenyl triazolium salt with 6-membered fused ring (**99**, 0.01 M) in d_4-methanol at 25 °C, with 0.16 M NEt_3.

R=	Time/ h	D%	Ald%	Add%	Ben%
4-OMe	0.7	44	46	1	53
	12.6	90	32	<0.1	68
2-Me	1.4	58	85	1	15
	12.6	71	76	<0.1	24
	14.4	72	74	<0.1	26

* The percentage of components distribution were calculated from Equation 4.1-4.4.

In Chapter 3, the reaction parameters of hydroxy aryl-adduct formation and consumption of all four aldehydes (**135-137, 139**) are measured (Section 3.5, with the buffer of NEt_3: $NEt_3 \cdot HCl$ = 2:1). Regardless of the catalyst backbone variation, the hydroxy aryl-adduct association constants of 2-methylbenzaldehyde **136** are generally 3- to 6-fold higher than those for 4-methoxybenzaldehyde. The adduct dissociation constants for 2-methylbenzaldehyde **136** are smaller or comparable to the 4-methoxybenzaldehyde ($k_{-1}^{2\text{-Me}}/\ k_{-1}^{4\text{-OMe}}$ = 0.52~1.02), and the equilibrium constants for 2-methylbenzaldehydes are at least 3-fold larger than those for 4-methoxybenzaldehyde (Section 3.5.4, Table 3.4 and 3.6). Moreover, the Breslow intermediate formation rates for 2-methylbenzaldehyde **136** are always larger than the 4-methoxybenzaldehyde cases ($k_2^{2\text{-Me}}/\ k_2^{4\text{-OMe}}$ = 1.04~11.5).

The lower level of deuterium incorporation in 2-methylbenzaldehyde case corresponds well to its smaller k_{-1}, which slower down the H/D-exchange rate of the benzylic proton on the hydroxy aryl-adduct. The higher equilibrium constants and higher Breslow intermediate formation rate of 2-methylbenzaldehyde **138** could have potentially increased D% and Ald%, however, this is not observed.

Unsurprisingly, the reduction of catalyst's initial concentration and the side reaction of catalysts decreases the final deuterium incorporation of 4-methoxybenzaldehyde and 2-methylbenzaldehyde. Reactions with 0.02 M of triazolium salts were conducted. Table 4.7 summarises the results of reactions of 2-methylbenzaldehyde **136**, 4-methylbenzaldehyde **137**, 4-methoxybenzaldehyde **139** and benzaldehyde **135** with pentafluorophenyl triazolium salt **99** (n=2). Within these reactions, 0.02 M of triazolium **99** was added into 0.08 M of aldehyde d_4-methanol solution with 0.16 M of triethylamine as base. For clearer comparison, Table 4.7 also provides the reaction results at different reaction times.

Table 4.7.% Components distribution of self-condensation reaction of 0.08 M of 2-methylbenzaldehyde **136**, 4-methylbenzaldehyde **137**, 4-methoxybenzaldehyde **139** and benzaldehyde **135** in the presence of 0.02 M of pentafluorophenyl triazolium salt with 6-membered fused ring (**99**) in d_4-methanol, at 25 °C, with 0.16 M NEt_3.

R=	Time/ h	D%	Ald%	Add%	Ben%
Ph	0.7	88	10	4	87
	5.4	98	11	1	76
4-OMe	0.7	80	29	1	69
2-Me	0.7	81	71	6	23
	1.4	87	69	2	30
4-Me	0.7	89	14	3	84
	0.9	90	13	2	85

* The percentage of components distribution were calculated from Equation 4.1-4.4.

Comparing the Table 4.6 and 4.7, double the loading of triazolium salts significantly increased the H/D-exchange efficiency. Although more benzoin product is generated, the shorter reaction period now possible reduced the consumption of triazolium salt *via* side reaction.

For the reactions conducted for 0.7 hours, the D% follows the trend: $D\%^{4\text{-Me}} > D\%^{Ph} > D\%^{2\text{-Me}} > D\%^{4\text{-OMe}}$; the Ald% follow the trend: $Ald\%^{2\text{-Me}} >> Ald\%^{4\text{-OMe}} > Ald\%^{4\text{-Me}} > Ald\%^{Ph}$; for adduct, the trend follow: $Add\%^{2\text{-Me}} > Add\%^{Ph} > Add\%^{4\text{-Me}} > Add\%^{4\text{-OMe}}$; for benzoin product, the trend follow: $Ben\%^{Ph} > Ben\%^{4\text{-Me}} > Ben\%^{4\text{-OMe}} >> Ben\%^{2\text{-Me}}$.

The trend of hydroxy aryl-adduct (Add%) can be explained simply by the equilibrium constants variation (Section 3.7.2). The combined effects of substituent electronic property and steric occupancy lead to the variation of adduct formation equilibrium constants followed the trend: $K^{2\text{-Me}} > K^{Ph} > K^{4\text{-Me}} > K^{4\text{-OMe}}$. On this basis, the remaining aldehyde trend could presume to be: $Ald\%^{4\text{-OMe}} > Ald\%^{4\text{-Me}} > Ald\%^{Ph} > Ald\%^{2\text{-Me}}$. However, the *ortho*-methyl group on the aldehyde aryl-ring largely suppresses benzoin product formation, and results in the limited consumption of 2-methylbenzaldehyde,

thus, lead to the remaining aldehyde follows the trend: $Ald\%^{2\text{-}Me} >> Ald\%^{4\text{-}OMe} > Ald\%^{4\text{-}Me} > Ald\%^{Ph}$. Apart from the *ortho*-substituted aldehyde, the benzoin product formation trend disfavours the electron-deficient aryl-substituents. Meanwhile, the combined variation of adduct formation, dissociation and Breslow intermediate formation rates lead to the trend of deuterium incorporation, and no simple explanation can be suggested.

Although the D% of benzaldehyde is very high (98%), the Ald% is quite low. 76% of benzaldehyde formed benzoin *via* self-condensation, and 12% of benzaldehyde was oxidized into benzoic acid. Moreover, the reaction finally reached equilibrium, which raises another possibility for the synthetically accessing d^1-deuterated aldehydes: from the retro-benzoin condensation.

Deuterium oxide was also explored as solvent and deuterium source for the deuterium exchange of benzaldehyde. Deuterated methanol was used as co-solvent as the solubilities of aldehyde, adduct, and benzoin are low in water. Despite the utilization of 50 v/v % d_4-methanol, and full dissolution of aldehyde, a yellow precipitate accumulated after the initiation. Mass spectrometry suggest the yellow precipitate to be a mixture of compounds of different molecular weights, none of which include the normal reaction intermediates.

4.5. Retro-benzoin Condensation Study

In Section 4.4, the results suggest the formation of acyloin-type product is unavoidable, while it is possible to add the acyloins directly into the reaction to suppress the formation of acyloins directly from the aldehyde. As introduced in Chapter 3, our previous research conditions were deliberately chosen to allow access to rate and equilibrium constants of steps up to the formation of Breslow intermediate, and limited results have been obtained for the retro-benzoin reaction. Thus, the retro-benzoin condensation reactions were

proceeded by adding benzoin **158** (0.04 M) into the d_2-dichloromethane solution of pentafluorophenyl triazolium **98, 99, 74** (0.02 M) with 0.16 M of triethylamine at 25 °C, respectively (Scheme 4.9).

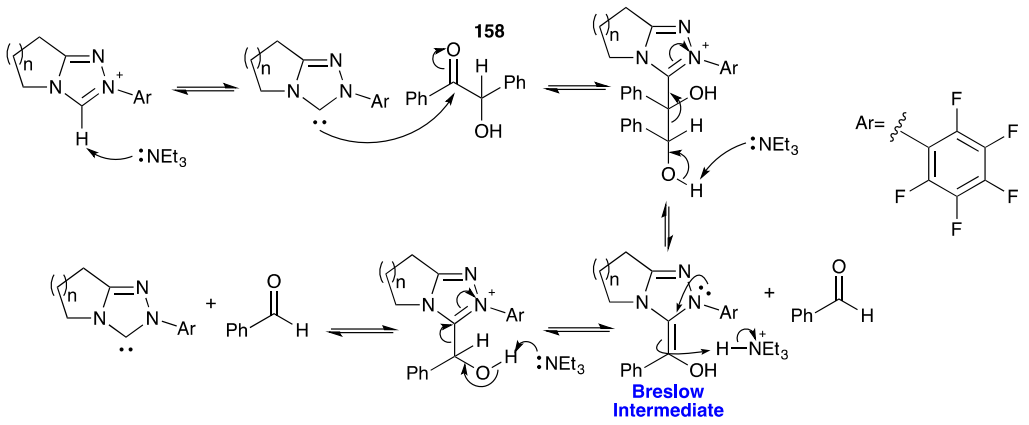

Scheme 4.9. Potential mechanism of retro-benzoin reaction

Table 4.8 summarises the components of reaction mixture after being initiated for 2 hours. Since benzaldehyde **135** is easily oxidised, Acid% was also considered for this experiment. "Acid%" represents the percentage of benzoic acid formed from aldehyde, which can be calculated *via* Equation 4.5. Meanwhile, within this retro-benzoin study, the remaining percentage of aldehyde (Ald%), hydroxy aryl adduct (Add%), and benzoin product (Ben%) are now calculated *via* Equation 4.5-4.8, which introduced the amount of benzoic acid formed.

$$Acid\% = \frac{[Ald]}{[Ald]_0} = \frac{[Acid]}{[Ald]+[Add]+2\times[Ben]+[Acid]} \times 100\% \qquad \textbf{Equation 4.5}$$

$$Ald\% = \frac{[Ald]}{[Ald]_0} = \frac{[Ald]}{[Ald]+[Add]+2\times[Ben]+[Acid]} \times 100\% \qquad \textbf{Equation 4.6}$$

$$Add\% = \frac{[Add]}{[Ald]_0} = \frac{[Add]}{[Ald]+[Add]+2\times[Ben]+[Acid]} \times 100\% \qquad \textbf{Equation 4.7}$$

$$Ben\% = \frac{2\times[Ben]}{[Ald]_0} = \frac{2\times[Ben]}{[Ald]+[Add]+2\times[Ben]+[Acid]} \times 100\% \qquad \textbf{Equation 4.8}$$

Table 4.8.% Components distribution of retro-benzoin reaction of benzoin (0.04 M) catalysed by pentafluorophenyl triazolium with 5-, 6-, and 7-membered fused ring (**98, 99, 74** , 0.02 M) in d_2-dichloromethane at 25 °C, with 0.16 M NEt_3.

n=	Time/ h	Ald%	Add%	Ben%	Acid%
1	1.94	18	1	71	10
2	1.98	24	7	55	14
3	1.98	26	3	64	7

* The percentage of components distribution were calculated from Equation 4.5-4.8.

The formation of benzaldehyde was observed by ^{1}H NMR spectroscopy, which suggested the full retro-benzoin reaction from benzoin towards benzaldehyde. For the same reaction time, the pentafluorophenyl triazolium salt with a 6-membered fused ring (**99)** resulted in the highest amount of the reverse reaction of benzoin (lowest Ben%), however, with most of aldehyde trapped as adduct or oxidized into benzoic acid. Interestingly, the quantity of benzoic acid also varies by using different triazoliums, however, the precise effect of catalyst on the oxidation rate of aldehyde is hard to measure because of the parallel reactions. The pentafluorophenyl triazolium salt with a 7-membered fused ring resulted in the highest Ald%, which can be used as potential candidate for the synthesis of d^1-deuterated benzaldehyde *via* the retro-benzoin reaction.

By changing d_2-dichloromethane to d_4-methanol, the solvent can also operate as a deuterium resource. Scheme 4.10 illustrates the possible mechanism of the retro-benzoin reaction in d_4-methanol. Thus, benzoin **158** (0.04 M) and pentafluorophenyl triazolium salt **99** with 6-membered fused ring (0.02 M) were added into the deuterated methanol solution with 0.16 M of triethylamine. Table 4.9 provides the D% into both aldehyde and benzoin at different reaction times.

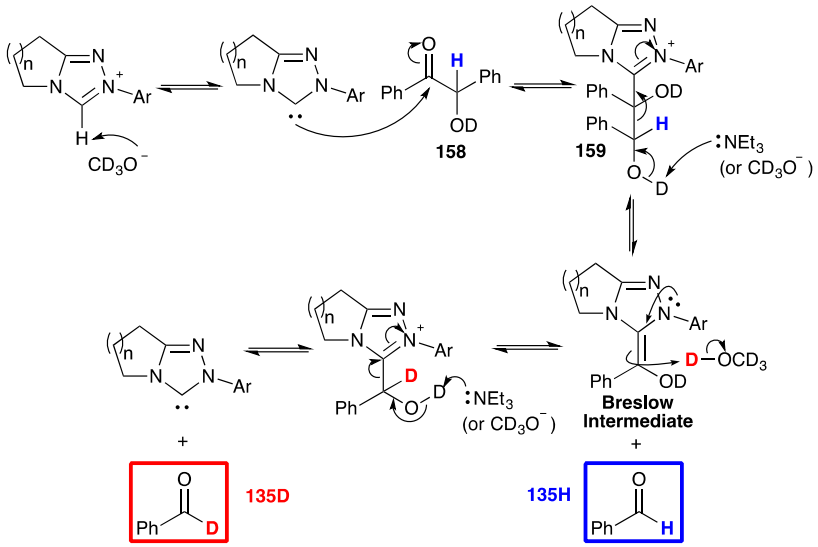

Scheme 4.10. Retro-benzoin mechanism in d_4-methanol resulting in d_1-deuteration of aldehyde.

Table 4.9. Ald%, Ben% and D% of the retro-benzoin reaction of benzoin (0.04 M) catalysed by pentafluorophenyl triazolium salt **99** (n=2, 0.02 M) in d_4-methanol, 25 °C, with 0.16 M NEt_3.

Time/ h	D% (Ald)	Ald%	D% (Ben)	Ben%
0.08	68	7	0	88
1.11	90	9	12	83
6.09	98	10	74	77
15.08	99	11	87	72

* The percentage of components distribution were calculated from Equation 4.5-4.8.

The decomposition of benzoin initially generates a certain amount of protonated benzaldehyde **135H**, and the deuterium exchange of aldehyde lowers down the percentage of protonated aldehyde. Meanwhile, the benzoin also underwent a deuterium exchange process, which reduces the amount of protonated aldehyde synthesized *via* decomposition.

^{2}D NMR spectra also confirmed the formation of d^1-deuterated aldehyde by observing the deuterium peak at 9.99 ppm, while the peak due to deuterated benzoin overlaps with the solvent peak.

To check the difference between the benzoin condensation and retro-benzoin reaction, the reaction of benzaldehyde **135** (0.08 M) and the pentafluorophenyl triazolium salt **99** (n=2, 0.02 M) in a d_4-methanol solution with 0.16 M of triethylamine were monitored by ^{1}H NMR, and the result was compared with the previous retro-benzoin condesnation. Table 4.10 compares the concentrations of each components for both the benzoin condensation and retro-benzoin reaction for different reaction times. In Table 4.10, "benzoin" represents benzoin condensation initiated with triazolium and benzaldehyde **135**, while the "retro" refers to the retro-benzoin reaction initiated from triazolium and benzoin **158**.

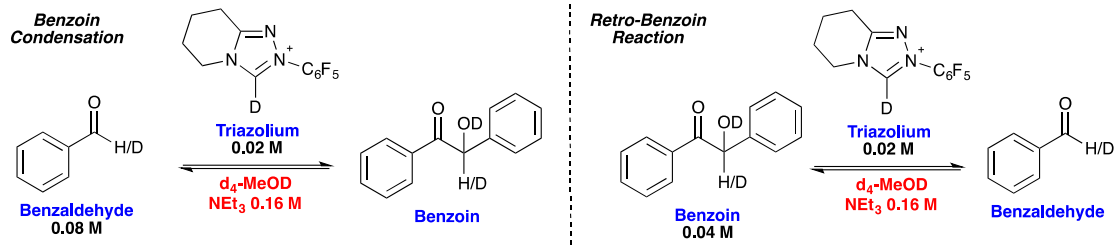

Table 4.10. % Components distribution of the retro-benzoin reaction of benzoin **158** (0.04 M) and benzoin condensation of benzaldehyde **135** (0.08 M) catalysed by pentafluorophenyl triazolium salt **99** (n=2, 0.02 M) in d_4-methanol at 25 °C, with 0.16 M NEt_3.

Exp.	Time/ h	D% (Ald)	D% (Ben)	Ald%	Add%	Ben%	Acid%
benzoin	0.07	34	9	17	6	74	4
retro	0.08	68	<0.1	7	3	88	3
benzoin	0.66	88	45	10	3	83	5
retro	0.67	86	5	9	4	87	4
benzoin	1.13	91	59	10	3	82	5
retro	1.11	90	12	9	3	83	5
benzoin	6.08	97	86	11	1	75	13
retro	6.09	98	74	10	1	77	12

* The percentage of components distribution were calculated from Equation 4.5-4.8.

Comparing ^{1}H NMR spectra of the benzoin condensation and retro-benzoin reaction, numbers and chemical shifts of reaction mixture signals are the same, indicating the

dialdehyde adduct **159** is not detectable. Either the ^{1}H NMR peaks of **159** overlapped with other components or the reaction rates for **159**'s consumption are quite large.

After a very short reaction time (< 1h), both the benzoin condensation and retro-benzoin reached equilibrium, with the concentration of all the components to be the same (~10% of aldehyde, ~3% of adduct, ~82% of benzoin, and ~5% of benzoic acid). The incremental change in benzaldehyde percentage after equilibrium should be owing to the decomposition of catalyst, which also decreased the adduct quantity.

Solvent effects on retro-benzoin reactions can be observed by changing d_2-dichloromethane to d_4-methanol, possibly owing to the higher dielectric constant of methanol. The formation rate of benzaldehyde in deuterated dichloromethane is around threefold that in deuterated methanol. Moreover, after 1.98 hours in both solvents, the two reactions have reached equilibrium, and the reaction mixture of retro-benzoin reaction in d_2-dichloromethane was formed by 24% of benzaldehyde, 7% of adduct, 55% of benzoin, and 14% of benzoic acid; while in d_4-methanol, only 10% of aldehyde has been synthesized, with 3% of adduct, 82% of benzoin left, and 6% of benzaldehyde oxidized into benzoic acid.

4.6. Summary

The extent of deuterium incorporation into reactant aldehyde (2-methoxybenzaldehyde **138**) was evaluated under different reaction conditions, including an examination of the following factors: the backbone modification of triazolium salts, concentrations of reactants, reaction temperature, choice of solvent, solution basicity and nucleophilicity. By changing the conditions and NHC catalyst, we hoped to suppress the formation of benzoin product **158**, and increase the formation and dissociation rate of the hydroxy aryl adduct **144** and Breslow intermediate **124**, thus, find a new catalytic approach

towards d_1-deuterated aldehyde.

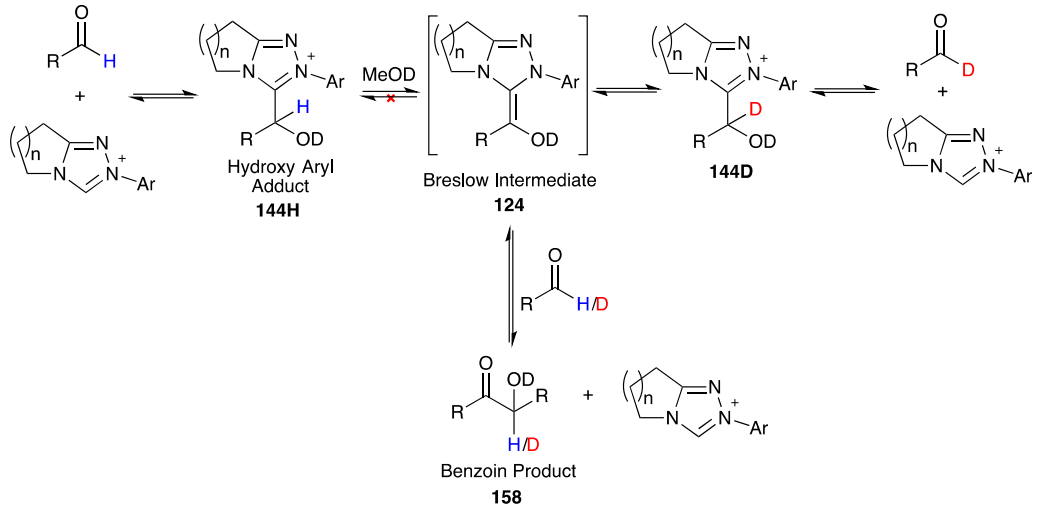

The sterically bulky *ortho*-substituted triazolium salt showed good suppression to the benzoin condensation, while they also trapped aldehyde in the hydroxy aryl adduct. By additionally checking the benzoin condensation reaction catalysed by N-*para*-fluorophenyl, N-*para*-methoxyphenyl, and N-phenyl triazolium salts, we observed that electron-deficient N-aryl substituents of triazolium salt increased the exchange rate of hydroxy aryl adduct, thus favouring the synthesis of d_1-deuterated aldehyde. Thus, pentafluorophenyl triazolium salt with different fused ring sizes **98, 99, 84** were chosen as the most promising candidate for deuterated evaluation. Further investigation suggested the pentafluorophenyl triazolium salt with a six-membered fused ring (**99**, n= 2) to be the ideal NHC precursors, with five-membered catalyst (n= 1) producing too much benzoin product, and the seven-membered analogue (n= 3) with very poor deuterium incorporation.

By analysing reactions performed under different buffer types (NEt_3: $NEt_3 \cdot HCl$ = 1:2, 1:1, 2:1), we observed that more basic solution favours both the H/D-exchange of the aldehydic proton, and the formation of benzoin product. Lower reaction temperatures slow down the entire process and trap more aldehyde in the hydroxy aryl adduct form.

Changing solvent from d_4-methanol to deuterium oxide showed an unidentified by-product.

Finally, the best deuterium exchange result was found at 2.2 hours with 0.02 M of pentafluorophenyl triazolium salt **99** (n= 2) loading and 0.08 M of aldehyde in d_4-methanol at 25 °C, with 0.16 M NEt_3. 73% of aldehyde remained, with 99% of deuterium incorporation, and only 14% of the initial aldehyde converted to benzoin product.

The H/D-exchange of other aromatic aldehydes was performed, however, only *ortho*-substituted aldehydes (*e.g.* 2-methylbenzaldehyde **136**) gave relatively satisfying results. Non-*ortho* substituted aldehyde all generated large quantities of benzoin-type products. We thus raised another possibility for synthetically accessing d_1-deuterated aldehydes from the retro-benzoin condensation. ^{1}H NMR spectroscopic analysis suggest the same distribution of products from the benzoin and retro-benzoin condensation. Initial exploration of the retro-benzoin with benzaldehyde and benzoin gave promising results with 97.4% deuteration of benzaldehyde.

4.7. Reference

1. H. J. Neuburg, J. Atherley and L. Walker, *Girdler-sulfide process physical properties*, Atomic Energy of Canada Ltd., 1977.
2. C. G. Swain and R. F. Bader, *Tetrahedron Lett.*, 1960, **10**, 182-199.
3. C. G. Swain, R. F. Bader and E. R. Thornton, *Tetrahedron*, 1960, **10**, 200-211.
4. M. Miyashita, M. Sasaki, I. Hattori, M. Sakai and K. Tanino, *Science*, 2004, **305**, 495-499.
5. D. H. Phillips, G. A. Potter, M. N. Horton, A. Hewker, C. Crofton-Sleigh, M. Jarman and S. Venitt, *Carcinogenesis*, 1994, **15**, 1487-1492.
6. M. Jarman, G. K. Poon, M. G. Rowlands, R. M. Grimshaw, M. N. Horton, G. A. Potter and R. McCague, *Carcinogenesis*, 1995, **16**, 683-688.
7. A. E. Mutlib, R. J. Gerson, P. C. Meunier, P. J. Haley, H. Chen, L. S. Gan, M. H. Davies, B. Gemzik, D. D. Christ, D. F. Krahn, J. A. Markwalder, S. P. Seitz, R. T. Robertson and G. T. Miwa, *Toxicol Appl Pharmacol*, 2000, **169**, 102-113.
8. Z. X. Tian, D. R. Reed and S. R. Kass, *Int. J. Mass Spectrom.*, 2015, **377**, 130-138.
9. J. Atzrodt, V. Derdau, T. Fey and J. Zimmermann, *Angew Chem Int Edit*, 2007, **46**, 7744-7765.

10. W. JamesáCatallo, *Chem. Soc. Rev.*, 1997, **26**, 401-406.
11. A. Di Giuseppe, R. Castarlenas and L. A. Oro, *C. R. Chim.*, 2015, **18**, 713-741.
12. T. Maegawa, Y. Fujiwara, Y. Inagaki, H. Esaki, Y. Monguchi and H. Sajiki, *Angew Chem Int Edit*, 2008, **47**, 5394-5397.
13. T. Maegawa, Y. Fujiwara, Y. Inagaki, Y. Monguchi and H. Sajiki, *Adv. Synth. Catal.*, 2008, **350**, 2215-2218.
14. P. Avenier, X. Solans-Monfort, L. Veyre, F. Renili, J.-M. Basset, O. Eisenstein, M. Taoufik and E. A. Quadrelli, *Top. Catal.*, 2009, **52**, 1482-1491.
15. T. Maegawa, N. Ito, K. Oono, Y. Monguchi and H. Sajiki, *Synthesis*, 2009, **2009**, 2674-2678.
16. J. Atzrodt and V. Derdau, *Journal of Labelled Compounds & Radiopharmaceuticals*, 2010, **53**, 674-685.
17. Y. Sawama, T. Yamada, Y. Yabe, K. Morita, K. Shibata, M. Shigetsura, Y. Monguchi and H. Sajiki, *Adv. Synth. Catal.*, 2013, **355**, 1529-1534.
18. J. M. Buchanan, J. M. Stryker and R. G. Bergman, *J. Am. Chem. Soc.*, 1986, **108**, 1537-1550.
19. B. A. Arndtsen and R. G. Bergman, *Science*, 1995, 1970-1972.
20. T. Furuta, A. Suzuki, M. Matsuzawa, H. Shibasaki and Y. Kasuya, *Steroids*, 2003, **68**, 693-703.
21. J. Zanetti and D. Sickman, *J. Am. Chem. Soc.*, 1936, **58**, 2034-2035.
22. A. F. Thompson and N. H. Cromwell, *J. Am. Chem. Soc.*, 1939, **61**, 1374-1376.
23. J. Xie, P.-K. Lo, C.-S. Lam, K.-C. Lau and T.-C. Lau, *Dalton Trans.*, 2018, **47**, 240-245.
24. J. Motoyoshiya, T. Yazaki and S. Hayashi, *J. Org. Chem.*, 1991, **56**, 735-740.
25. S. L. Scott, A. Bakac and J. H. Espenson, *J. Am. Chem. Soc.*, 1992, **114**, 4205-4213.
26. S. J. Gould and X.-C. Cheng, *Tetrahedron Lett.*, 1993, **49**, 11135-11144.
27. V. Stanjek, M. Miksch and W. Boland, *Tetrahedron*, 1997, **53**, 17699-17710.
28. K. Yamaguchi and N. Mizuno, *Angew Chem Int Edit*, 2002, **41**, 4538-4542.
29. J. T. Kendall, *Journal of Labelled Compounds and Radiopharmaceuticals*, 2000, **43**, 917-924.
30. R. M. Bullock and B. J. Rappoli, *J. Am. Chem. Soc.*, 1991, **113**, 1659-1669.
31. K. Choudhary, P. K. Sharma and K. K. Banerji, *International Journal of Chemical Kinetics*, 1999, **31**, 469-475.
32. G. Chowdhury, M. W. Calcutt and F. P. Guengerich, *J Biol Chem*, 2010, **285**, 8031-8044.
33. H. Goerner and H. Kuhn, *J. Phys. Chem.*, 1986, **90**.
34. D. W. Barnett, M. S. Refaei and R. W. Curley, Jr., *J Labelled Comp Radiopharm*, 2013, **56**, 6-11.
35. R. M. Magid, O. S. Fruchey, W. L. Johnson and T. G. Allen, *J. Org. Chem.*, 1979, **44**, 359-363.
36. M. Y. S. Ibrahim and S. E. Denmark, *Angew Chem Int Edit*, 2018, **57**, 10362-10367.
37. M. Zhang, X. A. Yuan, C. Zhu and J. Xie, *Angew Chem Int Edit*, 2019, **58**, 312-316.
38. W. J. Kerr, M. Reid and T. Tuttle, *Angew Chem Int Edit*, 2017, **56**, 7808-7812.
39. E. S. Isbrandt, J. K. Vandavasi, W. Y. Zhang, M. P. Jamshidi and S. G. Newman, *Synlett*, 2017, **28**, 2851-2854.
40. N. Iranpoor, H. Firouzabadi, E. Etemadi-Davan, A. Rostami and K. R. Moghadam, *Appl Organomet Chem*, 2015, **29**, 719-724.
41. J. T. Spletstoser, J. M. White, A. R. Tunoori and G. I. Georg, *J. Am. Chem. Soc.*, 2007, **129**, 3408-3419.
42. E. M. Higgins, J. A. Sherwood, A. G. Lindsay, J. Armstrong, R. S. Massey, R. W. Alder and A. C.

O'Donoghue, *Chem. Commun.*, 2011, **47**, 1559-1561.

43. J. ZHU, Durham University, 2016.

Chapter 5. Synthesis and Catalytic Reaction of BAC

5.1. Introduction

Bis(amino)cyclopropenylidenes (BACs) are an outstanding catalyst with similar characteristics to NHCs[1]. Normal NHCs' electronic stability is usually influenced by the mesomeric and inductive effects provided by the adjacent nitrogen atoms (Chapter 1). With two exocyclic nitrogen atoms, the stability of Bis(amino)cyclopropenylidene (BAC) derivatives, are electronically stabilised by a significant degree of surface electron delocalization (σ-aromaticity) of the three-membered ring[2]. The potential resonance structures formed with adjacent nitrogen atoms (Scheme 5.1)[3], and the small bond angle of the divalent carbon centre, speculatively, also contribute to BAC's stability[4, 5].

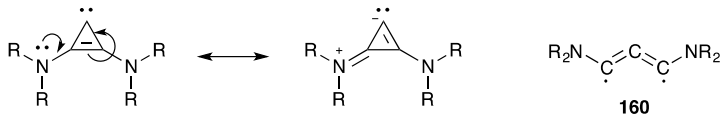

Scheme 5.1. Canonical resonance of BAC and potential ring-opening product **160**.

Apart from the electronic stabilisation for BACs, sterically bulky N-substituents could also increase the dimerization energy barrier for both carbene analogues[3, 6, 7]. A computational study by Bertrand raised the possibility for the BAC system to be sterically overloaded, *e.g*. with *t*-Bu and TMS substituents. These models suggested the steric strain exerted by bulky substituents has the tendency to rotate the amino groups out of the plane formed by the three-membered ring, and forced the centre ring to undergo a ring-opening process to afford the corresponding propadienylidene biradical **160**. Disappointingly, no mechanism towards the formation of biradical **160** has been provided.

Compared with NHCs, the published syntheses of BACs are slightly more straightforward, with only a two-step protocol[8], although the scope in terms of substituent variation is relatively limited. As a result of the long distance between the carbene centre and N-substituents, BACs are considered as the least sterically hindered carbenes. Furthermore, ^{31}P NMR studies indicated the BACs to be comparable π-acceptors to NHCs by investigating their corresponding adducts formed with phenylphosphinidene, respectively[9]. The studies of carbonyl stretching frequencies within rhodium complexes suggest BACs as stronger σ-donors[10]. Moreover, based on our group's unpublished results, the pK_as of the conjugated acid of BACs are comparable to imidazolyl carbenes.

Since the first free BAC was crystallised in 2006 (Scheme 5.2), both their modification and application developed rapidly, however, mainly focused on the organometallic complexes with BAC ligands[11]. Despite the fact that bis(amino)cyclopropenylidenes (BACs) have good stability and potentially can undergo classic NHC-like umpolung reactions, their applications are still limited. Only a few examples of organocatalytic transformations have been reported utilising BACs as catalysts (benzoin, Stetter, aza-benzoin, and conjugate addition).

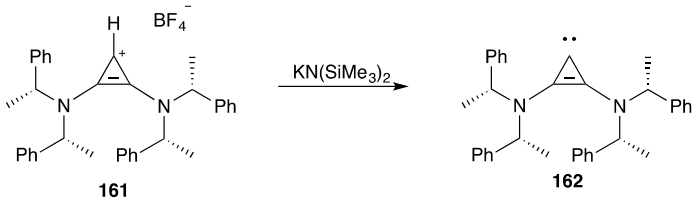

161 **162**

Scheme 5.2. First chiral bis(amino)cyclopropenylidene **161** and its precursor **162**.

In 2007, Tamm reported the first self-condensation of benzaldehyde catalysed by the chiral BAC **162**, however, with unsatisfactory enantioselectivity (18% *ee*) and limited details provided[12]. ^{13}C NMR data of the BAC **162** suggests the loss of signal degeneracy corresponded to the 1-phenylethyl moiety compared with cyclopropenium salt **161**,

which indicates the collapse of enantioselectivity, possibly as a consequence of rapid internal rotation of the carbene, and suggesting the need of less flexible BAC structures.

Six years after Tamm's work, Gravel reported the first Stetter reaction catalysed by BACs with excellent yields, regio- and chemo-selectivities (Scheme 5.3)[13]. Their work compared the catalytic efficacies between the isopropyl-substituted carbene **163** (yield <10%) and ethyl-substituted carbene **164** (yield= 98%), highlighting the influence of sterically hindered substituents in BACs (Scheme 5.3).

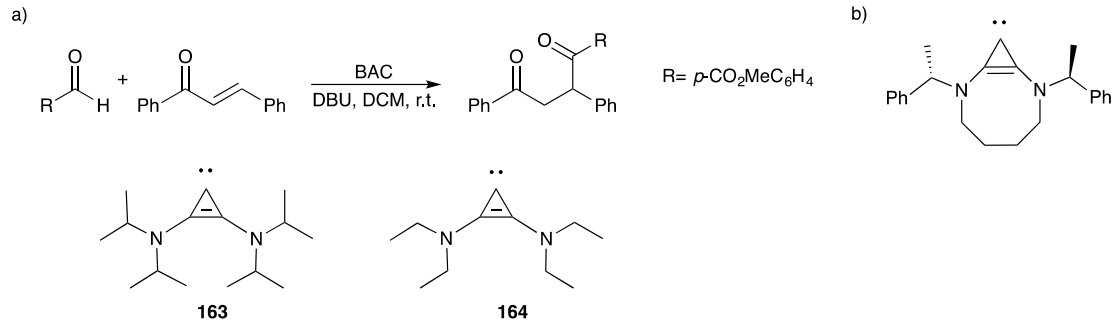

Scheme 5.3. a) Gravel's Stetter reaction catalysed by bis(amino)cyclopropenylidene **163** and **164**, b) Chiral bis(amino)cyclopropenylidene formed by a diamine.

In contrast to thiazolyl and triazolyl carbene derivatives, the BAC catalysed Stetter reaction can tolerate the utilisation of inactivated electron-rich aldehydes and β-alkyl substituted ketone acceptors, remarkably, without a competing homobenzoin reaction. Unpublished results from the O'Donoghue group support the latter report of Gravel of the absence of any homo benzoin product for these BAC-catalysed process. The competition experiment by loading two aldehydes simultaneously suggested BACs have the opposite tendency from NHCs to react with more hindered but less electron-rich aryl-aldehydes. Moreover, an enantioselective Stetter reaction involving unsaturated ketones was performed by the chiral BAC to afford the product with excellent yield (99 %) and moderate enantioselectivity (36% *ee*)[13].

To limit the formation of benzoin by-product, a traditional cross-aza-benzoin reaction restricts the selection of reagents due to the reversibility of the entire catalytic circle. Gravel claimed BAC **165** to be an excellent catalyst towards the aza-benzoin reaction with no by-product formation, and the reversibility of aza-benzoin product was confirmed. By contrast, both the formation and dissociation of dimerised aldehyde (benzoin-type product) was not observed (Scheme 5.4)[1].

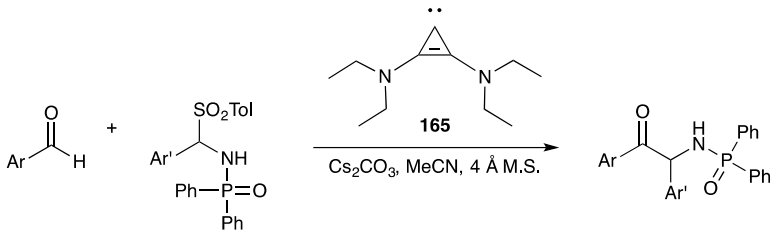

Scheme 5.4. BAC **165** catalysed cross-aza-benzoin condensation.

Schneider reported a general catalytic example of an aza-Morita-Baylis-Hillman (aza-MBH) reaction with low catalyst loading and mild conditions (Scheme 5.5). Interestingly, the counter ion of the BAC precursor influenced the product yield: the existence of tetrafluoroborate anion generated the product with 60% higher yield than tetraphenylborate. Moreover, 1 mol% loading of BAC **165** with tetrafluoroborate anion gave 90% yield, indicating the higher efficacy of BACs than conventional aza-MBH catalysts, *e.g.* N- or P-centered Lewis bases and NHCs[8].

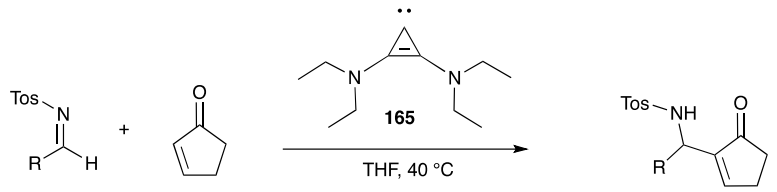

Scheme 5.5. BAC catalysed aza-Morita-Baylis-Hillman reaction.

An intermolecular MBH reaction between *α, β*-unsaturated carbonyl compounds **166** and *p*-quinone methides **167** catalysed by BAC was illustrated by Anand *et al.* recently.

Based on their outcomes, a plausible mechanism of the MBH reaction was proposed (Scheme 5.6). Moreover, different from Gravel's BAC-catalysed Stetter reactions, the attempts using chiral BAC **162** and **168** both led to racemic mixtures[14].

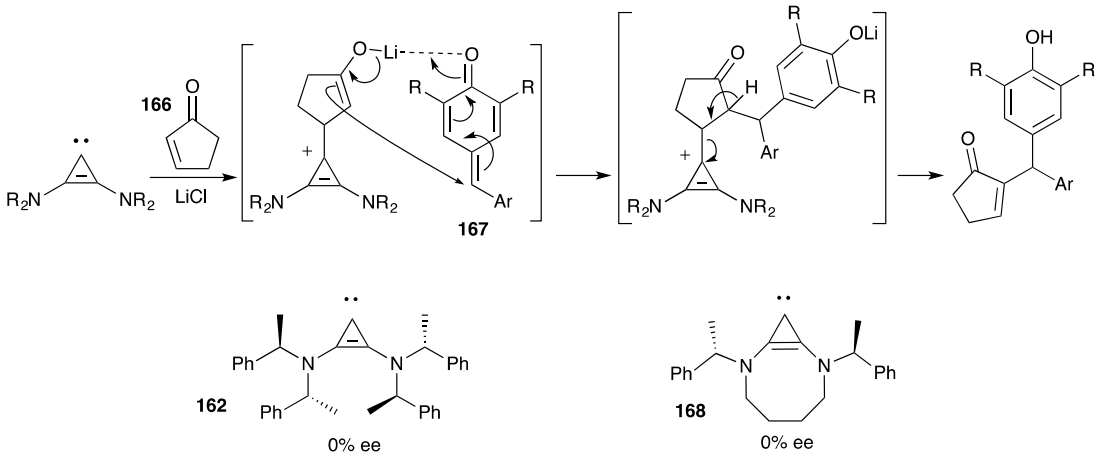

Scheme 5.6. Plausible mechanism of MBH reaction, and the chiral BACs used for the enantioselective investigation.

The high reactivity and excellent efficacy of BAC **165** can also be applied to the 1,6-conjugate addition between aryl-aldehydes and *p*-quinone methides (Scheme 5.7). Markedly, no corresponding products were formed in the case of aliphatic aldehydes, however, without any reason being suggested[15].

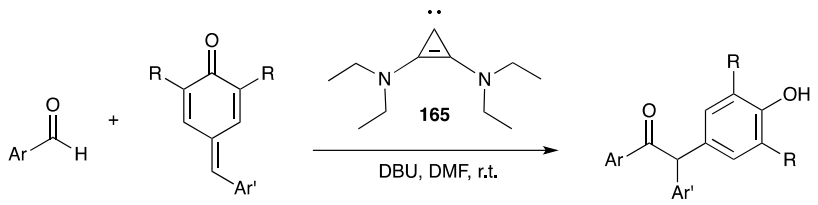

Scheme 5.7. BAC **165** catalysed 1,6-conjugate addition.

Recently, Anand demonstrated the 1,4- and 1,6-conjugate addition of carbon nucleophiles catalysed by BACs, which first applied BACs as a non-covalent Brønsted base (Scheme 5.8)[16]. Although the pK_a of BACs are comparable to the imidazolyl carbenes, the product's outcome yields catalysed by BACs (75~94%) are higher than

NHCs (50~65%). Thus BAC and NHC nucleophilicities may not parallel their basicities.

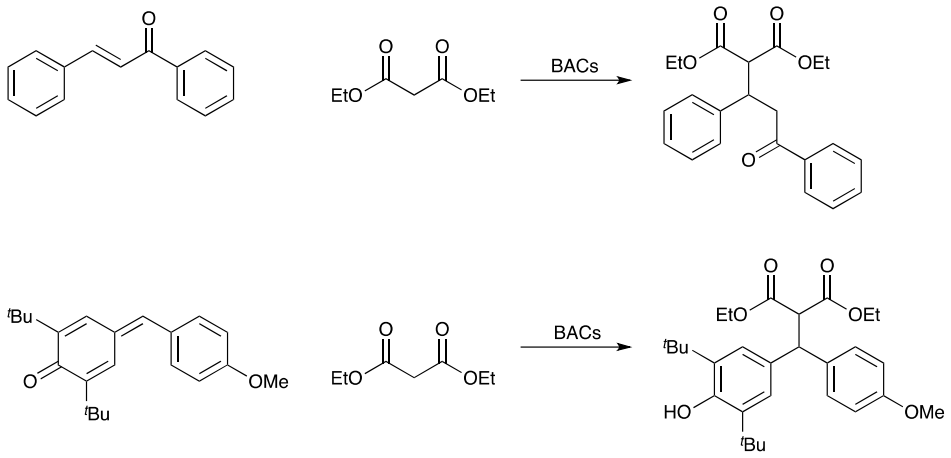

Scheme 5.8. 1,4- and 1,6-conjugate addition catalysed by BACs.

5.2. Syntheses of BAC Precursors

During my project, the syntheses of three bis(amino)cyclopropenium salts were attempted *via* two different procedures (Figure 5.1). The diisopropyl and diphenylethyl cyclopropenium salts (**169** and **170**) have been obtained by Bertrand and Tamm *via* Procedure A[12, 17], while there is currently no published synthetic procedure of morpholine substituted cyclopropenium **171**, and the salt was successfully generated *via* Procedure B (Scheme 5.9). This section mainly discusses the synthetic routes towards these cyclopropenium salts.

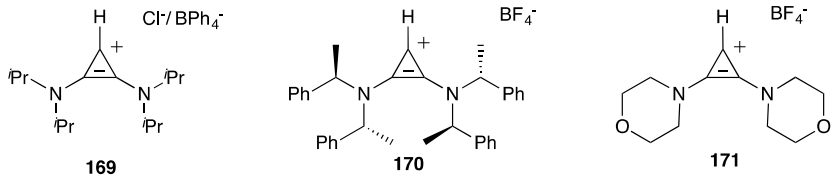

Figure 5.1. Selectively synthesized bis(amino)cyclopropenium salts **169, 170,** and **171**.

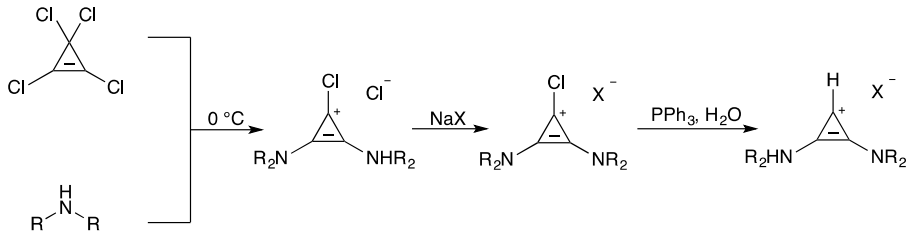

Synthetic procedure A.

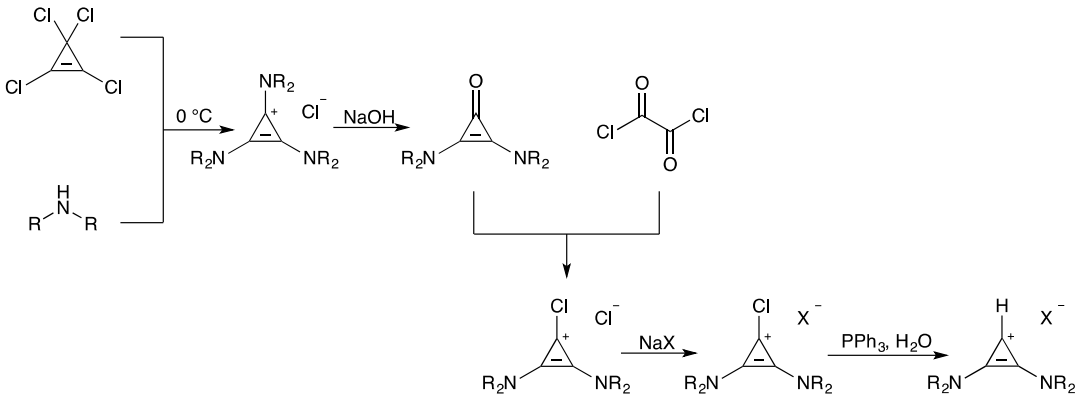

Synthetic procedure B.

Scheme 5.9. General procedures utilised for the preparation of cyclopropenium salts.

The syntheses of BAC precursors, bis(amino)cyclopropenium salts, was first developed in 1971[18]. Starting from the tetrachlorocyclopropene and the disubstituted amines, Yoshida prepared several di- and tri-substituted cyclopropenium rings. Yoshida suggested the bulky secondary amines, like diisopropylamine, have the trend to form di-substituted products. Meanwhile, the less bulky amines, like dimethylamine, favour the formation of tri-substituted product.

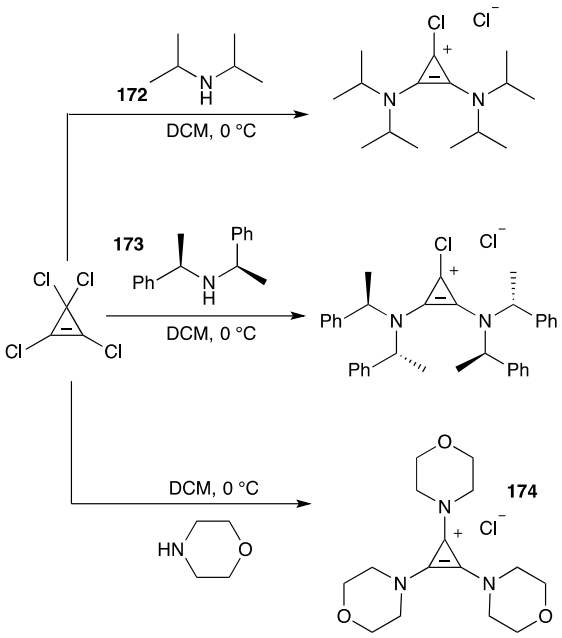

Scheme 5.10. Different product outcomes caused by changing the steric hindrance

During my project, the reaction of diisopropylamine **172** and diphenylethylamine **173** with tetrachlorocyclopropene gave di-substituted cyclopropenium rings with chloride as counter ion. Meanwhile, the reaction between morpholine and tetrachlorocyclopropene always give tri-substituted product. Wilde[1] suggested that decreasing the temperature of reaction mixtures to -78 °C could slow down the addition of diethylamine to the tetrachlorocyclopropene, therefore primarily leading to di-substituted product. However, LCMS suggested the major product of reaction with morpholine still to be the tri-substituted cyclopropenium **174** at -78 °C, and extra steps were required to obtain the di-substituted morpholine cyclopropenium salt (Scheme 5.11). Moreover, the unreacted morpholine hydrochloride salt cannot be removed by purification of **174** *via* extraction (water/DCM) or recrystallisation (DCM/diethyl ether).

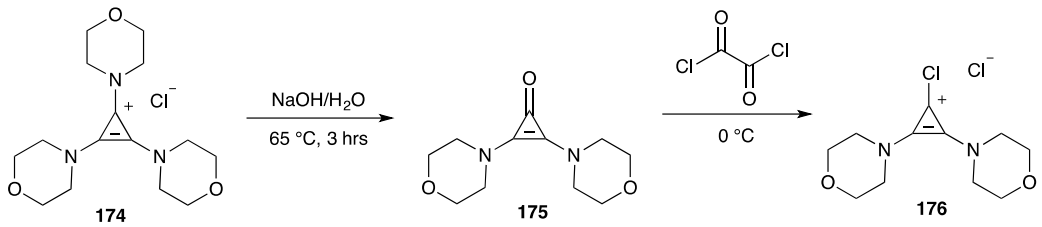

Scheme 5.11. Synthesis of bis(morpholino)cyclopropenium **176**.

Previous research suggested heating up the solution of tri-substituted cyclopropenium with base, and followed by the treatment with oxalyl chloride can probably give the corresponding di-substituted products[19]. Thus, an excess amount of sodium hydroxide was added to the aqueous solution of the mixture of **174** and morpholine hydrochloride salt. Analysis by LCMS suggest the solution need to be heated to 65 °C for at least three hours for reaction to occur. After DCM washing followed by carefully recrystallisation, the bis(morpholino)cyclopropenone **175** was obtained as a pale-yellow solid. Currently, there is no published methodology to the morpholino cyclopropenone **175**, and the structural data suggests the crystal is cross-linked by various intermolecular interactions between protons and oxygens (Figure 5.2). Oxalyl chloride was added to the solid of **175** at 0 °C, and generated the di-substituted chlorocyclopropenium salts **176** with chloride as counter ion.

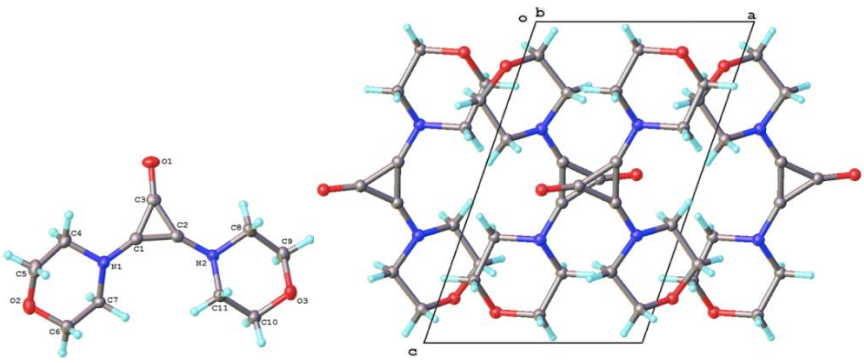

Figure 5.2. Crystal structure of bis(morpholino)cyclopropenone **175**.

According to previous research, sodium tetraphenylborate and sodium tetrafluoroborate were applied for counter ion replacement (Scheme 5.12). For

diisopropyl(amino)cyclopropenium chloride **169**, its counter ion only partially replaced by using $NaBPh_4$, which was suggested by the ^1H NMR spectrum of the final product and will be discussed later. Sodium tetrafluoroborate was used for the counter ion replacement of the diphenylethyl- and morpholine-(amino)cyclopropenium salts **170** and **171**.

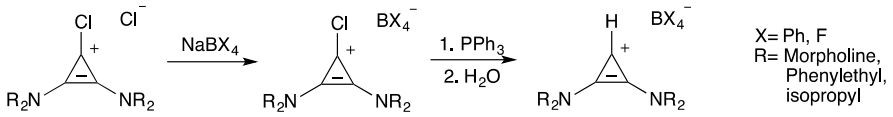

Scheme 5.12. Counter ion replacement and dichlorination of bis(amino)cyclopropenium.

The dechlorination by using triphenylphosphine followed by the addition of water afforded the final products **169-171**. Current research suggests the chemical shift of cyclopropenium hydrogen is influenced by counter ions. For example, literature suggests in the cases of diisopropyl(amino)cyclopropenium derivatives (with $CDCl_3$ as NMR solvent), that the chemical shift of the cyclopropenium proton is 7.45 ppm with BF_4^- as counter ion[20], and 8.97 ppm with Cl^- [21], 4.92 ppm with BPh_4^- [10]. The ^1H NMR spectrum ($CDCl_3$) shows the chemical shift of the cyclopropenium proton of diisorpopyl(amino)cyclopropenium **169** obtained in this project is 7.44 ppm, which suggest the counter ion could be a mixture of BPh_4^- and Cl^-. Meanwhile, the smaller integration of the BPh_4^- peaks than the alkyl peaks also supports this. Following counter ion exchange by using bis(triphenylphosphoranylidene)ammonium chloride (PPNCl) **177** failed due to the difficulty in separating BAC from the excess amount of the PPNCl salt.

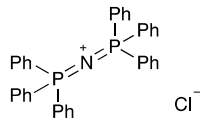

Figure 5.3. Bis(triphenylphosphoranylidene)ammonium chloride salt **177**

LC-MS analysis suggested the dechlorination to form the

diphenylethyl(amino)cyclopropenium **171** to be a success, however, the purification of the product failed by recrystallisation and column chromatography.

During the dechlorination of di(morpholino)cyclopropenium salts, a ring opened by-product **178** was obtained during recrystallisation. X-ray crystallography suggest the structure of this by-product to be a triphenylphosphine substituted ketone (Figure 5.4), and a possible mechanism of formation is shown in Scheme 5.13. The observation of a ring-opening product is surprising as the opening of the aromatic ring should be challenging. Perhaps the less sterically congested morpholino substituent (versus isopropyl) permits S_N2 attack to phosphonium adduct **179**, although evidence for this was not obtained. The presence of a cationic phosphorous may facilitate the difficult ring opening *via* a vinyl anion possibly concerted with protonation.

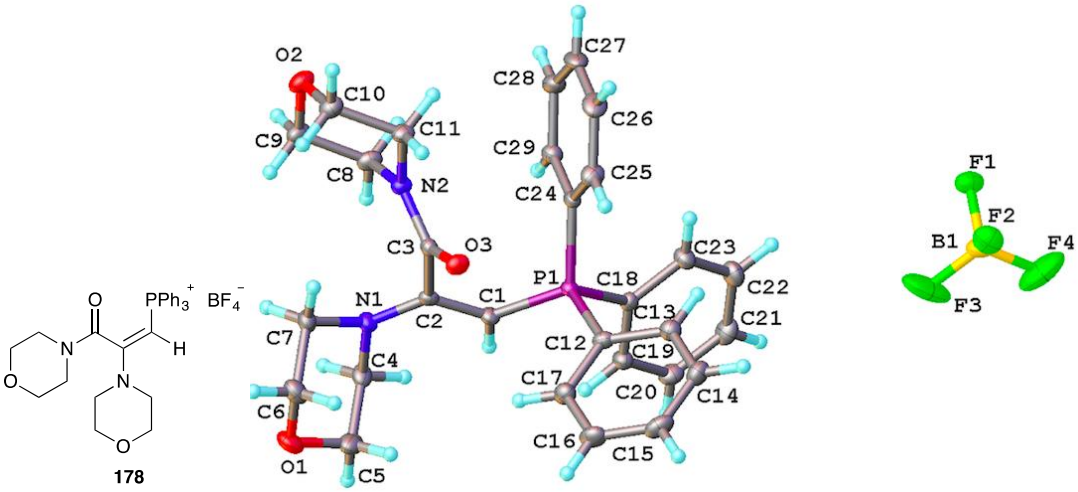

Figure 5.4. Crystal structure of α,β-unsaturated amide **178**.

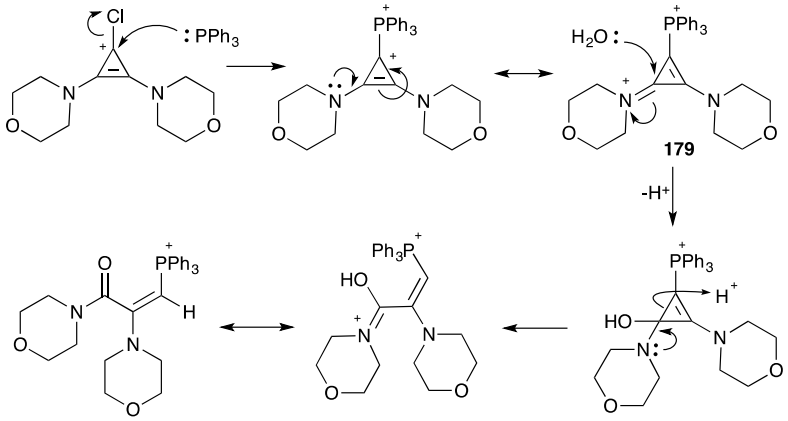

Scheme 5.13. Possible mechanism for formation of α,β-unsaturated amide **178**.

Furthermore, in the course of these studies, an inorganic crystal has been characterized, with no record on the inorganic crystal database (ICSD) (Figure 2.8). The molecular formula of this crystal is suggested to be $NaNH_4(BF_4)_2$, with a highly disordered ammonium cation.

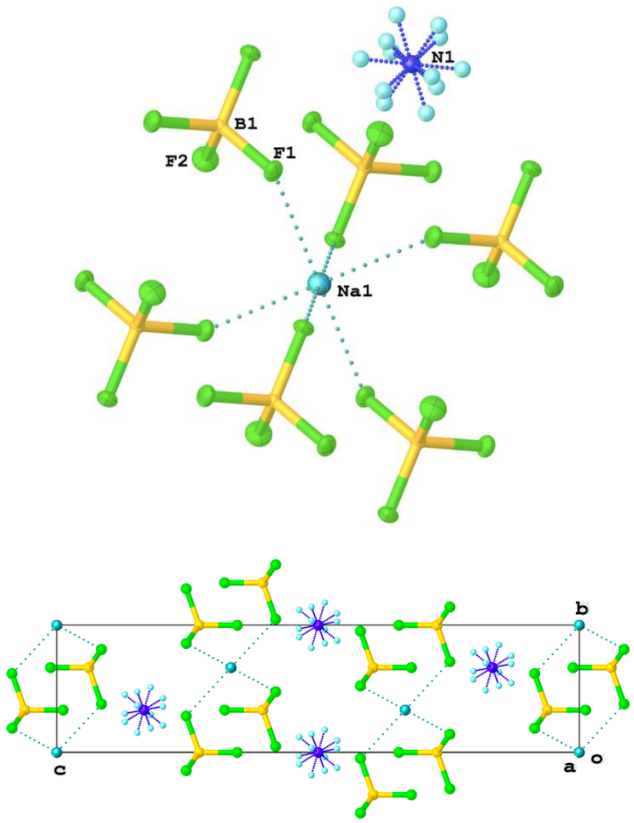

Figure 5.5. Inorganic crystals isolated during synthesis.

5.3. Summary

This chapter introduced the developments and applications of bis(amino)cyclopropenylidenes. The syntheses of three different bis(amino)cyclopropenium salts **169-171** were attempted by using two procedures. A new cyclopropenium derivative with morpholine substituents was synthesized and several crystal structures, including by-product and reaction intermediates, were obtained to help probe the synthetic route.

5.4. Reference

1. M. M. Wilde and M. Gravel, *Org Lett*, 2014, **16**, 5308-5311.
2. L. E. Johnson and D. B. DuPre, *J Phys Chem A*, 2007, **111**, 11066-11073.
3. W. W. Schoeller, G. D. Frey and G. Bertrand, *Chemistry*, 2008, **14**, 4711-4718.
4. A. Kausamo, H. M. Tuononen, K. E. Krahulic and R. Roesler, *Inorg Chem*, 2008, **47**, 1145-1154.
5. T. J. Lee, A. Bunge and H. F. Schaefer, *J. Am. Chem. Soc.*, 1985, **107**, 137-142.
6. A. Poater, F. Ragone, S. Giudice, C. Costabile, R. Dorta, S. P. Nolan and L. Cavallo, *Organometallics*, 2008, **27**, 2679-2681.
7. S. C. Carbenes, *Angew. Chem., Int. Ed.*, 2010, **49**, 8810-8849.
8. X. Lu and U. Schneider, *Chem Commun (Camb)*, 2016, **52**, 12980-12983.
9. O. Back, M. Henry‐Ellinger, C. D. Martin, D. Martin and G. Bertrand, *Angew. Chem., Int. Ed.*, 2013, **52**, 2939-2943.
10. G. Kuchenbeiser, B. Donnadieu and G. Bertrand, *J Organomet Chem*, 2008, **693**, 899-904.
11. B. T. Ramanjaneyulu, S. Mahesh and R. V. Anand, *Org Lett*, 2015, **17**, 3952-3955.
12. D. Holschumacher, C. G. Hrib, P. G. Jones and M. Tamm, *Chem Commun (Camb)*, 2007, DOI: 10.1039/b706708a, 3661-3663.
13. M. M. Wilde and M. Gravel, *Angew Chem Int Edit*, 2013, **52**, 12651-12654.
14. P. Goswami, S. Sharma, G. Singh and R. Vijaya Anand, *The Journal of organic chemistry* 2018, **83**, 4213-4220.
15. B. T. Ramanjaneyulu, S. Mahesh and R. Vijaya Anand, *Org Lett*, 2015, **17**, 6-9.
16. G. Singh, P. Goswami and R. Vijaya Anand, *Org Biomol Chem*, 2018, **16**, 384-388.
17. B. Goldfuss and M. Schumacher, *J Mol Model*, 2006, **12**, 591-595.
18. Z. I. Yoshida and Y. Tawara, *J. Am. Chem. Soc.*, 1971, **93**, 2573-&.
19. D. TUCKER, Durham University, 2018.
20. R. Mir and T. Dudding, *J Org Chem*, 2018, **83**, 4384-4388.
21. Y. D. Bidal, M. Lesieur, M. Melaimi, F. Nahra, D. B. Cordes, K. S. A. Arachchige, A. M. Z. Slawin, G. Bertrand and C. S. J. Cazin, *Adv. Synth. Catal.*, 2015, **357**, 3155-3161.

Chapter 6. Conclusions and Future Work

6.1. Conclusions

Overall, the syntheses of sixteen N-aryl substituted bicyclic triazolium salts **77-92** were attempted (Figure 6.1). Among these triazolium salts, **88** was first designed in my MSc degree, and the synthetic procedures of **81, 84-87, 89** have been published previously[1-3], while there are no previous reports of the preparation of **77-80, 82, 83, 90-92**. Among the sixteen triazolium salts, the 2,4,6-trichlorophenyl triazolium salt **82, 83** and mesityl triazolium salt **87** could not be purified as only trace amounts were identified by mass spectrometry, the indole triazolium **92** was not detected by mass spectrometry, and the other twelve triazolium salts were successfully isolated and purified. Furthermore, crystal structures were obtained for triazolium salt **77, 79, 84-86, 90, 91, 103-105**.

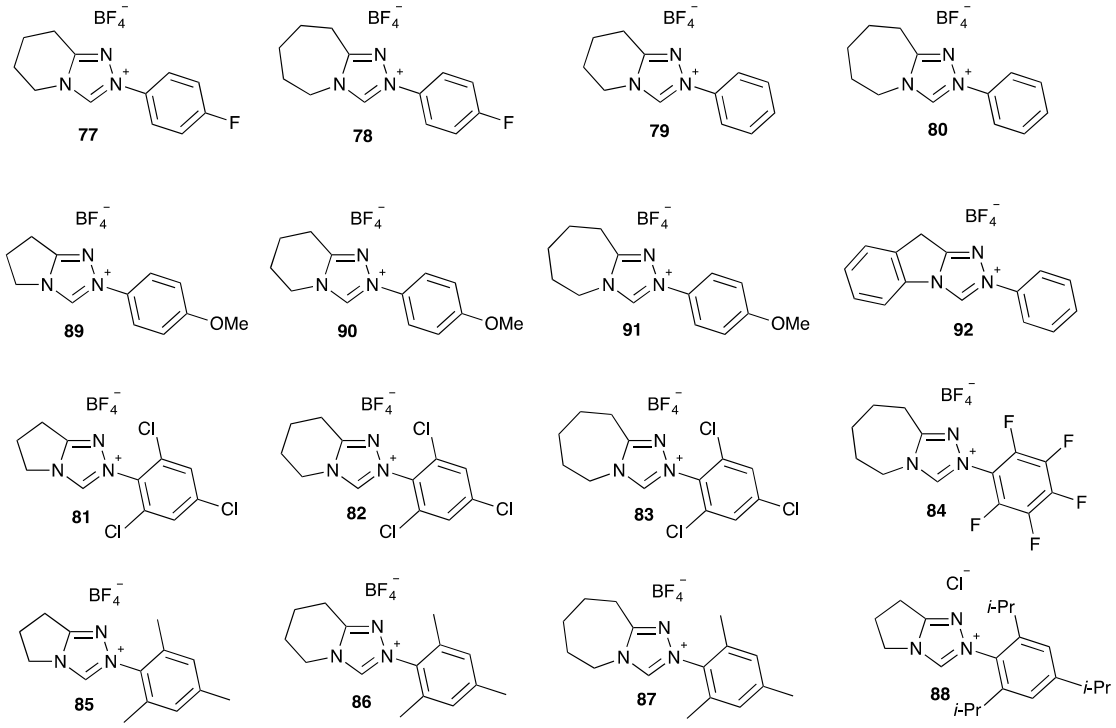

Figure 6.1. Selectively prepared bicyclic N-aryl triazolium salts **77-81, 84-86, 88-91**

During the preparation of these triazolium salts, a novel dialkoxy acetal adduct was isolated, whose formation probably can explain the difficult access towards certain triazolium salts. LC-MS analysis suggests the formation of this dialkoxy acetal adduct is favoured by the electron-withdrawing N-aryl groups and *ortho*-substituted aryl rings. We thus modified the synthetic procedure and the syntheses of six dialkoxy acetal adducts **111-116** were attempted. We successfully isolated and purified three dialkoxy acetal adducts **111, 112, 114** with 2,4,6-trichlorophenyl as N-aryl substituent, while ^{1}H NMR suggest the dialkoxy acetal adduct with 7-membered fused rings (**115,** and **116**) to be a mixture with the corresponding triazolium salt, and cannot be purified by recrystallisation. During the preparation of these dialkoxy acetal adducts, crystal structures of four intermediary amidrazones **107-110**, and four single X-ray crystal structures of dialkoxy acetal adduct **111, 112, 114, 116** were obtained.

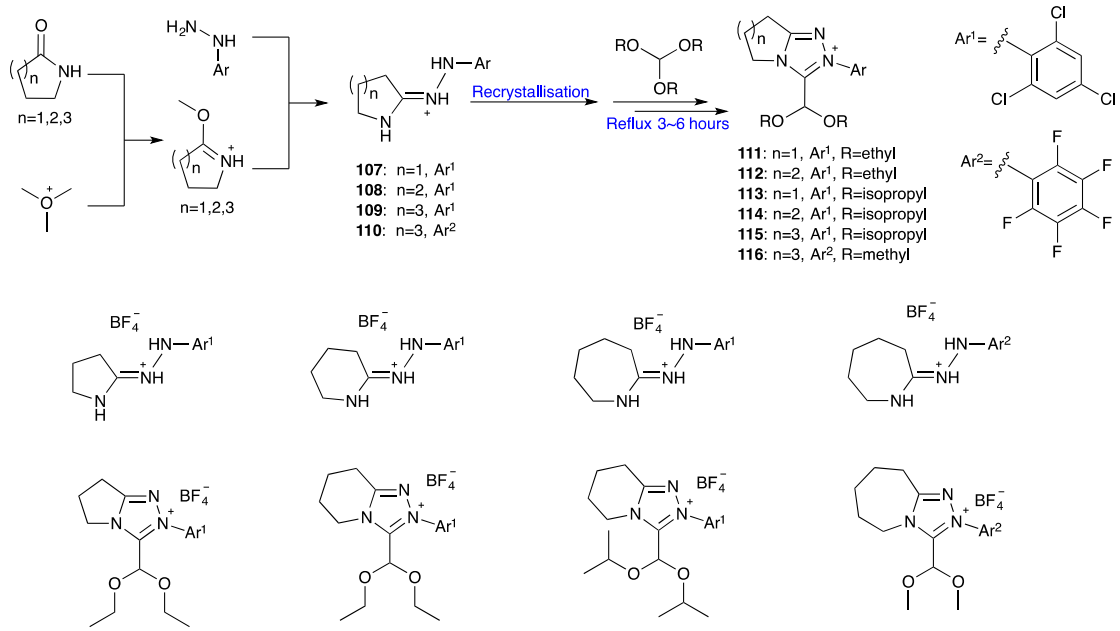

Scheme 6.1. Synthetic procedures towards dialkoxy acetal adduct **111-116**, and the crystal structures obtained.

In parallel, three synthetic trials of bis(amino)cyclopropenium salts, precursors of a new class of carbene, were performed, with bis(diisopropylamino)- and bis(morpholino)-

cyclopropenium salts **167** and **171** being prepared successfully. The bis(diisopropyl-amino)cyclopropenium **169** was suggested to have mixed counter ions, while the purification of bis[(*R*-1-phenylethyl)amino]cyclopropenium **170** was challenging. Meanwhile, there is no current report of bis(morpholino)cyclopropenium **171**, and the crystal structure of its intermediary cyclopropenone **175** was obtained.

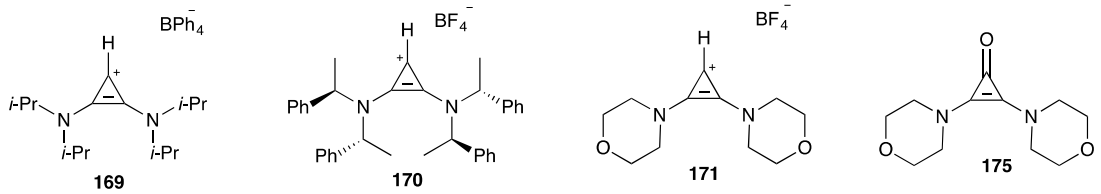

Figure 6.2. Structures of bis(amino)cyclopropenium salts **169-171**, and cyclopropenone **175**.

The second aim of the project was to kinetically evaluate the backbone structure of triazolium salts (*e.g.* fused ring size, N-aryl substituent) in the triethylamine-buffered benzoin reaction in d_4-methanol. In total, seventeen aryl-substituted aldehydes and fifteen N-aryl bicyclic triazolium salts were used to conduct over one hundred kinetic experiments. The formation and decay of reactants, intermediates, products and by-products were monitored *in situ* by ^{1}H NMR spectroscopy, in triethylamine-buffered d_4-methanol solution at 25 °C.

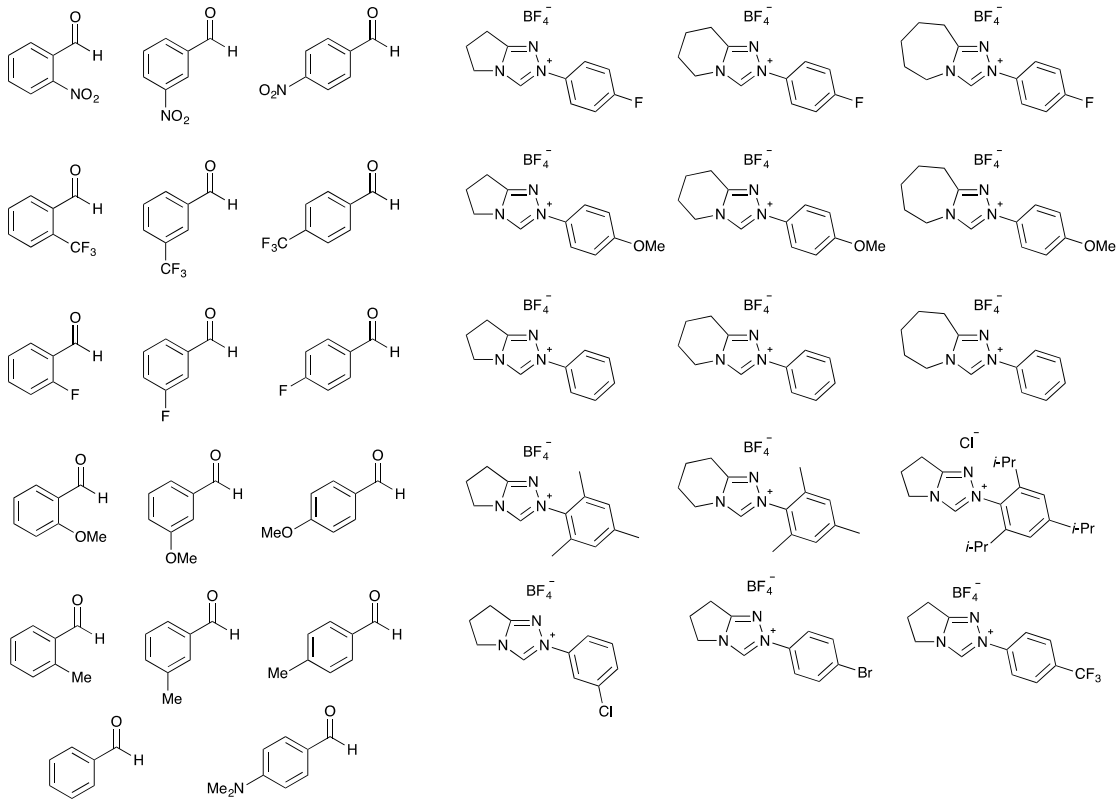

Figure 6.3. Aldehydes and triazolium salts used for the detailed kinetic evaluation of benzoin condensation.

During the benzoin condensation, the 3-hydroxy aryl adduct **144** was the only observed intermediate, with its fast transformation into Breslow intermediate being indirectly proven by the deuteration of hydroxyaryl adduct.

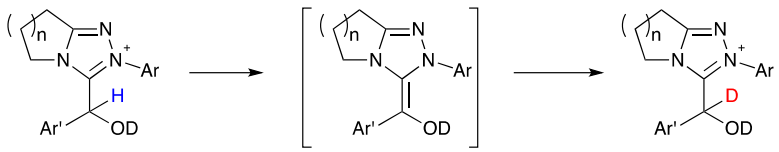

Scheme 6.2. Evidence of formation of Breslow intermediate **124** *via* H/D-exchange of hydroxy aryl adduct **144**.

The formation and decomposition rate constants, equilibrium constants of the hydroxy aryl adduct **144** were calculated and fitted by using three parallel methods from the concentration profile. The influence of the catalyst and aldehyde backbone structures towards the reaction parameters of adduct formation and consumption (k_1, k_{-1}, K, k_2)

were analysed and discussed. The structural data obtained from single X-ray crystallography and computer modelling (DFT) were analysed.

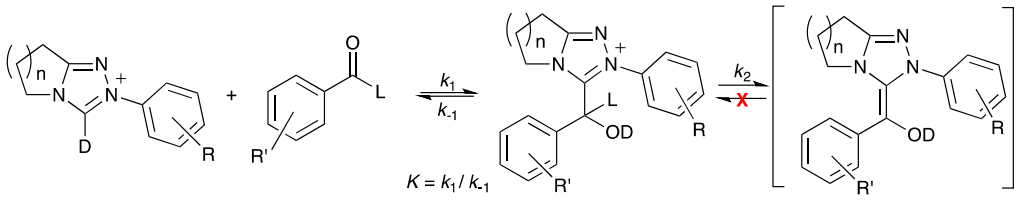

Scheme 6.3. Brief mechanism towards the formation and consumption of hydroxy aryl adduct **144**.

Increasing fused ring size from 5 (n= 1) to 6 (n= 2) largely decreased the adduct formation rate constants ($k_1^{n=1/n=2}$ = 4.2-7.8 fold), while the k_1 values for n= 2 and 3 are comparable ($k_1^{n=2/n=3}$= 1.1-2.9 fold). The opposite trend for the adduct dissociation constants (k_{-1}) can be observed ($k_{-1}^{n=1/n=2}$ = 0.42-0.97 fold, $k_{-1}^{n=2/n=3}$ = 0.33-0.74 fold). The combined variation of k_1 and k_{-1} lead to the overall equilibrium constants decreasing in the order $K^{n=1} >> K^{n=2} > K^{n=3}$ ($K^{n=1/n=2}$ = 5.4-13.3 fold, $K^{n=2/n=3}$ = 2.5-5.3 fold). By analysing the existing crystal structures of triazolium salts with different fused ring size, the first structural based explanation towards the catalyst performance were suggested. We postulated that the relatively small steric occupancy of the 5-membered fused ring (n= 1) than the 6- (n= 2) and 7-membered fused ring (n= 3) may facilitate the formation of the hydroxy aryl adduct **144** due to the better accommodation of the aldehydic moiety. Results from DFT calculation suggest the incremental CH_2 addition have no influence on the conformational flexibility of the fused ring of triazolium, while the flipping of the 7-membered fused ring is closer to the reaction centre, which provide the largest steric hindrance. Meanwhile, the conformational flexibility study of the fused ring, and the rotation behavior of aldehydic moiety of hydroxy aryl adduct both suggest the steric influence between adduct fused ring and aldehydic moiety.

The formation rate constant of Breslow intermediate **124** largely decreased with the

increment of fused ring size[I]. This can be an indirect evidence of the formation of Breslow intermediate as the larger steric hindrance provided by larger fused rings impede the flattening process of the double bond formation.

Regardless of the triazolium salt backbone structures (fused ring size and aryl-substituent), electron donating *para*-aryl substituents on the aldehyde decrease the adduct formation rate constant, k_1, the equilibrium constant, K, and the formation rate constant of Breslow intermediate, k_2. Meanwhile, no single trend describe the variation of the dissociation constant, k_{-1}, follow. The further Hammett analysis of the reaction data also support this, and the positive reaction constants, ρ, for all four parameters, suggest the increased electron density near the *para*-substituted aryl ring at the transition state, or in the product, relative to the reactant state.

The *ortho*-substituents of aryl-aldehyde were demonstrated to provide extra effects apart from electronic properties towards the reaction parameters, with different aldehydic aryl substituents having different impacts. We propose that the intramolecular hydrogen bond formation and the steric hindrance provided by *ortho*-aryl aldehydic substituents as two crucial factors.

We also established the linear free energy relationship between the catalyst *para*-/*meta*-aryl-substituents and the reaction parameters. Our data suggest that, regardless of the fused ring size of triazolium salts, the electron-withdrawing N-aryl substituents accelerate both the adduct association and dissociation rate constants, and agreed with the Hammett analyses. Meanwhile, the ρ value of equilibrium constant K are substantially smaller than 1, which suggest the position of equilibrium being relatively

[I] Limited data obtained due to the small values of k_2 being observed, thus, the variation range of k_2 was not state here.

independent with the catalyst aryl substituents. Moreover, the Hammett analyses of k_2 show non-linear behaviour.

Finally, the *ortho*-aryl-substituents of triazolium salts impede the approach of the aldehydic moiety towards catalyst, with extra impact on *ortho*-aryl substituted aldehydes. Thus, a decrease of adduct formation rate constant should be expected. Meanwhile, we also suggest the extra steric hindrance provided by *ortho*-aryl substituents force the aryl ring perpendicular to the triazolyl centre to provide a better accommodation for the aldehydic moiety during the development of the adduct formation. These two combined effects lead to the complicated effect of catalyst *ortho*-aryl substituents towards the reaction parameters.

The last aim of my project was to find a catalytic route towards the synthesis of d_1-deuterated aldehydes. The extent of deuterium incorporation into reactant aldehyde (2-methoxybenzaldehyde **138**) was evaluated under different reaction conditions, including the backbone modification of triazolium salts, concentrations of reactants, reaction temperature, choice of solvent, solution basicity and nucleophilicity. By changing the listed conditions and reactants, the best deuterium exchange result was found at 2.2 hours with 0.02 M of pentafluorophenyl triazolium salt **99** (n= 2) loading and 0.08 M of aldehyde in d_4-methanol at 25 °C, with 0.16 M NEt_3. 72.8% of aldehyde remained, with 99.1% of deuterium incorporation, and only 13.6% of the initial aldehyde formed benzoin product.

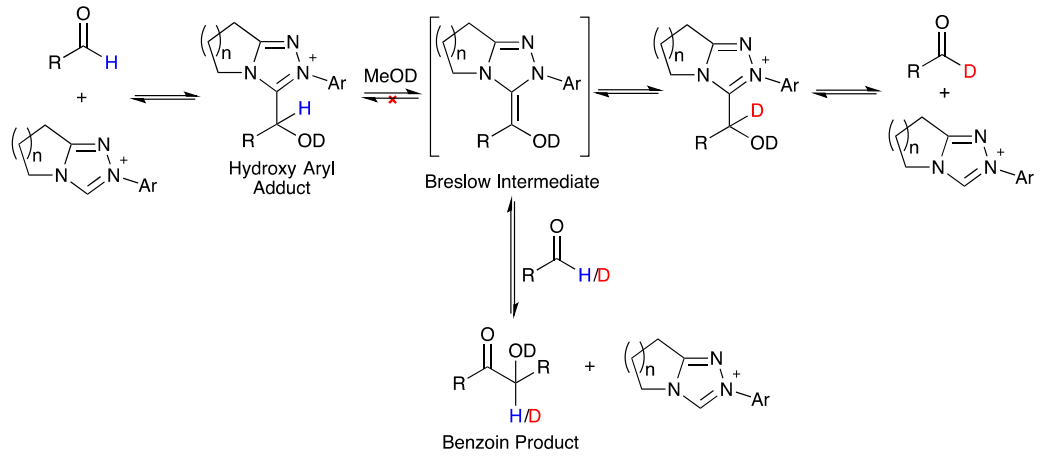

Scheme 6.4. Mechanism of benzoin condensation in d_4-methanol.

The H/D-exchange of other aromatic aldehydes were performed, however, only *ortho*-substituted aldehydes (*e.g.* 2-methylbenzaldehyde **136**) gave relatively satisfying results. Non-*ortho* substituted aldehyde all generated large quantities of benzoin-type products. We thus raised another possibility for synthetically accessing d_1-deuterated aldehydes from the retro-benzoin condensation. ^{1}H NMR spectroscopic analysis suggest the same distribution of products from the benzoin and retro-benzoin condensation. Initial exploration of the retro-benzoin with benzaldehyde and benzoin gave promising results with 97.4% deuteration of benzaldehyde.

6.2. Future Work

A large focus of this thesis has been understanding the steps up to the Breslow intermediate for the reactions of various aldehydes and N-heterocyclic carbenes (NHCs). Whilst a broad range of data has been acquired, there are some gaps remaining in terms of understanding the role of fused ring size.

Future work will consider further purification of N-mesityl triazolium **87**, and N-2,4,6-trichlorophenyl triazolium **82** and **83**. To further investigate the influence of the steric hindrance provided by the fused ring of triazolium salt, the 2-phenyl-[1,2,4]triazolo[4,3-

a]pyridin-2-ium tetrafluoroborate **176** should be synthesized. The kinetic profiles evaluating rate and equilibrium constants with aldehydes should be compared with the data obtained from N-phenyl bicyclic triazolium salt **101** and **79**.

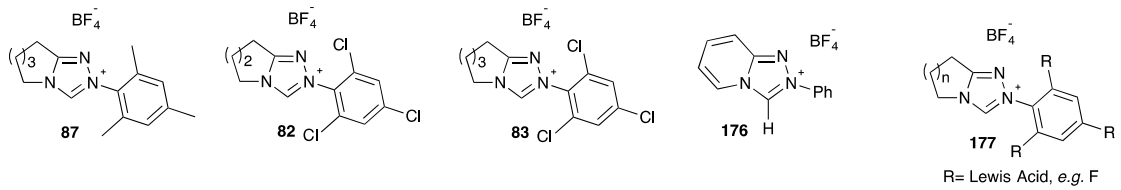

Figure 6.4. Triazolium precatalysts **87, 82, 83, 176, 177** for future syntheses.

The additional variation of catalyst architecture incorporating both N-aryl substituents and fused ring size should be considered, *e.g.* the Lewis acid substituted triazolium salt **177**. In parallel, the literature suggests bis(amino)cyclopropenylidene (BACs) have opposite chemoselectivities to NHC derivatives, and dispute the formation of benzoin products. Thus, variation of amino-substituents of bis(amino)cyclopropenium salts **178** should be investigated for the purpose of kinetic evaluation. Meanwhile, currently there are no synthetic approach towards the aniline-substituted BAC analogues **179**, and the potential application and catalytic property variation could be evaluated in detail.

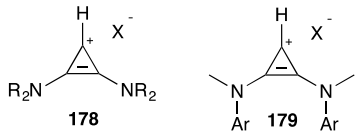

Figure 6.5. bis(amino)cyclopropenium salt **178** and **179** for future syntheses.

Moreover, potential deuterium incorporation towards a broad range of deuterio-aldehydes should be investigated. Recent unpublished work from our group shows the hydroxyaryl adducts from BACs are particularly stable, thus potentially allows cascade formation of d^1 deuterated aldehyde by changing reaction conditions, *e.g.* stronger base, higher temperature (Scheme 6.5). Overall, all of these studies of partitioning of Breslow-like intermediates towards deuteration versus other reactions provides a bigger scope

quantitative understanding of chemoselectivity in carbene-catalysed processes.

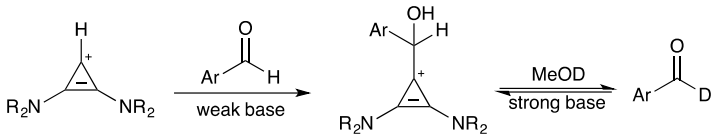

Scheme 6.5. Cascade synthetic approach towards d_1-deuerated aldehyde.

The investigation of the dialkoxyacetal NHC adduct **180** has been undertaken, the potential formation mechanism also being suggested. This will be further pursued to develop a more-detailed synthetic evaluation of this adducts' formation including mechanistic studies, and build up the possible application of this adduct.

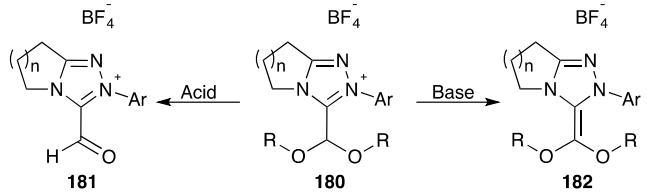

Scheme 6.6. Potential application of the dialkoxy acetal adduct **180** to form NHC-formaldehyde **181** and new type of Breslow intermediate **182**

Current results suggest the good stability of dialkoxy acetal adduct in 1 M DCl. Future work could use other acids rather than DCl (*e.g.* D_2SO_4, $DClO_4$, DBF_4), and the concentration of the acid could be increased. Alternative access towards the NHC-formaldehyde **181** *via* the reduction of dibenzyloxy acetal adduct could also be investigated (Scheme 6.7).

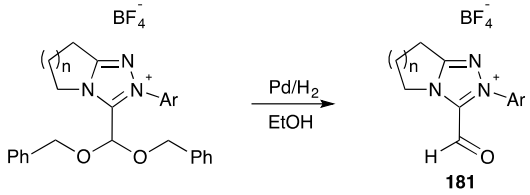

Scheme 6.7. Alternative synthetic approach towards the NHC-formaldehyde **181**.

The evidence of formation of Breslow intermediate in basic conditions was obtained. We assume by varying reaction conditions like using stronger bases, non-protic solvents and the utilisation of glove box probably can impede the oxidation and hydrolysis of the Breslow intermediate. Thus, the direct synthesis and further characterization of Breslow intermediate might be conducted.

6.3. References

1. P.-C. Chiang, M. Rommel and J. W. Bode, *J. Am. Chem. Soc.*, 2009, **131**, 8714-8718.
2. R. W. Davidson and M. J. Fuchter, *Chem. Commun.*, 2016, **52**, 11638-11641.
3. J. E. Thomson, C. D. Campbell, C. Concellon, N. Duguet, K. Rix, A. M. Slawin and A. D. Smith, *J Org Chem*, 2008, **73**, 2784-2791.

Chapter 7. Experimental Section

7.1. General Instrument

NMR: NMR samples were prepared in deuterium oxide-d_2, chloroform-d_1, methanol-d_4, dichloromethane-d_2, and dimethyl sulfoxide-d_6. The chemical shifts for residual solvent peak in ^{1}H and ^{13}C NMR spectra are reported in Table 7.1.

Table 7.1. Signals due to NMR solvents

Solvent	δ_H, ppm	δ_C, ppm
deuterated chloroform	7.26	77.2
deuterium oxide	4.79	-
deuterated dichloromethane	5.32	53.8
deuterated methanol	2.50	39.5
deuterated dimethyl sulfoxide	3.31	49.0

Data are presented as follows: chemical shift (ppm), integration, multiplicity (s = singlet, d = doublet, t = triplet, q = quartet, p = quintet, h= heptet, m = multiplet, br = broad), coupling constants (Hz), and assignment. Varian Mercury-400, Bruker Avance-400, Varian Inova-500, Varian VNMRS-600 and Varian VNMRS-700 instruments were used to record the NMR spectra at 400, 500, 600 and 700 MHz.

EA: Elemental analyses were obtained from the Microanalytical Unit (Department of Chemistry, Durham University), and performed on an Exeter CE-440 Elemental Analyser.

MS: A waters *TQD* mass spectrometer was used to perform the low resolution mass spectrometry, and Thermo-Finnigan *LTQ FT* mass spectrometer was used to perform the

high resolution mass spectrometry.

Chromatography: Thin layer chromatography was performed using silica-backed Machery-Nagel Polygram SILG/UV_{254} plates. Column chromatography was performed using silica gel.

Single Crystal X-ray Crystallography: The X-ray single crystal data in this project has been collected by the Crystallography Department of Durham University using λMoKα-radiation (λ=0.71073Å) at 120.0K. Bruker SMART CCD 6000 (fine-focus sealed tube, graphite monochromator), Bruker D8Venture (Photon100 CMOS detector, IμS-microsource, focusing mirrors), and Agilent XCalibur (4-circle kappa geometry goniometer, Mo sealed tube) diffractometers equipped with Cryostream (Oxford Cryosystems) open-flow nitrogen cryostat were the three instruments used for data collection. The structures were solved by direct method and refined by full-matrix least squares on F^2 for all data using Olex2S[1] and SHELXTL[2] software. All non-hydrogen atoms were refined with anisotropic displacement parameters, H-atoms were located on the difference map and refined isotropically.

Computational Methods: The geometry optimizations were proceeded *via* Gaussview using the Durham University Hamilton HPC. The level of theory applied was B3LYP/6-31(g), with solvent methanol modelled using an implicit polarizable continuum model (PCM)[3, 4].

7.2. Materials

NMR Solvents: Deuterium oxide-d_2 (99.9 atom % D), methanol-d_4 (99.8 atom % D), dimethyl sulfoxide-d_6 (99.9 atom % D) and dichloromethane-d_2 (99.8 atom % D) were purchased from Cambridge Isotope Laboratories. Chloroform-d_1 (99.8 atom % D) was

purchased from Apollo Scientific, and Euriso-top.

Reagents: Benzaldehyde and triethylamine were purchased from Sigma-Aldrich and distilled before use. Triethylamine hydrochloride from Sigma-Aldrich was vacuum dried prior to use. Unless stated, all other chemicals were reagent grade and used without further purification. Reactions involving air or moisture sensitive reagents were performed under an argon atmosphere using oven-dried glassware. Solvents were dried prior to use using an Innovative Technology Inc. solvent purification system. 2-(4-phenyl)-6,7-dihydro-*5H*-pyrrolo[2,1-c] [1,2,4] triazol-2-ium chloride **72** was prepared in my MSc project, and 2-(4-fluorophenyl)-6,7-dihydro-*5H*-pyrrolo[2,1-c] [1,2,4] triazol-2-ium chloride **73** was synthesized by Aron Morris.

7.3. Synthetic Procedures of N-heterocyclic Triazolium Salts

7.3.1. Synthesis of 2-perfluorophenyl-6,7,8,9-tetrahydro-5*H*-[1,2,4]triazolo[4,3-a]azepin-2-ium tetrafluoroborate

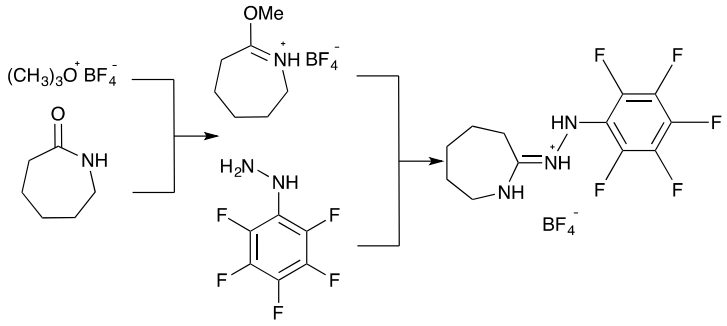

Using procedures adapted from Rovis and Gravel[5, 6], trimethyloxonium tetrafluoroborate (1.61 g, 11.0 mmol) was added to an anhydrous dichloromethane (50 mL) solution of ε-caprolactam (1.25 g, 11.0 mmol), and stirred 3 hours at room temperature under an argon environment. Pentafluorophenyl hydrazine (2.16 g, 11.0 mmol) was added and the solution turned orange immediately. After 12 hours stirring, some amidrazone product precipitated as orange crystals. Removal of all solvent yielded an orange residue, which was used without further purification. ***m/z*** (ES+): 294 ([M–BF_4]$^+$, 100%); **HRMS** (ES+): $[M+H]^+$ $C_{12}H_{13}N_3F_5$ requires: 294.1030, found: 293.1017.

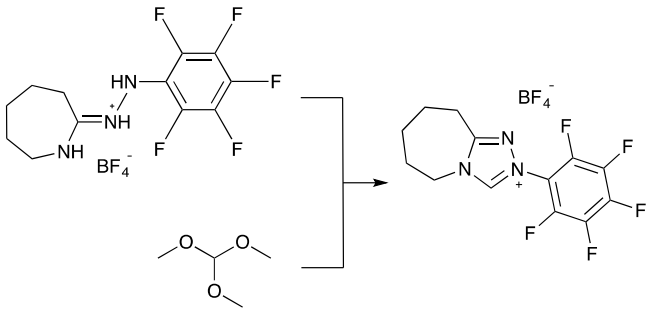

Trimethyl orthoformate (20 mL) was added into the solution of orange residue in chlorobenzene (5 mL), followed by the addition of few drops of hydrochloric acid solution (4 M in 1,4-dioxane). The mixture was refluxed for 48 hours and solvent was removed under reduced pressure to give the crude products as viscous brown oils. The oil was further purified by multi-phase recrystallization from dichloromethane: diethyl

ether, and chloroform: diethyl ether systems to give beige solid. Recrystallization from toluene and methanol: diethyl ether yielded the title product as colourless needle-like crystals (1.17g, 27%), slow evaporation of the remaining toluene washing phase further yielded more product. **^{1}H NMR** (400 MHz, $(CD_3)_2SO$): δ_H 1.78 (2H, m, CH_2), 1.93 (4H, m, 2 × CH_2), 3.18 (2H, m, CH_2), 4.51 (2H, m, CH_2), 10.59 (1H, s, NCH(N)); **^{13}C NMR** (176 MHz, $CDCl_3$): 24.1, 25.6, 26.7, 29.3, 45.0, 111.3, 136.9, 139.5, 141.4, 143.9, 147.6, 159.9; **^{19}F NMR** (376 MHz, $CDCl_3$): δ_F –146.00 (2F, m, ArF), -148.62 (1F, tt, *J*=3.24, 23.14, ArF), –160.14 (2F, m, ArF); ***m/z*** (ES+): 304 ($[M–BF_4]^+$, 100%). ***m/z*** (ES+): 304 ($[M–BF_4]^+$, 100%); **HRMS** (ES+): $[M–BF_4]^+$ $C_{13}H_{11}N_3F_5$ requires: 304.0873, found: 304.0881.

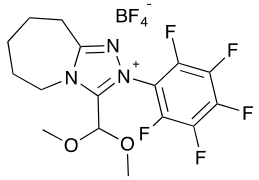

During recrystallization, trace amounts of dimethoxy acetal adduct was found. **HRMS** (ES+): $[M–BF_4]^+$ $C_{16}H_{17}N_3O_2F_5$ requires: 378.1241, found: 378.1234.

7.3.2. Synthesis of 2-(2,4,6-triisopropylphenyl)-6,7-dihydro-5*H*-pyrrolo[2,1-c] [1,2,4] triazol-2-ium chloride

7.3.2.1. Synthesis of 2,4,6-triisopropyl phenyl hydrazine

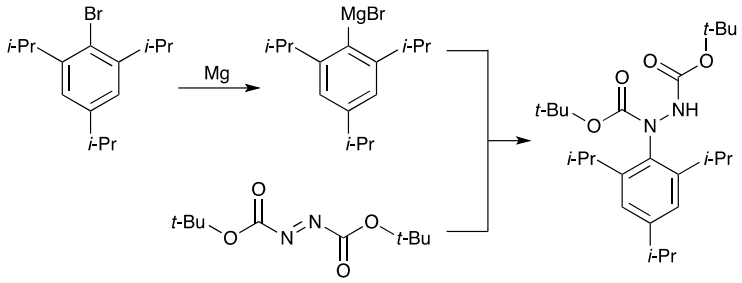

Based on synthetic procedure explored in my MSc research project[7], high-vacuum dried magnesium turnings (0.58 g, 24 mmol, 1.2 equiv) were heated to 90 ºC for one hour

under argon, and cooled down to room temperature. A catalytic amount of iodine was added, followed by the addition of 2-bromo-1,3,5-triisopropylbenzene (6 mL, 24 mmol, 1.2 equiv) and anhydrous tetrahydrofuran (9 mL) within one fraction. A water bath was utilized to control the reaction temperature at 55 ºC. The reaction was stirred for at least 4 hours, then cooled to room temperature, and the Grignard reagent was added to an anhydrous tetrahydrofuran (20 mL) solution of di-*tert*-butyl diazo-1,2-dicarboxylate (DBAD, 4.60 g, 20 mmol, 1 equiv) *via* cannula at -78 ºC. After 30 minutes of stirring, acetic acid (1.8 mL, 24 mmol, 1.2 equiv) was added to quench the reaction. The reaction mixture was diluted with water, and extracted with diethyl ether, then washed with brine, dried over sodium sulfate and filtered. Vacuum concentration gave the crude title compound as a yellow sticky oil, which has a distinctive smell and can be used directly without further purification. R_f (diethyl ether: ethyl acetate 90:10) = 0.39; ***m/z*** (ES+): 457 ($[M+Na]^+$, 78.21%; **HRMS** (ES+): $[M+H]^+$ $C_{25}H_{43}N_2O_4$ requires 435.3223, found 435.3213.

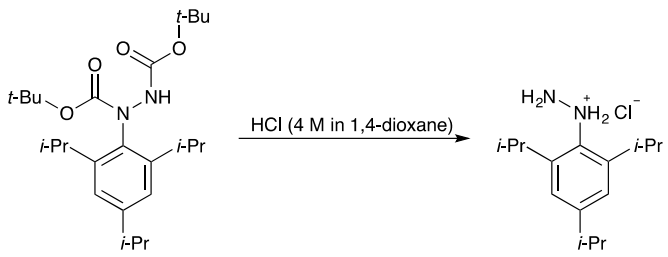

Di-*tert*-butyl 1-(2,4,6-triisopropylphenyl)hydrazine-1,2-dicarboxylate (1.84 g, 5 mmol) was dissolved in anhydrous methanol (12.5 mL) and hydrochloric acid (4 M in 1,4-dioxane, 12.5 mL, 50 mmol) was added slowly to the solution. After the mixture was stirred for 4 hours at room temperature, the color turned orange, and a white precipitate formed. The resulting mixture was kept in the freezer (-18 ºC) overnight, and the precipitate was removed by filtration and washed with hexane. All volatiles were then removed under reduced pressure to give a brown solid mixture. Hexane was used to dissolve all the non-polar impurities, and the remaining light brown solid was washed with cold diethyl ether to yield the title compound as a white powder. **^{1}H NMR** (400

MHz, DMSO): δ_H 1.19-1.29 (18H, m, CH_3), 2.88 (1H, h, *J*= 6.99 Hz, CH), 2.41 (2H, h, *J*= 6.95 Hz, CH), 7.01 (2H, s, ArH); **HRMS** (ES+): $[M\text{-}Cl]^+$ $C_{15}H_{27}N_3$ requires: 235.2174, found: 235.2187.

7.3.2.2. 2-Methoxy-4,5-dihydro-3H-pyrrole

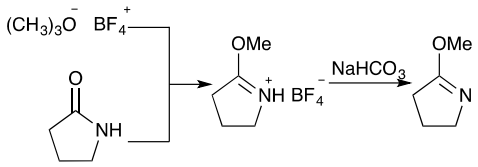

According to a literature procedure[8], 2-pyrrolidinone (0.4 mL, 5 mmol) was dissolved in anhydrous dichloromethane (25 mL) and trimethyloxonium tetrafluoroborate (0.82 g, 5.5 mmol). The mixture was stirred overnight under argon at room temperature until all the insoluble trimethyloxonium tetrafluoroborate solid was consumed. Saturated sodium bicarbonate solution (25 mL) was added slowly over 20 minutes. The organic phase was separated and the aqueous phase was extracted with dichloromethane (3 × 50 mL). The combined organic layers were dried over sodium sulphate and filtered. Most of the dichloromethane was removed on a rotary evaporator, with the pressure > 250 mbar as the imino product is volatile, to give the title compound as faint yellow oil with a distinctive odour, which can be directly used without further purification. **^{1}H NMR** (400 MHz, $(CD_3)_2SO$): δ_H 1.90 – 2.00 (2H, m, CH_2), 2.36 – 2.42 (2H, m, CH_2), 3.50 – 3.55 (2H, m, CH_2), 3.70 (3H, s, CH_3)

7.3.2.3. Amidrazone

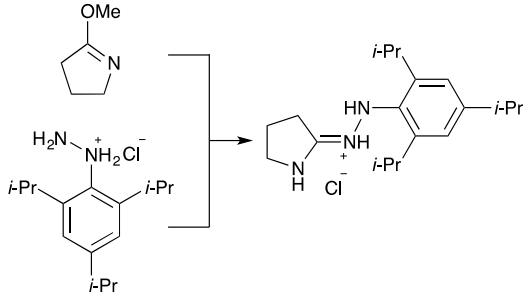

Imino ether (Section 7.3.2.2) was dissolved in methanol (20 mL) and added to the

hydrazine hydrochloride, which caused the evolution of a white gas. A few drops of hydrochloric acid solution (4 M, in 1,4-dioxane) were added. The mixture was stirred at 60 °C overnight, and the solution turned light yellow. All volatiles were removed under reduced pressure to give the amidrazone as a pale yellow solid, which can be directly used without further purification. **HRMS** (ES+): $[M\text{-}Cl]^+$ $C_{19}H_{32}N_3$ requires: 302.2596, found: 302.2594.

7.3.2.4. 2-(2,4,6-triisopropylphenyl)-6,7-dihydro-5H-pyrrolo[2,1-c][1,2,4] triazol-2-ium chloride

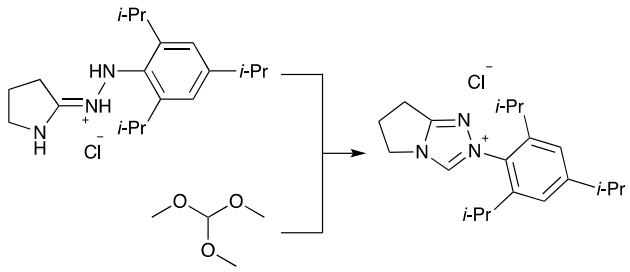

Amidrazone was dissolved in anhydrous chlorobenzene (5 mL) and trimethyl orthoformate (6.6 mL, 40 mmol) was added to the solution, followed by the addition of hydrochloric acid solution (0.5 mL, 4 M, in 1,4-dioxane). A reflux condenser with a calcium chloride drying tube was fitted and the mixture was heated to reflux for 2 hours, generating some solid. The solvent was removed under reduced pressure and the crude product was obtained as a yellow oil. Ethyl acetate washing of the oil yielded the title compound as a pale yellow powder (0.45g, 29%); **^{1}H NMR** (400 MHz, DMSO): δ_H 1.11 (6H, d, *J*= 6.8 Hz, CH_3), 1.17 (6H, d, *J*= 6.8 Hz, CH_3), 1.26 (6H, d, *J*= 6.9 Hz, CH_3), 2.41 (2H, h, *J*= 6.8 Hz, CH), 2.76 (2H, p, *J*= 7.6 Hz, CH_2), 3.01 (1H, h, *J*= 6.9 Hz, CH), 3.17 (2H, t, *J*=7.7 Hz, CH_2), 4.44 (2H, t, *J*= 7.4 Hz, CH_2), 10.37 (1H, s, NCH(N)); **^{13}C NMR** (176 MHz, $CDCl_3$): δ_c 21.9, 24.1, 24.2, 24.5, 28.2, 34.2, 48.0, 122.9, 129.8, 142.1, 145.6, 152.7, 163.9; **m/z** (ES+) 312 ($[M\text{-}Cl]^+$, 100 %); **HRMS** (ES+): $[M\text{-}Cl]^+$ $C_{20}H_{30}N_3$ requires: 312.2440, found: 312.2444.

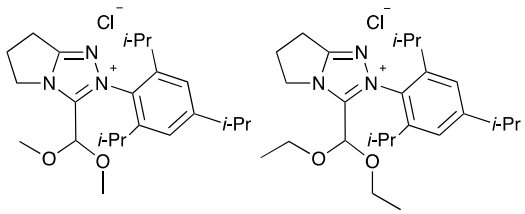

Trace amounts of dimethoxy acetal adduct could be detected from the ethyl acetate washing phase. **HRMS** (ES+): $[M\text{-}Cl]^+$ $C_{23}H_{36}N_3O_2$ requires: 386.2807, found: 386.2808. When using triethyl orthoformate instead of trimethyl orthoformate, corresponding diethoxy acetal adduct can also be detected. **HRMS** (ES+): $[M\text{-}Cl]^+$ $C_{25}H_{40}N_3O_2$ requires: 414.3110, found: 414.3121.

7.3.3. Synthesis of 2-mesityl-5,6,7,8-tetrahydro-[1,2,4]triazolo[4,3-a]pyridin-2-ium tetrafluoroborate

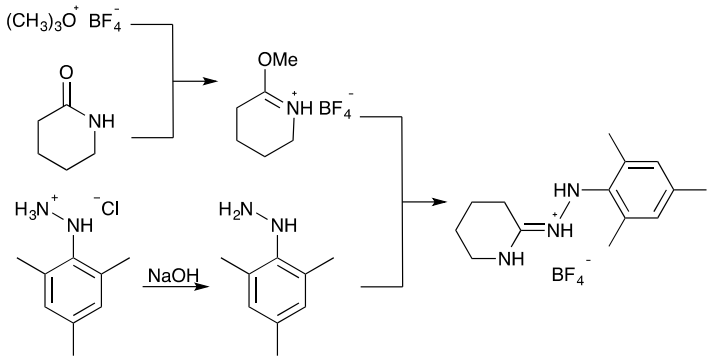

Using procedures adapted from Smith and co-workers[9], trimethyloxonium tetrafluoroborate (0.87 g, 6.0 mmol) was added into an anhydrous dichloromethane (25 mL) solution of 2-piperidone (0.50 g, 6.0 mmol), and stirred overnight. Mesityl hydrazine hydrochloride (1.50 g, 8.00 mmol) was dissolved in aqueous sodium hydroxide (1 M, 8 mL, 8.0 mmol), and extracted into dichloromethane. This latter dichloromethane solution was immediately added to the reaction mixture, and stirred for a further 48 hours at room temperature under argon to obtain a red solution. The solvent was removed under reduced pressure, yielding the amidrazone as an orange solid, which was used without further purification. **HRMS** (ES+): $[M\text{-}BF_4]^+$ $C_{14}H_{22}N_3$ requires: 232.1814, found: 232.1802.

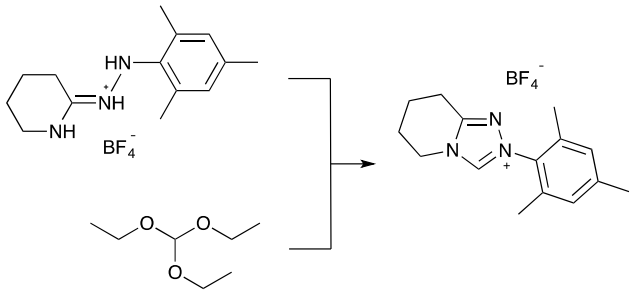

The residue was dissolved in chlorobenzene (10 mL) and triethyl orthoformate (5 mL). Following addition of a few drops of hydrochloric acid solution (4 M, in 1,4-dioxane), the whole mixture was refluxed for 48 hours. The solvent was removed under reduced pressure, and trituration using hexane and ethyl acetate yielded the title compound as an off-white solid (1.76 g, 92%), with spectroscopic details in accordance with the literature. **^{1}H NMR** (400 MHz, $CDCl_3$): δ_H 2.07 (6H, s, 2 × CH_3), 2.11-2.30 (4H, m, 2 × CH_2), 2.38 (3H, s, CH_3), 3.14 (2H, t, *J*=6.21 Hz, CH_2), 4.61 (2H, t, *J*=5.84, CH_2), 7.01 (2H, s, 2 × ArCH), 9.63 (1H, s, NCH(N)); ***m/z*** (ES+): 242 ([M–BF_4]$^+$, 100%); **HRMS** (ES+): [M-BF_4]$^+$ $C_{15}H_{20}N_3$ requires: 242.1657, found: 242.1652.

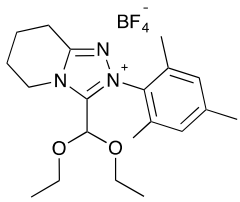

Trace amounts of diethoxy acetal adduct was detected from the ethyl acetate washing phase. **HRMS** (ES+): [M-BF_4]$^+$ $C_{20}H_{30}N_3O_2$ requires: 344.2338, found: 344.2329.

7.3.4. Synthesis of 2-mesityl-5,6,7,8-tetrahydro-[1,2,4]triazolo[4,3-a]pyridin-2-ium Chloride

7.3.4.1. *O*-methylvalerolactim

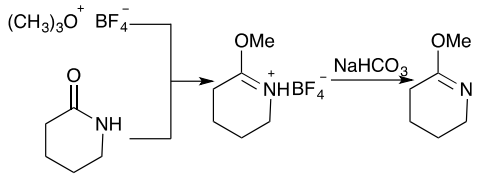

According to a literature procedure[10], 2-piperidone (0.5 g, 5 mmol) was dissolved in anhydrous dichloromethane (25 mL) and trimethyloxonium tetrafluoroborate (0.87 g, 6 mmol). The mixture was stirred overnight under argon at room temperature until all the insoluble trimethyloxonium tetrafluoroborate solid was consumed. Saturated sodium bicarbonate solution (25 mL) was added slowly over 20 minutes. The organic phase was separated and the aqueous phase was extracted with dichloromethane (3 × 50 mL). The combined organic layers were dried over sodium sulphate, filtered and most of the dichloromethane was removed on a rotary evaporator, with the pressure >250 mbar as the imino product is volatile. The title compound was obtained as faint yellow oil with a distinctive odor, which can be directly used without further purification.

7.3.4.2. Amidrazone

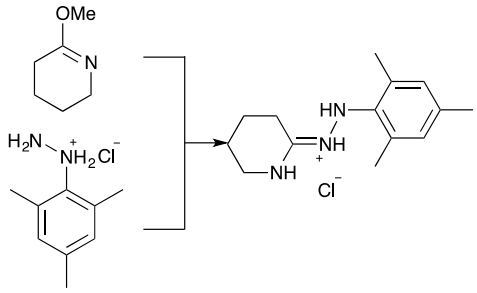

O-methylvalerolactim was dissolved in methanol (20 mL) and added to the mesityl hydrazine hydrochloride, which caused the evolution of a white gas. A few drops of hydrochloric acid solution (4 M, in 1,4-dioxane) were added. The mixture was stirred at 60 °C overnight, and the solution turned red. All volatiles were removed under reduced pressure to give the amidrazone as a red solid, which can be directly used without further purification. ***m/z*** (ES+): 232 ($[M–BF_4]^+$, 100%).

7.3.4.3. 2-mesityl-5,6,7,8-tetrahydro-[1,2,4]triazolo[4,3-a]pyridin-2-ium Chloride

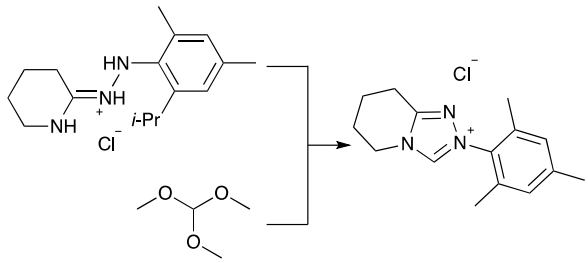

Amidrazone was dissolved in anhydrous chlorobenzene (5 mL) and trimethyl orthoformate (6.6 mL, 40 mmol) was added to the solution. A reflux condenser with a calcium chloride drying tube was fitted and the mixture was heated to reflux for 48 hours. The solvent was removed under reduced pressure yielding a brown oil. Traced amounts of product could be detected however purification was difficult. **HRMS** (ES+): $[M\text{-}BF_4]^+$ $C_{15}H_{20}N_3$ requires: 242.1657, found: 242.1655.

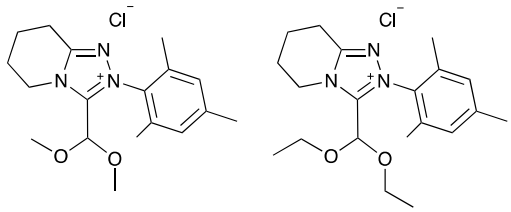

Trace amounts of dimethoxy acetal adduct could be detected from the ethyl acetate washing phase. **HRMS** (ES+): $[M\text{-}BF_4]^+$ $C_{18}H_{26}N_3O_2$ requires: 316.2025, found: 316.2021. Following the replacement of trimethyl orthoformate by triethyl orthoformate, corresponding diethoxy acetal adduct could also be detected. **HRMS** (ES+): $[M\text{-}BF_4]^+$ $C_{20}H_{30}N_3O_2$ requires: 344.2338, found: 344.2326.

7.3.5. Synthesis of 2-mesityl-6,7,8,9-tetrahydro-5*H*-[1,2,4]triazolo[4,3-a]azepin-2-ium tetrafluoroborate

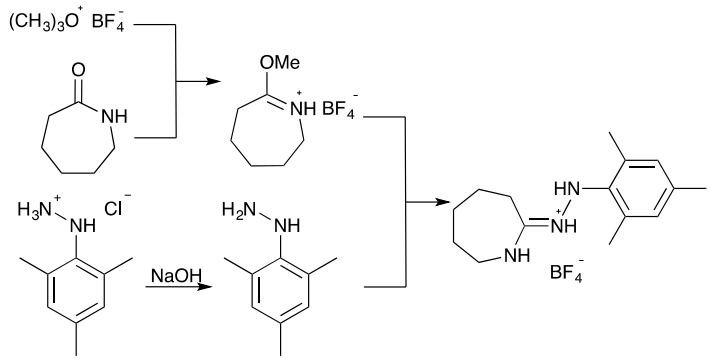

Using procedures adapted from Bode and co-workers[11], trimethyloxonium tetrafluoroborate (1.61 g, 11.0 mmol) was added into an anhydrous dichloromethane (50 mL) solution of ε-caprolactam (1.25 g, 11.0 mmol), and stirred overnight. Mesityl hydrazine hydrochloride (3.00 g, 16.0 mmol) was dissolved in aqueous sodium hydroxide (1 M, 16 mL, 16.0 mmol), and extracted into dichloromethane. This dichloromethane solution was immediately added to the reaction mixture, and stirred for a further 48 hours at room temperature under argon to obtain a dark purple solution. The solvent was removed under reduced pressure, yielding the amidrazone as a black solid, which was used without further purification. ***m/z*** (ES+): 246 ($[M–BF_4]^+$, 100%).

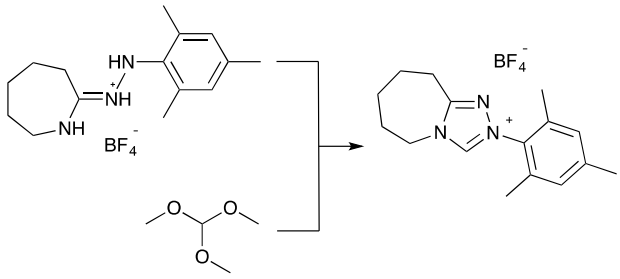

Trimethyl orthoformate (20 mL) was added into the solution of black residue in chlorobenzene (5 mL), followed by the addition of few drops of hydrochloric acid solution (4 M in 1,4-dioxane). The mixture was refluxed for 48 hours and solvent was removed under reduced pressure to give the crude product as a viscous transparent brown oil. Recrystallization from several solvent systems failed and gradient column chromatography was applied for further purification. By changing solvent from 100% DCM to 100% acetone, a clear brown oil was obtained, however still suggested a

mixture containing the title product. **^{1}H NMR** (400 MHz, $CDCl_3$): δ_H 1.88 (2H, m, CH_2), 2.02 (4H, m, 2 × CH_2), 2.07 (6H, s, 2 × CH_3), 2.38 (3H, s, CH_3), 3.18 (2H, m, CH_2), 4.61 (2H, m, CH_2), 7.00 (2H, s, 2 × ArH), 9.64 (1H, s, NCH(N)); ***m/z*** (ES+): 256 ([M–BF_4]$^+$, 100%); **HRMS** (ES+): [M-BF_4]$^+$ $C_{16}H_{22}N_3$ requires: 256.1814, found: 256.1824.

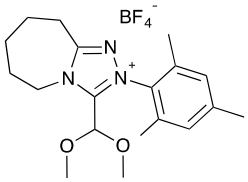

Trace amounts of dimethoxy acetal adduct could be detect from the reaction mixture. **HRMS** (ES+): [M-BF_4]$^+$ $C_{19}H_{28}N_3O_2$ requires: 330.2182, found: 330.2197.

7.3.6. Synthesis of 2-(4-fluorophenyl)-5,6,7,8-tetrahydro-[1,2,4]triazolo[4,3-a]pyridin-2-ium tetrafluoroborate

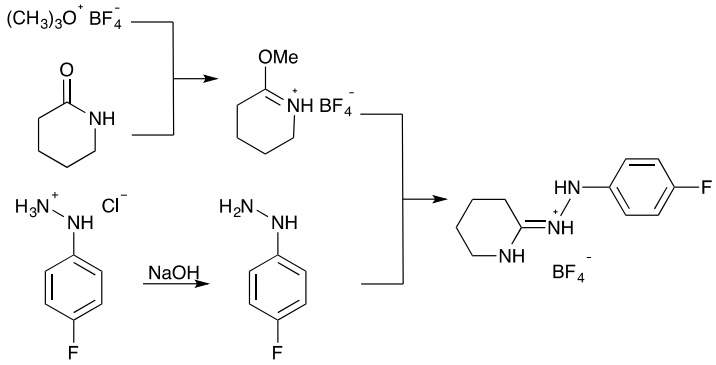

Using procedures adapted from Rovis and Gravel[5], trimethyloxonium tetrafluoroborate (0.87 g, 6.0 mmol) was added into an anhydrous dichloromethane (25 mL) solution of 2-piperidone (0.50 g, 6.0 mmol), and stirred overnight to obtain a yellow solution. 4-Fluorophenyl hydrazine hydrochloride (1.31 g, 8.00 mmol) was dissolved in aqueous sodium hydroxide (1 M, 8 mL, 8.0 mmol), and extracted into dichloromethane. This dichloromethane solution was immediately added to the reaction mixture, stirred for a further 36 hours at room temperature under argon to obtain a red solution, with a white precipitate. The solvent was removed under reduced pressure, yielding the amidrazone

as a red solid, which was used without further purification. **HRMS** (ES+): $[M\text{-}BF_4]^+$ $C_{11}H_{15}N_3F$ requires: 208.1250, found: 208.1259.

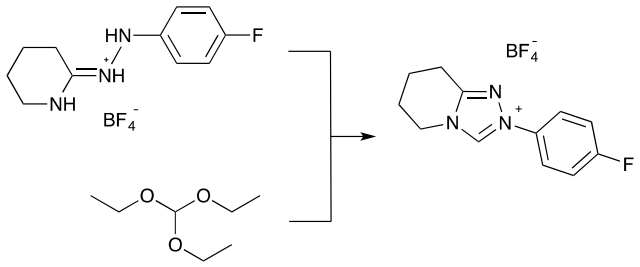

The residue was dissolved in chlorobenzene (5 mL) and triethyl orthoformate (25 mL), followed by the addition of hydrochloric acid solution (0.5 mL, 4 M, in 1,4-dioxane), and the colour changed immediately from red into purple. The mixture was stirred and refluxed for 48 hours and an emulsion was obtained. All volatiles were removed under reduced pressure, to yield the crude product as a dark brown oil. Further ethyl acetate and diethyl ether washes yield the product as a white solid (0.90 g, 49%). **^{1}H NMR** (400 MHz, $CDCl_3$): δ_H 2.11 (4H, qd, *J*= 6.6, 3.6 Hz, 2 × CH_2), 3.10 (2H, t, *J*= 6.0 Hz, CH_2), 4.48 (2H, t, *J*= 5.5 Hz, CH_2), 7.20 (2H, m, 2 × ArH), 7.84 (2H, m, 2 × ArH), 9.99 (1H, s, NCH(N)); **^{13}C NMR** (176 MHz, $CDCl_3$): 18.6, 21.0, 21.4, 46.1, 117.1 (d, *J*= 23.6 Hz), 123.2 (d, *J*= 9.1 Hz), 131.3 (d, *J*= 3.3 Hz), 139.7, 153.2, 162.1, 164.6; **^{19}F NMR** (376 MHz, $CDCl_3$): δ_F –108.86 (s, ArF), -158.60 (s, BF_4), –158.69 (s, BF_4); ***m/z*** (ES+): 304 ($[M–BF_4]^+$, 100%). ***m/z*** (ES+): 218 ($[M–BF_4]^+$, 100%); **HRMS** (ES+): $[M–BF_4]^+$ $C_{12}H_{13}N_3F$ requires: 218.1094, found: 218.1094.

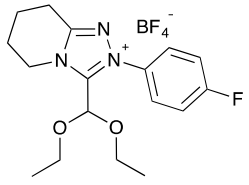

Trace amounts of diethoxy acetal adduct could be detected from the ethyl acetate washing phase. **HRMS** (ES+): $[M\text{-}BF_4]^+$ $C_{17}H_{23}N_3O_2F$ requires: 320.1774, found: 320.1781.

7.3.7. Synthesis of 2-(4-fluorophenyl)-6,7,8,9-tetrahydro-5*H*-[1,2,4]triazolo[4,3-a]azepin-2-ium tetrafluoroborate

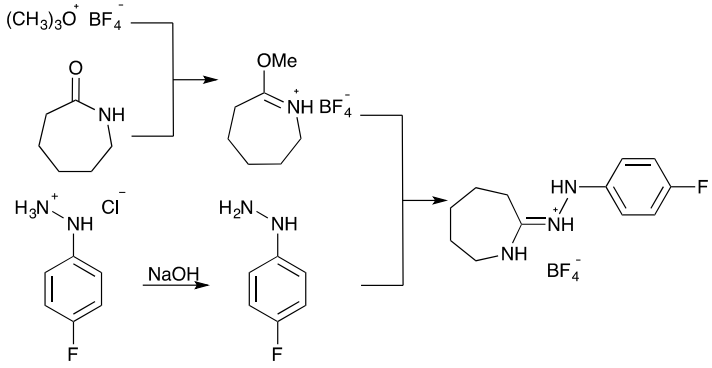

Using procedures adapted from Rovis and Gravel[1], trimethyloxonium tetrafluoroborate (1.61 g, 11.0 mmol) was added into an anhydrous dichloromethane (50 mL) solution of ε-caprolactam (1.25 g, 10 mmol), and stirred overnight to obtain a yellow solution. 4-Fluorophenyl hydrazine hydrochloride (1.79 g, 16.0 mmol) was dissolved in aqueous sodium hydroxide (1 M, 16 mL, 16.0 mmol), and extracted into dichloromethane. This dichloromethane solution was immediately added to the reaction mixture, stirred for a further 48 hours at room temperature under argon to obtain a red solution, with a white precipitate. The solvent was removed under reduced pressure, yielding the amidrazone as a red solid, which was used without further purification. ***m/z*** (ES+): 222 ($[M–BF_4]^+$, 100%).

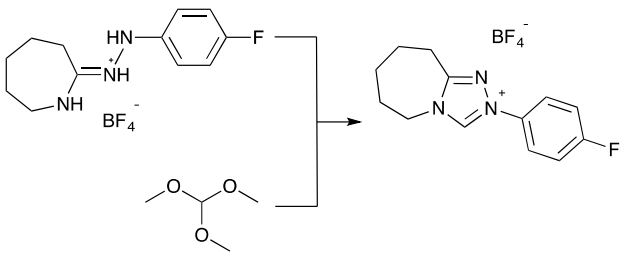

The residue was dissolved in trimethyl orthoformate (25 mL), a catalytic amount of hydrochloric acid solution (0.5 mL, 4 M, in 1,4-dioxane) was added, and the colour changed immediately from red into purple. After the mixture was stirred and refluxed for 48 hours, the solution colour changed from purple to dark red and finally a yellow emulsion was obtained. All volatiles were removed under reduced pressure, to yield the

crude product as a dark brown oil. An ethyl acetate wash yielded a brown sticky solid, and recrystallization from DCM: toluene provided a yellow gel. After several recrystallizations, a white gel formed, and removal of solvent by vacuum filtration yield the product as a white solid (0.342 g, 11%). **^{1}H NMR** (400 MHz, CDl_3): δ_H 1.88 (2H, m, CH_2), 1.99 (4H, m, 2 × CH_2), 3.16 (2H, m, CH_2), 4.52 (2H, dt, *J*= 15.2, 4.3 Hz, CH_2), 7.22 (2H, m, 2 × ArH), 7.86 (2H, m, 2 × ArH), 10.02 (1H, s, NCH(N)); **^{13}C NMR** (176 MHz, $CDCl_3$): 24.4, 26.1, 27.2, 29.7, 49.8, 117.1 (d, *J*= 23.6 Hz), 123.0 (d, *J*= 9.1 Hz), 131.0 (d, *J*= 3.3 Hz), 140.8, 158.6, 162.1, 164.6; **^{19}F NMR** (376 MHz, $CDCl_3$): δ_F – 108.85 (s, ArF), -151.01 (s, BF_4), –151.07 (s, BF_4 ***m/z*** (ES+): 232 ($[M–BF_4]^+$, 100%). **HRMS** (ES+): $[M–BF_4]^+$ $C_{13}H_{15}N_3F$ requires: 232.1250, found: 232.1251.

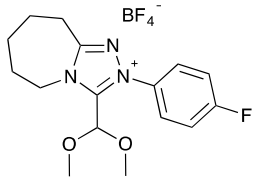

Trace amounts of dimethoxy acetal adduct could be detected from the ethyl acetate washing phase. **HRMS** (ES+): $[M\text{-}BF_4]^+$ $C_{16}H_{21}N_3O_2F$ requires: 306.1618, found: 306.1631.

7.3.8. Synthesis of 2-phenyl-5,6,7,8-tetrahydro-[1,2,4]triazolo[4,3-a]pyridin-2-ium tetrafluoroborate

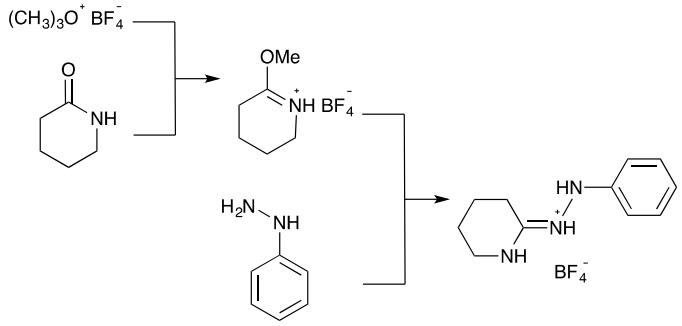

Based on a procedure by Rovis and co-workers[1], trimethyloxonium tetrafluoroborate (1.73 g, 12.0 mmol) was added to a 2-piperidone solution (1.10 g, 12.0 mmol) in dry

dichloromethane (50 mL), and stirred at room temperature overnight under argon. After the addition of phenylhydrazine (1.00 mL, 10.2 mmol), the reaction mixture was stirred for 48 hours at room temperature under an inert atmosphere, then concentrated under reduced pressure to yield the amidrazone as a red solid which was directly used without further purification. **HRMS** (ES+): $[M–BF_4]^+$ $C_{11}H_{16}N_3$ requires: 190.1344, found: 190.1346.

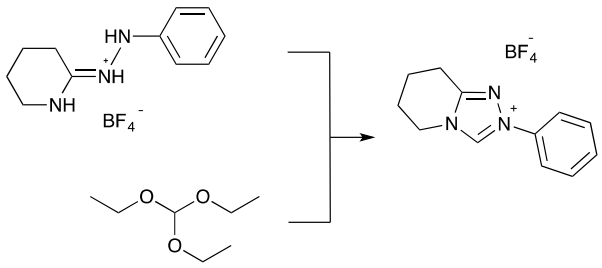

The residue was dissolved by using triethyl orthoformate (20 mL), followed by the addition of a catalytic amount of hydrochloric acid (0.5 mL, 4 M, in 1,4-dioxane), and the whole mixture was refluxed for 24 hours. Solvent was removed under reduced pressure. Ethyl acetate and diethyl ether were used to precipitate and wash the solid to yield the crude product as a sticky brown solid. Recrystallization from methanol: diethyl ether yielded the title compound as a brown needle-like crystals (1.20 g, 42%). **^{1}H NMR** (500 MHz, CD_2Cl_2): δ_H 2.17 (4H, m, 2 × CH_2), 3.17 (2H, t, *J*= 6.5 Hz, CH_2), 3.46 (2H, m, CH_2), 4.55 (2H, t, *J*= 5.0 Hz, CH_2), 7.65 (3H, m, 3 × ArH), 7.90 (2H, m, 2 × ArH), 10.12 (1H, s, NCH(N)); **^{13}C NMR** (176 MHz, CD_2Cl_2): δ_C 18.7 (CH_2), 21.2 (CH_2), 21.5 (CH_2), 46.4 (CH_2), 120.7 (2 × ArCH), 130.3 (ArCH), 130.9 (ArCH), 134.9 (ArCH), 139.1 (ArCN), 153.5 (NCN); ***m/z*** (ES+): 200 ($[M–BF_4]^+$, 100%). No trace of diethyl acetal adduct was observed.

7.3.9. Synthesis of 2-phenyl-6,7,8,9-tetrahydro-5*H*-[1,2,4]triazolo[4,3-a]azepin-2-ium tetrafluoroborate

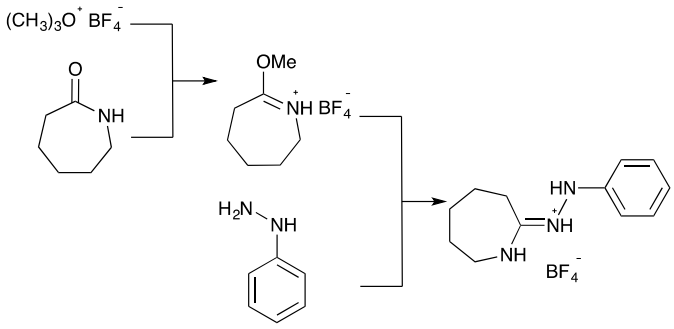

Based on a procedure by Rovis and co-workers[1], trimethyloxonium tetrafluoroborate (1.61 g, 11.0 mmol) was added into an anhydrous dichloromethane (50 mL) solution of ε-caprolactam (1.25 g, 10 mmol), and stirred overnight to obtain a yellow solution. After the addition of phenyl hydrazine (1 mL, 10.0 mmol), the reaction mixture was stirred for a further 48 hours at room temperature under argon to obtain a red solution. The solvent was removed under reduced pressure, yielding the amidrazone as a red solid, which was used without further purification. ***m/z*** (ES+): 204 ($[M–BF_4]^+$, 100%).

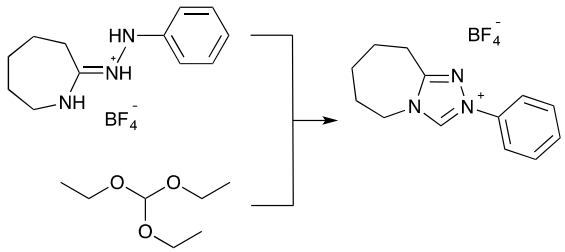

The residue was dissolved in triethyl orthoformate (25 mL), and a catalytic amount of hydrochloric acid solution (0.5 mL, 4 M, in 1,4-dioxane) was added. The mixture was stirred and refluxed for 48 hours and all volatiles were removed under reduced pressure to yield the crude product as a dark brown oil. An ethyl acetate wash yielded the product as an orange solid (2.589 g, 86%), with spectroscopic details in accordance with the literature[9]. **^{1}H NMR** (400 MHz, CDl_3): δ_H 1.85 (2H, m, CH_2), 1.96 (4H, m, 2 × CH_2), 3.16 (2H, m, CH_2), 4.51 (2H, m, CH_2), 7.51 (2H, m, 2 × ArH), 7.84 (2H, m, 2 × ArH), 10.04 (1H, s, NCH(N)); **^{13}C NMR** (176 MHz, $CDCl_3$): 24.4, 26.0, 27.3, 29.6, 49.7, 120.6, 123.0 (d, *J*= 9.1 Hz), 130.1, 130.4, 134.9, 140.6, 158.6; ***m/z*** (ES+): 214 ($[M–BF_4]^+$, 100%). **HRMS** (ES+): $[M–BF_4]^+$ $C_{13}H_{16}N_3$ requires: 214.1344, found: 214.1351. No trace of diethyl acetal adduct was observed.

7.3.10. Synthesis of 2-(4-methoxyphenyl)-6,7-dihydro-5*H*-pyrrolo[2,1-c][1,2,4] triazol-2-ium chloride

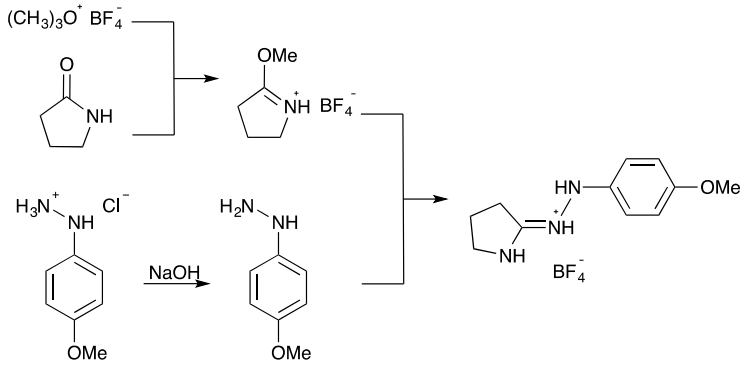

Using procedures adapted from Rovis and Gravel[1], trimethyloxonium tetrafluoroborate (0.87 g, 6.0 mmol) was added into an anhydrous dichloromethane (25 mL) solution of 2-pyrrolidinone (0.50 g, 6.0 mmol), and stirred overnight. 4-Methoxyphenyl hydrazine hydrochloride (0.87 g, 5.0 mmol) was dissolved in aqueous sodium hydroxide (1 M, 8 mL, 8.0 mmol), and extracted into dichloromethane. This dichloromethane solution was immediately added to the reaction mixture, and stirred for a further 48 hours at room temperature under argon. The colour of the solution changed from purple to dark grey, and a purple precipitate was observed to form. The solvent was removed under reduced pressure, yielding the amidrazone as a dark grey solid, which was used without further purification. ***m/z*** (ES+): 206 ([M–BF_4]$^+$, 100%).

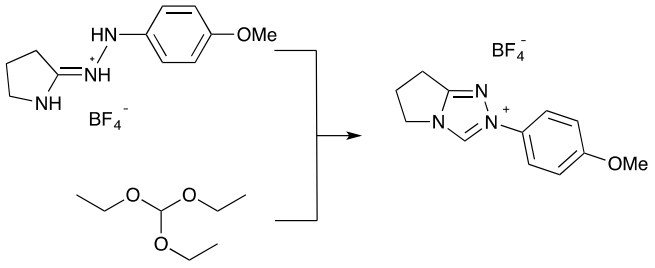

The residue was dissolved in triethyl orthoformate (25 mL). After a catalytic amount of hydrochloric acid solution (0.5 mL, 4 M, in 1,4-dioxane) was added, the colour changed immediately from brown into dark purple. The mixture was stirred and refluxed for 48 hours, and all volatiles were removed under reduced pressure, to yield the crude product

as a dark brown oil. An ethyl acetate wash yielded the product as a white powder (1.29 g, 85%), with spectroscopic details in accordance with the literature[8, 14]. **^{1}H NMR** (400 MHz, CDl_3): δ_H 2.87 (2H, m, CH_2), 3.23 (2H, t, *J*=7.8 Hz, CH_2), 3.86 (3H, s, OCH_3), 4.62 (2H, t, *J*=7.4 Hz, CH_2), 7.01 (2H, d, *J*=9.1 Hz, ArH), 7.71 (2H, d, *J*=9.1 Hz, ArH), 9.97 (1H, s, NCH(N)); **^{13}C NMR** (176 MHz, $CDCl_3$): δ_C 22.0 (CH_2), 26.8 (CH_2), 47.8 (CH_2), 55.90 (OCH_3), 115.4 (2 × ArCH), 122.8 (2 × ArCH), 128.8 (ArCN), 137.1 (NCH(N)), 161.5 (ArCO), 162.5 (NCN); ***m/z*** (ES+): 216 ([M–BF_4]$^+$, 100%). No trace of diethyl acetal adduct was observed.

7.3.11. Synthesis of 2-(4-methoxyphenyl)-5,6,7,8-tetrahydro-[1,2,4]triazolo[4,3-a]pyridin-2-ium tetrafluoroborate

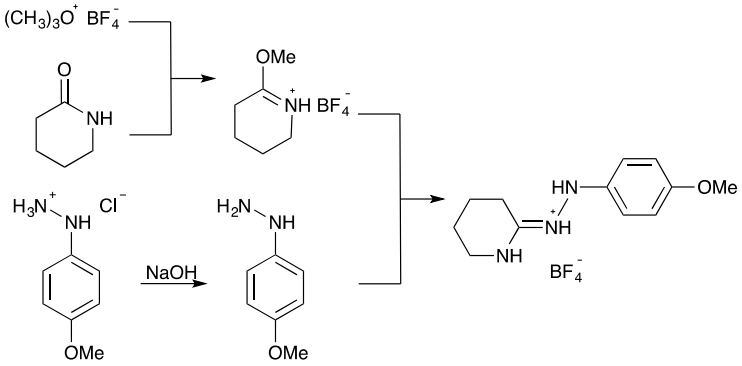

Using procedures adapted from Rovis and Gravel[1], trimethyloxonium tetrafluoroborate (0.87 g, 6.0 mmol) was added to a 2-piperidone solution (0.50 g, 6.0 mmol) in dry dichloromethane (25 mL), and stirred at room temperature overnight, under an argon environment. After the addition of 4-methoxyphenyl hydrazine hydrochloride (0.87 g, 5.0 mmol), the reaction mixture was stirred for 48 hours at room temperature under an inert atmosphere to obtain a blue solution, with purple precipitations. All volatiles were removed under reduced pressure to yield the amidrazone as a purple precepitate which was directly used without further purification. ***m/z*** (ES+): 220 ([M–BF_4]$^+$, 100%).

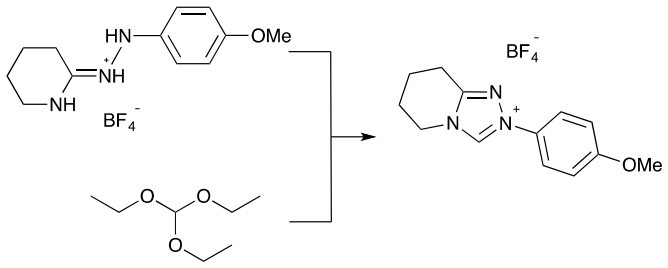

The residue was dissolved by using triethyl orthoformate (20 mL), followed by the addition of catalytic amount of hydrochloric acid (0.5 mL, 4 M, in 1,4-dioxane), and the whole mixture was refluxed for 48 hours to obtain a brown solvent with a white precipitate. Solvent was removed under reduced pressure and ethyl acetate and diethyl ether were used to further precipitate and wash the solid. The title compound was obtained as a white solid (1.05 g, 65%). **^{1}H NMR** (500 MHz, DMSO): δ_H 2.00 (4H, m, 2 × CH_2), 3.07 (2H, t, *J*= 6.3 Hz, CH_2), 4.29 (2H, t, *J*= 6.0 Hz, CH_2), 7.23 (3H, m, 3 × ArH), 7.80 (2H, m, 2 × ArH), 10.64 (1H, s, NCH(N)); **^{13}C NMR** (176 MHz, DMSO): δ_C 18.8, 21.1, 21.2, 45.8, 56.3, 115.7, 122.7, 128.6, 140.5, 153.5, 160.9; ***m/z*** (ES+): 230 ($[M–BF_4]^+$, 100%). No trace of diethyl acetal adduct was observed.

7.3.12. Synthesis of 2-(4-methoxyphenyl)-6,7,8,9-tetrahydro-5*H*-[1,2,4]triazolo[4,3-a]azepin-2-ium tetrafluoroborate

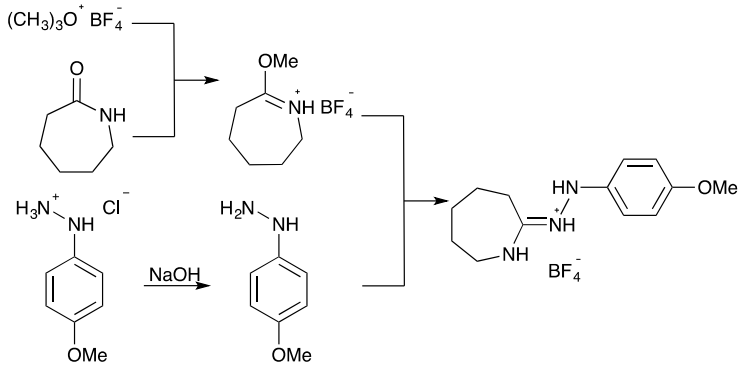

Using procedures adapted from Rovis and Gravel[1], trimethyloxonium tetrafluoroborate (1.74 g, 12.0 mmol) was added into an anhydrous dichloromethane (50 mL) solution of ε-caprolactam (1.25 g, 10.0 mmol), and stirred overnight to obtain a yellow solution. After the addition of 4-methoxyphenyl hydrazine hydrochloride (1.74 g, 10.0 mmol), the reaction mixture was stirred for a further 48 hours at room temperature under argon

to obtain a dark red solution. The solvent was removed under reduced pressure, yielding the amidrazone as a black solid, which was used without further purification.

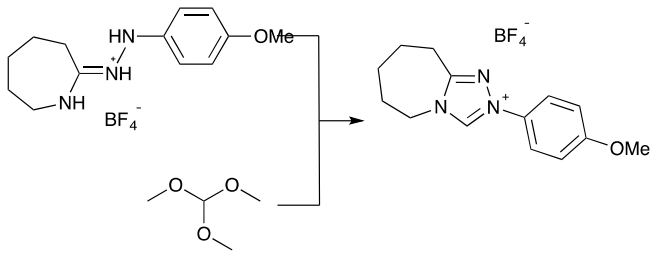

The residue was dissolved in trimethyl orthoformate (25 mL). After a catalytic amount of hydrochloric acid solution (0.5 mL, 4 M, in 1,4-dioxane) was added, the solvent changed from dark red to dark blue immediately. The mixture was stirred and refluxed for 48 hours and all volatiles were removed under reduced pressure to yield the crude product as a dark brown oil. An ethyl acetate wash yielded the crude product as a sticky yellow solid. Recrystallization from dichloromethane: toluene resulted in a pale-yellow powder with a small amount of impurities, and further recrystallizations from methanol: diethyl ether yielded the final product as an off-white powder (0.73 g, 22%). **^{1}H NMR** (400 MHz, CDl_3): δ_H 1.87 (2H, m, CH_2), 1.99 (4H, m, 2 × CH_2), 3.16 (2H, m, CH_2), 3.87 (3H, s, CH_3), 4.53 (2H, m, CH_2), 7.02 (2H, m, 2 × ArH), 7.76 (2H, m, 2 × ArH), 9.98 (1H, s, NCH(N)); **^{13}C NMR** (176 MHz, $CDCl_3$) δ_C 24.5, 26.1, 27.4, 29.7, 49.6, 55.7, 115.1, 122.3, 127.8, 139.9, 158.3, 161.1; ***m/z*** (ES+): 244 ([M–BF_4]$^+$, 100%). No trace of diethyl acetal adduct was observed.

7.3.13. Synthesis of 2-(2,4,6-trichlorophenyl)-6,7-dihydro-5*H*-pyrrolo[2,1-c][1,2,4] triazol-2-ium tetrafluoroborate

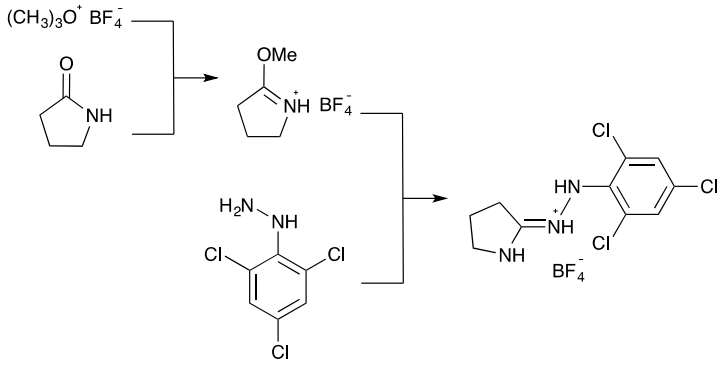

Using procedures adapted from Davidson and Fuchter[12], trimethyloxonium tetrafluoroborate (1.74 g, 12.0 mmol) was added into an anhydrous dichloromethane (50 mL) solution of 2-pyrrolidinone (1.10 g, 12.0 mmol), and stirred overnight. 2,4,6-Trichlorophenyl hydrazine (2.12 g, 10.0 mmol) was added into the mixture and stirred for a further 48 hours at room temperature under argon to obtain a red solution with some precipitate. The solvent was removed under reduced pressure, yielding the amidrazone as a red solid, which was used without further purification.

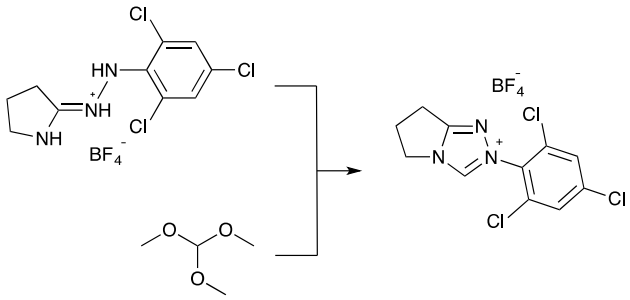

The residue was dissolved in trimethyl orthoformate (25 mL), and a catalytic amount of hydrochloric acid solution (0.5 mL, 4 M, in 1,4-dioxane) was added. The mixture was stirred and refluxed for 48 hours, and all volatiles were removed under reduced pressure, to yield the crude product as a dark brown oil. Addition of a mixture of methanol, ethyl acetate, and diethyl ether resulted in the formation of a brown oil suspended in the remaining solution. The brown oil contained impurities was removed and further diethyl ether was added to the remaining solution with sonication yielding the product as a pale-yellow powder (0.52, 14%), with spectroscopic details in accordance with the literature[15]. **^{1}H NMR** (400 MHz, $CDCl_3$): δ_H 2.95 (2H, m, CH_2), 3.31 (2H, dd, *J*=8.3, 7.3 Hz, CH_2), 4.77 (2H, dd, *J*= 8.2, 6.6 Hz, CH_2), 7.58 (2H, s, 2 × ArH), 9.84 (1H, s, NCH(N)); ***m/z*** (ES+): 288 ($[M–BF_4]^+$, 100%), 290 ($[M–BF_4]^+$, 97%).

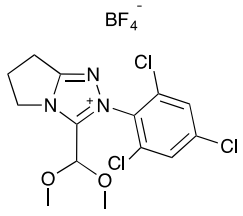

Trace amounts of dimethoxy acetal adduct could be detected from the ethyl acetate washing phase. ***m/z*** (ES+): 362 ($[M–BF_4]^+$, 89%), 364 ($[M–BF_4]^+$, 100%).

7.3.14. Synthesis of 2-(2,4,6-trichlorophenyl)-5,6,7,8-tetrahydro-[1,2,4] triazolo[4,3-a]pyridin-2-ium tetrafluoroborate

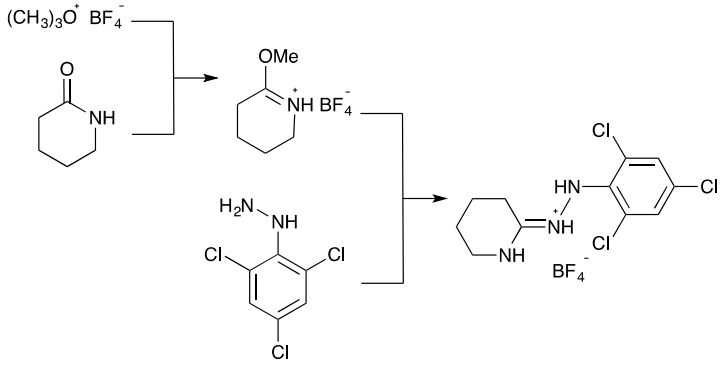

Using procedures adapted from Davidson and Fuchter[8], trimethyloxonium tetrafluoroborate (1.74 g, 12.0 mmol) was added to a 2-piperidone solution (1.10 g, 12.0 mmol) in dry dichloromethane (50 mL), and stirred at room temperature overnight, under an argon environment. After the addition of 2,4,6-trichlorophenyl hydrazine (2.12 g, 10.0 mmol), the reaction mixture was stirred for 48 hours at room temperature under an inert atmosphere to yield a red solution, with a purple precipitate. All volatiles were removed under reduced pressure to yield the amidrazone as a red solid, which was directly used without further purification. ***m/z*** (ES+): 292 ($[M–BF_4]^+$, 100%), 294 ($[M–BF_4]^+$, 93%).

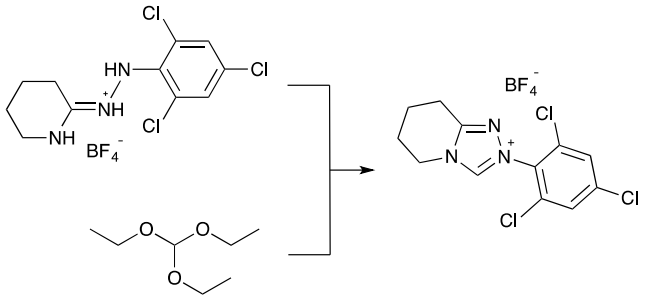

The residue was dissolved using triethyl orthoformate (20 mL), followed by the addition of a catalytic amount of hydrochloric acid (0.5 mL, 4 M, in 1,4-dioxane). The reaction mixture was refluxed for 48 hours to obtain a red emulsion. All volatiles were removed

under reduced pressure to give a brown oil. Trace amounts of title compound could be detected by mass spectroscopy, however purification was difficult. ***m/z*** (ES+): 302 ([M–BF_4]$^+$, 100%), 304 ([M–BF_4]$^+$, 92%).

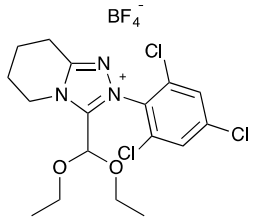

Trace amounts of diethoxy acetal adduct could be detected from the emulsion. ***m/z*** (ES+): 404 ([M–BF_4]$^+$, 100%), 406 ([M–BF_4]$^+$, 86%).

7.3.15. Synthesis of 2-(2,4,6-trichlorophenyl)-6,7,8,9-tetrahydro-5*H*-[1,2,4]triazolo [4,3-a]azepin-2-ium tetrafluoroborate

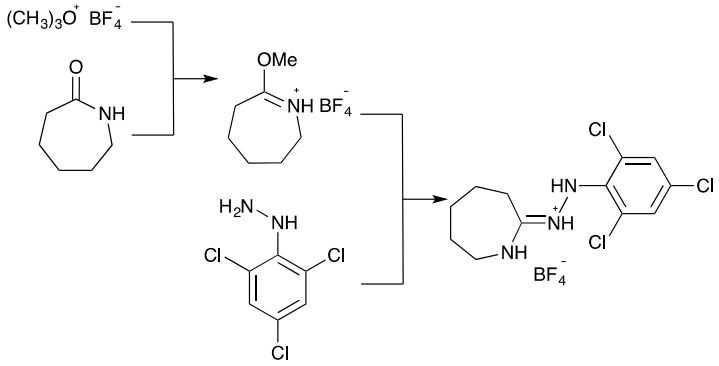

Using procedures adapted from Davidson and Fuchter[8], trimethyloxonium tetrafluoroborate (1.74 g, 12.0 mmol) was added into an anhydrous dichloromethane (50 mL) solution of ε-caprolactam (1.25 g, 10.0 mmol), and stirred overnight to obtain a yellow solution. After the addition of 2,4,6-trichlorophenyl hydrazine (2.12 g, 10.0 mmol), the reaction mixture was stirred for a further 48 hours at room temperature under argon to obtain a dark red solution. The solvent was removed under reduced pressure, yielding the amidrazone as a red solid, which was used without further purification. ***m/z*** (ES+): 306 ([M–BF_4]$^+$, 100%), 308 ([M–BF_4]$^+$, 92%).

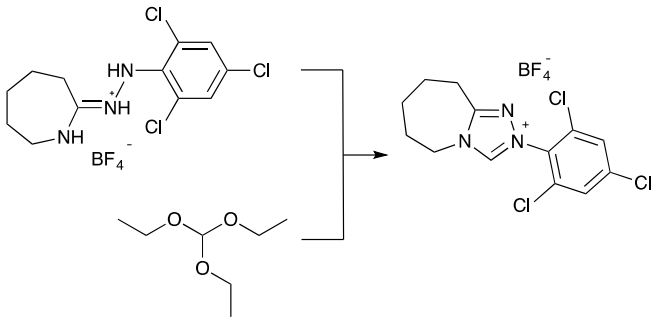

The residue was dissolved in trimethyl orthoformate (25 mL), and a catalytic amount of hydrochloric acid solution (0.5 mL, 4 M, in 1,4-dioxane) was added. The mixture was stirred and refluxed for 120 hours, and a dark red emulsion was obtained. All volatiles were removed under reduced pressure to yield the crude product as a dark brown oil. Trace amounts of title compound can be detected by mass spectroscopy, however the purification was difficult. ***m/z*** (ES+): 316 ($[M–BF_4]^+$, 97%), 318 ($[M–BF_4]^+$, 100%).

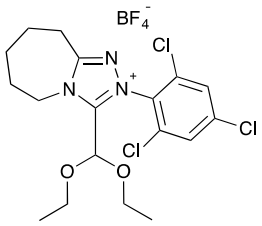

Trace amounts of diethoxy acetal adduct could be detected from the emulsion. ***m/z*** (ES+): 418 ($[M–BF_4]^+$, 100%), 420 ($[M–BF_4]^+$, 94%). ***m/z*** (ES+): 362 ($[M–BF_4]^+$, 89%), 364 ($[M–BF_4]^+$, 100%).

7.4. Synthetic Procedure of Dialkoxy Acetal Adduct

7.4.1. Synthesis of 2-perfluorophenyl-6,7,8,9-tetrahydro-5H-3-dimethoxyacetal[1,2,4]triazolo [4,3-a]azepin-2-ium tetrafluoroborate

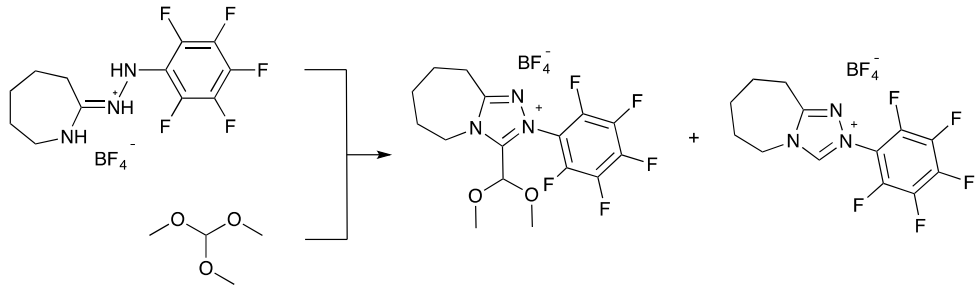

Amidrazone obtained using procedure introduced in Section 7.3.1 is recrystallized from methanol: diethyl ether system, and yield a white solid. The purified amidrazone (0.5 g, 1.31 mmol) was added into trimethyl orthoformate (10 mL). The yellow mixture was refluxed for 3 hours and solvent was removed under reduced pressure to give the crude products as viscous yellow solid. The solid was further purified by multi-phase recrystallization from dichloromethane: diethyl ether, and chloroform: diethyl ether systems, however spectroscopies suggest to be a mixture of triazolium salt **84** and dimethoxy acetal adduct **116**. **^{1}H NMR** (400 MHz, $(CD_3)_2SO$): δ_H 1.78 (2H, m, CH_2), 1.86 (2H, m, CH_2), 1.93 (2H, m, CH_2), 3.16 (2H, m, CH_2), 3.39 (6H, s, 2 × CH_3), 4.47 (2H, m, CH_2), 6.16 (1H, s, CH), with the triazolium salt peak appear at 10.59 (1H, s, NCH(N)); ***m/z*** (ES+): 378 ($[M–BF_4]^+$, 100%); **HRMS** (ES+): $[M–BF_4]^+$ $C_{16}H_{17}N_3O_2F_5$ requires: 378.1241, found: 378.1234.

7.4.2. Synthesis of 2-(2,4,6-trichlorophenyl)-6,7-dihydro-5H-3-diethoxyacetal-pyrrolo[2,1-c][1,2,4]triazol-2-ium tetrafluoroborate

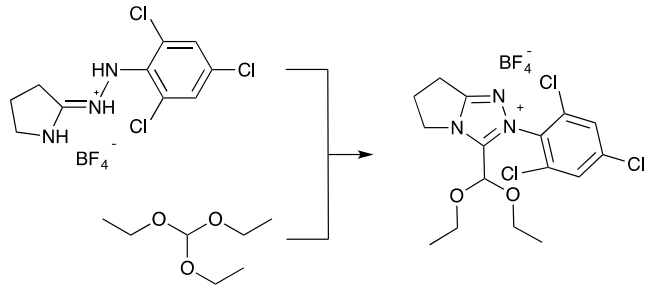

Amidrazone obtained using procedure introduced in Section 7.3.13 is recrystallized from methanol: diethyl ether system, and yield a white solid. The purified amidrazone (0.68 g, 1.86 mmol) was added into triethyl orthoformate (10 mL). The yellow mixture

was refluxed for 3 hours and solvent was removed under reduced pressure to give the crude products as viscous yellow solid. The solid was further purified by multi-phase recrystallization from dichloromethane: diethyl ether, and chloroform: diethyl ether systems yielding the product as a brown solid (0.66 g, 76.3%). **^{1}H NMR** (400 MHz, $(CD_3)_2SO$): δ_H 0.99 (6H, t, 2 × CH_3), 2.76 (2H, tq, CH_2), 3.24 (2H, t, CH_2), 3.60 (4H, m, 2 × CH_2), 4.48 (2H, t, CH_2), 6.16 (1H, s, CH), 8.15 (2H, s, 2 × ArH); **^{13}C NMR** (176 MHz, $CDCl_3$) δ_C 14.9, 22.2, 27.0, 49.5, 64.3, 94.2, 129.8, 131.0, 133.9, 138.6, 164.8; **HRMS** (ES+): $[M–BF_4]^+$ $C_{16}H_{19}N_3O_2Cl_3$ requires: 390.0553, found: 390.0543, 392.0529.

7.4.3. Synthesis of 2-(2,4,6-trichlorophenyl)-6,7-dihydro-5H-3-diisopropoxyacetal-pyrrolo[2,1-c][1,2,4]triazol-2-ium tetrafluoroborate

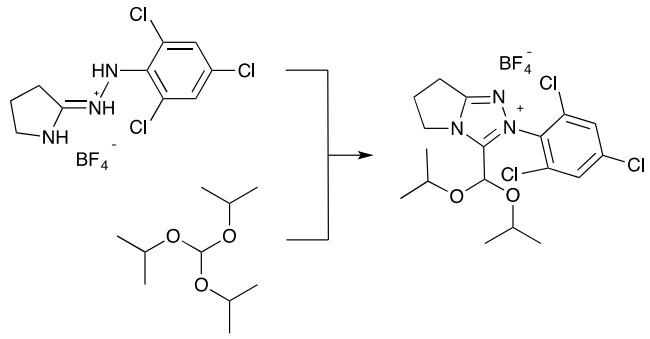

Amidrazone obtained using procedure introduced in Section 7.3.13 is recrystallized from methanol: diethyl ether system, and yield a white solid. The purified amidrazone (0.62 g, 1.69 mmol) was added into triisopropyl orthoformate (10 mL). The yellow mixture was refluxed for 6 hours and solvent was removed under reduced pressure to give the crude products as viscous yellow oil. Further recrystallisation from methanol: diethyl ether gives yellow crystals, however, is not pure.

7.4.4. Synthesis of 2-(2,4,6-trichlorophenyl)-5,6,7,8-tetrahydro-3-diethoxyacetal-[1,2,4]triazolo[4,3-a]pyridin-2-ium tetrafluoroborate

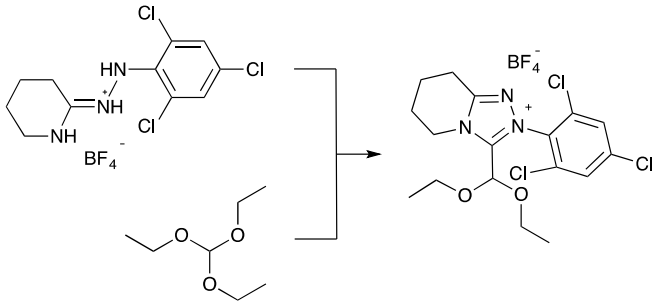

Amidrazone obtained using procedure introduced in Section 7.3.14 is recrystallized from methanol: diethyl ether system, and yield a white solid. The purified amidrazone (1.06 g, 2.78 mmol) was added into triethyl orthoformate (10 mL). The yellow mixture was refluxed for 3 hours and solvent was removed under reduced pressure to give the crude products as viscous yellow solid. The solid was further purified by multi-phase recrystallization from dichloromethane: diethyl ether, and chloroform: diethyl ether systems yielding the product as a white needle-like solid (0.71 g, 52.2%). **^{1}H NMR** (400 MHz, $(CD_3)_2SO$): δ_H 1.02 (6H, t, 2 × CH_3), 2.06 (4H, m, 2 × CH_2), 3.13 (2H, t, CH_2), 3.63 (4H, m, 2 × CH_2), 4.38 (2H, t, CH_2), 6.27 (1H, s, CH), 8.17 (2H, s, 2 × ArH); **^{13}C NMR** (176 MHz, $CDCl_3$) δ_C 14.9, 17.7, 20.7, 21.6, 47.1, 64.4, 94.2, 129.7, 131.4, 133.7, 138.3, 150.8, 155.7; ***m/z*** (ES+): 404 ($[M–BF_4]^+$, 100%), 406 ($[M–BF_4]^+$, 86%).

7.4.5. Synthesis of 2-(2,4,6-trichlorophenyl)-5,6,7,8-tetrahydro-3-diisopropoxyacetal-[1,2,4]triazolo[4,3-a]pyridin-2-ium tetrafluoroborate

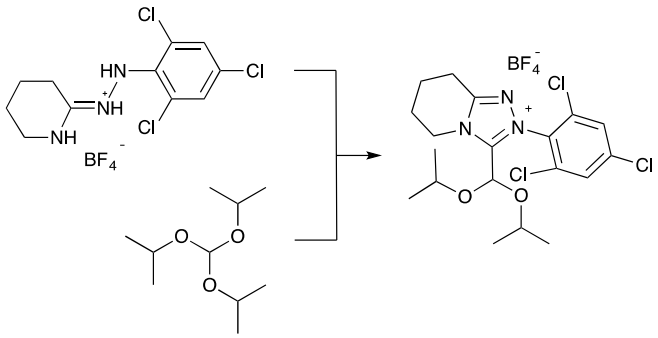

Amidrazone obtained using procedure introduced in Section 7.3.14 is recrystallized from methanol: diethyl ether system, and yield a white solid. The purified amidrazone

(0.62 g, 1.63 mmol) was added into triisopropyl orthoformate (10 mL). The yellow mixture was refluxed for 5 hours and solvent was removed under reduced pressure to give the crude products as viscous yellow solid. The solid was further purified by multi-phase recrystallization from dichloromethane: diethyl ether, and chloroform: diethyl ether systems yielding the product as a white solid (0.51 g, 60.1%). **^{1}H NMR** (400 MHz, $(CD_3)_2SO$): δ_H 1.12 (12H, dd, 4 × CH_3), 2.17 (2H, m, CH_2), 2.30 (2H, m, CH_2), 3.17 (2H, t, CH_2), 4.05 (2H, hept, 2 × CH), 4.55 (2H, t, CH_2), 6.30 (1H, s, CH), 7.56 (2H, s, 2 × ArH); ***m/z*** (ES+): 432 ($[M–BF_4]^+$, 100%), 434 ($[M–BF_4]^+$, 88%).

7.4.6. Synthesis of 2-perfluorophenyl-6,7,8,9-tetrahydro-5H-3-diisopropoxyacetal [1,2,4]triazolo [4,3-a]azepin-2-ium tetrafluoroborate

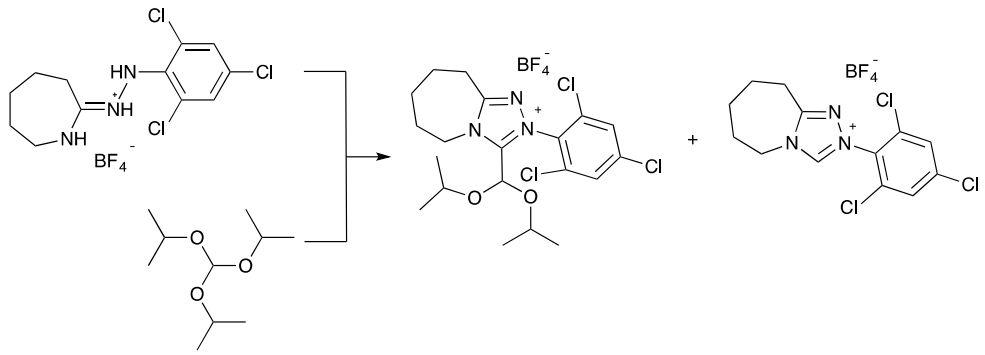

Amidrazone obtained using procedure introduced in Section 7.3.15 is recrystallized from methanol: diethyl ether system, and yield a white solid. The purified amidrazone (0.60 g, 1.52 mmol) was added into trimethyl orthoformate (10 mL). The yellow mixture was refluxed for 4 hours and solvent was removed under reduced pressure to give the crude products as viscous yellow solid. The solid was further purified by multi-phase recrystallization from dichloromethane: diethyl ether, and chloroform: diethyl ether systems, however spectroscopies suggest to be a mixture of triazolium salt **83** and dimethoxy acetal adduct **115**. **^{1}H NMR** (400 MHz, $(CD_3)_2SO$): δ_H 1.13 (12H, dd, 4 × CH_2), 1.89 (2H, m, CH_2), 2.02 (4H, m, 2 × CH_2), 3.25 (2H, m, CH_2), 4.05 (2H, hept, 2 × CH), 4.67 (2H, m, CH_2), 6.26 (1H, s, CH), 7.59 (2H, m, 2 × ArH), with the triazolium

salt peak appear at 10.14 (1H, s, NCH(N)); ***m/z*** (ES+): 446 ([M–BF_4]$^+$, 100%), 448 ([M–BF_4]$^+$, 90%).

7.5. Synthetic Procedures of Bis(amino)cyclopropenium Salts

7.5.1. Synthesis of bis(diisopropylamino)cyclopropenium tetraphenylborate 61

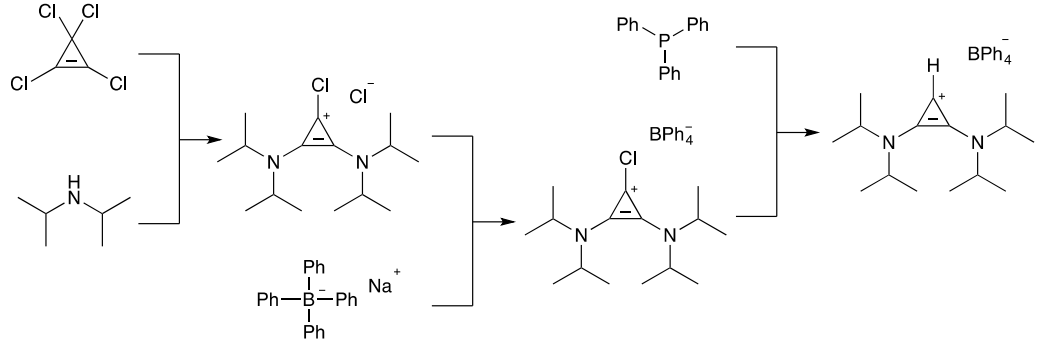

Based on a procedure by Betrand[13, 14], diisopropylamine (7.01 mL, 50.0 mmol) was added dropwise at 0 ºC to a stirred solution of tetrachlorocyclopropene (1.78 g, 10.0 mmol) in dichloromethane (100 mL). A vigorous ejection of hydrogen chloride was observed. The solution developed a yellow colour and a white precipitate was observed to form. After stirring for 6 hours at 0 ºC, the solution was warmed to ambient temperature and sodium tetraphenylborate (3.42 g, 10.0 mmol) was added. The suspension was stirred overnight to form a red solution with white precipitate and then refluxed for 4 hours. After cooling down to room temperature, triphenylphosphine (2.62 g, 10 mmol) was added to form a yellow solution, followed by immediate addition of water (70 mL). The mixture was stirred overnight with a vent open to air. The organic layer was separated and washed with water (3 × 150 mL), then dried with sodium sulphate and solvent was removed under reduced pressure to yield the title compound as pale-grey crystals, with NMR suggesting the counter ion to be a mixture of tetrafluoroborate and chlorine as the chemical shift of Cp-H different from literature[13]. **^{1}H NMR** (700 MHz, $CDCl_3$): δ_H 1.27 (12H, d, *J*=6.8 Hz, 4 × CH_3), 1.32 (12H, d, *J*=6.8

Hz, N-CH_3), 3.72 (2H, h, *J*=6.8 Hz, 4 × CH_3), 3.89 (2H, h, *J*=6.8 Hz, N-CH_3), 6.58 (1H, s, Cp-H), 7.44 (8H, m, ArH), 7.03 (8H, t, *J* = 7.4 Hz, ArH), 6.88 (3H, t, *J*= 7.2 Hz, ArH)); **^{13}C NMR** (176 MHz, $CDCl_3$): δ_C 20.9, 21.1, 49.9, 55.7, 100.9, 121.7, 125.6, 127.4, 130.2, 133.3, 134.1, 136.2, 164.9.

7.5.2. Synthesis of bis[(*R*-1-phenylethyl)amino]cyclopropenium tetrafluoroborate 62

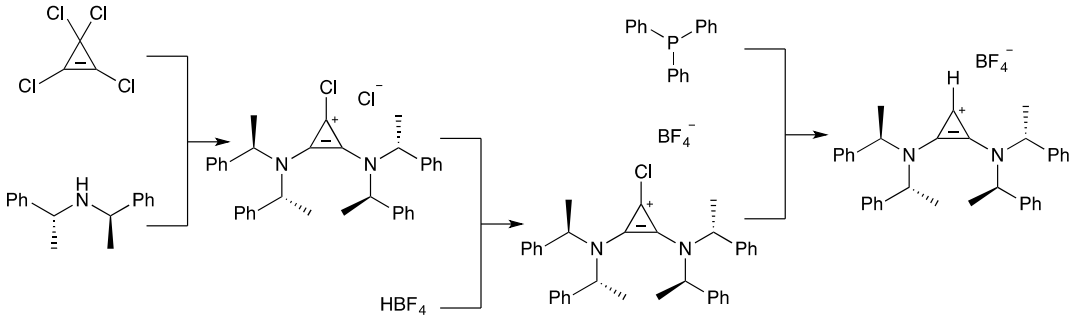

Based on a procedure by Tamm[15], bis(*R*-1-phenylethyl)amine (2 mL, 10.0 mmol) was added dropwise at 0 ºC to a stirred solution of tetrachlorocyclopropene (0.6 mL, 5.0 mmol) in dichloromethane (50 mL). A vigorous ejection of hydrochloric gas was observed and the solution turned yellow. After stirring overnight, tetrafluoroboric acid (0.42 mL, 48% in water) was added. The suspension was stirred overnight to form a red solution. Triphenylphosphine (1.31 g, 5.0 mmol) was added to form a yellow solution, followed by immediate addition of water (30 mL). The mixture was stirred overnight with a vent open to air to yield a brown solution, in which trace amounts of title product could be found. ***m/z*** (ES+): 485 ($[M–BF_4]^+$, 100%), 485 ($[M–BF_4]^+$, 94%).

7.5.3. Synthesis of bis(morpholine)cyclopropenium tetrafluoroborate 63

There is no detailed synthetic procedure towards the title compound currently, and the following procedure details attempts adapted from unpublished work in our group.

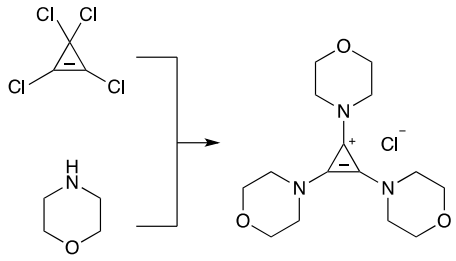

Morpholine (4.30 mL, 25.0 mmol) was added dropwise at 0 ºC to a stirred solution of tetrachlorocyclopropene (1.22 mL, 10.0 mmol) in chloroform (50 mL) under argon. The solution was warmed to room temperature and stirred for 1 hour, and formed a white precipitate. Hydrochloric acid was added to protonate the remaining morpholine. Solvent was removed under reduced pressure and the morpholine hydrochloride solid was washed by ethyl acetate. The washing phase was collected and ethyl acetate was removed under reduced pressure. The above procedure to remove morpholine hydrochloride was repeated several times and an excess of saturated potassium bicarbonate solution was utilised to deprotonated the morpholine hydrochloride salt remaining in organic phase. The solvent was removed under reduced pressure and the orange oil was dried over high vacuum line to yield the tris(morpholilno)cyclopropenium salt as a highly hydroscopic orange solid. ***m/z*** (ES+): 294 ($[M–Cl]^+$, 100%), 294 ($[M–BF_4]^+$, 93%).

Another attempt neglected the removal of remaining morpholine result in the formation of by-product rather than the target compound.

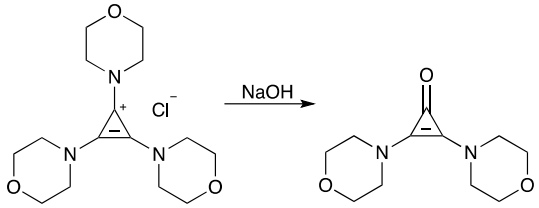

Tris(morpholino)cyclopropenium chloride was added to a stirred solution of sodium hydroxide (8.00 g, 0.20 mol) in water (150 mL), and the solution colour turned yellow immediately. The mixture was warmed to 65 ºC and stirred for 1 hour. The reaction mixture was then concentrated under reduced pressure and extracted by

dichloromethane (3 × 50 mL). The organic phase was collected and dried over sodium sulphate. After removal of solvent, the remaining brown oil was recrystallized from dichloromethane: diethyl ether to yield the bis(morpholino)cyclopropenone as pale-yellow crystals (0.36g, 16%). **^{1}H NMR** (700 MHz, $CDCl_3$): δ_H 3.36 (8H, m, 4 × CH_2), 3.76 (8H, m, 4 × CH_2); **^{13}C NMR** (176 MHz, DMSO): δ_C 49.4, 66.2, 120.4, 135.0; ***m/z*** (ES+): 225 ($[M+H]^+$, 100%), 225 ($[M+H]^+$, 100%).

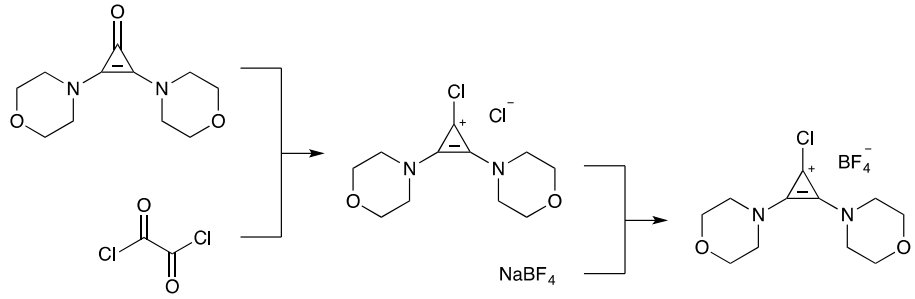

Bis(morpholino)cyclopropenone (0.248 g, 1.10 mmol) was placed in a dry flask under argon, and oxalyl chloride (1 mL) was added dropwise with stirring. The mixture was dried under reduced pressure to remove the remaining oxalyl chloride, and acetonitrile (8 mL) was used to dissolve the white-brown solid. After the addition of sodium tetrafluoroborate (0.132 g, 1.20 mmol), the mixture was stirred for 6 hours, and solvent was removed to yield the 1-chloro-2,3-bis(morpholino)cyclopropenium chloride as a brown solid.

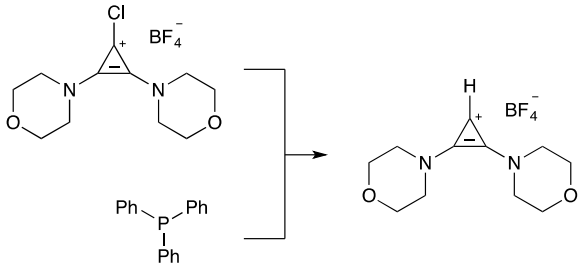

1-chloro-2,3-bis(morpholino)cyclopropenium chloride (0.18 g, 0.55 mmol) was dissolved in dichloromethane (10 mL), and triphenylphosphine (0.262 g, 1.00 mmol) was added followed by immediate addition of water (10 mL). The mixture was stirred overnight with a vent open to air, and the resulting mixture was extracted by water (3 × 10 mL). The water phase was collected and solvent was removed under reduced pressure

to yield the product as a pale-yellow solid. Further recrystallization from methanol: diethyl ether yielded the title compound as a pale-yellow needle-like crystal (0.10 g, 8%). **^{1}H NMR** (700 MHz, DMSO): δ_H 3.61 (8H, ddd, *J*=17.8, 5.8, 3.9 Hz, 4 × CH_2), 3.74 (8H, m, 4 × CH_2), 7.64 (1H, s, Cp-H); ***m/z*** (ES+): 209 ([M-BF_4]$^+$, 100%), 209 ([M-BF_4]$^+$, 100%).

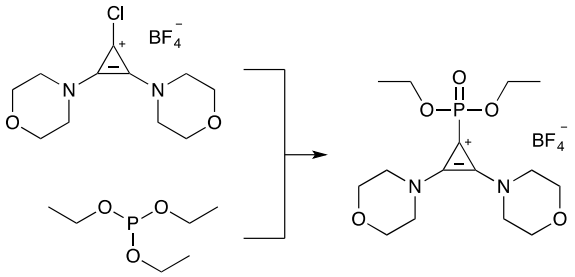

To probe a potential new synthetic procedure towards bis(amino)cyclopropenium salt, 1-chloro-2,3-bis(morpholino)cyclopropenium chloride (0.10g, 0.30 mmol) was dissolved by using dichloromethane (10 mL), and triethyl phosphite (10 mL) was added. The mixture was stirred overnight but none of the target product could be detected.

7.6. Kinetic Studies of the NHC-catalysed Benzoin Condensation

Solutions of triethylamine buffer in methanol-d_4 were prepared using dried triethylamine hydrochloride and distilled triethylamine. ^{1}H NMR spectra were recorded on an Oxford Varian Inova 500 spectrometer thermostated at 25 °C, with a relaxation delay (d1) of 5 s, sweep width of 10000.0 Hz, acquisition time (at) of 2 s and 45° pulse angle (pw). Spectra were run with 32 transients (nt, total running time ~4 min) for kinetic evaluation, and 8 for pre-equilibrium studies. Measurement times were taken from the mid-point of the acquisition.

7.7. Reference

1. O. V. Dolomanov, L. J. Bourhis, R. J. Gildea, J. A. K. Howard and H. Puschmann, *J. Appl. Crystallogr.*, 2009, **42**, 339-341.

2. G. M. Sheldrick, *Acta Crystallogr A*, 2008, **64**, 112-122.
3. A. D. Becke, *J. Chem. Phys.*, 1993, **98**, 1372-1377.
4. a. Petersson, A. Bennett, T. G. Tensfeldt, M. A. Al‐Laham, W. A. Shirley and J. Mantzaris, *J. Phys. Chem.*, 1988, **89**, 2193-2218.
5. M. S. Kerr, J. Read de Alaniz and T. Rovis, *J Org Chem*, 2005, **70**, 5725-5728.
6. S. M. Langdon, M. M. Wilde, K. Thai and M. Gravel, *J. Am. Chem. Soc.*, 2014, **136**, 7539-7542.
7. J. ZHU, Durham University, 2016.
8. M. Schedler, R. Frohlich, C. G. Daniliuc and F. Glorius, *Eur. J. Org. Chem.*, 2012, **2012**, 4164-4171.
9. K. B. Ling and A. D. Smith, *Chem. Commun.*, 2011, **47**, 373-375.
10. K. Suenaga, H. Shimogawa, S. Nakagawa and D. Uemura, *Tetrahedron Lett.*, 2001, **42**, 7079-7081.
11. P.-C. Chiang, M. Rommel and J. W. Bode, *J. Am. Chem. Soc.*, 2009, **131**, 8714-8718.
12. R. W. Davidson and M. J. Fuchter, *Chem. Commun.*, 2016, **52**, 11638-11641.
13. V. Lavallo, Y. Canac, B. Donnadieu, W. W. Schoeller and G. Bertrand, *Science*, 2006, **312**, 722-724.
14. D. Martin, A. Baceiredo, H. Gornitzka, W. W. Schoeller and G. Bertrand, *Angew Chem Int Edit*, 2005, **44**, 1700-1703.
15. D. Holschumacher, C. G. Hrib, P. G. Jones and M. Tamm, *Chem Commun (Camb)*, 2007, DOI: 10.1039/b706708a, 3661-3663.

Acknowledgements

I would like to thank my parents for their support on both my study and life. Thank you for your willingness to afford all my living expenses and tuition fees, and your support is far more than these. I could keep doing what I like and devote myself to chemistry without any worries, mainly because I know that I always have two people behind me with no complaint. Even though I am thousand miles away from home, I understand that, whenever I was tired and would like to have a rest, there is always a shelter for me to hide myself in.

I would like to thank my supervisor, Dr. AnnMarie O'Donoghue, for your expert knowledge and guidance over my whole PhD. The help and opportunities you provided, offered me a chance to train myself into a better shape. Also, your invaluable support and encouragement enabled me to complete my work successfully. I think being your student is one of the most brilliant decisions I have ever made.

To Qing He, thank you very much for willing to be my roommate, and take care of my life and study. You taught me a lot, in every sense. You are one of the most important people in my life. I think I don't need to mention too much here, as I know you understand.

My colleagues David Tucker, Peter Quinn, Lami Mnamounu, Oliver Maguire, David Wang-Pascua, Kevin Maduka, and all the students worked in our lab, thank you for your kind help on my project. I should never forget to mention the "Fluorine Group". You shared the office and lab with us and you are the group of the people who brought all the funs to us.

I should also say thanks to all the staffs working in Durham, especially the staffs in NMR, Mass Spectrometry, Elemental Analysis, X-ray Crystallography, HPLC, Glass-blowing Workshop, Electronic Workshop, and Mechanic Workshop. Thank you very much for your help, and thank you to always bear me with my stupid questions and enquiries.

I also appreciate all the lecturers I met in both China and Britain. Your educations and guidance helped me figure out my interest in chemistry.

Finally, I would like to say thanks to all my friends in my life. Siying Liu and Ji Sun, when we are roommates in Liverpool, I was still not grow up enough. Thank you for bearing with all my childish behaviours. You two are my friends, also my sisters, who helped me establish a better world view. Huiyu Liu, you are my undergraduate classmate, and we both applied to Durham for Master and PhD. Thank you for these eight-years' accompaniment. I should say thanks to Dr. Ge Bai and Xiaoxiao Ma, you are always willing to help me dealing with my problems and listened to my complains. Thank you to all the staffs in Yum cafe, you know even better than my parents about which drink I like, I really enjoy the short talks with you guys every day.

I've met so many friends in Durham, Rongjuan Huang, Huizhe Yang, Xiangwen Fan, Wenfeng Tan, Jin Wang, Fei Zhang, Xiang Li, Mengying Xia, Xi Lu, Mengsi Li, Jun Wang…… There is no way for me to mention all your names here, but I wish you all the best in future, and I think one day we will meet each other in a place in the world.

Appendix

Concentration Profiles

Concentration profile for the self-condensation of 2-methoxybenzaldehyde **138** (0.08 M), catalysed by *meta*-chlorophenyl triazolium precatalyst **103** (n= 1, 0.04 M), in 0.107 M NEt_3 and 0.053 M $NEt_3 \cdot HCl$ in methanol-d_4.

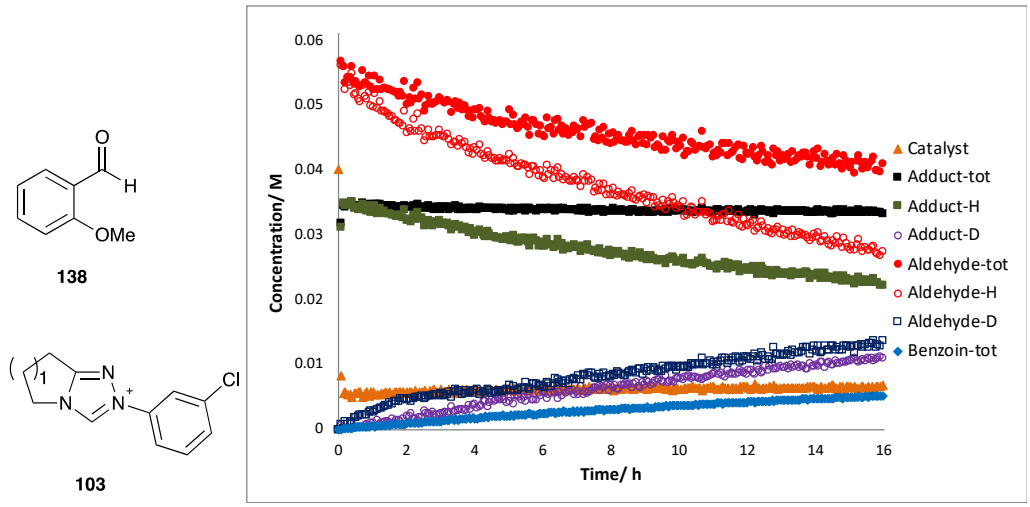

Concentration profile for the self-condensation of 4-methoxybenzaldehyde **139** (0.10 M), catalysed by *meta*-chlorophenyl triazolium precatalyst **103** (n= 1, 0.04 M), in 0.107 M NEt_3 and 0.053 M $NEt_3 \cdot HCl$ in methanol-d_4.

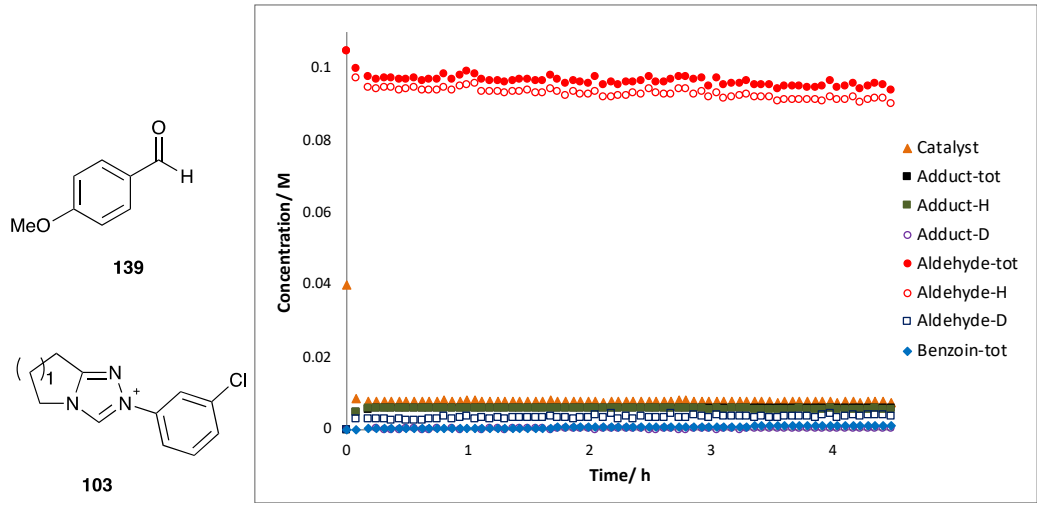

Concentration profile for the self-condensation of benzaldehyde **135** (0.075 M), catalysed by *meta*-chlorophenyl triazolium precatalyst **103** (n= 1, 0.04 M), in 0.107 M NEt_3 and 0.053 M NEt_3·HCl in methanol-d_4.

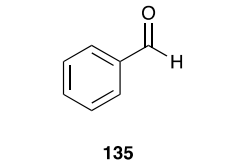

135

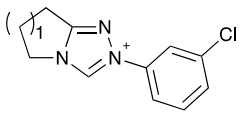

103

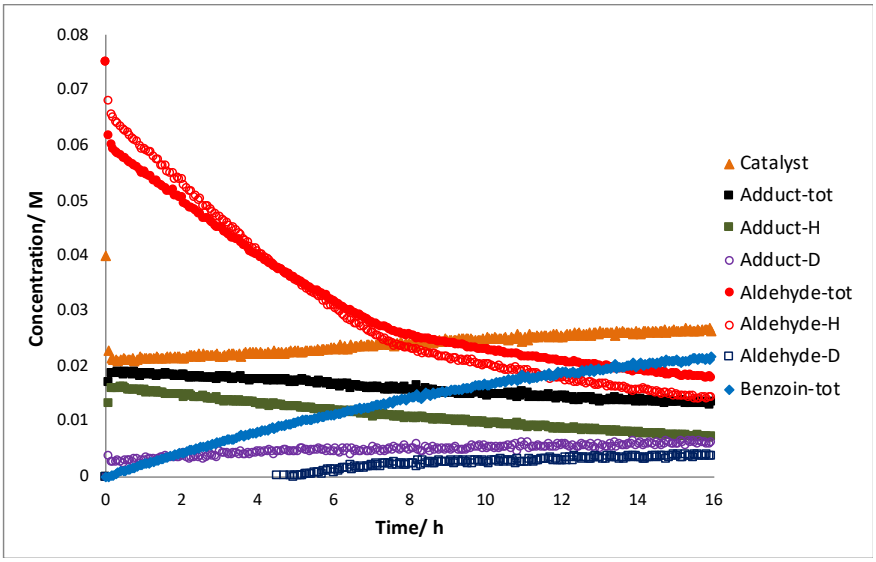

Concentration profile for the self-condensation of 2-methoxybenzaldehyde **138** (0.08 M), catalysed by *para*-bromophenyl triazolium precatalyst **104** (n= 1, 0.08 M), in 0.107 M NEt_3 and 0.053 M NEt_3·HCl in methanol-d_4.

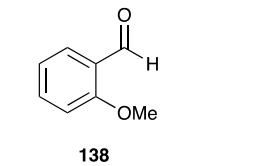

138

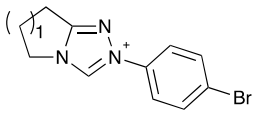

104

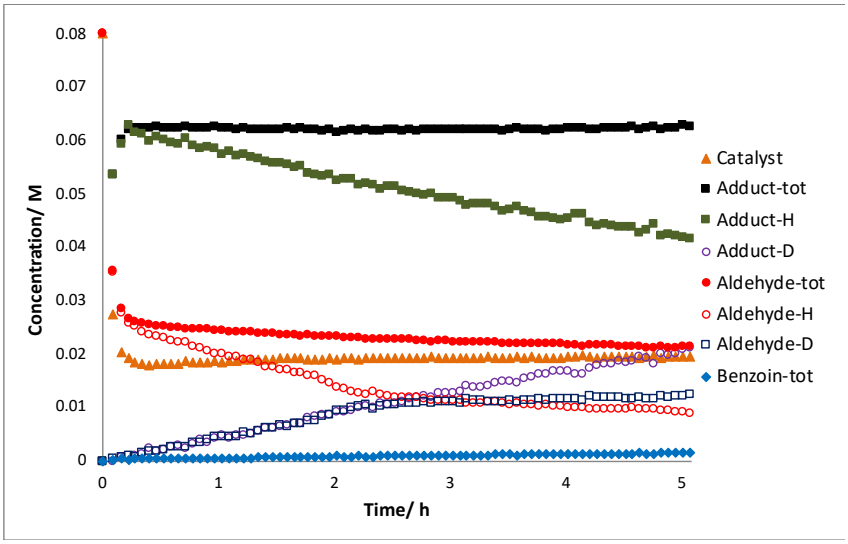

Concentration profile for the self-condensation of 4-methoxybenzaldehyde **139** (0.09 M), catalysed by *para*-bromophenyl triazolium precatalyst **104** (n= 1, 0.08 M), in 0.107 M NEt_3 and 0.053 M $NEt_3 \cdot HCl$ in methanol-d_4.

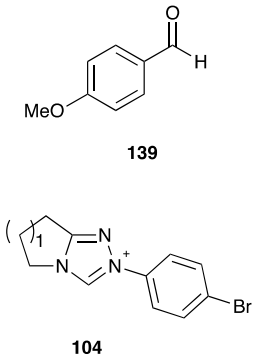

139

104

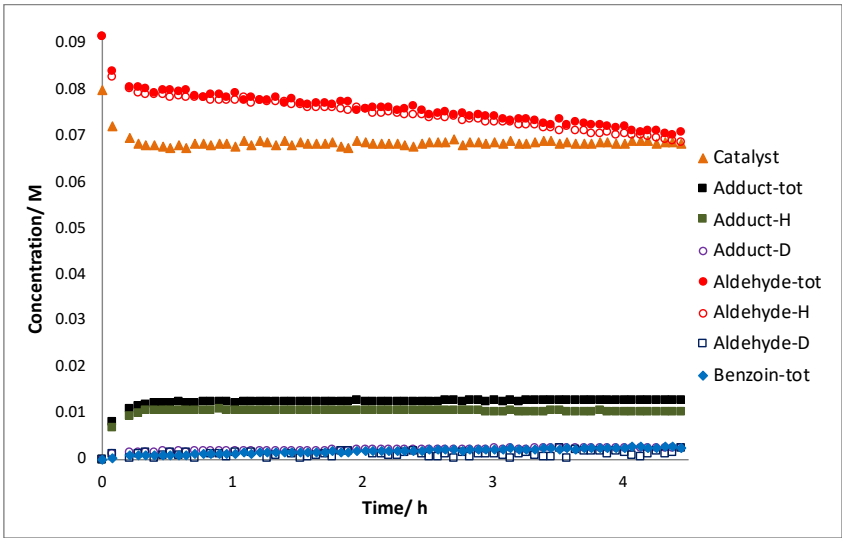

Concentration profile for the self-condensation of benzaldehyde **135** (0.07 M), catalysed by *para*-bromophenyl triazolium precatalyst **104** (n= 1, 0.08 M), in 0.107 M NEt_3 and 0.053 M $NEt_3 \cdot HCl$ in methanol-d_4.

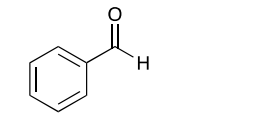

135

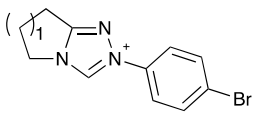

104

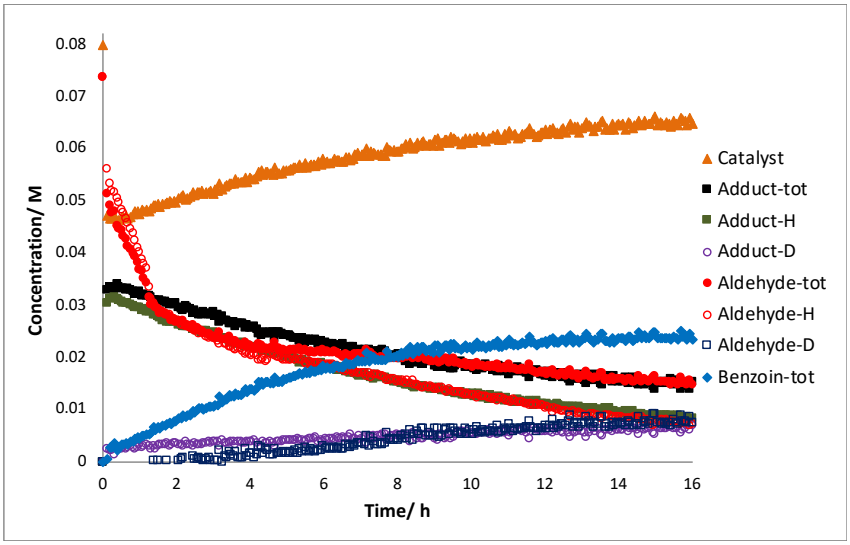

Concentration profile for the self-condensation of 2-methoxybenzaldehyde **138** (0.053 M), catalysed by *para*-trifluoromethylphenyl triazolium precatalyst **105** (n= 1, 0.043 M), in 0.107 M NEt_3 and 0.053 M $NEt_3 \cdot HCl$ in methanol-d_4.

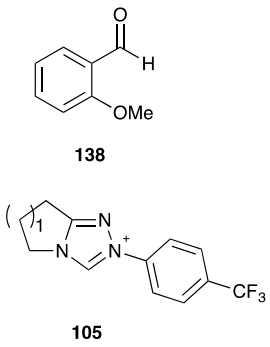

138

105

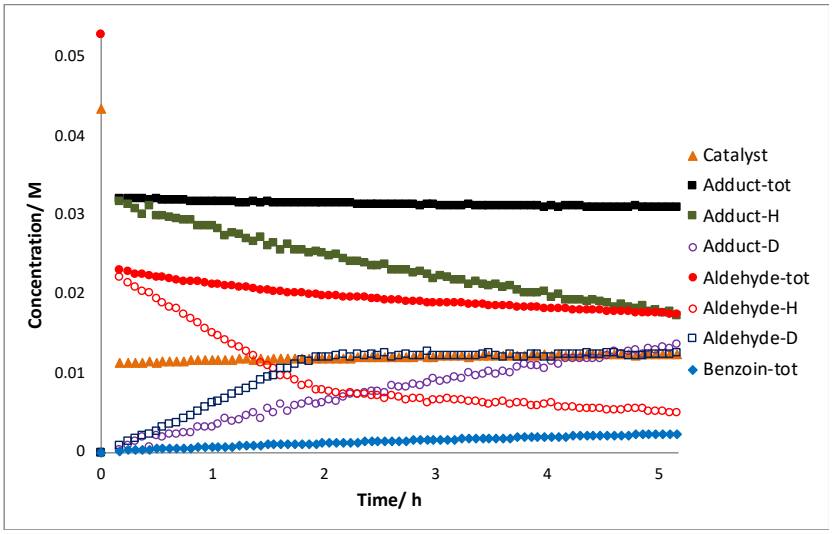

Concentration profile for the self-condensation of 4-methoxybenzaldehyde **139** (0.053 M), catalysed by *para*-trifluoromethylphenyl triazolium precatalyst **105** (n= 1, 0.041 M), in 0.107 M NEt_3 and 0.053 M $NEt_3 \cdot HCl$ in methanol-d_4.

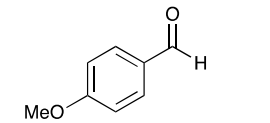

139

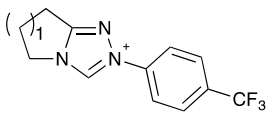

105

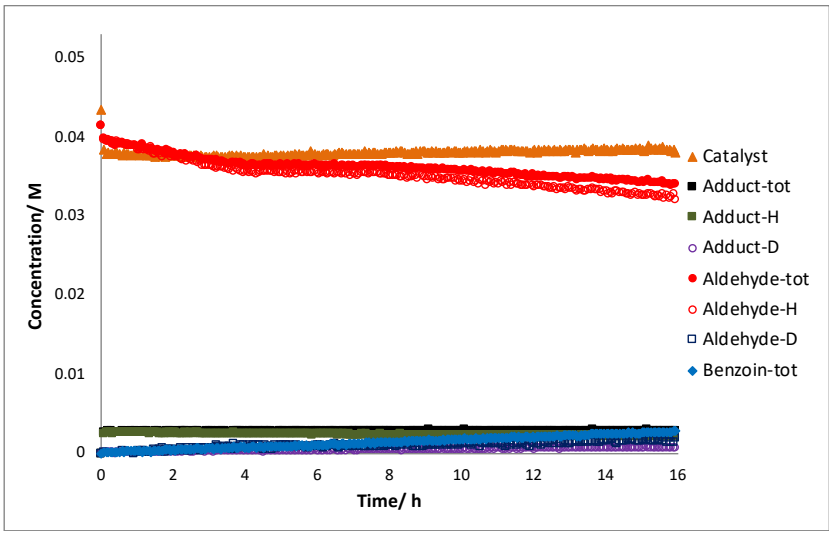

Concentration profile for the self-condensation of benzaldehyde **135** (0.036 M), catalysed by *para*-trifluoromethylphenyl triazolium precatalyst **105** (n= 1, 0.043 M), in 0.107 M NEt_3 and 0.053 M $NEt_3 \cdot HCl$ in methanol-d_4.

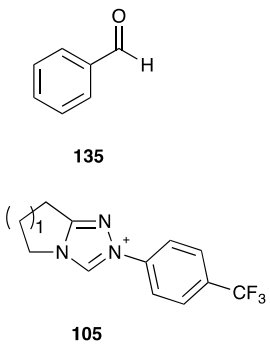

135

105

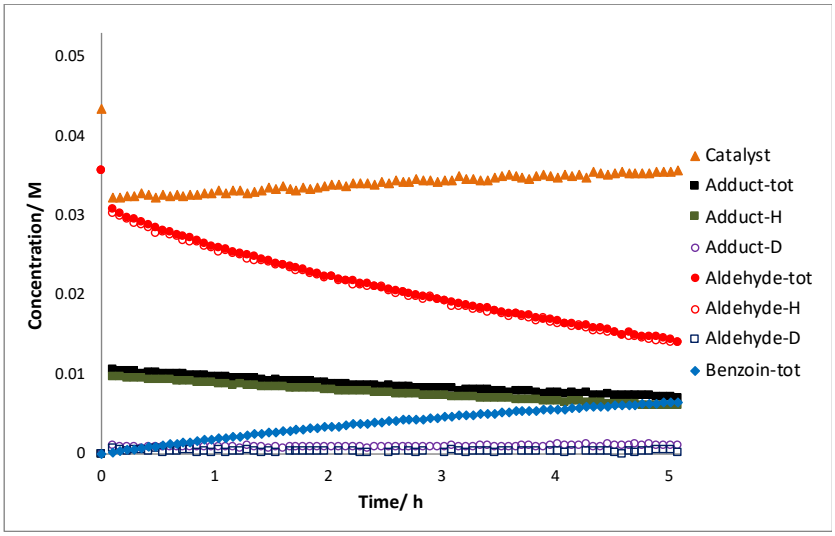

Concentration profile for the self-condensation of 2-methylbenzaldehyde **136** (0.077 M), catalysed by *para*-fluorophenyl triazolium precatalyst **100** (n= 1, 0.08 M), in 0.107 M NEt_3 and 0.053 M $NEt_3 \cdot HCl$ in methanol-d_4.

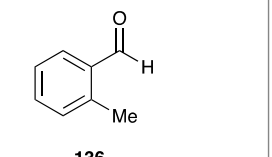

136

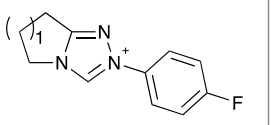

100

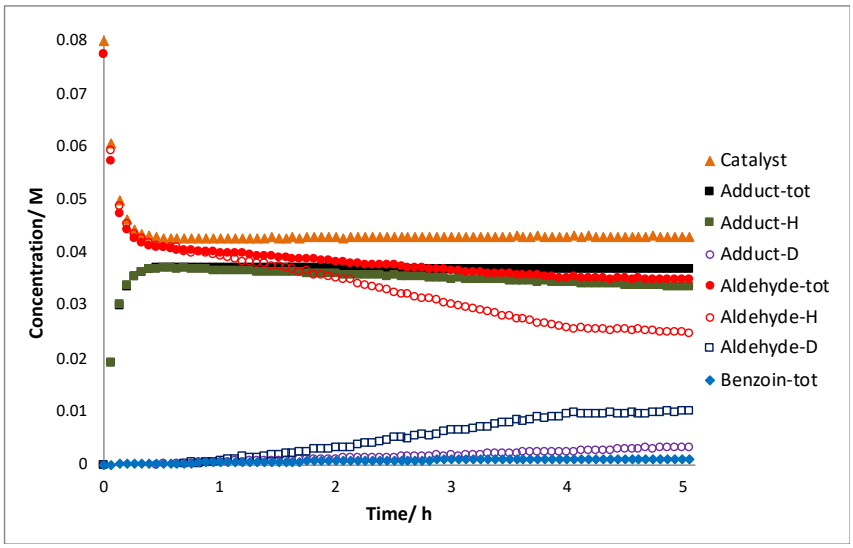

Concentration profile for the self-condensation of 4-methylbenzaldehyde **137** (0.079 M), catalysed by *para*-fluorophenyl triazolium precatalyst **100** (n= 1, 0.08 M), in 0.107 M NEt_3 and 0.053 M $NEt_3 \cdot HCl$ in methanol-d_4.

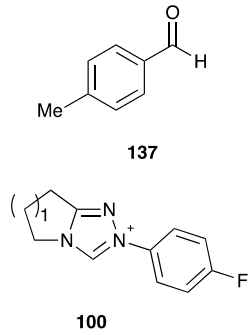

137

100

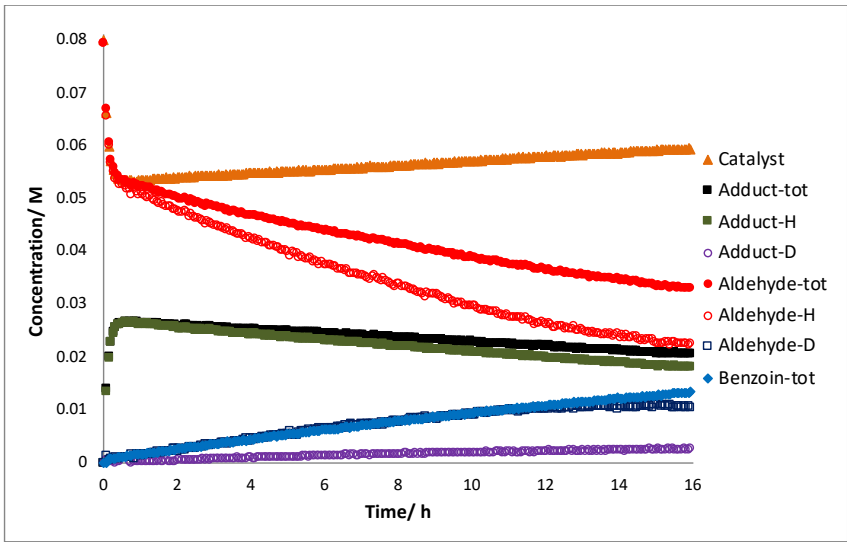

Concentration profile for the self-condensation of 2-trifluoromethylbenzaldehyde **150** (0.071 M), catalysed by phenyl triazolium precatalyst **101** (n= 1, 0.08 M), in 0.107 M NEt_3 and 0.053 M $NEt_3 \cdot HCl$ in methanol-d_4.

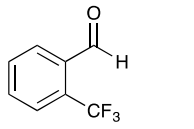

150

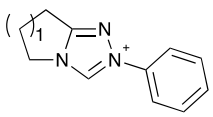

101

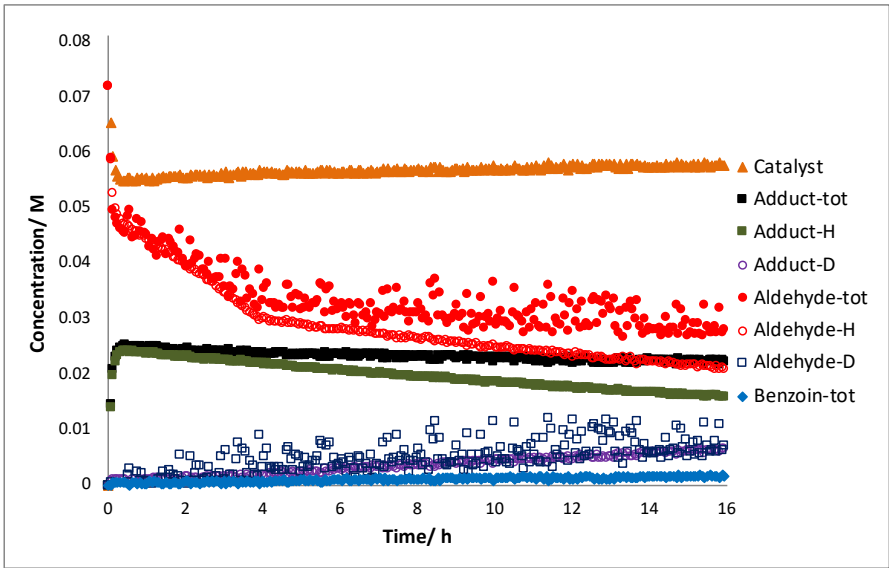

Concentration profile for the self-condensation of 2-fluorobenzaldehyde **154** (0.07 M), catalysed by phenyl triazolium precatalyst **101** (n= 1, 0.08 M), in 0.107 M NEt_3 and 0.053 M $NEt_3 \cdot HCl$ in methanol-d_4.

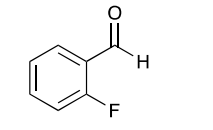

154

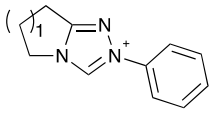

101

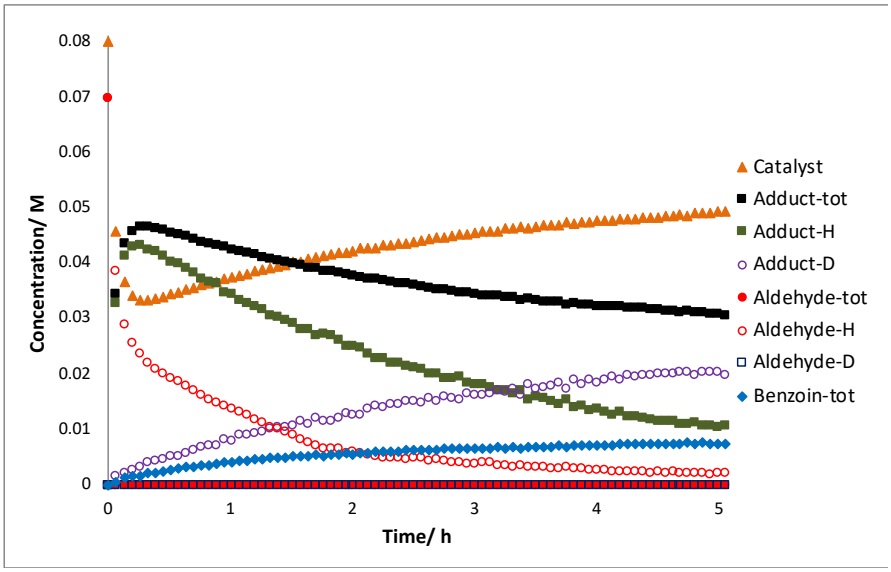

Concentration profile for the self-condensation of 2-methylbenzaldehyde **136** (0.078 M), catalysed by phenyl triazolium precatalyst **101** (n= 1, 0.08 M), in 0.107 M NEt_3 and 0.053 M $NEt_3 \cdot HCl$ in methanol-d_4.

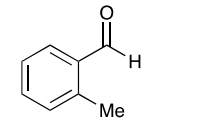

136

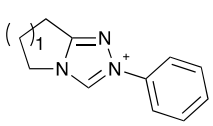

101

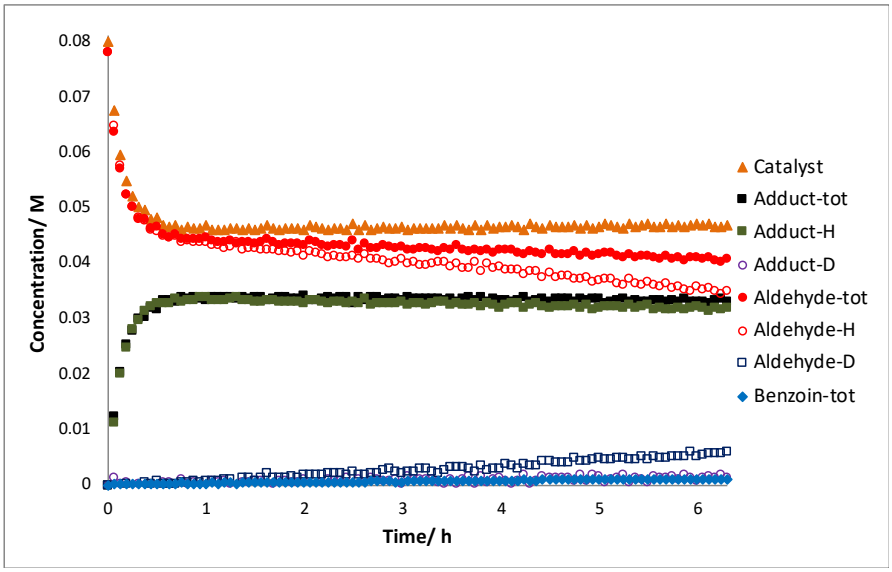

Concentration profile for the self-condensation of 2-methoxybenzaldehyde **138** (0.08 M), catalysed by phenyl triazolium precatalyst **101** (n= 1, 0.08 M), in 0.107 M NEt_3 and 0.053 M $NEt_3 \cdot HCl$ in methanol-d_4.

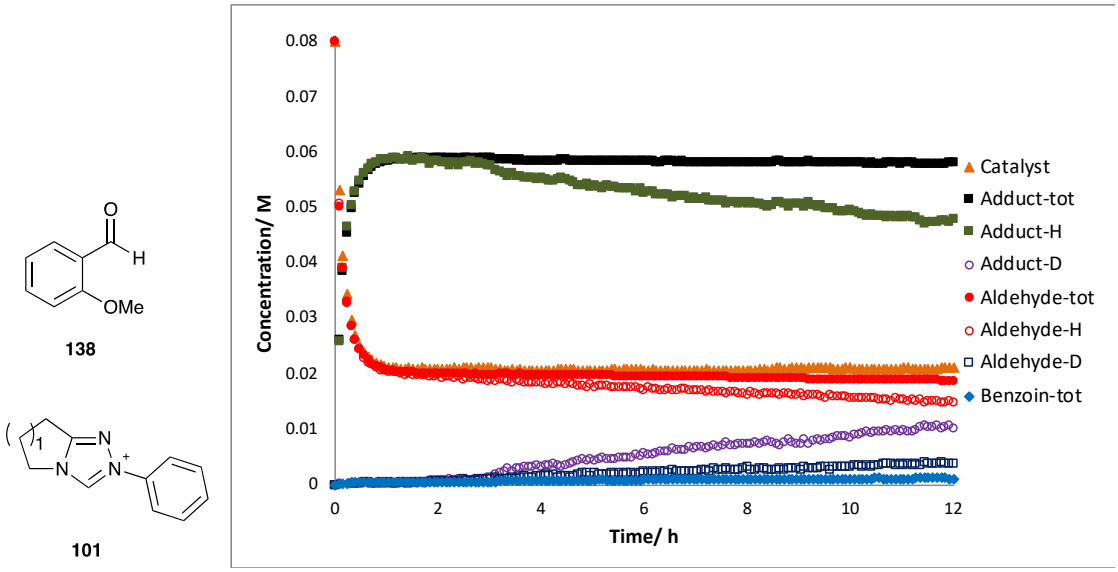

Concentration profile for the self-condensation of 3-trifluoromethylbenzaldehyde **151** (0.069 M), catalysed by phenyl triazolium precatalyst **101** (n= 1, 0.08 M), in 0.107 M NEt_3 and 0.053 M $NEt_3 \cdot HCl$ in methanol-d_4.

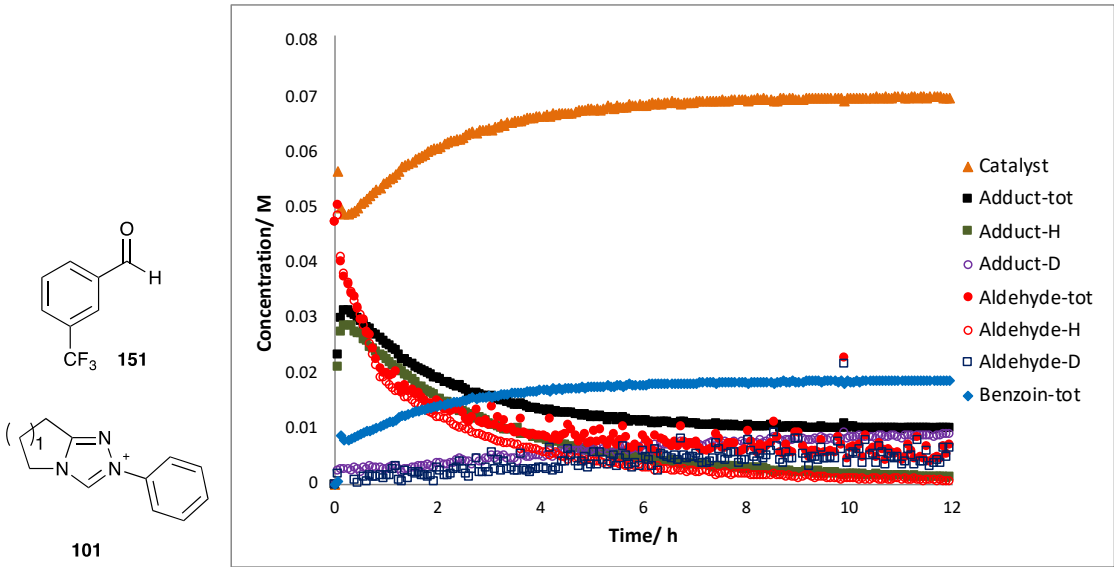

Concentration profile for the self-condensation of 3-fluorobenzaldehyde **155** (0.072 M), catalysed by phenyl triazolium precatalyst **101** (n= 1, 0.08 M), in 0.107 M NEt_3 and 0.053 M $NEt_3 \cdot HCl$ in methanol-d_4.

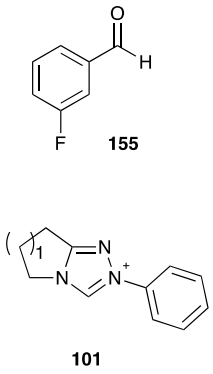

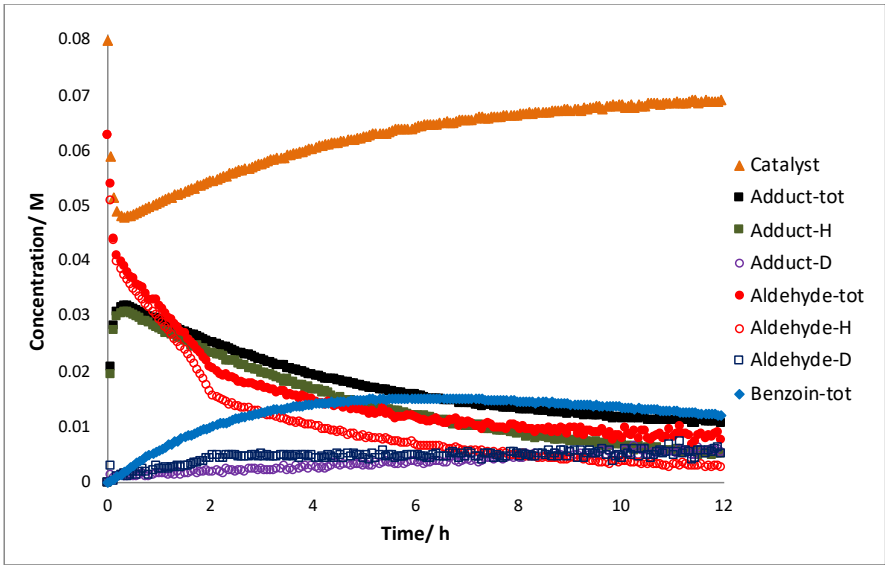

Concentration profile for the self-condensation of 3-methylbenzaldehyde **153** (0.08 M), catalysed by phenyl triazolium precatalyst **101** (n= 1, 0.08 M), in 0.107 M NEt_3 and 0.053 M $NEt_3 \cdot HCl$ in methanol-d_4.

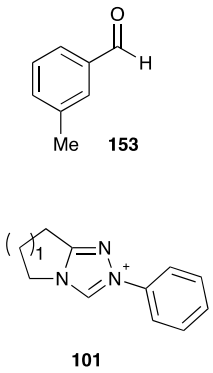

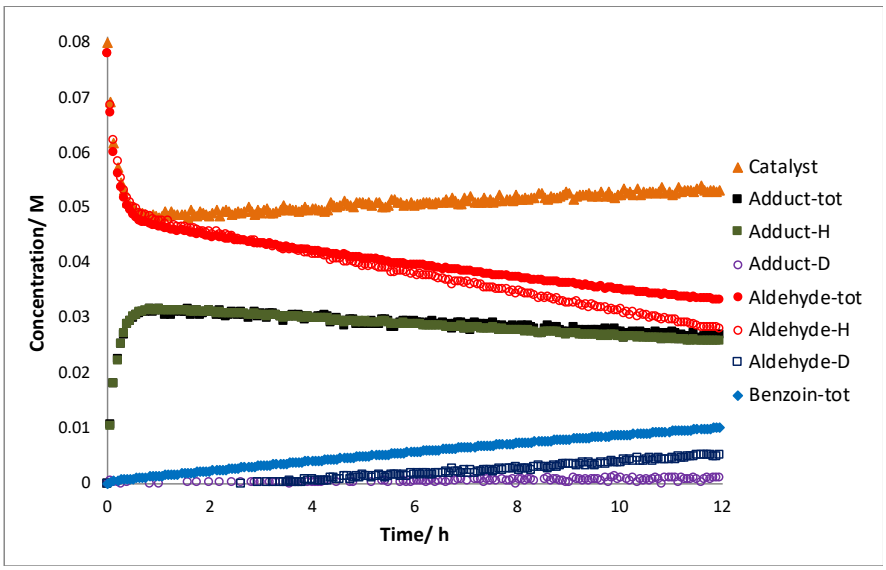

Concentration profile for the self-condensation of 3-methoxybenzaldehyde **149** (0.083 M), catalysed by phenyl triazolium precatalyst **101** (n= 1, 0.08 M), in 0.107 M NEt_3 and 0.053 M $NEt_3 \cdot HCl$ in methanol-d_4.

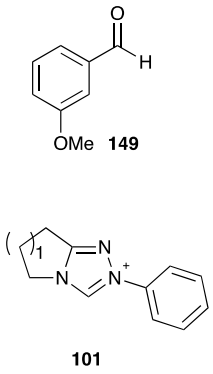

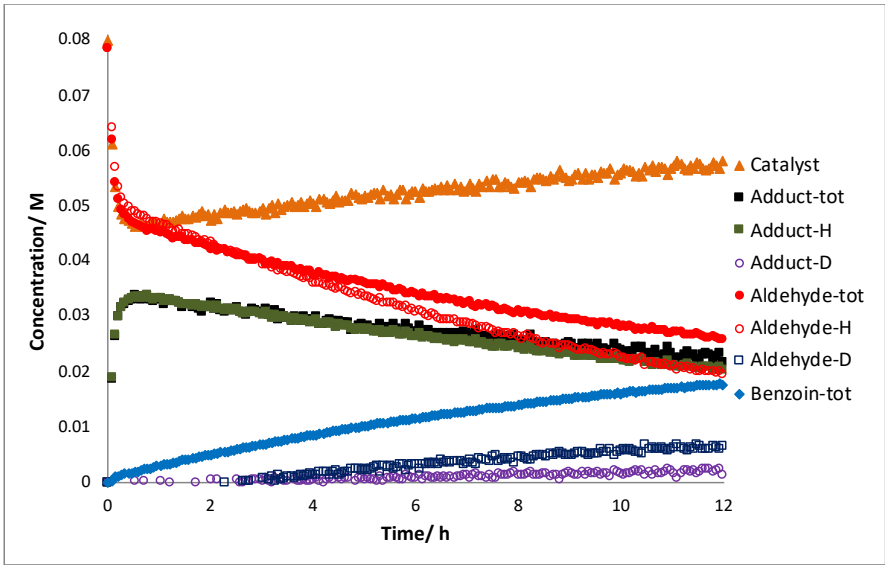

Concentration profile for the self-condensation of 4-trifluoromethylbenzaldehyde **152** (0.072 M), catalysed by phenyl triazolium precatalyst **101** (n= 1, 0.08 M), in 0.107 M NEt_3 and 0.053 M $NEt_3 \cdot HCl$ in methanol-d_4.

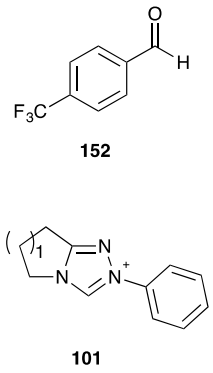

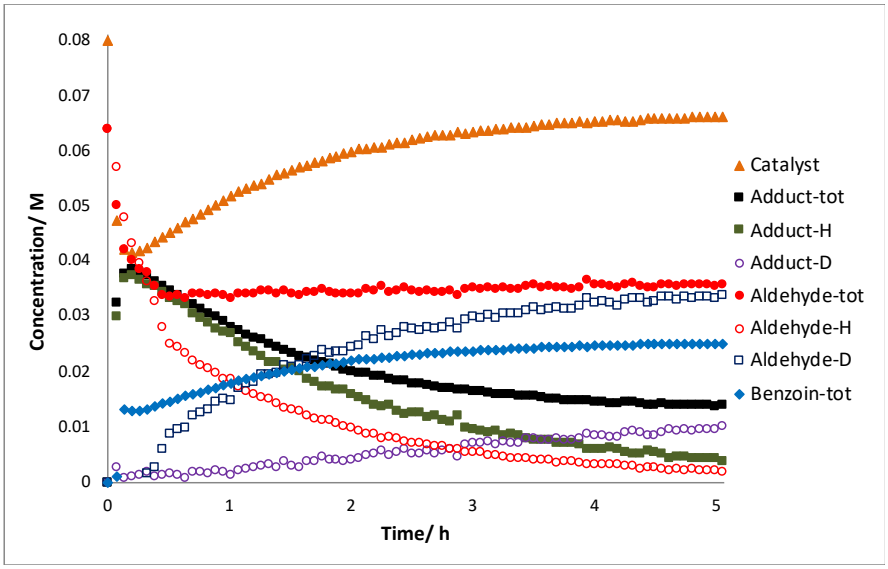

Concentration profile for the self-condensation of 4-fluorobenzaldehyde **156** (0.071 M), catalysed by phenyl triazolium precatalyst **101** (n= 1, 0.08 M), in 0.107 M NEt_3 and 0.053 M $NEt_3 \cdot HCl$ in methanol-d_4.

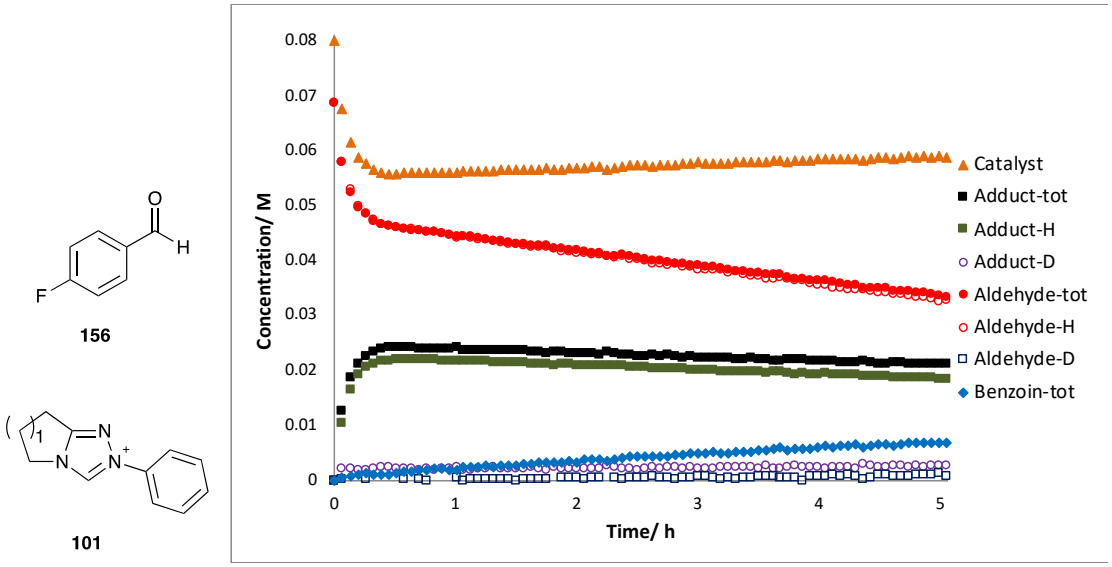

Concentration profile for the self-condensation of 4-methylbenzaldehyde **137** (0.092 M), catalysed by phenyl triazolium precatalyst **101** (n= 1, 0.08 M), in 0.107 M NEt_3 and 0.053 M $NEt_3 \cdot HCl$ in methanol-d_4.

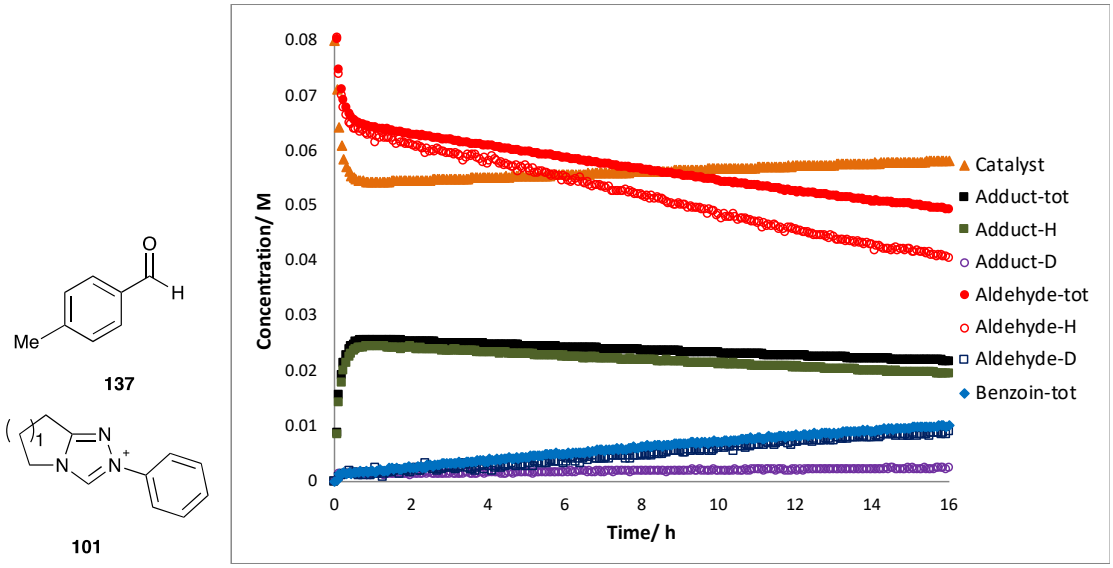

Concentration profile for the self-condensation of 4-dimethylaminobenzaldehyde **157** (0.087 M), catalysed by phenyl triazolium precatalyst **101** (n= 1, 0.08 M), in 0.107 M NEt_3 and 0.053 M NEt_3·HCl in methanol-d_4.

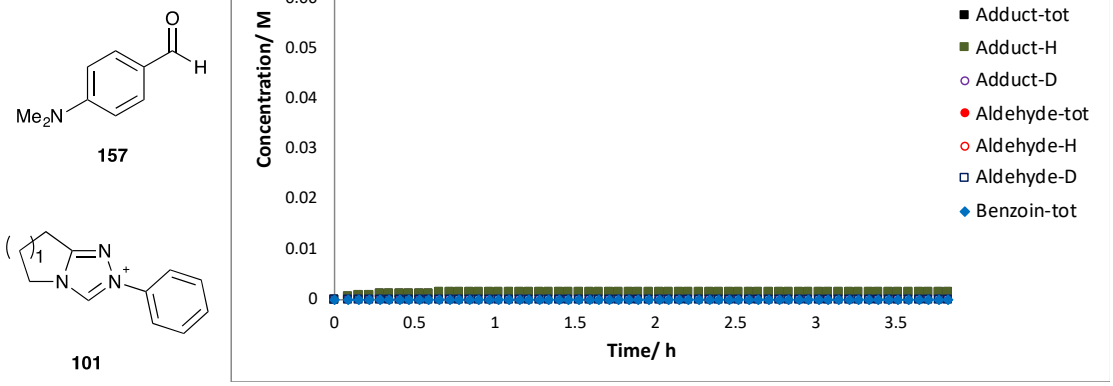

Concentration profile for the self-condensation of 2-methylbenzaldehyde **136** (0.12 M), catalysed by *para*-methoxyphenyl triazolium precatalyst **89** (n= 1, 0.08 M), in 0.107 M NEt_3 and 0.053 M NEt_3·HCl in methanol-d_4.

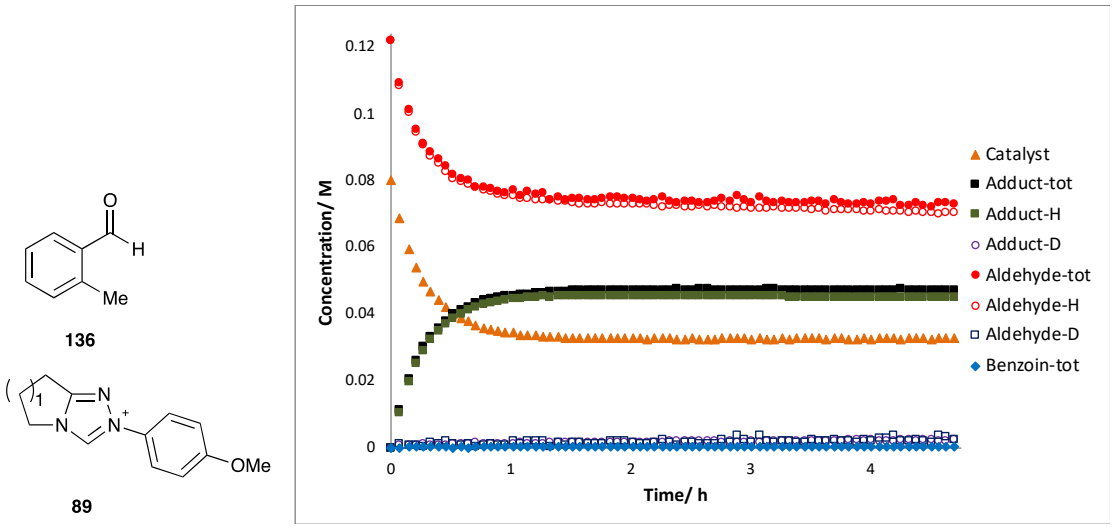

Concentration profile for the self-condensation of 2-methoxybenzaldehyde **138** (0.08 M), catalysed by *para*-methoxyphenyl triazolium precatalyst **89** (n= 1, 0.08 M), in 0.107 M NEt_3 and 0.053 M $NEt_3 \cdot HCl$ in methanol-d_4.

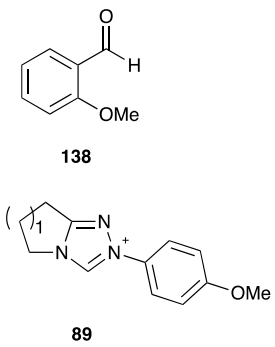

138

89

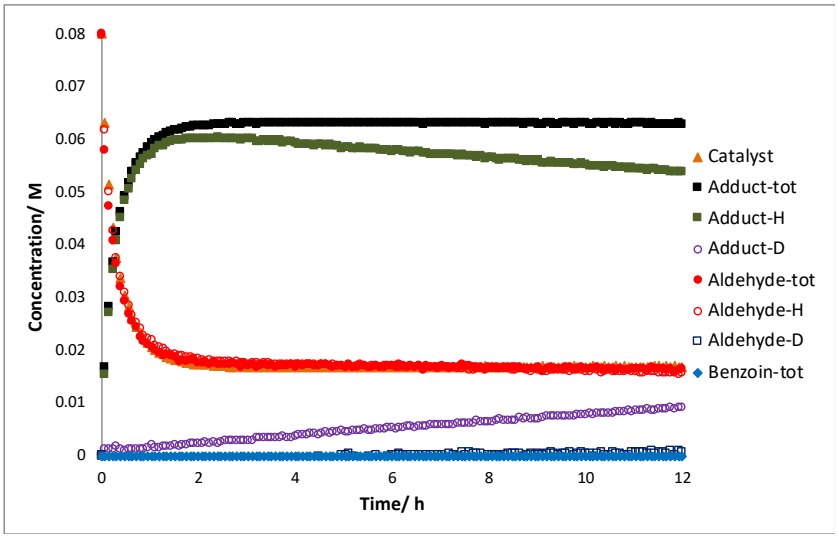

Concentration profile for the self-condensation of 4-methylbenzaldehyde **137** (0.11 M), catalysed by *para*-methoxyphenyl triazolium precatalyst **89** (n= 1, 0.08 M), in 0.107 M NEt_3 and 0.053 M $NEt_3 \cdot HCl$ in methanol-d_4.

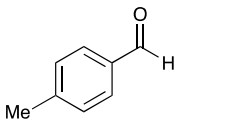

137

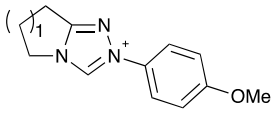

89

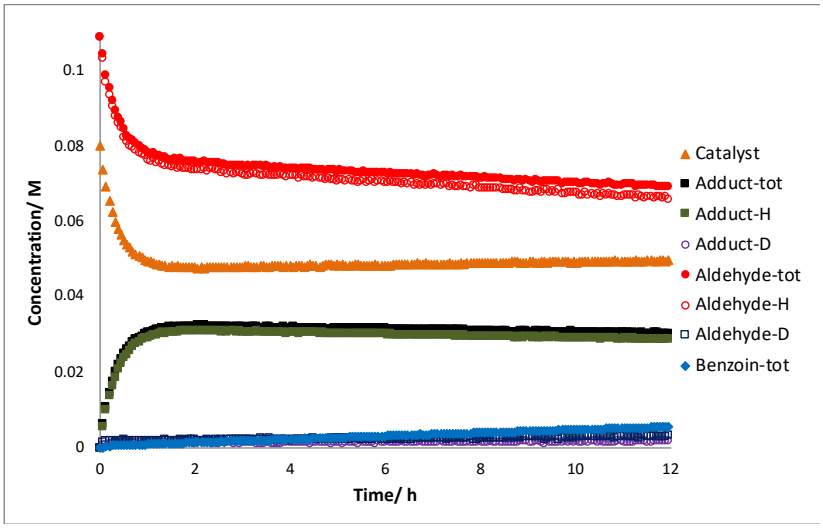

Concentration profile for the self-condensation of 2-methoxybenzaldehyde **138** (0.082 M), catalysed by triisopropylphenyl triazolium precatalyst **88** (n= 1, 0.08 M), in 0.107 M NEt_3 and 0.053 M $NEt_3 \cdot HCl$ in methanol-d_4.

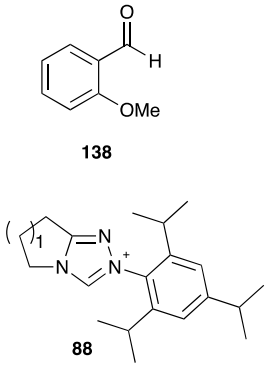

138

88

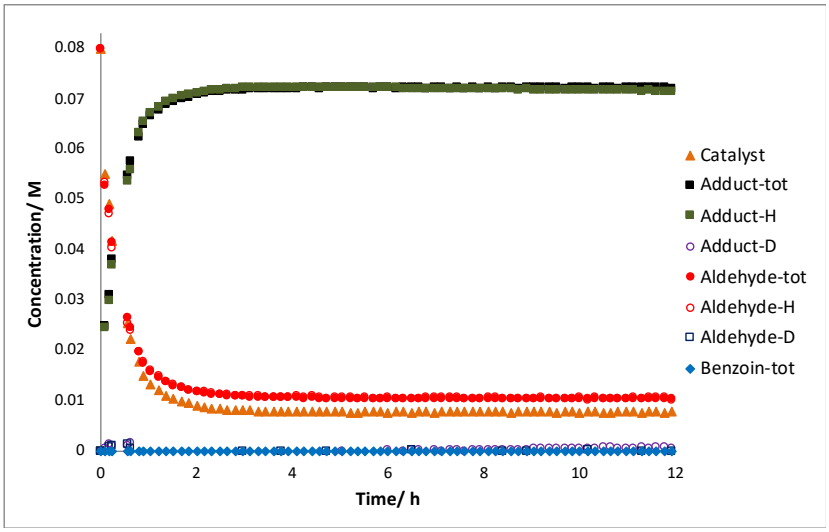

Concentration profile for the self-condensation of 4-methoxybenzaldehyde **139** (0.077 M), catalysed by triisopropylphenyl triazolium precatalyst **88** (n= 1, 0.076 M), in 0.107 M NEt_3 and 0.053 M $NEt_3 \cdot HCl$ in methanol-d_4.

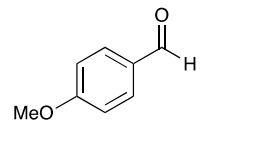

139

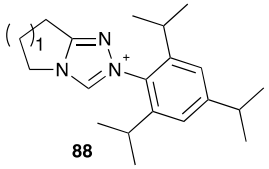

88

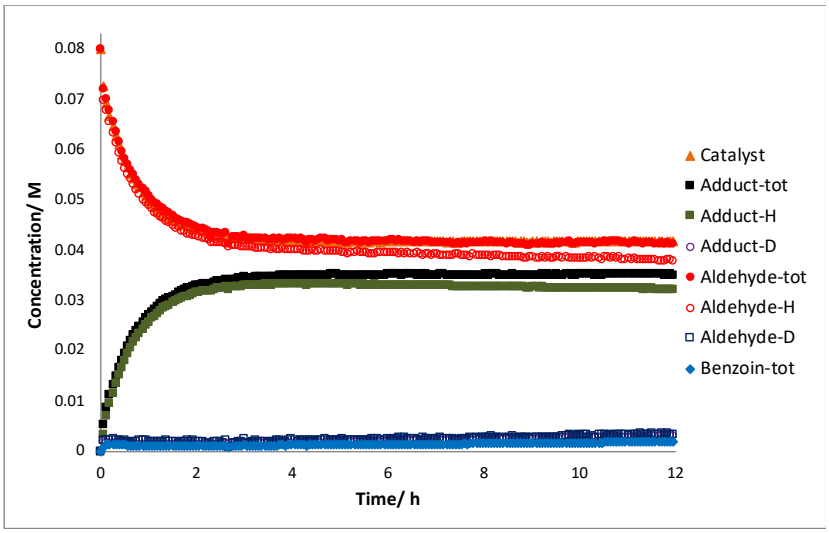

Concentration profile for the self-condensation of benzaldehyde **135** (0.08 M), catalysed by triisopropylphenyl triazolium precatalyst **88** (n= 1, 0.076 M), in 0.107 M NEt_3 and 0.053 M $NEt_3 \cdot HCl$ in methanol-d_4.

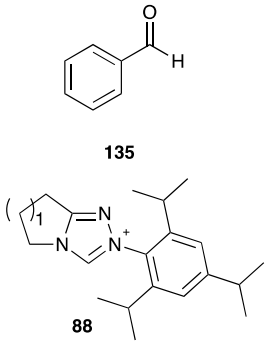

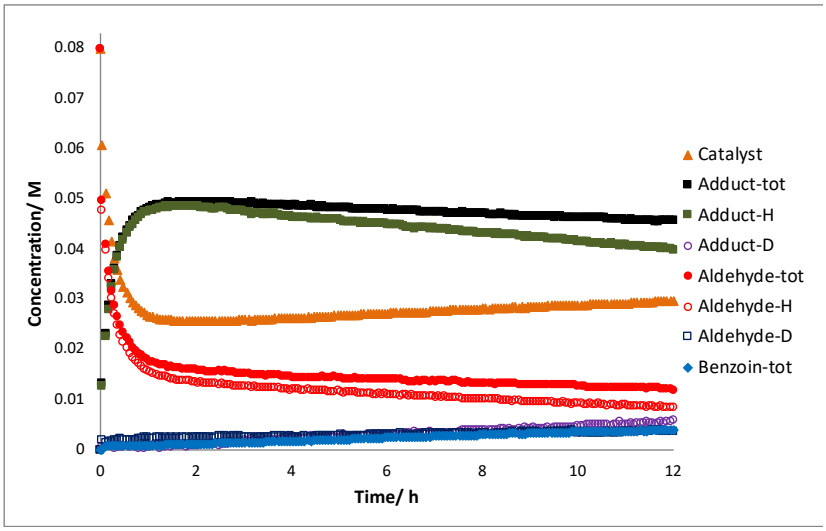

Concentration profile for the self-condensation of 2-methoxybenzaldehyde **138** (0.08 M), catalysed by mesityl triazolium precatalyst **86** (n= 2, 0.068 M), in 0.107 M NEt_3 and 0.053 M $NEt_3 \cdot HCl$ in methanol-d_4.

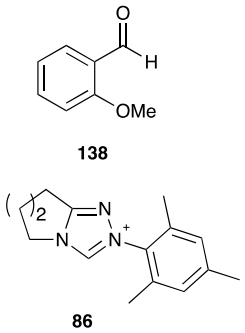

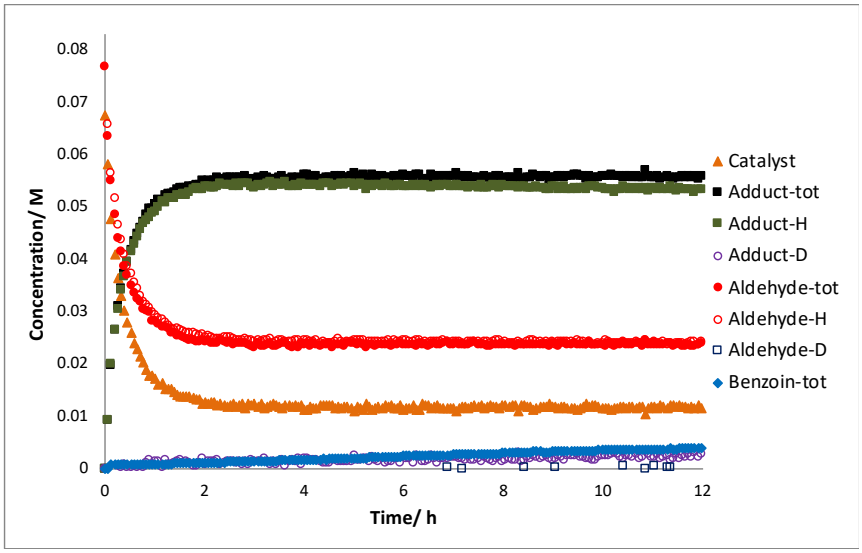

Concentration profile for the self-condensation of 4-methoxybenzaldehyde **139** (0.077 M), catalysed by mesityl triazolium precatalyst **86** (n= 2, 0.068 M), in 0.107 M NEt_3 and 0.053 M $NEt_3 \cdot HCl$ in methanol-d_4.

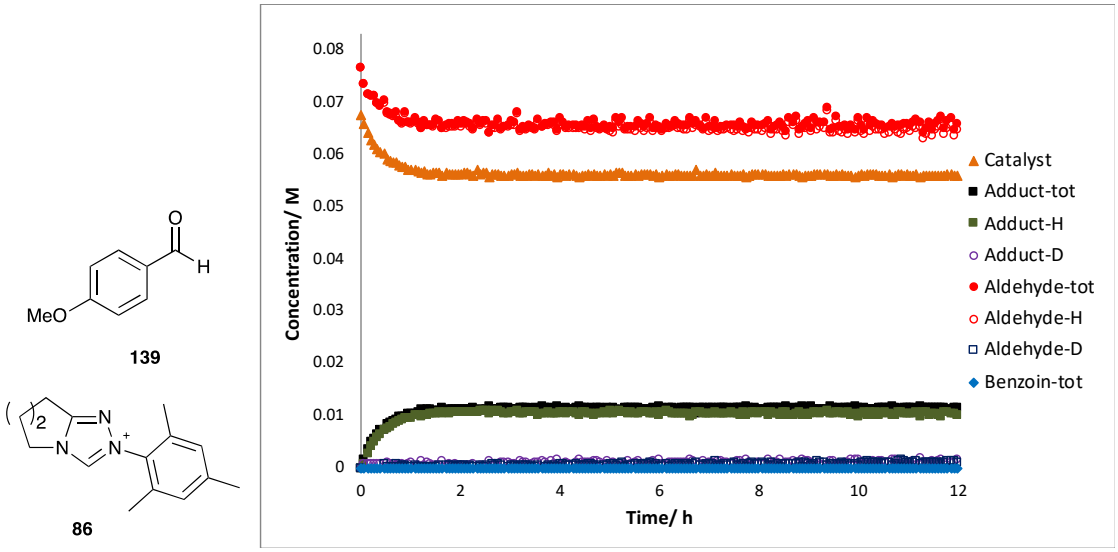

Concentration profile for the self-condensation of benzaldehyde **135** (0.071 M), catalysed by mesityl triazolium precatalyst **86** (n= 2, 0.068 M), in 0.107 M NEt_3 and 0.053 M $NEt_3 \cdot HCl$ in methanol-d_4.

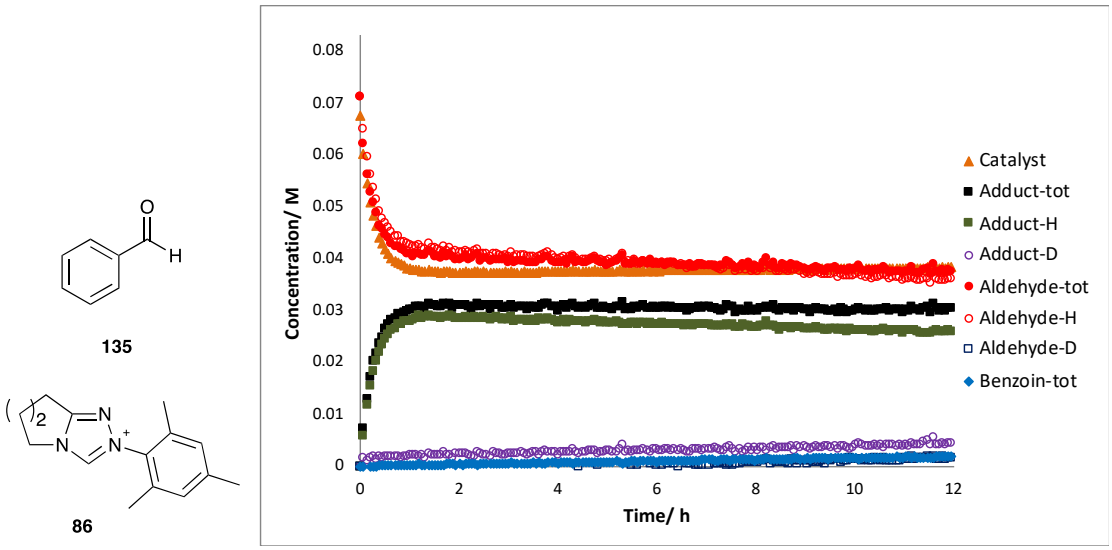

Concentration profile for the self-condensation of 2-methylbenzaldehyde **136** (0.076 M), catalysed by *para*-fluorophenyl triazolium precatalyst **77** (n= 2, 0.08 M), in 0.107 M NEt_3 and 0.053 M NEt_3·HCl in methanol-d_4.

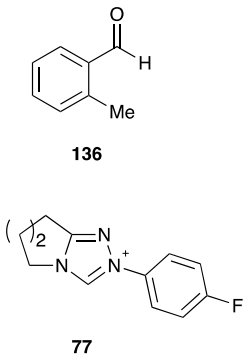

136

77

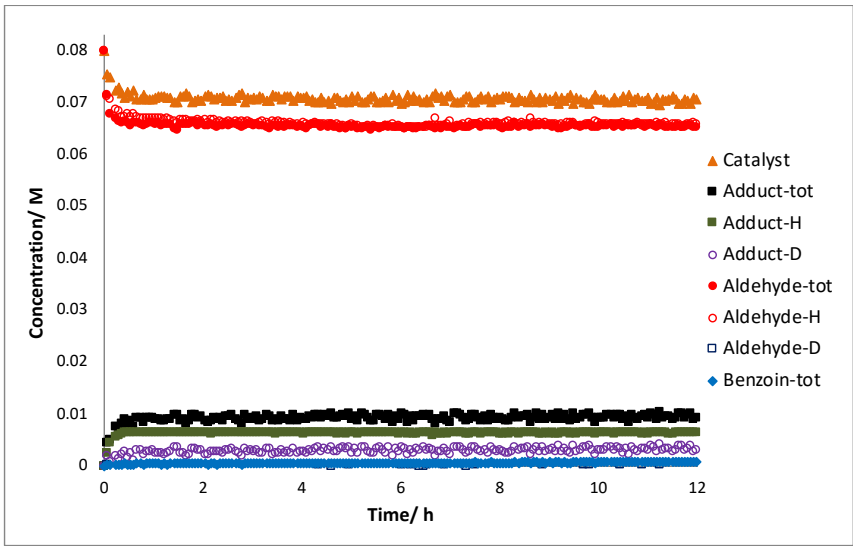

Concentration profile for the self-condensation of 2-methoxybenzaldehyde **138** (0.077 M), catalysed by *para*-fluorophenyl triazolium precatalyst **77** (n= 2, 0.08 M), in 0.107 M NEt_3 and 0.053 M NEt_3·HCl in methanol-d_4.

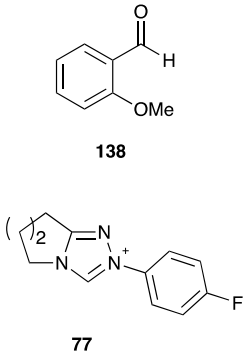

138

77

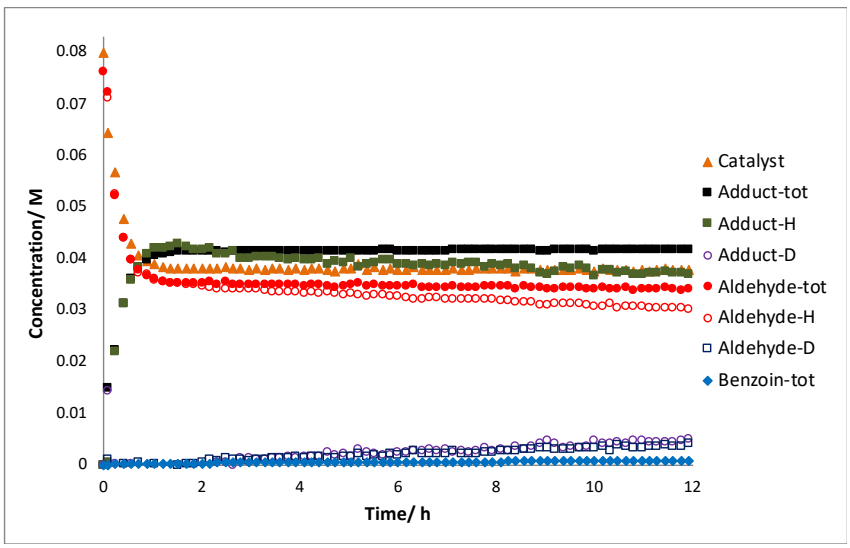

Concentration profile for the self-condensation of 4-methylbenzaldehyde **137** (0.076 M), catalysed by *para*-fluorophenyl triazolium precatalyst **77** (n= 2, 0.08 M), in 0.107 M NEt_3 and 0.053 M $NEt_3 \cdot HCl$ in methanol-d_4.

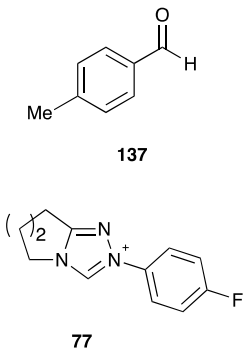

137

77

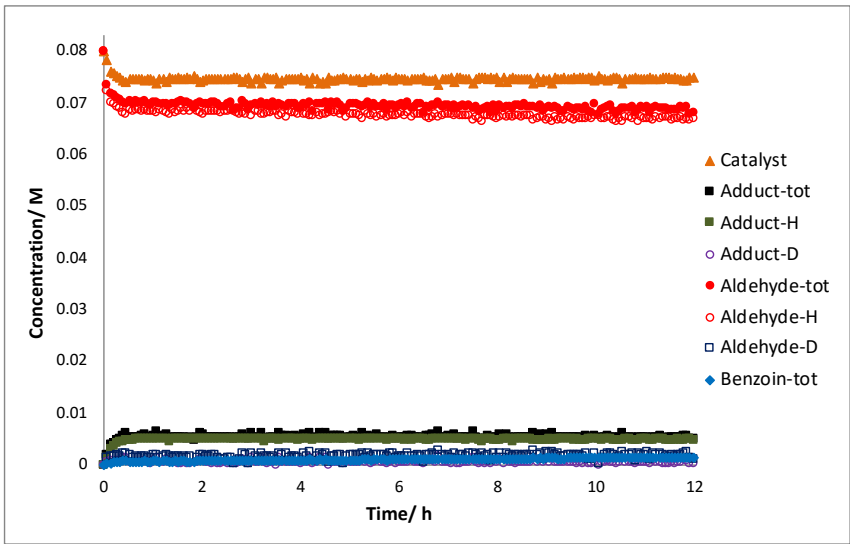

Concentration profile for the self-condensation of 4-methoxybenzaldehyde **139** (0.073 M), catalysed by *para*-fluorophenyl triazolium precatalyst **77** (n= 2, 0.08 M), in 0.107 M NEt_3 and 0.053 M $NEt_3 \cdot HCl$ in methanol-d_4.

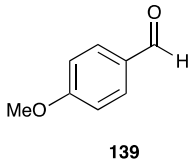

139

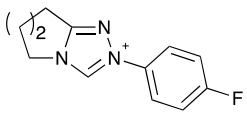

77

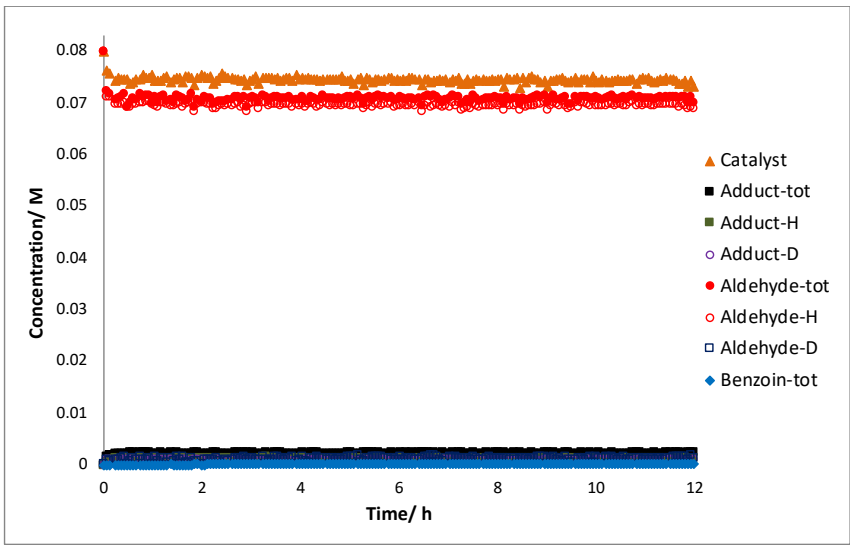

Concentration profile for the self-condensation of benzaldehyde **135** (0.068 M), catalysed by *para*-fluorophenyl triazolium precatalyst **77** (n= 2, 0.08 M), in 0.107 M NEt_3 and 0.053 M $NEt_3 \cdot HCl$ in methanol-d_4.

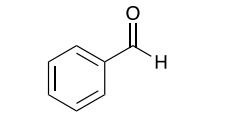

135

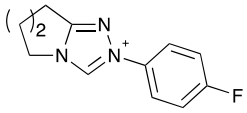

77

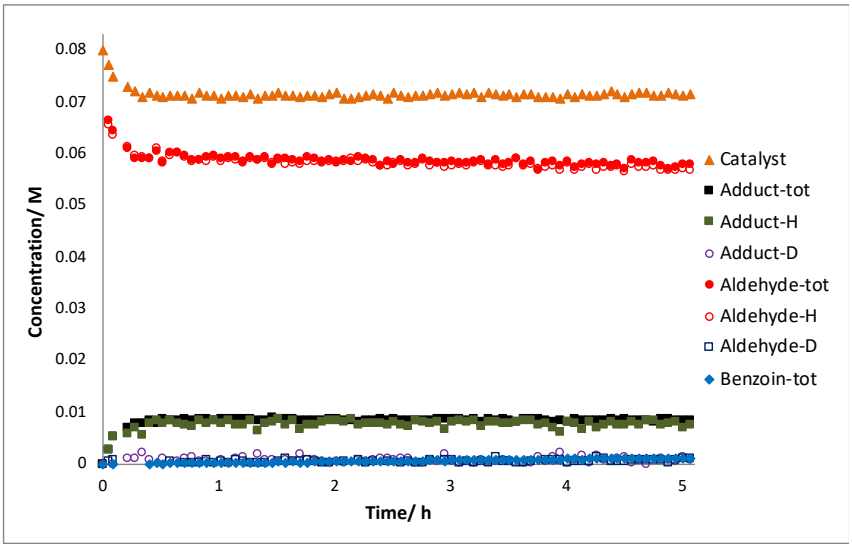

Concentration profile for the self-condensation of 2-methylbenzaldehyde **136** (0.079 M), catalysed by phenyl triazolium precatalyst **79** (n= 2, 0.08 M), in 0.107 M NEt_3 and 0.053 M $NEt_3 \cdot HCl$ in methanol-d_4.

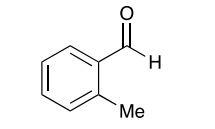

136

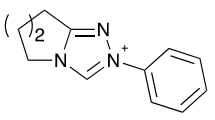

79

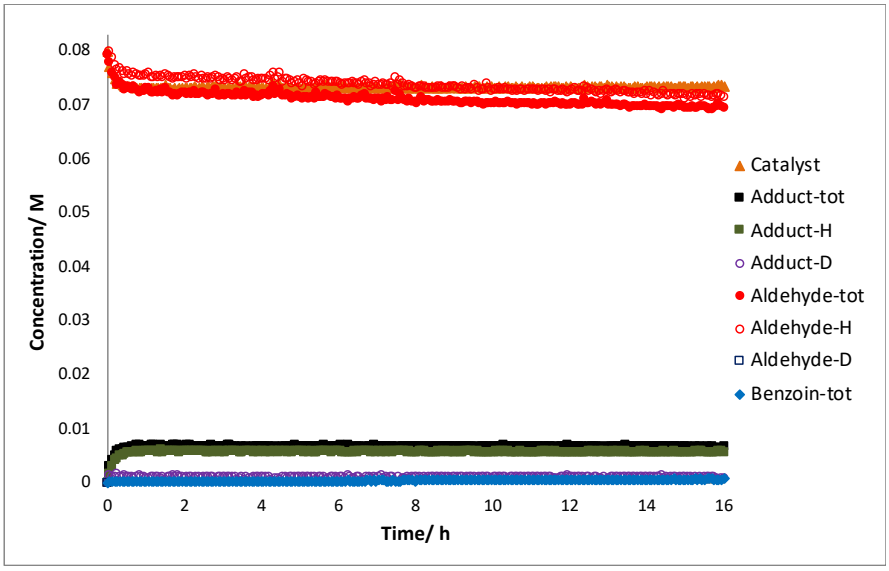

Concentration profile for the self-condensation of 2-methoxybenzaldehyde **138** (0.08 M), catalysed by phenyl triazolium precatalyst **79** (n= 2, 0.08 M), in 0.107 M NEt_3 and 0.053 M $NEt_3 \cdot HCl$ in methanol-d_4.

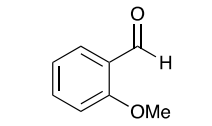

138

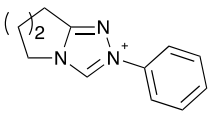

79

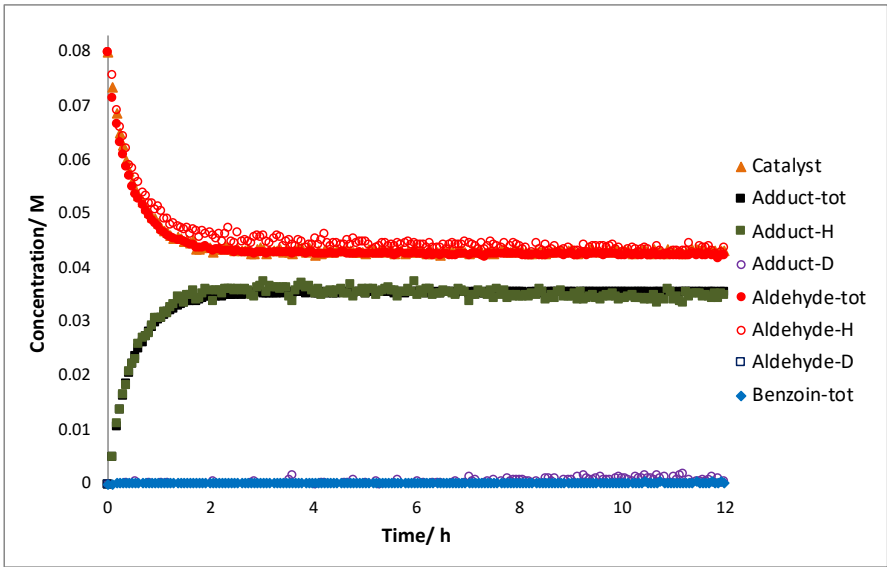

Concentration profile for the self-condensation of 4-methylbenzaldehyde **137** (0.081 M), catalysed by phenyl triazolium precatalyst **79** (n= 2, 0.08 M), in 0.107 M NEt_3 and 0.053 M $NEt_3 \cdot HCl$ in methanol-d_4.

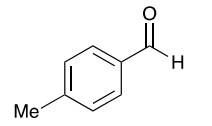

137

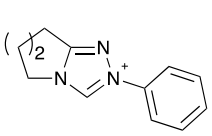

79

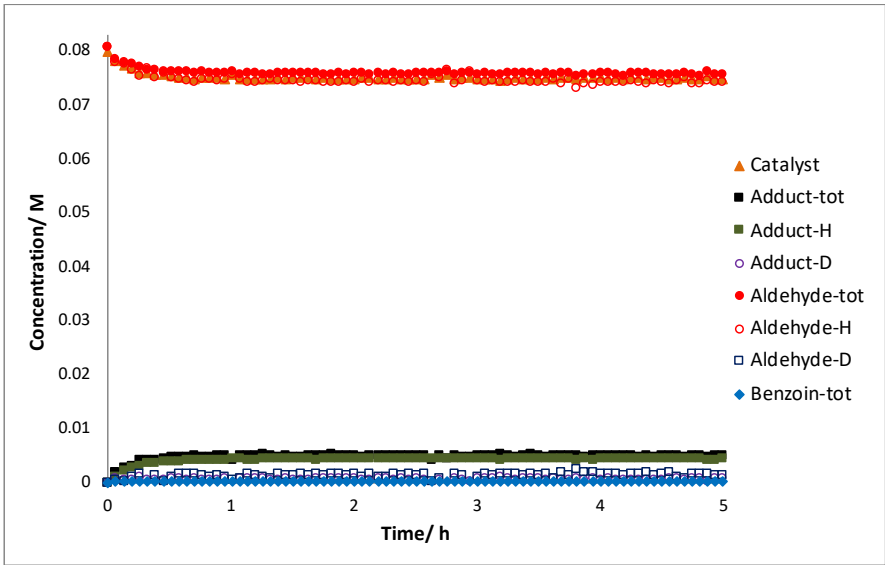

Concentration profile for the self-condensation of 4-methoxybenzaldehyde **139** (0.093 M), catalysed by phenyl triazolium precatalyst **79** (n= 2, 0.08 M), in 0.107 M NEt_3 and 0.053 M $NEt_3 \cdot HCl$ in methanol-d_4.

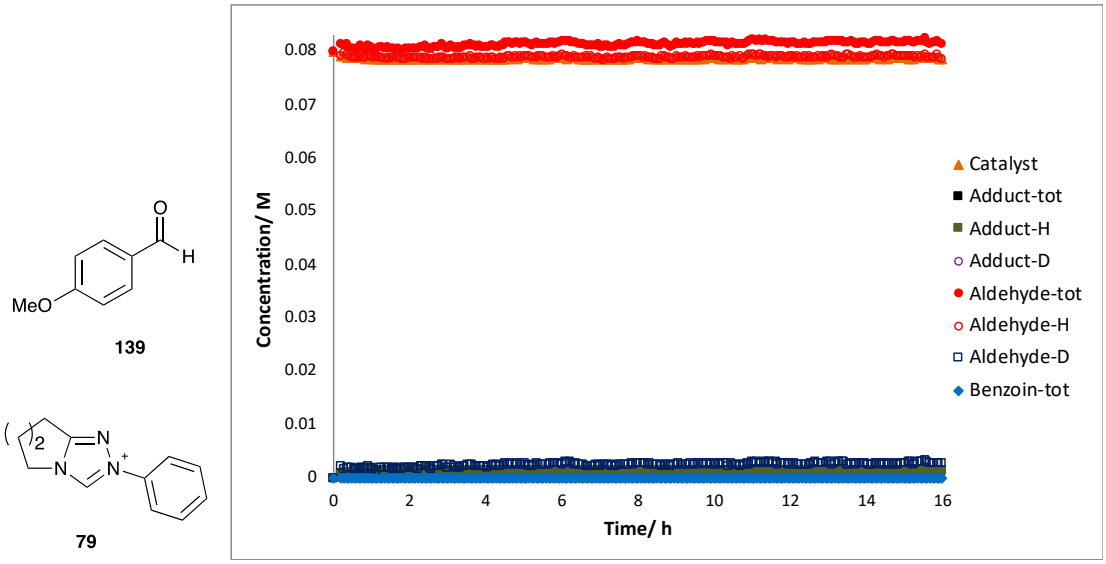

Concentration profile for the self-condensation of benzaldehyde **135** (0.08 M), catalysed by phenyl triazolium precatalyst **79** (n= 2, 0.08 M), in 0.107 M NEt_3 and 0.053 M $NEt_3 \cdot HCl$ in methanol-d_4.

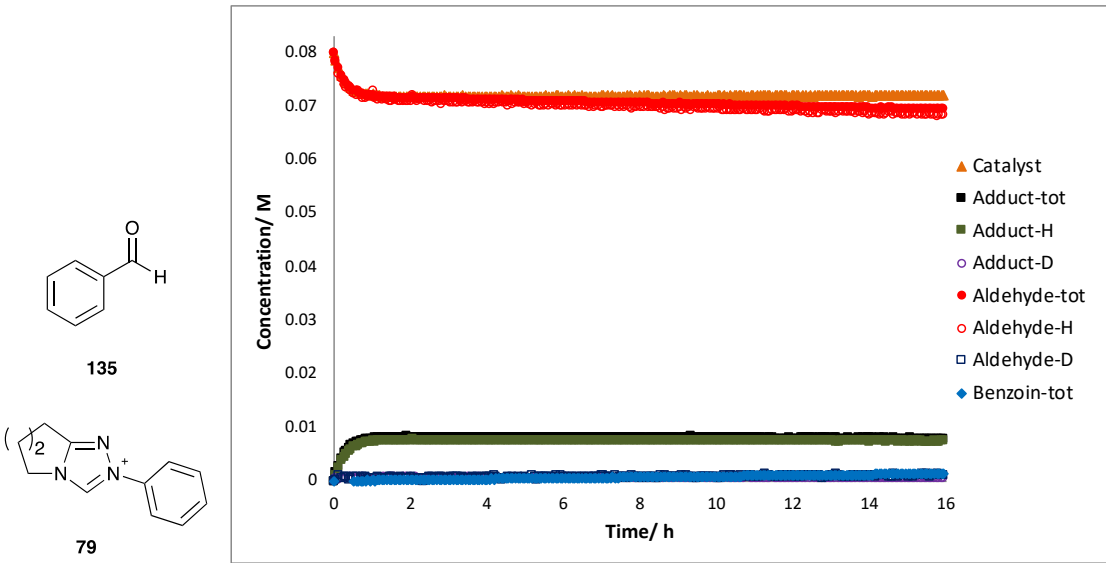

Concentration profile for the self-condensation of 2-methylbenzaldehyde **136** (0.036 M), catalysed by *para*-methoxyphenyl triazolium precatalyst **90** (n= 2, 0.04 M), in 0.107 M NEt_3 and 0.053 M $NEt_3 \cdot HCl$ in methanol-d_4.

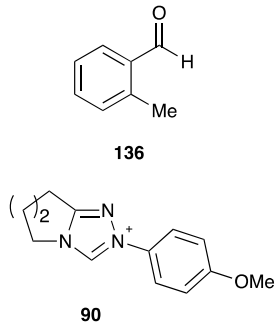

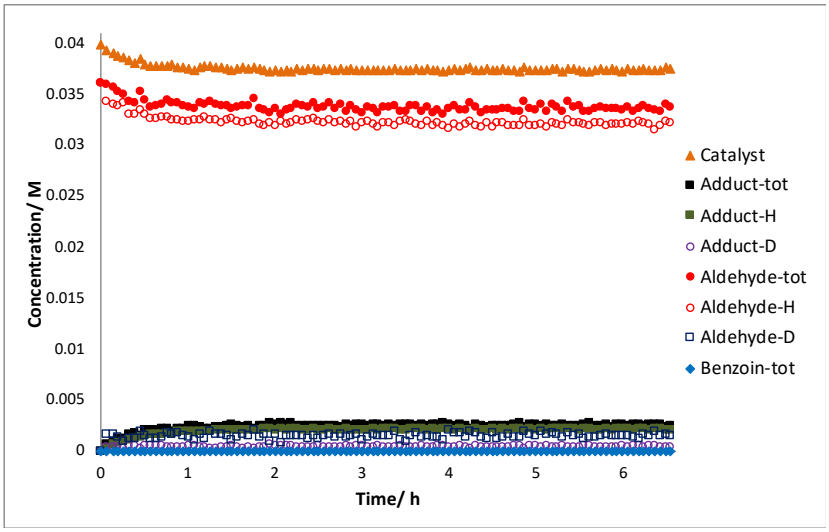

Concentration profile for the self-condensation of 2-methoxybenzaldehyde **138** (0.038 M), catalysed by *para*-methoxyphenyl triazolium precatalyst **90** (n= 2, 0.039 M), in 0.107 M NEt_3 and 0.053 M $NEt_3 \cdot HCl$ in methanol-d_4.

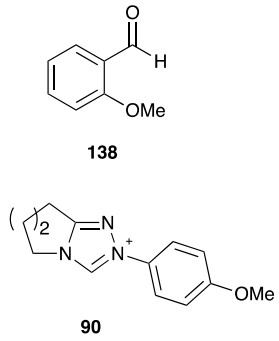

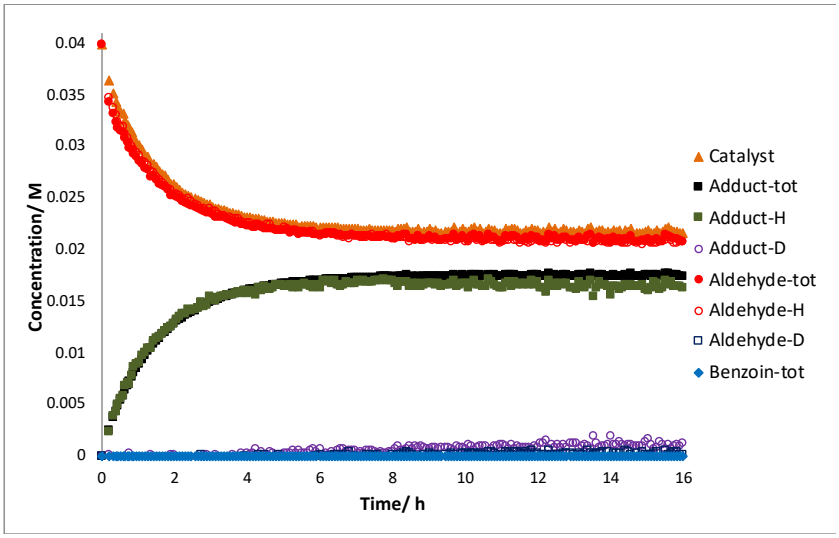

Concentration profile for the self-condensation of 4-methylbenzaldehyde **137** (0.04 M), catalysed by *para*-methoxyphenyl triazolium precatalyst **90** (n= 2, 0.04 M), in 0.107 M NEt_3 and 0.053 M $NEt_3 \cdot HCl$ in methanol-d_4.

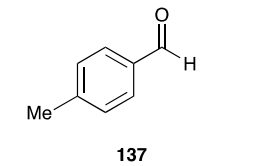

137

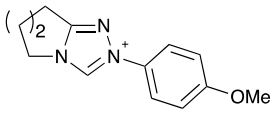

90

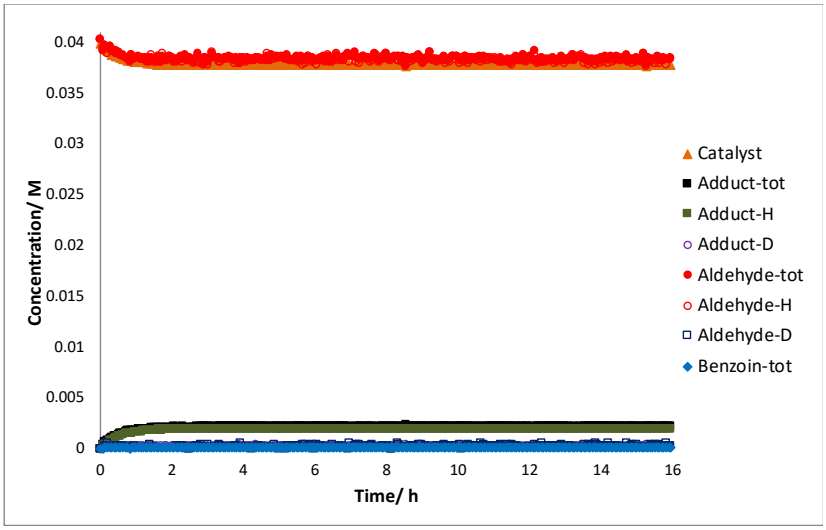

Concentration profile for the self-condensation of 4-methoxybenzaldehyde **139** (0.093 M), catalysed by *para*-methoxyphenyl triazolium precatalyst **90** (n= 2, 0.04 M), in 0.107 M NEt_3 and 0.053 M $NEt_3 \cdot HCl$ in methanol-d_4.

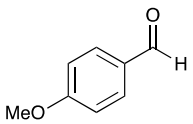

139

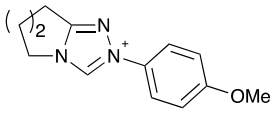

90

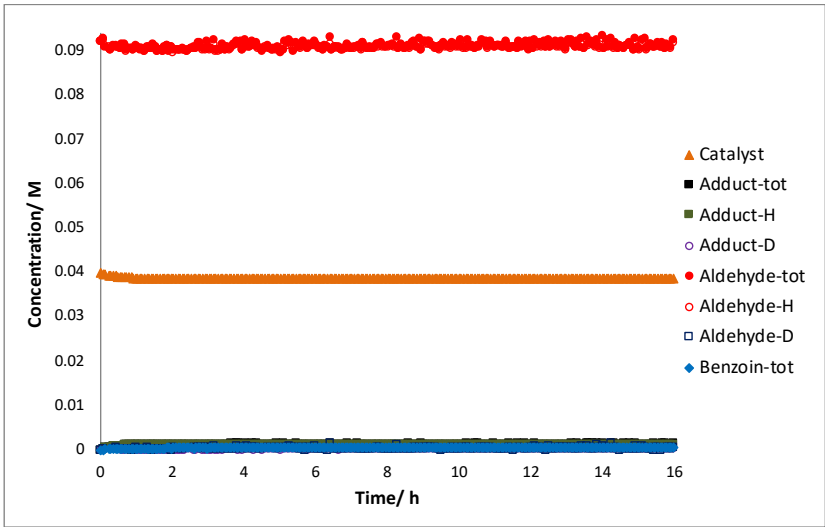

Concentration profile for the self-condensation of benzaldehyde **135** (0.063 M), catalysed by *para*-methoxyphenyl triazolium precatalyst **90** (n= 2, 0.04 M), in 0.107 M NEt_3 and 0.053 M $NEt_3 \cdot HCl$ in methanol-d_4.

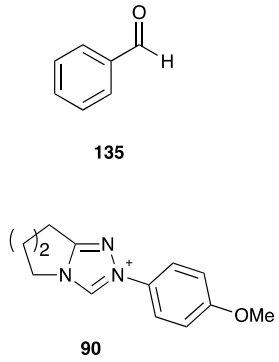

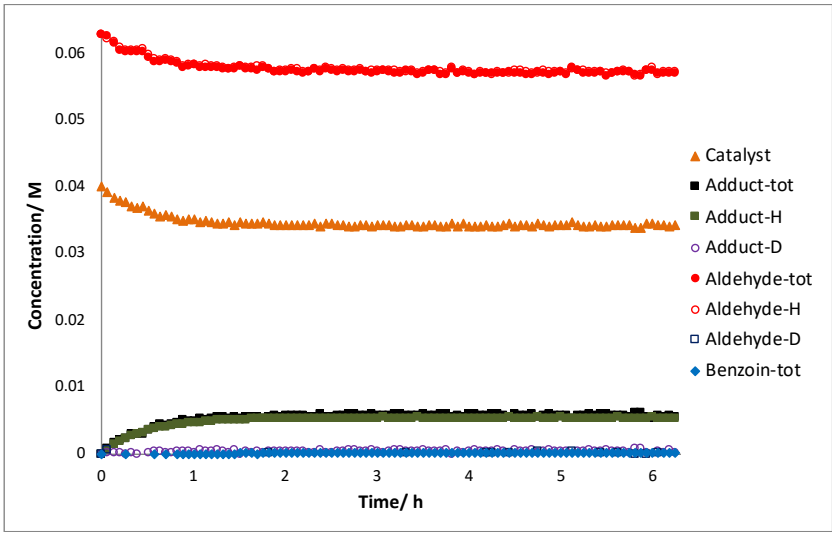

Concentration profile for the self-condensation of 2-methylbenzaldehyde **136** (0.077 M), catalysed by *para*-fluorophenyl triazolium precatalyst **78** (n= 3, 0.078 M), in 0.107 M NEt_3 and 0.053 M $NEt_3 \cdot HCl$ in methanol-d_4.

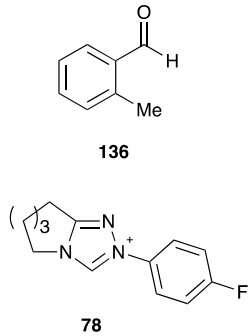

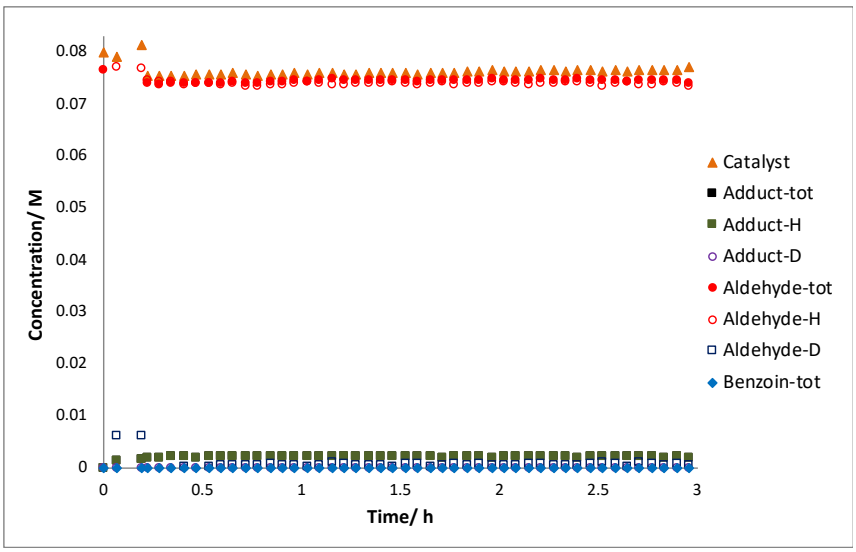

Concentration profile for the self-condensation of 2-methoxybenzaldehyde **138** (0.081 M), catalysed by *para*-fluorophenyl triazolium precatalyst **78** (n= 3, 0.078 M), in 0.107 M NEt_3 and 0.053 M $NEt_3 \cdot HCl$ in methanol-d_4.

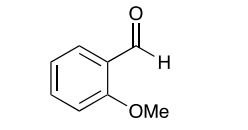

138

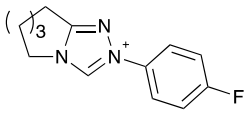

78

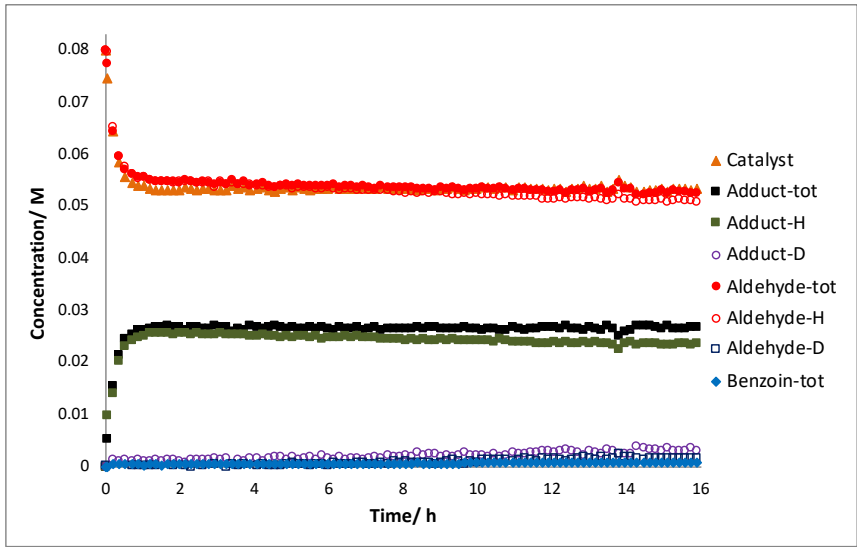

Concentration profile for the self-condensation of 4-methylbenzaldehyde **137** (0.081 M), catalysed by *para*-fluorophenyl triazolium precatalyst **78** (n= 3, 0.08 M), in 0.107 M NEt_3 and 0.053 M $NEt_3 \cdot HCl$ in methanol-d_4.

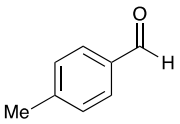

137

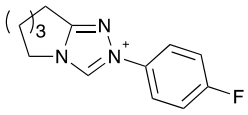

78

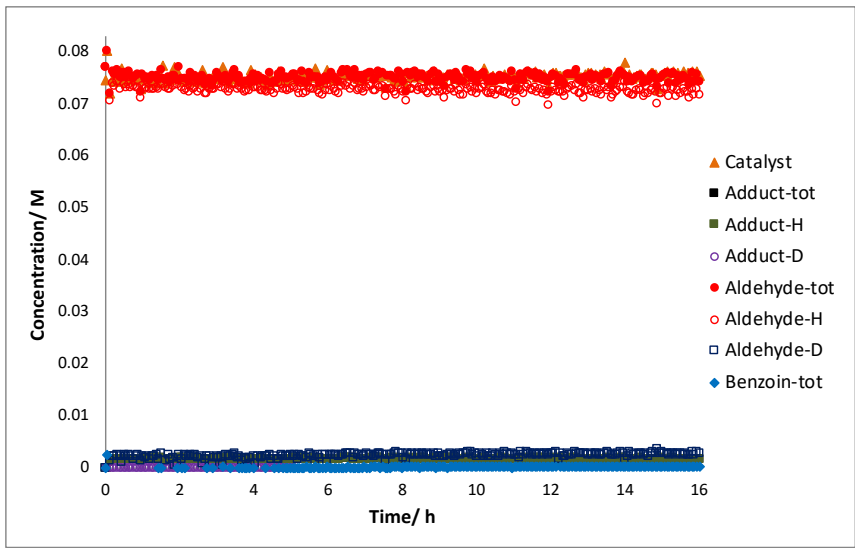

Concentration profile for the self-condensation of 4-methoxybenzaldehyde **139** (0.073 M), catalysed by *para*-fluorophenyl triazolium precatalyst **78** (n= 3, 0.076 M), in 0.107 M NEt_3 and 0.053 M $NEt_3 \cdot HCl$ in methanol-d_4.

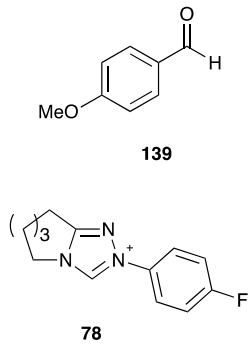

139

78

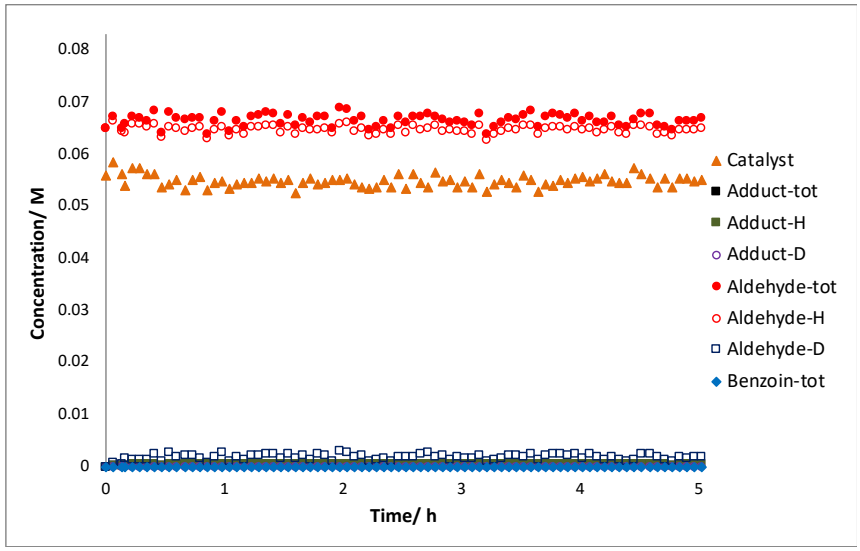

Concentration profile for the self-condensation of benzaldehyde **135** (0.069 M), catalysed by *para*-fluorophenyl triazolium precatalyst **78** (n= 3, 0.08 M), in 0.107 M NEt_3 and 0.053 M $NEt_3 \cdot HCl$ in methanol-d_4.

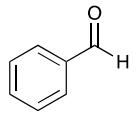

135

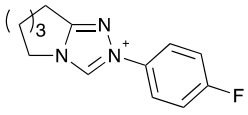

78

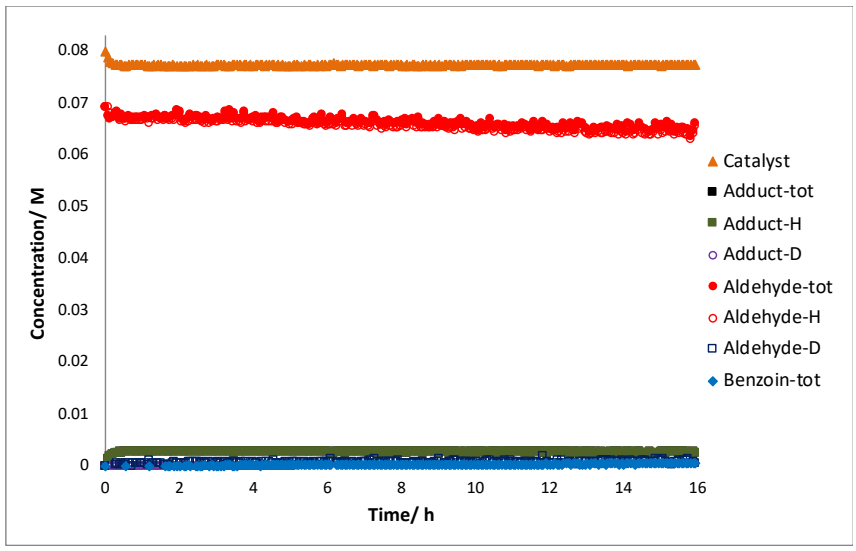

Concentration profile for the self-condensation of 2-methylbenzaldehyde **136** (0.074 M), catalysed by phenyl triazolium precatalyst **80** (n= 3, 0.08 M), in 0.107 M NEt_3 and 0.053 M $NEt_3 \cdot HCl$ in methanol-d_4.

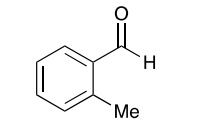

136

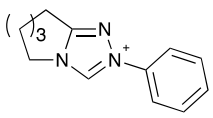

80

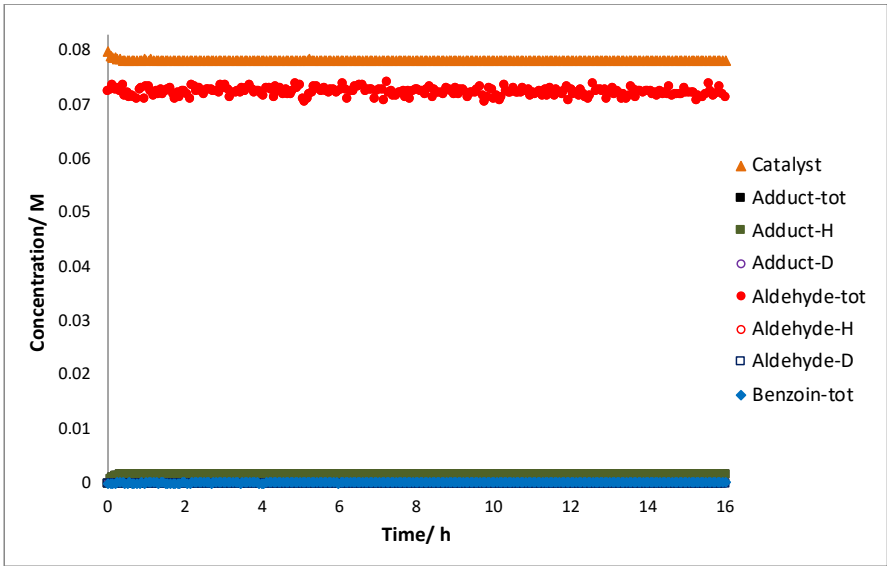

Concentration profile for the self-condensation of 2-methoxybenzaldehyde **138** (0.081 M), catalysed by phenyl triazolium precatalyst **80** (n= 3, 0.08 M), in 0.107 M NEt_3 and 0.053 M $NEt_3 \cdot HCl$ in methanol-d_4.

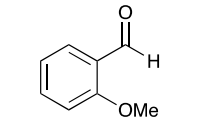

138

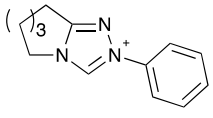

80

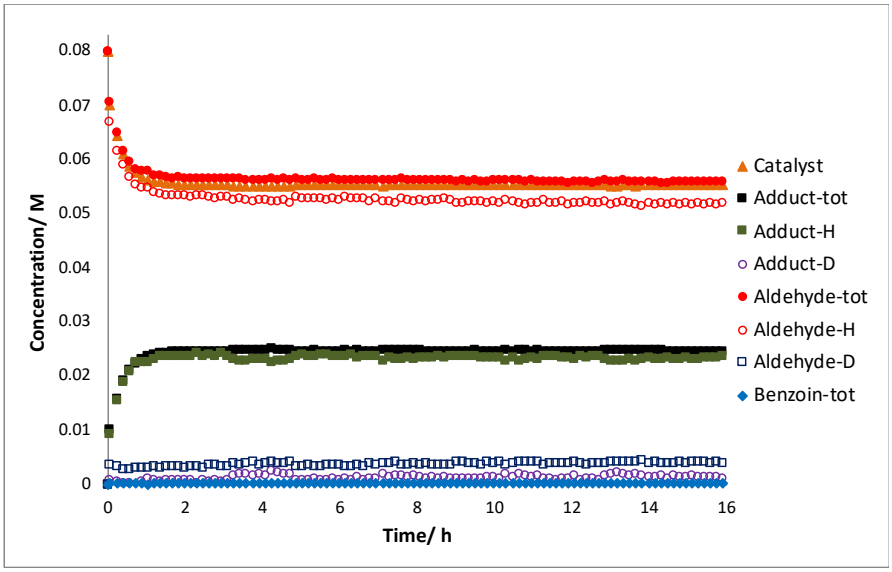

Concentration profile for the self-condensation of 4-methylbenzaldehyde **137** (0.073 M), catalysed by phenyl triazolium precatalyst **80** (n= 3, 0.08 M), in 0.107 M NEt_3 and 0.053 M $NEt_3 \cdot HCl$ in methanol-d_4.

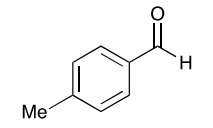

137

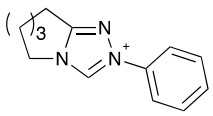

80

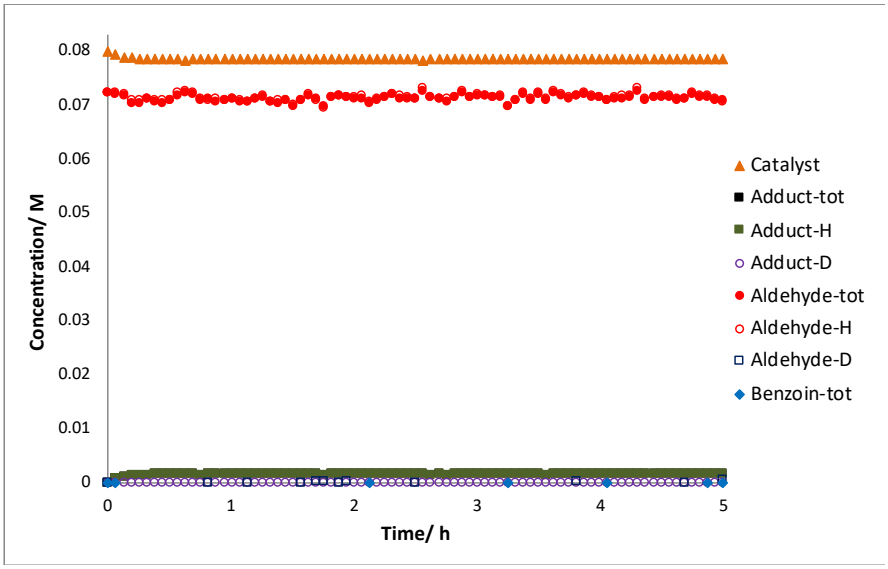

Concentration profile for the self-condensation of 4-methoxybenzaldehyde **139** (0.08 M), catalysed by phenyl triazolium precatalyst **80** (n= 3, 0.08 M), in 0.107 M NEt_3 and 0.053 M $NEt_3 \cdot HCl$ in methanol-d_4.

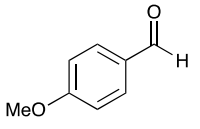

139

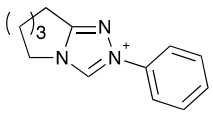

80

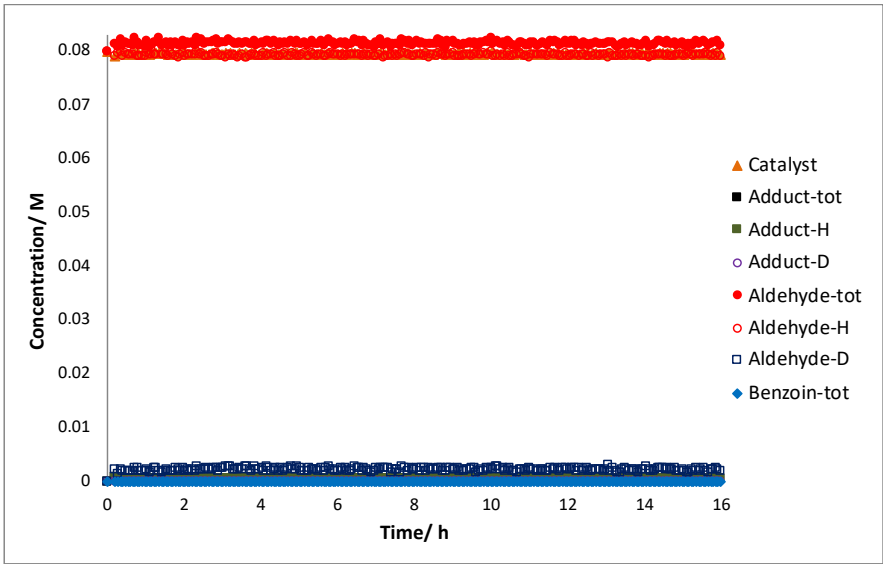

Concentration profile for the self-condensation of benzaldehyde **135** (0.071 M), catalysed by phenyl triazolium precatalyst **80** (n= 3, 0.08 M), in 0.107 M NEt_3 and 0.053 M $NEt_3 \cdot HCl$ in methanol-d_4.

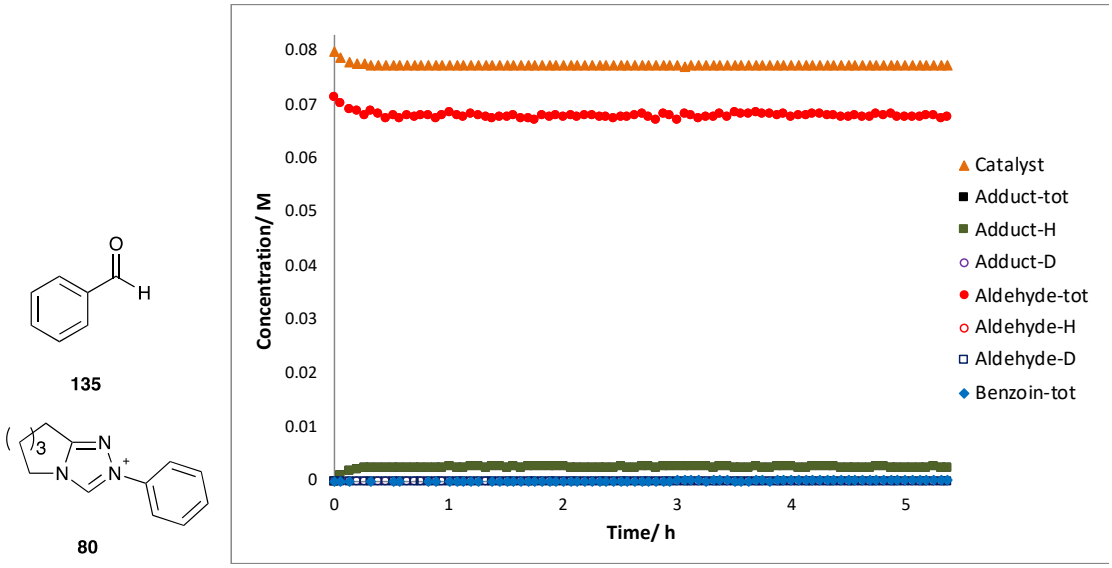

Concentration profile for the self-condensation of 2-methylbenzaldehyde **136** (0.081 M), catalysed by *para*-methoxyphenyl triazolium precatalyst **91** (n= 3, 0.06 M), in 0.107 M NEt_3 and 0.053 M $NEt_3 \cdot HCl$ in methanol-d_4.

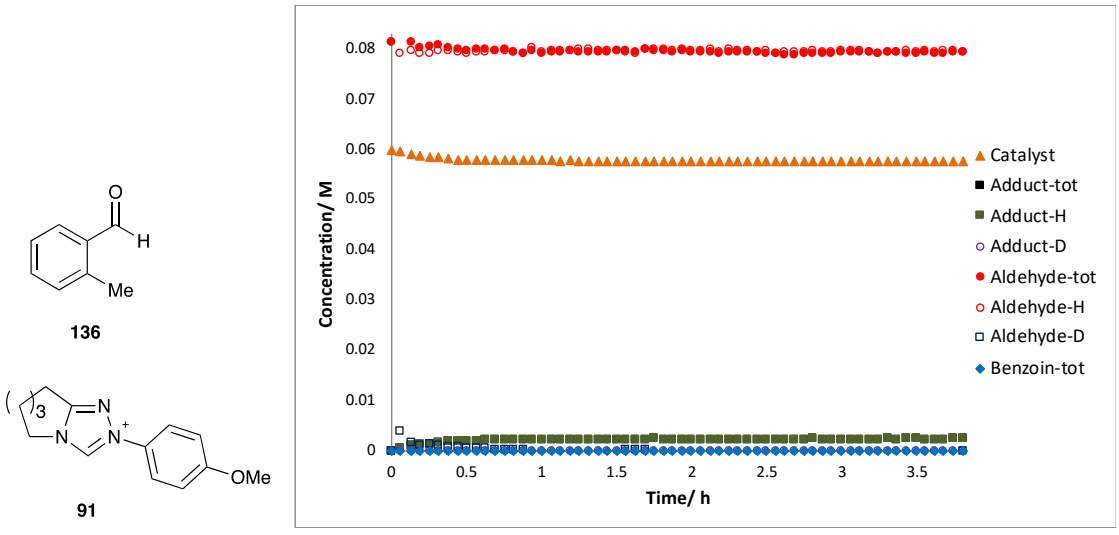

Concentration profile for the self-condensation of 2-methoxybenzaldehyde **138** (0.06 M), catalysed by *para*-methoxyphenyl triazolium precatalyst **91** (n= 3, 0.06 M), in 0.107 M NEt_3 and 0.053 M $NEt_3 \cdot HCl$ in methanol-d_4.

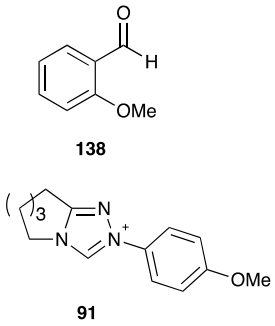

138

91

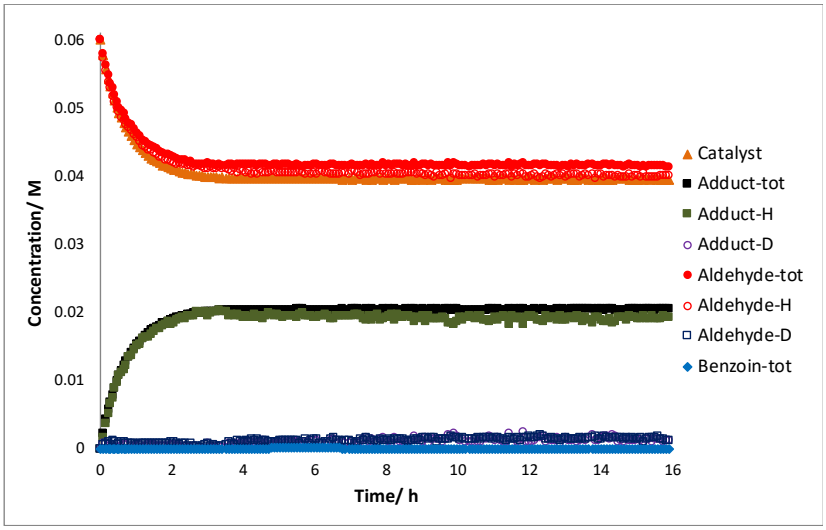

Concentration profile for the self-condensation of 4-methylbenzaldehyde **137** (0.086 M), catalysed by *para*-methoxyphenyl triazolium precatalyst **91** (n= 3, 0.06 M), in 0.107 M NEt_3 and 0.053 M $NEt_3 \cdot HCl$ in methanol-d_4.

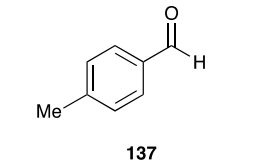

137

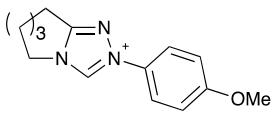

91

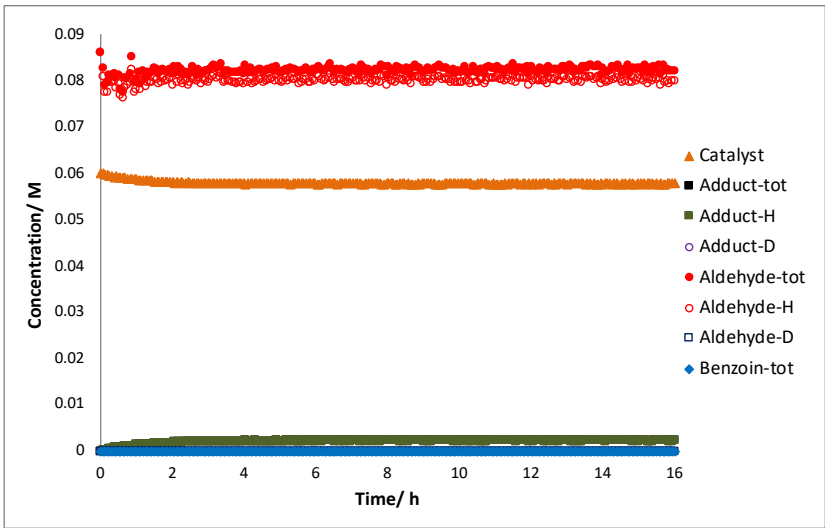

Concentration profile for the self-condensation of 4-methoxybenzaldehyde **139** (0.067 M), catalysed by *para*-methoxyphenyl triazolium precatalyst **91** (n= 3, 0.06 M), in 0.107 M NEt_3 and 0.053 M $NEt_3 \cdot HCl$ in methanol-d_4.

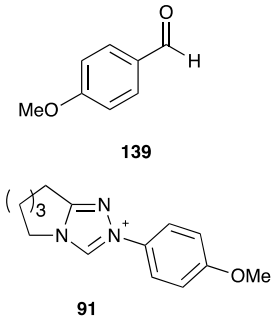

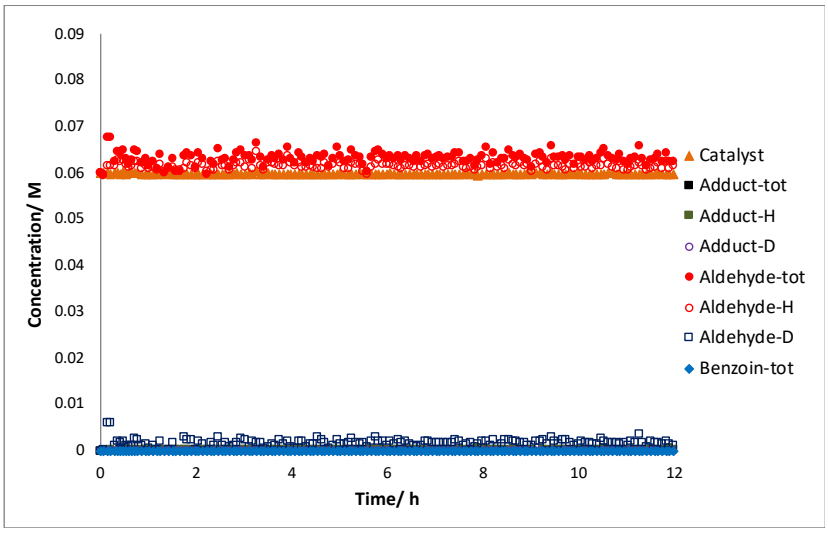

Concentration profile for the self-condensation of benzaldehyde **135** (0.06 M), catalysed by *para*-methoxyphenyl triazolium precatalyst **91** (n= 3, 0.06 M), in 0.107 M NEt_3 and 0.053 M $NEt_3 \cdot HCl$ in methanol-d_4.

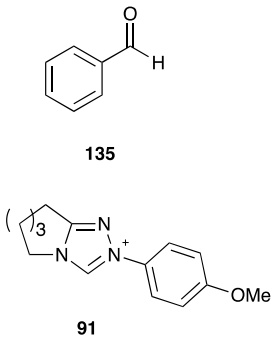

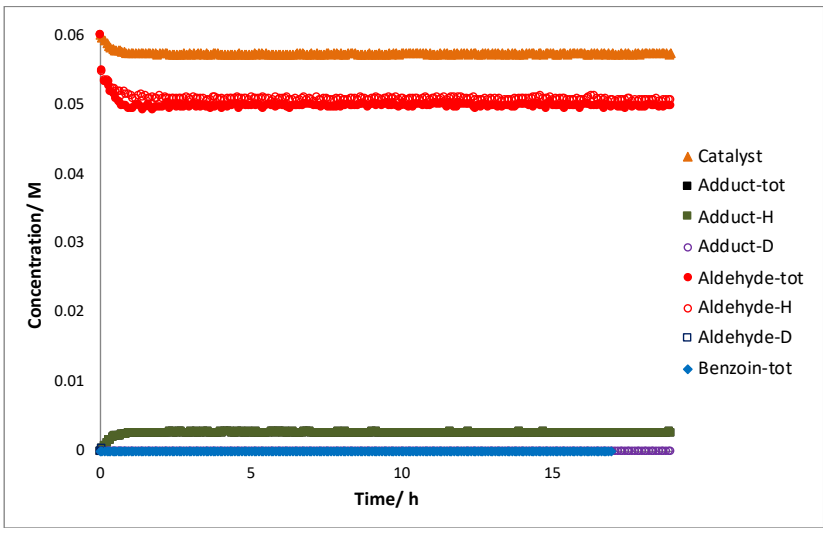

Global Fitting Profiles

Global fitting profile for the self-condensation of 2-methoxybenzaldehyde **138** (0.08 M), catalysed by *meta*-chlorophenyl triazolium precatalyst **103** (n= 1, 0.04 M), in 0.107 M NEt_3 and 0.053 M NEt_3·HCl in methanol-d_4.

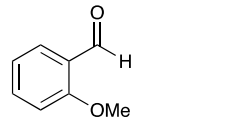

138

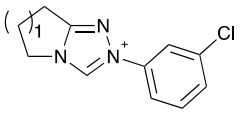

103

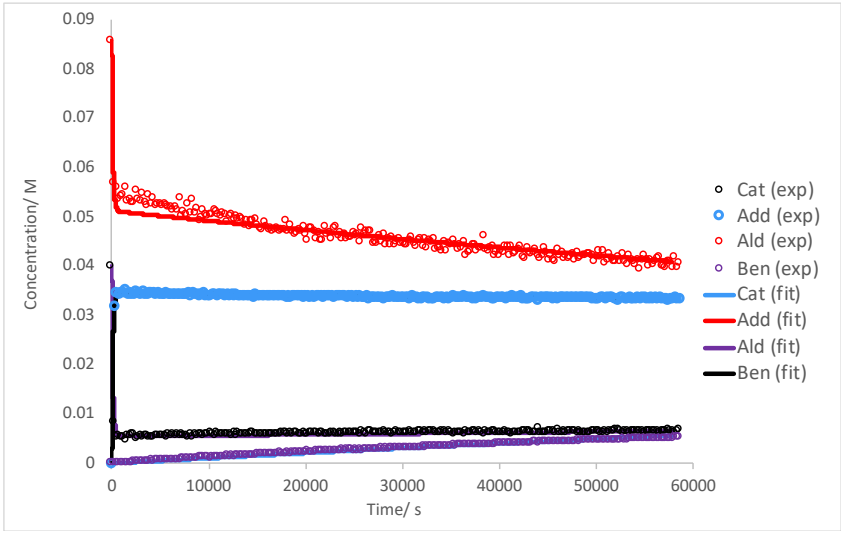

Global fitting profile for the self-condensation of 4-methoxybenzaldehyde **139** (0.10 M), catalysed by *meta*-chlorophenyl triazolium precatalyst **103** (n= 1, 0.04 M), in 0.107 M NEt_3 and 0.053 M NEt_3·HCl in methanol-d_4.

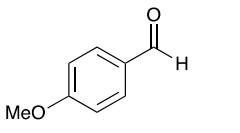

139

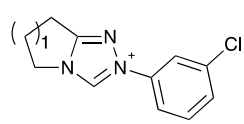

103

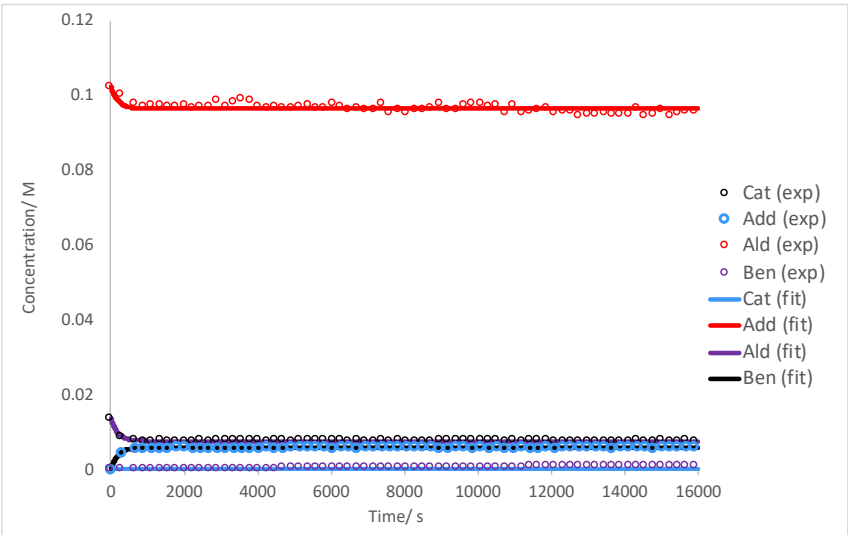

Global fitting profile for the self-condensation of benzaldehyde **135** (0.075 M), catalysed by *meta*-chlorophenyl triazolium precatalyst **103** (n= 1, 0.04 M), in 0.107 M NEt_3 and 0.053 M NEt_3·HCl in methanol-d_4.

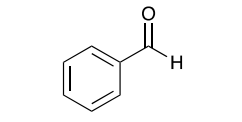

135

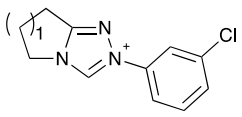

103

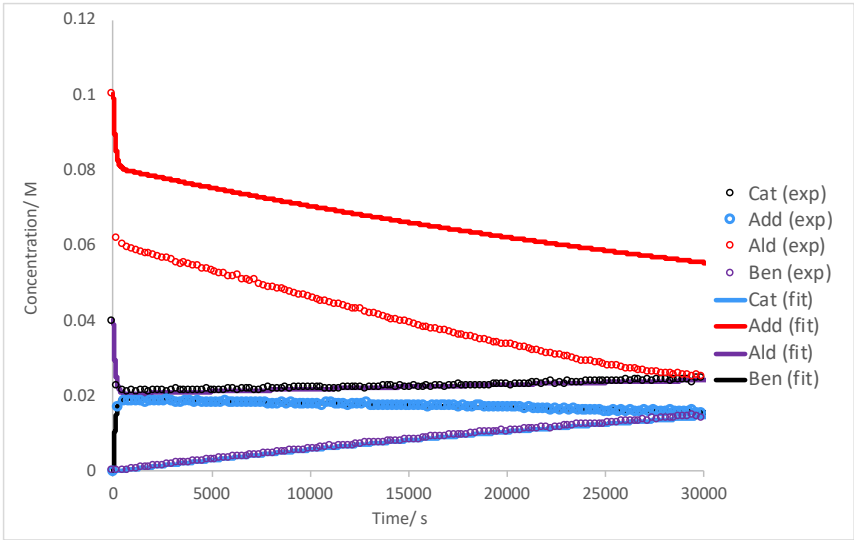

Global fitting profile for the self-condensation of 2-methoxybenzaldehyde **138** (0.08 M), catalysed by *para*-bromophenyl triazolium precatalyst **104** (n= 1, 0.08 M), in 0.107 M NEt_3 and 0.053 M NEt_3·HCl in methanol-d_4.

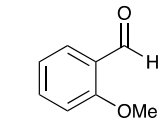

138

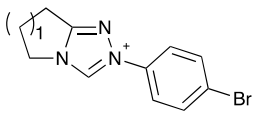

104

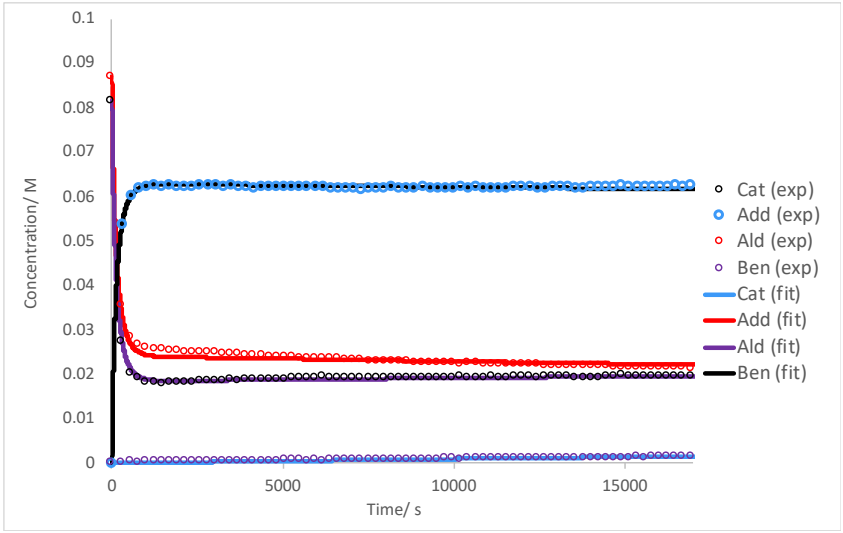

Global fitting profile for the self-condensation of 4-methoxybenzaldehyde **139** (0.09 M), catalysed by *para*-bromophenyl triazolium precatalyst **104** (n= 1, 0.08 M), in 0.107 M NEt_3 and 0.053 M NEt_3·HCl in methanol-d_4.

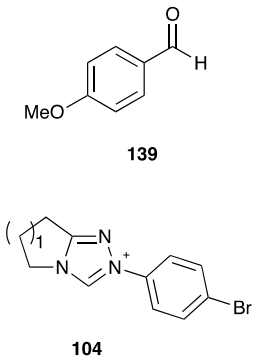

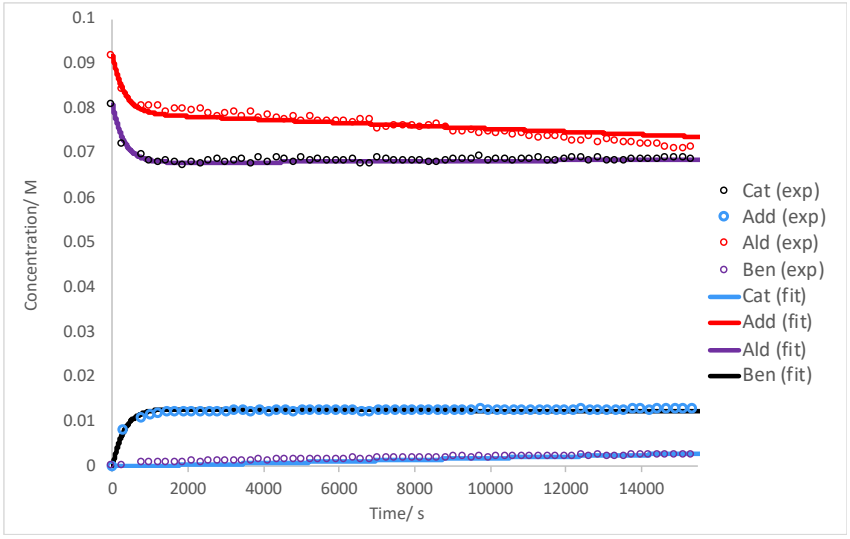

Global fitting profile for the self-condensation of benzaldehyde **135** (0.07 M), catalysed by *para*-bromophenyl triazolium precatalyst **104** (n= 1, 0.08 M), in 0.107 M NEt_3 and 0.053 M NEt_3·HCl in methanol-d_4.

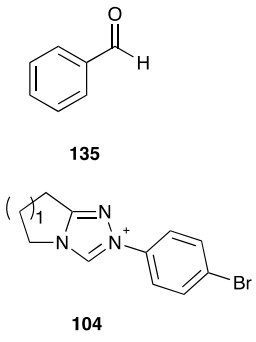

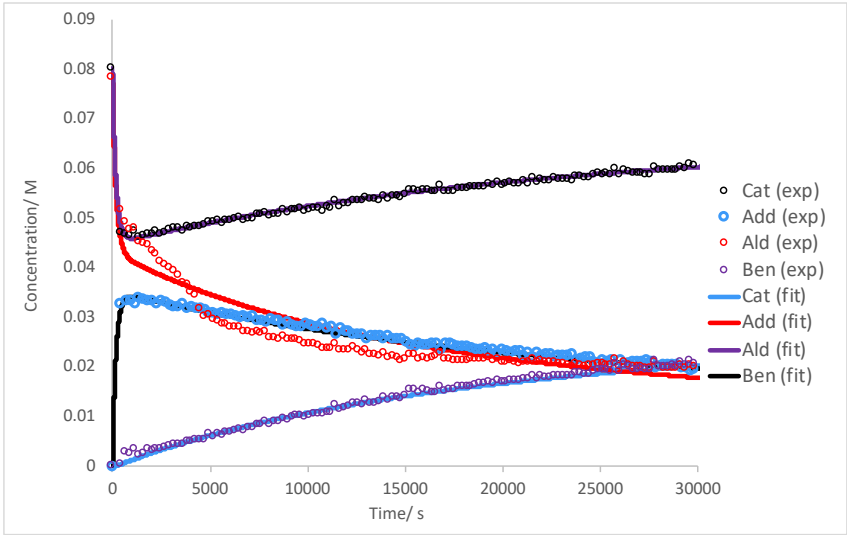

Global fitting profile for the self-condensation of 2-methoxybenzaldehyde **138** (0.053 M), catalysed by *para*-trifluoromethylphenyl triazolium precatalyst **105** (n= 1, 0.043 M), in 0.107 M NEt_3 and 0.053 M NEt_3·HCl in methanol-d_4.

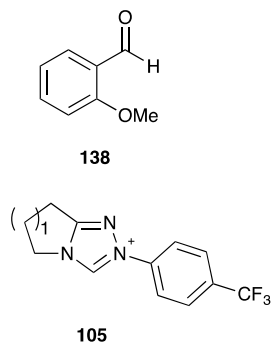

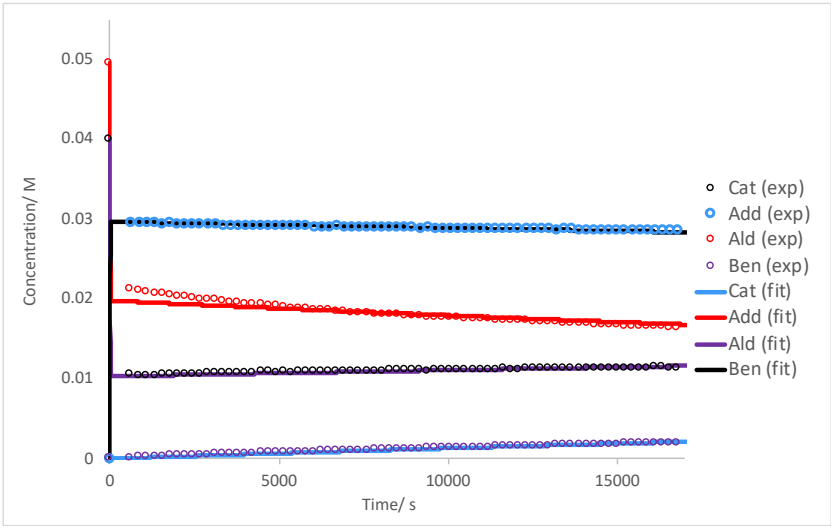

Global fitting profile for the self-condensation of 4-methoxybenzaldehyde **139** (0.053 M), catalysed by *para*-trifluoromethylphenyl triazolium precatalyst **105** (n= 1, 0.041 M), in 0.107 M NEt_3 and 0.053 M NEt_3·HCl in methanol-d_4.

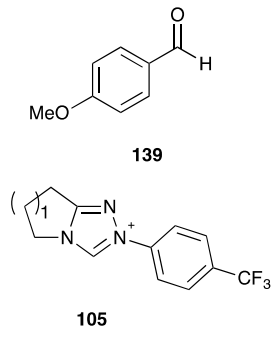

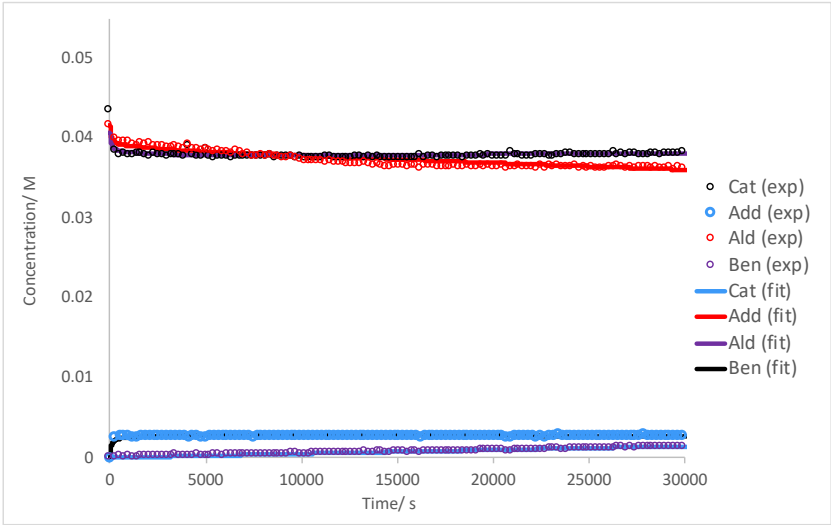

Global fitting profile for the self-condensation of benzaldehyde **135** (0.036 M), catalysed by *para*-trifluoromethylphenyl triazolium precatalyst **105** (n= 1, 0.043 M), in 0.107 M NEt_3 and 0.053 M NEt_3·HCl in methanol-d_4.

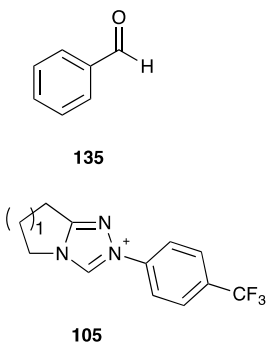

135

105

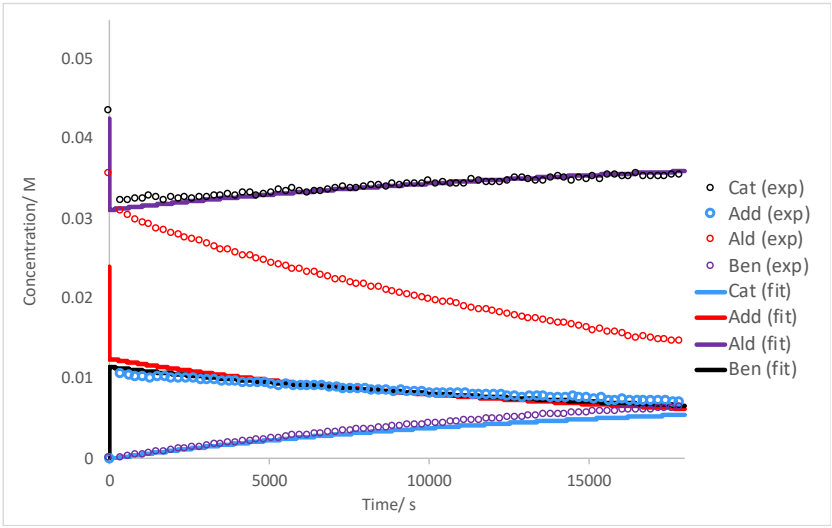

Global fitting profile for the self-condensation of 2-methylbenzaldehyde **136** (0.077 M), catalysed by *para*-fluorophenyl triazolium precatalyst **100** (n= 1, 0.08 M), in 0.107 M NEt_3 and 0.053 M NEt_3·HCl in methanol-d_4.

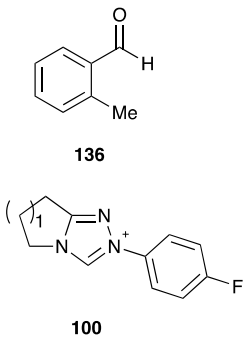

136

100

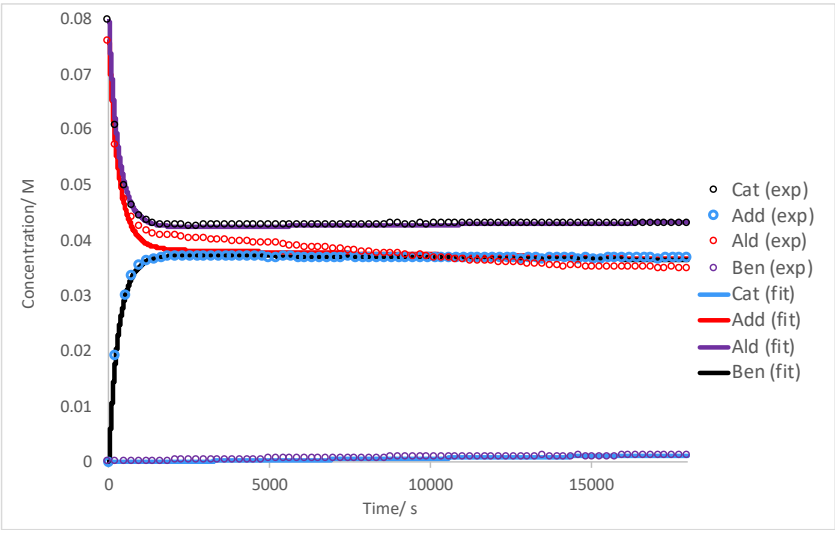

Global fitting profile for the self-condensation of 4-methylbenzaldehyde **137** (0.079 M), catalysed by *para*-fluorophenyl triazolium precatalyst **100** (n= 1, 0.08 M), in 0.107 M NEt_3 and 0.053 M NEt_3·HCl in methanol-d_4.

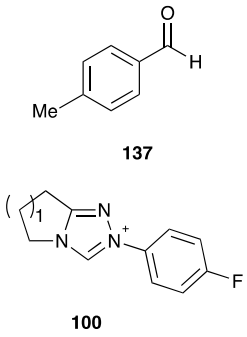

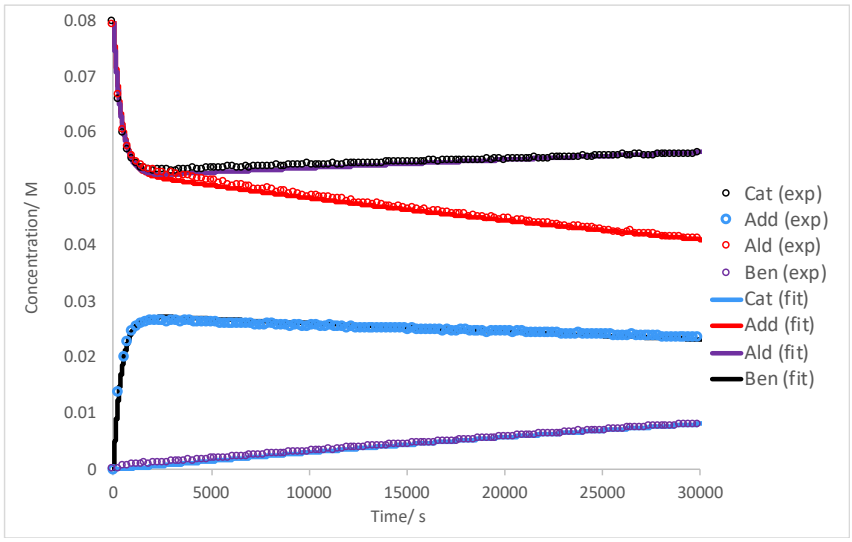

Global fitting profile for the self-condensation of 2-trifluoromethylbenzaldehyde **150** (0.071 M), catalysed by phenyl triazolium precatalyst **101** (n= 1, 0.08 M), in 0.107 M NEt_3 and 0.053 M NEt_3·HCl in methanol-d_4.

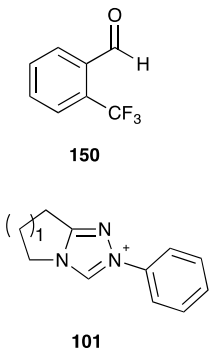

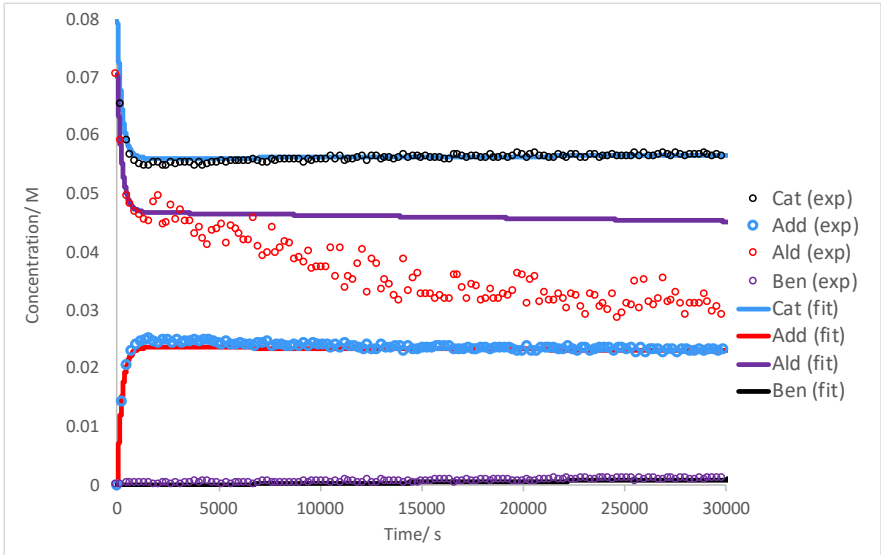

Global fitting profile for the self-condensation of 2-fluorobenzaldehyde **154** (0.07 M), catalysed by phenyl triazolium precatalyst **101** (n= 1, 0.08 M), in 0.107 M NEt_3 and 0.053 M $NEt_3 \cdot HCl$ in methanol-d_4.

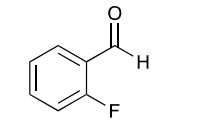

154

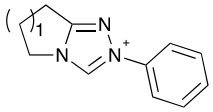

101

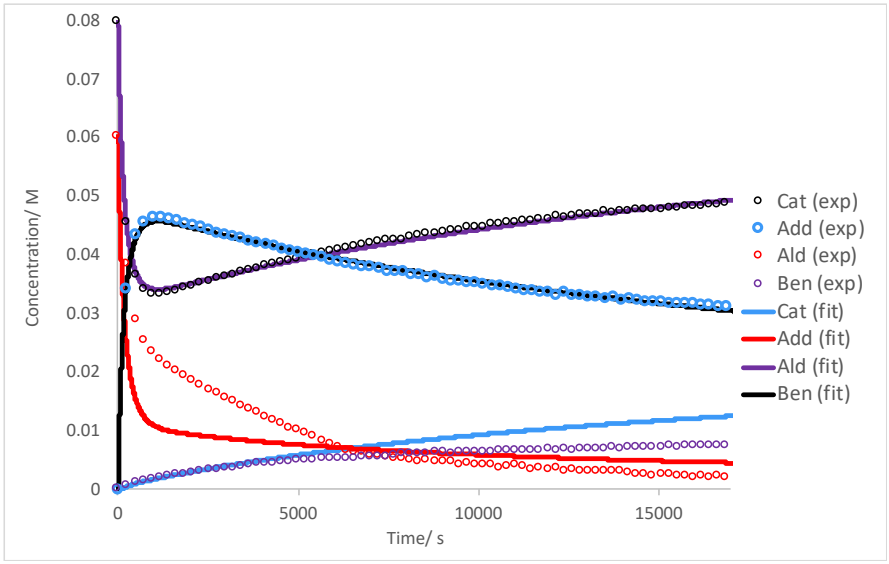

Global fitting profile for the self-condensation of 2-methylbenzaldehyde **136** (0.078 M), catalysed by phenyl triazolium precatalyst **101** (n= 1, 0.08 M), in 0.107 M NEt_3 and 0.053 M $NEt_3 \cdot HCl$ in methanol-d_4.

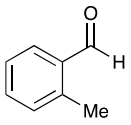

136

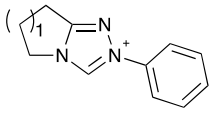

101

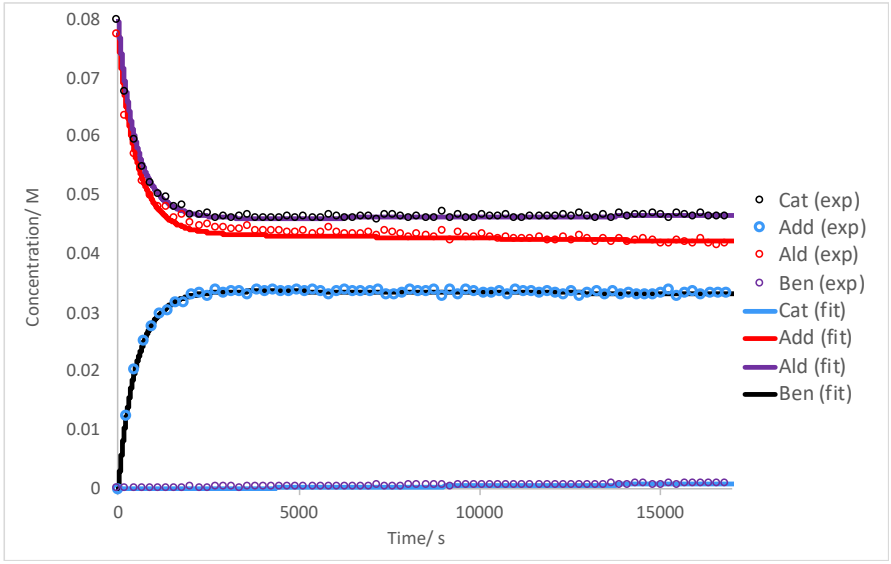

Global fitting profile for the self-condensation of 2-methoxybenzaldehyde **138** (0.08 M), catalysed by phenyl triazolium precatalyst **101** (n= 1, 0.08 M), in 0.107 M NEt_3 and 0.053 M $NEt_3 \cdot HCl$ in methanol-d_4.

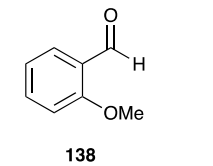

138

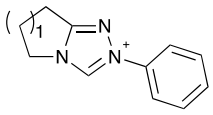

101

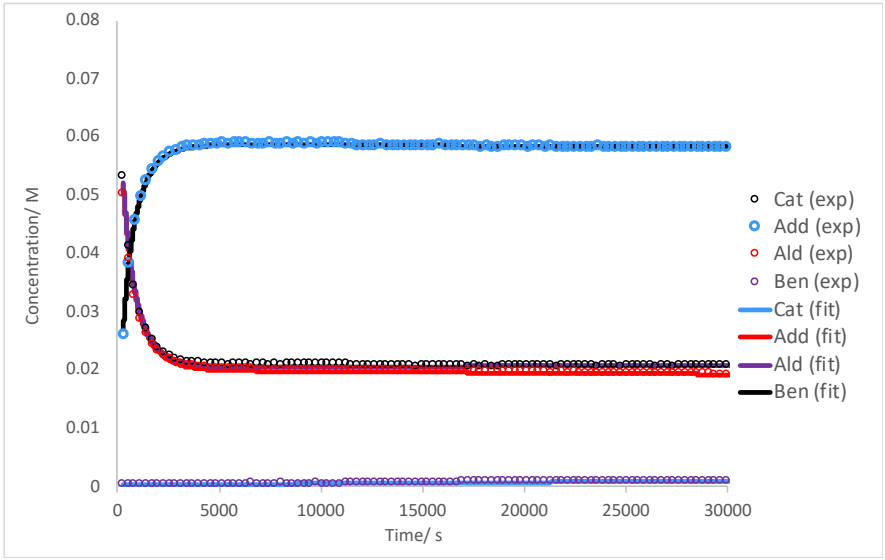

Global fitting profile for the self-condensation of 3-trifluoromethylbenzaldehyde **151** (0.069 M), catalysed by phenyl triazolium precatalyst **101** (n= 1, 0.08 M), in 0.107 M NEt_3 and 0.053 M $NEt_3 \cdot HCl$ in methanol-d_4.

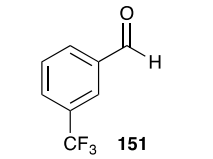

151

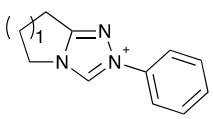

101

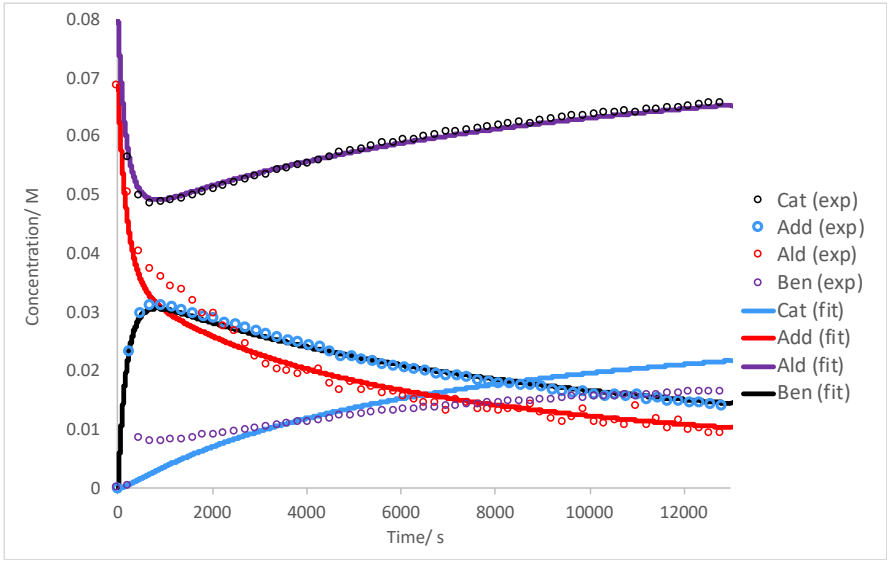

Global fitting profile for the self-condensation of 3-fluorobenzaldehyde **155** (0.072 M), catalysed by phenyl triazolium precatalyst **101** (n= 1, 0.08 M), in 0.107 M NEt_3 and 0.053 M $NEt_3 \cdot HCl$ in methanol-d_4.

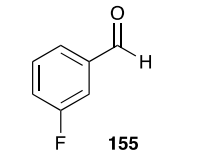

155

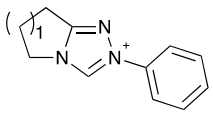

101

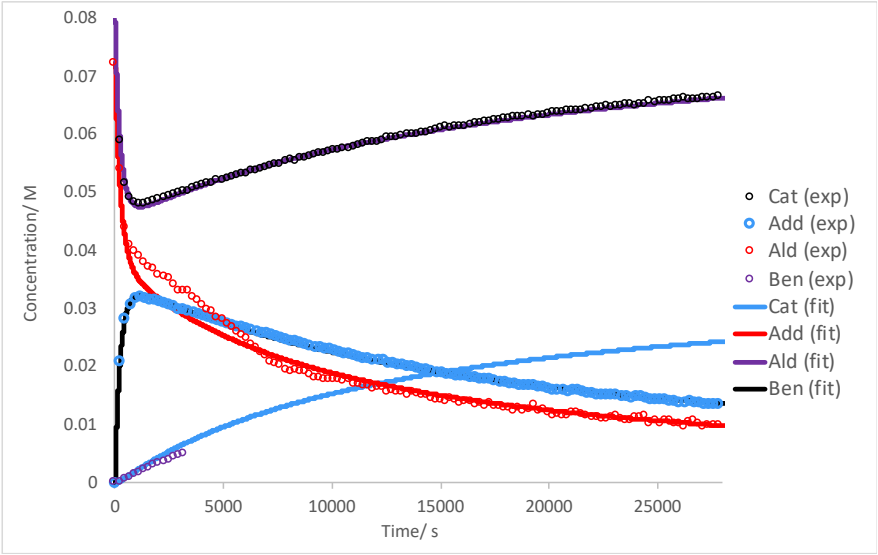

Global fitting profile for the self-condensation of 3-methylbenzaldehyde **153** (0.08 M), catalysed by phenyl triazolium precatalyst **101** (n= 1, 0.08 M), in 0.107 M NEt_3 and 0.053 M $NEt_3 \cdot HCl$ in methanol-d_4.

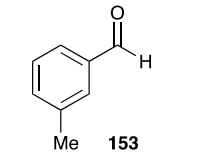

153

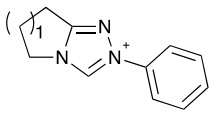

101

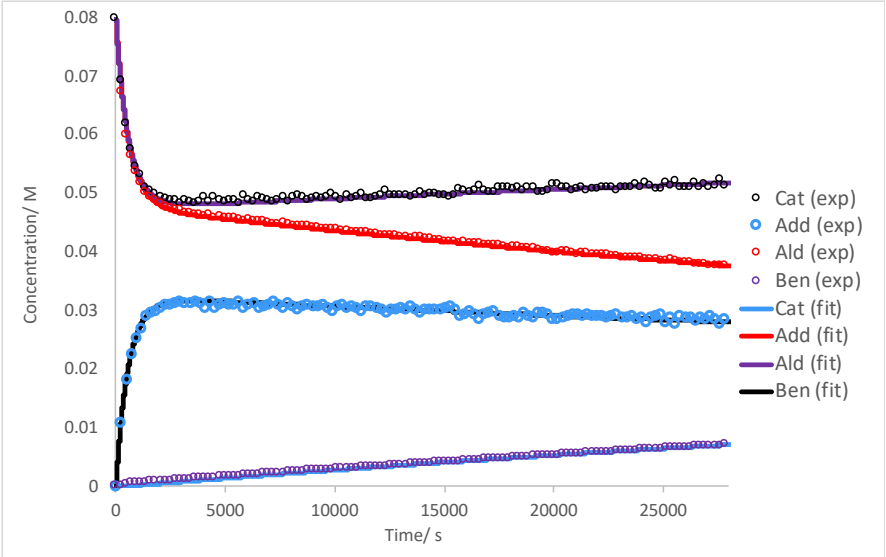

Global fitting profile for the self-condensation of 3-methoxybenzaldehyde **149** (0.083 M), catalysed by phenyl triazolium precatalyst **101** (n= 1, 0.08 M), in 0.107 M NEt_3 and 0.053 M NEt_3·HCl in methanol-d_4.

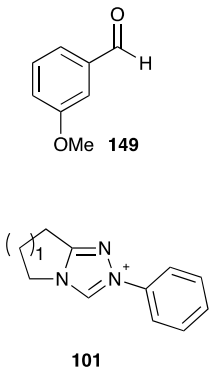

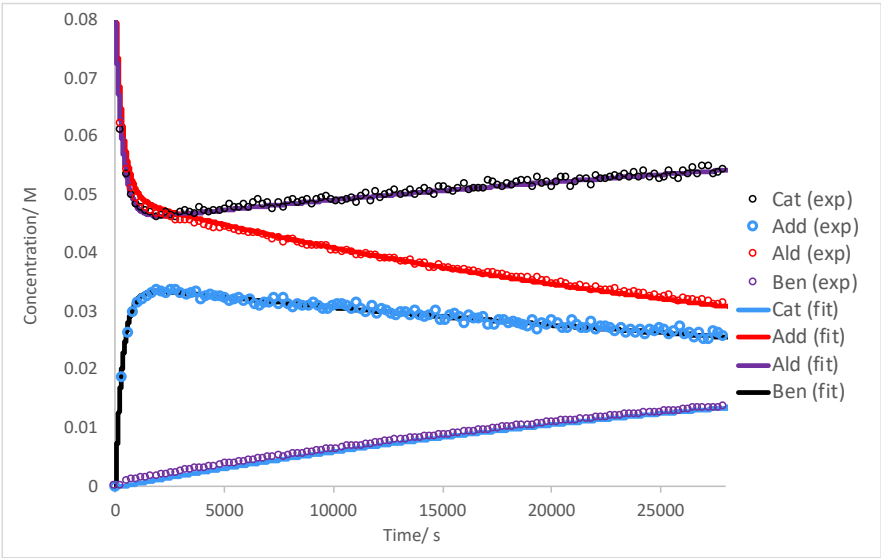

Global fitting profile for the self-condensation of 4-trifluoromethylbenzaldehyde **152** (0.072 M), catalysed by phenyl triazolium precatalyst **101** (n= 1, 0.08 M), in 0.107 M NEt_3 and 0.053 M NEt_3·HCl in methanol-d_4.

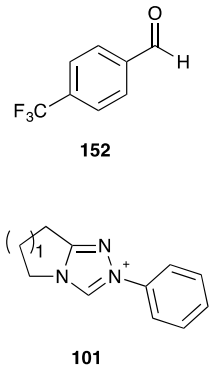

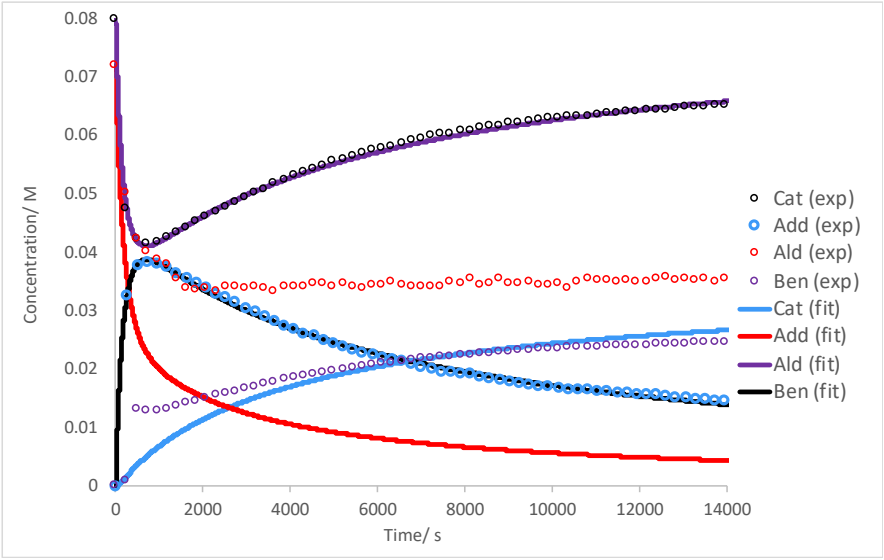

Global fitting profile for the self-condensation of 4-fluorobenzaldehyde **156** (0.071 M), catalysed by phenyl triazolium precatalyst **101** (n= 1, 0.08 M), in 0.107 M NEt_3 and 0.053 M $NEt_3 \cdot HCl$ in methanol-d_4.

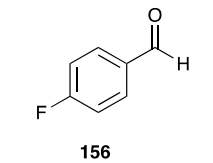

156

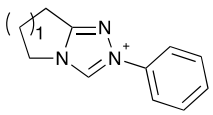

101

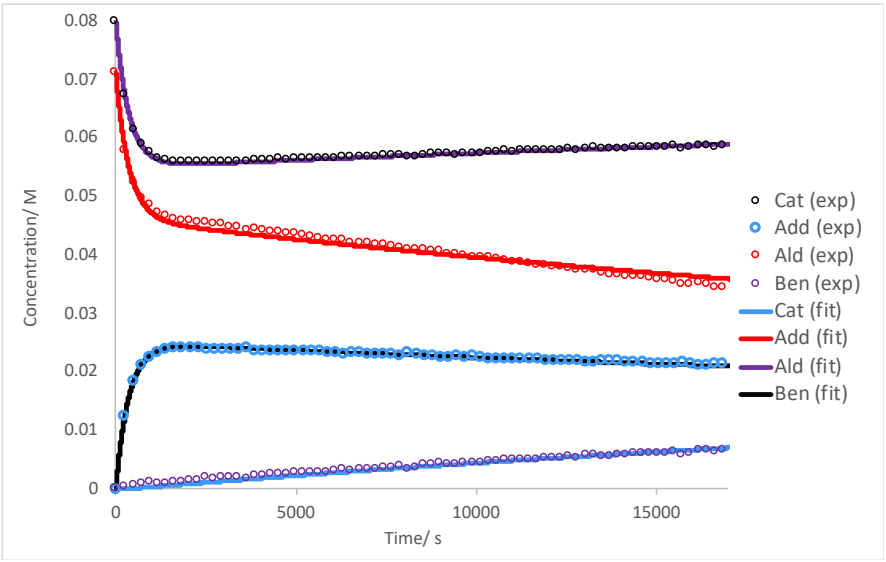

Global fitting profile for the self-condensation of 4-methylbenzaldehyde **137** (0.092 M), catalysed by phenyl triazolium precatalyst **101** (n= 1, 0.08 M), in 0.107 M NEt_3 and 0.053 M $NEt_3 \cdot HCl$ in methanol-d_4.

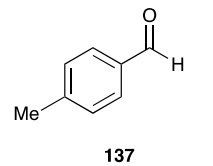

137

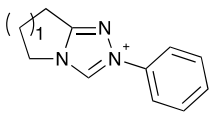

101

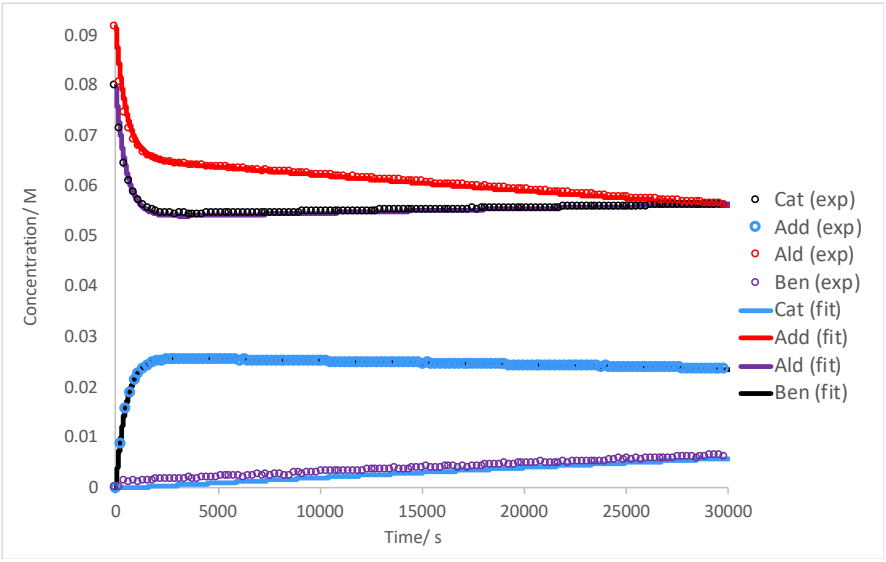

Global fitting profile for the self-condensation of 4-dimethylaminobenzaldehyde **157** (0.087 M), catalysed by phenyl triazolium precatalyst **101** (n= 1, 0.08 M), in 0.107 M NEt_3 and 0.053 M NEt_3·HCl in methanol-d_4.

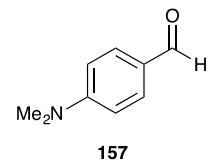

157

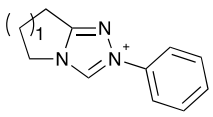

101

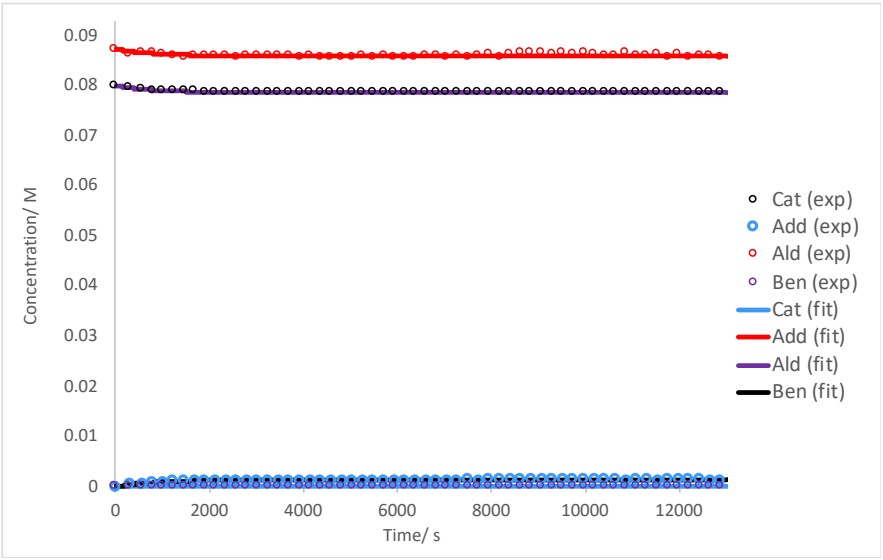

Global fitting profile for the self-condensation of 2-methylbenzaldehyde **136** (0.12 M), catalysed by *para*-methoxyphenyl triazolium precatalyst **89** (n= 1, 0.08 M), in 0.107 M NEt_3 and 0.053 M NEt_3·HCl in methanol-d_4.

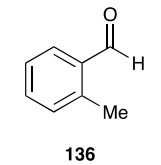

136

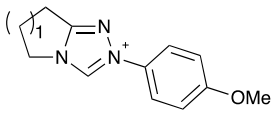

89

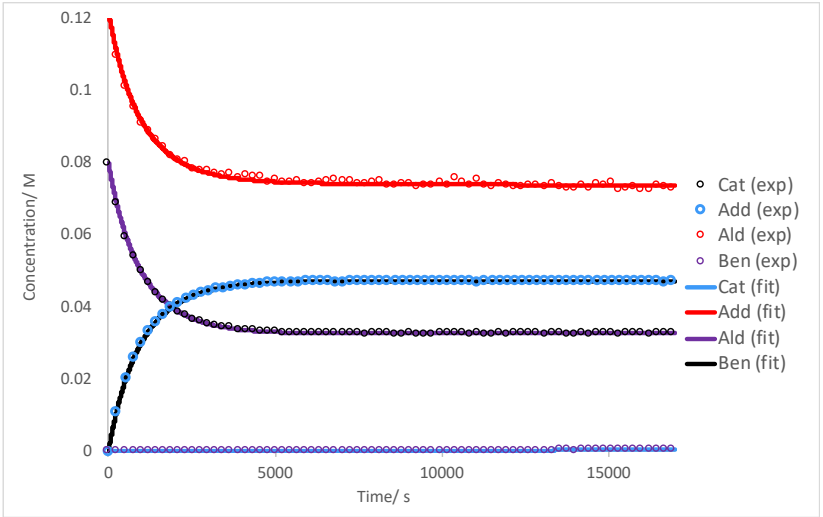

Global fitting profile for the self-condensation of 2-methoxybenzaldehyde **138** (0.08 M), catalysed by *para*-methoxyphenyl triazolium precatalyst **89** (n= 1, 0.08 M), in 0.107 M NEt_3 and 0.053 M $NEt_3 \cdot HCl$ in methanol-d_4.

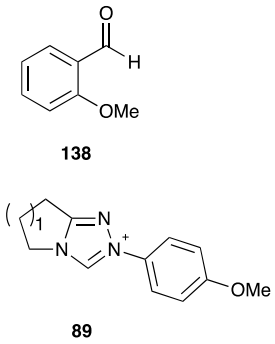

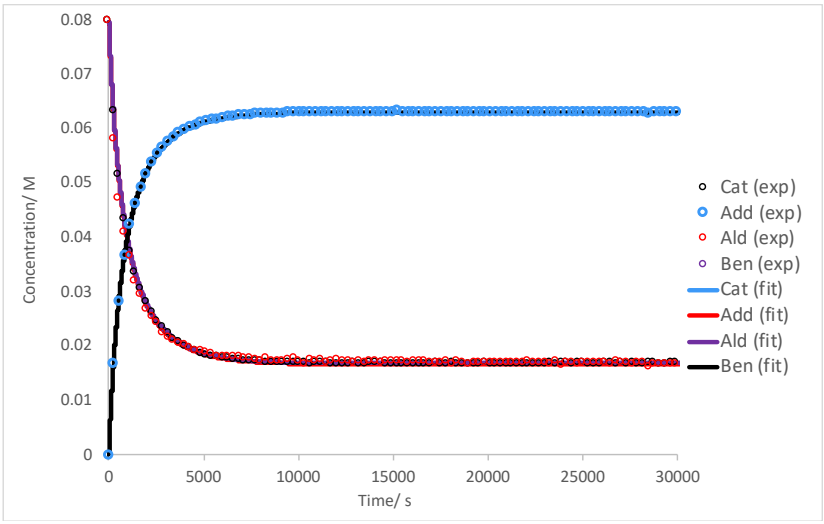

Global fitting profile for the self-condensation of 4-methylbenzaldehyde **137** (0.11 M), catalysed by *para*-methoxyphenyl triazolium precatalyst **89** (n= 1, 0.08 M), in 0.107 M NEt_3 and 0.053 M $NEt_3 \cdot HCl$ in methanol-d_4.

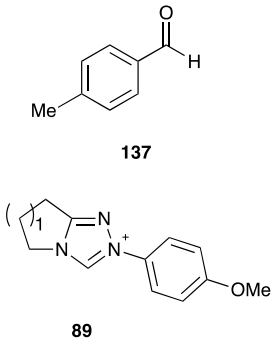

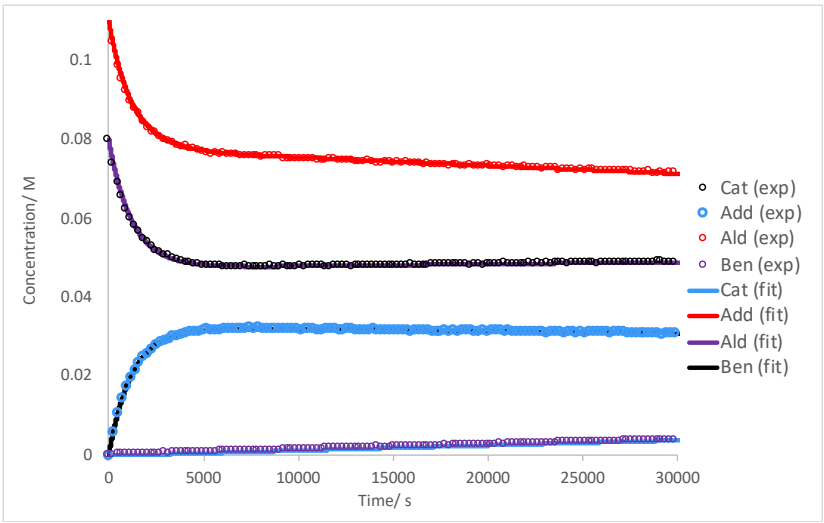

Global fitting profile for the self-condensation of 2-methoxybenzaldehyde **138** (0.082 M), catalysed by triisopropylphenyl triazolium precatalyst **88** (n= 1, 0.08 M), in 0.107 M NEt_3 and 0.053 M $NEt_3 \cdot HCl$ in methanol-d_4.

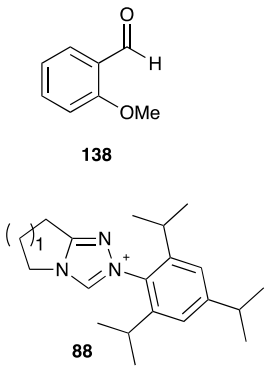

138

88

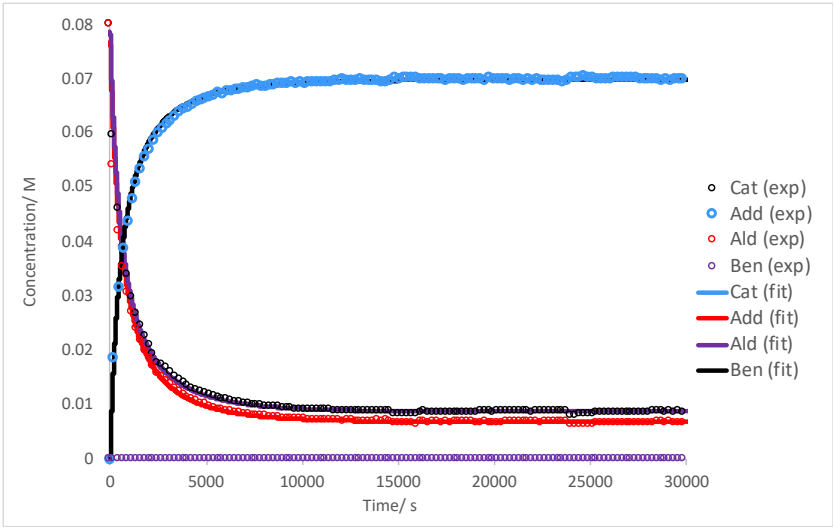

Global fitting profile for the self-condensation of 4-methoxybenzaldehyde **139** (0.077 M), catalysed by triisopropylphenyl triazolium precatalyst **88** (n= 1, 0.076 M), in 0.107 M NEt_3 and 0.053 M $NEt_3 \cdot HCl$ in methanol-d_4.

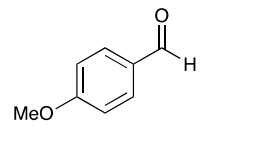

139

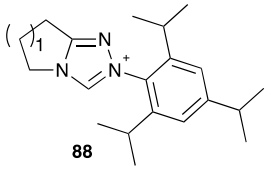

88

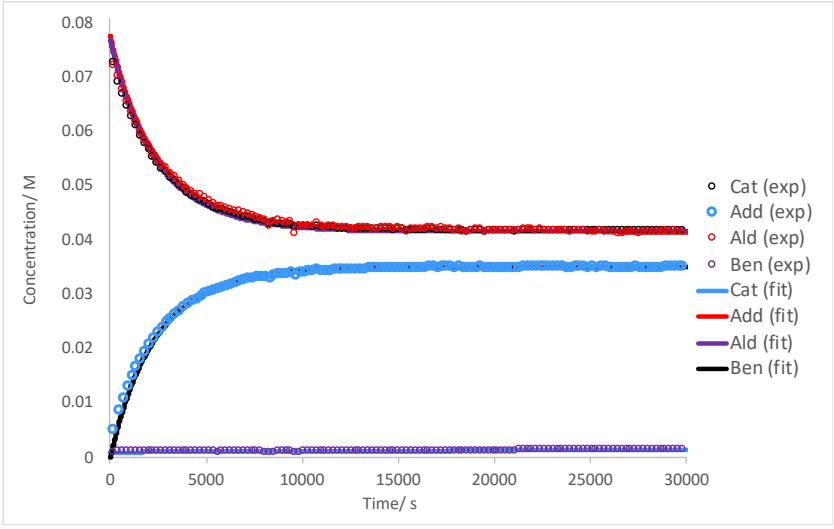

Global fitting profile for the self-condensation of benzaldehyde **135** (0.08 M), catalysed by triisopropylphenyl triazolium precatalyst **88** (n= 1, 0.076 M), in 0.107 M NEt_3 and 0.053 M $NEt_3 \cdot HCl$ in methanol-d_4.

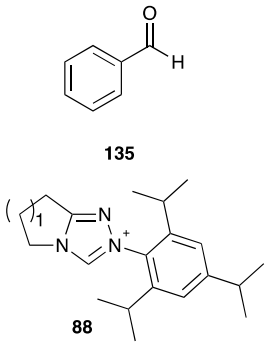

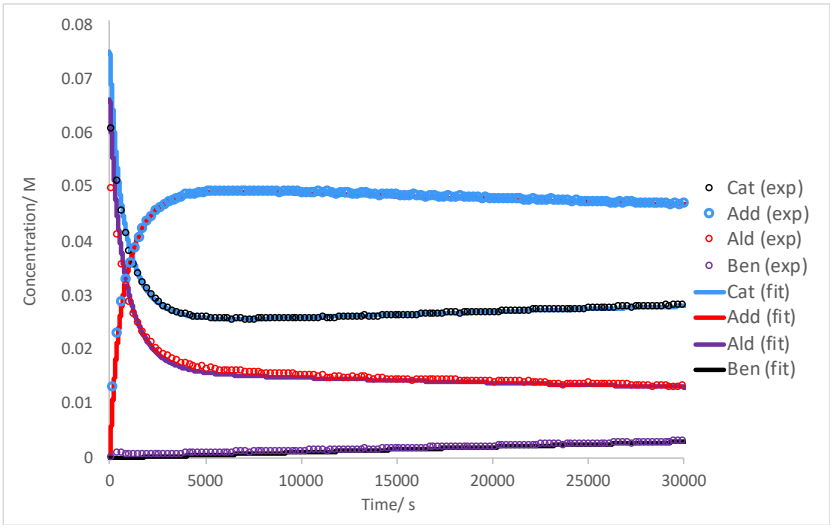

Global fitting profile for the self-condensation of 2-methoxybenzaldehyde **138** (0.08 M), catalysed by mesityl triazolium precatalyst **86** (n= 2, 0.068 M), in 0.107 M NEt_3 and 0.053 M $NEt_3 \cdot HCl$ in methanol-d_4.

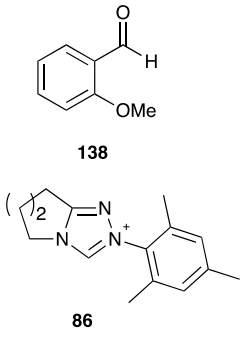

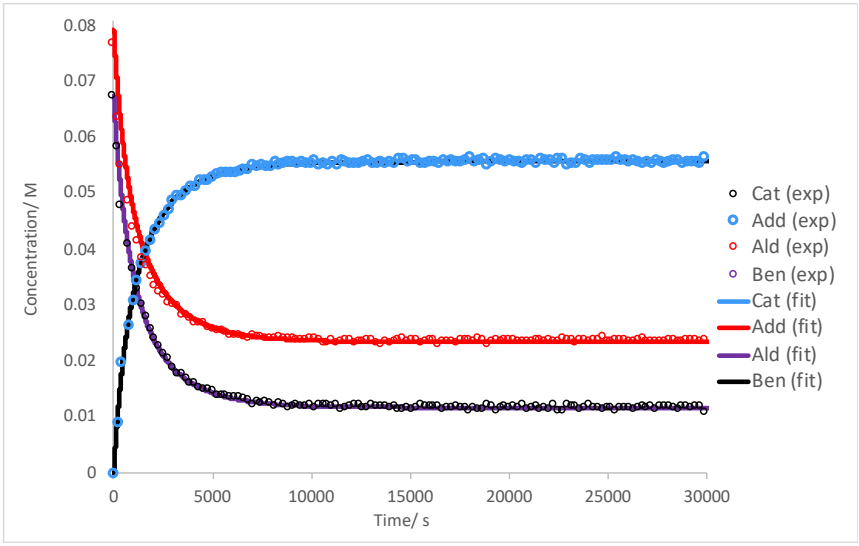

Global fitting profile for the self-condensation of 4-methoxybenzaldehyde **139** (0.077 M), catalysed by mesityl triazolium precatalyst **86** (n= 2, 0.068 M), in 0.107 M NEt_3 and 0.053 M $NEt_3 \cdot HCl$ in methanol-d_4.

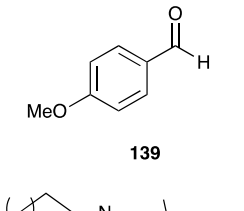

139

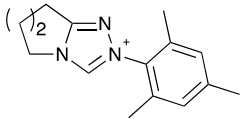

86

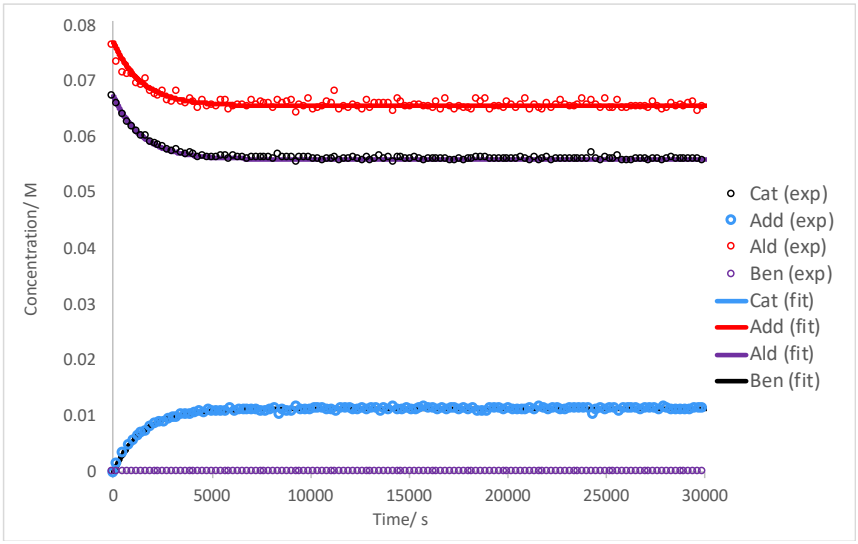

Global fitting profile for the self-condensation of benzaldehyde **135** (0.071 M), catalysed by mesityl triazolium precatalyst **86** (n= 2, 0.068 M), in 0.107 M NEt_3 and 0.053 M $NEt_3 \cdot HCl$ in methanol-d_4.

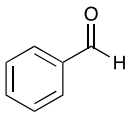

135

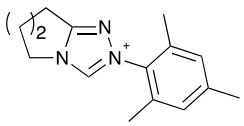

86

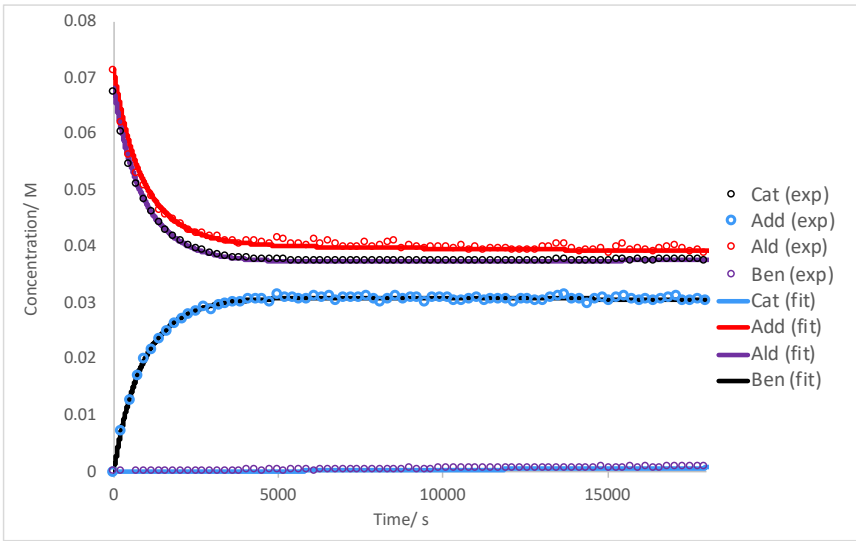

Global fitting profile for the self-condensation of 2-methylbenzaldehyde **136** (0.076 M), catalysed by *para*-fluorophenyl triazolium precatalyst **77** (n= 2, 0.08 M), in 0.107 M NEt_3 and 0.053 M NEt_3·HCl in methanol-d_4.

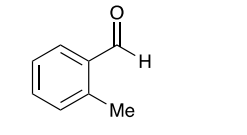

136

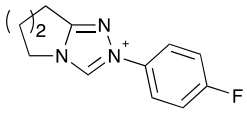

77

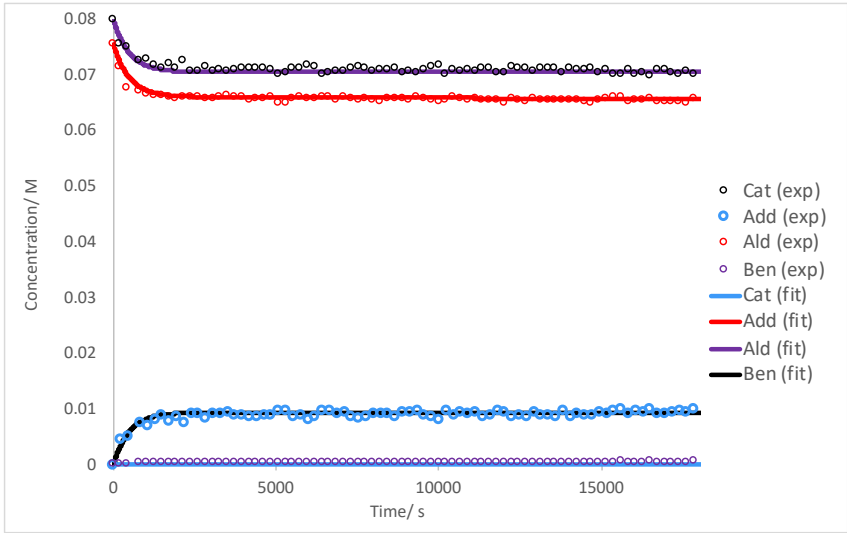

Global fitting profile for the self-condensation of 2-methoxybenzaldehyde **138** (0.077 M), catalysed by *para*-fluorophenyl triazolium precatalyst **77** (n= 2, 0.08 M), in 0.107 M NEt_3 and 0.053 M NEt_3·HCl in methanol-d_4.

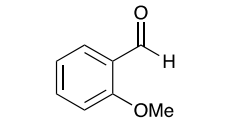

138

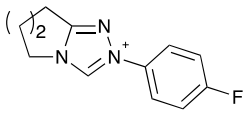

77

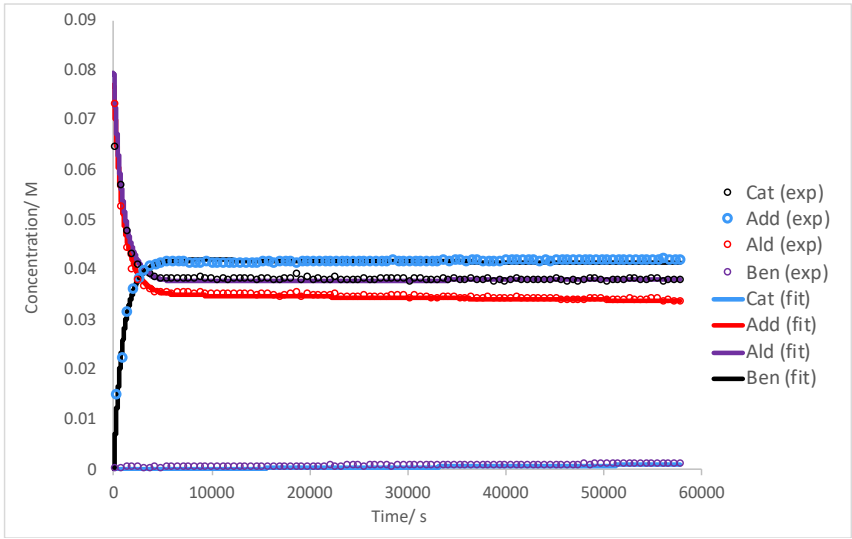

Global fitting profile for the self-condensation of 4-methylbenzaldehyde **137** (0.076 M), catalysed by *para*-fluorophenyl triazolium precatalyst **77** (n= 2, 0.08 M), in 0.107 M NEt_3 and 0.053 M NEt_3·HCl in methanol-d_4.

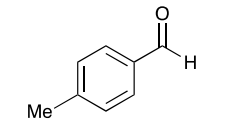

137

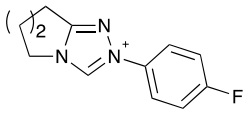

77

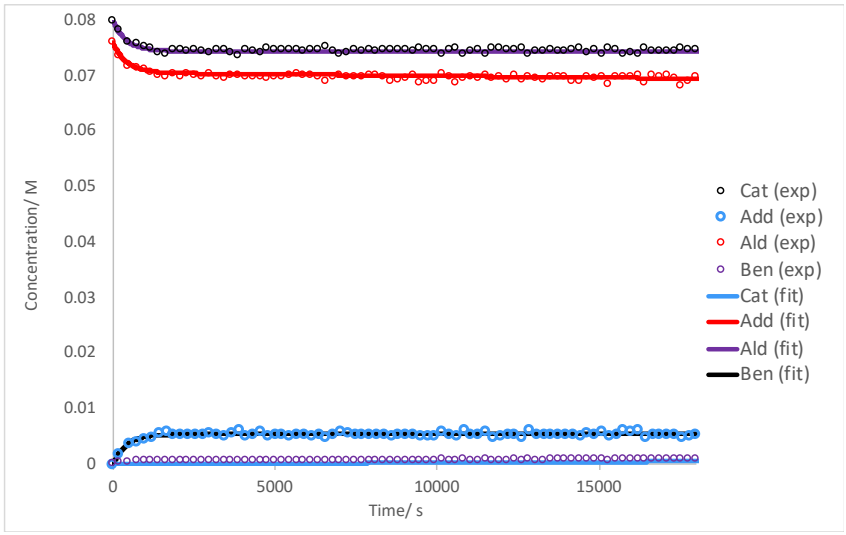

Global fitting profile for the self-condensation of 4-methoxybenzaldehyde **139** (0.073 M), catalysed by *para*-fluorophenyl triazolium precatalyst **77** (n= 2, 0.08 M), in 0.107 M NEt_3 and 0.053 M NEt_3·HCl in methanol-d_4.

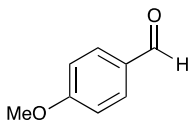

139

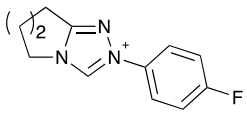

77

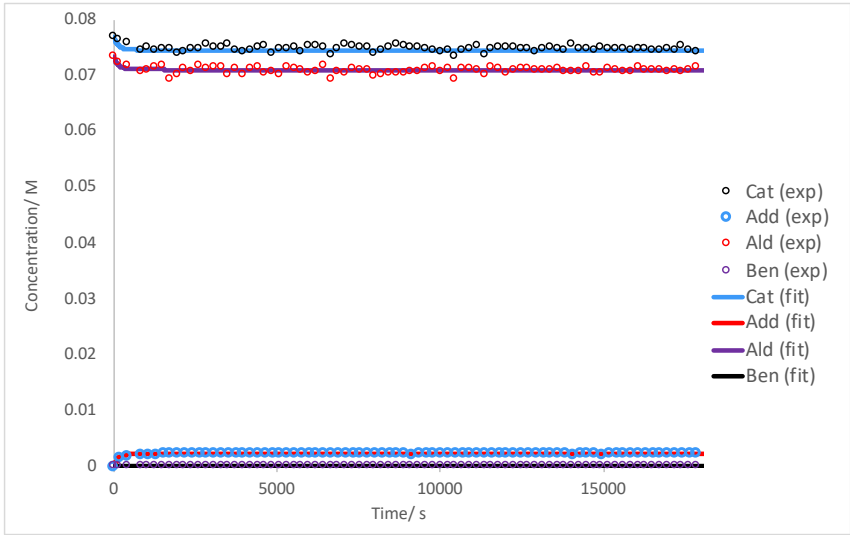

Global fitting profile for the self-condensation of benzaldehyde **135** (0.068 M), catalysed by *para*-fluorophenyl triazolium precatalyst **77** (n= 2, 0.08 M), in 0.107 M NEt_3 and 0.053 M $NEt_3 \cdot HCl$ in methanol-d_4.

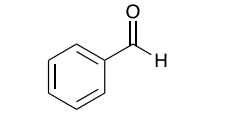

135

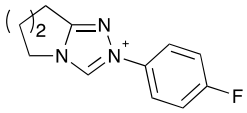

77

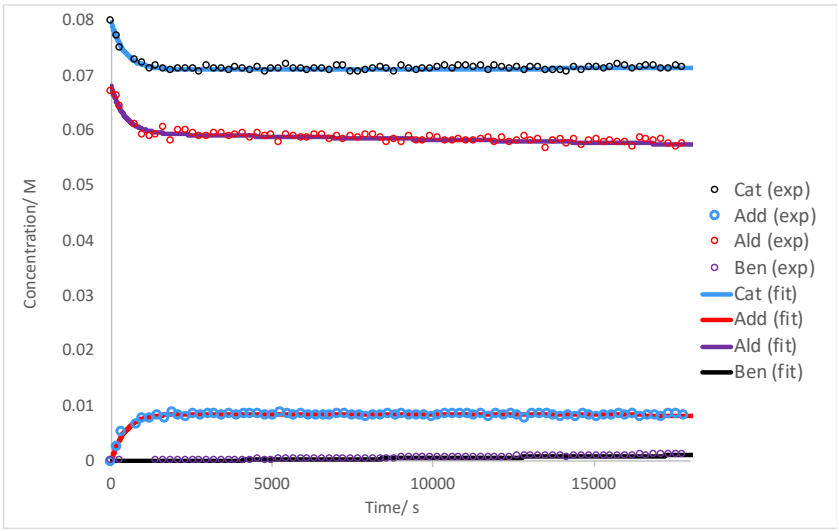

Global fitting profile for the self-condensation of 2-methylbenzaldehyde **136** (0.079 M), catalysed by phenyl triazolium precatalyst **79** (n= 2, 0.08 M), in 0.107 M NEt_3 and 0.053 M $NEt_3 \cdot HCl$ in methanol-d_4.

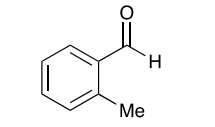

136

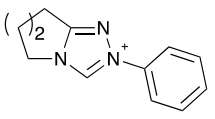

79

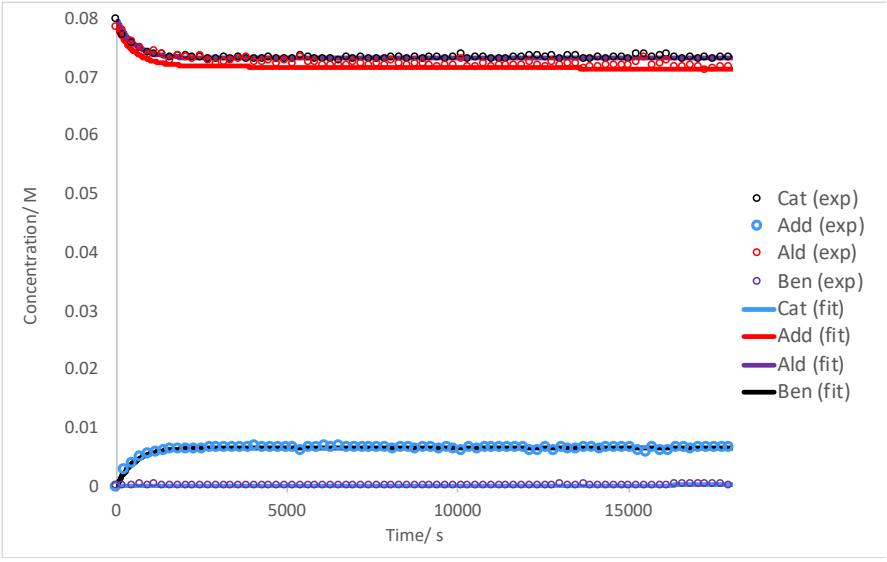

Global fitting profile for the self-condensation of 2-methoxybenzaldehyde **138** (0.08 M), catalysed by phenyl triazolium precatalyst **79** (n= 2, 0.08 M), in 0.107 M NEt_3 and 0.053 M $NEt_3 \cdot HCl$ in methanol-d_4.

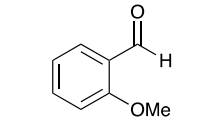

138

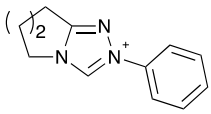

79

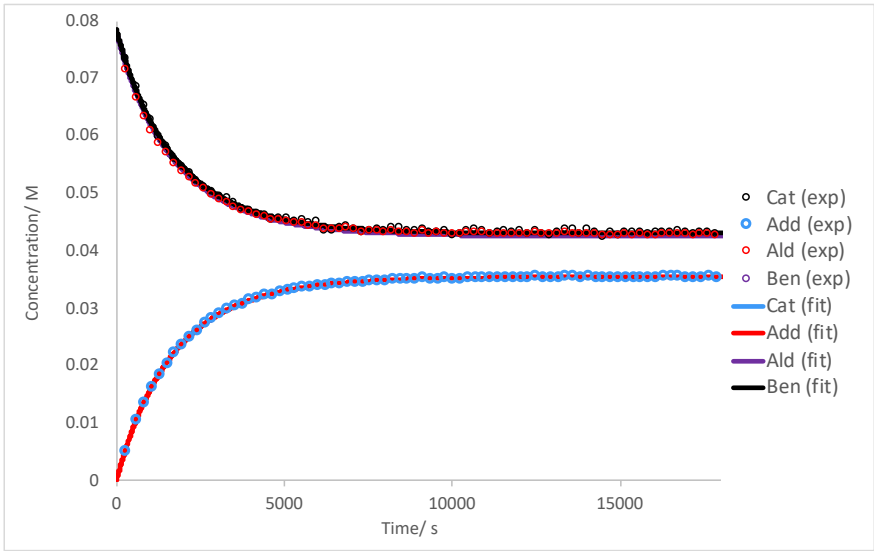

Global fitting profile for the self-condensation of 4-methylbenzaldehyde **137** (0.081 M), catalysed by phenyl triazolium precatalyst **79** (n= 2, 0.08 M), in 0.107 M NEt_3 and 0.053 M $NEt_3 \cdot HCl$ in methanol-d_4.

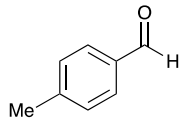

137

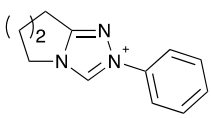

79

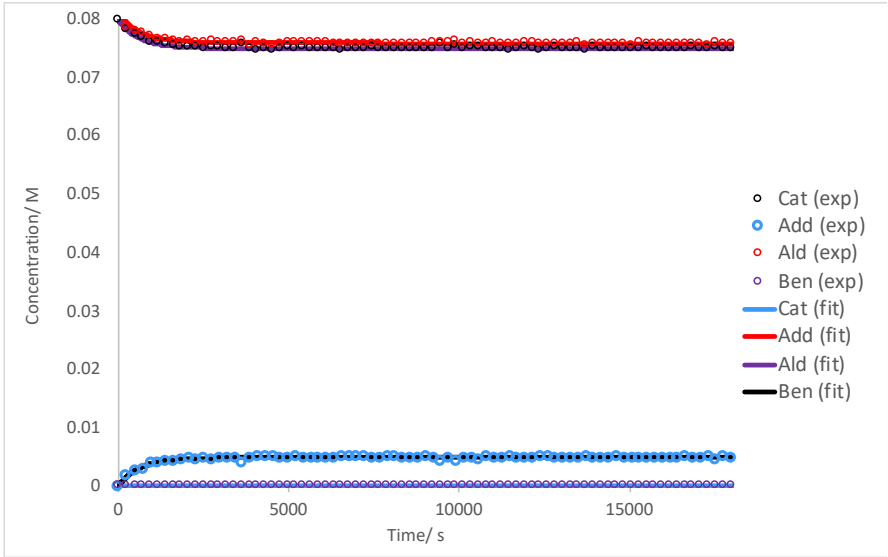

Global fitting profile for the self-condensation of benzaldehyde **135** (0.08 M), catalysed by phenyl triazolium precatalyst **79** (n= 2, 0.08 M), in 0.107 M NEt_3 and 0.053 M NEt_3·HCl in methanol-d_4.

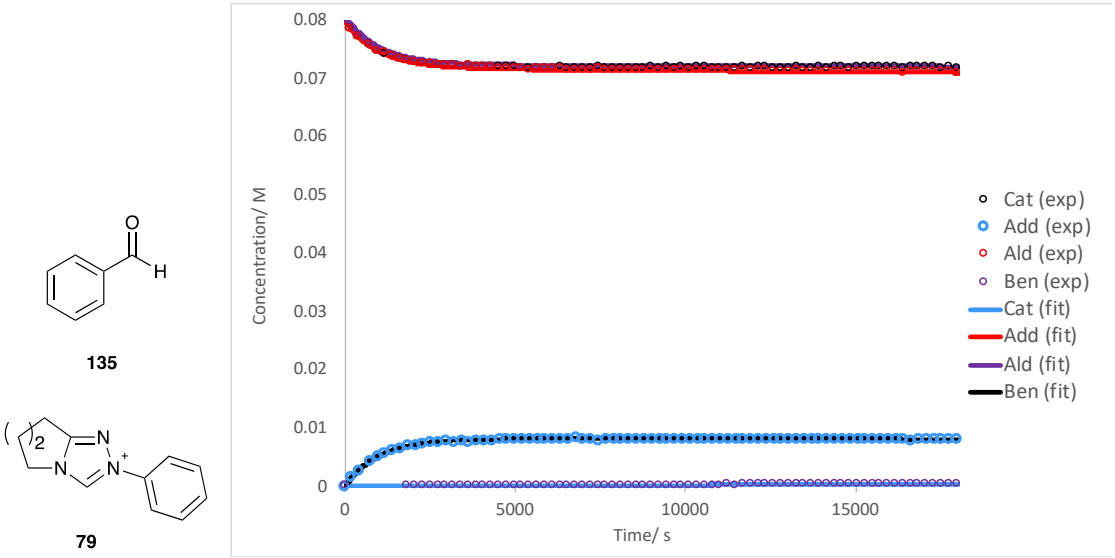

Global fitting profile for the self-condensation of 2-methylbenzaldehyde **136** (0.036 M), catalysed by *para*-methoxyphenyl triazolium precatalyst **90** (n= 2, 0.04 M), in 0.107 M NEt_3 and 0.053 M NEt_3·HCl in methanol-d_4.

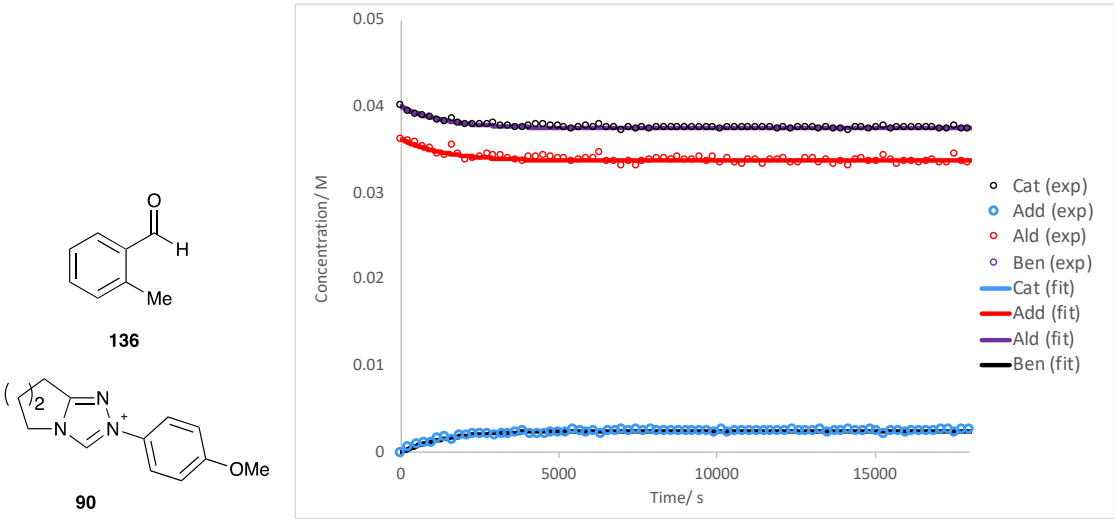

Global fitting profile for the self-condensation of 2-methoxybenzaldehyde **138** (0.038 M), catalysed by *para*-methoxyphenyl triazolium precatalyst **90** (n= 2, 0.039 M), in 0.107 M NEt_3 and 0.053 M NEt_3·HCl in methanol-d_4.

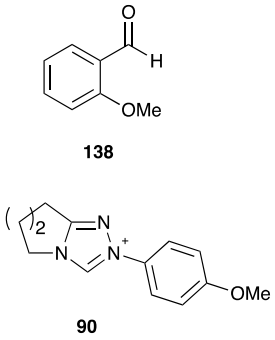

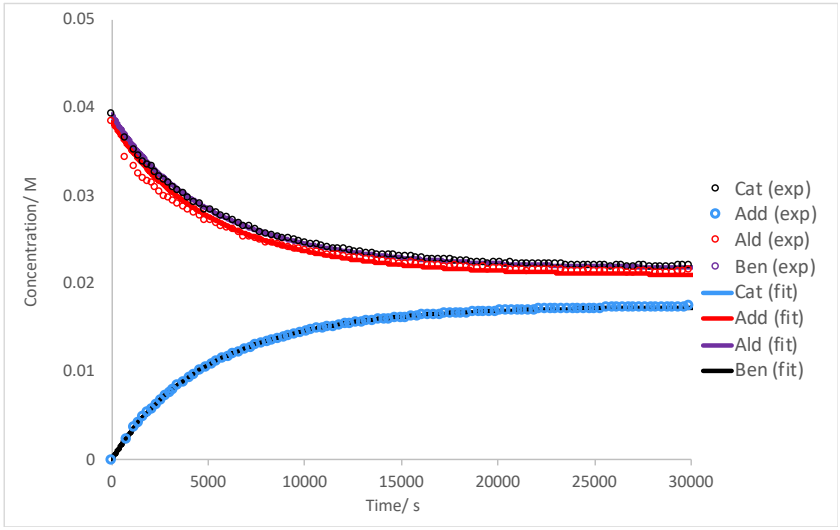

Global fitting profile for the self-condensation of 4-methylbenzaldehyde **137** (0.04 M), catalysed by *para*-methoxyphenyl triazolium precatalyst **90** (n= 2, 0.04 M), in 0.107 M NEt_3 and 0.053 M NEt_3·HCl in methanol-d_4.

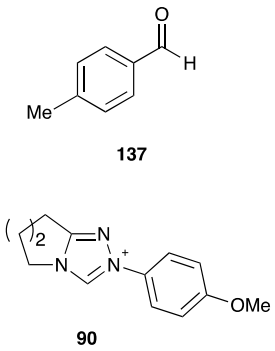

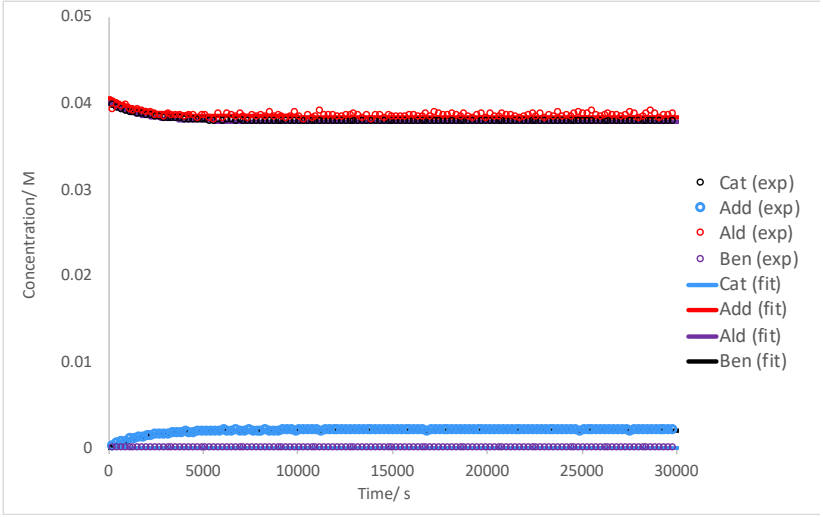

Global fitting profile for the self-condensation of 4-methoxybenzaldehyde **139** (0.093 M), catalysed by *para*-methoxyphenyl triazolium precatalyst **90** (n= 2, 0.04 M), in 0.107 M NEt_3 and 0.053 M $NEt_3 \cdot HCl$ in methanol-d_4.

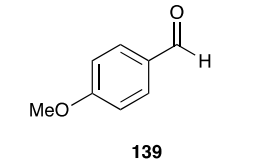

139

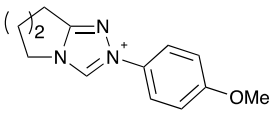

90

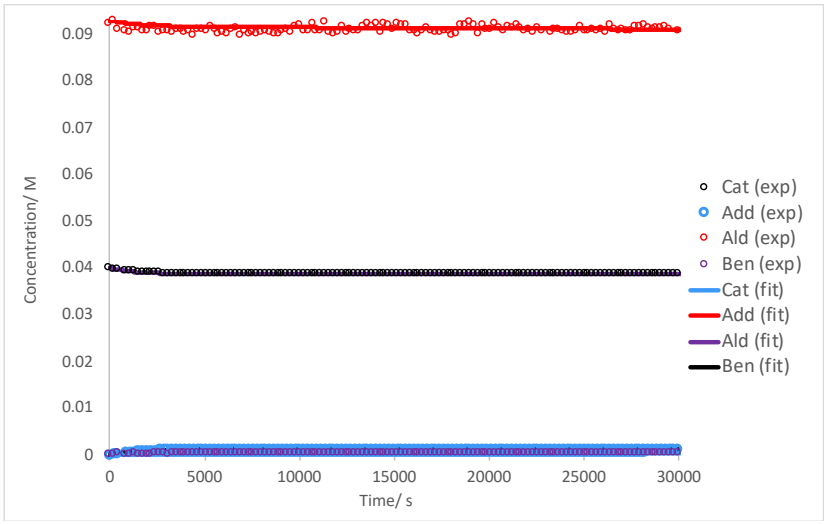

Global fitting profile for the self-condensation of benzaldehyde **135** (0.063 M), catalysed by *para*-methoxyphenyl triazolium precatalyst **90** (n= 2, 0.04 M), in 0.107 M NEt_3 and 0.053 M $NEt_3 \cdot HCl$ in methanol-d_4.

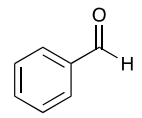

135

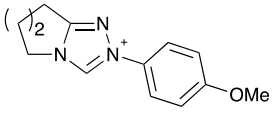

90

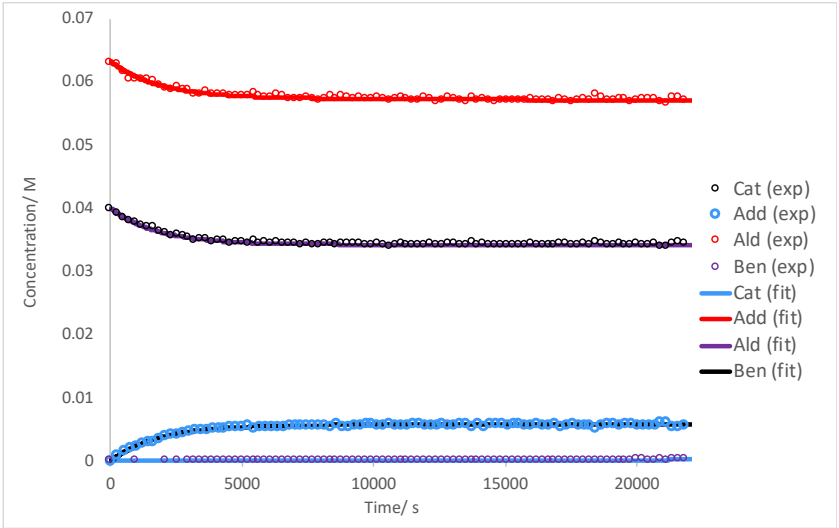

Global fitting profile for the self-condensation of 2-methylbenzaldehyde **136** (0.077 M), catalysed by *para*-fluorophenyl triazolium precatalyst **78** (n= 3, 0.078 M), in 0.107 M NEt_3 and 0.053 M NEt_3·HCl in methanol-d_4.

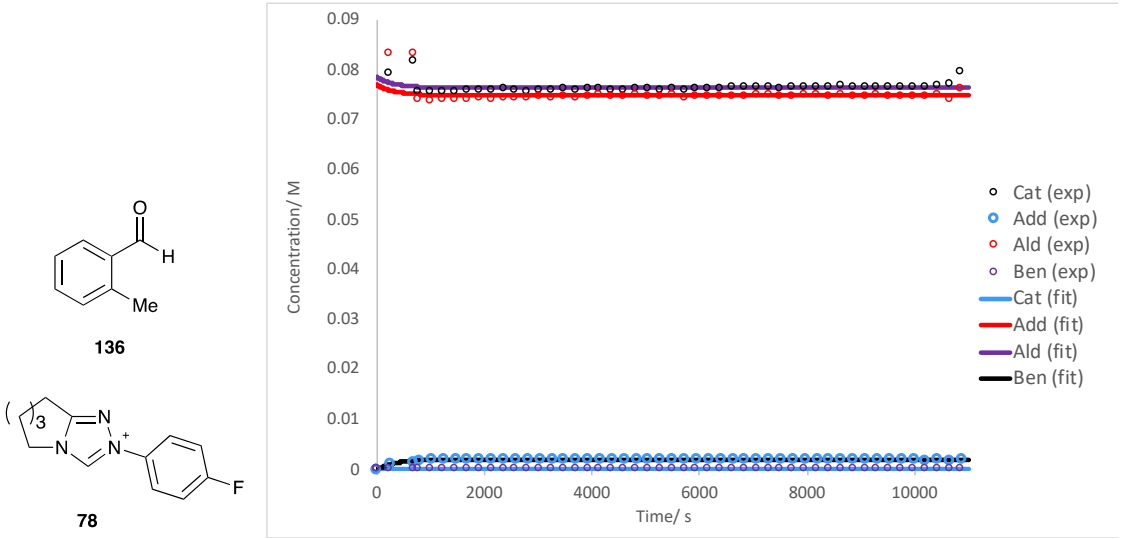

Global fitting profile for the self-condensation of 2-methoxybenzaldehyde **138** (0.081 M), catalysed by *para*-fluorophenyl triazolium precatalyst **78** (n= 3, 0.078 M), in 0.107 M NEt_3 and 0.053 M NEt_3·HCl in methanol-d_4.

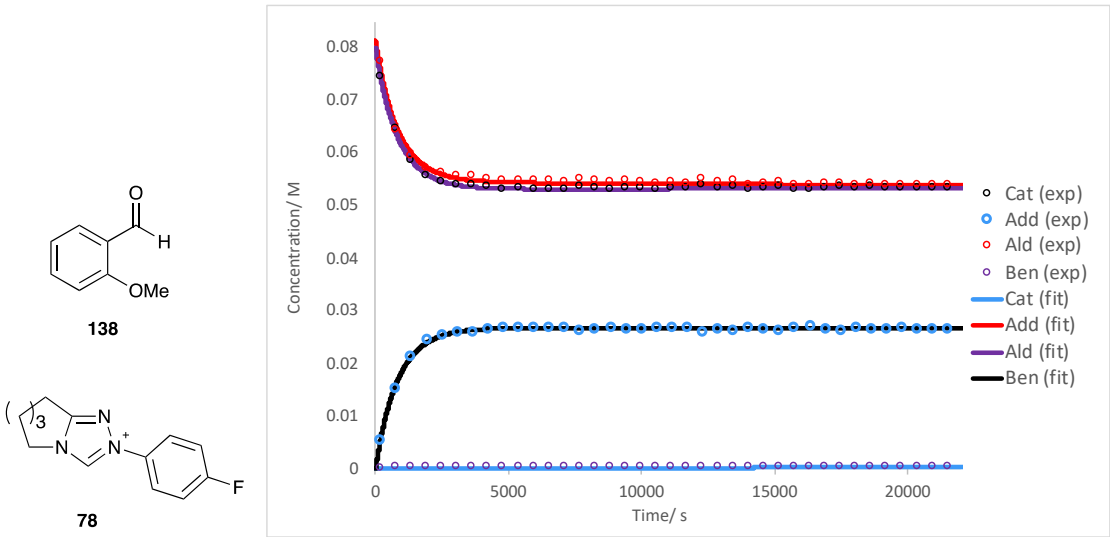

Global fitting profile for the self-condensation of 4-methylbenzaldehyde **137** (0.081 M), catalysed by *para*-fluorophenyl triazolium precatalyst **78** (n= 3, 0.08 M), in 0.107 M NEt_3 and 0.053 M NEt_3·HCl in methanol-d_4.

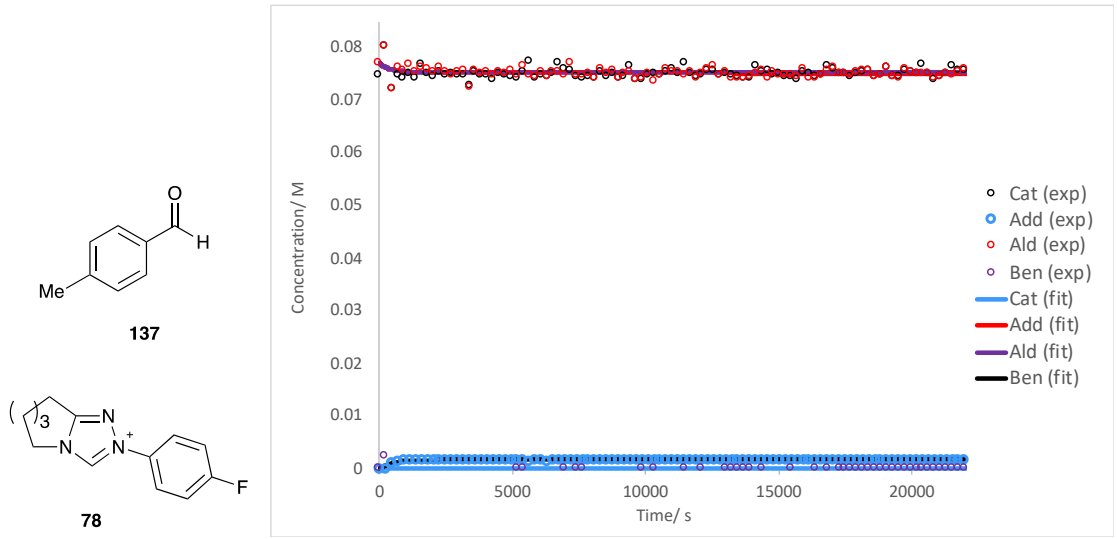

Global fitting profile for the self-condensation of 4-methoxybenzaldehyde **139** (0.073 M), catalysed by *para*-fluorophenyl triazolium precatalyst **78** (n= 3, 0.076 M), in 0.107 M NEt_3 and 0.053 M NEt_3·HCl in methanol-d_4.

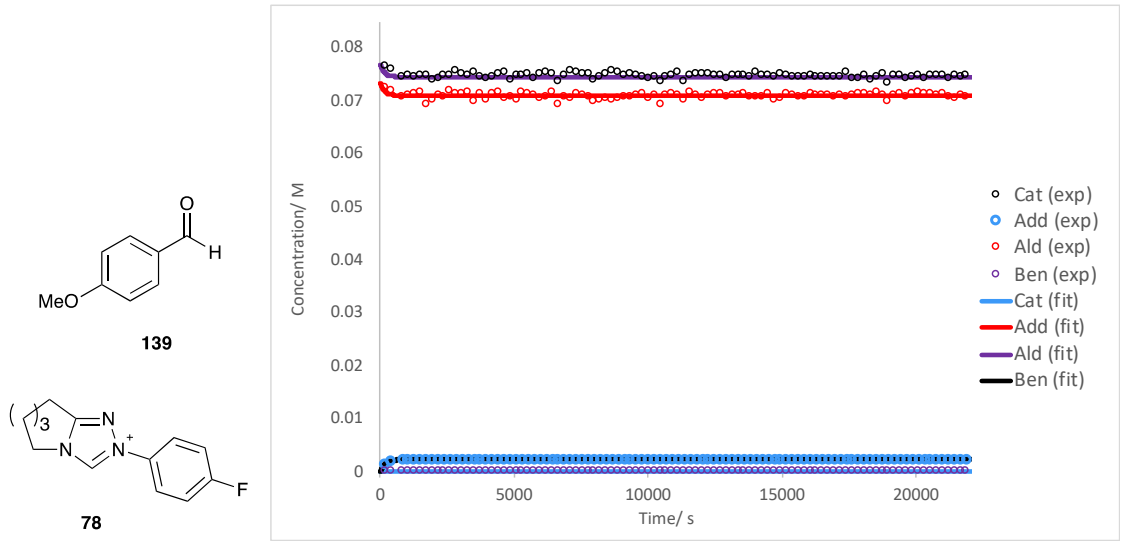

Global fitting profile for the self-condensation of benzaldehyde **135** (0.069 M), catalysed by *para*-fluorophenyl triazolium precatalyst **78** (n= 3, 0.08 M), in 0.107 M NEt_3 and 0.053 M $NEt_3 \cdot HCl$ in methanol-d_4.

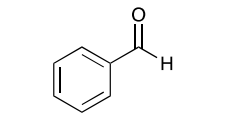

135

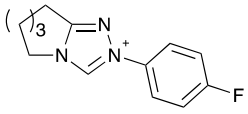

78

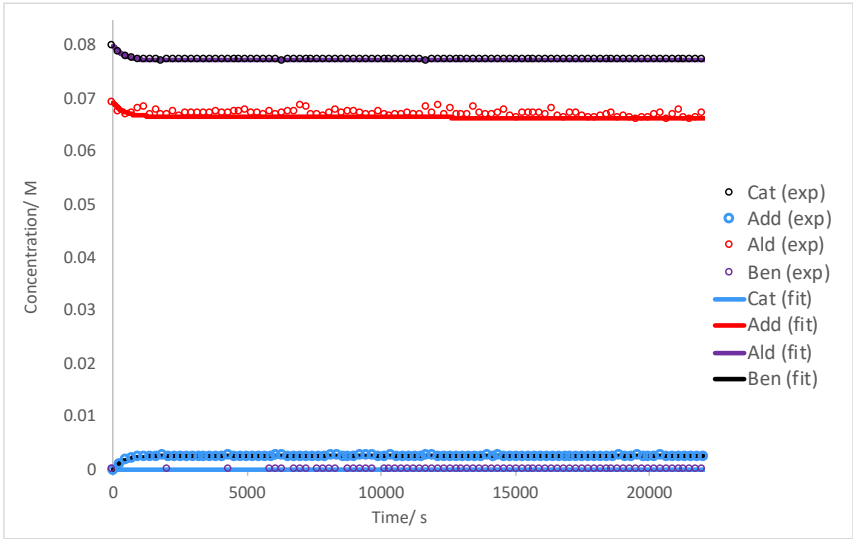

Global fitting profile for the self-condensation of 2-methylbenzaldehyde **136** (0.074 M), catalysed by phenyl triazolium precatalyst **80** (n= 3, 0.08 M), in 0.107 M NEt_3 and 0.053 M $NEt_3 \cdot HCl$ in methanol-d_4.

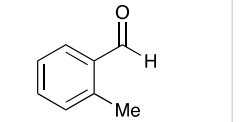

136

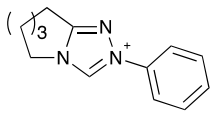

80

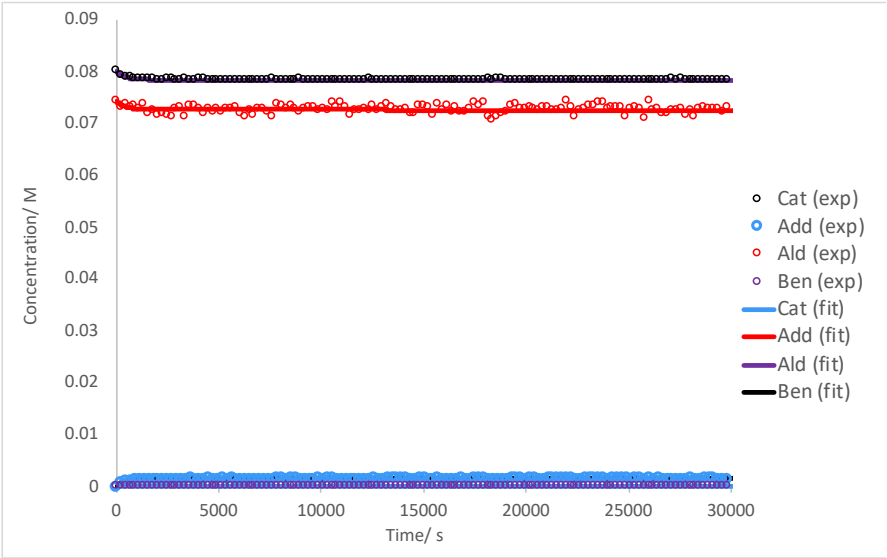

Global fitting profile for the self-condensation of 2-methoxybenzaldehyde **138** (0.081 M), catalysed by phenyl triazolium precatalyst **80** (n= 3, 0.08 M), in 0.107 M NEt_3 and 0.053 M $NEt_3 \cdot HCl$ in methanol-d_4.

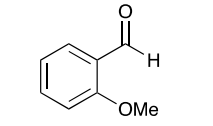

138

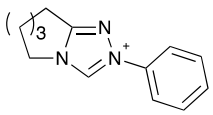

80

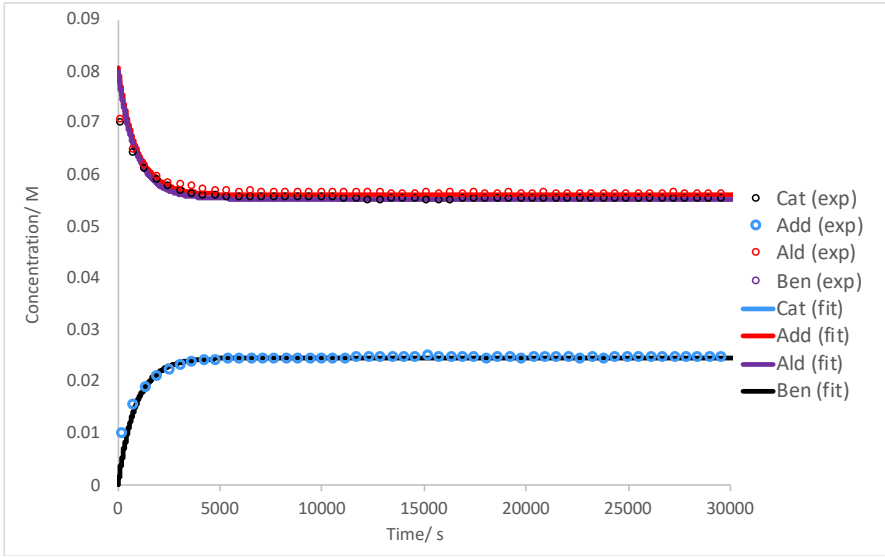

Global fitting profile for the self-condensation of 4-methylbenzaldehyde **137** (0.073 M), catalysed by phenyl triazolium precatalyst **80** (n= 3, 0.08 M), in 0.107 M NEt_3 and 0.053 M $NEt_3 \cdot HCl$ in methanol-d_4.

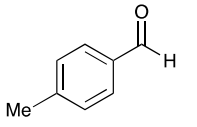

137

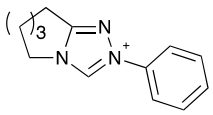

80

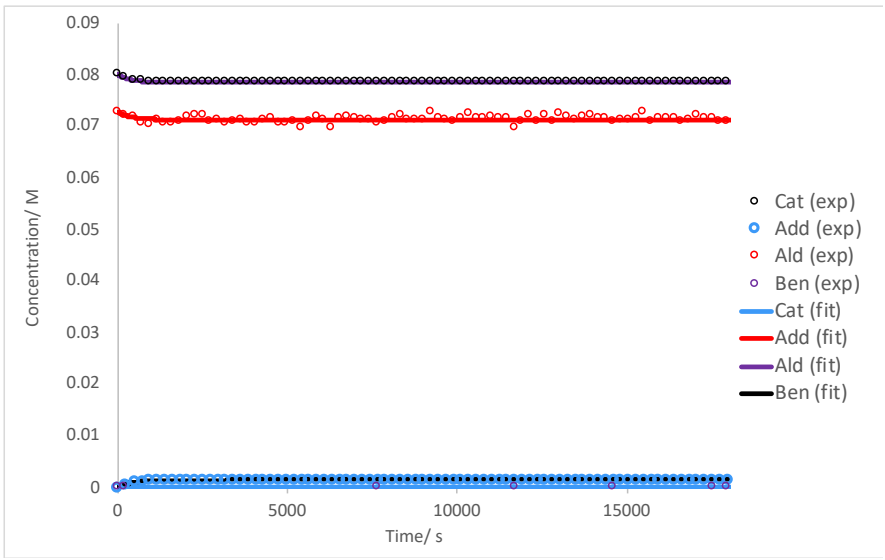

Global fitting profile for the self-condensation of benzaldehyde **135** (0.071 M), catalysed by phenyl triazolium precatalyst **80** (n= 3, 0.08 M), in 0.107 M NEt_3 and 0.053 M $NEt_3 \cdot HCl$ in methanol-d_4.

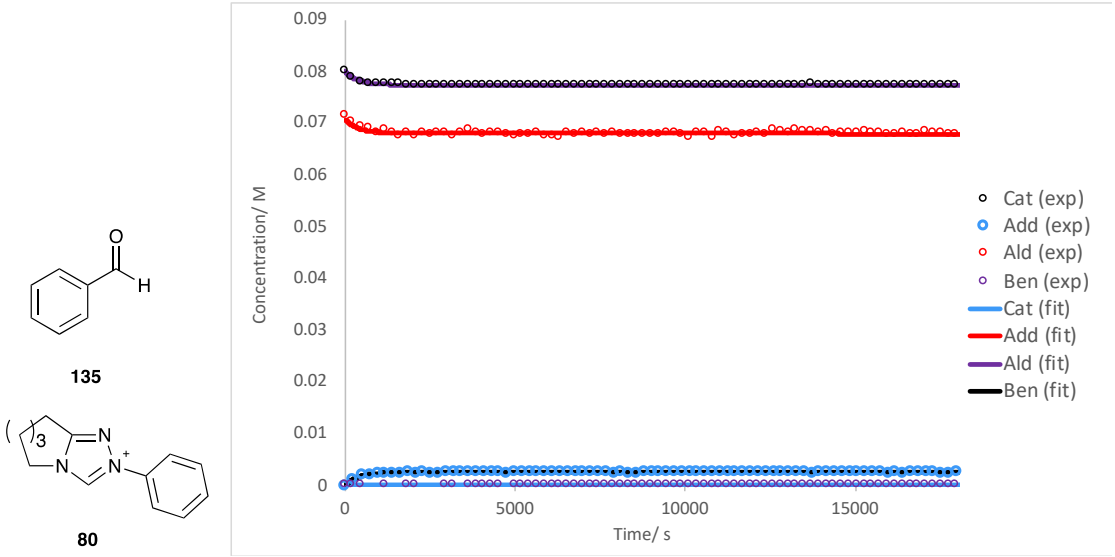

Global fitting profile for the self-condensation of 2-methylbenzaldehyde **136** (0.081 M), catalysed by *para*-methoxyphenyl triazolium precatalyst **91** (n= 3, 0.06 M), in 0.107 M NEt_3 and 0.053 M $NEt_3 \cdot HCl$ in methanol-d_4.

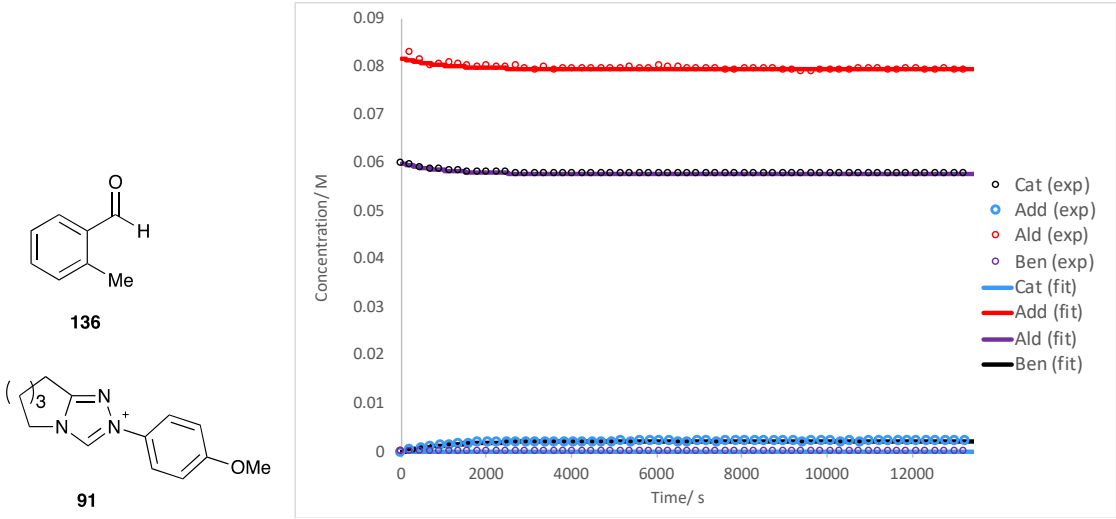

Global fitting profile for the self-condensation of 2-methoxybenzaldehyde **138** (0.06 M), catalysed by *para*-methoxyphenyl triazolium precatalyst **91** (n= 3, 0.06 M), in 0.107 M NEt_3 and 0.053 M $NEt_3 \cdot HCl$ in methanol-d_4.

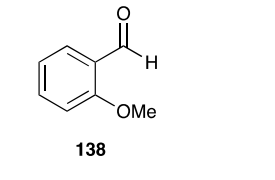

138

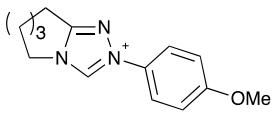

91

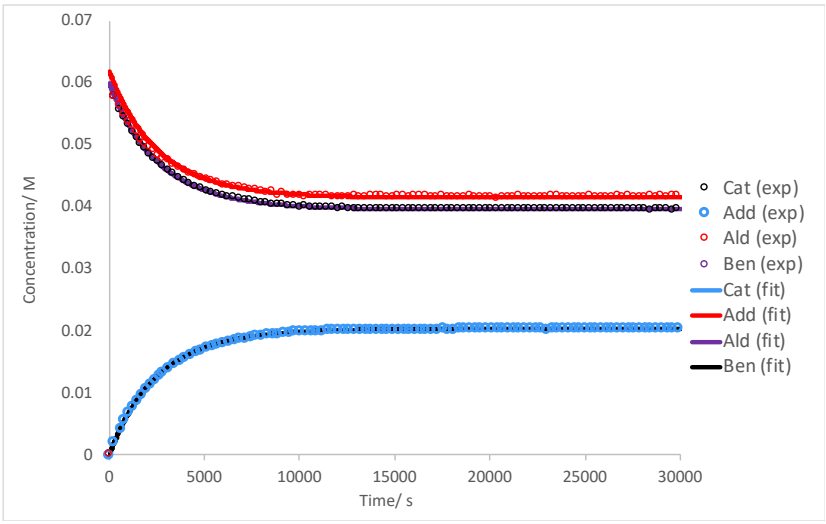

Global fitting profile for the self-condensation of 4-methylbenzaldehyde **137** (0.086 M), catalysed by *para*-methoxyphenyl triazolium precatalyst **91** (n= 3, 0.06 M), in 0.107 M NEt_3 and 0.053 M $NEt_3 \cdot HCl$ in methanol-d_4.

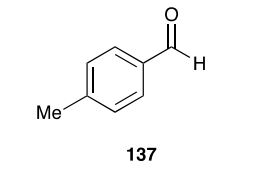

137

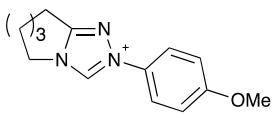

91

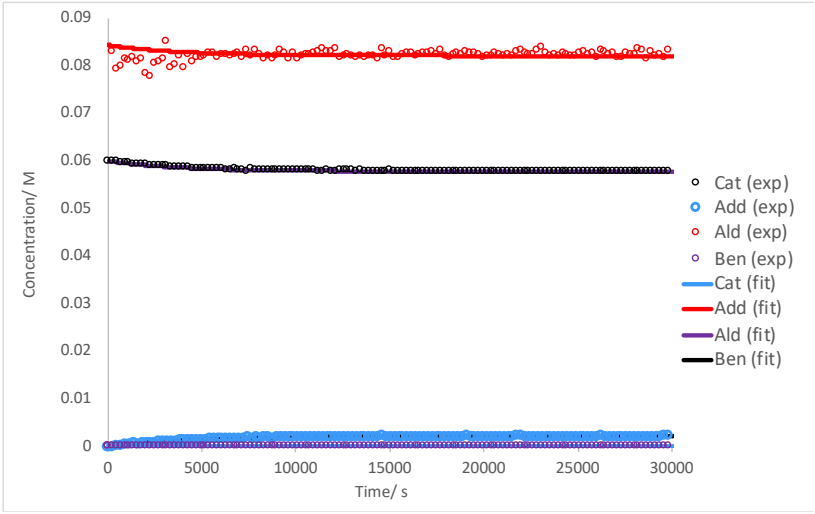

Global fitting profile for the self-condensation of benzaldehyde **135** (0.06 M), catalysed by *para*-methoxyphenyl triazolium precatalyst **91** (n= 3, 0.06 M), in 0.107 M NEt_3 and 0.053 M $NEt_3 \cdot HCl$ in methanol-d_4.

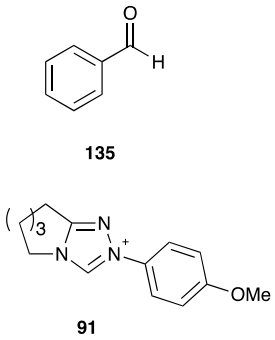

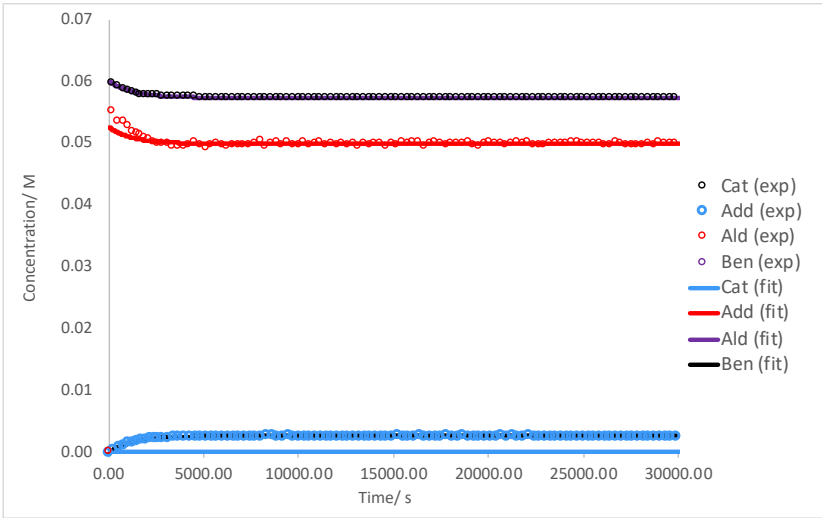

Hammett Analysis

Substituent constants and the logarithmic ratio of reaction parameters of benzaldehyde **135** in the presence of triazolium salts **89, 100, 103-105**.

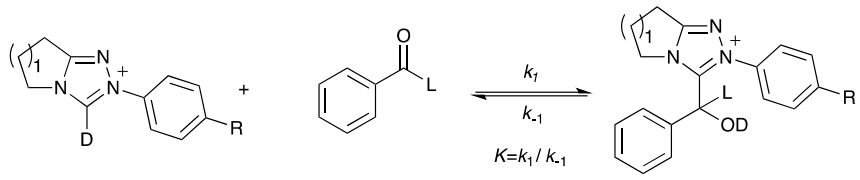

R=	σ	lg(k_1/k_1^H)	lg(k_{-1}/k_{-1}^H)	lg(K/K^H)
4-OMe	-0.268	-0.015	-0.285	0.269
4-F	0.062	0.472	0.346	0.125
4-Br	0.232	0.619	0.601	0.019
3-Cl	0.373	0.722	0.701	0.021
4-CF3	0.54	0.962	1.053	-0.091

Substituent constants and the logarithmic ratio of reaction parameters of *para*-methoxybenzaldehyde **139** in the presence of triazolium salts **89, 100, 103-105**.

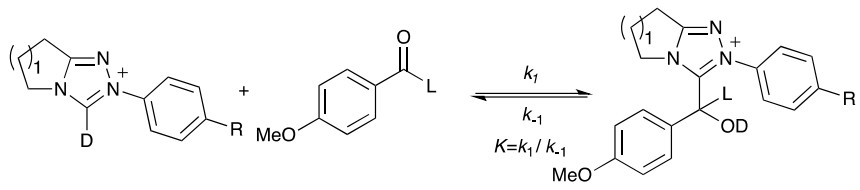

R=	σ	lg(k_1/k_1^H)	lg(k_{-1}/k_{-1}^H)	lg(K/K^H)
4-OMe	-0.268	0.012	-0.149	0.161
4-F	0.062	0.452	0.357	0.096
4-Br	0.232	0.724	0.707	0.018
3-Cl	0.373	0.834	0.857	-0.023
4-CF3	0.54	0.853	1.044	-0.191

Substituent constants and the logarithmic ratio of reaction parameter k_2 of aldehyde **135, 138, 139** in the presence of triazolium salts **89, 100, 103-105**.

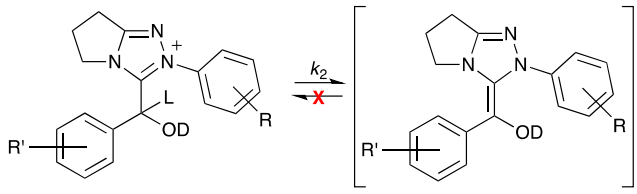

R=	σ	$lg(k_2/k_2^H)^{2\text{-OMe}}$	$lg(k_2/k_2^H)^H$	$lg(k_2/k_2^H)^{4\text{-OMe}}$
4-OMe	-0.268	0.384	0.050	-0.745
4-F	0.062	-0.165	0.456	0.089
4-Br	0.232	0.458	0.230	0.012
3-Cl	0.373	0.465	0.328	-0.117
4-CF3	0.54	0.823	0.573	0.037

Summary of the reaction constants, ρ, of each reaction parameters.

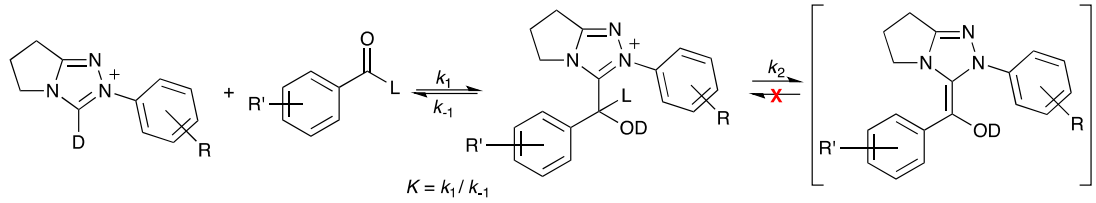

R'=	n=	N(Data)[a]	$\rho(k_1)^R$	$\rho(k_{-1})^R$	$\rho(K)^R$	$\rho(k_2)^R$
2-OMe	1	5	1.5	1.8	-0.3	1.1
	2	2	1.6	1.8	-0.2	2.4
	3	2	1.1	1.5	-0.4	1.1
Ph	1	5	1.2	1.6	-0.4	0.5
	2	2	1.4	1.9	-0.5	
	3	2	0.8	1.6	-0.8	1.8
4-OMe	1	5	1.1	1.5	-0.4	0.8
	2	2			0.2	
	3	2				
2-Me	1	5	1.9	1.7	0.2	1.9
	2	2	1.2	1.2	0.01	
	3	2	1.6	2.1	-0.6	
4-Me	1	2	1.6	1.5	0.2	1.6
	2	2	1.4	1.8	-0.5	1.7
	3	2	2.9	3.5	-0.6	1.3

Proof of Equation

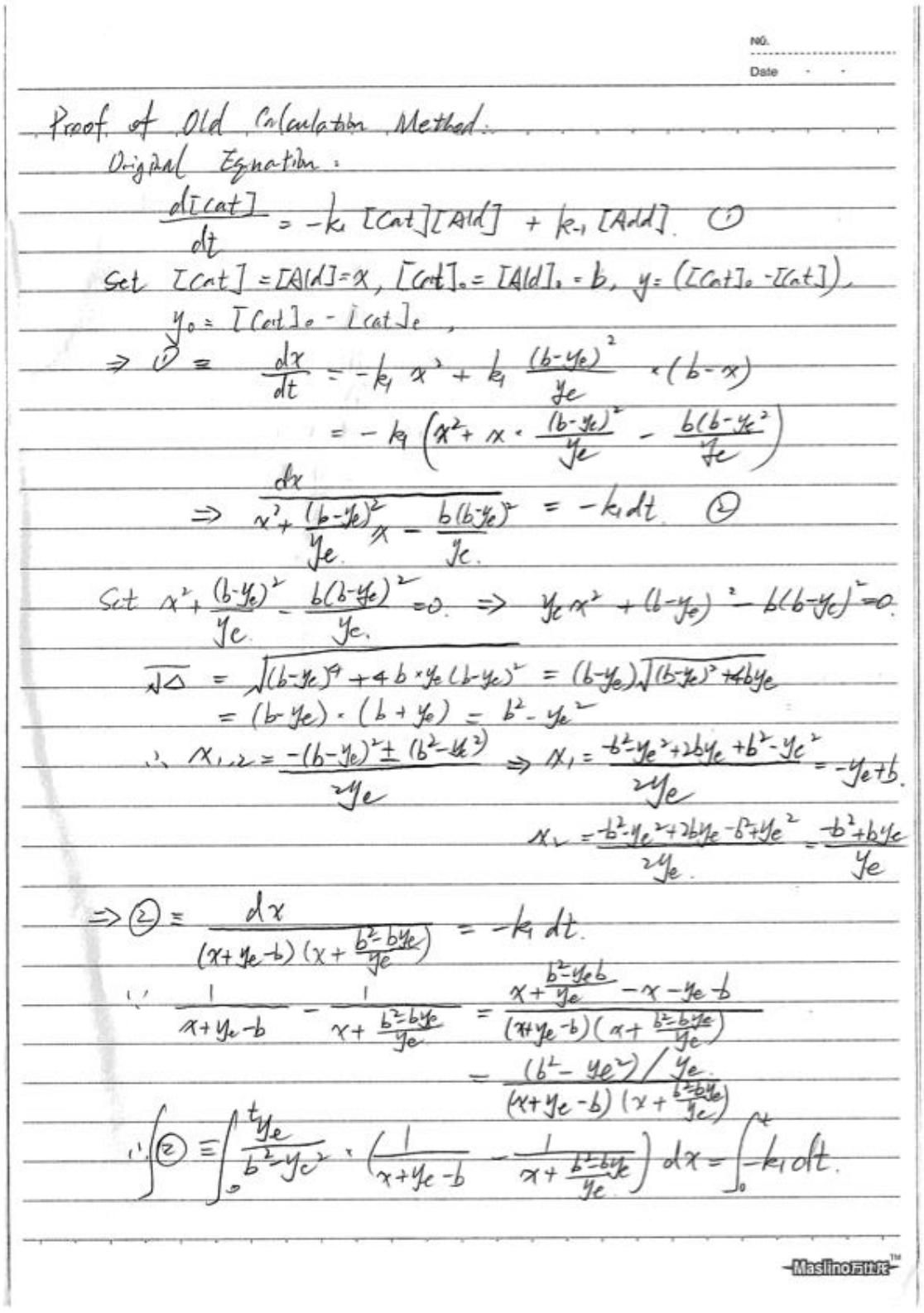

Proof of Old Calculation Method:

Original Equation:

$$\frac{d[Cat]}{dt} = -k_1[Cat][Ald] + k_{-1}[Add] \quad ①$$

Set $[Cat] = [Ald] = x$, $[Cat]_0 = [Ald]_0 = b$, $y = ([Cat]_0 - [Cat])$,

$y_0 = [Cat]_0 - [Cat]_e$,

$$\Rightarrow ① \equiv \frac{dx}{dt} = -k_1 x^2 + k_1 \frac{(b-y_e)^2}{y_e} \times (b-x)$$

$$= -k_1\left(x^2 + x \cdot \frac{(b-y_e)^2}{y_e} - \frac{b(b-y_e)^2}{y_e}\right)$$

$$\Rightarrow \frac{dx}{x^2 + \frac{(b-y_e)^2}{y_e}x - \frac{b(b-y_e)^2}{y_e}} = -k_1 dt \quad ②$$

Set $x^2 + \frac{(b-y_e)^2}{y_e} - \frac{b(b-y_e)^2}{y_e} = 0 \Rightarrow y_e x^2 + (b-y_e)^2 - b(b-y_e)^2 = 0$.

$$\sqrt{\Delta} = \sqrt{(b-y_e)^4 + 4b \times y_e (b-y_e)^2} = (b-y_e)\sqrt{(b-y_e)^2 + 4by_e}$$

$$= (b-y_e) \cdot (b+y_e) = b^2 - y_e^2$$

$$\therefore x_{1,2} = \frac{-(b-y_e)^2 \pm (b^2-y_e^2)}{2y_e} \Rightarrow x_1 = \frac{-b^2-y_e^2+2by_e+b^2-y_e^2}{2y_e} = -y_e + b.$$

$$x_2 = \frac{-b^2-y_e^2+2by_e-b^2+y_e^2}{2y_e} = \frac{-b^2+by_e}{y_e}$$

$$\Rightarrow ② \equiv \frac{dx}{(x+y_e-b)\left(x+\frac{b^2-by_e}{y_e}\right)} = -k_1 dt.$$

$$\therefore \frac{1}{x+y_e-b} - \frac{1}{x+\frac{b^2-by_e}{y_e}} = \frac{x+\frac{b^2-y_e b}{y_e} - x - y_e + b}{(x+y_e-b)\left(x+\frac{b^2-by_e}{y_e}\right)}$$

$$= \frac{(b^2-y_e^2)/y_e}{(x+y_e-b)\left(x+\frac{b^2-by_e}{y_e}\right)}$$

$$\therefore \int ② \equiv \int_0^t \frac{y_e}{b^2-y_e^2} \cdot \left(\frac{1}{x+y_e-b} - \frac{1}{x+\frac{b^2-by_e}{y_e}}\right) dx = \int_0^t -k_1 dt.$$

No.

Date

Proof of Old Calculation Method:

Original Equation:

$$\frac{d[Cat]}{dt} = -k_1[Cat][Ald] + k_{-1}[Add] \quad ①$$

Set $[Cat] = [Ald] = x$, $[Cat]_0 = [Ald]_0 = b$, $y = ([Cat]_0 - [Cat])$,

$y_0 = [Cat]_0 - [Cat]_e$,

$$\Rightarrow ① \equiv \frac{dx}{dt} = -k_1 x^2 + k_1 \frac{(b-y_e)^2}{y_e} \times (b-x)$$

$$= -k_1\left(x^2 + x \cdot \frac{(b-y_e)^2}{y_e} - \frac{b(b-y_e)^2}{y_e}\right)$$

$$\Rightarrow \frac{dx}{x^2 + \frac{(b-y_e)^2}{y_e}x - \frac{b(b-y_e)^2}{y_e}} = -k_1 dt \quad ②$$

Set $x^2 + \frac{(b-y_e)^2}{y_e}x - \frac{b(b-y_e)^2}{y_e} = 0 \Rightarrow y_e x^2 + (b-y_e)^2 x - b(b-y_e)^2 = 0$

$$\sqrt{\Delta} = \sqrt{(b-y_e)^4 + 4b \cdot y_e (b-y_e)^2} = (b-y_e)\sqrt{(b-y_e)^2 + 4by_e}$$

$$= (b-y_e)\cdot(b+y_e) = b^2 - y_e^2$$

$$\therefore x_{1,2} = \frac{-(b-y_e)^2 \pm (b^2-y_e^2)}{2y_e} \Rightarrow x_1 = \frac{-b^2+y_e^2+2by_e+b^2-y_e^2}{2y_e} = -y_e + b.$$

$$x_2 = \frac{-b^2+y_e^2+2by_e-b^2+y_e^2}{2y_e} = \frac{-b^2+by_e}{y_e}$$

$$\Rightarrow ② \equiv \frac{dx}{(x+y_e-b)\left(x+\frac{b^2-by_e}{y_e}\right)} = -k_1 dt.$$

$$\because \frac{1}{x+y_e-b} - \frac{1}{x+\frac{b^2-by_e}{y_e}} = \frac{x+\frac{b^2-y_e b}{y_e} - x - y_e + b}{(x+y_e-b)\left(x+\frac{b^2-by_e}{y_e}\right)}$$

$$= \frac{(b^2-y_e^2)/y_e}{(x+y_e-b)\left(x+\frac{b^2-by_e}{y_e}\right)}$$

$$\therefore \int ② \equiv \int_0^{t} \frac{y_e}{b^2-y_e^2} \cdot \left(\frac{1}{x+y_e-b} - \frac{1}{x+\frac{b^2-by_e}{y_e}}\right) dx = \int_0^{t} -k_1 dt.$$

No.

Date

Proof of Old Calculation Method.

Original Equation:

$$\frac{d[Cat]}{dt} = -k_1[Cat][Ald] + k_{-1}[Add] \quad ①$$

Set $[Cat] = [Ald] = x$, $[Cat]_0 = [Ald]_0 = b$, $y = ([Cat]_0 - [Cat])$.

$y_0 = [Cat]_0 - [Cat]_e$,

$$\Rightarrow ① \equiv \frac{dx}{dt} = -k_1 x^2 + k_1 \frac{(b-y_e)^2}{y_e} \times (b-x)$$

$$= -k_1\left(x^2 + x \cdot \frac{(b-y_e)^2}{y_e} - \frac{b(b-y_e)^2}{y_e}\right)$$

$$\Rightarrow \frac{dx}{x^2 + \frac{(b-y_e)^2}{y_e}x - \frac{b(b-y_e)^2}{y_e}} = -k_1 dt \quad ②$$

Set $x^2 + \frac{(b-y_e)^2}{y_e}x - \frac{b(b-y_e)^2}{y_e} = 0 \Rightarrow y_e x^2 + (b-y_e)^2 x - b(b-y_e)^2 = 0$.

$$\sqrt{\Delta} = \sqrt{(b-y_e)^4 + 4b \cdot y_e (b-y_e)^2} = (b-y_e)\sqrt{(b-y_e)^2 + 4by_e}$$

$$= (b-y_e)\cdot(b+y_e) = b^2 - y_e^2$$

$$\therefore x_{1,2} = \frac{-(b-y_e)^2 \pm (b^2-y_e^2)}{2y_e} \Rightarrow x_1 = \frac{-b^2+y_e^2+2by_e+b^2-y_e^2}{2y_e} = -y_e + b.$$

$$x_2 = \frac{-b^2+y_e^2+2by_e-b^2+y_e^2}{2y_e} = \frac{-b^2+by_e}{y_e}$$

$$\Rightarrow ② \equiv \frac{dx}{(x+y_e-b)\left(x+\frac{b^2-by_e}{y_e}\right)} = -k_1 dt.$$

$$\therefore \frac{1}{x+y_e-b} - \frac{1}{x+\frac{b^2-by_e}{y_e}} = \frac{x+\frac{b^2-y_e b}{y_e} - x - y_e + b}{(x+y_e-b)\left(x+\frac{b^2-by_e}{y_e}\right)}$$

$$= \frac{(b^2-y_e^2)/y_e}{(x+y_e-b)\left(x+\frac{b^2-by_e}{y_e}\right)}$$

$$\therefore \int ② \equiv \int_0^t \frac{y_e}{b^2-y_e^2} \cdot \left(\frac{1}{x+y_e-b} - \frac{1}{x+\frac{b^2-by_e}{y_e}}\right) dx = \int_0^t -k_1 dt.$$

No.

Date

Proof of Old Calculation Method:

Original Equation:

$$\frac{d[Cat]}{dt} = -k_1[Cat][Ald] + k_{-1}[Add] \quad ①$$

Set $[Cat] = [Ald] = x$, $[Cat]_0 = [Ald]_0 = b$, $y = ([Cat]_0 - [Cat])$,

$y_0 = [Cat]_0 - [Cat]_e$,

$$\Rightarrow ① \equiv \frac{dx}{dt} = -k_1 x^2 + k_1 \frac{(b-y_e)^2}{y_e} \times (b-x)$$

$$= -k_1\left(x^2 + x \cdot \frac{(b-y_e)^2}{y_e} - \frac{b(b-y_e)^2}{y_e}\right)$$

$$\Rightarrow \frac{dx}{x^2 + \frac{(b-y_e)^2}{y_e}x - \frac{b(b-y_e)^2}{y_e}} = -k_1 dt \quad ②$$

Set $x^2 + \frac{(b-y_e)^2}{y_e} - \frac{b(b-y_e)^2}{y_e} = 0 \Rightarrow y_e x^2 + (b-y_e)^2 - b(b-y_e)^2 = 0$.

$$\sqrt{\Delta} = \sqrt{(b-y_e)^4 + 4b \times y_e (b-y_e)^2} = (b-y_e)\sqrt{(b-y_e)^2 + 4by_e}$$

$$= (b-y_e)\cdot(b+y_e) = b^2 - y_e^2$$

$$\therefore x_{1,2} = \frac{-(b-y_e)^2 \pm (b^2-y_e^2)}{2y_e} \Rightarrow x_1 = \frac{-b^2+y_e^2+2by_e+b^2-y_e^2}{2y_e} = -y_e + b.$$

$$x_2 = \frac{-b^2-y_e^2+2by_e-b^2+y_e^2}{2y_e} = \frac{-b^2+by_e}{y_e}$$

$$\Rightarrow ② \equiv \frac{dx}{(x+y_e-b)\left(x+\frac{b^2-by_e}{y_e}\right)} = -k_1 dt.$$

$$\therefore \frac{1}{x+y_e-b} - \frac{1}{x+\frac{b^2-by_e}{y_e}} = \frac{x+\frac{b^2-y_e b}{y_e} - x - y_e + b}{(x+y_e-b)\left(x+\frac{b^2-by_e}{y_e}\right)}$$

$$= \frac{(b^2-y_e^2)/y_e}{(x+y_e-b)\left(x+\frac{b^2-by_e}{y_e}\right)}$$

$$\therefore \int ② \equiv \int_0^t \frac{y_e}{b^2-y_e^2} \cdot \left(\frac{1}{x+y_e-b} - \frac{1}{x+\frac{b^2-by_e}{y_e}}\right) dx = \int_0^t -k_1 dt.$$